1993

Solid state chemistry of alkali-metal-indium systems: synthesis, characterization and bonding of indium cluster phases

Slavi Christov Sevov
Iowa State University

Order Number 9335019

Solid state chemistry of alkali-metal-indium systems: Synthesis, characterization and bonding of indium cluster phases

Sevov, Slavi Christov, Ph.D.

Iowa State University, 1993

U·M·I
300 N. Zeeb Rd.
Ann Arbor, MI 48106

Solid state chemistry of alkali-metal–indium systems:

Synthesis, characterization and bonding of indium cluster phases

by

Slavi Christov Sevov

A Dissertation Submitted to the

Graduate Faculty in Partial Fulfillment of the

Requirements for the Degree of

DOCTOR OF PHILOSOPHY

Department: **Chemistry**
Major: **Inorganic Chemistry**

Approved:

Signature was redacted for privacy.

In Charge of Major Work

Signature was redacted for privacy.

For the Major Department

Signature was redacted for privacy.

For the Graduate College

Iowa State University
Ames, Iowa

1993

TABLE OF CONTENTS

ACKNOWLEDGMENTS

I thank Professor John D. Corbett for supporting and encouraging my efforts throughout the course of this research. His suggestions and advice, and especially his ability to discriminate the important from the unimportant, have been a great help to me and an example to follow. I appreciate the freedom he has given me to explore new fields in solid state chemistry.

I thank Victor Young for helping with single crystal X-ray data collections; Jerry Ostenson for the magnetic measurements; Gordie Miller for helping with the extended-Hückel calculations; Joseph Shinar for providing the "Q" apparatus for the conductivity measurements.

I am indebted to Shirley Standley and all former and present members of Dr. Corbett's and Dr. Franzen's groups. They have always been supportive and helpful, and I have had great times and great discussions with them.

Also, I would like to thank my parents, Christo and Stanka Sevov, for their deep belief that education and hard labor pays off some day. They taught me this even during the hopeless and dark days of communist Bulgaria. Благодаря ви майко, татко и Любчо. I am grateful to my grandma, Lozka, and grandpa, Sevo, whose love and care made my childhood joyful.

I extend my thanks to my wife Nonka and to my daughter Elitza and son Christo for their love, patience and understanding. Without them the world would have been empty.

This work was performed at Ames Laboratory under contract no. W-7405-eng-82 with the U.S. Department of Energy. The United States govrnment has assigned the DOE Report number IS-T 1648 to this thesis.

INTRODUCTION

Organization of the dissertation

The dissertation is organized as a collection of separate papers. Some of them have been published, and others are in press, submitted or to be submitted for publication. Each paper describes the experimental details for the particular subject, contains its own references and is followed by tables, figures and, where appropriate, supplementary material. The publication status of each paper is as follows:

PAPER 1. (communication)	*Inorg. Chem.* **1991**, *30*, 4875–4877
PAPER 2.	*J. Alloys Comp.*, submitted
PAPER 3. (communication)	*Inorg. chem.* **1993**, *32*, 1059–1061
PAPER 4.	*J. Am. Chem. Soc.*, submitted
PAPER 5.	*Inorg. Chem.* **1992**, *31*, 1895–1901
PAPER 6.	*J. Solid State Chem.*, **1993**, *103*, 114–130
PAPER 7.	to be submitted
PAPER 8.	*Inorg. Chem.* **1993**, *32*, 1612–1615
PAPER 9.	*Z. Anorg. Allg. Chem.* **1993**, *619*, 128–132
PAPER 10.	to be submitted
PAPER 11.	to be submitted
PAPER 12.	to be submitted

The papers are followed by a general summary and future research section and list of references cited in the present introduction.

Background

The interest in clusters and their bonding and properties has been growing in recent years. One of the first examples of clusters of a main-group element were the boranes, $B_nH_n^{2-}$. Their

structural uniqueness caught the attention of many scientists at that time. It was found that boron forms deltahedral clusters of up to 12 atoms in these compounds. The shapes of the clusters match some of the so-called Platonic solids, geometric objects of high symmetry built of equilateral triangles. Some examples of these are the tetrahedron, the octahedron, the tricapped trigonal prism, the icosahedron etc. Each boron atom is bonded to 3, 4 or 5 other boron atoms from the cluster and is exo bonded to a hydrogen atom. Empirical rules for counting the number of electrons needed for the cluster bonding have been developed by Wade[1] and have become a very useful tools for the boranes and carboranes ($C_2B_{n-2}H_n$). These rules state that the number of skeletal electrons needed for bonding in a *closo*-cluster depends only on the number of vertices (n) of the cluster and is $2n + 2$. Moreover, the number remains the same even if some of the vertices are removed, $2n + 4$ and $2n + 6$ for the corresponding *nido*- and *arachno*-derivatives, respectively, where n is the number of remaining vertices.

The logical next step was to explore the remaining main-group elements and to try to synthesize similar clusters. It was realized that an M–H bond is not likely to be favorable for the heavier main-group elements because of the large energy difference between the H 1*s* and M n*p* orbitals. Syntheses of alternative "naked" clusters (no ligands) or interconnected clusters (each cluster has other clusters for exo-ligands) have been successful. Following is a brief discussion on the advantages and disadvantages for formation of deltahedral clusters in the different groups of post-transition elements.

Groups 6 and 7. The elements in these groups are very rich in electrons and a formation of one bond in group 7 or two bonds in group 6 leads to an octet configuration for the elements. Two-atom molecules for the halogens and chains of 2-bonded atoms for the chalcogens are common features in the chemistry of these elements. The abundance of electrons means that there is no need to share them with more atoms and, therefore, no need of cluster formation.

The only way that would lead to a cluster would be a removal of some of the electrons or, in other words, an oxidation. This, of course, is difficult since these are some of the best oxidants.

Group 5. The elements in this group are also relatively rich in electrons. They have fewer electrons than the elements in groups 6 and 7 but enough to achieve an octet by formation of three bonds. All deltahedra, except the tetrahedron, contain 4- and higher-bonded atoms and, therefore, are not preferred by these elements. Instead, they very easily form nondeltahedral clusters where each vertex is 2- or 3-bonded. Some examples are P_7^{3-} and Sb_7^{3-} with a geometry of a monocapped (triangular face) and distorted trigonal prism (four 3-bonded and three 2-bonded vertices),[2] the adamantane type P_{10}^{6-} (four 3-bonded and six 2-bonded vertices)[3] and P_{11}^{3-} (eight 3-bonded and three 2-bonded vertices).[4] The Wade's rules are not valid for such formations since simple 2-center-2-electron bonds are formed. Again, as in groups 6 and 7, electrons need to be removed in order to form deltahedra. A naked *closo*-deltahedral cation would have a charge of +(n-2), i.e., $M_n^{(n-2)+}$. Possible counteranions are the chalcogens and the halogens but the problem with them is that they tend to bond covalently with the pnictogens and form either neutral compounds ($Bi_5^{3+} + 3X^- \rightarrow 4Bi + BiX_3$[5]) or large coordination-type anions with low charges (BiX_5^{2-}). Many of the latter would be needed to balance the relatively high positive charge on the larger clusters. This requires packing of many large anions with fewer smaller cations and may be infeasible.

One solution is to form only smaller clusters that will need fewer counteranions because of the lower charges and may pack well with them. Examples are Bi_3^+ and Bi_5^{3+}.[6,7] Another way is to form *nido*- or *arachno*-species which will require lower charges, $+(n - 4)$ and $+(n - 6)$, respectively. An example is the *arachno*-Bi_8^{2+}.[6] For smaller clusters this may even lead to negative charges as in the square planar *arachno*-Bi_4^{2-}.[8] A third solution is to form different distorted deltahedra for which the Wade's rules do not apply. This may lead to lower cluster

charges. An example is the unusually elongated tricapped trigonal prism found for *closo*-Bi_9^{5+} ($2n + 4$ bonding electrons).[9]

Group 4. A *closo*-deltahedron from elements of this group would have an *n*-independent charge of -2. The problem is clear, only two cations are needed to balance the charge and, therefore, not enough to pack with the clusters, especially larger ones, and to separate them efficiently from each other in a solid.

Two solutions have been found for this problem. The first one is to form *arachno*- or *nido*-derivatives of relatively small clusters. These will have higher charges of -4 and -6, respectively, and 4 or 6 cations may separate them. An example is the *nido*-Sn_4^{4-} found in NaSn.[10] The second, more efficient, way is to synthesize the clusters from solutions where large countercations such as crypt-(Na or K)$^+$ are available.[5] Examples for clusters formed by this method are *closo*-Pb_5^{2-} and Ge_9^{2-} and *nido*-Sn_9^{4-}.[11-13]

Group 3. The elements in this group appear to have the appropriate number of electrons for formation of deltahedral clusters. Surprisingly, though, not much exploration has been done prior to this work. The elements of this group are frequently called electron poor-elements. They have only one *p*-electron per atom and need to share it with as many atoms as possible in order to achieve good bonding. This, of course, is the prerequisite for cluster formation. A *closo*-deltahedron of these atoms will have a charge of $-(n + 2)$ and require that many alkali-metal countercations. An obvious problem associated with this is that large clusters will have unreasonably high charges and are unlikely to form. Smaller clusters like *nido*-In_4^{8-}, Tl_4^{8-}, on the other hand, are stable and have been found in Na_2In (Paper 6) and Na_2Tl,[14] respectively.

Four different ways to alleviate the problem of the high cluster charges are presented here for indium. The first one is to form hitherto unknown types of clusters with geometries different from the boranes that would require fewer than $2n + 2$ electrons. Examples are In_{11}^{7-} and

$In_{10}Hg^{8-}$ in K_8In_{11} and $K_8In_{10}Hg$, respectively (Papers 1 and 2). The second way is again a hypoelectronic cluster with geometry deviating from the boranes but in addition, with a central heteroatom. The heteroatom provides additional bonding as in $In_{10}Ni^{10-}$ (Paper 4) or additional bonding and additional electrons as in $In_{10}Zn^{8-}$. The third way, by far the most frequently encountered, is to form interconnected clusters. Each exo bond reduces the charge on the cluster by one through oxidation of a *s*-pair on a vertex. A different way to look at the exo-bonded cluster is as a borane where the hydrogen ligands are missing and some are replaced by other clusters. Examples of such exo bonded clusters are 4-bonded *closo*-In_6^{4-} (Paper 9), 12-bonded *closo*-In_{12}^{2-} and 12-bonded *arachno*-In_{12}^{6-} (Paper 8), 12-bonded *nido*-In_{11}^{4-} and 8- or 12-bonded *closo*-In_{16}^{12-} and In_{16}^{8-} (Papers 5 and 6), respectively, 6-bonded *closo*-In_{12}^{8-} (Paper 7) and 12-bonded *closo*-In_{18}^{10-} (Paper 10). The fourth way to reduce the charge of a cluster is to substitute some of the indium atoms by electron-richer elements. This has been achieved in a partially tin-substituted icosahedra of indium (Paper 10).

Boron, aluminum and gallium, in a contrast to indium, apparently undertake only the last two routes when forming clusters. The alkali-metal–gallium–(third element) systems have been explored quite extensively and only interconnected clusters have been found.[14] No isolated naked clusters have been observed. Thallium, on the other hand, forms isolated Tl_4^{8-} and Tl_{11}^{7-} similarly to indium.[15,16] Apparently the larger *s*–*p* energy separation for In and Tl than for B, Al and Ga leads to better stabilization of the *s*-pairs as lone pairs at the vertices of a naked cluster of the former.

Groups 1 and 2. No homoatomic clusters have been found for the elements of these groups, probably because of the enormous negative charges that would apparently be required. Nevertheless, these elements can substitute for indium in some clusters. Zn and Au substitute

partially for In in some of the sites in *closo*-icosahedron (Paper 10). Hg substitutes for $1/6^{th}$ of the In in the trigonal prismatic sites of $In_{10}Hg^{8-}$ (Paper 2).

A surprise in indium chemistry came with the discovery that in presence of the right ingredients this element forms fullerene-type cages of different sizes, analogous to the well known carbon fullerenes. The latter have focused the attention of many scientists and a considerable amount of work has been done on different sizes of molecules of this new form of carbon and their derivatives obtained by substitution, addition, intercalation and insertion.[17] The structural characterization of the carbon fullerenes has been quite difficult owing to the rotation of the molecules even in solid state, and so far this has relied mainly on NMR results. Nevertheless, it is known that they are hollow spherical formations of even numbers of carbon atoms (60, 70, 72, ...) with 12 pentagonal and the rest hexagonal faces. Similarly built indium cages of 70, 74 and 78 indium atoms are found in the compounds reported in Papers 11 and 12. Moreover, these cages contain isolated, Ni(Pd, Pt)-centered indium clusters at their centers which, in turn, are shielded from the inside surface of the cage by spherical layers of sodium cations. The whole formation can be compared with an onion bulb with layers of In, Na, In and Ni inward from the surface.

PART I. ISOLATED CLUSTERS OF INDIUM

PAPER 1. A REMARKABLE HYPOELECTRONIC INDIUM CLUSTER IN K_8IN_{11}

Slavi C. Sevov and John D. Corbett*

ABSTRACT

The new phase K_8In_{11} ($R\bar{3}c$, Z = 6, a = 10.006 (1) Å, c = 50.839 (7) Å) is constructed from layers of isolated indium clusters separated by potassium ion layers both in and between the cluster layers. The phase is metallic ($\rho_{295} \sim 600$ μohm-cm) and shows weak temperature-independent paramagnetism ((1—2) × 10^{-4} emu mol^{-1} corrected). The last potassium electron is evidently delocalized in the conduction band, perhaps mainly on the double potassium layers. The observed In_{11} cluster is derived from the ideal pentacapped trigonal prism (D_{3h}) through substantial compression along the C_3 axis, which produces bonding between the two types of capping atoms at the expense of that within the ends of the expanded trigonal prism. Extended-Hückel MO calculations show that the pentacapped polyhedron is closed shell with $2n - 2$ skeletal electrons, and the observed distortion converts this to the more stable In_{11}^{7-} with $2n - 4$ p electrons. This appears to be the first example of a homoatomic cluster well below the conventional $2n + 2$ (closo) skeletal electron limit. Some contrasting behavior of gallium is noted.

COMMUNICATION

We have discovered that the unprecedented, electron-poor "naked" cluster anion In_{11}^{7-} exists in the binary phase K_8In_{11}, with the added feature that one electron per formula unit is apparently delocalized in a conduction band. This result provides the first homoatomic indium cluster and evidently the first example of a stable unit well below the $2n + 2$ skeletal minimum described by Wade's rules, in this case $2n - 4$. The published K—In phase diagram,[1] based largely on thermal analysis, shows only KIn_4 ($BaAl_4$-type) plus an unknown phase near 36 at.% K that was first assigned as K_8In_{11}[2] and then $K_{22}In_{39}$ (or K_7In_{13})[1] based on a supposedly analogous sodium—gallium phase.[3] Fusion of the two elements with ~40 at.% K proportions at 530°C followed by equilibration of the solid mixture for 2—3 days each at 400°C and 300°C readily provides the corresponding high yield of the plate-like, brittle, dark gray K_8In_{11} (42.1 at.% K). Single crystal studies[4,5] reveal a new type of polyhedron, the compressed pentacapped trigonal prism shown in two views in Figure 1. Atom parameters and a listing of distances and angles are included in the supplementary material.

The In—In separations range between 2.963 (1) Å (In1—In3) and 3.097 (2) Å (In3—In3) except for the slightly longer 3.284 (1) Å distance between the two types of capping atoms, In1—In2. These values compare reasonably with 2.884 Å for the single bond distance,[6] 2.89—3.17 Å within the octahedra in Cs_2In_3,[7] and 2.990 Å in Li_3In_2 (three-bonded nets).[8] As shown in Figure 2, layers of indium polyhedra lying on three-fold axes are rhombohedrally stacked along the 50.8 Å c axis, with K2 layers within and double K1 layers between the cluster layers. Potassium caps faces of the indium polyhedron at both ends (K1) and around the waist (K2), as can be seen in Figure 1B. The 3.1° torsional twist of the trigonal prism, which lowers the symmetry from D_{3h} to D_3, can be correlated with packing effects between the large clusters and the potassium layers. The shortest intercluster In—In separation is 5.260 Å.

The new polyhedron's nearest relative appears to be the ideal (but unknown) pentacapped trigonal prism from which the new cluster is generated by a sizable compression along the three-fold axis. The triangular ends of the In3 trigonal prism are greatly expanded in the process (to 5.00 Å) but six new intercap (In1 — In2) interactions at 3.28 Å are gained. The more compact result is sort of a deltahedron if we tolerate the "creases" formed by the triangles that share In1 — In2 edges, which have a dihedral angle of 21.90° lying outside of the cluster.[9] The 19 electrons available for In p orbital bonding (assuming complete transfer from potassium) and the unlikely (but not impossible, judging from Sn_9^{3-} [10]) prospect of a paramagnetic cluster prompted additional studies. The diamagnetic susceptibilities of two K_8In_{11} samples, −(4−5) x 10^{-4} emu/mol at room temperature, decrease in magnitude by only ~10% on cooling to 25 K. Corrections of 3.1 x 10^{-4} emu/mol for the ion cores and 3.0 x 10^{-4} emu/mol estimated for the Larmor precession contribution of nine electron pairs in cluster orbitals[11] give a net of +(1−2) x 10^{-4} emu/mol, appropriate for a small Pauli paramagnetism. Extended-Hückel MO calculation results (below) place the last electron roughly 1.2 eV above a plausible HOMO. An alternative to this improbable result in the solid state is for the Fermi energy to fall within that gap, the last electron being delocalized over the crystal. Resistivities of two ground samples measured by the electrodeless "Q" method[12] over the range of 110−295°K indicated a metallic behavior, ρ_{295} ~ 600 μohm-cm, with a coefficient of +0.32% per degree. (It is noteworthy that liquid K−In alloys show a comparable resistivity at 475°C, ~450 μohm-cm, at a large maximum near 50±5 at.% K that has been attributed to cluster formation.[13] The thermodynamic excess stability of the liquid at 500°C occurs near 35% K,[14] where the solid system has a network structure $K_{22}In_{39}$.)

We conclude that one electron per cluster is delocalized, probably over the double K1 layers (perhaps with antibonding In−In contributions) in which the shortest interlayer K−K distances, 4.05 Å, are comparable to the single bond value, 4.00 Å.[6] The need for an extra

potassium atom must arise from packing requirements and "solvation" of the polyanion by sufficient cations; intercalation of these layers by one halide per K_8In_{11} has not been successful. Substitution reactions with sodium have given other phases. On the other hand, the larger cation in RbK_7In_{11} disorders in half of the K2 positions with expansion of only the a–b (cluster) net, while two more rubidium atoms appear to complete the K2 substitution and randomly occupied one-sixth of the K1 sites with a substantial lattice expansion in *c*.

The In_{11}^{7-} ion represents a new cluster bonding configuration in an evidently unknown hypoelectronic (homoatomic) cluster regime. An analogue of the better known C_{2v} closo deltahedron with 11 vertices and 24 electrons (as for $B_{11}H_{11}^{2-}$) would require an unreasonable −13 charge with In_{11}. This charge problem is alleviated for many gallium (and indium) clusters through the formation of network structures via intercluster bonds, e.g., at all eleven vertices of the ideal C_{2v} Ga_{11} unit in K_3Ga_{13}.[15] The only alternative mentioned in the literature appears to be the ideal pentacapped trigonal prism, but this is thought to be disfavored by the presence of two vertices of order three.[16] According to extended Hückel calculations,[17] the latter cluster exhibits a 1.2 eV HOMO–LUMO gap with only 20 p electrons ($2n - 2$).[18] The axial compression and lateral expansion necessary to achieve the observed ($2n - 4$) cluster, Figure 3, drives a single bonding a_1' orbital higher via both loss of bonding in the ends of the trigonal prism and increased antibonding In1–In2 interactions, while several occupied levels become more stable.

The general assessment of alkali metal–indium compounds (AB_x) as similar to gallium examples appears to be unwarranted. There are some isostructural AB_4 and AB (NaTl-type) examples and common network structures for the pairs $CsGa_3$ – $CsIn_3$[19-21] and $Na_{22}Ga_{39}$[22] – $K_{22}In_{39}$.[23] The many evidently unique indium examples are presently under study. We also find that the unreported phase Na_2In exists and is isostructural with Na_2Tl.[24] This makes it

formally a Zintl phase and another cluster example as it contains isolated In_4 tetrahedra with edges of 3.066 (2) to 3.153 (1) Å that are isoelectronic with Sn_4^{4-} in KSn,[25] $Sb_4(g)$, P_4, etc. Isolated gallium polyhedra are not known in any alkali metal compound, although Ga_3 and Ga_4 units occur in Ba_8Ga_7.[26]

Supplementary Material Available. Data collection and refinement information, atom parameters, distances and angles for K_8In_{11} (4 pages); observed and calculated structure factor results for the same (5 pages). Ordering information is given on any current masthead page.

REFERENCES

1. Pelton, A. D.; Larose, S. *Bull. Alloy Phase Diagr.* **1990**, *11*, 232.

2. Thümmel, R.; Klemm, W. *Z. Anorg. Allg. Chem.* **1970**, *376*, 44.

3. a) Ling, R. G.; Belin, C. *Acta Crystallogr.* **1982**, *B38*, 1104.
b) Frank-Cordier, U.; Cordier, G.; Schäfer, H. *Z. Naturforsch.* **1982**, *37b*, 127.

4. The structure was solved by direct methods following data collection at 23°C on a Rigaku AFC6R instrument with monochromatized Mo Kα radiation. Crystal data are $R\bar{3}c$ (No. 167), Z = 6, a = 10.006 (1) Å, c = 50.839 (7) Å (hexagonal setting, from Guinier powder data), R(F), R_w = 3.3, 3.6% for 607 independent observed reflections ($2\theta \leq 50°$), 31 variables, and with absorption (μ = 94.6 cm^{-1}) corrected by DIFABS (Walker, N.; Stuart, D. *Acta Crystallogr.* **1983**, *A39*, 158) (0.491 ≤ transm. ≤ 1.000). All lattice sites are fully occupied.

5. After our investigations were complete, a very brief report of the same structure (with In_{11}^{8-}) appeared, without comment or discussion, in: Blase, W.; Cordier, G.; Somer, M. *Z. Kristallogr.* **1991**, 194, 150.

6. Pauling, L.; Kamb, B. *Proc. Nat'l Acad. Sci.* **1986**, *83*, 3569.

7. Yatsenko, S. P.; Tschuntonow, K. A.; Orlov, A. N.; Yarmolyuk, Ya. P.; Hryn, Yu. N. *J. Less-Common Met.* **1985**, *108*, 339.

8. Stöhr, J.; Schäfer, H. *Z. Naturforsch.* **1979**, *34b*, 653.

9. Another cluster that is geometrically related but chemically distant to that in K_8In_{11} is the $Cs_{11}O_3$ unit found in several metal-rich oxide system by Simon, A., *Structure and Bonding* **1979**, *36*, 81. Although these have the same symmetry and projection, they actually consist of three centered Cs_6O units sharing faces, and the length of the common Cs–Cs edge (≙ In2–In2 = 5.06 Å, Figure 1) is actually 0.4 – 0.6 Å less than those defining the tricapped trigonal prism, i.e., the ends of the polyhedron are concave outward. A similar construction is found in $Ru_{11}(CO)_{23}^{3-}$, with an axial Ru–Ru separation that is only slightly longer than around the outside (Fumagelli, A.; Martinengo, S., Ciani, G.; Sironi, A., *J. Chem. Soc., Chem. Commun.* **1983**, *453*).

10. Critchlow, S. C.; Corbett, J. D. *J. Am. Chem. Soc.* **1983**, *105*, 5715.

11. Selwood, P. W. *Magnetochemistry*, Interscience Publishers: New York, 2nd ed., **1956**, pp. 70, 79. The In^{3+} core value used may be too small.

12. Shinar, J.; Dehner, B.; Beaudry, B. J.; Peterson, D. T. *Phys. Rev. B* **1988**, *37*, 2066.

13. Meijer, J. A.; Geertsma, W.; van der Lugt, W. *J. Phys. F.: Met. Phys.* **1985**, *15*, 899.

14. Takenaka, T.; Petric, A.; Saboungi, M.-L. *J. Phys.: Condens. Matter* **1991**, *3*, 1603.

15. Belin, C.; Ling, R. G. *J. Solid-State Chem.* **1983**, *48*, 40.

16. King, R. B.; Rouvray, D. H. *J. Am. Chem. Soc.* **1977**, *99*, 7834.

17. Orbital parameters and energies from Janiak, C.; Hoffmann, R. *J. Am. Chem. Soc.* **1990**, *112*, 5924. Predominantly s-based orbitals in a cluster with the observed dimensions lie between −17.7 and −9.0 eV, while the higher block of nine bonding orbitals have on average only 2.5% In 5s population.

18. We were reminded that this closed shell count can be easily derived by the addition of two axial In^{+} ions to the closo In_9^{11-} (D_{3h}), which process adds no new bonding orbitals or p electrons (J. K. Burdett, private communication).

19. Ling, R. C.; Belin, C. *Z. Anorg. Allg. Chem.* **1981**, *480*, 181.

20. Van Vucht, J. H. N. *J. Less-Common Met.* **1985**, *108*, 163.

21. Tschuntonow, K. A.; Yatsenko, S. P.; Hryn, Yu. N.; Yarmolyuk, Ya. P.; Orlov, A. N. *J. Less-Common Met.* **1984**, *99*, 15.

22. Ling, R. G.; Belin, C. *Acta Crystallogr.* **1982**, *B38*, 1101.

23. Sevov, S. C.; Corbett, J. D., unpublished results.

24. Hansen, D. A.; Smith, J. F. *Acta Crystallogr.* **1967**, *22*, 836.

25. Hewaidy, I. F.; Busmann, E.; Klemm, W. *Z. Anorg. Allg. Chem.* **1964**, *328*, 283.

26. Fornasini, M. L. *Acta Crystallogr.* **1983**, *C39*, 943.

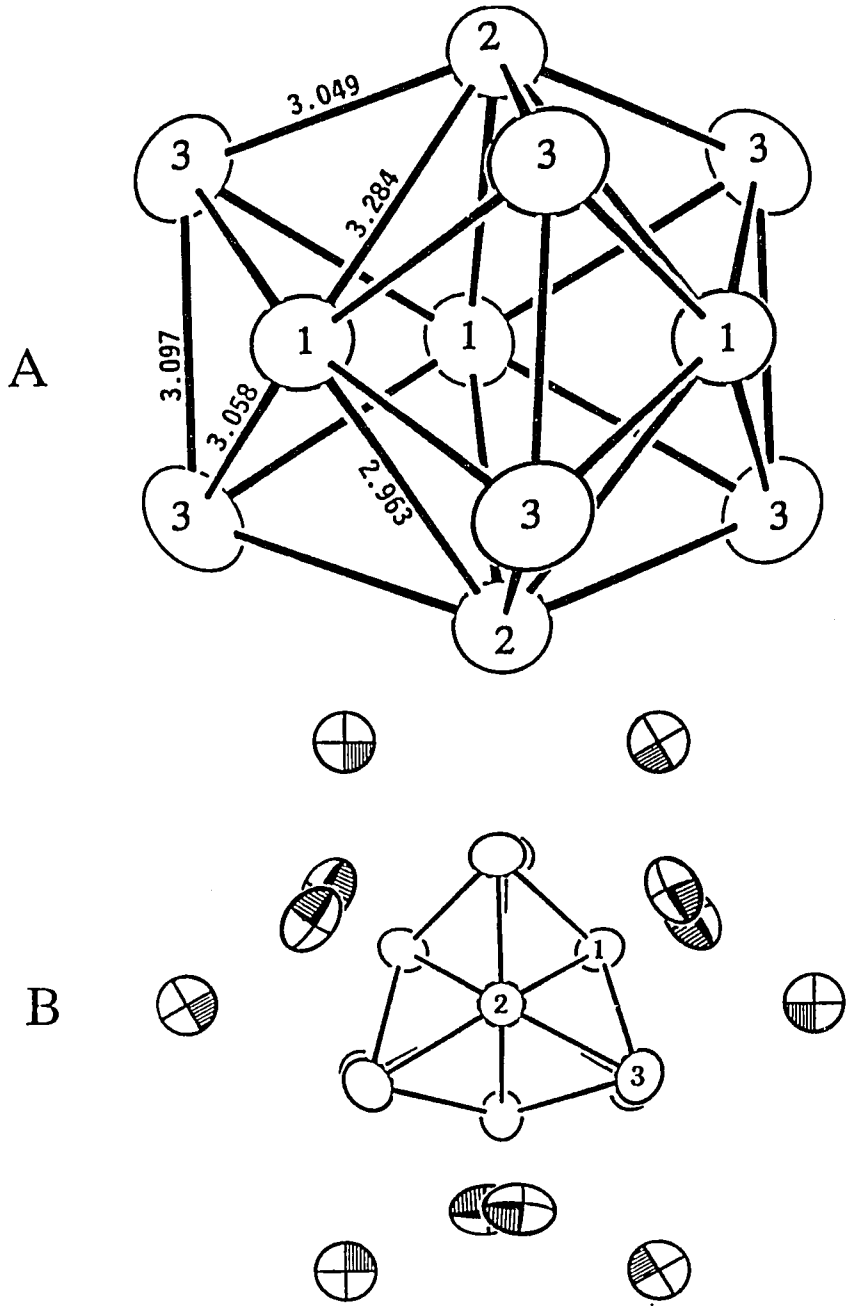

Figure 1. Two views of the indium cluster in K_8In_{11} (95% probability ellipsoids): A, the atom numbering system, with the three-fold axis vertical; B, along the C_3 axis (infinite view distance) with the surrounding potassium atoms (shaded). The K2 atoms in the outer ring lie in the plane of the clusters.

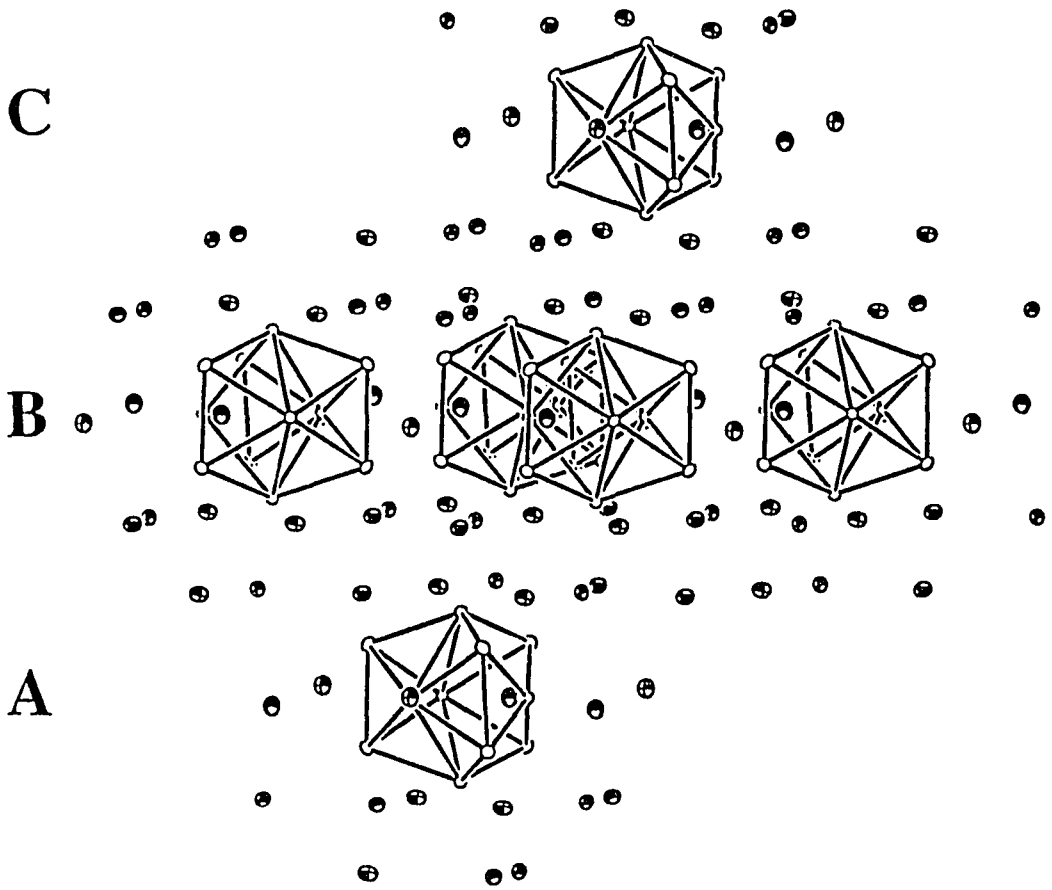

Figure 2. The rhombohedral stacking of cluster and potassium layers in K_8In_{11}. One-half of the hexagonal cell along *c* (vertical) is shown.

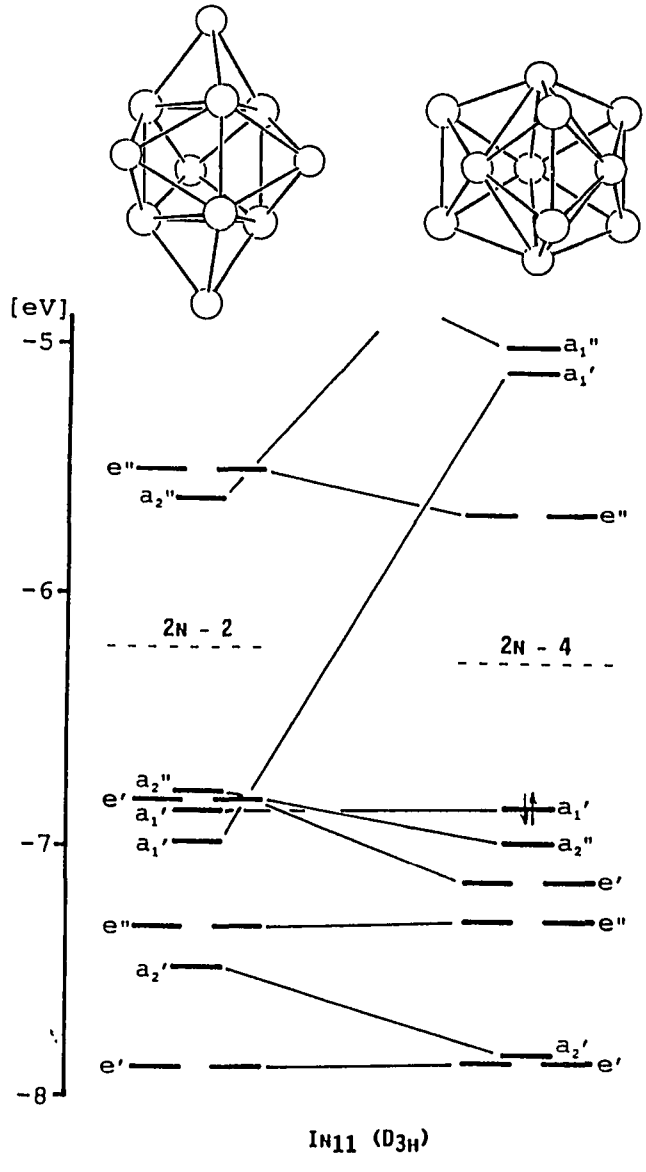

Figure 3. The lower MO levels for p orbitals in In_{11} clusters with D_{3h} symmetry: left, the classical pentacapped trigonal prism (d_{ave} = 3.082 Å) and right, the observed axially compressed cluster with 2n — 4 electrons and d_{ave} = 3.090 Å (D_{3h} assignments). Note the increased bonding in the latter.

SUPPLEMENTARY MATERIAL

Data collection and refinement parameters for K_8In_{11}

Formula weight	1575.81
Crystal size, mm	0.04 × 0.1 × 0.2
Lattice parameters:[a]	
a, Å	10.006 (1)
c, Å	50.839 (7)
V, Å^3	4408 (1)
Space group, Z	$R\bar{3}c$ (#167), 6
d(calc.), g cm^{-3}	3.56
μ(Mo–Kα), cm^{-1}	94.6
Transmission range	0.491–1.000
Diffractometer	Rigaku AFC6R
Radiation	Mo–Kα (λ = 0.71069 Å) graphite-monochromated
Temperature, °C	23
Octants measured	$\pm h, k, l$
Scan method	ω
$2\theta_{max}$	50°
Number of reflections:	
measured	2770
observed ($I \geq 3\sigma_I$)	1675
unique observed ($I \geq 3\sigma_I$)	607
Number of variables	31
R_{ave} (all data), %	5.4
R; R_w,[b] %	3.3; 3.6
Goodness of fit indicator	1.1
Maximum shift/σ in final cycle	0.00
Largest peaks in final ΔF map	+1.1 e/Å^3 (0.76 Å from In1)
	-1.1 e/Å^3

[a] Room temperature Guinier data with Si as an internal standard (λ = 1.540562 Å).

[b] $R = \Sigma||F_o| - |F_c||/\Sigma|F_o|$; $R_w = [\Sigma w(|F_o| - |F_c|)^2/\Sigma w(F_o)^2]^{1/2}$; $w = \sigma_F^{-2}$.

Positional and thermal parameters for K_8In_{11}

atom	N	x	y	z	B_{eq}
In1	18e	0.7907 (1)	0	1/4	1.78 (5)
In2	12c	0	0	0.70025 (2)	1.78 (3)
In3	36f	0.3737 (1)	0.3242 (1)	0.05292 (1)	2.15 (3)
K1	36f	0.3001 (3)	0.9295 (3)	0.02146 (5)	3.1 (1)
K2	12c	0	0	0.0793 (1)	3.4 (1)

atom	U_{11}	U_{22}	U_{33}	U_{12}	U_{13}	U_{23}
In1	0.0246 (5)	0.0192 (6)	0.0220 (5)	0.0096 (3)	-0.0010 (2)	-0.0020 (4)
In2	0.0228 (5)	0.0228 (5)	0.0221 (7)	0.0114 (3)	0.0	0.0
In3	0.0234 (5)	0.0325 (5)	0.0275 (4)	0.0152 (4)	-0.0054 (3)	0.0028 (3)
K1	0.032 (1)	0.037 (2)	0.032 (2)	0.006 (1)	0.000 (1)	-0.003 (1)
K2	0.039 (2)	0.039	0.051 (3)	0.020 (1)	0.0	0.0

Distances to nearest neighbors about each atom in K_8In_{11}

In1 – In2	(x2)	3.284 (1)	K1 – K1	(x2)	4.049 (4)
In1 – In3	(x2)	2.9632 (8)	K1 – K1	(x1)	4.136 (5)
In1 – In3	(x2)	3.0582 (8)	K1 – K1[e]	(x3)	4.869 (5)
In2 – In3	(x3)	3.0494 (9)	K1 – K2	(x1)	4.372 (4)
In3 – In3	(x1)	3.097 (2)	K1 – K2	(x2)	4.504 (4)
In3 – In3[b]	(x2)	5.000 (2)	K2 – K1	(x3)	4.372 (4)
			K2 – K1	(x2)	4.504 (4)
K1 – In1[c]	(x1)	3.619 (3)			
K1 – In2[c]	(x1)	3.917 (3)	In1 – K1[c]	(x2)	3.619 (3)
K1 – In2[d]	(x1)	3.967 (3)	In1 – K2	(x2)	4.104 (1)
K1 – In3[c]	(x1)	3.659 (3)	In2 – K1[c]	(x3)	3.917 (3)
K1 – In3[c]	(x1)	3.690 (3)	In2 – K1[d]	(x3)	3.967 (3)
K1 – In3[d]	(x1)	3.788 (3)	In3 – K1[c]	(x1)	3.659 (3)
K1 – In3	(x1)	3.974 (3)	In3 – K1[c]	(x1)	3.690 (3)
K2 – In1	(x3)	4.104 (1)	In3 – K1	(x1)	3.974 (3)
K2 – In3	(x3)	4.044 (2)	In3 – K1[d]	(x1)	3.788 (3)
K2 – In3	(x3)	3.766 (2)	In3 – K2	(x1)	3.766 (2)
			In3 – K2	(x1)	4.044 (2)

[a] d(K–In) [b] Edge of triangular faces in trigonal prism.

[c] Face-capping distances.

[d] Second K1 layer.

[e] The only intralayer K–K distance listed.

Intracluster bond angles in K_8In_{11} (deg)

atom	atom	atom	angle
In2	In1	In2	100.75 (4)
In2	In1	In3	106.05 (3)
In2	In1	In3	58.17 (2)
In2	In1	In3	103.85 (3)
In2	In1	In3	57.35 (2)
In3	In1	In3	157.31 (5)
In3	In1	In3	112.26 (3)
In3	In1	In3	61.88 (3)
In1	In2	In1	67.05 (3)
In1	In2	In3	55.65 (2)
In1	In2	In3	57.61 (2)
In1	In2	In3	110.81 (4)
In3	In2	In3	110.13 (2)
In1	In3	In1	74.06 (4)
In1	In3	In2	66.18 (3)
In1	In3	In3	60.57 (2)
In1	In3	In2	65.04 (3)
In3	In1	In3	152.78 (5)
In2	In3	In3	108.70 (3)

PAPER 2. $K_8In_{10}Hg$: A ZINTL PHASE WITH ISOLATED $In_{10}Hg$ CLUSTERS

Slavi C. Sevov, Jerome E. Ostenson and John D. Corbett*

ABSTRACT

The title compound results from the substitution of one mercury atom for indium in the known metallic K_8In_{11} [$8K^+ + In_{11}^{7-} + e^-$]. It contains the same isolated eleven-atom clusters as before, pentacapped trigonal prisms compressed along the three-fold axis, but with mercury disordered over the trigonal prismatic sites ($P6_3/m$, $Z = 2$, $a = 9.9812$ (4) Å, $c = 16.851$ (1) Å, $R/R_w = 2.4/2.8\%$). The cluster $In_{10}Hg^{8-}$ is likewise hypoelectronic and requires the $2n-4 = 18$ skeletal bonding electrons available for this stoichiometry. The close-packed layers of clusters are again separated by double layers of potassium, but these follow an h.c.p. order rather than the c.c.p. arrangement found in K_8In_{11}. The phase is diamagnetic ($\sim -3.5 \times 10^{-4}$ emu/mol.), in contrast to the Pauli-like behavior of K_8In_{11}, but it too exhibits a conductivity characteristic of a poor metal, ρ_{295} ~270/μΩ-cm with a coefficient of +0.48% deg.$^{-1}$.

INTRODUCTION

The supposedly simple alkali-metal–indium systems are proving to be rich in novel cluster chemistry, revealing a considerable disposition toward homoatomic bonding in closed-shell, valence-precise situations [1–6]. Most of the indium products appear to be very distinctive relative to those formed by its congener gallium [7], especially in the formation of isolated and centered clusters. The first example was the remarkable K_8In_{11} in which close-packed layers of isolated pentacapped trigonal prisms ($\sim D_{3h}$) both contain potassium atoms and are separated by double potassium layers [1]. A formal In_{11}^{8-} anion with an odd number of electrons would be improbable, and, in fact, M.O. calculations as well as magnetic and conductivity measurements show that the metallic compound should be formulated in terms of one delocalized electron and hypoelectronic ($2n$-4) clusters In_{11}^{7-}. Both axial capping and compression of a conventional tricapped trigonal prism account for the unusual electronic configuration, well below the classical $2n$+2 "floor" predicted by Wade's rules for normal closo deltahedra [8]. Two other types of isolated clusters have been found in addition to numerous phases containing interconnected clusters, some of novel design [2,3,6]. The first is the zinc-centered $In_{10}Zn^{8-}$ as the potassium salt. The anion is based on a bicapped antiprism (D_{4d}) in which a cluster expansion and the zinc interstitial reduce the classical 12– charge to 8– [4]. Another type of clusters found in $K_{10}In_{10}M$, M = Ni, Pd, Pt, are best described as M-centered, tetracapped trigonal prisms of approximately C_{3v} symmetry [6].

The novelty of a closed-shell cluster In_{11}^{7-} in a solid that is also metallic by virtue of an extra electron, viz. $(K^+)_8In_{11}^{7-}e^-$, has prompted us to search for derivatives in which the odd electron might instead be bound. One obvious way to accomplish this would be by substitution of a zinc family element into the cluster since these are one electron poorer. Zinc itself gives instead the centered $In_{10}Zn^{8-}$ (above), cadmium produces a complex network structure [6], but mercury gives us the desired result $In_{10}Hg^{8-}$ in the potassium salt.

EXPERIMENTAL SECTION

The reaction techniques in welded tantalum tubing have been described before [2,3]. All materials were handled in a N_2-filled glovebox. A mixture of the elements (K – J.T.Baker, lump under oil, 98+%; In – Cerac, 99.999%; Hg – Fisher, instrument grade) in proportions appropriate to produce $K_8In_{10}Hg$ was allowed to react at 600°C for 2 days, quenched to room temperature, and then annealed at 400°C for 10 days. The product was dark gray, very brittle and had a metallic lustre. A few crystallites were selected, sealed in capillaries, and checked by oscillation and Wessenberg film techniques for singularity and an eventual space group assignment.

A plate-like single crystal (0.05 × 0.12 × 0.20 mm) was chosen and mounted on a CAD4 single crystal diffractometer. (Some details of the data collection and refinement are listed in Table 1.) The 25 reflections from a random search were indexed with a hexagonal unit cell of the same dimensions as already estimated from the Weissenberg photographs. Two octants of data were collected at room temperature with monochromated Mo Kα radiation ($2\theta_{max}$ = 50°). The data were consistent with three possible space groups, $P6_3$, $P6_3/m$ and $P6_322$, after corrections for Lorentz and polarization effects as well as for absorption with the aid of the average of two ψ–scans collected at different θ values . Wilson plot statistics showed a centrosymmetric type distribution, so $P6_3/m$ was chosen and was later shown to be correct.

Application of direct methods (SHELX-86 [9]) gave three positions with distances around each appropriate to In–In bonds. Subsequent least-squares refinement and difference Fourier synthesis using these revealed three additional positions that were assigned to potassium. A few least-squares cycles with anisotropic thermal parameters led to R = 3.6% but a quite small B_{eq} for In3 compared with those for In1 and 2. Refinement of the occupancies of the indium atoms with all K atoms fixed showed 115% (18σ high) occupancy for the In3 site and

comparable B_{eq} values for all three. The behavior suggested that a heavier atom, Hg in our case, was mixed with indium on the In3 position. Consequently, a mixture of indium and mercury was refined in this position with the constraint of 100% occupancy. This led to a drop of R(F) to the final value, 2.4% (R_w = 2.8%). The occupancies of the other In sites did not deviate from unity by more than 2% (1.5σ) when the K atoms were kept fixed, and the K sites, by more than 5% (4σ) when the In atoms were held fixed. The refined composition with only proportions at the In3 site varying was $K_8In_{9.97(3)}Hg_{1.03(3)}$ which agreed very well with the composition determined by EDX – $K_8In_{10.0(2)}Hg_{1.0}$. The largest peaks in the final difference Fourier map were 1.06 e/Å^3 (1.0 Å from In3) and -0.72 e/Å^3. Note that the mercury-free K_8In_{11} occurs in a different space group, $R\bar{3}c$.

The powder pattern of the compound was obtained from a small portion of a powdered sample mounted between pieces of cellophane tape. An Enraf-Nonius Guinier camera, Cu $K\alpha_1$ radiation (λ = 1.540 562 Å) and NBS (NIST) silicon as an internal standard were employed for this purpose. The least-squares refinement of measured 2θ values indexed on the basis of a calculated pattern gave the reported lattice dimensions.

The electrical resistivity of the phase was measured by an electrodeless "Q" method [10] over the temperature range 160–295 K with readings taken every 20°. The magnetization of the compound was measured at field of 3 Tesla over the range 6–295 K on a Quantum Design MPMS SQUID magnetometer. The containment procedures are described in more detail elsewhere [2].

RESULTS AND DISCUSSION

Atom parameters and important distances and angles for $K_8In_{10}Hg$ are listed in Tables 2 and 3, respectively. Structure factor data (5 pages) are available from J.D.C.

A view of the $In_{10}Hg$ cluster is shown on Fig. 1. Open ellipsoids represent In1 and 2, the face and axial capping atoms, respectively, while the crossed members define the trigonal prism over which In3 and Hg are disordered in a 5:1 atomic ratio. There are two clusters per unit cell centered at 2*d* ($\bar{6}$) positions 2/3, 1/3, 1/4 and 1/3, 2/3, 3/4. The geometry of the cluster is effectively the same as In_{11} in K_8In_{11} although there are minor differences in the point group symmetries. The triangle of face-capping In1 atoms in $In_{10}Hg$ is rotated around the three-fold axis by 0.29° relative to the trigonal prism so that the In1 atoms are not exactly above the center of the rectangular faces, meaning that In1 has two different distances to In3(Hg) – 3.032 (1) Å and 3.014 (1) Å. This reduces the symmetry from D_{3h} to C_{3h}. In the In_{11} cluster, the two triangles that define the trigonal prism are instead twisted by 3.1° with respect to each other, and the symmetry is again reduced, this time to D_3 [1].

The average In–In bond distances in the two clusters differ by only 0.006 Å. The distances from the mixed In3,Hg position to In1 and In2 are naturally slightly larger (3.023(ave) and 3.138 Å, respectively) than the corresponding values in K_8In_{11} (3.011(ave) and 3.097 Å), befitting the mercury substitution. The seemingly large thermal ellipsoid for the In3,Hg site also reflects this.

Figure 2 shows general views of the structures of K_8In_{11} (left) and of $K_8In_{10}Hg$ (right). The clusters in both structures lie in close-packed layers but the stacking is different. In K_8In_{11} they follow a cubic (ABC) stacking and the cell is rhombohedral, while in $K_8In_{10}Hg$ the packing order and the space group are hexagonal (AB). Double layers of K1 atoms with very similar distances separate the layers of clusters in both structures . The other potassium atoms (K2 in

K_8In_{11}, K2 and K3 in $K_8In_{10}Hg$) lie within the cluster layers. The quadrilateral (In3–In2–In3–In1) faces at both ends of the cluster are each capped by K1 atoms that are also neighbors of In2 and In2–In3 edges in other clusters through the double K1 layers. The triangular (In3–In1–In3) faces around the cluster waist are capped by six more potassium (K2 and K3 here), each of which is similarly bonded to two other clusters. The compounds can also be approximated as close packed layers of *h.c.p.* $K_6K_{6/3}In_{10}Hg$ or *c.c.p.* $K_6K_{6/3}In_{11}$ units. This specificity of alkali-metal bonding through edge-bridging or face-capping of indium cluster units seems quite general.

Since the structure of $K_8In_{10}Hg$ looks very much like a polymorph of the K_8In_{11}, additional work was done in order to establish that the compound is indeed a ternary phase. A reaction designed to produce the phase without mercury was run under exactly the same conditions as described in the Experimental Section, but the product was only the known K_8In_{11}. The EDX results (Experimental) and the change in space group also reassured us that a real substitution had occurred. The mercury compound has a 7.8 $Å^3$ larger formula volume, but reasonable data for such an $Hg–In^+$ interchange cannot be found.

The location of the mercury substitution into In_{11}^{7-} is interesting relative to other examples. Extended-Hückel calculations on the parent give (within the Mulliken approximation) charges of −0.31, −0.54 and −0.83 on the capping (In1), axial (In2) and prismatic (In3) sites. Thus, the electron-poorer (and also heavier) mercury substitutes at the most negative site, the one that also has the fewest bonding neighbors. This mode agrees on both counts with the disposition observed for the parallel substitution of thallium within the clusters $TlSn_9^{3-}$ (axial Tl in a bicapped square antiprism) and $TlSn_8^{3-}$ (Tl capping in a tricapped trigonal prism) that have been isolated from nonaqueous solutions as salts with largely organic cations [11]. These dispositions contradict the usual wisdom in, e.g., carboranes, where the electron-richer

heteroatom carbon substitutes at the more negative sites. However, these contrary examples also involve substantial differences in bond strength and character and orbital size. It is also interesting to note that the clusters In_{11}^{7-} and $In_{10}Hg^{8-}$ as well as the centered members $In_{10}Zn^{8-}$ (D_{4d}) and $In_{10}Ni^{10-}$ ($\sim C_{3v}$) are all isoelectronic in total electrons yet, the stable eleven-atom polyhedra for these involve three different examples, one substitutional and two interstitial. The configurations that these systems have to choose from appear to be substantial in number, with energy differences and structural preferences that appear to be small and subtle, respectively.

Extended-Hückel MO calculations performed earlier on In_{11} showed that a cluster with this geometry is hypoelectronic and requires $2n-4 = 18$ p-electrons for skeletal bonding, i.e., In_{11}^{7-}. The eighth electron in K_8In_{11} was presumed to be delocalized, possibly within the double K1 layers, making the compound metallic. Some properties were consistent, a temperature-independent $\chi_M(corr) = +(1-2) \times 10^{-4}$ emu mol^{-1} and $\rho_{295} \sim 600$ $\mu\Omega$·cm with a positive temperature coefficient [1]. The complete reduction of the anion by all eight potassium valence electrons in $K_8In_{10}Hg$ leads to the isoelectronic $In_{10}Hg^{8-}$ species with a closed shell of skeletal electrons. The substitution of one and only one mercury atom in the same cluster is strong support for our earlier analysis of K_8In_{11}.

The measured magnetic susceptibilities of $K_8In_{10}Hg$ were again corrected for the diamagnetism from the ion cores (-3.3×10^{-4} emu mol^{-1}) and for the Larmor precession of the nine electron pairs in the skeletal orbitals of the cluster (-3.0×10^{-4} emu mol^{-1}). The net result is plotted on Fig. 3 together with comparable data for K_8In_{11}, the two data sets having received the same corrections save for the small difference of the mercury core. Considerable electron pairing is evident between the Pauli paramagnetic K_8In_{11} and the diamagnetic $K_8In_{10}Hg$ where a Zintl (valence) phase would be expected. (The tails at low temperature are common features

usually attributed to small amounts of para- or ferromagnetic impurities.) No superconductivity was seen for $K_8In_{10}Hg$ (or the phases containing centered indium clusters) at fields of 50–100 Oe over the range 2–10 K. The diamagnetic properties of $K_8In_{10}Hg$, $K_8In_{10}Zn$ and $K_{10}In_{10}Ni$ are virtually superimposable [12].

In contrast, $K_8In_{10}Hg$ was found to have an electrical resistivity of $\rho_{295} \sim 270$ μΩ·cm with a coefficient of +0.48% per degree. While the absolute value for ρ may be uncertain by a factor of about three, the coefficient should be fairly reliable. Such seemingly conflicting properties, i.e., strong diamagnetism and (poor) metal-like conductivities, have also been observed for another salt that is surmised to have a closed-shell polyanion, $K_8In_{10}Zn$ [4]. (Two probe data indicate that $K_{10}In_{10}Ni$ is a very poor conductor [12], as is the $^{2}_{\infty}[In_6^{4-}]$ network in Rb_2In_3 [13].) A metal like indium in negative oxidation states will of course have elevated valence energies, conceivably enough to afford some overlap of valence and conduction bands. The magnetic and conduction properties of $K_8In_{10}Hg$ are probably best attributed to a semimetallic behavior. In any case, the results should not obliterate the clear importance of covalent In–In bonding below some high-lying conduction in what could be a "metallic Zintl phase" [14].

Finally, we note that the magnitudes of both the observed diamagnetism and the electronic conduction may be exaggerated via the same effects that influence many heavy main-group metals themselves. Indium is both diamagnetic ($\chi_{293}(corr) = -45 \times 10^{-6}$ emu mol^{-1}) and metallic ($\rho_{293} = 8.4$ μΩ·cm [15]). Large orbital overlaps and low densities of states at E_F classically go hand-in-hand with small effective electron masses. This in turn affords smaller Pauli-paramagnetic but larger diamagnetic Landau contributions for the conduction electrons as well as high charge mobilities and thence enhanced conductivity [16].

REFERENCES

1 S. C. Sevov and J. D. Corbett, *Inorg. Chem. 30* (1991) 4875.

2 S. C. Sevov and J. D. Corbett, *Inorg. Chem. 31* (1992) 1895.

3 S. C. Sevov and J. D. Corbett, *J. Solid State Chem.* **103** (1993), 114.

4 S. C. Sevov and J. D. Corbett, *Inorg. Chem. 32* (1993), 1059.

5 J. D. Corbett and S. C. Sevov, *Z. Phys. D.–Atoms, Molecules and Clusters* (1993), in press.

6 S. C. Sevov, J. D. Corbett, unpublished research.

7 C. Belin and M. Tillard-Charbonnel, *Prog. Solid State Chem. 22* (1993) 59.

8 K. Wade, *Adv. Inorg. Chem., Radiochem. 18* (1976) 1.

9 G. M. Sheldrick, SHELXS-86; Universität Göttingen, BRD (1986).

10 J. Shinar, B. Dehner, B. J. Beaudry, D. T. Peterson, *Phys. Rev. 37B* (1988) 2066.

11 R. C. Burns and J. D. Corbett, *J. Am. Chem. Soc. 104* (1982) 2804.

12 S. C. Sevov and J. D. Corbett, *J. Am. Chem. Soc.*, submitted.

13 S. C. Sevov and J. D. Corbett, *Z. Anorg. Allg. Chem. 619* (1993) 128.

14 Nesper, R. *Prog. Solid State Chem. 20* (1990) 1.

15 *CRC Handbook of Chemistry and Physics*, CRC Press, Boca Raton, Florida; 65th ed. (1984), E-108, F-120.

16 Kittel, C. *Introduction to Solid State Physics*, 2nd ed. (1956), p. 293.

Table I. Data collection and refinement parameters for $K_8In_{10}Hg$

crystal size, mm	0.05 × 0.12 × 0.20
lattice parameters[a]	
a, Å	9.9812 (4)
c, Å	16.851 (1)
V, Å^3	1453.8 (1)
space group, Z	$P6_3/m$, (No. 176), 2
diffractometer, temp. (°C)	CAD4, 21
radiation, 2θ(max)	Mo Kα, graphite monochromated; 50°
octants measured	$\pm h, k, l$
scan method	ω–2θ
no. reflec. meas.	2804
obs. ($I>3.00\ \sigma_I$)	1897
indep. obs.	611
abs. coeff. (Mo Kα), cm^{-1}	140.5
transm. factor range	0.5002 – 1.0
R(ave), (all data) %	4.7
no. variables	34
residuals R; R_w[b](%)	2.4; 2.8
maximum shift/σ in final cycle	0.00
largest peaks in final ΔF, e/Å^3	+1.06 (1.0 Å from In3), -0.72
sec. ext. coeff. (10^{-8})	8 (2)

[a] Guiner data with Si internal standard, λ = 1.540562 Å.

[b] $R = \Sigma||F_o| - |F_c||/\Sigma|F_o|$; $R_w = [\Sigma w(|F_o| - |F_c|)^2/\Sigma w(F_o)^2]^{1/2}$; $w = \sigma_F^{-2}$.

Table II. Positional and thermal parameters for $K_8In_{10}Hg$

Atom	Position	*x*	*y*	*z*	B_{eq}	Occupancy (≠1)
In1	6h	0.4638(1)	0.3457(1)	1/4	2.05(3)	
In2	4f	2/3	1/3	0.10048(6)	2.07(3)	
In3	12i	0.36822(6)	0.05369(7)	0.15690(4)	2.61(3)	0.828 (5)
Hg	12i	(0.36822)	(0.05369)	(0.15690)	(2.61)	0.172
K1	12i	0.6296(3)	0.0695(3)	0.4349(1)	3.42(9)	
K2	2a	0	0	1/4	3.6(2)	
K3	2c	1/3	2/3	1/4	4.0(2)	

Atom	U_{11}[a]	U_{22}	U_{33}	U_{12}	U_{13}	U_{23}
In1	0.0298(5)	0.0239(5)	0.0277(5)	0.0121(5)	0	0
In2	0.0283(4)	U_{11}	0.0221 (6)	$U_{11}/2$	0	0
In3, Hg	0.0297(4)	0.0323(4)	0.0327(4)	0.0121(3)	-0.0032(3)	-0.0077(3)
K1	0.063(2)	0.042(1)	0.033(1)	0.032(1)	-0.000(1)	0.002 (1)
K2	0.043 (2)	U_{11}	0.049(4)	$U_{11}/2$	0	0
K3	0.048 (2)	U_{11}	0.056(4)	$U_{11}/2$	0	0

[a] $T = \exp[-2\pi^2(U_{11}h^2a^{*2} + U_{22}k^2b^{*2} + U_{33}\ell^2c^{*2} + 2U_{12}hka^*b^* + 2U_{13}h\ell a^*c^* + 2U_{23}k\ell b^*c^*)]$.

Table III. Important distances (Å) and intracluster angles (deg) in $K_8In_{10}Hg$[a]

	In1		**In3**		**K1**		**K2**
2 In1	3.618 (2)	In1	3.0142 (9)	In1[b]	3.580 (2)	3 In1	4.1672 (9)
2 In2	3.273 (1)	In1	3.0317 (9)	In2[b]	3.895 (2)	6 In3	3.7798 (6)
2 In3	3.0142 (9)	In2	3.0420 (7)	In2[c]	3.960 (3)	6 K1	4.615 (2)
2 In3	3.0317 (9)	In3	3.138 (1)	In3[d]	3.641 (2)		**K3**
2 K1[b]	3.580 (2)	In3[e]	5.005 (1)	In3[b]	3.730 (2)	3 In1	4.0166 (8)
K2	4.1672 (9)	K1[d]	3.641 (2)	In3[c]	3.744 (2)	6 In1	4.0199 (6)
K3	4.0166 (8)	K1[b]	3.730 (2)	In3[b]	3.868 (2)	6 K1	4.195 (2)
	In2	K1[c]	3.744 (2)	2 K1	4.040 (3)		
3 In1	3.273 (1)	K1[b]	3.868 (2)	K1	4.125 (4)		
3 In3	3.0420 (7)	K2	3.7798 (6)	2 K1[f]	4.865 (2)		
3 K1[b]	3.895 (2)	K3	4.0199 (6)	K2	4.615 (2)		
3 K1[c]	3.960 (3)			K3	4.195 (2)		

Table III. (continued)

atom	atom	atom	angle
In2	In1	In2	100.68 (3)
In2	In1	In3	57.70 (1), 57.55 (2)
In2	In1	In3	105.48 (3), 105.08 (3)
In3	In1	In3	62.73 (3), 62.32 (3)
In3	In1	In3	111.75 (2)
In3	In1	In3	155.40 (3)
In1	In2	In1	67.11 (3)
In1	In2	In3	56.88 (2), 57.24 (2)
In1	In2	In3	111.45 (4)
In3	In2	In3	110.70 (2)
In1	In3	In1	73.51 (3)
In1	In3	In2	65.42 (2), 65.21 (2)
In1	In3	In3	58.64 (1), 58.84 (1)
In2	In3	In3	108.21 (2)

[a] d(K–In) ≤ 5.72 Å; d(In–In) ≤ 5.76 Å. All In3 sites contain 5/6 In, 1/6 Hg.
[b] Face capping distances.
[c] Second K1 layer.
[d] Exo bond.
[e] Edge of the triangle that caps the trigonal prism.
[f] The only intralayer K–K distance within range.

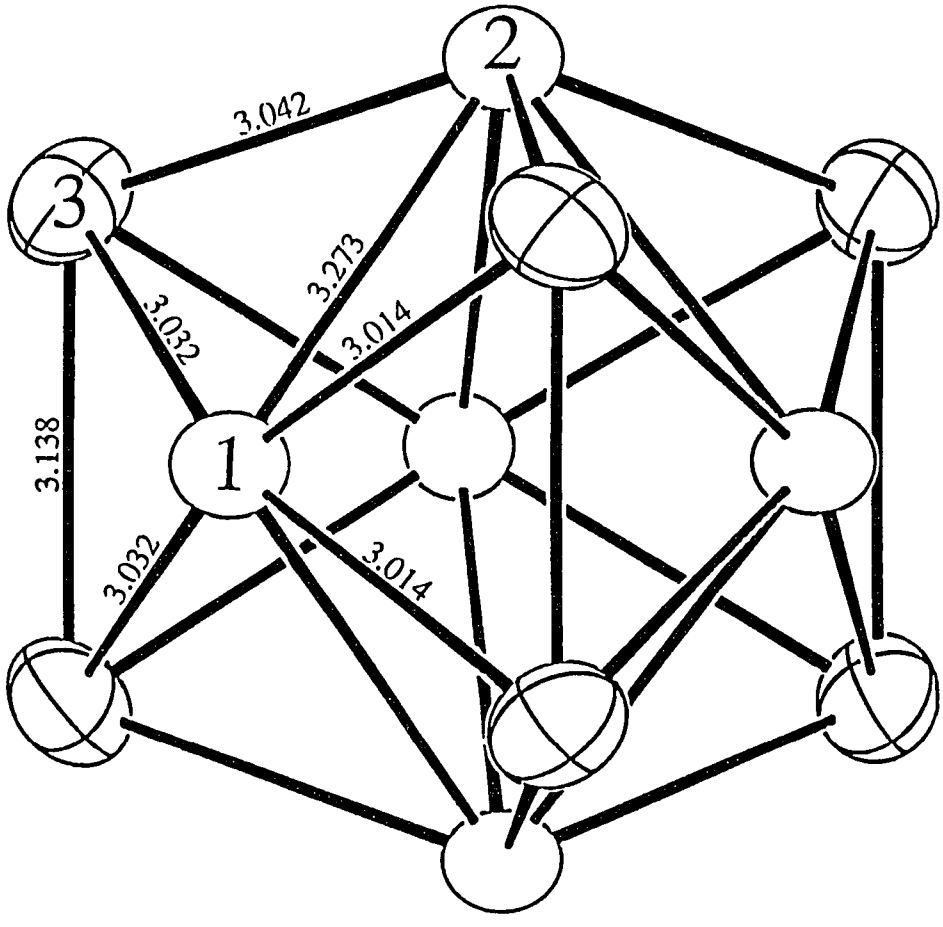

Figure 1. The $In_{10}Hg$ cluster in $K_8In_{10}Hg$ with the three-fold axis vertical (94% probability ellipsoids). The trigonal prismatic atoms 3 are 5/6 In, 1/6 Hg while In1 and In2 cap all faces thereof. Distances in Ångstroms.

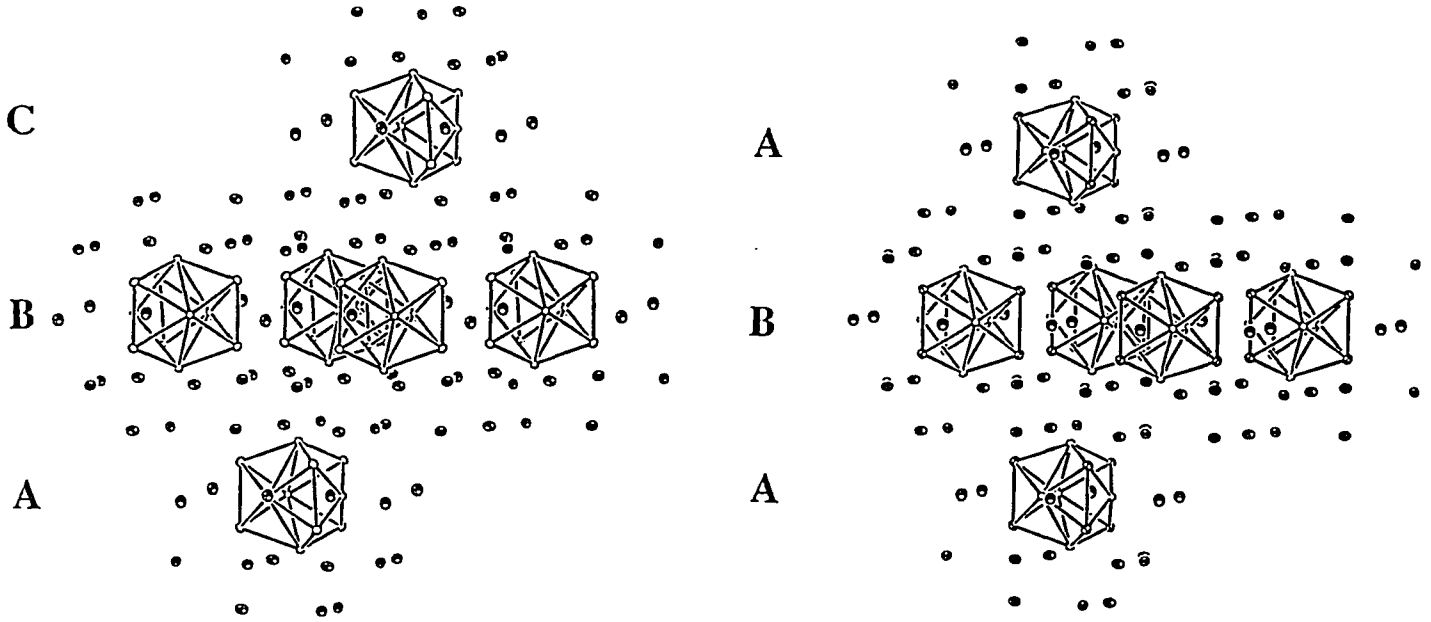

Figure 2. The close-packed layering of clusters and potassium ions in (left) K_8In_{11} ($R\bar{3}c$) and (right) $K_8In_{10}Hg$ ($P6_3/m$) ($\vec{c}$ vertical).

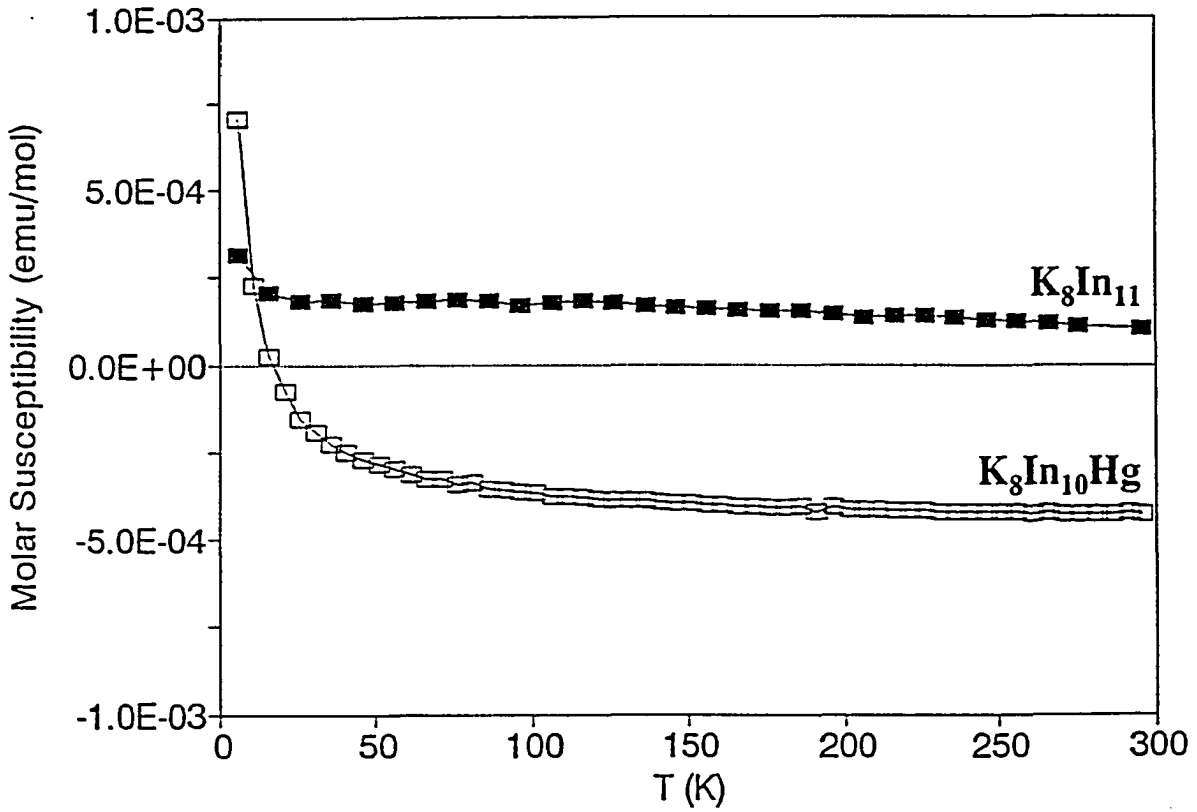

Figure 3. Molar magnetic susceptibility vs T for K_8In_{11} and $K_8In_{10}Hg$. Both data sets have been corrected for core diamagnetism and with the same orbital (Larmour) precession contribution from the cluster-bonding electron pairs.

PAPER 3. $K_8In_{10}Zn$: INTERSTITIALLY-STABILIZED ANALOGUES OF EARLY TRANSITION-METAL HALIDE CLUSTERS

Slavi C. Sevov and John D. Corbett*

ABSTRACT

Reaction of the elements in the indicated proportions in sealed Ta at 600°C followed by slow cooling gives $K_8In_{10}Zn$ as a single phase. The structure (*P4/nnc*, $Z = 2$, $a = 10.2916$ (5), $c = 13.837$ (1) Å, $R(F)/R_w = 2.1/2.1\%$) contains isolated $In_{10}Zn^{8-}$ polyhedra with D_4 symmetry, that is, bicapped antiprismatic clusters of indium that are centered by zinc (aver. In–In and In–Zn distances = 3.072 and 2.836 Å, respectively). Charge-consistent, extended-Hückel calculations on polyhedra of (a) the ideal In_{10}, (b) the observed distorted example, and (c) that centered with zinc illuminate the bonding in the hypoelectronic $In_{10}Zn^{8-}$ relative to a classical (hypothetical) In_{10}^{12-} with $2n + 2$ electrons. The effects are quite parallel to those found for the many interstitially-stabilized M_6X_{12}-type cluster phases among early transition-metal halides. $K_8In_{10}Zn$ is diamagnetic and a poor metal.

COMMUNICATION

Convergence of the principles that afford both interstitially-stabilized halide clusters of the early transition metals and hypoelectronic clusters of main-group-elements has been realized in the centered clusters in the new compound $K_8(In_{10}Zn)$. Zintl or "naked" clusters of the post-transition elements (Sn_9^{4-}, Pb_5^{2-}, Bi_4^{2-}, etc.) generally follow Wade's rules and therefore contain a minimum of $2n + 2$ skeletal bonding electrons in p-orbital-based MO's.[1] Although analogous ions for members of the aluminum family are unknown, perhaps because of the requisite high charges, i.e., *closo*-$M_n^{-(n+2)}$, the hypoelectronic ($2n - 4$ e$^-$) example In_{11}^{7-} (D_{3h}) in K_8In_{11}[2] and a closely related substituted cluster in the semiconducting $K_8In_{10}Hg$[3] have recently been discovered. In these instances, fortuitous electronic consequences of both polyhedral capping and distortion have allowed access to this new cluster regime. Several other nearly-electron-precise structures consisting of interconnected clusters, both familiar and new, further attest to the strength and dominance of In–In[3–5] (and Ga–Ga[6–8]) bonding. At the other extreme, a large family of nominally electron-poor M_6X_{12}-type clusters of the group 3 and 4 transition metals have been synthesized in which one of a diverse list of atom centered within each cluster is necessary for thermodynamic stability.[9–11] Centered indium cluster ions have now been discovered in which exactly the same effects are operative, namely, the provision of additional electrons and central bonding by the interstitial. This article reports on the first example, $In_{10}Zn^{8-}$, which is nominally D_{4d} and has $2n = 20$ skeletal bonding electrons.

Fusion of the elements in the indicated proportions at 600°C in a welded Ta container followed by slow cooling (3°/hr) affords a single-phase sample of $K_8In_{10}Zn$ according to a comparison of the Guinier powder photograph of the product with that calculated based on the refined structural parameters. The compound is very brittle and dark with a slight yellow luster. Analogous products are not obtained with Na, Rb, Cd, or Hg.

Single crystal studies[12] reveal the presence of discrete bicapped archimedian antiprisms of indium, the classic polyhedron for a *closo*-M_{10} unit, but these are both distorted and centered by a zinc atom, Figure 1. The polyhedron has 422 (D_4) symmetry with In2 and Zn lying on the 4-fold axis. The deviations from D_{4d} correspond to only a 1.73° torsional twist of the opposed squares and a 0.092 Å difference in the In1–In1 distances, which we presume arise from packing effects. The skeletal distortions serve to put the zinc atom nearly equidistant from all members of the indium shell. This makes the edges of the square faces of the antiprism 0.57 Å longer than the average of the In–In separations marked by solid lines, 3.072 Å. The last is close to the average in In_{11}^{7-}, 3.090 Å,[2,13] indicating the presence of both comparable bonding about the indium shell and a Zn prop that is of an appropriate size. We are unable to find In–Zn distances in any other compound with which to compare the observed 2.836 Å average, but the uncritical use of the sum of Pauling single bond metallic radii for the two metals gives an average bond order of 0.46, not unreasonable in view of the electronic structure (below).

There is only one type of potassium in the structure, and this has what appear to be fairly specific interactions with the cluster anions, as generally observed. Each cation has three cluster neighbors in which it caps a triangular face of In1 atoms about the waist of one (3.56–3.96 Å), bridges an In1–In2 edge in a second (3.77 Å), and is exo to a single In1 in a third (3.76 Å). This arrangement in effect means that In2 vertices in the staggered clusters penetrate the double potassium layers that lie between cluster layers (see frontispiece), in contrast to the greater separation of clusters between double cation layers along $\vec{c}$ in K_8In_{11}.[2] The shortest K–K and intercluster In–In separations are 4.26 and 5.58 Å, respectively, 0.2 and 0.3 Å greater than in the metallic K_8In_{11}.

The electronic consequences of this composition and structure are readily appreciated with the results of extended Hückel calculations.[14] Figure 2 shows these for the dominantly p-

orbital states in (a), the classic bicapped square antiprism (with the same average edge lengths as $In_{10}Zn^{8-}$), (b) after the observed lateral expansion and axial compression to make all vertices substantially equidistant from the centroid, and (c), following encapsulation of the zinc atom in the distorted polyhedron. (The b_2 MO near −4.2 eV is in fact the top of a block of mainly s-based orbitals, the others ranging between −5.57 and −9.05 eV; only the set of three b_2 orbitals exhibit appreciable s-p mixing.) The distortion from (a) to (b) raises the penultimate a_1 to a future LUMO role through expansion of the square faces of the antiprism where this MO is both σ- and π-bonding. Interactions of the other high-lying bonding orbitals a_1, b_2, e_1 in the distorted cluster with the valence orbitals of the inserted Zn obviously stabilize this hypothetical intermediate and give a result that is consistent with the observed closo but centered cluster with 20 skeletal (p) electrons [8(K) + 10(In p) + 2(Zn)]. This contrasts with the ideal but unknown empty cluster In_{10}^{12-} with $2n + 2 = 22$ electrons and a charge that is greater by four.

The role of the interstitial is strikingly similar to the apparent stabilization of many other electron-poor M_6X_{12}-type clusters of zirconium, hafnium and the rare-earth-metals where encapsulation of a main-group (or transition-metal) element likewise provides additional electrons and central bonding but no new bonding orbitals.[9,11] (As in $In_{10}Zn^{8-}$, some skeletal bonding orbitals in the empty cluster have the same representations as s and p on the interstitials, and the corresponding bonding and high-lying antibonding levels are generated in the encapsulation process.) Examples are $Sc(Sc_6Cl_{12}N)$, $Zr_6Cl_{12}Be$ and $Zr_6I_{14}C$, all with $2n + 2 =$ 14 bonding electrons counting those of the interstitial as well. These and the $In_{10}Zn^{8-}$ examples are all stable in a thermodynamic sense, that is, with respect to all alternate products. Ordinary chemistry does not afford much guidance in predicting where other cluster examples may be found, but several other apparent interstitial or substitution derivatives of indium clusters are presently under study. One tantalizing series are the isoelectronic $K_{10}In_{10}M$, M = Ni, Pd, Pt, in

which the d orbitals on Ni, etc. are effectively core-like and nonbonding. The nickel-centered polyhedron is closest to C_{3v} symmetry but is in fact also a recognizable distortion of the ~D_{4d} polyhedron of $In_{10}Zn^{8-}$.[3] It is interesting to note that In_{11}^{7-} is also isoelectronic with $In_{10}Zn^{8-}$, one skeletal atom in the former being converted to the role of a smaller interstitial.

The magnetic susceptibility data for $K_8In_{10}Zn$ are shown in Figure 3 after correction for core (-3.04×10^{-4} emu mol^{-1}) and orbital or Langevin (-3.23×10^{-4} emu mol^{-1}) effects, as before.[2,5] Shown for comparison is that for the metallic and similarly corrected $(K_8^+)In_{11}^{7-}$ e^-. The additional electronic localization in the zinc compound is clear. On the other hand, "Q" measurements indicate a metal-like conductivity for $K_8In_{10}Zn$, with ρ_{295} ~255 $\mu\Omega$–cm and a coefficient of 0.32% per degree over the range of 140–295 K. Of course, the last effect represents what goes on near the top of the valence band and presumably reflects some overlap with the conduction band. An analogous conductivity behavior is observed for Na_4Sn_4 and Na_8In_4 with tetrahedral cluster anions.[5] A small or negligible gap at E_F seems highly reasonable in densely packed solids containing *anions* of a metallic main-group element like indium. Contributions of cation orbitals to the valence bands and of cluster antibonding MO's to the conduction band in these phases may be general and appreciable (as in Na_4Sn_4[15]) but this cannot be handled in simple Hückel calculations. The contrast between χ and ρ results may originate with insufficient diamagnetic corrections in the former, only a few carriers, or both. But conduction via high lying and substantially nonbonding levels should not obscure or lessen the obvious importance of localization in covalent In–In (or other) cluster bonds that lie lower in the valence levels/band. The value and import of the descriptor "metallic Zintl phase"[16] is clear.

Supplementary Material Available. Tables of data collection and refinement information, atom parameters, and distances and angles in $K_8In_{10}Zn$ (4 pages); a listing of F_o and F_c data for the same structure (4 pages). Ordering information is given on any current masthead page.

REFERENCES

1. Corbett, J. D. *Chem. Rev.* **1985**, *85*, 383.
2. Sevov, S. C.; Corbett, J. D. *Inorg. Chem.* **1991**, *30*, 4875.
3. Sevov, S. C.; Corbett, J. D., unpublished research.
4. Sevov, S. C.; Corbett, J. D. *Inorg. Chem.* **1992**, *31*, 1895.
5. Sevov, S. C.; Corbett, J. D. *J. Solid State Chem.* **1992,** in press.
6. Belin, C.; Ling, G. *J. Solid State Chem.* **1983**, *48*, 40.
7. Schäfer, H. *J. Solid State Chem.* **1987**, 57, 210.
8. Burdett, J. K.; Canadell, E. *J. Am. Chem. Soc.* **1990**, *112*, 7207.
9. Ziebarth, R. P.; Corbett, J. D. *Acc. Chem. Res.* **1989**, *22*, 256.
10. Zhang, J.; Corbett, J. D. *Inorg. Chem.* **1991**, *30*, 437.
11. Corbett, J. D. in "Modern Perspectives in Inorganic Crystal Chemistry", E. Parthé, ed. (NATO ASI Series C), Kluwer Academic Publishers, **1992**, in press.
12. The structure was solved by direct methods (SHELX-86) following data collection at 22°C on a CAD 4 diffractometer with Mo Kα radiation. The crystal data are *P4/nnc* (no. 126), $Z = 2$; $a = 10.2916$ (5) Å, $c = 13.837$ (1) Å (from Guinier data, $\lambda = 1.54056$ Å), $R(F)/R_w = 2.1 / 2.1$ % for 427 independent reflections ($2\theta \leq 50°$), 25 variables and with absorption ($\mu = 95.5$ cm^{-1}) corrected with the average of two ψ-scans. The largest ΔF residual, 0.66 e/Å^3, was 1.3 Å from K.
13. The longer but still relevant d(In1–In1), 3.627 (2) Å, was missing from the previous listing for In_{11}^{7-}.[2]
14. The orbital exponents for In were as before[2] while those for Zn came from Janiac, C.; Hoffman, R. *J. Am. Chem. Soc.* **1990**, *112*, 5924. The H_{ii} values for both were iterated to charge consistency (Zn 4s = –6.14, 4p = –2.72 eV; In 5s = –6.47, 5p = –2.40 eV) with the aid of parameters given by Munita, R.; Letelier, J. R. *Theor. Chim. Acta.* (Berlin) **1981**, *58*, 167. The same H_{ii} values for In were used for the In_{10} clusters shown in Figure 2a,b.

15. Springelkamp, F.; De Groot, R. A.; Geertsma, W.; van der Lugt, W.; Mueller, F. M. *Phys. Rev. B.* **1985**, *32*, 2319.

16. Nesper, R. *Prog. Solid State Chem.* **1990**, *20*, 1.

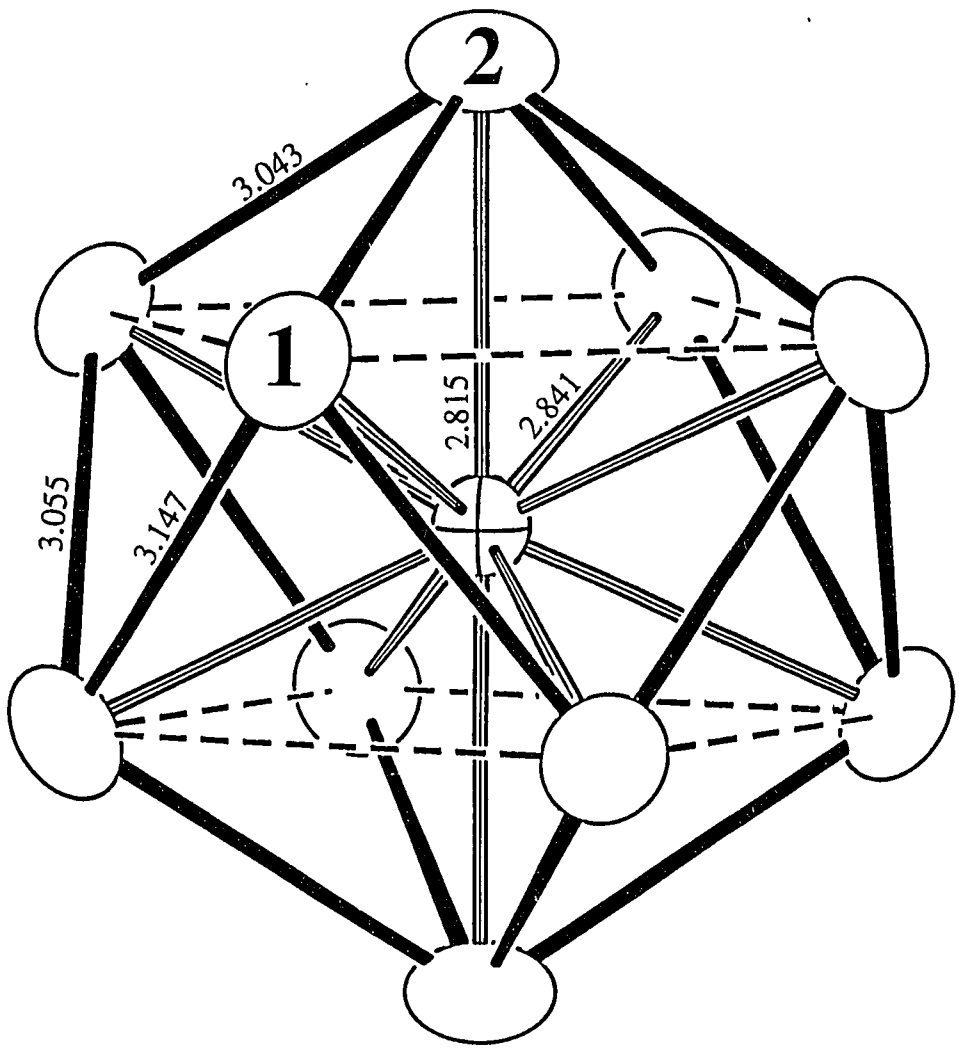

Figure 1. The cluster anion $In_{10}Zn^{8-}$. The cluster has D_4 symmetry and its the principal axis lies vertical. (Thermal ellipsoids at the 94% probability level.)

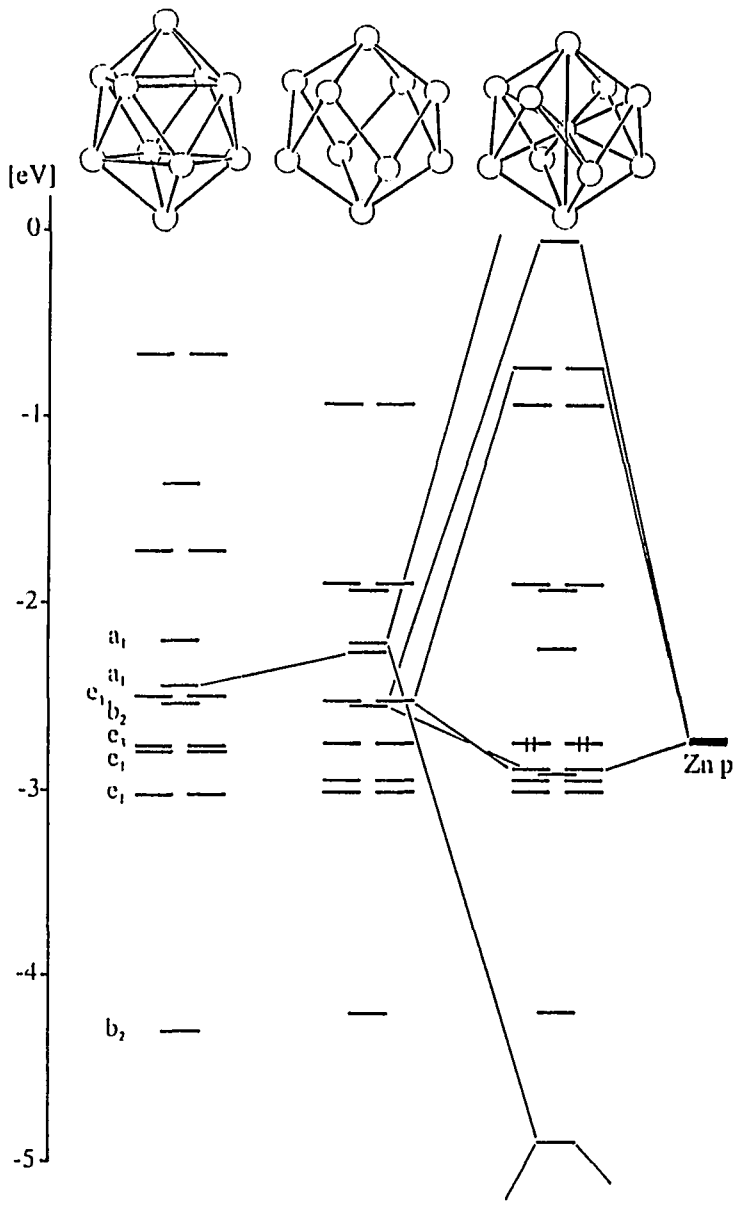

Figure 2. Charge-consistent extended-Hückel MO results for $In_{10}Zn^{8-}$ (D_{4d}) for (a) the classical 10-atom polyhedron, (b) after distortion to the observed shell dimensions, (c) after zinc insertion. The $b_2(2)$ level contains appreciable In 5s contributions and lies at the top of the s-based orbitals.

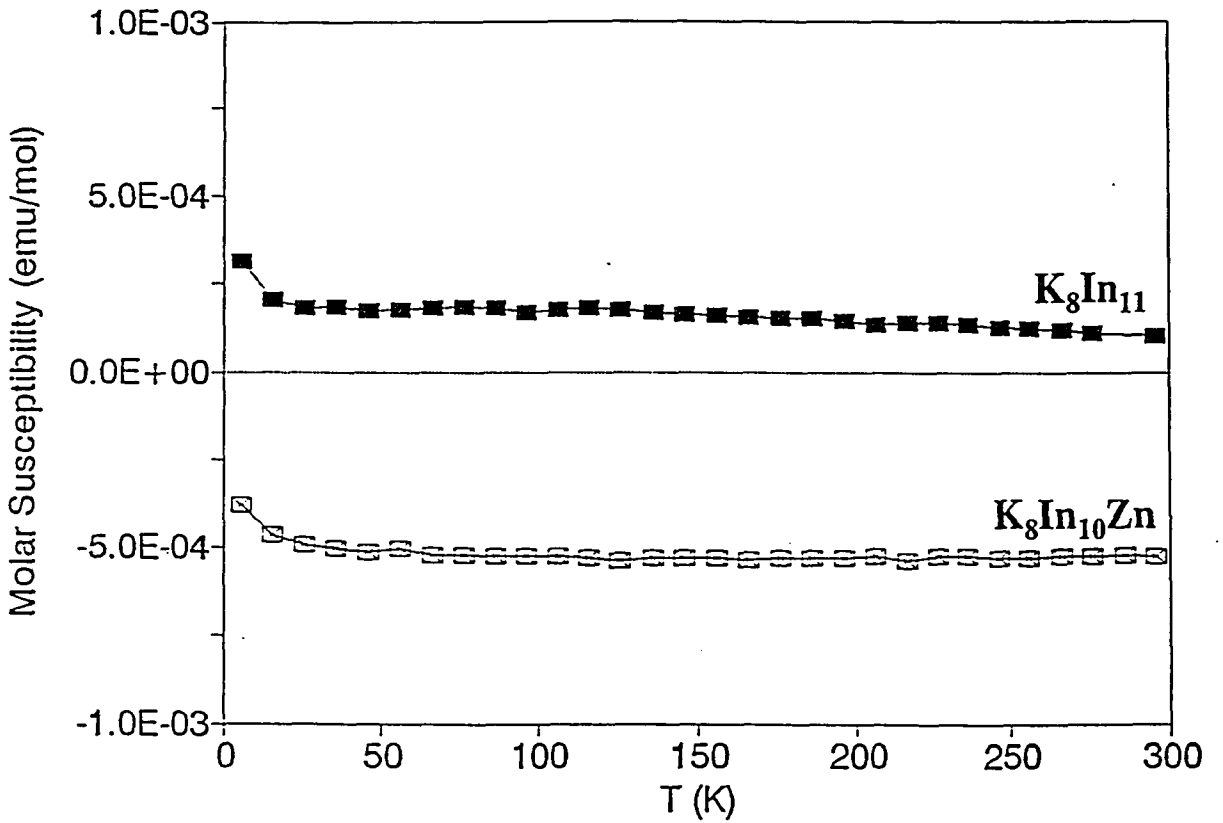

Figure 3. Molar magnetic susceptibility data for $K_8In_{10}Zn$ relative to those for the metallic K_8In_{11}. Both have been corrected for core and orbital (Langevin) diamagnetic contributions.

SUPPLEMENTARY MATERIAL

Data Collection and Refinement Information

formula Weight	1526.37
crystal size	0.1 × 0.1 × 0.2 mm
lattice parameters:[a]	
a, Å	10.2916 (5)
c, Å	13.837 (1)
V, Å^3	1465.6 (1)
space group, Z	*P4/nnc* (#126), 2
d(calc)	3.46 g/cm^3
f_{000}	1344
μ (Mo Kα)	95.484 cm^{-1}
transmission range	0.749–1.00
diffractometer	CAD 4
temperature, °C	20
octants measured	±h, k, ℓ
scan method	Ω–2θ
2-θ (max)	50°
no refl. (no conditions)	2845
obser. ($I > 3.00\ \sigma_I$)	1312
unique reflec.	427
R(ave) (all data)	10.6%
no. variables	25
residuals: *R*; R_w[b]	2.1; 2.1%
goodness of fit indicator	0.8
maximum shift in final cycle	0.00
largest peaks in final diff. map	+0.66 e/Å^3 (1.3 Å from K)
sec. extinc. coeff. (10^{-7})	−0.66, 0.1 (1) e/Å^3

[a] Guinier powder data with Si as internal standard, λ = 1.540562 Å.

[b] $R = \Sigma||F_o| - |F_c||/\ \Sigma|F_o|$; $R_w = [\Sigma w(|F_o| - |F_c|)^2 / \Sigma w(F_o)^2]^{1/2}$; $w = \sigma_F^{-2}$.

Positional parameters and B(eq) for $K_8In_{10}Zn$[a]

atom	sym	*x*	*y*	*z*	$B_{(eq)}$
In1	1	0.01731 (5)	0.15771 (5)	0.66354 (4)	2.30 (2)
In2	4	¼	¼	0.54655 (8)	2.75 (3)
Zn	42	¼	¼	¾	1.47 (5)
K	1	0.0469 (2)	−0.1781 (2)	0.6041 (1)	3.25 (8)

U values for $K_8In_{10}Zn$[b]

atom	U_{11}	U_{22}	U_{33}	U_{12}	U_{13}	U_{23}
In1	0.0243(3)	0.0296(3)	0.0334(3)	−0.0036(2)	−0.0084(3)	−0.0029(3)
In2	0.0424(5)	U_{11}	0.0198(6)	0	0	0
Zn	0.0179(8)	U_{11}	0.020(1)	0	0	0
K	0.045(1)	0.034(1)	0.044(1)	−0.000(1)	−0.006(1)	−0.005(1)

---

[a] Origin at $\bar{1}$, s.g. 126.

[b] $T = \exp[(-2\pi^2(U_{11}h^2a^{*2} + U_{22}k^2b^{*2} + U_{33}\ell^2c^{*2} + 2U_{12}hka^*b^* + 2U_{13}h\ell a^*c^* + 2U_{23}k\ell b^*c^*)]$.

Important Distances in K8In10Zn[a] (Å)

In1		In2		Zn		K	
2 In1	3.6433(7)[b]	4 In1	3.0426(8)	8 In1	2.8405(5)	In1	3.565(2)[c]
In1	3.055(1)	Zn	2.815(1)	2 In2	2.815(1)	In1	3.736(2)[c]
In1	3.147(1)	4 K	3.773(2)			In1	3.764(2)
In2	3.0426(8)					In1	3.768(2)[d]
Zn	2.8405(5)					In1	3.960(2)[c]
K	3.565(2)					In2	3.773(2)[d]
K	3.736(2)					2 K	4.258(3)
K	3.764(2)					K	4.301(4)
K	3.960(2)					K	4.434(4)
K	3.768(2)					2 K	4.447(3)
						K	4.761(4)

[a] d(K–In) < 4.94 Å, d(K–K) < 5.20 Å

[b] Edge of the square faces.

[c] Face-capping distances.

[d] Edge-bridging distances.

Intracluster Bond Angles in K8In10Zn (deg)

atom	atom	atom	angle
In1	In1	In1	71.94(2)
In1	In1	In2	102.86(2)
In1	In1	In2	100.75(2)
In1	In1	Zn	57.47(1)
In1	In1	Zn	56.37(1)
In2	In1	Zn	57.05(2)
In1	In2	In1	115.72(4)
In1	In2	In1	73.56(2)
In1	In2	Zn	57.86(2)
In1	Zn	In1	130.18(2)
In1	Zn	In1	79.78(1)
In1	Zn	In1	65.07(2)
In1	Zn	In1	140.93(2)
In1	Zn	In1	67.27(2)
In1	Zn	In1	137.84(2)
In1	Zn	In2	65.09(1)
In1	Zn	In2	114.91(1)
In2	Zn	In2	180.00

PAPER 4. $K_{10}In_{10}Z$ (Z = Ni, Pd or Pt): ZINTL PHASES CONTAINING ISOLATED DECAINDIUM CLUSTERS CENTERED BY TRANSITION ELEMENTS

Slavi C. Sevov and John D. Corbett*

ABSTRACT

The isostructural title compounds are obtained in high yield by slowly cooling the appropriate fused mixture in welded Ta. They occur in the orthorhombic space group *Pnma*, Z = 12, with a = 15.948 (6), 16.043 (6), 16.056 (3) Å, b = 32.565 (6), 32.73 (1), 32.692 (1) Å, c = 18.822 (3), 18.895 (5), 18.896 (3) Å for the Ni, Pd, Pt derivatives, respectively. The structure of the Ni phase was refined by single crystal means (R,R_w = 2.9, 3.3 %) and shown to be constructed from close-packed layers of Ni-centered In_{10} clusters that are separated by potassium ions both within and between the cluster layers. The compounds have large resistivities at room temperature by two-probe methods and are diamagnetic. The geometry of the clusters can be derived from an ideal tetracapped trigonal prism (C_{3v}) of In centered by Z through axial compression along the three-fold axis and opening of the capped triangular face so as to yield substantially equal Ni–In distances. The clusters are also related to Sb_7^{3-}, etc. Charge-consistent extended-Hückel MO calculations show that the Ni-centered cluster has a closed shell with $2n$ = 20 skeletal electrons, only the s and p orbitals on the interstitial mixing with appropriate cluster orbitals. The d orbitals on Ni do not appear to participate significantly, presumably because they are fully reduced (lie too low) relative to In p (d(In–Ni) ~2.8 Å). This means that Ni, Pd and Pt behave as quasi-main-group elements.

INTRODUCTION

Although indium lies three periods below boron, its ability to form a variety of isolated clusters with homoatomic covalent bonding parallels that of the familiar boranes $B_nH_n^{2-}$ surprisingly well. Of course, indium analogs with exo-bonded H, R, etc. are not stable, but alternative "naked" clusters are. However, a potential problem remains with such clusters, the apparent requirement of at least $2n+2$ skeletal electrons for closo-polyhedra (Wade's rules) that is repeatedly observed with boranes, carboranes, etc.[1] or in analogues with later, heavier elements like Sn_9^{4-}, Pb_5^{2-} and so forth (Zintl ions).[2] This minimum would require that closo clusters of n In atoms have unusually high charges, especially when n is large, viz. In_n^{-n-2}. Indium generally avoids this circumstance by forming either clusters with new geometries that are hypoelectronic with respect to these rules[3] or borane-type clusters with several two-center exo bonds between them that reduce the charge on each cluster by one per bond.[4,5]

Small tetrahedral (nido) clusters, formally In_4^{8-}, are still found in Na_2In. The charge on the cluster is apparently not too high, and a common geometry is retained.[5] The situation is different in 10- and 11-atom indium clusters. The latter are represented by In_{11}^{7-} and the substitution product $In_{10}Hg^{8-}$ in K_8In_{11} and $K_8In_{10}Hg$, respectively.[3,6] Both clusters have a geometry unknown for boranes, a pentacapped trigonal prism compressed along the three-fold axes that requires $2n-4$ skeletal electrons. A third type of cluster is the Zn-centered $In_{10}Zn^{8-}$ found in $K_8In_{10}Zn$.[7] Although this has a classical geometry, a bicapped Archemedian antiprism, it is distorted through compression along the four-fold axis so that all Zn–In separations are about equal. This unit now requires $2n$ rather than $2n+2$ skeletal bonding electrons, two of the former being provided by the zinc. This particular situation is in many respects quite similar to that in the many interstitially-stabilized cluster halides of the early transition metals.[8]

Gallium, in a great contrast with indium, has been reported to form alkali-metal compounds with structures consisting exclusively of cluster networks. Many binary and ternary alkali-metal–gallium–third element systems have been explored without finding any examples of isolated gallium clusters.[9] It is not yet clear whether such gallium analogs exist, but have been missed, or simply are not stable with respect to other compounds.

The discovery that indium clusters can be centered by zinc sparked a search for other elements that might act similarly in ternary alkali-metal–indium–third element systems. The compounds reported here were obtained directly from reactions designed to produce $K_{10}In_{10}Z$ (Z = Ni, Pd or Pt) isoelectronic with $K_8In_{10}Zn$. In fact, Z-centered clusters in these have a different configuration and thus represent a fourth example of a family of relatively large, naked indium clusters.

EXPERIMENTAL SECTION

Mixtures of the elements (K – J. T. Baker, lump under oil, 98+%; In – Cerac, shot, 99.999%; Ni – Matheson, Coleman & Bell, sheet, reagent grade; Pd – Johnson Mathey, wire, 99.995%; Pt – government issue, sheet, reagent grade) in atomic ratios K : In : (Ni, Pd, Pt) = 10 : 10 : 1 were fused in closed Ta-containers at 600°C for 2 days and then cooled slowly (3°/h) to room temperature. The melting points are about 480 °C. (The technique is described in more detail elsewhere.[5]) The products were in the form of loose bar- or gem-like crystallites with dull and dark yellowish appearances. They react rapidly with moist air, boiling in a minute or two, and surface contamination from handling within a Vacuum Atmospheres glovebox is even sufficient to preclude useful XPS data.

Other reactions loaded to produce analogous compounds containing Sc, Ti, Cr, Mn, Fe, Co, Ru or Rh yielded only known binary products according to their powder patterns. The above compositions loaded with Na instead of K produced compounds with different networks of clusters or known binary products.

Powder patterns were obtained from ground samples mounted between pieces of cellophane tape. An Enraf-Nonius Guinier camera, Cu Kα radiation (λ = 1.540 562 Å), and NBS (NIST) silicon as an internal standard were employed for this purpose. X-ray powder patterns calculated on the basis of the refined positional parameters for Z = Ni (below) matched the respective ones for the K–In–Pd and K–In–Pt products very well, leading to the conclusion that the same structure pertains to all three. A least-squares refinement of the measured and indexed 2θ values calibrated with standard Si lines resulted in a = 15.948 (6), b = 32.565 (6), c = 18.822 (3) Å, V = 9775 (7) Å^3 for $K_{10}In_{10}Ni$, a = 16.043 (6), b = 32.73 (1), c = 18.895 (5) Å, V = 9921 (5) Å^3 for $K_{10}In_{10}Pd$ and a = 16.056 (3), b = 32.692 (5), c = 18.896 (3) Å, V = 9918

(3) $Å^3$ for $K_{10}In_{10}Pt$. All of the patterns contained weak lines for indium metal as well, probably from adventitious oxidation of the very sensitive samples during the X-ray exposure.

A few crystals from the Ni product were sealed in glass capillaries and checked for singularity by oscillation film techniques. A zero-layer Weissenberg photograph of one 0.15 × 0.15 × 0.20-mm example revealed an *mmm* Laue class. Two octants of data up to $2\theta = 50°$ (18435 reflections) were collected at 23°C with monochromated Mo Kα radiation on CAD4 single crystal diffractometer with $\omega-\theta$ scans. Subsequent processing of the data and the structure refinement were done with the aid of the TEXSAN package.[10] Correction for Lorentz and polarization effects and for absorption ($\mu = 86.7\ cm^{-1}$) with the aid of the average of three ψ-scans at different 2θ angles gave a data set that showed systematic absences (*0kl*: $k + l \neq 2n$ and *hk0*: $h \neq 2n$) consistent with two possible space groups – $Pn2_1a$ (No. 33) and *Pnma* (No. 62). Since the Wilson plot statistics indicated the existence of a center of symmetry, *Pnma* was chosen for the structure solution.

Application of direct methods (SHELXS-86[11]) provided 17 peaks with distances between them suitable for In and two smaller peaks with shorter distances to In than the others which were assigned to Ni. There were also eleven peaks with heights and distances suitable for K, but they were not assigned for the first few cycles. Successive least-square cycles and a difference Fourier synthesis revealed all seventeen potassium positions. Refinement of all atoms with anisotropic thermal parameters and a secondary extinction coefficient gave final residuals of R, R_w = 2.9, 3.3 % (4634 reflections $I > 3\sigma_I$, 299 variables). Occupancies of In or Ni did not deviate from unity by more than 1.0 % (2.5σ) when the cations were held fixed, or those of K by more than 3.6 % (4σ) when the In and Ni occupancies were kept fixed. All atoms were therefore retained at full occupancies for the final cycles. The remaining peaks in a final

difference Fourier map were 1.4 e/Å^3, 1.07 Å from In5B, and −1.1 e/Å^3. Structure factor data are available from J.D.C.

The magnetizations of ~25 mg ground samples of single phase samples of all three $K_{10}In_{10}Z$ phases were measured at a field of 3 T over 6–295 K and also at 100 Oe over 1.4–6 K on a Quantum Design MRMS SQUID magnetometer. The holder used for the purpose and the techniques are described elsewhere.[5]

Extended-Hückel calculations were carried out as before.[3-5,12] The H_{ii} values used for Ni and In in all three calculations were iterated to charge consistency and resulted in -6.4 and -2.33 eV for In 5*s* and 5*p*, respectively, and −7.38, −6.19 and −2.35 ev for Ni 3*d*, 4*s* and 4*p*, respectively.[13] The charge iterations were done with the observed cluster plus 10 dummy potassium atoms placed far from the cluster and with the same symmetry. The H_{ii} values and s orbitals used for the potassium atoms were such as to ensure complete charge transfer to, and no significant overlap with, the cluster.

RESULTS AND DISCUSSION

Structure description

A general view of the unit cell for $K_{10}In_{10}Ni$ approximately along the *c* axis is shown in Figure 1 with connections drawn between all indium atoms that are less than 4.00 Å apart. Important near-neighbor distances are listed in Table I.

The structure contains isolated 10-atom indium clusters that are centered by nickel and ordered in close-packed layers perpendicular to the *a* axis (vertical in the Figure). Although all clusters are $In_{10}Ni$, they are of two crystallographically different versions (below), eight clusters of type A (centered by Ni(A)) and four of type B (centered by Ni(B)) per cell. Each cluster has six neighbors in the same layer as required for a close-packed layer, three of each type about the A-type clusters and six A-type neighbors about each B-type cluster. The layers are not quite flat but puckered along $\vec{a}$ by ~0.5 Å. The layers are stacked in a hexagonal packing order, which leads to quite large trigonal antiprismatic (ideally octahedral) voids between the layers.

The two indium clusters shown in Figure 2 have very similar geometries although different symmetries. Atoms in the cluster about Ni(A) lie on general positions, while In2B, In4B, In7B, In5B and the central Ni(B) atoms lie on a mirror plane that gives the cluster C_s symmetry, Figure 2b. Both can be considered as derived from trigonal prism capped on all three rectangular and one triangular faces (C_{3v}). The former prisms, now distorted, are defined by In1A to 6A and In1B to 4B, while In7A – 9A and InB5 and B6 cap the former rectangular faces of the prisms. Finally, In10A and In7B cap one expanded end face of each prism. All indium atoms have similar distances to the respective nickel atoms, which means the clusters must be substantially compressed along the quasi 3-fold axes through the axial In10A or 7B and the corresponding nickel atom. This in turn opens up the capped triangular face of the prism and puts the edge distances out of a bonding range, 4.19–4.53 Å. In order to keep the In–In

distances around the cluster in a "normal" range, the atoms capping the former rectangular faces (In(7–9)A, In(5,6)B) also move closer to the edges of the expanded triangular face. The foregoing cluster description seems much more useful than one based on pentagonal indium pyramids (e.g., with In2A as the vertex) that are capped on the open face by a square (e.g., In(4,9,6,10)A).

The $In_{10}Ni$ cluster geometries may be compared with those of the In_{11} and $In_{10}Hg$ clusters found in K_8In_{11} and $K_8In_{10}Hg$, respectively.[3,6] These are based on distorted pentacapped ($\sim D_{3h}$) rather than tetracapped trigonal prisms and do not have central atoms. The two axial atoms that cap the triangular faces of the trigonal prisms are shifted towards the center of the clusters to a much greater degree than in $In_{10}Ni$ so that the two expanded triangular faces have edge distances around 5 Å. In these cases, the compressions are sufficient to add bonding between the two types of face-capping atoms, at ~ 3.3 Å rather than 3.82–4.23 Å here (10A – 7,8,9A, 7B – 5,6B).

The Ni–In distances have a relatively small dispersion – from 2.697(2) to 2.816(2) Å and from 2.703(3) to 2.814(2) Å for the A and B types clusters, respectively, with an overall average of 2.78 Å. These distances compare reasonably well with the 8-fold Ni–In distance in more symmetric NiIn (CsCl-type) of 2.65 Å[14] and with the single bond radii sum for the two elements, 2.58 Å,[15] although the direct relationships among these are not so simple. The small dispersion means that the indium atoms are very close to the surface of an imaginary sphere around the central atom.

The In–In distances in the two Ni-centered clusters (Table I) are, in general, larger than commonly seen in other systems with bridged or isolated clusters, which are 2.85 to 3.1 Å, the shorter appearing particularly in intercluster bonding.[3–7] Many of them here are in the range 3.1 to 3.3 Å and some are even greater than 3.3 Å. Apparently the size of the central element,

the central bonding and possibly the cation interactions (below) affect both the geometry of the cluster and the bonding between the In atoms. (The first variation is well known in centered transition-metal halide clusters.[8]) The consequence of adding a central atom can be appreciated by a comparison of In–In distances in this cluster with those in the empty In_{11} since they have similar geometries and derivations. The average distances in the more-or-less vertical edges of the trigonal prisms, 3.323 Å and 3.300 Å here, are much greater than that in In_{11}, 3.097 Å. The average distances in the uncapped triangular ends of the prisms of the Ni-centered clusters are also relatively long, 3.144 Å and 3.233 Å for the A- and B-types, respectively. A useful comparison can also be obtained with the In–In distances in $In_{10}Zn^{8-}$ ($\sim D_{4d}$).[7] The two clusters are isoelectronic and in fact differ only slightly in average In–In distances, 3.072 Å with Zn vs 3.090 and 3.094 Å for Ni, although the average Zn–In distance is somewhat greater than for Ni–In, 2.835 vs. 2.777 Å. (Zn is also correspondingly 0.06 Å larger in metallic radius.[15]) This contrast appears to be a result of the different number of In–In bonds in the two cluster types. We find eight 3-bonded and two 4-bonded indium atoms in the Zn-centered cluster, but one 3-bonded, six 4-bonded and three 5-bonded indium atoms in the Ni-centered clusters. The distances logically increase when there are more bonded neighbors, the five-bonded atoms in the latter also having the more distant neighbors.

Cation effects

It is not immediately clear, though, why the two clusters (although isoelectronic) need to have different geometries and, therefore, differently bonded indium atoms. One possibility is that weaker (though shorter) Ni–In than Zn–In bonding may require more In–In bonds in the former to compensate for the lost central bonding. A more attractive explanation is simply packing requirements. We have repeatedly found that the ordering of the alkali-metal cations about faces, edges, and vertices of indium clusters in many structures are geometrically quite

specific. The fact that there are two more cations per cluster in $K_{10}In_{10}Ni$ than in $K_8In_{10}Zn$ means that the former clusters will have more potassium neighbors. In order to accommodate them, the number and lengths of the In–In separations may have to be greater, meaning more edges and faces. More evidence regarding this can be found in bond populations (below).

The layers of clusters as well as clusters within each layer are separated by the potassium cations (Figure 1). Similar ordering of the cations is also present in K_8In_{11} and $K_8In_{10}Hg$.[3,6] The thermal parameters for all potassium atoms in $K_{10}In_{10}Ni$ are relatively large (B_{eq} = 3.5(1)–8.6(4) Å^2) compared with those in the previous two and in $K_8In_{10}Zn$ which all fell in the range 3.0 to 5.0 Å^2.[3,6,7] This must result from the larger number of cations per cluster here than for the others, meaning more potassium and fewer indium neighbors for each cation. This, in turn, leads to longer K–K distances, more space around each potassium and, consequently, greater positional freedom. The potassium atoms are again arranged so that they cap faces, bridge edges, and bond exo at vertices of the indium clusters. The potassium functionalities summarized in Table II reveal some clear regularities and order to these that also relate to ellipsoid differences. Distances are of course also important, and these can be recovered from Table I. Suffice for note here is the fact that all cations with apparent coordination numbers above five have two relatively long K–In distances >3.85 Å (the others range down to 3.45 Å).

The first eleven potassium atoms have smaller thermal parameters, 3.5(1) to 4.9(2) Å^2. On the other hand, the last four, which are only three or four coordinate, have B_{eq} values between 7.2 and 8.6 Å^2, and these are also more anisotropic than the rest. The large thermal parameters probably result from the fact that these four atoms fill larger trigonal antiprismatic voids between close-packed layers of indium clusters and, therefore, have each other for neighbors as well as fewer indium neighbors. The anisotropic displacement parameters for these

atoms are also somewhat greater along *a*, the antiprismatic axis, because they either bridge In–In cluster edges that are parallel to each other or bridge an edge and cap a vertex that are nearly coplanar with the cation. Such nearly planar environments usually allow greater motion normal to the plane of the surrounding atoms. In addition, these four cations do not have any potassium neighbors along the direction of the larger thermal motion, while K13 (B_{eq} = 5.6 Å^2), which also has only three indium neighbors, has surrounding potassium atoms that present a quite isotropic environment.

Because of the large number of potassium atoms per cluster, the shortest intercluster distance, 5.744(2) Å between In3A and In6A, is also greater than the 5.26 and 5.58 Å between the clusters in K_8In_{11} and $K_8In_{10}Zn$, respectively. In other words, the clusters in $K_{10}In_{10}Ni$ are more loosely packed and more diluted by a sea of potassium cations than those other compounds. The distortions observed within the two clusters also suggest that this is a somewhat "soft" structure.

Properties

The magnetic susceptibilities of the Ni, Pd and Pt derivatives are temperature-independent over the range 25–295 K and, after holder corrections, fall in the range of –(9–12) × 10^{-4} emu mol^{-1}. Two types of diamagnetic corrections can be applied to these numbers. The first, for the ion core diamagnetism, total -3.3, -3.5 and -3.6 × 10^{-4} emu mol^{-1} for the Ni, Pd and Pt derivatives, respectively. A second correction, for the Larmor precession of the electron pairs in the large cluster orbitals, was calculated as before[3,7] with r_{ave} = 2.35 Å to yield χ_L = –3.0 × 10^{-4} emu mol^{-1} for each compound. These give final χ_M values of –(2.7–4.7), –(4.5–5.5) and –(4.5–5.5) × 10^{-4} emu mol^{-1} for Z = Ni, Pd and Pt, respectively, clearly diamagnetic results. The susceptibilities of $K_{10}In_{10}Ni$ are shown in Figure 4 together with those similarly corrected for the diamagnetic $K_8In_{10}Hg$ and $K_8In_{10}Zn$ and the Pauli-paramagnetic K_8In_{11} ($8K^+ + In_{11}^{7-}$ +

e^-). No superconductivity was observed at low fields and at temperatures as low as 1.4 K. The crystal habits of these very reactive phases precluded gaining conductivity estimates by the Q-method that we have found useful in other cases. Resistances of the compounds were therefore checked by two-probe measurements on a few bar-like crystals with lengths of 3 to 5 mm. These yielded resistances of 2 to 4 kΩ ($\rho \sim 10^2$ Ω·cm), values that are 50–500 times those similarly measured for other poorly metallic or semimetal indium cluster phases.[3–7] The high resistivities and the diamagnetic susceptibilities are in a good agreement with the crystal structure and the proposed electronic structure of the clusters (below).

Electronic structure

Extended-Hückel MO calculations were performed on three different species: a) an undistorted tetracapped trigonal prism (C_{3v}), b) the empty C_{3v} symmetry cluster with the observed compression along the pseudo 3-fold axis, and c) the cluster in b) centered by Ni. All species had average distances equal to those observed. (Calculations with the geometries of the real clusters instead led to no more than 0.06 eV splitting of the degenerate orbitals and no significant differences between the A and B types.) The resulting MO energy diagrams are shown in Figure 4.

As expected, the ideal (but improbably proportioned) tetracapped trigonal prism has a closed shell with $2n$ electrons.[16] The top 10 orbitals (between -2.3 and -3.0 eV) below a small gap of ~0.5 eV (Figure 4a) are of mainly *p* character and carry the skeletal bonding electrons. A block of orbitals of mainly *s*-character spreads from -4.3 to -9.0 eV, combinations of the so-called lone pairs on the indium. (As before,[7] the HOMO for the *s* block near -4.3 eV exhibits significant hybridization of *s* and *p*.) Upon distortion, nothing significant happens to the *s* block, as it should be, and also to the lower 9 of 10 skeletal bonding orbitals. Those that do change are the a_1 HOMO and some of the antibonding levels. A closer look reveals that this a_1 is

bonding within the triangular ends of the prism and antibonding between the unique capping atom and those in the capped triangle. The observed axial compression raises the a_1 energy on both accounts.

Orbitals with similar behaviors are also found in the pentacapped trigonal prism of In_{11} and the bicapped square antiprism of $In_{10}Zn$ when these are axially compressed. The a_1 orbital in the former is destabilized to a greater degree (by 2 eV) because the atoms capping the triangular faces of the prism are pushed much closer to the center of the cluster (above) and both triangular ends are capped. In the Zn-centered cluster, the change in the energy of the a_1 orbital at this stage is about the same as with the Ni-centered example because, first, the compression of the cluster is not as pronounced as in the pentacapped trigonal prism simply because it is limited by the central atom, and second, the destabilization is not as large since the larger squares need not expand as much in order to accommodate the compression. As an example, the edges within the squares increase to 3.625 Å while that in the triangles of the pentacapped trigonal prisms go to 5.00 Å. (Some of the antibonding orbitals fall in energy during compression (Fig. 3b) because they are in character opposite to that of a_1, antibonding within the triangles of the prism and bonding between the capping atom and the triangle.)

Introduction of the Ni atom at the center of the cluster produces a very interesting result (Figure 4c). The Ni *d* orbitals remain unperturbed as they exhibit negligible mixing with cluster orbitals. In effect, this appears to come about because of the appreciable difference between the energies of the skeletal cluster orbitals around −2.5 eV and of the Ni *d* orbitals located around −7.5 eV; in other words, the nickel is fully reduced and d^{10}. The resulting In–Ni distances are thus too long for good overlap between Ni *d* and In s, p. A similar conclusion regarding inertness of the Ni *d* orbitals has been deduced for several Ni-centered nickel carbonyl clusters, $Ni_9(GeEt)_6(CO)_8$ (a body-centered cube capped on all faces by GeEt)[17] as well as in

$[Ni_{11}(SbNi(CO)_3)_2CO)_{18}]^{2-}$ [18] and $[Ni_{11}(SnR)_2CO_{18}]^{2-}$,[19] centered icosahedra containing two trans Sb or Sn atoms and 2.057–2.58 Å Ni–Ni distances. The conclusion that there are no significant Ni–Ni bond populations for interstitial–cage distances above ~2.5 Å[19] translates into Ni–In distances ~2.77 Å based on the metallic radii, comparable to what are found here.

On the other hand, the Ni *s* and *p* orbitals are of appropriate energies and apparently appropriate sizes to overlap well with certain cluster molecular orbitals. The Ni *s* orbital mixes with two a_1 orbitals from the cluster. The upper one was the HOMO for the ideal tetracapped trigonal prism (Figure 5a) that was pushed higher during the distortion leading to the observed cluster geometry (Figure 5b), while the other cluster a_1 is the lowest orbital in the *s*-block. The charge distribution in the middle a_1 result is ~50% Ni *s*, 30% In *p*, while the radial orbital that is pushed up appreciably is about 80% In *p*. The Ni *p* orbitals transform as a_1 and e for this point group and mix with appropriate combinations from the cluster (Figure 5c) to increase the HOMO–LUMO gap to ~0.5 eV. The net result of the insertion of the central element is the stabilization of some cluster orbitals and a gain of In bonding to the central Ni atom, although it is difficult to be more specific regarding the latter bond energies. The cluster has a closed shell with $2n = 20$ skeletal electrons and therefore a -10 charge, $In_{10}Ni^{10-}$. A comparable result was obtained from calculations on the Zn-centered $In_{10}Zn^{8-}$ with a geometry of a bicapped square antiprism. In that case, a Zn atom not only lowered the energies of some of the cluster orbitals but also provided two of the bonding electrons. The resulting cluster is isoelectronic with $K_{10}Ni^{10-}$, both having closed $3d^{10}$ cores on the interstitial atoms.

The EHMO results compared with those for $In_{10}Zn^{8-}$ also provide some information regarding the different geometries of the indium shells and the increases in both In–In distances and the number of nearest neighbors about each vertex in the nickel case. Our assertion then was that the last appeared to be related to the larger number of cations to be accommodated. The calculated In–In bond populations average 0.826 per vertex in $In_{10}Ni^{10-}$ vs 0.761 in

$In_{10}Zn^{8-}$, i.e., greater bonding does appear in the In shell that is "solvated" by the greater number of cations. The Ni–In populations are 2.23 while those for Zn–In (with an intrinsically different overlap) total 2.32. The latter separations are longer, in amount appropriate to the single bond radii.

We also note that $In_{10}Ni^{10-}$ can be readily related to Sb_7^{3-} electronically and geometrically which is a monocapped trigonal prism.[20] Removal of the three nonbonding electron pairs on the two-bonded antimony atoms (compare P_4S_3) corresponds to the indium fragment In_7^{11-}. This in turn translates to $In_{10}Ni^{10-}$ when a) the three trapezoidal faces of the M_7 species are capped by In^+, b) the polyhedron is centered by d^{10} Ni(0), and c) one electron pair is added. The last is necessary to fill the newly developed a_1 radial orbital in the 11-atom closed polyhedron.

The apparent inertness of the *d* orbitals on the central Ni, Pd, Pt atoms in these indium clusters may be behind our failure to synthesize clusters centered by earlier transition metals with fewer d electrons. If the interstitial orbitals are again low in energy, electron transfer from the well-reduced indium cluster to the *d* shell should again fill it to d^{10}. This circumstance is likely to be unfavorable since these indium clusters already require a sizable number of additional electrons from the alkali metal, and an earlier Z element would require an even greater cation content and negative charge on the cluster.

We recently discovered that the corresponding isostructural $Na_{10}Ga_{10}Z$ compounds may also be synthesized directly.[21] Furthermore, the Ni, Pd or Pt-centered indium clusters reported here evidently may also be obtained encapsulated in larger alkali metal–indium cages. Although substantial disorder is a problem, the size and geometry of some of the former resemble the Z-centered clusters in $K_{10}In_{10}Z$. The average Ni–In distances are observed to vary slightly from example to example, 2.66–2.78 Å compared with 2.78 Å here, suggesting the clusters be compressed somewhat under certain circumstances.[22]

REFERENCES

1. Greenwood, N. N.; Eaxnshaw, A. *Chemistry of the Elements* **1984**, Pergamon Press: Oxford, UK, p. 171–209.

2. Corbett, J. D. *Chem. Rev.* **1985**, *85*, 383.

3. Sevov, S. C.; Corbett, J. D. *Inorg. Chem.* **1991**, *30*, 4875.

4. Sevov, S. C.; Corbett, J. D. *Inorg. Chem.* **1992**, *31*, 1895.

5. Sevov, S. C.; Corbett, J. D. *J. Solid State Chem.* **1993**, *103*, 114.

6. Sevov, S. C.; Ostenson, J. E.; Corbett J. D. *J. Alloys Comp.*, submitted.

7. Sevov, S. C.; Corbett, J. D. *Inorg. Chem.* **1993**, *32*, 1059.

8. Ziebarth, R. P.; Corbett, J. D. *Acc. Chem. Res.* **1989**, *22*, 256.

9. Belin, C.; Tillard-Charbonnel, M. *Prog. Solid State Chem.* **1993**, *22*, 59 and references therein.

10. TEXAN, version 6.0 package, Molecular Structure Corp., The Woodlands: Texas (1990).

11. Sheldrick, G. M. SHELXS-86, Universität Göttingen, BRD (1986).

12. The orbital exponents used for In were from Janiac, C.; Hoffman, R. *J. Am. Chem. Soc.* **1990**, *112*, 5924 and for Ni, from Summerville, R. H.; Hoffman, R. *J. Am. Chem. Soc.* **1976**, *98*, 7240.

13. The parameters for charge iterations with one configuration for each orbital were from Munita, R.; Letelier, J. R. *Theor. Chim. Acta* **1981**, *58*, 167 for In, and from Mayers, C. E.; Norman, L. J.; Loew, L. M. *Inorg. Chem.* **1978**, *17*, 1581 for Ni.

14. Ruhl, R. C.; Giessen, B. C.; Cohen, M.; Grant, N. J. *Mat. Sci. Eng.* **1967**, *2*, 314.

15. Pauling, L. *The Nature of the Chemical Bond*, Cornell University Press: Ithaca, New York, **1960**, p. 400.

16. A tricapped trigonal prism (9 atoms), a regular *closo* deltahedron, requires $2n + 2 = 20$ electrons according to the Wade's rules. Addition of an In^+ cation along the 3-fold axis generates no new orbitals. The skeletal electron count thus remains at 20 which is now $2n$.

17. Zebrowski, J. P.; Hayashi R. K.; Bjarnason, A.; Dahl, L. F. *J. Am. Chem. Soc.* **1992**, *114*, 3121.

18. Albano, V. G.; Demartin, F.; Iapalucci, M. C.; Longoni, G.; Sironi, A, Zanotti, V. *J. Chem. Soc., Chem. Commun.* **1990**, 547.

19. Dahl, L. F., private communication.

20. Adolphson, D. G.; Corbett, J. D.; Merryman, D. J. *J. Am. Chem. Soc.* **1976**, *98*, 7234.

21. Henning, R. W.; Corbett, J. D., unpublished research.

22. Sevov, S. C.; Corbett, to be submitted for publication.

Table I. Distances to nearest neighbors about each atom in $K_{10}In_{10}Ni$ ($d_{In-In} \leq 3.8$ Å, $d_{In-K} \leq 4.25$ Å, $d_{K-K} \leq 4.9$ Å).

In1A		**In4A**		**In8A**			**In2B**			**In6B**				
In2A	3.158(1)	In1A	3.354(1)	In2A	3.126(2)	2	In1B	3.192(2)		In1B	3.116(1)			
In3A	3.120(1)	In7A	2.968(1)	In3A	3.041(1)		In4B	3.570(2)		In2B	3.056(1)			
In4A	3.354(1)	In9A	2.949(1)	In5A	2.972(1)	2	In6B	3.056(1)		In3B	2.992(1)			
In7A	3.160(1)	In10A	2.968(1)	In6A	2.958(1)		NiB	2.803(3)		In4B	2.963(1)			
In9A	3.096(2)	NiA	2.754(2)	NiA	2.811(2)					NiB	2.763(1)			
NiA	2.784(2)					2	K8	3.637(4)						
		K2	3.730(3)	K7	3.573(3)	2	K14	3.771(4)		K1	3.645(3)			
K4	3.944(4)	K3	4.038(4)	K10	3.771(3)		K15	4.221(8)		K3	3.896(4)			
K4	3.709(4)	K5	3.793(3)	K11	3.518(3)					K8	4.123(4)			
K5	3.782(3)	K8	4.135(4)	K12	3.549(4)		**In3B**			K10	3.769(3)			
K8	3.666(4)	K15	3.782(4)	K13	4.010(4)					K14	3.692(4)			
K13	3.636(4)	K16	4.039(5)				In1B	3.165(1)						
				In9A			In5B	3.060(1)		**In7B**				
In2A		**In5A**					In6B	2.992(1)						
				In1A	3.096(2)		In7B	2.937(1)	2	In3B	2.937(1)			
In1A	3.158(1)	In2A	3.231(1)	In3A	3.068(1)		NiB	2.785(2)		In4B	3.095(2)			
In3A	3.154(1)	In7A	3.020(1)	In4A	2.949(1)					NiB	2.703(3)			
In5A	3.231(1)	In8A	2.972(1)	In6A	2.959(1)		K3	3.810(3)						
In7A	3.247(1)	In10A	2.931(1)	NiA	2.816(2)		K5	3.630(3)		K2	3.817(5)			
In8A	3.126(2)	NiA	2.745(2)				K6	3.629(4)	2	K3	3.452(3)			
NiA	2.813(2)			K3	3.726(3)		K9	4.073(4)	2	K6	4.027(4)			
		K1	3.710(3)	K5	3.692(3)		K10	3.666(3)		K9	3.735(5)			
K4	3.794(4)	K7	4.101(4)	K6	3.777(4)									
K4	3.768(4)	K7	3.962(4)	K11	3.605(3)		**In4B**			**NiA**				
K7	3.682(3)	K11	3.761(3)	K12	3.637(4)									
K10	3.992(3)	K14	4.202(4)				In2B	3.570(2)		In1A	2.784(2)			
K11	4.035(3)	K17	3.740(4)	**In10A**		2	In6B	2.963(1)		In2A	2.813(2)			
K13	3.734(4)						In7B	3.095(2)		In3A	2.806(2)			
		In6A		In4A	2.968(1)		NiB	2.764(2)		In4A	2.754(2)			
In3A				In5A	2.931(1)					In5A	2.745(2)			
		In3A	3.384(1)	In6A	3.029(1)	2	K3	3.721(3)		In6A	2.697(2)			
In1A	3.120(1)	In8A	2.958(1)	NiA	2.737(2)	2	K17	3.798(4)		In7A	2.777(2)			
In2A	3.154(1)	In9A	2.959(1)							In8A	2.811(2)			
In6A	3.384(1)	In10A	3.029(1)	K3	3.763(3)		**In5B**			In9A	2.816(2)			
In8A	3.041(1)	NiA	2.697(2)	K7	3.668(3)					In10A	2.737(2)			
In9A	3.068(1)			K14	3.738(4)	2	In1B	3.013(2)						
NiA	2.806(2)	K1	3.850(4)	K16	3.531(2)	2	In3B	3.060(1)		**NiB**				
		K3	3.488(3)				NiB	2.809(2)						
K1	3.678(3)	K7	3.477(3)	**In1B**					2	In1B	2.814(2)			
K4	3.716(4)	K12	3.747(4)				K2	3.659(5)		In2B	2.803(3)			
K10	3.836(3)	K12	3.564(4)	In1B	3.314(2)	2	K5	3.774(3)	2	In3B	2.785(2)			
K11	3.694(3)			In2B	3.192(2)		K9	3.453(5)		In4B	2.764(2)			
K12	3.768(4)	**In7A**		In3B	3.165(2)					In5B	2.809(2)			
				In5B	3.013(2)				2	In6B	2.763(1)			
		In1A	3.160(1)	In6B	3.116(1)					In7B	2.703(3)			
		In2A	3.247(1)	NiB	2.814(2)									
		In4A	2.968(1)											
		In5A	3.020(1)	K6	3.638(4)									
		NiA	2.777(2)	K8	3.488(3)									
				K9	3.489(4)									
		K7	3.499(3)	K10	3.870(3)									
		K8	3.562(3)											
		K15	4.130(2)											
		K17	3.746(4)											

Table I. (continued)

K1

	In3A	3.678(3)
	In5A	3.710(3)
	In6A	3.850(4)
	In6B	3.645(3)
	K3	4.010(5)
	K4	4.483(5)
	K7	4.462(5)
	K10	4.243(4)
	K11	3.811(5)
	K12	4.046(5)
	K14	4.568(6)
	K17	4.017(5)

K2

2	In4A	3.730(3)
	In5B	3.659(5)
	In7B	3.817(5)
2	K3	4.401(5)
2	K5	4.127(4)
2	K6	4.165(5)
	K15	4.439(8)
	K16	4.016(8)

K3

	In4A	4.038(4)
	In6A	3.488(3)
	In9A	3.726(3)
	In10A	3.763(3)
	In3B	3.810(3)
	In4B	3.721(3)
	In6B	3.896(4)
	In7B	3.452(3)
	K1	4.010(5)
	K2	4.401(5)
	K6	3.913(5)
	K12	4.443(5)
	K16	3.995(7)
	K17	4.204(6)

K4

	In1A	3.944(4)
	In1A	3.709(4)
	In2A	3.794(4)
	In2A	3.768(4)
	In3A	3.716(4)
	K1	4.483(5)
	K4	3.858(7)
	K7	4.197(5)
	K8	4.134(5)
	K10	4.152(5)
	K11	4.889(5)
	K13	4.520(5)
	K13	4.043(5)

K5

	In1A	3.782(3)
	In4A	3.793(3)
	In9A	3.692(3)
	In3B	3.630(3)
	In5B	3.774(3)
	K2	4.127(4)
	K6	3.922(5)
	K6	4.835(5)
	K8	4.089(5)
	K9	4.289(5)
	K10	4.546(5)
	K11	4.783(5)
	K13	4.212(5)

K6

	In9A	3.777(4)
	In1B	3.638(4)
	In3B	3.629(4)
	In7B	4.027(4)
	K2	4.165(5)
	K3	3.913(5)
	K5	3.922(5)
	K5	4.835(5)
	K9	3.833(5)
	K10	4.824(5)
	K12	4.629(5)
	K13	4.714(6)

K7

	In2A	3.682(3)
	In5A	4.101(4)
	In5A	3.962(4)
	In6A	3.477(3)
	In7A	3.499(3)
	In8A	3.573(3)
	In10A	3.668(3)
	K1	4.462(5)
	K4	4.197(5)
	K11	4.829(5)
	K13	3.991(5)
	K14	4.131(6)
	K17	4.072(6)

K8

	In1A	3.666(4)
	In4A	4.135(4)
	In7A	3.562(3)
	In1B	3.488(3)
	In2B	3.637(4)
	In6B	4.123(4)
	K4	4.134(5)
	K5	4.089(5)
	K9	4.481(5)
	K10	4.674(5)
	K13	4.936(5)
	K14	4.075(6)
	K15	4.020(6)

K9

2	In1B	3.489(4)
2	In3B	4.073(4)
	In5B	3.453(5)
	In7B	3.735(5)
2	K5	4.289(5)
2	K6	3.833(5)
2	K8	4.481(5)

K10

	In2A	3.992(3)
	In3A	3.836(3)
	In8A	3.771(3)
	In1B	3.870(3)
	In3B	3.666(3)
	In6B	3.769(3)
	K1	4.243(4)
	K4	4.152(5)
	K5	4.824(5)
	K8	4.674(5)
	K11	4.317(5)
	K12	4.265(6)
	K13	4.737(6)

K11

	In2A	4.035(3)
	In3A	3.694(3)
	In5A	3.761(3)
	In8A	3.518(3)
	In9A	3.605(3)
	K1	3.811(5)
	K4	4.889(5)
	K5	4.783(5)
	K7	4.829(5)
	K10	4.317(5)
	K12	4.190(6)
	K13	4.179(6)
	K13	4.695(6)

K12

	In3A	3.768(4)
	In6A	3.747(4)
	In6A	3.564(4)
	In8A	3.549(4)
	In9A	3.637(4)
	K1	4.046(5)
	K3	4.443(5)
	K6	4.629(5)
	K10	4.265(6)
	K11	4.190(6)
	K12	4.015(8)
	K13	4.401(5)

K13

	In1A	3.636(4)
	In2A	3.734(4)
	In8A	4.010(4)
	K4	4.520(5)
	K4	4.043(5)
	K5	4.212(5)
	K6	4.714(6)
	K7	3.991(5)
	K10	4.737(6)
	K11	4.179(6)
	K11	4.695(6)
	K12	4.401(5)

K14

	In5A	4.202(4)
	In10A	3.738(4)
	In2B	3.771(4)
	In6B	3.692(4)
	K1	4.568(6)
	K7	4.131(6)
	K8	4.075(6)
	K14	4.719(9)
	K15	4.774(7)
	K16	4.819(7)
	K17	4.202(8)
	K17	4.675(7)

K15

2	In4A	3.782(4)
2	In7A	4.130(2)
	In2B	4.221(8)
	K2	4.439(8)
2	K8	4.020(6)
2	K14	4.774(7)
	K16	4.340(9)
2	K17	4.606(7)

K16

2	In4A	4.039(5)
2	In10A	3.531(2)
	K2	4.016(8)
2	K3	3.995(7)
2	K14	4.819(7)
	K15	4.340(9)
2	K17	4.619(9)

K17

	In5A	3.740(4)
	In7A	3.746(4)
	In4B	3.798(4)
	K1	4.017(5)
	K3	4.204(6)
	K7	4.072(6)
	K14	4.202(8)
	K14	4.675(7)
	K15	4.606(7)
	K16	4.619(9)
	K17	4.502(8)

Table II. Indium Neighbors of the Potassium Cations in $K_{10}In_{10}Ni$.[a]

Atom	CN[b]	N[c]	In
K1	4	1	3,5,6A; 6B
K2	4	1	4,4A; 5,7B
K3	8	4	4,6,9,10A; 3,4,6,7B
K4	5	3+2	1,2,3A; 1,2A
K5	5	3+2	1,4,9A; 3,5B
K6	4	2+1	3,7B; 9A,1B
K7	7	4+3	5,7,8,10A; 2,5,7A
K8	6	3	1,4,7A; 1,2,6B
K9	6	4+2	3,3,5,7B; 1,1B
K10	6	3	2,3,8A; 1,3,6B
K11	5	3+2	2,5,8A; 3,9A
K12	5	3+2	3,6,8A; 6,9A
K13	3	1	1,2,8A
K14	3	2+1	2,6B; 10A
K15	4	2	4,7A
K16	4	2	4,10A
K17	3	2+1	5,7A; 4B

[a] $d < 4.2$ Å.

[b] All K with 6 or more In neighbors have two d(K–In) values >3.85 Å within the set listed.

[c] The orders of indium bonding to each potassium: 1–vertex, 2–edge, 3–triangular face, 4–quadrilateral face. Multiplicities of each type can be deduced from the second and last columns.

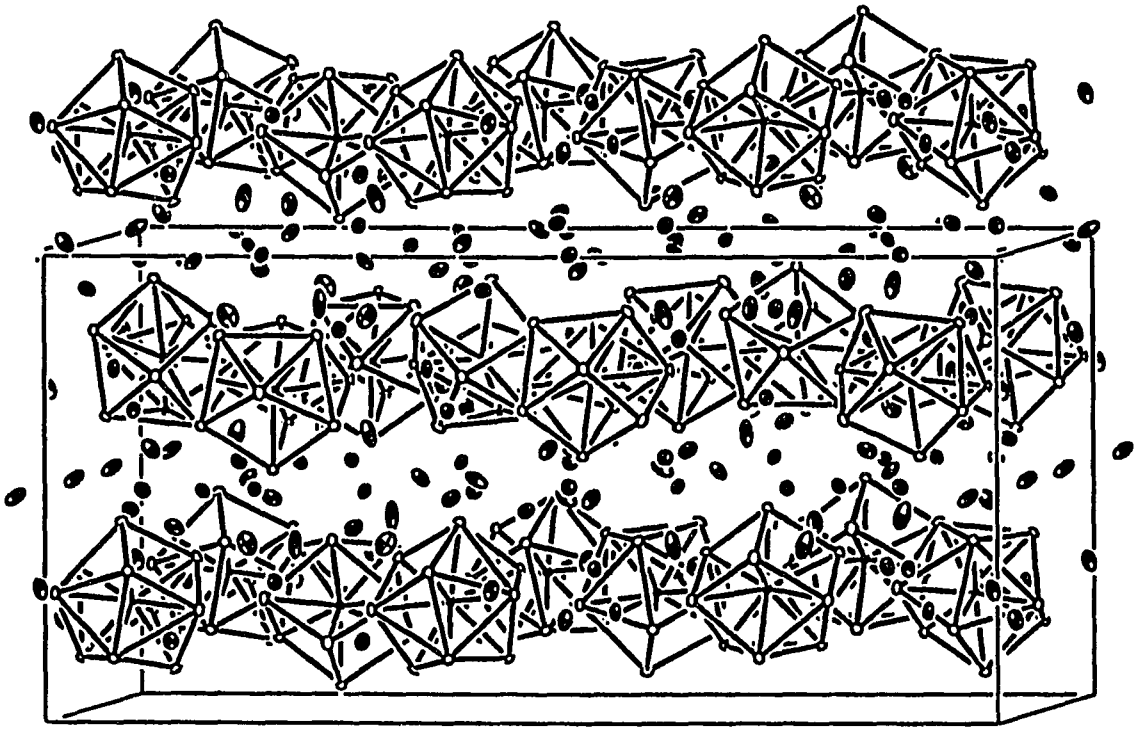

Figure 1. A general view of the unit cell of $K_{10}In_{10}Ni$ approximately along the 18.8 Å *c* axis. The well-separated Ni-centered clusters of 10 indium atoms (open ellipsoids) form close-packed layers stacked in hexagonal sequence along the *a* axis (vertical). The potassium cations (dark ellipsoids) separate both the layers and the clusters within each layer. Mirror planes lie at b = 1/4, 3/4. (20% probability ellipsoids).

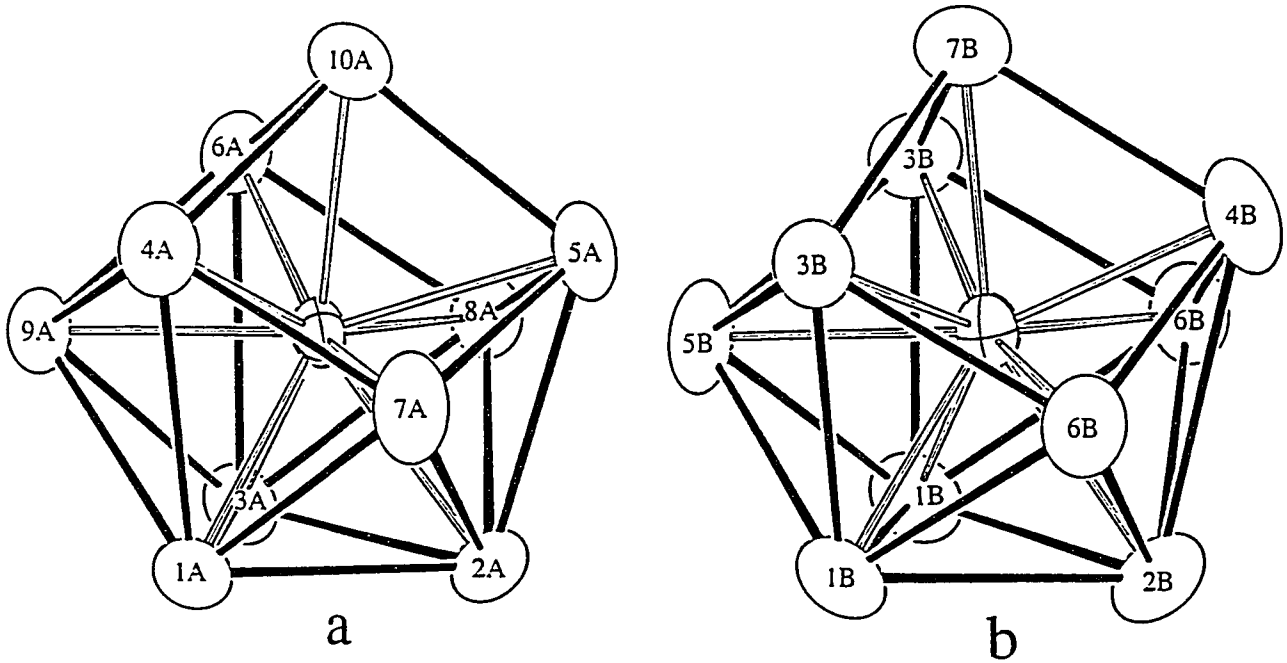

Figure 2. The independent Ni-centered clusters in $K_{10}In_{10}Ni$. a) type A, with no symmetry and b) type B with C_s symmetry; In2B, 4B, 7B, 5B and Ni(B) lie on a mirror plane. (94% ellipsoids)

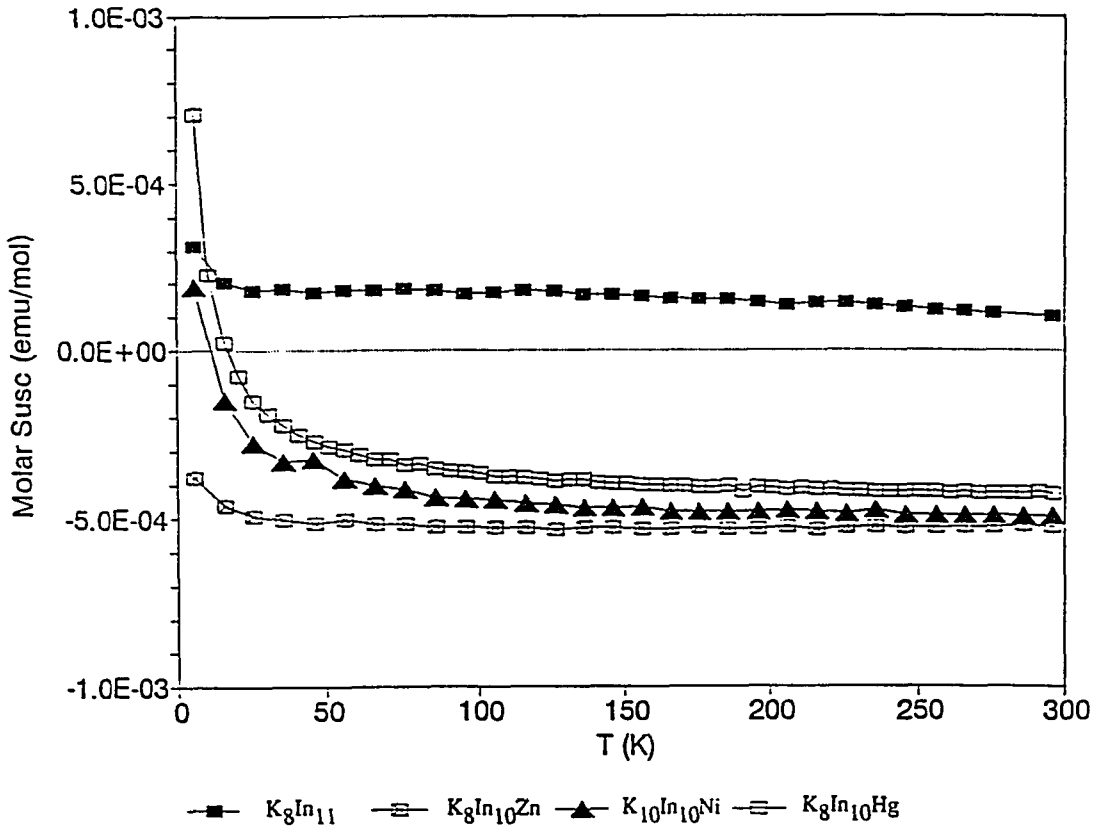

Figure 3. A plot of the molar magnetic susceptibilities of $K_{10}In_{10}Ni$ (filled triangles). Added for comparison are the susceptibilities of the diamagnetic $K_8In_{10}Hg$ (open squares) and $K_8In_{10}Zn$ (crossed squares) and of the Pauli-paramagnetic K_8In_{11} (filled squares). All have received similar core and cluster skeletal orbital corrections.

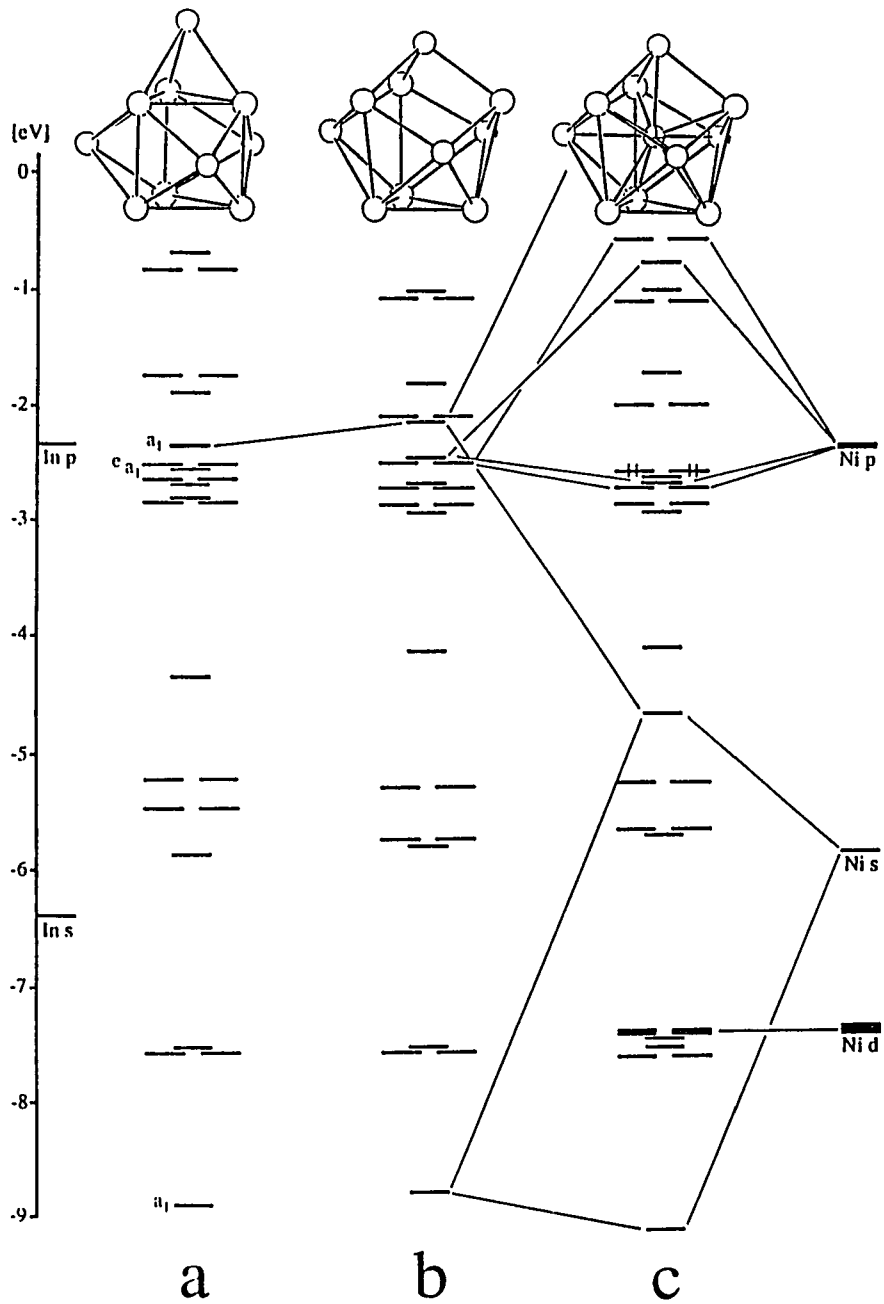

Figure 4. Charge-consistent EHMO results for $K_{10}In_{10}Ni$. a) the undistorted tetracapped trigonal prism; b) In_{11} distorted to the observed polyhedron; c) as in $In_{10}Ni^{10-}$.

SUPPLEMENTARY MATERIAL

Data collection and refinement parameters for $K_{10}In_{10}Ni$

Formula weight	1597.88
Crystal size, mm	0.15 × 0.15 × 0.20
Lattice parameters:[a]	
a, Å	15.948 (6)
b, Å	32.565 (6)
c, Å	18.822 (3)
V, Å^3	9775 (7)
Space group, Z	*Pnma* (#62), 12
d(calc.), g cm^{-3}	3.26
μ(Mo Kα), cm^{-1}	86.74
Transmission range	0.8126–1.0000
Diffractometer	CAD4
Radiation	Mo Kα (λ = 0.71069 Å) graphite-monochromated
Temperature, °C	23
Octants measured	*h*,±*k*, *l*
Scan method	ω–θ
$2\theta_{max}$	50°
Number of reflections:	
measured	18435
observed ($I \geq 3\sigma_I$)	9369
unique	4634
Number of variables	299
R_{ave} (all data), %	7.5
R; R_w,[b] %	2.9; 3.3
Goodness of fit indicator	1.00
Maximum shift/σ in final cycle	0.00
Largest peaks in final ΔF map	+1.4 e/Å^3 (1.07 Å from In5B) -1.1 e/Å^3
Secondary ext. coeff.	5(4) × 10^{-10}

[a] Room temperature Guinier data with Si as an internal standard (λ = 1.540562 Å).

[b] $R = \Sigma||F_o| - |F_c||/\Sigma|F_o|$; $R_w = [\Sigma w(|F_o| - |F_c|)^2/\Sigma w(F_o)^2]^{1/2}$; $w = \sigma_F^{-2}$.

Table II. Positional and isotropic equivalent displacement parameters for $K_{10}In_{10}Ni$

atom	N	x	y	z	B_{eq}
In1A	8d	0.86108(5)	0.42568(3)	0.97816(4)	2.10(4)
In2A	8d	0.86800(5)	0.47382(3)	0.12366(4)	2.09(4)
In3A	8d	0.72377(6)	0.49090(2)	0.01286(4)	1.95(4)
In4A	8d	0.75840(6)	0.34003(3)	0.02532(5)	2.51(4)
In5A	8d	0.77419(6)	0.41061(3)	0.22941(4)	2.39(4)
In6A	8d	0.57592(5)	0.42701(3)	0.07930(4)	2.19(4)
In7A	8d	0.89031(6)	0.37476(3)	0.11891(5)	2.72(4)
In8A	8d	0.68012(6)	0.48130(2)	0.16923(4)	1.95(4)
In9A	8d	0.67343(6)	0.40758(3)	0.94983(4)	2.09(4)
In10A	8d	0.65800(6)	0.35556(3)	0.15533(5)	2.76(4)
NiA	8d	0.7435(1)	0.41655(4)	0.08630(7)	1.41(6)
In1B	8d	0.83931(6)	0.69912(3)	0.14500(5)	2.42(4)
In2B	4c	0.85918(8)	3/4	0.00102(7)	2.53(6)
In3B	8d	0.64460(6)	0.68043(3)	0.14817(5)	2.40(4)
In4B	4c	0.6428(1)	3/4	0.95246(7)	2.90(6)
In5B	4c	0.7227(1)	3/4	0.23509(6)	2.74(6)
In6B	8d	0.73572(6)	0.67839(3)	0.00927(5)	2.45(4)
In7B	4c	0.54575(8)	3/4	0.09487(7)	2.31(6)
NiB	4c	0.7149(1)	3/4	0.0860(1)	1.52(9)
K1	8d	0.6641(2)	0.58567(9)	0.9194(2)	3.5(1)
K2	4c	0.6932(3)	1/4	0.9160(2)	3.8(2)
K3	8d	0.5064(2)	0.3346(1)	0.0065(2)	3.5(1)
K4	8d	0.9247(2)	0.5426(1)	0.9682(2)	4.5(2)
K5	8d	0.8150(2)	0.3503(1)	0.8304(2)	4.3(2)
K6	8d	0.5711(2)	0.3437(1)	0.8066(2)	4.9(2)
K7	8d	0.5207(2)	0.4237(1)	0.2579(2)	3.9(2)
K8	8d	0.0095(2)	0.3398(1)	0.9707(2)	4.9(2)
K9	4c	0.5168(3)	3/4	0.2918(3)	4.2(2)
K10	8d	0.7675(2)	0.58609(9)	0.1271(2)	3.9(2)
K11	8d	0.7030(3)	0.4863(1)	0.8175(2)	4.9(2)
K12	8d	0.5241(2)	0.5393(1)	0.0796(2)	5.8(2)
K13	8d	0.5413(3)	0.5416(1)	0.3130(2)	5.6(2)
K14	8d	0.8618(3)	0.6775(1)	0.8447(2)	7.2(3)
K15	4c	0.8938(4)	1/4	0.0795(3)	7.2(4)
K16	4c	0.6265(5)	1/4	0.1217(4)	8.6(4)
K17	8d	0.6056(4)	0.6809(1)	0.7931(2)	8.4(3)

Table III. Anisotropic displacement parameters for $K_{10}In_{10}Ni$

atom	U_{11}	U_{22}	U_{33}	U_{12}	U_{13}	U_{23}
In1A	0.0250(5)	0.0291(5)	0.0258(4)	-0.0022(4)	0.0075(4)	-0.0021(4)
In2A	0.0244(5)	0.0274(5)	0.0278(5)	-0.0073(4)	-0.0029(4)	-0.0018(4)
In3A	0.0345(5)	0.0182(4)	0.0216(4)	0.0018(4)	-0.0001(4)	0.0042(4)
In4A	0.0441(6)	0.0197(4)	0.0315(5)	0.0020(4)	0.0004(5)	-0.0065(4)
In5A	0.0426(6)	0.0312(5)	0.0172(4)	0.0037(5)	-0.0065(4)	0.0004(4)
In6A	0.0239(5)	0.0336(5)	0.0258(5)	-0.0003(4)	-0.0023(4)	-0.0048(4)
In7A	0.0337(5)	0.0402(5)	0.0295(5)	0.0145(5)	-0.0090(4)	-0.0048(4)
In8A	0.0291(5)	0.0227(4)	0.0224(4)	0.0021(4)	0.0001(4)	-0.0047(4)
In9A	0.0296(5)	0.0300(5)	0.0197(4)	-0.0012(4)	-0.0039(4)	-0.0027(4)
In10A	0.0490(7)	0.0271(5)	0.0288(5)	-0.0116(5)	0.0055(5)	0.0032(4)
NiA	0.0230(9)	0.0165(7)	0.0139(7)	0.0000(6)	-0.0011(6)	-0.0006(6)
In1B	0.0287(5)	0.0284(5)	0.0349(5)	0.0057(4)	-0.0080(4)	0.0010(4)
In2B	0.0326(7)	0.0257(7)	0.0377(8)	0.0	0.0136(6)	0.0
In3B	0.0306(5)	0.0283(5)	0.0322(5)	-0.0008(4)	0.0012(4)	0.0096(4)
In4B	0.053(1)	0.0335(8)	0.0235(7)	0.0	-0.0124(7)	0.0
In5B	0.053(1)	0.0348(7)	0.0166(6)	0.0	0.0040(6)	0.0
In6B	0.0423(6)	0.0218(4)	0.0289(5)	-0.0011(4)	0.0008(4)	-0.0063(4)
In7B	0.0258(7)	0.0237(7)	0.0382(8)	0.0	-0.0004(6)	0.0
NiB	0.023(1)	0.018(1)	0.017(1)	0.0	-0.001(1)	0.0
K1	0.058(2)	0.039(2)	0.035(2)	0.003(2)	-0.001(2)	0.002(1)
K2	0.056(3)	0.042(3)	0.047(3)	0.0	0.007(2)	0.0
K3	0.046(2)	0.038(2)	0.048(2)	-0.012(2)	0.000(2)	-0.012(1)
K4	0.047(2)	0.062(2)	0.062(2)	-0.011(2)	0.011(2)	0.004(2)
K5	0.069(2)	0.053(2)	0.041(2)	-0.007(2)	0.011(2)	-0.018(2)
K6	0.058(2)	0.078(3)	0.048(2)	-0.021(2)	0.008(2)	-0.014(2)
K7	0.057(2)	0.054(2)	0.039(2)	-0.006(2)	0.024(2)	-0.002(2)
K8	0.066(2)	0.065(2)	0.057(2)	0.034(2)	0.015(2)	-0.002(2)
K9	0.047(3)	0.039(3)	0.073(3)	0.0	0.017(3)	0.0
K10	0.073(2)	0.024(2)	0.050(2)	0.002(2)	-0.002(2)	-0.000(1)
K11	0.103(3)	0.050(2)	0.032(2)	-0.017(2)	0.014(2)	0.008(2)
K12	0.067(3)	0.102(3)	0.051(2)	0.046(2)	0.004(2)	0.022(2)
K13	0.086(3)	0.076(3)	0.052(2)	-0.031(2)	0.000(2)	-0.004(2)
K14	0.134(4)	0.099(3)	0.039(2)	-0.028(3)	0.016(3)	-0.023(2)
K15	0.121(6)	0.047(3)	0.106(5)	0.0	-0.041(4)	0.0
K16	0.200(8)	0.030(3)	0.097(5)	0.0	0.033(5)	0.0
K17	0.189(6)	0.061(3)	0.069(3)	0.039(3)	-0.028(3)	-0.023(2)

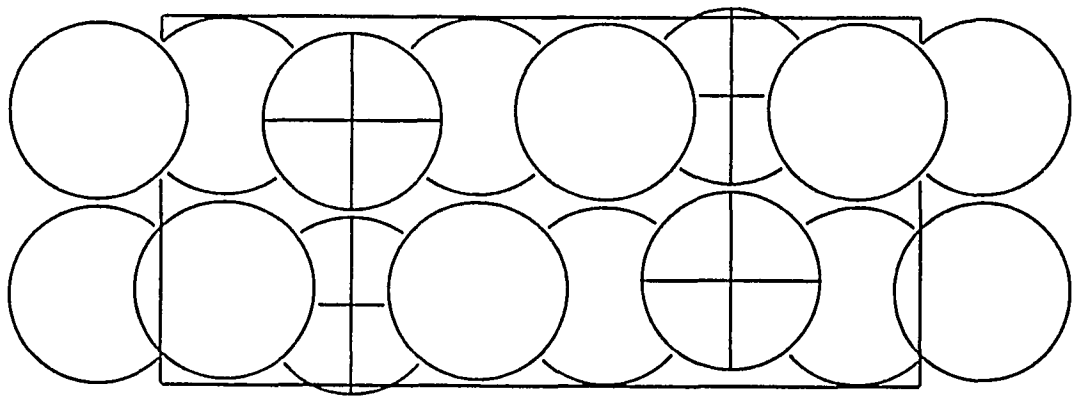

a

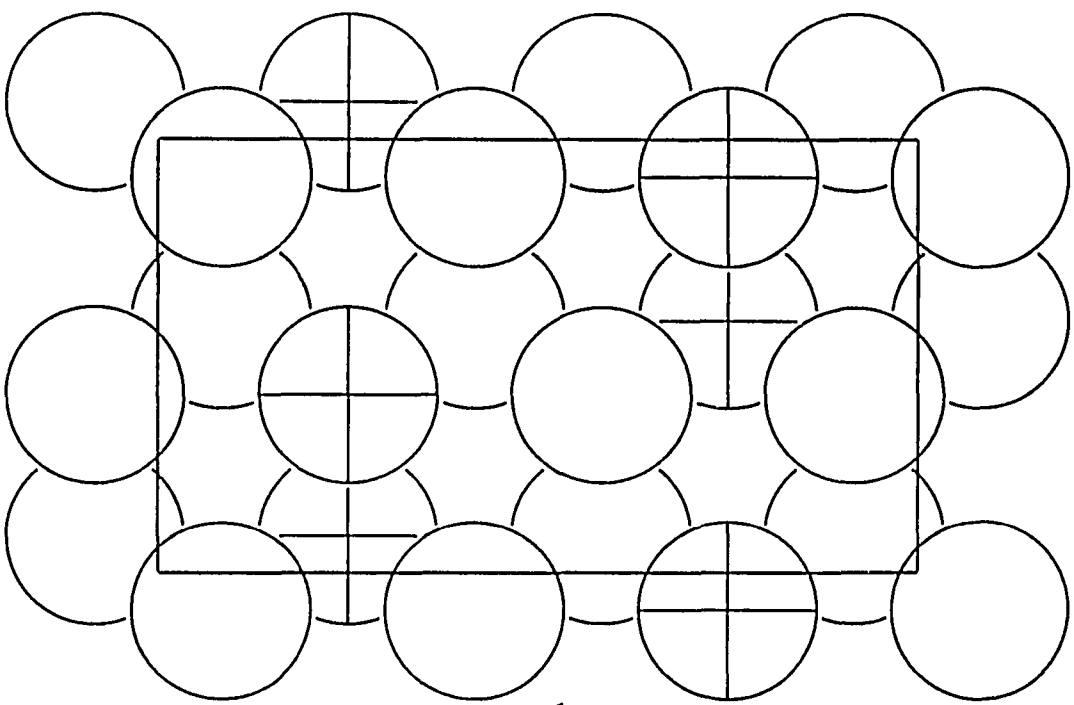

b

Two projections of the structure of $K_{10}In_{10}Ni$ with the clusters represented as open (A-type clusters) and crossed (B-type clusters) circles: a) along the *c* axis and b) along the *a* axis.

PART II. NETWORKS OF INDIUM CLUSTERS

PAPER 5. SYNTHESIS, CHARACTERIZATION AND BONDING OF INDIUM CLUSTERS: $Na_7In_{11.8}$, A NOVEL NETWORK STRUCTURE CONTAINING *CLOSO*-In_{16} AND *NIDO*-In_{11} CLUSTERS

Slavi C. Sevov and John D. Corbett*

ABSTRACT

Reactions of the elements in proportions near 37.3 at.% Na at ~500°, 410° and then at 250°C readily produce the well-crystallized title phase. The tetragonal structure at the indium-rich limit was solved by standard single-crystal X-ray means at room temperature ($P4_2/nmc$, Z = 12; a = 16.093 (4) Å, c = 23.384 (8) Å; $R(F)/R_w$ = 3.4/3.6%). The network structure consists of interbonded clusters — the first example of *closo*-In_{16} icosioctahedra ($\bar{4}m2$ symmetry) that are 8-exo-bonded, 10-bonded nido-icosahedra (fractional occupancy of the eleventh cluster site generates ~36% 1,3-arachno units), and four-bonded indium atoms in pairs of triangles (In_{16} : $In_{11(10)}$:In_1 = 1 : 4 : 12). Extended Hückel calculations that include significant interactions between directional nonbonding pairs on atoms in neighboring In_{16} and In_{11} units indicate $2n$ + 4 skeletal electrons are necessary for each, with no nonbonding pairs on the latter, and a closed shell for 504 electrons per cell vs 507 for the refined stoichiometry. Observed properties are in good agreement; at the indium-rich limit, the phase is a poor metal (ρ_{295} ~ 540 μohm-cm) with a Pauli-like paramagnetism χ_M = (1.7 — 1.8) x 10^{-4} emu mol^{-1} after correction for core and orbital diamagnetism. The intercluster interactions appear to be closely correlated with a small region of nonstoichiometry and changes in the c lattice parameter. Some general factors in a diverse indium cluster chemistry are noted.

INTRODUCTION

Reduced compounds of the boron family elements have long been famous for their important and novel examples of structures and bonding. Probably the most remarkable in both historic importance and diversity of chemistry are the boron hydrides, broadly defined. Here we need to recall mainly the family of simple borane (2-) ions. These are typified by the geometrically closo-$B_nH_n^{2-}$ species which require $2n + 2$ skeletal electrons according to Wade's Rules as well as nido- and arachno-species which are missing one or two vertices and possess $2n + 4$ or $2n + 6$ cluster-based electrons, respectively.[1,2] The same rules have also been generalized for the "naked" Zintl ion clusters of main group elements (Bi_8^{2+}, Sn_5^{2-}, Sn_9^{4-}, etc.) in which "inert s pairs" replace those in the exo B—H bonds in the boranes.[3,4] The lower $2n + 2$ limit appears to have been a general "floor" for the electron count in such isolated clusters.

An interesting contrast is the sparcity of aluminum analogues.[5,6] On the other hand, gallium as a post-transition element forms many binary and ternary compounds that contain gallium clusters, fused clusters, and cluster fragments.[7-10] However, virtually no isolated clusters of gallium have been found, perhaps because the charges on such units would be too high (e.g., Ga_8^{10-} and Ga_{12}^{14-} for closo analogues of $B_8H_8^{2-}$ and $B_{12}H_{12}^{2-}$, respectively). Instead, intercluster bonding is common as this formally converts the s-orbital to a bonding role and reduces the cluster charge by one for each exo bond. The results are three-dimensional network structures. Unfortunately, apparent fractional occupancy of both gallium and cation positions as well as disorder complicate the understanding and interpretation of the bonding requirements of many of the gallide structures. However, some clear-cut and successful assignments have been achieved,[7,11-13] although confirmatory property measurements have generally not been obtained.

Knowledge of the compositions and structures of even binary alkali metal—indium phases is generally poor. We have already reported[14] that the potassium system contains the metallic

phase K_8In_{11} with isolated and unprecedented hypoelectronic In_{11}^{7-} clusters and $K_{22}In_{39}$ which is essentially isostructural with $Na_{21}Ga_{39}$.[8] The latter consists of a network of heavily interbonded In_{12} and In_{15} clusters. Our present results for many binary (and some ternary) compounds formed between indium and the alkali metals (A) suggest that close structural relationships between gallium and indium (E) systems may exist only for the foregoing $A_{22}E_{39}$ as well as the layered AE_3[16-18] and AE (NaTl-type[19]) phases. Instead, a plethora of new indium units are found in relatively well-behaved structures.

The present article reports on our first results for Na—In system, the network structure of $Na_7In_{11.8}$ (37.3 at.% Na). Subsequent manuscripts will provide information about other specimens, the closely related network structure of $Na_{15}In_{28}$ (34.9% Na) and the isolated tetrahedral clusters in Na_2In (66.7%).[15] All of their compositions bear little relationship to those presently assigned in the phase diagram which is largely based on thermal analysis. Here, the compound nearest Na_7In_{12} has been approximated[20] as Na_5In_8 (38.5%) or Na_2In_3 (40.0%) based on different estimates of the melting point maximum.[21,22] Earlier evidence for a phase near Na_3In (75%) is contradictory. The system has long been known to contain the Zintl phase NaIn (50%).[19]

EXPERIMENTAL SECTION

Synthesis

All materials were handled in a N_2-filled glovebox. The surface of the indium metal (Cerac, 99.999%) was cleaned with a scalpel before use as was the sodium (Alpha, 99.9+%, sealed under Ar). In an exploratory reaction, a mixture with 38.5 at.% Na was loaded into a tantalum tube welded at one end. (Loss of some Na on transfer is the most probable error.) The other end of the tube was then weld-sealed in a He atmosphere, the tube was placed in a fused silica ampule, and this sealed under high vacuum after baking.

The components were fused at 490°C, and the mixture was then annealed at 410°C for 3 days and at 250°C for 5 days. (The liquidus is at ca. 440°C for this composition.[20]) The resulting ingot was metallic in appearance and very brittle. Its powder pattern was obtained from finely ground sample mounted between pieces of cellophane tape. An Enraf-Nonius Guinier camera, Cu Kα radiation (λ = 1.540562 Å), and NBS (NIST) silicon as an internal standard were employed for this purpose.

Structure determination

Few plate-like pieces were picked from the crushed sample, sealed in thin-walled glass capillaries, and checked by means of oscillation, Weissenberg and precession photographs for singularity and, eventually, a space group assignment. The photographs showed a tetragonal cell with systematic absences consistent with only one possible space group — $P4_2/nmc$ (no. 137). A crystallite ca. 0.1 x 0.1 x 0.05 mm was chosen, and X-ray data were collected (2 octants, $2\theta \leq 50°$) at room temperature with the aid of a Rigaku AFC6R single-crystal diffractometer together with monochromated Mo Kα radiation. A few details of the data collection and refinement are listed in Table I.

The 25 reflections found from a random search by the diffractometer were indexed with a tetragonal cell with the expected dimensions. The diffraction data confirmed the chosen space group after their correction for Lorentz and polarization effects and for absorption with the aid of the average of ψ-scans of three reflections at different θ values.

Application of direct methods[23] gave twelve positions that were (correctly) assigned to indium in the starting model. A few cycles of least-squares refinement (TEXSAN[24]) and a difference Fourier synthesis revealed eleven atom positions with distances to the indium atoms that were appropriate for sodium, and these were so assigned. Refinement with isotropic thermal parameters proceeded smoothly (R = 8.5%), but this produced an unreasonably large thermal parameter for In11. However, the electron density at this position was too high to replace it by a sodium atom and, moreover, the distances from this position to the neighboring indium atoms were undoubtedly of the order of In–In distances. Consequently this position was refined as indium with partial occupancy, 63.6 (8)% in the final analysis. The multiplicity of the other In atoms did not deviate from unity by more than 3% (3σ) when the Na atoms were kept fixed, and for Na, by 4–6% (≤ 2σ) when the In atoms were fixed. Therefore, these multiplicities were not varied from unity in the final refinement.

The final residuals listed were obtained after anisotropic refinement of all atoms as well as variation of the multiplicity of In11. The refined composition is $Na_7In_{11.757(5)}$ (37.32(1) at.% Na). The largest residual peaks in the final difference Fourier map were 2.6 e/Å^3 (1.68 Å from In10) and -1.5 e/Å^3.

A powder X-ray diffraction pattern calculated for the compound based on the refined positional parameters allowed indexing of 40 lines in the observed powder pattern. The 2θ values of these and the standard Si lines afforded the lattice constants listed for $Na_7In_{11.76}$ by a least-squares refinement. The powder pattern also contained weak lines from indium metal as a

second phase, probably from adventitious oxidation or hydrolysis of the sample during the X-ray exposure.

Nonstoichiometry

Two reactions containing 36.8 and 41 at.% Na were subsequently carried out under the conditions described above. Both of them showed Na_7In_{12} as a major phase, but the first also contained the indium-richer $Na_{15}In_{28}$,[15] and the second had some of the sodium-richer NaIn[19] as a second phase. The lattice parameters of the Na_7In_{12-x} component in these two products should represent the limits of any range of stoichiometry. The phase on the indium-rich side had lattice parameters of a = 16.096 (2), c = 23.385 (4) Å, virtually identical to those of the sample from which the structure was refined. On the other hand, the lattice at the sodium-rich side had a = 16.107 (2) Å, c = 23.286 (4) Å, a significant contraction of the c-axis (0.4%, 11—18σ) while the a-axis remained about the same (0.07%, 4.2σ difference).

Electrical resistivity

Since the compound is quite air and moisture sensitive, the routine four-probe method for measuring resistivity was not applicable. We used instead an electrodeless "Q" method.[25] For this purpose, the sample was ground, a fraction with an average particle diameter of 340 μm was separated, and this was mixed with an equal volume of powdered (chromatography) alumina in order to reduce contact between the sample particles. The mixture was loaded into a glass ampule and sealed under 480 torr of Ar. The Q measurements were made at 35 MHz over the temperature range of 130 − 295 K. A plastic bag with holes for all parts and a nest outside the coil for the thermocouple was used to avoid interference both from the thermocouple and from moisture condensation on the ampule while cooling with off-gas from liquid N_2. Readings were taken every 10 degrees after waiting sufficient time to reach temperature equilibrium.

Magnetic susceptibility

The container was constructed of fused silica tubing (3 mm i.d.) in which a closely fitting silica rod had been sealed in one half. A 25 mg sample was then loaded into the open end in the glovebox, and another such rod was inserted from the other end of the tube. The assembly was evacuated, backfilled with He, and sealed at the second end. The sample was thus fixed between the rods. This type of holder gives a very uniform background and much more reproducible results than the usual container in which the sample sits on a fused septum. The magnetization was measured at field of 3 Tesla over the range 6 — 295 K on a Quantum Design MPMS SQUID magnetometer. The raw data were corrected for the susceptibility of the container.

RESULTS AND DISCUSSION

Structure description

The final positional and isotropic-equivalent displacement parameters and the important distances for the refined composition $Na_7In_{11.76}$ are listed in Tables II and III, respectively. The general view of the unit cell in Figure 1 outlines all In–In separations that are less than 3.5 Å. The structure can be described as a three-dimensional indium network composed of three different building blocks: *closo*-16-vertex deltahedra (Figure 2a), the 11-membered nido derivative of an icosahedra (Figure 2b), and pairs of triangles (Figure 2c). These units are 8-, 10-, and 10-bonded, respectively, to other members via exo In–In bonds that are generally somewhat shorter than those within the polyhedra.

The 16-vertex cluster (In9, 10, 12) has D_{2d} ($\bar{4}m2$) point group symmetry but is in fact very close to T_d symmetry. This polyhedron can be derived from a 12-membered truncated tetrahedron formed by In9 and In10 on which all hexagonal faces are also capped by In12. The total number of triangular faces is 28, and so it can be called an icosioctahedron (or twenty-eight-hedron). All In9 atoms therein are exo bonded to In6 in eight different icosahedra (Figure 2a and Figure 3) leaving eight atoms (In10,12) that are members only of this polyhedron. The somewhat larger and nonuniform ellipsoids for the latter group may suggest some torsional motion (or distortion) although In12 is distinctive in that it also has longer bonds to six other indium atoms. The cluster is centered by a Na2 ion.

The nido-icosahedra (In1, 2, 3, 6, 7, 8, 11) have only *m* symmetry and are grouped in fours about the other point of $\bar{4}m2$ symmetry (site *2b*). All but In11 have exo bonds (Figure 2b); In1 and In3 are bonded to the same atoms in three other icosahedra, each In6 is bonded to a 16-vertex polyhedron, and In2, 7, 8 are bonded to different In_3 triangles. The only atom without an exo bond (In11) is the one that refines as a partially occupied site (63.6%). The cluster is

distorted somewhat such that In11 (when present) projects somewhat from the polyhedron. Its closest exo-neighbor is In12 in In_{16} at 3.87 Å, too long to afford a strong bonding interaction between these two atoms but probably the source of some electronic effects and nonstoichiometry (below).

The third building block (Figure 2c) consists of pairs of triangles, each made up of two In4 atoms and one In5. These can all be considered as four-bonded, isolated In atoms. The group is bonded to eight different nido icosahedra, the dashed lines in Figure 2c between pairs of exo In8 atoms representing edges of two different icosahedra, Figure 2b.

Figure 3 shows a condensed version of the connectivity between these building blocks in two different views. Large and medium circles represent the centers of the In_{16} and In_{11} clusters, respectively, while the small crossed circles denote the positions of each of the In_3 triangles. The structure can be viewed (Figure 3a) as composed of macrolayers lying normal to the c axis. Each layer consists of squares of 16-vertex clusters, each of which is centered by a tetrahedron composed of four interconnected nido-icosahedra (heavier outline), or vice versa (Figure 3b). The bonding within the layers is mainly through direct $(In_{11})_{4/4} - (In_{16})_{4/4}$ intercluster bonds as well as through $(In_{11})_4 - (In_3)_2$ interactions. The different layers are held together only by the pairs of In_3 triangles or, in other words, via isolated indium atoms.

All sodium atoms except Na2, 3, 4 cap triangular faces of the polyhedra. The same type of positioning for the alkali metal is seen in K_8In_{11}.[14] The Na2 cation is in the center of the icosioctahedron, and Na3 and Na4 center the tetrahedral holes formed by four icosahedra or three icosahedra and one triangle, respectively. The In—In distances within and between the clusters are typical for In clusters (2.84 − 3.06 Å) except for (a) some longer distances associated with distortion of the In_{11}, In_{10} units (3.16 − 3.19 Å) and (b) greater values about In12 (3.30 − 3.47 Å), which has six rather than five bonding neighbors within its cluster.

Properties

Resistivities of $Na_7In_{11.76}$ calculated from the Q-measurements are nicely linear with temperature over 130 – 295 K and indicate a metallic behavior, ρ_{295} ~ 540 μohm-cm with a coefficient of +0.26% per degree. Such a resistivity is characteristic of what would be termed a "poor metal". The value is logically greater than the maximum resistivity observed in liquid Na–In mixtures, ρ_{748} ~ 180 μohm-cm at ~60 at.% Na.[26] (The last is close to the composition of Na_2In which contains discrete tetrahedral clusters in the solid state.[15]) It should be noted that absolute resistivities determined by the "Q" method are probably accurate by no more than a factor of three, but the temperature coefficient should be quite reliable.

Magnetic measurements on $Na_7In_{11.76}$ gave temperature-independent susceptibilities of $-(5.4 - 5.5) \times 10^{-4}$ emu/mol over the range of 12 – 295 K. Two types of diamagnetic corrections may be subtracted from this number. The first, for the ion cores of Na^+ and In^{3+}, totals -2.6×10^{-4} emu/mol.[27] The second, a diamagnetic correction for the Larmor precession of the electron pairs in the orbitals of each cluster, can be estimated from $\chi_L = -0.79Z_i \times 10^{-6} (r_{ave}/a_0)^2$ emu/mol-cluster[28] where Z_i is the number of skeletal electrons in the cluster, r_{ave} is the average radius of the orbitals (Å), and a_0 = 0.529 Å. For r_{ave}, we appropriately averaged the distances from the center of each cluster to the middle of the different types of In–In edges on its surface. This gave 2.4 Å and 3.1 Å for the nido-icosahedra and the icosioctahedra, and thence $\chi_L = -4.2$ and -9.8 ($\times 10^{-4}$ emu/mol-cluster), respectively. Based on the proportions of each cluster per formula unit, the total Larmor correction per mol of Na_7In_{12} becomes $\chi_L = -(0.67 \cdot 4.23 + 0.17 \cdot 9.8) \times 10^{-4} = -4.5 \times 10^{-4}$ emu/mol. Combination of this, the ion core value, and the measured susceptibility provides $\chi_M = +(1.7 - 1.8) \times 10^{-4}$ emu/mol. This is indicative of a very small Pauli-type paramagnetism, consistent with the conductivity measured and the electron count based on theory (below). The diamagnetic corrections must be viewed as

approximate; valence electrons in lone pairs and bonds between clusters and to the isolated indium atoms have not been included and will certainly increase the end result. A similar procedure has given a similar susceptibility value for K_8In_{11}, which is stoichiometric and also a poor metal.[14]

Structural features

The most interesting aspect of this structure is the first example of the 16-vertex deltahedron. The geometry of such a cluster has been discussed before[29] in connection with the possible existence of higher order boranes. Since four six-bonded and possibly energetically less favored boron atoms would be necessary in *closo*-$B_{16}H_{16}^{2-}$, these authors proposed transition-metal-substituted analogues instead such as $(CpCo)_4B_{12}H_{12}$ or $[(OC)_3Fe]_4B_{12}H_{12}$. However, calculations suggested that a pure 16-atom boron cluster might still exist, there seeming to be a net advantage in maximizing the number of near-neighbor bonds in spite of their decreasing strengths.[30]

Here we should mention that the icosioctahedron qualifies as a closed polyhedron according to the criteria for it.[31] As far as we have been able to find in the literature, the largest closed clusters formed by any element in the boron group are the 15-vertex, 26-face polyhedra (icosihexahedra) observed in BeB_3[32] and in SiB_6.[33] It is interesting to note the similarity in the genesis of the 15- and the 16-vertex clusters. The former can be viewed as a tricapped truncated trigonal prism (3:3(3)3:3) while the icosioctahedron is, as noted above, a tetracapped truncated tetrahedron. The clusters in BeB_3 are Be_3B_{12} units where beryllium takes the three capping positions. The cluster in SiB_6 is actually $Si_{3+x}B_{12-x}$ in which three silicon atoms are capping, but some silicon is also mixed with boron on four other positions, and there are two other partially occupied silicon sites as well. Interconnected clusters are present in both phases.

Highly condensed polyhedra with the same geometry as the In_{16} cluster are found in some MM'_2 intermetallic compounds such as $MgCu_2$ and $MgZn_2$.[34-36] In these compounds (known also as "Laves phases"), the M′ atoms generate truncated tetrahedra that share all hexagonal faces, while M atoms center these and also cap the four hexagonal faces of the tetrahedra, viz., $M'_{12/6}M_{5/5}$. These condensed units are also called Friauf polyhedra and can alternatively be viewed, perhaps more simply, in terms of vertex-linked tetrahedra.

Surprisingly, individual 16-atom metal clusters with the same $\bar{4}m2$ symmetry were also recently discovered in $Y_{16}Ru_4I_{20}$.[37] Here the 16-atom yttrium polyhedra are both centered by a tetrahedron of Ru atoms and sheathed by iodine. Besides the centering, there is subtle geometric difference as well; the cluster in $Y_{16}Ru_4I_{20}$ can be considered to be the result of a tetrahedral condensation of four Ru-centered octahedra Y_6Ru about edges rather than as an approximately spherical deltahedron. This viewpoint follows from the fact that the yttrium atoms that cap the hexagonal faces of the truncated tetrahedron lie almost in the planes of those hexagons and thus represent smaller distortions of the starting octahedra. This condition doubtlessly relates to the presence of strong Y—Ru central forces.

Discussion in some detail of one more feature of the structure is necessary, namely the partially occupied site of In11. The icosahedra bearing In11 (Figure 2b) are nido-species, but the 63.6 (8)% occupancy of this site means that 36% of them are actually 1,3-arachno clusters. This distribution represents the upper limit for the former judging from lattice constant variations with composition (Experimental Section). The lack of an In atom on this position doesn't affect the connectivity of the overall network since this is the only site in this cluster without an exo bond. Loss of an atom from this position reduces the total bonding as well as some intercluster repulsions, and less than 50% occupancy of the In11 site will decrease the number of available electrons below that evidently needed for the indium network bonding (below). Of course, frac-

tional occupancy of some other indium sites may instead pertain at the sodium-rich limit although this does not seem indicated or necessary.

Electronic structure

Extended-Hückel MO calculation have been performed on the separate (8-bonded) *closo*-In_{16}, the (10-bonded) *nido*-In_{11} units and the (10-bonded) arachno-In_{10} clusters as well as on the observed arrangement of four *nido*- (arachno-)In_{11} units about one In_{16} cluster, all with the observed configurations.[38] Exo bonds in cluster network are important in the bonding descriptions; therefore, dummy atoms about each species with only 5s-type orbitals were used at the positions of all exo bonded atoms to "saturate" the exo bonding. These 5s orbitals were given Slater-type orbital exponents and energies equal to those for In 5p, although the latter quantity can in fact be that of In 5s without affecting the results significantly. Such a setup for cluster bridging is intended to make the results as close as possible to reality. Calculations on the bonding in the pairs of indium triangles (Figure 2c) showed that these each have the same electronic requirements (a'^2,e'^4) as would the component four-bonded atoms, and they were so treated thereafter. (Although 3-D band calculations would provide the ultimate results, these would be almost impossible to visualize for a calculation with 144 atoms.) The energy results for the calculations are shown in Figures 4 and 5.

In_{16}. As noted earlier by Brown and Lipscomb,[29] closed polyhedra with 16, 19, 22 atoms do not obey the $n + 1$ skeletal bonding orbital (Wade's) rule. These deviations were later generalized as "intrinsic" by Fowler.[39] Indeed, our calculations on the isolated unit show that there are 18 instead of 17 such orbitals below a 2.5 eV gap. The 36 skeletal electrons needed to fill these orbitals then put the cluster in the so-called hyperelectronic class. The earlier studies of this polyhedron only noted that an instability would be expected with $2(n + 1)$ electrons and that either $2n$ or $2n + 4$ was probable, although the one expectation of $2n$ (with boron)[29] would

be quite improbable for the indium example, as the gap at that point is very small (Figure 4). Eight of the nine top bonding orbitals for this cluster shown in Figure 4 are located mainly on indium atoms that lack exobonds (In10, 12) (the eighth orbital down is excluded). In other words, substantial p-mixing is present and these filled orbitals represent combinations of outward pointing electron pairs, in contrast to dominantly s-like pairs found on atoms in the isolated cluster In_{11}^{7-} and others. Burdett and Canadell[13] showed that the highest bonding orbitals in interconnected gallium clusters are usually isolated lone pairs on atoms without exo bonds. As the nuclearity and hence the radius of the curvature of the cluster increase, they predicted that the energy of such a lone pair could become so high that it is left empty, as for that in the imaginary $B_{15}H_{14}^{3-}$ icosihexahedron. This could also lead to fractional occupancy or even expulsion of that atom. Although the present In_{16} icosioctahedron is of higher nuclearity, all lone pairs are of a bonding type. This apparent contradiction can be explained by the fact that the one lone pair in $B_{15}H_{14}^{3-}$ is surrounded by exo-bonds with which it is antibonding. On the other hand, in In_{16} we have groups of four neighboring lone pairs on the top and bottom of the cluster and, although each set as a whole is antibonding with respect to the neighboring exo bonds, the lone pairs within each set are π-bonding with respect to each other. Thus, removal of one or more atoms in these sets should reduce the bonding interactions for the remaining lone pairs and raise their energies, and calculations carried out on such defect indium clusters proved this to be the case. This effect could be the reason why In(10, 12) sites, although similar to the In11 site in terms of bonding, are not partially occupied.

In_{11} and In_{10}. As expected, the two clusters are calculated to each have 13 skeletal bonding orbitals ($n + 2$, $n + 3$, respectively). The HOMO for In_{11} (Figure 4) is purely a lone pair on In11 that points radially from the cluster. This orbital is very much π-anti bonding to the five neighboring exo bonds even though distortions at this point leave the In11 somewhat

protruding. Even so, the energy gap to the next bonding orbital is nearly 0.5 eV. The HOMO calculated for the pairs of metal triangles (Figure 2c) falls at nearly the same energy, −6.9 eV.

In_{16} combined with In_{11}. Comparison of the electron counts needed and available were at this point somewhat troublesome. However, in connection with the nonstoichiometry, we noticed that the distances from In11 in each nido-iscosahedron to In12 (3.872 (6) Å) and to two In10 atoms (4.099 (5) Å) in the In_{16} cluster appeared to afford some significant repulsive interactions between these atoms relative to distances already considered as "bonding" in the individual units, 2.9 − 3.5 Å. One example of these repulsive contacts is dashed in Figure 1. Each In11 atom approximately caps a triangular face formed by the In10 and two In12 atoms in the nearest icosioctahedron, so that the former's lone pair lies almost normal to that face, while the lone pairs on In10 and In12 are directed radially outward from the In16 cluster. This arrangement suggests that interactions between these orbitals are important. Extended Hückel MO calculations were therefore performed on the collection of an In16 cluster surrounded by one, two, three, or four *nido*-In_{11} clusters[40] (the differences from four in each case were taken to be the number of noninteracting arachno-In_{10} clusters). The noteworthy result is that the lone pair orbitals on all In11 atoms are in the process pushed up in energy by ca. 1.65 eV and thus become antibonding and empty and the LUMO for the macrocluster. The highest bonding orbitals on In_{16} are correspondingly lowered by this effect. The important consequences of these intercluster interactions are shown in Figure 5 where only the altered levels are shown in the middle portion, the blocks representing intracluster levels that are basically unchanged by these effects. The HOMO–LUMO gap for the macrocluster is now approximately 1.2 eV, although this detail clearly depends on orbital parameters utilized.

Electron count

The compound is now very slightly electron-rich judging from the numbers of electrons needed and available. We count the electrons in the following way. Each unit cell contains two icosioctahedra, eight icosahedra (which round off to 5 nido- and 3 arachno-), and 24 isolated, four-bonded indium atoms. The electron requirements of each unit and the total for a closed shell system are as follows:

	skeletal	exo	lone pair	Σ, ea.	total
2 In_{16}	36	8	16	60	120
5 In_{11}	26	10	0	36	180
3 In_{10}	26	10	0	36	108
24 In_1				4	96
closed shell sum:					504
available: 141 x3 + 84 x 1					507
difference:					+3

The unit cell contains 141 indium atoms (with 5/8th occupancy of In11) that provide three valence electrons each, and the 84 sodium atoms furnish one electron each. The total is 507 available electrons per cell, three (0.6%) more than necessary for closed shells for all species. A 50% occupancy of In11 with all other atoms fixed would close the sum and give a Zintl phase. The above result is changed insignificantly (0.2e) if the refined occupancy (63.6 (8)%) is used instead of approximated as 62.5%. Of course, there are other ways to account for and to express this evident electron surplus in the solid state. It is very encouraging to note the strong support provided to the bonding model by the measured metallic conductivity and the Pauli-like magnetic susceptibility (above).

The effects of the nonstoichiometry observed on the sodium-rich, or indium-poor, side of the composition studied structurally are also completely consonant with the above picture. One way to accomplish such a composition change would be to add more sodium ions to the cell, but this would seem to be inconsistent with the significant (0.4%) contraction of *c*. The last instead appears to be clearly associated with the unique In11 and its significantly short "nonbonding" distances to In12 and In10 in the In_{16} cluster since their result is directed along *c*. Although we cannot tell the amount, additional atoms are evidently removed from the In11 site preferentially in sodium-richer systems.

The bottom line in our assessment of the structure of and bonding in $Na_7In_{11.76}$ at the indium-rich limit is that the valence electron count lies only very slightly above that necessary to give a closed shell configuration to the individual units. This in itself is quite satisfying; a structure of this complexity must have quite specific electronic requirements. The character of the excess electron distribution cannot be better defined at this time. Figure 5 represents the situation only at k = 0, although it does not seem likely that the relatively large gap at Γ will be bridged elsewhere in k-space. Whether the excess electrons lie in the conduction band implied by the Figures or in states with a substantial sodium component (as in K_8In_{11} apparently) is not known, although there are many Na—Na separations that are less than that in the b.c.c. metal (3.72 Å). In a broader sense, $Na_7In_{11.76}$ seems to be another example of a "metallic Zintl phase"[41] in which the small perturbations at E_F (sea level) that make it (weakly) metallic scarcely obscure the strong covalent bonding associated with the network and the clusters at lower energies (in the depths of the sea — see Nesper[41]). The structure itself represents the best ordered solution to a complex problem of not only filling space with cations and cluster anions, but also the requirements of cluster stability, size, and the need for some intercluster bonding.

The variety of clusters and structures found for indium as well as for gallium illustrate well the considerable number of possibilities available in these systems.

We should again re-emphasize that the exo bonding of the clusters of indium and gallium is the major route by which what would otherwise be isolated ions with a high charge, e.g., In_{16}^{20-}, achieve smaller and more reasonable values. The "inert s pair" is in effect changed into a bonding role in the process, reducing the charge by one for each such bond. This means is already known to be dominant in polygallium chemistry, and what we have seen of indium systems so far indicates a parallel yet very distinctive cluster chemistry with perhaps fewer nonstoichiometry complexities and more simple ions.

The Na–In system alone illustrates a considerable variety. In addition to $Na_7In_{11.8}$ (37.3 at.% Na), the slightly indium-richer $Na_{15}In_{28}$ (34.9%), apparently the last binary compound in this direction, exhibits very similar building blocks and structural array: 10-bonded *nido*-In_{11}, 12-bonded (not 8) *closo*-In_{16}, and similar triangles of isolated atoms. The indium-richer phases appear to be only NaIn, isostructural with "the" Zintl phase NaTl (stuffed diamond), and Na_2In which contained isolated indium tetrahedra, nominally In_4^{8-} and isoelectronic with Sb_4, etc.[15] Subtle details of crystal packing appear to be responsible for the occurrence of another isolated cluster, the hypoelectronic In_{11}^{7-} (D_{3h}), in a phase A_8In_{11} with 42.1% A only for potassium or a limited amount of rubidium. More details on this unusual indium chemistry will follow.

Acknowledgement. We are indebted to J. Shinar for the use of the Q apparatus, to J. E. Ostenson for the magnetic data, and to G. J. Miller for suggestions on some of the calculations.

Supplementary material available: Data collection and refinement details and anisotropic displacement parameters for $Na_7In_{11.76}$ (2 pages); structure factor data for the same (10 pages).

REFERENCES

1. Wade, K. Adv. Inorg. Chem. Radiochem. **1976**, 18, 1.
2. Olah, G. A.; Wade, K.; Williams, R. E., Eds. Electron Deficient Boron and Carbon Clusters, J. Wiley: New York, **1991**.
3. Corbett, J. D. Inorg. Chem. **1968**, 7, 198.
4. Corbett, J. D. Chem. Rev. **1985**, 85, 383.
5. Hiller, W.; Klinkhammer, K.-W.; Uhl, W.; Wagner, J. Angew. Chem. Int. Ed. Engl. **1991**, 30, 179.
6. Nesper, R. Angew. Chem. Int. Ed. Engl. **1991**, 30, 795.
7. Belin, C.; Ling, R. G. J. Solid State Chem. **1983**, 48, 40 and references therein.
8. Frank-Cordier, U.; Cordier, G.; Schäfer, H. Z. Naturforsch. **1982**, 37b, 119, 127.
9. Belin, C.; Charbonnel, M. J. Solid State Chem. **1986**, 64, 57.
10. Charbonnel, M.; Belin, C. J. Solid State Chem. **1987**, 67, 210.
11. Schäfer, H. J. Solid State Chem. **1985**, 57, 97.
12. Burdett, J. K.; Canadell, E. J. Am. Chem. Soc. **1990**, 112, 7207.
13. Burdett, J. K.; Canadell, E. Inorg. Chem. **1991**, 30, 1991.
14. Sevov, S. C.; Corbett, J. D. Inorg. Chem. **1991**, 30, 4875.
15. Sevov, S. C.; Corbett, J. D., unpublished research.
16. Ling, R. C.; Belin, C. Z. Anorg. Allg. Chem. **1981**, 480, 181.
17. Van Vucht, J. H. N. J. Less-Common Met. **1985**, 108, 163.
18. Tschuntonow, K. A.; Yatsenko, S. P.; Hryn, Yu. N.; Yarmolyuk, Ya. P.; Orlov, A. N. J. Less-Common Met. **1984**, 99, 15.
19. Zintl, E.; Neumayr, S. Z. Phys. Chem. **1933**. B20, 270.
20. Larose, S.; Pelton, A. D. J. Phase Equilib. **1991**, 12, 371.
21. Lamprecht, G. J.; Crowther, P. J. Inorg. Nucl. Chem. **1969**, 31, 925.

22. Thümmel, R.; Klemm, W. Z. Anorg. Allg. Chem. **1970**, 376, 44.

23. SHELXS-86, Sheldrick,G.M., Universität Göttingen, BRD, **1986**.

24. TEXSAN, Version 6.0 package, Molecular Structure Corp., The Woodlands, TX, **1990**.

25. Shinar, J.; Dehner, B.; Beaudry, B. J.; Peterson, D. T. Phys. Rev. **1988**, 37B, 2066.

26. van der Marel, C.; Braunderburg, E. P.; van der Lugt, W. J. Phys. F: Met. Phys. **1978**, 8, L273.

27. Selwood, P. W. Magnetochemistry, Interscience Publishers: New York, 2nd ed., 1956, p. 70.

28. Ashcroft, N. W.; Mermin, D. N. Solid State Physics, Holt, Rinehart and Winston: Philadelphia, 1976, p. 649.

29. Brown, L. D.; Lipscomb, W. N. Inorg. Chem. **1977**, 16, 2989.

30. Bicerano, J.; Marynick, D. S.; Lipscomb, W. N. Inorg. Chem. **1978**, 17, 2041.

31. King, R. B. J. Amer. Chem. Soc. **1969**, 91, 7211.

32. Mattes, R.; Tebbe, K. F.; Neidhard, H.; Rethfeld, H. J. Less-Common Met. **1976**, 47, 29.

33. Vlasse, M.; Slack, G. A.; Garbauskas, M.; Kasper, J. S.; Viala, J. C. J. Solid-State Chem. **1986**, 63, 31.

34. Frank, F. C.; Kasper, J. S. Acta Cryst. **1958**, 11, 184.

35. Muetterties, E. L.; Wright, C. M. Quart. Rev. **1967**, 21, 109.

36. Hyde, B. G.; Andersson, S. Inorganic Crystal Structures, J. Wiley: New York, **1989**, p. 375.

37. Payne, M. W.; Ebihara, M.; Corbett, J. D. Angew. Chem. Int. Ed. Engl. **1991**, 30, 856.

38. Orbital parameters and energies from Janiak, C.; Hoffmann, R. J. Am. Chem. Soc. **1990**, 112, 5924.

39. Fowler, P. W. Polyhedron **1985**, 4, 2051.

40. The calculation for $In_{16} + 4In_{11}$ actually exceeded the capacity of the program, and so the essential portion, the four In11 atoms, were represented by adjusted 5s orbitals on four isolated atoms. But the results with fewer In_{11} units make it clear that the In11 interactions are quite independent, especially those at opposite ends of the In_{16} cluster.

41. Nesper, R. Prog. Solid State Chem. **1990**, 20, 1.

Table I. Selected Data Collection and Refinement Parameters for $Na_7In_{11.76}$

Space group, Z	$P4_2/nmc$ (No. 137), 12
a, Å[a]	16.093 (4)
c, Å	23.384 (8)
V, Å^3	6056 (4)
absorp coeff (Mo Kα), cm^{-1}	133.6
transm coeff range	0.442 – 1.00
indep obs refl; variables	1352; 153
R,[b] %	3.4
R_w,[c] %	3.6

[a] Guinier data, λ = 1.540562 Å.

[b] $R = \Sigma||F_o| - |F_c|| / \Sigma|F_o|$.

[c] $R_w = [\Sigma w(|F_o| - |F_c|)^2 / \Sigma w(F_o)^2]^{1/2}$; $w = [\sigma(F)]^{-2}$.

Table II. Positional parameters and B_{eq} ($Å^2$) for $Na_7In_{11.76}$[a]

atom	posn	x	y	z	B_{eq},[b] $Å^2$
In1	16 h	0.6563 (1)	0.0659 (1)	0.29244 (6)	1.19 (6)
In2	8 g	1/4	0.0970 (1)	0.73247 (9)	1.2 (1)
In3	8 g	1/4	0.8384 (1)	0.61746 (9)	1.23 (9)
In4	16 h	0.8438 (1)	−0.0601 (1)	0.05747 (6)	1.29 (6)
In5	8 g	1/4	0.1561 (1)	0.85100 (9)	1.34 (9)
In6	16 h	0.5990 (1)	−0.0975 (1)	0.34123 (6)	1.41 (7)
In7	16 h	0.5959 (1)	0.0697 (1)	0.41476 (6)	1.31 (6)
In8	16 h	0.9116 (1)	−0.1581 (1)	−0.03786 (6)	1.44 (6)
In9	16 h	0.4331 (1)	−0.1549 (1)	0.29687 (7)	2.02 (7)
In10	8 g	1/4	0.8416 (2)	0.1106 (1)	3.0 (1)
In11[c]	8 g	1/4	0.9228 (3)	0.5016 (2)	2.8 (2)
In12	8 g	1/4	−0.0816 (2)	0.3361 (1)	3.8 (2)
Na1	8 g	1/4	0.4205 (7)	0.4056 (5)	1.9 (5)
Na2	2 a	3/4	1/4	3/4	1.2 (5)
Na3	2 b	3/4	1/4	1/4	1.8 (6)
Na4	4 d	1/4	1/4	0.9807 (8)	1.9 (8)
Na5	8 g	1/4	0.9439 (8)	0.8393 (5)	2.2 (6)
Na6	8 g	1/4	0.3873 (9)	0.2531 (5)	2.3 (6)
Na7	16 h	0.9435 (6)	−0.0583 (6)	0.1908 (4)	2.6 (4)
Na8	4 d	1/4	1/4	0.6294 (8)	3 (1)
Na9	16 h	0.0603 (6)	−0.0619 (6)	0.0600 (5)	3.4 (5)
Na10	8 g	1/4	0.6253 (8)	0.9791 (5)	2.2 (6)
Na11	8 g	1/4	0.0398 (8)	0.0764 (5)	2.2 (6)

[a] Origin at $\bar{1}$.

[b] $B_{eq} = (8\pi^2/3)\Sigma_i\Sigma_j U_{ij} a_i^* a_j^* a_i a_j$.

[c] Occupancy = 63.6 (8) %, giving the composition $Na_7In_{11.757(5)}$.

Table III. Distances of nearest neighbors about each atom in $Na_7In_{11.76}$[a]

	In1		In4		In7		In10	
	In1	2.858 (3)	In4	3.018 (3)	In1	3.022 (2)	2 In9	3.031 (3)
	In1	3.016 (3)	In5	3.041 (3)	In3	2.985 (2)	In10	2.949 (6)
	In2	3.080 (3)	In7	2.943 (2)	In4	2.943 (2)	2 In12	3.327 (3)
	In3	3.014 (3)	In8	2.941 (2)	In6	3.194 (2)		
	In6	3.012 (2)			In8	2.950 (2)	Na2	3.577 (3)
	In7	3.022 (2)	Na1	3.408 (5)	In11	3.161 (3)	2 Na9	3.62 (1)
			Na5	3.41 (1)			Na11	3.29 (1)
	Na3	3.469 (2)	Na7	3.506 (9)	Na5	3.456 (7)		
	Na5	3.546 (7)	Na9	3.48 (1)	Na7	3.506 (9)	**In11**	
	Na5	3.43 (1)	Na9	3.71 (1)	Na9	3.44 (1)		
	Na7	3.48 (1)	Na10	3.45 (1)	Na9	3.34 (1)	In3	3.030 (5)
	Na7	3.50 (1)	Na11	3.49 (1)	Na10	3.303 (6)	2 In7	3.161 (3)
							2 In8	3.163 (4)
	In2		**In5**		**In8**			
							Na1	3.38 (1)
2	In1	3.080 (3)			In4	2.941 (2)2	Na9	3.36 (1)
	In5	2.930 (3)	In2	2.930 (3)	In6	2.987 (2)	2 Na10	3.460(9)
2	In6	2.980 (2)	2 In4	3.041 (3)	In7	2.950 (2)		
			In5	3.023 (5)	In8	2.959 (3)		
	Na5	3.51 (1)			In11	3.163 (4)	**In12**	
2	Na6	3.34 (1)	2 Na1	3.38 (1)				
2	Na7	3.647 (9)	Na4	3.39 (2)	Na1	3.43 (1)	2 In9	3.304 (2)
	Na8	3.45 (1)	Na5	3.43 (1)	Na4	3.277 (8)	2 In9	3.473 (4)
			2 Na6	3.52 (1)	Na8	3.68 (1)	2 In10	3.327 (3)
	In3		2 Na7	3.623 (9)	Na9	3.65 (1)		
					Na9	3.61 (1)	Na1	3.06 (1)
2	In1	3.014 (3)	**In6**		Na11	3.347 (8)	Na2	3.376 (3)
	In3	2.845 (5)					Na6	3.68 (1)
2	In7	2.985 (2)	In1	3.012 (2)	**In9**		2 Na7	3.85 (1)
	In11	3.030 (5)	In2	2.980 (2)			2 Na9	3.90 (1)
			In7	3.194 (2)	In6	3.009 (3)		
	Na3	3.410 (2)	In8	2.987 (2)	In9	3.061 (4)		
2	Na5	3.57 (1)	In9	3.009 (3)	In9	2.969 (3)		
2	Na10	3.34 (1)			In10	3.031 (3)		
			Na6	3.306 (8)	In12	3.304 (20		
			Na7	3.621 (9)	In12	3.473 (4)		
			Na7	3.639 (8)				
			Na8	3.522 (4)	Na2	3.497 (2)		
			Na9	3.52 (1)	Na6	3.47 (1)		
			Na11	3.262 (8)	Na7	3.42 (1)		
					Na7	3.538 (9)		
					Na9	3.68 (1)		
					Na11	3.75 (1)		

Table III. (continued)

	Na1		Na6		Na8		Na10	
2	In4	3.408 (5)	2 In2	3.34 (1)	2 In2	3.45 (1)	2 In3	3.34 (1)
2	In5	3.38 (1)	2 In5	3.52 (1)	4 In6	3.522 (4)	2 In4	3.45 (1)
2	In8	3.43 (1)	2 In6	3.306 (8)	4 In8	3.68 (1)	2 In7	3.303 (6)
	In11	3.38 (1)	2 In9	3.47 (1)			In10	3.12 (1)
	In12	3.06 (1)	In12	3.68 (1)	Na4	3.48 (3)	2 In11	3.460 (9)
					2 Na6	3.64 (2)		
	Na4	3.26 (1)	Na1	3.61 (2)	2 Na11	3.60 (1)	Na5	3.45 (2)
	Na6	3.61 (2)	Na7	3.47 (1)			2 Na9	3.73 (1)
2	Na7	3.84 (1)	Na8	3.64 (2)	Na9		Na11	3.50 (2)
2	Na9	3.85 (1)						
			Na7		In4	3.48 (1)	Na11	
	Na2				In4	3.71 (1)		
			In1	3.48 (1)	In6	3.52 (1)	2 In4	3.49 (1)
8	In9	3.497 (2)	In1	3.50 (1)	In7	3.44 (1)	2 In6	3.262 (8)
4	In10	3.577 (3)	In2	3.647 (9)	In7	3.34 (1)	2 In8	3.347 (8)
4	In12	3.376 (3)	In4	3.506 (9)	In8	3.65 (1)	2 In9	3.75 (1)
			In5	3.623 (9)	In8	3.61 (1)	In10	3.29 (1)
	Na3		In6	3.621 (9)	In9	3.68 (1)		
			In6	3.639 (8)	In10	3.62 (1)	Na8	3.60 (1)
4	In1	3.469 (2)	In9	3.42 (1)	In11	3.36 (1)	2 Na9	3.49 (1)
4	In3	3.410 (2)	In9	3.538 (9)	In12	3.90 (1)	Na10	3.50 (2)
			In12	3.85 (1)				
4	Na5	3.75 (1)			Na1	3.85 (1)		
			Na1	3.84 (1)	Na7	3.59 (1)		
	Na4		Na5	3.68 (1)	Na9	3.95 (2)		
			Na6	3.47 (1)	Na10	3.73 (1)		
4	In4	3.524 (5)	Na7	3.81 (2)	Na11	3.499 (1)		
2	In5	3.39 (2)	Na9	3.59 (1)				
4	In8	3.277 (8)						
2	Na1	3.26 (1)						
	Na8	3.48 (3)						
	Na5							
2	In1	3.43 (1)						
2	In1	3.546 (7)						
	In2	3.51 (1)						
2	In3	3.57 (1)						
2	In4	3.41 (1)						
	In5	3.43 (1)						
	In7	3.456 (7)						
	Na3	3.75 (1)						
2	Na7	3.68 (1)						
	Na10	3.45 (2)						

[a] Limits are 3.5 Å for In–In and 3.9 Å for Na–In and Na–Na.

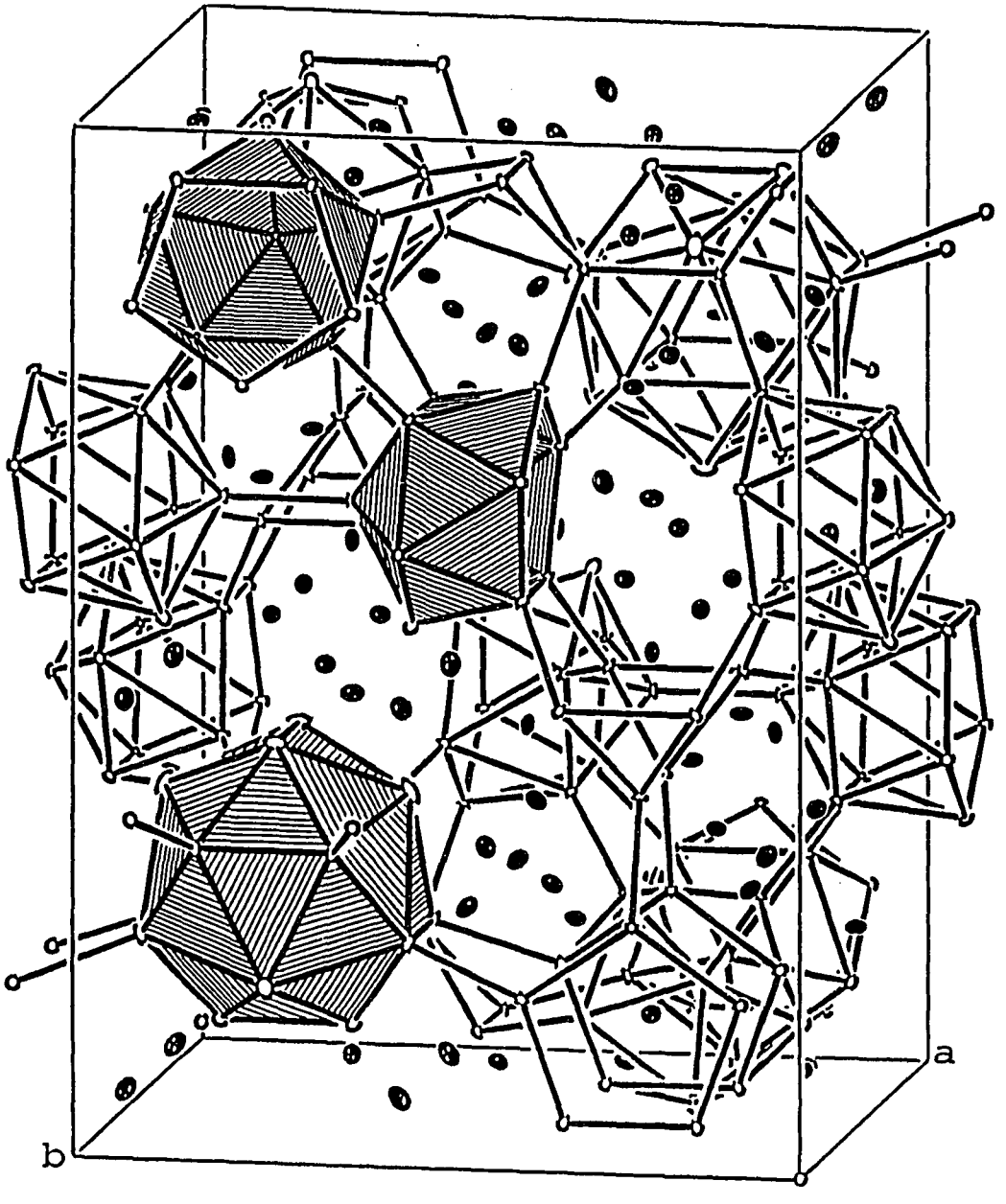

Figure 1. A general view of the unit cell of $Na_7In_{11.76}$, slightly off [100] with *c* vertical. The In atoms are depicted as open, Na as solid ellipsoids. Lines are drawn for all In–In separations less than 3.5 Å. One set of significant intercluster interactions between In11 in a nido-icosahedron and In12 and 2 x In10 in the In_{16} unit are dashed.

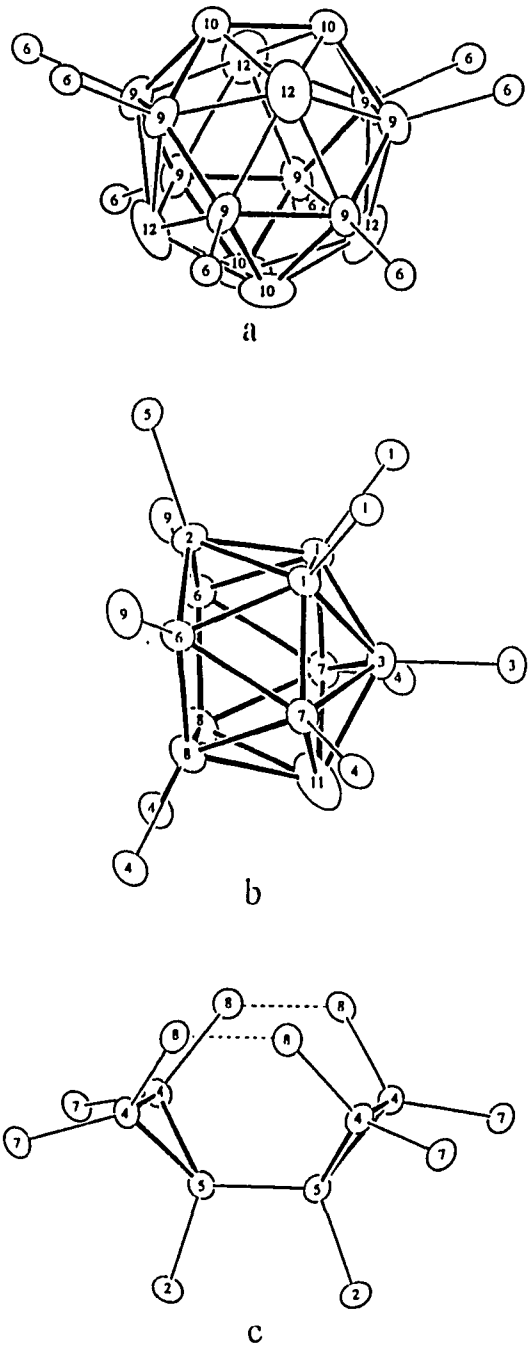

Figure 2. (a) The 16-vertex closo-icosioctahedron (the centering Na^+ is not shown); (b) the nido-icosahedron in which In11 is ~ 63.6% occupied; (c) pairs of In_3 triangles, all in $Na_7In_{11.76}$. The dangling atoms in all three represent intercluster bonds between these units (94% thermal ellipsoids).

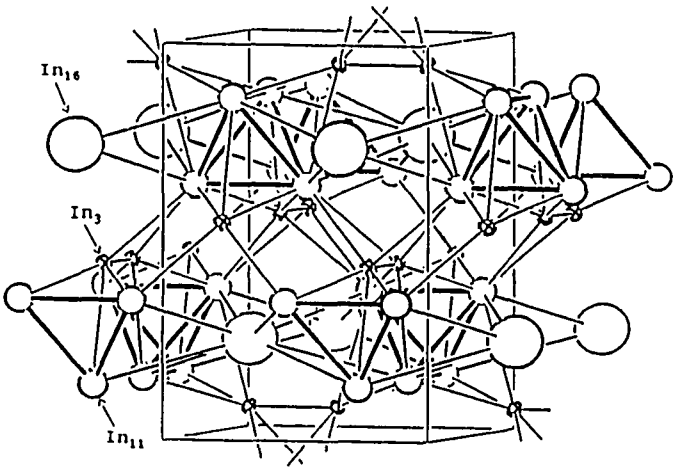

a

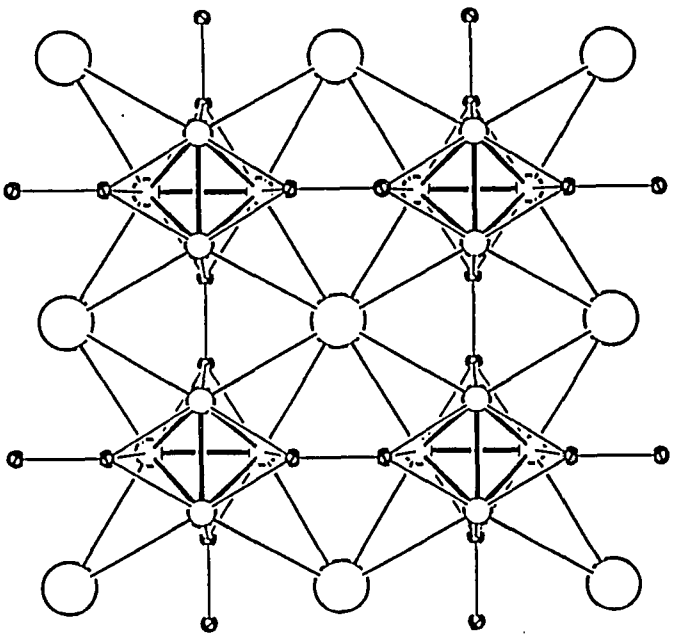

b

Figure 3. Representations of the layering of interbonded units in $Na_7In_{11.76}$. Large and medium circles mark the centers of In_{16} and $In_{11}(In_{10})$ clusters while small, crossed circles represent the In_3 triangles (Figure 2a, b, c, respectively). (a) Same orientation as Figure 1; (b) the [001] view. The $[In_{11(10)}]_4$ groups are emphasized.

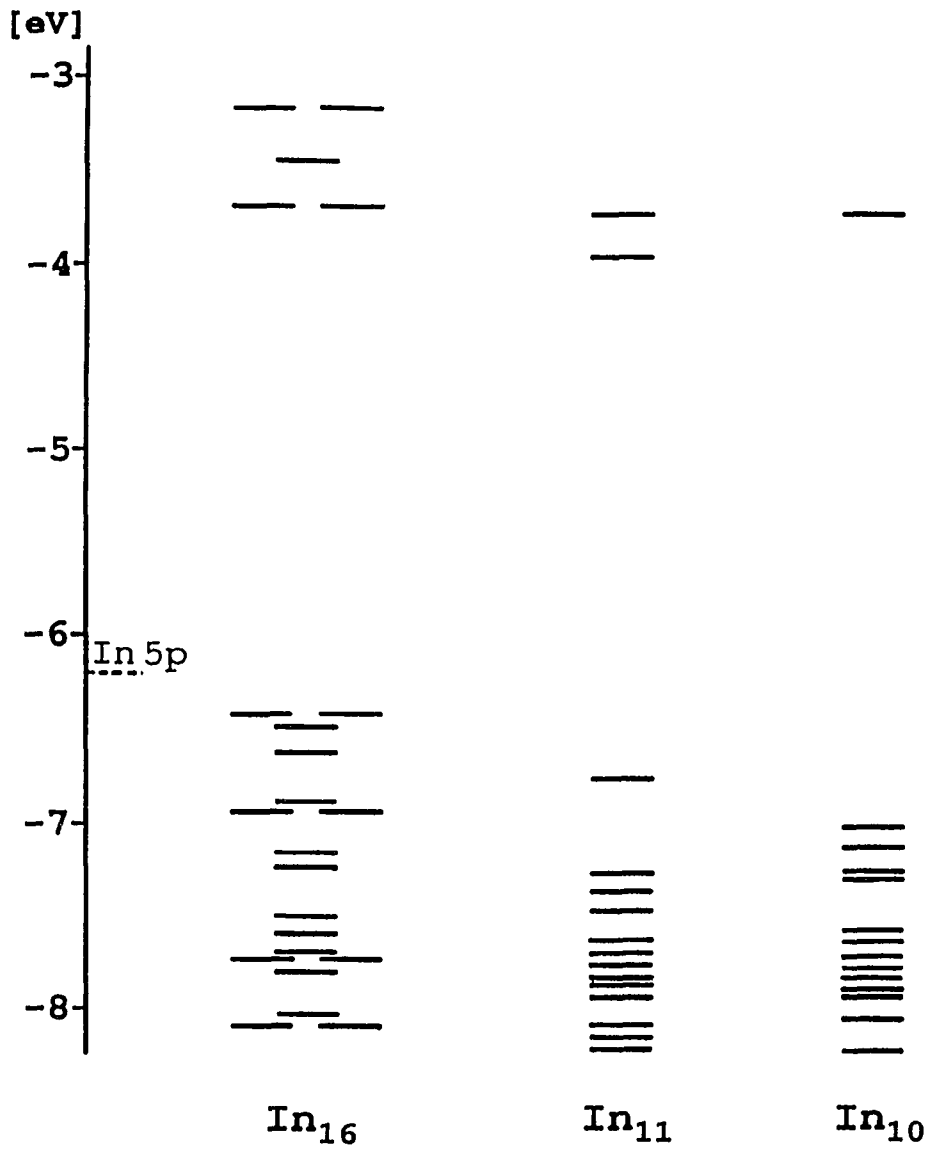

Figure 4. Extended Hückel results for the skeletal bonding levels in separate In_{16}, In_{11} and In_{10} units in $Na_7In_{11.76}$, including exo bonds. For In_{11} and In_{16}, the highest lying one and eight of nine orbitals, respectively, are nonbonding pairs on atoms without exo In–In bonds.

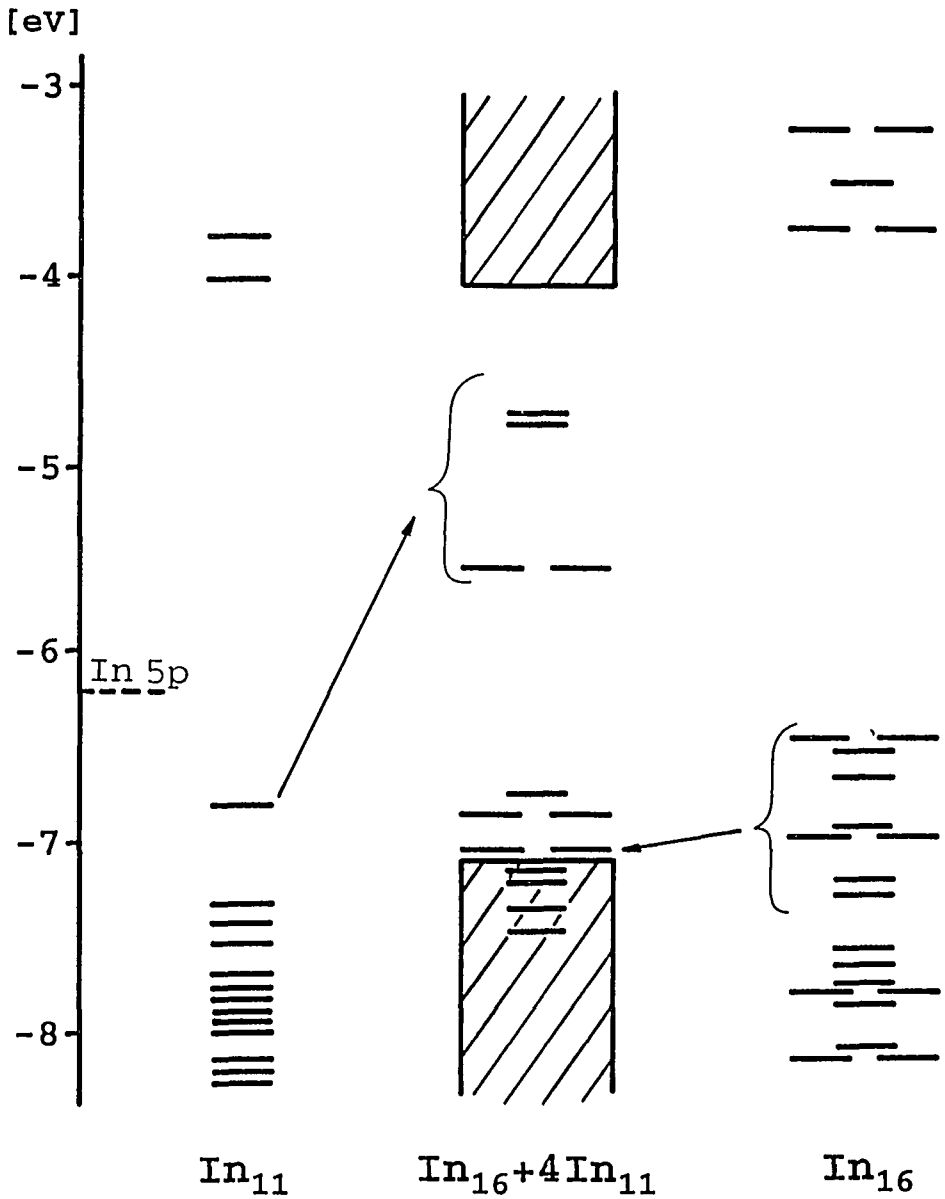

Figure 5. Perturbations on the extended Hückel results in Figure 4 when In11 — In10,12 interactions between "nonbonding" lone pairs on In_{16} and four surrounding In_{11} units are included. The explicit levels in the middle portion show only those energies that are significantly affected; the blocked areas represent the locales of unchanged skeletal bonding levels for In_{10}, In_{11} and In_{16} in which nonbonding pairs are not important components.

SUPPLEMENTARY MATERIAL

Further Data Collection and Refinement Information for $Na_7In_{11.76}$

Space group, Z	*$P4_2/nmc$* (#137), 12
a, Å[a]	16.093 (4)
c, Å	23.384 (8)
V, Å^3	6056 (4)
Crystal dimension (mm)	0.1 x 0.1 x 0.05
Diffractometer	Rigaku AFC6R
2θ max, deg	50.1
octants measured	±*h*, *k*, *l*
reflections:	
measured	11370
observed (>3σ_I)	4536
independent	1352
R_{ave},[b] %	5.4
absorp coeff (Mo Kα), cm^{-1}	133.6
transm. coeff. range	0.442 – 1.00
param. refined	153
R,[c] %	3.4
R_w,[d] %	3.6
G.O.F.[e]	1.115
Largest param. shift/esd	0.00
Secondary ext. coeff	0
Largest residual peak	+2.6 e/Å^3

[a] Guinier data, λ = 1.540562 Å.

[b] All data.

[c] $R = \Sigma||F_o| - |F_c|| / \Sigma|F_o|$.

[d] $R_w = [\Sigma w(|F_o| - |F_c|)^2 / \Sigma w(F_o)^2]^{1/2}$; $w = \sigma_F^{-2}$.

[e] Goodness of fit $S = \Sigma((|F_o| - |F_c|) / \sigma_i) / (N_{obs} - N_{para})$.

Thermal Parameters for $Na_7In_{11.76}$ ($Å^2$)

atom	U_{11}[a]	U_{22}	U_{33}	U_{12}	U_{13}	U_{23}
In1	1.52 (8)	1.55 (8)	1.46 (7)	0.02 (7)	−0.11 (7)	0.28 (6)
In2	1.4 (1)	1.8 (1)	1.4 (1)	0.0	0.0	−0.4 (1)
In3	1.4 (1)	1.2 (1)	2.1 (1)	0.0	0.0	−0.0 (1)
In4	1.70 (8)	1.39 (7)	1.82 (8)	−0.21 (7)	0.45 (7)	−0.26 (7)
In5	2.3 (1)	1.3 (1)	1.5 (1)	0.0	0.0	−0.2 (1)
In6	1.87 (9)	1.75 (9)	1.72 (7)	−0.23 (6)	0.18 (7)	0.06 (7)
In7	1.54 (7)	1.47 (8)	1.97 (8)	0.20 (6)	0.41 (7)	0.20 (7)
In8	1.91 (8)	1.60 (8)	1.97 (7)	−0.07 (7)	0.64 (7)	0.17 (7)
In9	2.2 (1)	1.90 (9)	3.5 (1)	−0.23 (8)	−0.90 (8)	0.49 (8)
In10	6.4 (2)	2.5 (1)	2.4 (1)	0.0	0.0	0.3 (1)
In11	2.3 (2)	3.3 (3)	4.9 (3)	0.0	0.0	1.9 (2)
In12	4.0 (2)	3.3 (2)	7.0 (2)	0.0	0.0	2.8 (2)
Na1	2.7 (7)	1.1 (6)	3.4 (7)	0.0	0.0	0.3 (6)
Na2	2.0 (9)	U_{11}	0.4 (10)	0.0	0.0	0.0
Na3	3 (1)	U_{11}	2 (1)	0.0	0.0	0.0
Na4	1 (1)	2 (1)	4 (1)	0.0	0.0	0.0
Na5	3.8 (8)	3.2 (8)	1.4 (6)	0.0	0.0	−0.3 (6)
Na6	3.3 (8)	3.2 (8)	2.3 (7)	0.0	0.0	0.9 (6)
Na7	3.1 (6)	3.3 (6)	3.4 (5)	−0.2 (4)	−0.7 (5)	1.3 (5)
Na8	3 (1)	5 (1)	3 (1)	0.0	0.0	0.0
Na9	3.3 (6)	4.0 (6)	5.6 (7)	0.4 (5)	−0.5 (5)	−2.0 (6)
Na10	2.2 (7)	3.7 (8)	2.3 (7)	0.0	0.0	0.5 (6)
Na11	3.1 (7)	2.6 (7)	2.5 (7)	0.0	0.0	−0.7 (6)

[a] $T = \exp[(-2\pi^2(U_{11}h^2a^{*2} + U_{22}k^2b^{*2} + U_{33}{}^2c^{*2} + 2U_{12}hka^*b^* + 2U_{13}ha^*c^* + 2U_{23}k b^*c^*)]$.

PAPER 6. SYNTHESIS, CHARACTERIZATION AND BONDING OF INDIUM CLUSTER PHASES: $Na_{15}In_{27.4}$, A NETWORK OF In_{16} AND In_{11} CLUSTERS; Na_2In WITH ISOLATED INDIUM TETRAHEDRA

Slavi C. Sevov and John D. Corbett*

ABSTRACT

The remaining phases in the Na—In system have been identified and characterized. The indium-richest is $Na_{15}In_{27.4}$, with a structure containing novel *closo*-In_{16} clusters interconnected to two kinds of *nido*-In_{11} units and isolated, 4-bonded atoms (*Cmcm*, Z = 8, a = 16.108(4) Å, b = 35.279(8) Å, c = 15.931(3) Å, R/R_w = 0.041/0.044 at the indium-rich limit $Na_{15}In_{27.54}$). Fractional occupancy of two atoms in cluster chain positions were found, one as a function of a narrow nonstoichiometry. The structure is related to that recently established for $Na_7In_{11.8}$. Resistivity and magnetic properties are consistent with a small (0.5 — 3.2%) excess of electrons relative to the calculated bonding requirements. The sodium-richest phase is the stable, diamagnetic, and weakly metallic Na_2In, isostructural with Na_2Tl ($C222_1$, Z = 16, a = 13.855(1) Å, b = 8.836(1) Å, c = 11.762(1) Å, R/R_w = 0.030/0.034). A corrected phase diagram is given.

INTRODUCTION

Knowledge of the binary Na–In system has been quite limited. The present phase diagram (*1*, *2*) is based largely on thermal analysis (*3*, *4*) and indicates a congruently melting phase at approximately Na_5In_8 or Na_2In_3, the Zintl phase NaIn (NaTl-type) (*5*), and a sodium-rich member Na_3In (*3*) or Na_2In (*4*). We have already reported on the structure and properties of $Na_7In_{11.8}$, the maximum melting compound (*6*). While exploring the region of stoichiometries over which this compound is stable, we observed that a second phase is formed on the indium-richer side. This article reports on this compound, namely $Na_{15}In_{27.4}$ (35.4 at.% Na), which exhibits a network structure closely related to that in $Na_7In_{11.8}$. We also discuss the identification and properties of Na_2In, the sodium-richest phase in the system.

EXPERIMENTAL SECTION

Syntheses

The reagents and the reaction techniques in welded tantalum tubing were described before (*6*). All materials were handled in a N_2-filled glovebox.

Composition space in Na—In was further explored following our identification and characterization of $Na_7In_{11.76}$ (37.3 at.% Na) as well as observation of the well-known NaIn (50.0% Na). Compositions of 35 and 67% Na were melted at 550°C and then slowly cooled to room temperature at 5°C per hour. (The liquidus temperatures for these are at about 440°C and 330°C, respectively (*1*).) The products were metallic in appearance and very brittle. Both samples react with moist air rapidly, with bubbling; in no way do any of these exhibit the air stability reported for the maximum melting "Na_2In_3" (*3*). Single crystals of $Na_{15}In_{27.54}$ (35.3% Na) and Na_2In (66.7%) were obtained from the respective samples.

Powder patterns were obtained after grinding the samples and mounting the powder between pieces of cellophane tape. An Enraf-Nonius Guinier camera, Cu Kα radiation (λ = 1.540562 Å) and NBS (NIST) silicon as an internal standard were employed for this purpose. Patterns of the above phases were later indexed with the aid of patterns calculated on the basis of the refined structures. Least-square refinements for 29 lines from the $Na_{15}In_{27.5}$ phase limit and 35 lines from Na_2In afforded the lattice constants a = 16.108 (4) Å, b = 35.279 (8) Å, c = 15.931 (3) Å for $Na_{15}In_{27.5}$ and a = 13.855 (1) Å, b = 8.836 (1) Å, and c = 11.762 (1) Å for Na_2In. Errors for the former are somewhat large because this particular combination of a large cell and near-tetragonality produce many diffraction lines, and these are often grouped very close to one other, making their measurement and assignment rather ambiguous at times.

A reaction designed to produce the reported Na_3In was carried out at that composition and under the reaction conditions described above. The product by eye clearly contained unreacted

sodium metal, but many small crystallites could be seen in the soft matrix. The X-ray powder pattern showed the presence of NaIn, Na_2In and Na. The sample was sealed in a Pyrex ampoule under vacuum and equilibrated at 140°C for 10 days. This time the amounts of NaIn and Na seen by powder pattern were negligible compared with that of Na_2In. A second equilibration was made at 240°C for 10 days, above what we conclude is the peritectic decomposition temperature of Na_2In (see Phase Diagram), and the sample quenched. If Na_2In existed up to 286°C, as in one proposal (*4*), it should have been seen in this product, but only NaIn and Na with traces of Na_2In were evident in the powder pattern. No evidence of either a peritectic decomposition point of 96°C for "Na_3In" (*3*) or of a suggested lower (peritectoid) stability limit for Na_2In at 160°C (*4*) could be found, either in the initial Na_3In reaction above which was cooled to room temperature at 5°C hr^{-1} or after an equilibration of the Na_2In in that sample for 14 days at 90°C. The "Na_3In" composition assignment was based on direct analysis and must have resulted from the virtual inseparability of Na and Na_2In by physical means.

Nonstoichiometry

A change in the occupancy of the In19 position in the $Na_{15}In_{27.54}$ structure (below) over a range of compositions was thought possible. Therefore, additional reactions with both 20 and 36.8 at.% Na were carried out. The former was treated as first described while the latter was heated at 490°C for two hours and then at 410°C and 250°C for 3 and 5 days, respectively.

The indium-richer sample provided the $Na_{15}In_{27.4}$ phase and a lot of unreacted indium metal, proving that the former is the indium-richest compound in the system. The lattice parameters of the former phase, a = 16.129 (3) Å, b = 35.308 (6) Å and c = 15.952 (2) Å), differ by only +4, +3 and +6 σ, respectively, from the values obtained earlier for the sample used for the structure refinement, indicating that the refined composition (below) is close to upper indium limit. (Higher occupancy of the fractional In19 position therein would cause a significant expansion of the c-axis

— see Structure Descriptions.) The other reaction produced the known $Na_7In_{11.76}$ (37.3 at.% Na) as a major phase, but lines from the $Na_{15}In_{27.4}$ structure could also be measured, and these gave *a* = 16.119 (3) Å, *b* = 35.141 (7) Å and *c* = 15.945 (4) Å. These demonstrate a significant contraction of the b axis at the indium-poor limit (0.167 Å, 18σ), while the a and c axes remain about the same (<3σ differences). A second structural study was therefore carried out on this sample to clarify this point since reduced occupation of a site other than that of In19 was implied.

Structure determinations

Three sets of diffraction data were collected at room temperature on CAD4 single crystal diffractometer with monochromated Mo Kα radiation ($2\theta_{max}$ = 50°), and the structures were refined with the aid of the TEXAN package (*7*). Some details of the data collection and refinement are listed in Table I. Unique aspects of the crystallography follow:

$Na_{15}In_{27.54}$. A few wedge-shaped pieces picked from the crushed sample were sealed in thin-walled glass capillaries and checked by means of oscillation, Weissenberg, and precession photographs for quality and, eventually, a space group assignment. The photographs showed a C-centered orthorhombic cell with additional systematic absences consistent with three possible space groups — *Cmcm* (no. 63), $Cmc2_1$ (no. 36) and *C2cm* (no. 40, nonstd.). A crystallite ca. 0.3 x 0.1 x 0.07 mm was chosen, and 25 reflections from a random search by the diffractometer were indexed with a C-centered orthorhombic cell of the expected dimensions. One octant of data was collected with no imposed conditions. The two possible space groups were confirmed after corrections for Lorentz and polarization effects as well as for absorption with the aid of the average of three ψ-scans at different θ values. Only a few relatively weak reflections (I/σ(I) ~3) violated the C-centering. The Wilson plot clearly suggested a centrosymmetric space group, and thus *Cmcm* was chosen for the first trial.

Application of direct methods(*8*) gave 19 positions with distances around each appropriate to indium. The weight of one of these was approximately half of the average of the others, and so only the 18 larger positions were assigned as In for the first few least-squares cycles. A subsequent difference-Fourier synthesis again revealed the position in question together with fourteen others, the latter having appropriate distances for sodium atoms. The odd peak was approximately twice the average height of the sodium positions, and so it was assigned as indium (In19). Refinement with isotropic thermal parameters led to R = 9.8% and to an unreasonably large thermal parameter for In19. Consequently this atom was refined with partial occupancy, 54.1(9)% in the final analysis. The occupancies of the other In atoms did not deviate from unity by more than 4% ($3-4\sigma$) when the Na atoms were kept fixed, and of Na, by 5 – 8% (~3σ) when the In atoms were fixed. Therefore, these other occupancies were all held at unity in the final refinement. The final residuals were R(F) = 4.1%, R_w = 4.4% with variation of positions, anisotropic thermal parameters and the multiplicity of In19 after application of DIFABS for an empirical absorption correction (*9*). The refined composition is $Na_{15}In_{27.541(9)}$ (35.26 (2) at.% Na). The largest residual peaks in the final difference Fourier map were 1.6 e/A^3 (1.9 Å from In7) and -2.3 e/Å^3.

The facts that In19 refines with occupancy within 4σ of 50% and that the distance to an equivalent position generated by the center of symmetry – 2.76 (1) Å – is significantly shorter than the shortest distance observed in $Na_7In_{11.8}$ – 2.845 (5) Å – suggested that the structure might be acentric in only this respect. Consequently, the $Cmc2_1$ group was assigned, and atomic positions calculated from the refined coordinates in *Cmcm*. In19 was placed at one of the two possible positions. (This nonetheless seemed unlikely as linear chains of nidoicosahedra running along the c-axis (see structure description) and all facing one way would make the crystal polar.) However, a difference Fourier map contained the other peak with a considerable height. The result was the same when the other enantiomorph was used. Not surprising, attempts to refine the structure as

acentric led to a very pronounced coupling between parameters of pairs of equivalent atoms in *Cmcm*. Film work excluded the possibility of a superlattice along $\vec{c}$. All these results were interpreted as evidence that the structure has a center of symmetry, and the In19 position is randomly occupied.

In order to establish the nature of the apparent nonstoichiometry of $Na_{15}In_{27.4}$, diffraction data were collected from a single crystal picked from the sample at indium-poor limit (see above).[1] The final positional and thermal parameters (available from J.D.C.) as well as interatomic distances were very close to those for $Na_{15}In_{27.54}$ (within 5σ) except for some larger changes associated with the smaller *b* axis. The major difference is the partial occupancy of the In15 site (64.4 (7)%) in addition to that of In19 (51.5 (7)%). The corresponding composition is $Na_{15}In_{27.16(1)}$ (35.6 at.% Na). The occupancy of In19 is again very close to one-half and within 3σ of that at the indium-rich limit.

Na_2In. Some single crystals without a particular shape were sealed in capillaries and checked for singularity by oscillation photographs. One of them (ca. 0.2 x 0.1 x 0.1 mm) was selected, and 25 reflections from the random search were indexed with a C-centered orthorhombic cell. Two octants of data were collected with the appropriate absence condition imposed. The diffraction data were corrected for Lorentz and polarization effects and also for absorption with the aid of ψ-scans of three reflections. The output showed an additional systematic extinction condition consistent with only one space group — $C222_1$ (no. 20). Direct methods gave two positions that were assigned to indium in the starting model. A few least-squares cycles and a difference Fourier map gave five more positions with distances to the indium atoms appropriate for sodium, and they

[1]Two octants of data were collected with the absence condition for C-centering imposed. Results were R_{ave} = 5.5%; (all data), R(F), R_w = 3.9, 5.0% for 2734 independent reflections, 229 variables and with absorption (μ = 134.3 cm^{-1}) corrected as before.

were so assigned. Refinement with isotropic thermal parameters proceeded smoothly, and a DIFABS empirical absorption correction was applied after convergence. Occupancies deviated from unity by $< 2\sigma$. The final residuals after anisotropic refinement of all atoms were $R = 3.0\%$, $R_w = 3.4\%$. No peaks larger than $1e/A^3$ appeared in the final difference Fourier map. The result was later recognized as the Na_2Tl structure (*10*). (Structure factor data as well as anisotropic displacement parameters for both structures are available from J.D.C.)

Property measurements

The electrical resistivities of the two compounds were again measured by an electrodeless "Q" method (*11*). These utilized a sized, powdered sample mixed with chromatographic Al_2O_3 and were made at 34 MHz and every 10° between 130 to 295 K. Sample magnetizations were measured at 3 Tesla over the range 6-295 K on a Quantum Design MPMS SQUID magnetometer. The raw data were corrected for the susceptibilities of the containers. The diamagnetic correction procedures are described in more detail elsewhere (*6*).

RESULTS AND DISCUSSION

Structure description

$Na_{15}In_{27.4}$. This phase exhibits a small homogeneity range corresponding to about ±0.2 in the indium coefficient. The phase is referred to by its mean composition unless changes therewith are important.

The final positional and isotropic-equivalent displacement parameters and the important distances at the indium-rich $Na_{15}In_{27.54}$ limit are listed in Tables II and III, respectively. The general view of the unit cell in Fig. 1 outlines all In—In distances less than 3.5 Å.

The structure can be described as a network of four types of clusters: 12-bonded closo-icosioctahedra (In_{16}) (that is, with 12 exo bonds to other cluster units), 10-bonded nido-icosahedra (In_{11}, denoted as type *A* hereafter), 10-, 11- or 12-bonded closo-, nido- or arachno-icosahedra (In_{12}, In_{11} or In_{10}, type *B* hereafter), depending on the interpretation of the fractional occupancy of In19, and 6-bonded In_3 triangles.

The novel 16-vertex cluster has C_{2v} (*m2m*) point group symmetry (Fig. 2a). The first example of such a species (although 8-bonded) was found in $Na_7In_{11.8}$. The cluster can be described as a tetracapped truncated tetrahedron, the capping atoms (pairs of In15 and 16) being six-bonded while the rest (In7, 9, 11, 18) are five-bonded within the cluster. All but In16 and In18 also have exo-bonds; In7 and In9 (4 of each) and the pair of In11 are thus bond the cluster to ten different In_{11} while the In15 pair are bonded to In15 in two other such In_{16} clusters (Fig. 2a, 3) to form zig-zag chains. Bonds within the cluster involving the six-bonded In15 and In16 are characteristically longer (3.277 (2) — 3.448 (3) Å) than between the rest (2.885 (5) — 3.070 (3) Å), and the former exhibit larger thermal ellipsoids. In18 has the third largest ellipsoid, which probably derives from the lack of an exo-bonds to it. The In_{16} cluster is centered by the Na1 ion and is stoichiometric at the indium-rich limit $Na_{15}In_{27.54}$, but In15 therein exhibits a 64.4 (7)% occupancy

at the indium-poor limit $Na_{15}In_{27.16}$. The bonding at In15 is at this time unique, the first example of indium bonded to six atoms within the cluster plus an exo-bond as well. Partial and random occupancy of this site toward one limit means that some of the icosioctahedra will be *nido*-In_{15} and perhaps a few, arachno In_{14} modifications, which are automatically only 11- or 10-bonded units. Since the In15 — In15 bonds have components only along [0,*y*,*z*], changes in the occupancy will only affect the *b* and *c* axes. Moreover, the length of the *c* axis seems to be defined mainly by the chains of In_{11} units running along it (below), and the major effect of reduced In15 occupancy is an observed decrease in the *b* axis as these chains flatten (see Experimental Section).

There are two types of polyhedra derived from icosahedra in this structure. The first, type *A*, are 10-bonded *nido*-In_{11} (In1, 2, 3, 4, 6, 8, 12) with only *m* symmetry (Fig. 2b). The missing vertex is opposite to In1, and all atoms but In12 are exo-bonded. The *A* clusters are bonded back-to-back via In1—In1. The In3 and a pair of In6 atoms therein are bonded to three different In_{11} (all type *A*), the two In2 are bonded to two different In_{11} (type *B*, Fig. 2c), and In4 and 8 are bonded to different indium triangles (Figure 2d). Finally, In12, which lacks an exo bond, has a position that can be described as remotely capping an open triangular face on a neighboring In_{16} cluster defined by two In18 and one In16 atoms, all of which also have no exo bonds. This will be important later in electronic considerations.

The second In_{11}, type *B*, has C_{2h} (2/*m*) point symmetry and forms chains along the **c** axis (Fig. 2c, 3a). Although it is related to an icosahedron, it is better viewed starting with a distorted pentagonal antiprism with its bases normal to $\vec{c}$. All atoms of the antiprism (In13, 14, 17) are exo-bonded; In13 to four different In_{11} (type A), In14 to four different icosioctahedra, and In17 to two different indium triangles. The In19 atoms that cap pentagonal antiprism appear to have a fixed and virtually 50% occupancy across the stoichiometry range (54.1 (9) to 51.5 (7)%). The refined distances from In19 to In13, 14 and 17 in the capped face (2.841 (5) Å, 2.889 (3) Å and 2.788 (6)

Å, respectively) are short compared with those either within the antiprism (2.95 – 3.10 Å) or the characteristically smaller (2-center, 2-electron) values between clusters (2.88 – 3.05 Å), meaning that In19 is closer to the plane of the capped pentagon (compare In17). The distance to In19 in the adjacent cluster is even shorter if both are present simultaneously – 2.76 (1) Å. There are many configurational possibilities in this chain in principle: 10-bonded arachno-, nido- and closo-clusters if In19 — In19 contacts are avoided, or 11-bonded nido- and closo-, and 12-bonded closo-clusters if In19 — In19 contacts exist. These uncertainties cause complications when counting the electrons needed for the indium network bonding (below). However, the simplest arrangement may be the best – small to large regions of ordered nido- In_{11} units that are not directly bonded together, with long range disorder within or between chains or sheets so as to gain a nonpolar crystal.

The last building block consists of pairs of triangles, Fig. 2d. As before (*6*), these can also be considered as isolated four-bonded In atoms. The pair is bonded to eight different In_{11} (*A*) and two In_{11} (*B*). The dashed lines in Figure 2d between pairs of exo In8 atoms represent edges of two different In_{11} (*A*), Figure 2b.

Figure 3a shows the connectivity between the cluster building blocks more clearly and in the same orientation as Fig. 1. Large circles now represent In_{16} clusters, medium circles In_{11} (*A*), medium crossed circles In_{11} (*B*), and small crossed circles, the positions of each of the In_3 units. The structure is seen to contain identical layers normal to $\vec{b}$, each consisting of interconnected zig-zag chains of alternating cluster types parallel to the c-axis. One layer is shown in two views in Fig. 3b and 3c. One chain is constructed of interbonded 16-vertex clusters, and the second chain is formed from tetrahedra (heavier outline) of In_{11} clusters, two each of *A* and *B*. These tetrahedra alternate in their orientation along the chain, the shared corners being the type *B* units. Each layer can also be constructed from pairs of levels along $\vec{b}$, as seen in profile in Fig. 3c. Each level consists of squares of the 16-vertex clusters, centered by the tetrahedron of In_{11} clusters (or vice

versa), and the two levels are shifted from each other by half the square's edge or, in other words, by $\vec{c}/2$.

At this point, a comparison of the structures of $Na_{15}In_{27.4}$ and the recently reported $Na_7In_{11.8}$ (*6*) is appropriate. The indium network of the latter contains most of the same building blocks as the present case, namely *closo*-In_{16} (although 8-bonded), *nido*-In_{11} (type *A* only), and pairs of In_3 triangles. These also form layers that are equivalent to a single level of the double layer in $Na_{15}In_{27.4}$, Fig. 3c. In other words, the nearly tetragonal layers in $Na_{15}In_{27.4}$ can be viewed as double layers formed by the condensation of two single layers from $Na_7In_{11.8}$. The pattern of intra- and interlevel bonding in the two structures is the same. The bonding within the layers in both is mainly through direct intercluster bonds as well as via some $In_{11} - In_3$ interactions. The separate layers in both are bonded together only by pairs of In_3 triangles or, in other words, via isolated indium atoms.

All sodium atoms except Na1, 4, 14 cap triangular faces of the various polyhedra. The same type of positioning of the alkali metals is seen in both K_8In_{11} (*12*) and $Na_7In_{11.8}$ (*6*). The Na1 cation is centered in the icosioctahedron, while Na4 and Na14 center the tetrahedral holes formed by four In_{11}, and three In_{11} and pair of triangles, respectively.

Na_2In. The final positional and thermal parameters and nearest neighbor distances are given in Tables IV and V, respectively. The prototype Na_2Tl structure discussed in detail before by Hansen and Smith (*10*) contains isolated, deformed Tl_4 clusters (C_2 point symmetry) surrounded by sodium atoms above all faces, edges and vertices of the cluster. Each sodium atom is shared by two or three tetrahedra. The In—In distances (3.066 (2) – 3.152 (1) Å) are close to other intracluster bonding distances. The shortest intercluster distance is 5.393 (1) Å.

Properties

The resistivities of the $Na_{15}In_{27.5}$ and Na_2In are both linear with the temperature over 130 —295°C and indicate metallic behavior. The resistivities at 295 K are about 290 and 270 μohm-cm with coefficients of +0.26 and +0.27% K^{-1}, respectively, characteristic of "poor metals". These are comparable to ρ_{295} ~540 μohm-cm for the metallic $Na_7In_{11.8}$ and a ρ_{748} maximum of ~180 μohm-cm for a liquid Na—In mixture at ~60 at.% Na (*13*). It should be noted that absolute values of resistivities determined by the "Q" method may be accurate only within a factor of three, but the temperature coefficients should be quite reliable.

Magnetic measurements gave temperature-independent susceptibilities for $Na_{15}In_{27.5}$ and Na_2In of —(12.0 — 13.0) x 10^{-4} and —(0.4 — 0.5) x 10^{-4} emu/mol, respectively, over 25 — 295 K. Two types of diamagnetic corrections are appropriate. Those for the Na^+ and In^{3+} ion cores total —6.0 x 10^{-4} emu/mol for $Na_{15}In_{27.5}$ and —0.3 x 10^{-4} emu/mol for Na_2In. As before (*6,12*), correction for the Larmor precession of the electron pair in each cluster orbital (Langevin contribution) is necessary. For r_{ave}, we averaged the appropriate distances from the center of each cluster to the middle of the different types of In-In edges on its surface. This gave 2.4 Å for the In_{11} clusters, 3.1 Å for the icosioctahedron, and 1.2 Å for the tetrahedron and, thence, —4.2, —9.8 and —0.5 (x 10^{-4}) emu/mol-cluster, respectively. Based on the proportions of each cluster per formula unit, the total Larmor corrections become χ_L = —[(1.5 x (4.2) + 0.5 x (9.8)] x 10^{-4} = —11.2 x 10^{-4} emu/mol for $Na_{15}In_{27.5}$ and χ_L = —0.25 (0.5) x 10^{-4} = —0.12 x 10^{-4} emu/mol for Na_2In. Combination of these, the ion core values, and the measured susceptibilities provides χ_M = +(4.2 — 5.2) x 10^{-4} emu/mol for $Na_{15}In_{27.5}$ and essentially zero (—0.08 to +0.02 x 10^{-4} emu/mol) for Na_2In. We note here that the molar susceptibility of the isostructural Na_2Tl, —0.03 x 10^{-4} emu/mol [at 50 to —300 K (*14*) after similar corrections] is remarkably close to the Na_2In result. All of the diamagnetic corrections are somewhat approximate, and the χ_M results would probably be slightly

more positive if the valence electrons in the $5s^2$ pairs or in the intercluster bonds were included. The Langevin correction is probably less than necessary as well. The results are as they stand consistent with small Pauli paramagnetic terms, as also observed early for $Na_7In_{11.8}$ and K_8In_{11}.

Electronic structure

$Na_{15}In_{27.4}$. Extended-Hückel MO calculations were performed on the separate 12-bonded *closo*–In_{16}, the 10-bonded *nido*-In_{11} (type *A*), different possibilities for the type *B* In_{11} and the observed arrangement of a pair of *nido*-In_{11} (type *A*) clusters about one In_{16} cluster, all with the observed configurations. The procedures and parameters are described in detail elsewhere (*6*). The indium atoms in the pairs of triangles (Fig. 2d) were treated as isolated four-bonded atoms following our earlier investigation.

In_{16}. We have earlier shown that 8-bonded closo-In_{16} has 18 bonding skeletal orbitals below a 2.5 eV gap and thus requires 2n + 4 = 36 electrons rather than the usual 2n + 2 by Wade's rule (*15*). (This is a standard exception (*16*).) The eight exo-bonds serve to lower the local charge on the cluster from —20 to —12. The 12-bonded *closo*-In_{16} in the present structure has the same electronic requirements for the skeletal bonding and a gap of ~2.8 eV, but the closed shell charge is further decreased to—8 by four more exo bonds. Combinations of the four lone pairs on the atoms without exo-bonds (In16, 18) form the cluster HOMO, as expected (Fig. 4). These orbitals are mainly p-type and are directed radially outward.

About 35% of the In15 atoms in In_{16} are missing at the indium poor limit (Experimental Section), meaning that the zig-zag chain of these is interrupted (Fig. 2a). Calculations on the 11-bonded nido- and 10-bonded arachno-clusters so formed indicated no change in the skeletal bonding requirements, 2n + 6 for nido and 2n + 8 for arachno. Unless the absences are correlated, there will also be In_{16} clusters in which the In15 atoms have no exo-bonds, rather only lone pairs. Calculations on such species showed that these lone pairs remain filled (although at higher energy)

despite some antibonding interactions with the surrounding six exo-bonds. In other words, the In15 absences do not alter electron requirements of these clusters.

In_{11} (type A). This cluster was calculated to have 13 skeletal bonding orbitals, as expected. The HOMO is a pure lone pair on In12, the only atom without an exo-bond, that points radially outward and lies about 0.5 eV above the next bonding orbital (Fig. 4 left). Again, π^* interactions with the five neighboring exo-bonds are responsible for the higher energy.

In_{11} (type B). As discussed earlier, half-occupancy of the In19 site (Fig. 2c) leads to several possible icosahedra derivatives. Calculations were performed on all possible species. The number of skeletal bonding orbitals for all of these is 13 but the numbers of exo-bond orbitals and of filled lone pairs are different and depend upon whether the In19 atom occupancies are correlated or not. When one In19 lacks an exo-bond, the lone pair on this atom is the HOMO and lies nearly 0.8 eV above the next bonding orbital in the same cluster. This difference is relatively great because In19 lies only ~1.3 Å above the plane defined by In13, 14, 17, while In12 in the type *A* cluster is ~2.0 Å above the In1, 4, 8 plane, which affords weaker antibonding interactions between the lone pair and the neighboring exo-bonds. If a single cluster lacks two exo bonds at In19, the lone pair combinations give rise to one antibonding and one bonding molecular orbitals.

Intercluster interactions. Although the structure is built of macrolayers interconnected by isolated indium atoms, Fig. 3a, significant interactions appear possible between In_{16} in one layer and the two *nido*-In_{11} (type *A*) units in the next layer, similar to an effect seen in $Na_7In_{11.8}$. The arrangement here is such that each In12 in the paired nido icosahedra approximately caps an In16–In18–In18 triangular face in the nearest icosioctahedron. The lone pair on In12 lies almost normal to that triangular face, while the lone pairs on In16 and In18 are directed radially outward from the icosioctahedron. The distances from In12 to In16 (4.032 (4) Å) and In18 (4.152 (3) Å) are quite long relative to "bonding" distances (2.9 – 3.5 Å), but still in a range to afford some

repulsive interactions. Extended-Hückel MO calculations were therefore also performed on the observed In_{16} — $2In_{11}$ configuration. As shown in the center of Fig. 4, one combination of In12 lone pairs becomes antibonding and presumably empty while the second falls in the nonbonding region (~0.5 eV above the highest bonding and ~1.0 eV below the lowest antibonding orbitals) where it could be either filled or empty. This means that either every or every other nido-In_{11} (A) has an empty lone pair orbital on the In12 atom.

The same arrangement of 10-bonded nido-In_{11} around In_{16} clusters occurs in $Na_7In_{11.8}$, but there the equivalent intercluster In—In distances are shorter — 3.872 (6) and 4.099 (5) Å — and the lone pairs of all nearest icosahedra are pushed up in energy and emptied.

Na_2In. The tetrahedron is considered a nido-unit resulting from a removal of a three-fold vertex from a closo-trigonal bipyramid. The In_4 units then have 2n + 4 = 12 skeletal electrons according to the Wade's rules (*15*), giving $(Na^+)_8In_4^{8-}$ either in the extreme of electron transfer or, better, by conventional oxidation state assignments.

Electron count

$Na_{15}In_{27.4}$. The number of electrons needed is somewhat less than that available, and the compound is electron-rich. Each unit cell contains four icosioctahedra, eight type *A* and four type *B* icosahedra, and 24 isolated, four-bonded indium atoms. We also take into account the effects of fractional occupancies on the cluster requirements and of the stoichiometry range of the phase relative to the electrons available. The electron requirements for each unit and the total are as follows:

		skeletal	exo	lone pair	Σ, ea	Σ/unit cell	
$4In_{16}$		36	12	8	56	224	224
$8In_{11}$ (A)	min	26	10	0	36	288	
	max	26	10	1	37		296
$4In_{11}$ (B)	min	26	11	0	37	148	
	max	26	10	2	38		152
$24In_1$					4	96	96
	closed shell total					756	768
	available at $Na_{15}In_{27.54}$ limit					781	781
	difference					+25	+13
	available at $Na_{15}In_{27.16}$ limit					772	772
	difference					+ 16	+ 4

The above numbers need some further comment. The In_{16} cluster in $Na_{15}In_{27.16}$ may have one (even two) In15 atom(s) missing at the indium-poor limit, but then the corresponding In15 atom/atoms on the adjacent units In_{16} will have stable lone pairs. These we can formally count as split between the two clusters, which means an occupancy-independent contribution from these units to the overall sum. The only case where this number can change is if the In15 atom from the second cluster is also missing so that a lone pair orbital is not available, but this seems less unlikely.

All *nido*—In_{11} (type *A*) may have an empty lone pair orbital on In12 because of nonbonded interactions with In_{16} (Fig. 4). Such an arrangement will lead to the minimum number of required electrons per cluster, 36. If every other cluster has this orbital empty, the maximum number of electrons per cluster is 37. The most complicated case is the electron count for type B icosahedra since the number of electrons needed per cluster depends upon whether the 50% of the In19 present are exo-bonded or not. The lower limit (26 skeletal + 11 for exo-bonds) is reached when all In19 atoms are exo-bonded, which means the local order gives pairs. This may not be very likely. The upper limit is reached when all clusters are nido-species, and none of them has In19 with an exo-

bond. The real count could be anywhere between those two limits, although, as noted before, the last seems more probable.

Taking into account that every indium atom provides three valence electrons and every sodium atom one, the number of available electrons per cell (Z=8) are 781 and 772 for $Na_{15}In_{27.54}$ and $Na_{15}In_{27.16}$, respectively, presuming the refined compositions are correct. The excess of electrons falls in the range of +13 to +25 (1.7 — 3.2%) at the former, indium-rich limit to +4 to +16 (0.5 — 2.0%) at the most reduced. In each case, our reasoning on uncertain electronic requirements favor the larger need and thence the smaller excess. If the maximum number of required electrons is correct, a 50% occupancy of the In15 site (rather than the 64% observed) would give a Zintl phase at the indium-poor limit. We are remarkably close to that point already, illustrating again the apparent drive to achieve a closed shell configuration even if this requires such a complicated structure.

Na_2In. We count the electrons for the formula Na_8In_4 and one In_4 tetrahedron. Those needed for skeletal bonding and lone pairs total 12 + 4 x 2 = 20. The number available is also 20 (= 4 x 3 + 8 x 1), suggesting that Na_2In could be semiconducting if the electron transfer from sodium to the In_4 unit is complete or, better, that the valence and conduction bands do not overlap. Alternatively, six 2-e bonds can be ascribed to the edges of the In_4 tetrahedron. The observed In—In bond distances, 3.066 (2) to 3.152 (1) Å (3.106 Å ave.) might seem long relative to the two-center two-electron intercluster bonds in the network structures, 2.85 to 3.02 Å, or the standard single bond, 2.84 Å (*17*). This does not necessarily imply delocalization of some bonding electrons out onto sodium. Bent bonds (reduced overlap) is one consideration, and charge repulsion is another. The comparative Sn_4^{4-} in β-NaSn exhibits edge distances of 2.967 (2) Å (*18*) relative to a metallic single bond distance of 2.842 Å and 2.80 Å in gray tin (*17*). Charge repulsion effects of 0.15 — 0.20 Å have been estimated in lengthening Tt_2^{4-} dimers (*19*) (Tt = tetredide).

Physical properties

The poor but metal-like conductivity characteristics of $Na_{15}In_{27.5}$ as well as its small Pauli-like magnetic susceptibility are nicely consistent with the foregoing electronic expectations for this phase. A few excess electrons in this complex arrangement should not detract from the considerable importance of covalent In—In bonding in and between the clusters. The term "metallic Zintl phase" (*19*) is again apt. The Na_2In phase is substantially diamagnetic, but a weak metallic conductivity contradicts the expectation from straightforward electron counting. Some small back donation from the In_4 anion with a formal 8– charge onto the sodium cations (of the same symmetry) and into the conduction band would not be surprising. A useful comparison can be made with the structure and properties of β-NaSn. Calculations based on an augmented spherical wave method involving both Na and Sn states place the Fermi level in a gap between broadened cluster (plus sodium) valence and sodium-plus-cluster conduction bands, so that the compound is predicted to be a semiconductor (*20*). Conductivity measurements show a contrary metallic property (*21*). This mismatch is not substantial and could be explained by some modest broadening of the calculated valence (cluster dominated) and conduction (Na) bands to give a small density of states at E_F. Again, this would in no way detract from the significance or importance of the cluster bonding.

Phase diagram

Figure 5 shows our proposal for a revised phase diagram for the In—Na system. We have chosen as a starting model the diagram reported by Thummel and Klem (in (*4*) and have kept all of the reported points and the resulting liquidus curve. Their data for the two eutectics and the NaIn peritectic are substantially the same as in the most recent compilation where the In(Na) liquidus end is also described (*1*, *2*). The following have been changed: the congruently melting composition of about Na_5In_8 is corrected to $Na_7In_{11.8}$, and the neighboring $Na_{15}In_{27.5}$ is added. Each is somewhat nonstoichiometric but not sufficiently so for this diagram. The eutectic transformations stop at

$Na_{15}In_{27.5}$ and Na_2In although they were observed beyond these compositions in thermal analysis (*3,4*), not too surprisingly. The peritectic temperature for $Na_{15}In_{27.5}$ is placed somewhat arbitarily.

The character and placement of the sodium-richest phase has needed some attention. Thummel and Klemm (*4*) correctly assessed the composition as near Na_2In ("around about $Na_{2.3}In$") but concluded from differential thermal measurements that the phase was stable only between ~285°C and ~165°C. They are the only investigators to have reported thermal effects in the latter region (Fig. 5). On the other hand, Lamprecht and Crowter (*3*) concluded that the phase was Na_3In, largely on the basis of an analysis of crystalline product supposedly isolated from excess sodium. In addition, they appear to have confused a peritectic decomposition of their Na_3In with the sodium-rich eutectic at 96°C. Our equilibration and X-ray studies establish that the phase is Na_2In and that it is stable from room temperature (or below) to somewhere between 180°C and 240°C where a peritectic decomposition to NaIn(s) and Na(In(ℓ) takes place. Our placement of the fixed point near 220°C was guided by the behavior of the reported liquidus data near 90% Na.

Acknowledgement. We are indebted to J. Shinar for the use of the Q apparatus, to J. E. Ostensen and D. J. Finnemore for the magnetic data.

REFERENCES

1. "Binary Alloy Phase Diagrams" 2nd ed., American Society for Metals, Metals Park, Ohio 44073 (1990), vol. 3, p. 2261.

2. S. LAROSE, A. D. PELTON: *Phase Equilib.* **12**, 371 (1991).

3. G. J. LAMPRECHT, P. J. CROWTHER: *J. Inorg. Nucl. Chem.* **31**, 925 (1969).

4. THÜMMEL, W. KLEMM: *Z. Anorg. Allg. Chem.* **44**, 376 (1970).

5. E. ZINTL AND S. NEUMAYR: *Z. Phys. Chem.* **B20**, 270 (1933).

6. S. C. SEVOV AND J. D. CORBETT: *Inorg. Chem.* **31**, 1895 (1992).

7. TEXSAN, Version 6.0 package, Molecular Structure Corp., The Woodlands, TX, 1990.

8. SHELX-86, G. M. SHELDRICK: Universität Göttingen, BRD (1986).

9. N. WALKER AND D. STUART: *Acta Crystallogr.* **A39**, 158 (1983).

10. D. A. HANSEN AND J. F. SMITH; *Acta Crystallogr.* **22**, 836 (1967).

11. J. SHINAR, B. DEHNER, B. J. BEAUDRY AND D. T. PETERSON: *Phys. Rev.* **37B**, 2066 (1988).

12. S. C. SEVOV AND J. D. CORBETT: *Inorg. Chem.* **30**, 4875 (1991).

13. C. VAN DER MAREL, E. P. BRAUNDERBURG AND W. J. VAN DER LUGT: *Phys. F: Met. Phys.* **8**, L273 (1978).

14. J. D. GREINER, D. A. HANSEN AND J. F. SMITH: *J. Less-Common Met.* **19**, 23 (1969).

15. K. WADE: *Adv. Inorg. Chem. Radiochem.* **18**, 1 (1976).

16. P. W. FOWLER: *Polyhedron*, **4**, 2051 (1985).

17. L. PAULING: "The Nature of the Chemical Bond," Cornell Univ. Press, Ithaca, New York (1960), 3rd Ed., pp. 400, 403.

18. W. MÜLLER AND K. VOLK: *Z. Naturforsch.* **32b**, 709 (1977).

19. R. NESPER: *Prog. Solid State Chem.* **20**, 1 (1990).

20. F. SPRINGELKAMP, R. A. DE GROOT, W. GEERTSMA, W. VAN DER LUGT AND F. M. MUELLER: *Phys. Rev.* **B32**, 2319 (1985).

21. R. NESPER; private communication (1990).

Table I. Selected data collection and refinement parameters for $Na_{15}In_{27.54}$ and Na_2In

Formula	$Na_{15}In_{27.54}$	Na_2In
Space group	*Cmcm*	$C222_1$
Z	8	16
a (Å)	16.108 (4)	13.855 (1)
b (Å)	35.279 (8)	8.836 (1)
c (Å)	15.931 (3)	11.762 (1)
V ($Å^3$)	9053 (6)	1440 (4)
Crystal dimensions (mm)	0.07 x 0.1 x 0.3	0.1 x 0.1 x 0.2
Radiation	Mo Kα, graphite-monochromated	Mo Kα, graphite-monochromated
$2\theta_{max}$, (deg.)	50	50
Scan mode	ω-θ	ω-θ
Octants	*h, k, l*	±*h, k, l*
Reflections		
Measured	8733	2683
Observed	2252	2254
Independent	2252	999
R_{ave} (all data) (%)	—	5.6
R (%)	4.1	3.0
R_w (%)	4.4	3.4
μ(cm^{-1})	137.37	64.20
Transmission coefficient range	0.9102 — 1.0563	0.8576 — 1.0807

Table II. Positional parameters and B_{eq} for $Na_{15}In_{27.54}$

atom	posn	x	y	z	B_{eq}
In1	8 g	0.0895(1)	0.17207(6)	1/4	1.2(1)
In2	16 h	0.1854(1)	0.11231(4)	0.1561(1)	1.23(6)
In3	8 g	0.3486(2)	0.09527(7)	1/4	1.4(1)
In4	16 h	0.1819(1)	0.19304(4)	0.0934(1)	1.33(7)
In5	16 h	0.0930(1)	0.21236(4)	0.9400(1)	1.43(7)
In6	16 h	0.3482(1)	0.14358(4)	0.0967(1)	1.46(7)
In7	16 h	0.3182(1)	0.04888(5)	0.8455(1)	1.84(7)
In8	16 h	0.3405(1)	0.22383(4)	0.1572(1)	1.39(7)
In9	16 h	0.4059(1)	0.11170(5)	0.9335(1)	2.01(8)
In10	8 f	0	0.15108(6)	0.8444(1)	1.5(1)
In11	8 g	0.4087(2)	0.01440(6)	1/4	1.7(1)
In12	8 g	0.1736(2)	0.24970(7)	1/4	1.6(1)
In13	16 h	0.0915(1)	0.05374(5)	0.0788(1)	2.13(8)
In14	16 h	0.1547(1)	0.02509(5)	0.9150(1)	2.28(8)
In15	8 f	0	0.47589(8)	0.0794(2)	3.0(1)
In16	8 g	0.1691(2)	0.36395(8)	1/4	2.9(1)
In17	8 f	0	0.07440(7)	0.9138(2)	2.4(1)
In18	8 f	0	0.67349(7)	0.8406(2)	2.7(1)
In19[a]	8 f	0	0.9965(1)	0.1635(3)	2.1(2)
Na1	4 c	0	0.5820(3)	1/4	1.9(5)
Na2	4 c	0	0.6636(5)	1/4	1.9(9)
Na3	16 h	0.3129(7)	0.0431(3)	0.0602(6)	2.6(5)
Na4	4 c	0	0.0876(6)	1/4	3.0(10)
Na5	8 f	0	0.1435(3)	0.0595(9)	2.0(6)
Na6	8 f	0	0.5794(4)	0.1127(9)	2.3(6)
Na7	8 g	0.134(1)	0.9156(4)	1/4	2.9(7)
Na8	16 h	0.1932(7)	0.1222(3)	0.5598(6)	2.5(5)
Na9	8 f	0	0.2382(4)	0.129(1)	2.7(7)
Na10	8 f	0	0.6988(4)	0.0370(8)	2.1(6)
Na11	8 g	0.1723(8)	0.8131(4)	1/4	2.3(6)
Na12	8 g	0.2036(8)	0.0242(4)	1/4	2.1(6)
Na13	16 h	0.3121(6)	0.2084(3)	0.5695(6)	2.8(5)
Na14	4 c	0	0.7625(6)	1/4	3.0(10)

[a] Occupancy = 54.1(9)%, giving the composition $Na_{15}In_{27.541(9)}$

Table III. Distances of nearest neighbors about each atom in $Na_{15}In_{27.5}$[a]

	In1		In6		In10		In15	
	In1	2.882(5)	In2	2.998(3)	In5	3.039(3)	2 In7	3.283(2)
	In2	3.012(3)	In3	2.979(2)	In10	3.007(5)	2 In9	3.448(3)
	In4	2.999(2)	In4	3.198(3)	In17	2.923(3)	2 In11	3.377(3)
	In12	3.055(3)	In8	2.993(2)			In15	3.047(6)
			In9	2.982(2)	Na5	3.44(1)		
	Na4	3.31(2)			Na7	3.53(1)	Na1	3.400(7
	Na5	3.51(1)	Na2	3.528(4)	Na8	3.61(1)	2 Na3	3.80(1)
	Na9	3.35(1)	Na3	3.638(9)	Na11	3.40(1)	2 Na3	3.85(1)
			Na6	3.34(1)	Na14	3.40(2)	Na6	3.69(1)
	In2		Na8	3.61(1)			Na6	3.63(2)
			Na10	3.268(9)	In11			
	In1	3.012(3)	Na13	3.546(9)			In16	
	In2	2.993(3)			In3	3.012(3)		
	In3	3.085(3)	In7		2 In7	3.070(3)	2 In7	3.437(3)
	In4	3.019(2)			In11	2.943(5)	2 In9	3.277(2)
	In6	2.998(3)	In7	3.042(3	2 In15	3.377(3)	2 In18	3.353(3)
	In13	2.841(2)	In9	2.979(2)				
			In11	3.070(3)	Na1	3.71(1)	Na1	3.325(7)
	Na3	3.54(1)	In14	2.978(3)	2 Na3	3.54(1)	Na7	3.66(2)
	Na4	3.452(6)	In15	3.283(2)	2 Na6	3.49(1)	2 Na8	3.79(1)
	Na5	3.535(7)	In16	3.437(3)	Na12	3.32(1)	Na11	3.12(1)
	Na8	3.46(1)					2 Na13	3.86(1)
	Na12	3.46(1)	Na1	3.501(4	In12			
			Na3	3.427(9)			In17	
	In3		Na3	3.577(9)	In1	3.055(3)		
			Na7	3.56(1)	2 In4	3.200(2)	In10	2.923(3)
2	In2	3.085(3)	Na8	3.61(1)	2 In8	3.202(3)	In13	3.100(3)
2	In6	2.979(2)	Na12	3.52(1)	*In16*	*4.032(4)*	In14	3.039(2)
	In11	3.012(3)			2 *In18*	*4.152(3)*	In19	2.788(6)
	Na2	3.43(1)			2 Na9	3.418(9)	Na5	3.37(1)
2	Na3	3.59(1)			Na11	3.34(1)	Na7	3.40(1)
2	Na6	3.32(1)			2 Na13	3.242(9)	Na8	3.57(1)
	Na12	3.43(1)						
	In4		In8		In13		In18	
	In1	2.999(2)	In4	2.957(2)	In2	2.841(2)	2 In9	3.040(3)
	In2	3.019(2)	In5	2.935(2)	In13	2.948(4)	2 In16	3.353(3)
	In5	2.913(2)	In6	2.993(2)	In14	2.978(3)	In18	2.885(5)
	In6	3.198(3)	In8	2.956(3)	In14	2.963(2)		
	In8	2.957(2)	In12	3.202(3)	In17	3.100(3)	Na1	3.54(1)
	In12	3.200(2)			In19	2.841(5)	Na9	3.15(1)
			Na2	3.65(1)			Na10	3.25(1)
	Na5	3.453(7)	Na10	3.324()	Na3	3.60(1)	2 Na13	3.57(1)
	Na8	3.50(1)	Na11	3.48(1)	Na4	3.323(8)		
	Na9	3.383(7)	Na13	3.68(1)	Na5	3.51(1)	In19	
	Na13	3.38(1)	Na13	3.70(1)	Na8	3.66(1)		
	Na13	3.500(9)	Na14	3.2626(9	Na12	3.433(8)	2 In13	2.841(5)
							2 In14	2.889(3)
	In5		In9		In14		In17	2.788(6)
							In19	2.760(10)
	In4	2.913(2)	In6	2.982(2)	In7	2.978(3)		
	In5	2.996(3)	In7	2.979(2)	In13	2.978(3)	Na4	3.50(2)
	In8	2.935(2)	In9	3.033(4)	In13	2.963(2)	2 Na7	3.83(2)
	In10	3.039(3)	In15	3.448(3)	In14	3.236(4)	2 Na12	3.69(1)
			In16	3.277(2)	In17	3.039(2)		
	Na5	3.43(1)	In18	3.040(3)	In19	2.889(3)		
	Na8	3.57(1)						
	Na9	3.49(1)	Na1	3.456(4)	Na3	3.50(1)		
	Na10	3.49(1)	Na3	3.49(1)	Na3	3.53(1)		
	Na11	3.406(6)	Na6	3.43(1)	Na7	3.375(9)		
	Na13	3.53(1)	Na8	3.45(1)	Na8	3.51(1)		
	Na13	3.80(1)	Na10	3.80(1)	Na12	3.248(8)		
	Na14	3.492(6)	Na13	3.73(1)				

Table III. (continued)

	Na1			**Na5**			**Na8**			**Na11**	
4	In7	3.501(4)	2	In1	3.51(1)		In2	3.46(1)	2	In5	3.406(6)
4	In9	3.456(4)	2	In2	3.535(7)		In4	3.50(1)	2	In8	3.48(1)
2	In11	3.71(1)	2	In4	3.453(7)		In5	3.57(1)	2	In10	3.40(1)
2	In15	3.400(7)	2	In5	3.43(1)		In6	3.61(1)		In12	3.34(1)
2	In16	3.325(7)		In10	3.44(1)		In7	3.61(1)		In16	3.12(1)
2	In18	3.54(1)	2	In13	3.51(1)		In9	3.45(1)			
				In17	3.37(1)		In10	3.61(1)		Na7	3.67(2)
	Na2						In13	3.66(1)	2	Na8	3.81(1)
				Na4	3.62(2)		In14	3.51(1)	2	Na13	3.73(1)
2	In3	3.43(1)	2	Na8	3.72(1)		In16	3.79(1)		Na14	3.30(2)
4	In6	3.528(4)		Na9	3.51(2)		In17	3.57(1)			
4	In8	3.65(1)								**Na12**	
				Na6			Na3	3.89(1)	2	In2	3.46(1)
2	Na6	3.69(2)					Na5	3.72(1)		In3	3.43(1)
2	Na10	3.61(1)	2	In3	3.32(1)		Na7	3.45(1)	2	In7	3.52(1)
	Na14	3.49(3)	2	In6	3.34(1)		Na11	3.81(1)		In11	3.32(1)
			2	In9	3.43(1)		Na13	3.59(1)	2	In13	3.433(8)
	Na3		2	In11	3.49(1)				2	In14	3.248(8)
				In15	3.69(1)			**Na9**	2	In19	3.69(1)
	In2	3.54(1)		In15	3.63(2)						
	In3	3.59(1)				2	In1	3.35(1)	2	Na3	3.56(1)
	In6	3.638(9)		Na2	3.69(2)	2	In4	3.383(7)		Na4	3.97(2)
	In7	3.427(9)	2	Na3	3.38(1)	2	In5	3.49(1)		Na7	3.99(2)
	In7	3.577(9)				2	In12	3.418(9)			
	In9	3.49(1)		**Na7**			In18	3.15(1)		**Na13**	
	In11	3.54(1)									
	In13	3.60(1)	2	In7	3.56(1)		Na5	3.52(2)		In4	3.38(1)
	In14	3.50(1)	2	In10	3.53(1)		Na9	3.85(3)		In4	3.500(9)
	In14	3.53(1)	2	In14	3.375(9)		Na10	3.46(2)		In5	3.53(1)
	In15	3.80(1)		In16	3.66(2)	2	Na13	3.69(1)		In5	3.80(1)
	In15	3.85(1)	2	In17	3.40(1)					In6	3.546(9)
			2	In19	3.83(2)			**Na10**		In8	3.68(1)
	Na3	3.59(2)					In8	3.70(1)		In9	3.73(1)
	Na6	3.38(1)	2	Na8	3.45(1)	2	In5	3.49(1)		In12	3.242(9)
	Na8	3.89(1)		Na11	3.67(2)	2	In6	3.268(9		In16	3.86(1)
	Na12	3.56(1)		Na12	2.99(2)	2	In8	3.324(8)		In18	3.57(1)
						2	In9	3.80(1)			
							In18	3.25(1)		Na8	3.59(1)
										Na9	3.69(1)
	Na4						Na2	3.61(1)		Na10	3.49(1)
							Na9	3.46(2)		Na11	3.73(1)
2	In1	3.31(2)				2	Na13	3.49(1)			
4	In2	3.452(6)								**Na14**	
4	In13	3.323(8)									
2	In19	3.50(2)							4	In5	3.492(6)
									4	In8	3.262(9)
2	Na5	3.62(2)							2	In10	3.40(2)
2	Na12	3.97(2)									
										Na2	3.49(3)
									2	Na11	3.30(2)

Table IV. Positional parameters and B_{eq} for Na_2In

atom	posn	x	y	z	B_{eq}
In1	8 c	0.28762(6)	0.04329(8)	0.12622(7)	2.13(3)
In2	8 c	0.05297(7)	0.6735(1)	0.52604(7)	2.98(4)
Na1	4 a	0.0659(5)	0	0	3.3(3)
Na2	4 b	0	0.5897(7)	1/4	3.6(3)
Na3	8 c	0.3020(4)	0.1963(5)	0.4181(5)	4.0(3)
Na4	8 c	0.1219(3)	0.2749(5)	0.2077(4)	3.5(2)
Na5	8 c	0.3625(4)	0.4131(6)	0.1673(5)	4.1(3)

Table V. Distances of Nearest Neighbors About Each Atom in Na_2In

	In1			**Na1**		**Na3**		**Na5**
In1	3.066(2)	2	In1	3.434(6)	In1	3.349(5)	In1	3.399(5)
In2	3.068(1)	2	In2	3.336(3)	In1	3.582(5)	In1	3.462(5)
In2	3.152(1)	2	Na3	3.389(6)	In1	3.695(5)	In2	3.320(5)
Na1	3.434(6)	2	Na4	3.532(5)	In2	3.696(5)	In2	4.180(6)
Na2	3.309(1)	2	Na5	3.521(8)	In2	3.707(6)	Na1	3.521(8)
Na3	3.349(5)	2	Na5	4.110(6)	Na1	3.389(6)	Na1	4.110(6)
Na3	3.582(5)				Na2	3.510(6)	Na2	3.570(7)
Na3	3.695(5)				Na3	3.97(1)	Na3	3.531(7)
Na4	3.318(5)				Na4	3.582(7)	Na3	3.616(7)
Na4	3.222(5)				Na4	3.575(7)	Na3	3.837(8)
Na5	3.399(5)				Na4	4.143(7)	Na4	3.526(7)
Na5	3.462(5)				Na5	3.531(7)	Na4	3.582(7)
	In2			**Na2**	Na5	3.616(7)	Na5	4.22(1)
In1	3.068(1)	2	In1	3.309(1)	Na5	3.837(8)	Na5	4.28(1)
In1	3.152(1)	2	In2	3.410(2)		**Na4**		
In2	3.127(2)	2	In2	3.590(4)	In1	3.318(5)		
Na1	3.336(3)	2	Na3	3.510(6)	In1	3.222(5)		
Na2	3.410(2)	2	Na4	3.292(7)	In2	3.306(5)		
Na2	3.590(4)	2	Na5	3.570(7)	In2	3.263(5)		
Na3	3.696(5)				Na1	3.532(5)		
Na3	3.707(6)				Na2	3.292(7)		
Na4	3.306(5)				Na3	3.582(7)		
Na4	3.263(5)				Na3	3.575(7)		
Na5	3.320(5)				Na4	3.52(1)		
Na5	4.180(6)				Na5	3.526(7)		
					Na5	3.582(7)		

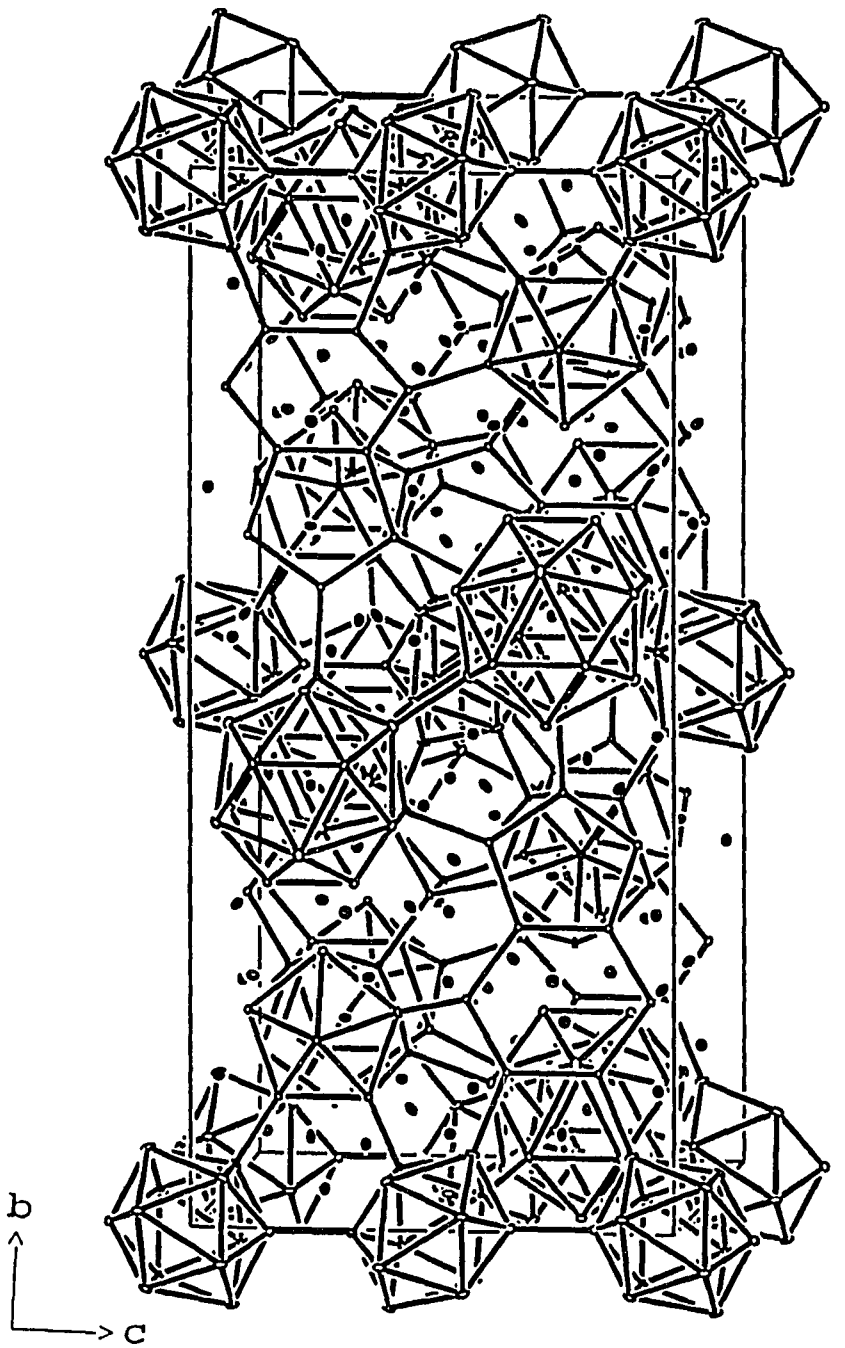

Figure 1. A view of the unit cell of $Na_{15}In_{27.4}$ slightly off [011]. Lines connect all In atoms <3.5 Å apart, while Na atoms are shown as dots.

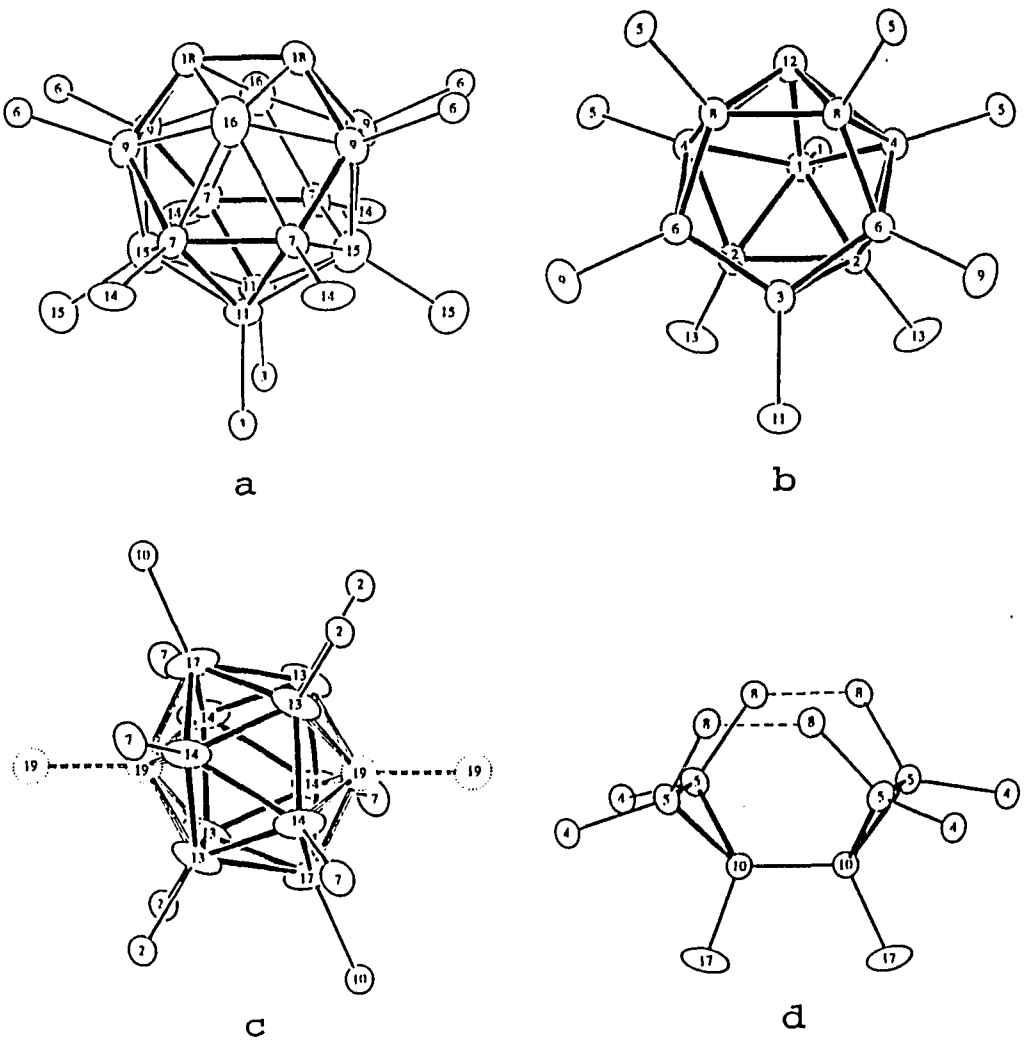

Figure 2. The individual clusters in $Na_{15}In_{27.4}$ with exo bonds included (a) icosioctahedral In_{16}, where In_{15} is 100% occupied at the indium-rich limit $Na_{15}In_{27.4}$, but ~64% at the sodium-rich boundary $Na_{15}In_{27.16}$, (b) *nido*-In_{11} type *A*, (c) *nido*-In_{11}, type *B*, in which the In19 position refines to slightly over 50% occupancy throughout the range, (d) the pairs of indium triangles, all of four-bonded indium.

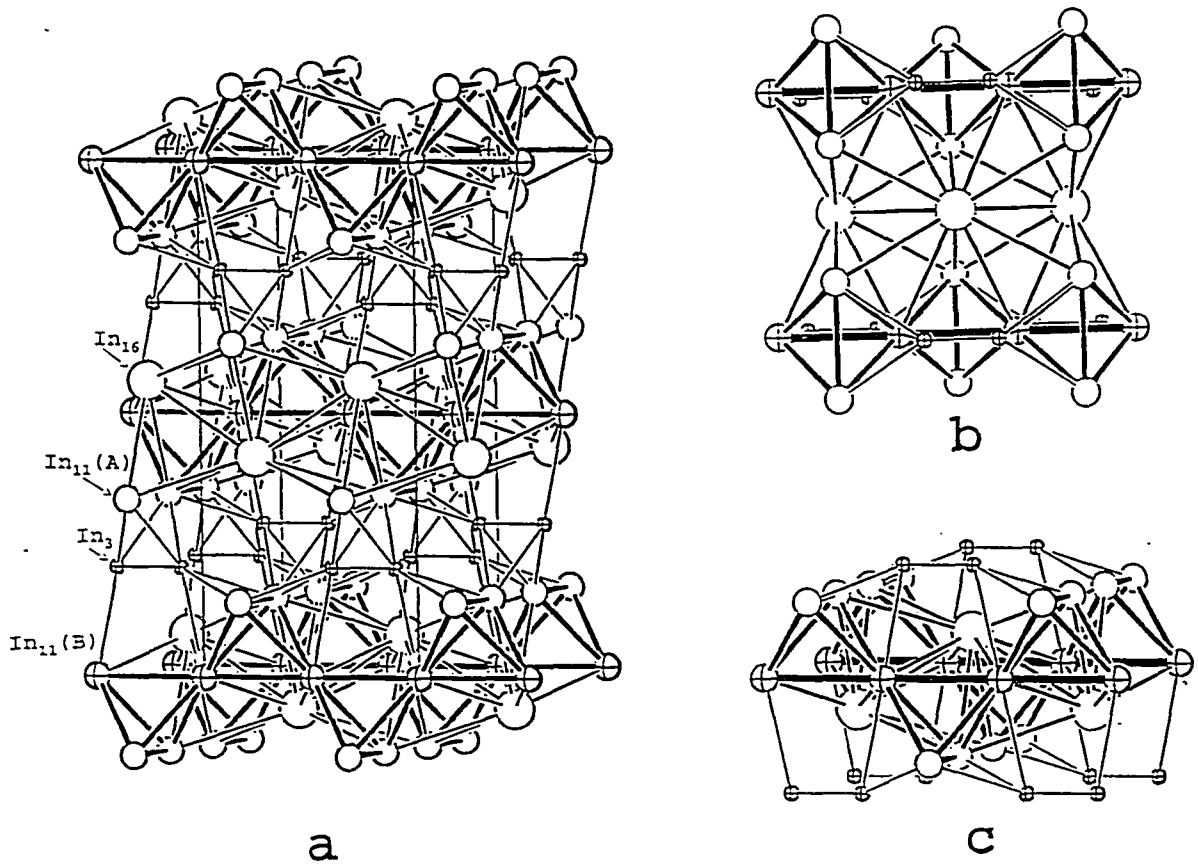

Figure 3. (a) A view of the indium sublattice in $Na_{15}In_{27.4}$ in which large, medium and medium crossed circles represent In_{16}, In_{11} (A) and In_{11}(B) cluster, respectively, and small crossed circles, the In_3 units. The orientation is the same as in Fig. 1, (b) a [101] view of a portion of the cluster layers in Fig. 3a. The tetrahedral arrays of 2 In_{11} (A) and 2 In_{11} (B) clusters are emphasized, (c) the same unit viewed slightly off [011].

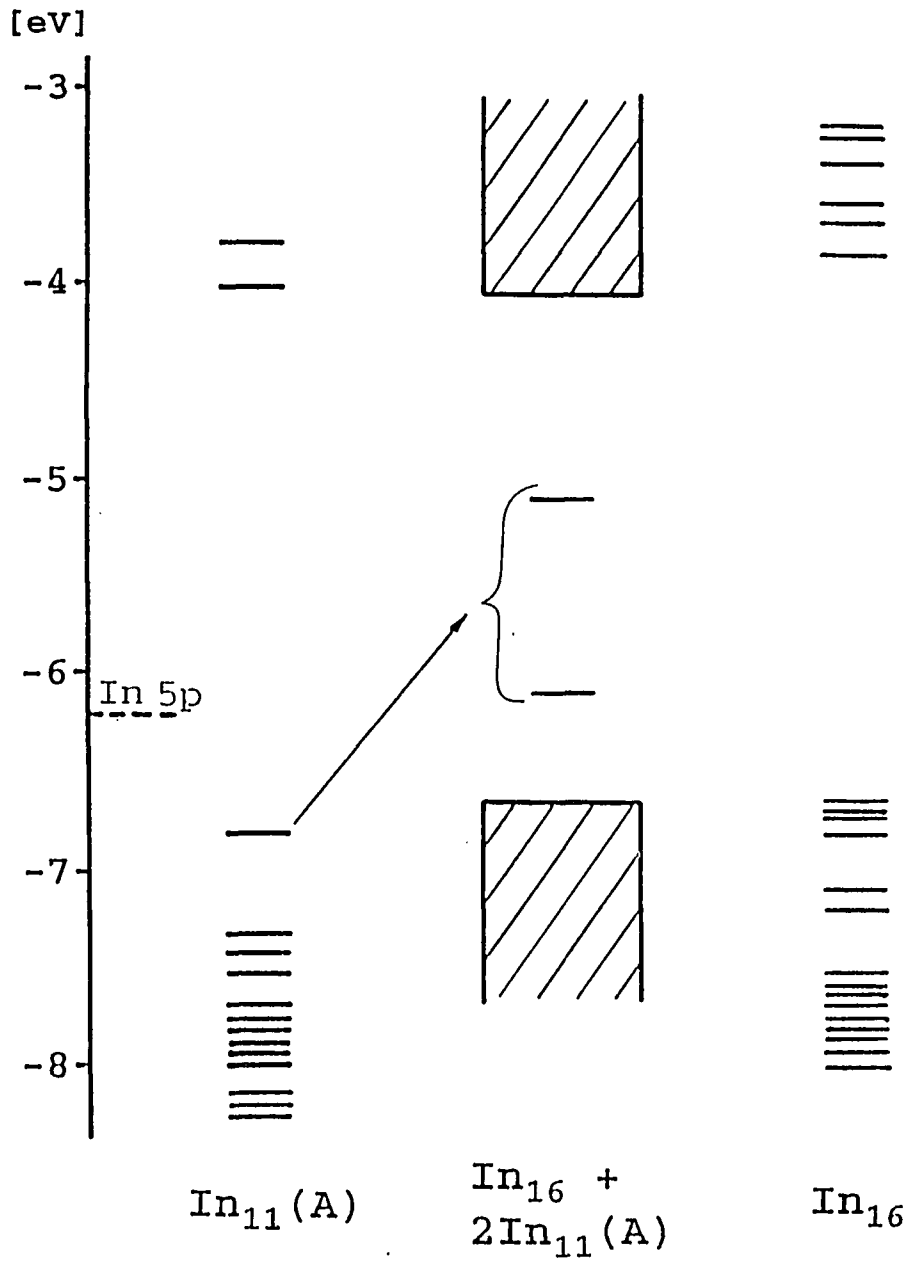

Figure 4. The results near the valence gap from EHMO calculations for In_{11} (A) (left), In_{16} (right), and the result of the nonbonding interactions between 2 In_{11} (A) In_{16} (center). Hatched areas denote the region of unchanged M.O. energies. (Three pairs of In_{16} levels are not separable on this scale.)

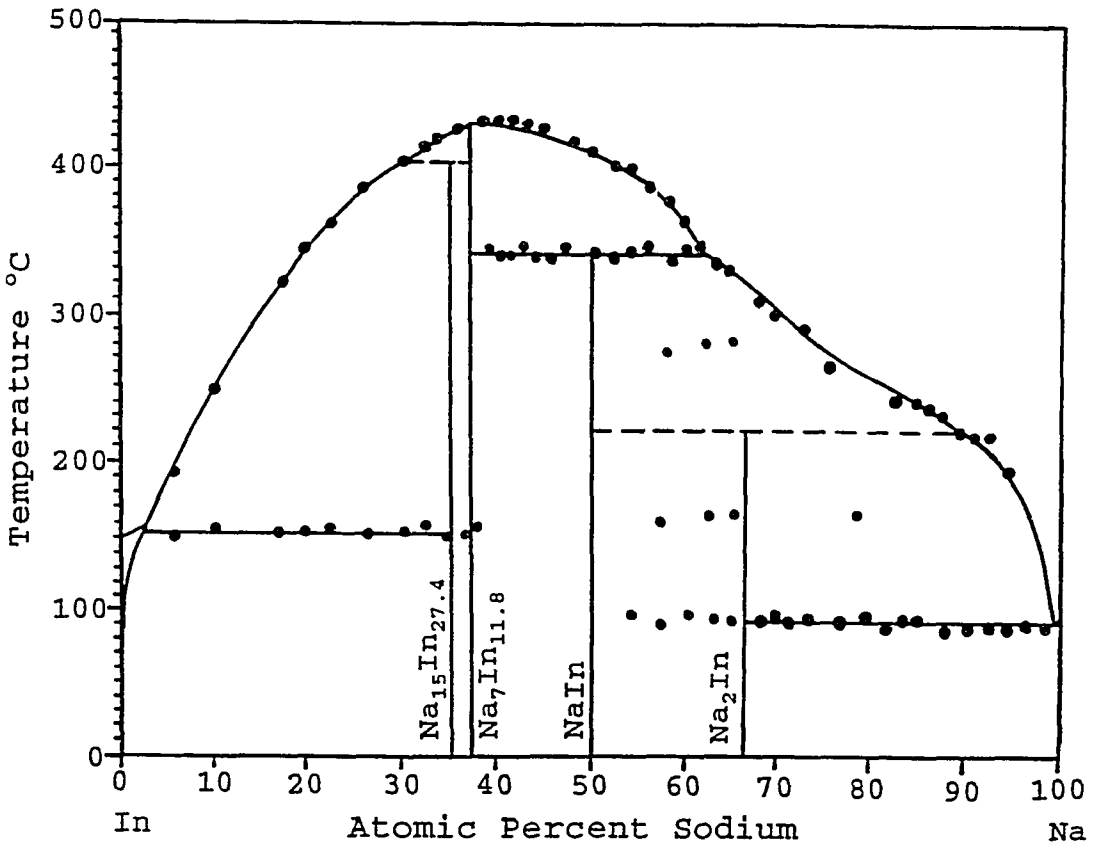

Figure 5. The revised In–Na phase diagram based on the cooling curve results of Thümmel and Klemm (*4*) accepted fixed point data (*1,2*), and the synthetic and structural studies of $Na_7In_{11.8}$ (*6*), $Na_{15}In_{27.4}$ and Na_2In. The peritectic temperature for $Na_{15}In_{27.4}$ is arbitrary, while that for Na_2In is estimated from the liquidus behavior and a few equilibration results (see text).

SUPPLEMENTARY MATERIAL

Thermal parameters for Na_2In $(A^2)x10^2$

atom	U_{11}	U_{22}	U_{33}	U_{12}	U_{13}	U_{23}
In1	2.55(4)	2.70(4)	2.84(4)	0.15(3)	-0.43(4)	-0.01(4)
In2	4.21(6)	3.97(5)	3.15(5)	-1.94(5)	-0.51(4)	0.42(5)
Na1	3.8(4)	2.5(3)	6.4(5)	0	0	-0.1(3)
Na2	5.1(5)	3.6(4)	4.8(4)	0	1.1(4)	0
Na3	6.0(4)	4.2(3)	5.1(3)	0.6(2)	-0.1(3)	-0.5(3)
Na4	3.9(3)	4.7(3)	4.6(3)	-0.7(2)	0.3(2)	-1.2(2)
Na5	5.2(3)	5.1(3)	5.2(3)	-1.1(2)	-0.1(3)	-0.6(3)

Thermal parameters for $Na_{15}In_{27.8}$

atom	U_{11}	U_{22}	U_{33}	U_{12}	U_{13}	U_{23}
In1	0.014(1)	0.017(1)	0.013(1)	0.001(1)	0.0	0.0
In2	0.0156(9)	0.0173(8)	0.0138(8)	-0.0005(7)	0.0002(7)	-0.0014(7)
In3	0.017(1)	0.021(1)	0.015(1)	0.003(1)	0.0	0.0
In4	0.0174(9)	0.0196(8)	0.0136(8)	-0.0003(8)	-0.0008(7)	0.0017(7)
In5	0.0187(9)	0.0202(9)	0.0156(8)	-0.0036(7)	-0.0034(7)	0.0034(7)
In6	0.020(1)	0.0185(9)	0.0169(9)	0.0004(7)	0.0027(8)	0.0006(7)
In7	0.025(1)	0.0253(9)	0.0195(8)	-0.0046(8)	0.0051(8)	-0.0046(7)
In8	0.0189(9)	0.0187(8)	0.0151(8)	-0.0035(7)	-0.0000(7)	-0.0012(7)
In9	0.023(1)	0.033(1)	0.021(1)	-0.0061(9)	0.0050(8)	-0.0067(8)
In10	0.027(1)	0.016(1)	0.014(1)	0.0	0.0	-0.001(1)
In11	0.018(1)	0.017(1)	0.031(1)	0.001(1)	0.0	0.0
In12	0.020(2)	0.024(1)	0.018(1)	-0.005(1)	0.0	0.0
In13	0.017(1)	0.0204(9)	0.043(1)	0.0005(8)	-0.0050(9)	-0.0155(8)
In14	0.023(1)	0.0154(8)	0.048(1)	-0.0005(8)	0.013(1)	-0.0001(8)
In15	0.041(2)	0.041(2)	0.033(2)	0.0	0.0	0.006(1)
In16	0.028(2)	0.053(2)	0.029(2)	0.015(1)	0.0	0.0
In17	0.019(1)	0.017(1)	0.054(2)	0.0	0.0	0.011(1)
In18	0.058(2)	0.025(1)	0.021(1)	0.0	0.0	-0.004(1)
In19	0.030(3)	0.026(3)	0.026(3)	0.0	0.0	-0.001(2)
Na1	0.020(6)	0.032(6)	0.020(6)	0.0	0.0	0.0
Na2	0.02(1)	0.01(1)	0.04(1)	0.0	0.0	0.0
Na3	0.045(7)	0.027(5)	0.027(5)	-0.004(5)	0.005(5)	0.002(4)
Na4	0.04(1)	0.05(1)	0.01(1)	0.0	0.0	0.0
Na5	0.027(8)	0.018(7)	0.030(8)	0.0	0.0	0.001(6)
Na6	0.011(7)	0.042(8)	0.035(8)	0.0	0.0	0.022(7)
Na7	0.05(1)	0.041(9)	0.017(7)	0.010(8)	0.0	0.0
Na8	0.034(6)	0.034(6)	0.028(5)	0.005(5)	0.004(5)	0.001(4)
Na9	0.04(1)	0.022(8)	0.04(1)	0.0	0.0	-0.003(7)
Na10	0.018(7)	0.035(8)	0.025(7)	0.0	0.0	0.004(6)
Na11	0.019(8)	0.036(8)	0.033(8)	0.003(7)	0.0	0.0
Na12	0.017(8)	0.038(8)	0.023(7)	0.009(7)	0.0	0.0
Na13	0.033(6)	0.036(6)	0.036(6)	-0.002(5)	-0.005(5)	-0.017(5)
Na14	0.03(1)	0.04(1)	0.04(1)	0.0	0.0	0.0

PAPER 7. SYNTHESIS, CHARACTERIZATION AND BONDING OF INDIUM CLUSTERS: MULTIPHASE REGION IN THE QUASI-BINARY K_8In_{11} – $Na_7In_{11.8}$ SYSTEM WITH A NEW COMPOUND $(K,Na)_{23}In_{39}$

ABSTRACT

A series of compositions $K_{8-x}Na_xIn_{11}$ and $K_{7-x}Na_xIn_{12}$ (x = integer) were reacted at 550°C for 10 hours and then cooled slowly (3°/h) to room temperature. Five different phases have been identified in the system. Three of them, K_8In_{11}, $K_3Na_{26}In_{48}$, and $Na_7In_{\sim 12}$, have already been reported. The structures of the remaining two are reported here. The first one, $(K,Na)_{22}In_{39}$, occurs in the rhombohedral space group $R\bar{3}m$, Z = 6, with a = 16.620 (3), c = 42.904 (8) Å with the refined composition $K_{8.2(2)}Na_{13.8}In_{39}$. The second one, $(K,Na)_{23}In_{39}$, occurs in the orthorhombic space group *Pnma*, Z = 4, with a = 17.69 (1), b = 17.028 (8), c = 24.82 (1) Å for the composition $K_{15}Na_8In_{39}$. The structures were refined by single crystal means to R, R_w = 3.8, 5.3 and 4.8, 4.9% respectively. The rhombohedral phase is isostructural with Na_7In_{13} ($Na_{21}In_{39}$) when a probable error of one missing cation in the latter is corrected, and is also isostructural with the reported $K_{22.33}In_{39.67}$ when the improbable mixing of indium on a potassium site is avoided. This structure exists at the potassium end of the binary system as well as on the potassium-poorer side of the ternary system (*ca.* $0.4 \leq K/Na \leq 1.3$). The orthorhombic phase is almost isostructural with the reported $Na_{22}Ga_{39}$ but there are two changes. One is that one Ga atom on a general position becomes two indium atoms on special positions, and the second is that one alkali metal atom on special position in $Na_{22}Ga_{39}$ becomes on a general position and provides one more cation per formula in $(K,Na)_{23}In_{39}$. This structure exists at the potassium rich side of the ternary system (*ca.* $2.5 \leq K/Na \leq 6.0$). The main factor governing which phase appears at a particular stoichiometry is the atomic ratio of K to Na. The rhombohedral phase as refined has one electron in excess of the needed 138 electrons for bonding. The orthorhombic phase, on the other hand, is electronically balanced, 140 needed and also available. The two phases show metallic conductivity and small Pauli-like paramagnetism (ρ_{295} = 280 and 360 μΩ-cm, χ_M = (1.1 and 0.9) × 10^{-4} emu mol^{-1} for the rhombohedral and the orthorhombic phases, respectively).

INTRODUCTION

The binary alkali metal–gallium[1] and –indium[2-5] systems have already been studied quite extensively. Some ternary compounds in the gallium system have also been reported.[1] We have studied the mixed alkali metal–indium ternary systems and have already reported on $A_3Na_{26}In_{48}$ (A = K, Rb, or Cs), in a structure containing *closo*- and *arachno*-In_{12} clusters.[6] Since we also found two binary compounds, K_8In_{11} and $Na_7In_{11.8}$, with very similar stoichiometries,[2,3] we were interested to see to what extend each of them can accommodate atoms from the other alkali metal and at the same time preserve its structure. This exploration led to the two phases reported here.

Since the structures that we will be discussing are closely related to the reported phases $Na_{22}Ga_{39}$ and Na_7Ga_{13} in the gallium system,[7-9] a more detailed background for these phases is proper. These compounds have been surrounded with some controversy for some time. Ling and Belin[7] refined the structure of $Na_{22}Ga_{39}$ in the orthorhombic space group *Pnma*. Schäfer et al, on the other hand, refined the structure of a phase prepared in excess sodium in the same space group and with similar atomic positions but ended up with different stoichiometry of Na_7Ga_{13} which can be rewritten as $Na_{21}Ga_{39}$, or one cation short from the compound refined by Belin. The same group stated that the same composition, $Na_{21}Ga_{39}$, existed in a rhombohedral form ($R\bar{3}m$) when prepared in excess of gallium.[9] The refinements of the two structures, orthorhombic and rhombohedral $Na_{21}In_{39}$, were done on data sets with no absorption corrections applied and the final residuals were around 10%. Later, a very brief note on the structure of a compound written as $K_{22.33}In_{39.67}$ appeared the same group.[10] The compound was isostructural with the rhombohedral $Na_{21}Ga_{39}$, but one vacant position in the latter was refined with mixed occupancy of 1/3 potassium and 2/3 indium. Such mixing of alkali metal and indium atoms on one and the same position, although not impossible, seems very unlikely.

The rhombohedral $(K,Na)_{22}In_{39}$ phase that we report here is isostructural with both $K_{22.33}In_{39.67}$ and the rhombohedral $Na_{21}Ga_{39}$ when mixing of indium and alkali metal in the first is avoided and one more cationic position in the second is filled. This phase exists at the sodium-rich end and also in the binary K–In system. The orthorhombic $(K,Na)_{23}In_{39}$ phase is very closely related to the orthorhombic $Na_{22}Ga_{39}$ (and $Na_{21}Ga_{39}$). All gallium sites but one, and all sodium sites but one, are practically the same in these structures. The differences are that one gallium position of general type becomes two indium positions of special type, and one sodium position of special type becomes a general position.

EXPERIMENTAL SECTION

Syntheses

The reagents and the reaction techniques in welded tantalum tubing were described before.[3,6] All materials were handled in a N_2-filled glovebox.

Mixtures with compositions $K_{8-x}Na_xIn_{11}$ ($1 \leq x$ (integer) ≤ 7), $K_{7-x}Na_xIn_{12}$ ($1 \leq x$ (integer) ≤ 6), K_7In_{11} and $KNaIn_2$ were prepared and melted at 550°C for 10 hour. (The highest melting points in the Na–In and K–In systems are about 441 and 478°C respectively.) The samples were then slowly cooled to room temperature at 3° per hour rate. The products at the sodium-rich side appeared as brittle gray chunks with metallic luster. Those at the potassium-rich side were in form of bars fused together with metallic luster and a slightly yellowish color on reflected light.

Powder patterns were obtained from ground samples that were mounted between pieces of cellophane tape. An Enraf-Nonius Guinier camera, Cu $K_{\alpha 1}$ radiation (λ = 1.540562 Å), and NBS (NIST) silicon as internal standard were employed for this purpose. A least-squares refinement of the measured 2θ values together with those of the standard silicon lines was used to determine the lattice parameters of the different phases.

Structure determination

Diffraction data for $K_{8.2}Na_{13.8}In_{39}$ and $K_{15}Na_8In_{39}$ were collected on CAD4 and Rigaku AFC6R/RA single crystal diffractometers, respectively, at 23°C with monochromated Mo Kα radiation up to 2θ = 50°. The structures were refined with the aid of the TEXSAN package. Some details of the data collection and refinement for the two structures are listed in Table I. Unique aspects of the study follow:

$K_{8.2}Na_{13.8}In_{39}$. Few pieces were selected from the crushed product of a reaction loaded as $K_2Na_5In_{12}$ (K : Na : In = 6.5 : 16.25 : 39). These were sealed in glass capillaries and then

checked for singularity and eventual space group assignment by oscillation and Weissenberg techniques. One of them was chosen, aligned along an axis (which later appeared to be the *c* axis) and Weissenberg photographs from the zero and the first layers (*hk0* and *hk1*) were taken. These revealed a hexagonal cell with rhombohedral type extinction, and two mirror planes containing the *c* axis. The same crystal was mounted on the diffractometer, and the 25 reflections found in random search were indexed with the expected hexagonal cell. Data from one large octant in reciprocal space were collected with the extinction for rhombohedral space group being imposed. These were corrected for Lorentz and polarization effects, and for absorption with the aid of the average of three ψ-scans at different angles. The Wilson plot indicated a centrosymmetric space group and therefore $R\bar{3}m$ was chosen.

Direct methods provided ten peaks with distances appropriate for indium atoms, and they were so assigned. A few cycles of least-squares refinement and a difference Fourier map revealed nine atoms with different weights and distances appropriate for Na or K. Initially all of them were assigned as Na. This led to negative thermal parameters on two sodium atoms and to quite small thermal parameter on another one. The first two were then changed to potassium atoms, and the third was refined with mixed Na and K occupancy. The final refinement of the data, including a DIFABS empirical absoption correction, with anisotropic thermal parameters and a secondary extinction correction converged at R/R_w = 3.8/5.3%. The largest residual peaks in the final difference Fourier map were 2.9 e/Å^3, 1.48 Å from In10, and -3.4 e/Å^3. The occupancies of the indium atoms did not deviate by more than 1.8% (5σ) when the cations were held constant, and those of the potassium and of the sodium atoms by more than 6% (6σ) when the indium atoms were held constant, so all these were held at full occupancy. The refined stoichiometry of the compound is $K_{8.2(2)}Na_{13.8}In_{39}$. Later it was recognized that it is isostructural with the rhombohedral $Na_{21}Ga_{39}$[9] when one more cation is added to the latter, and

also isostructural with $K_{22.33}In_{39.67}$[10] when mixing of K and In on one cationic position is avoided.

$K_{15}Na_8In_{39}$. Bar-like crystals were picked from different reactions that gave this phase as a product. Many of them were checked by oscillation for singularity, but most were multiple crystals and also diffracted extremely poorly, although they were sometimes nicely shaped. One of them, from a reaction loaded as K_7NaIn_{11} (K : Na : In = 24.8 : 3.5 : 39), was chosen, and from two Weissenberg photographs on different layers, the crystal system was determined to be orthorhombic, and very much like body centered. This crystal was mounted on Rigaku AFC6R/RA diffractometer, and the 25 reflections found in random search were indexed with body centered orthorhombic cell with the expected dimensions. Data were collected, and the structure was refined (after direct method solution) in *Imma* down to R = 3.9%, but four indium atoms at that stage were abnormally close to each other and with partial occupancies. Another crystal chosen from a reaction loaded as $KNaIn_2$ (K : Na : In = 19.5 : 19.5 : 39) mounted on CAD4 single crystal diffractometer, showed the same body centered orthorhombic cell. At that time, it was thought that the previous crystal may have been multiple and data were collected from the second crystal for the same cell. The structure refinement revealed exactly the same problems. This was a very strong indication that the space group chosen is incorrect and probably misleading because of the weak diffraction of the crystals.

A third crystal, chosen again from the reaction loaded as $KNaIn_2$, was mounted on Rigaku AFC6R/RA single crystal diffractometer, and this time data were collected on a primitive orthorhombic cell, although the 25 reflections from the random search suggested the corresponding body centered cell. The crystal diffracted as weakly as the previous two (from two octants of data with 14419 reflections measured, only 2320 were with $I \geq 3\sigma_I$), and moreover, only 14% of the already low percentage of observed data were violations of the body

centering. After corrections for Lorentz and polarization effects, and for absorption with the aid of the average of three ψ-scans at different angles, the data were consistent with only one centrosymmetric space group, *Pnma*. Direct methods in this space group provided 23 peaks with distances appropriate for indium, and they were so assigned. A few cycles of least-squares refinement and a difference Fourier synthesis provided fifteen additional atoms with distances appropriate for K or Na. For the first trial, these were refined as potassium atoms but some of them produced very large thermal ellipsoids. Next, the multiplicities on all cations were varied. Six of the atoms showed less than 100% occupation with deviations more than 3σ. These six positions were then refined with mixed K and Na content. For all of them the potassium occupancies became either zero within 3σ or negative, and this was a good indication that these sites are probably occupied by only sodium atoms. After assigning them to sodium, the final refinement of the data, including a DIFABS empirical absorption correction, and anisotropic parameters on the indium atoms only led to R/R_w = 4.8/4.9%. The alkali metal atoms could not be refined anisotropically because of insufficient data owing to the poor diffraction. The ratio of unique reflections to th number variables was already 5 to 1, which also caused large standard deviations on all refined parameters (as an example, the deviations of the positional parameters are around 0.008 Å). The occupancies of the atoms did not deviate by more than 6% (3σ) for In when the cations were held constant, and by more than 16% (3σ) for K or Na with In fixed, so all were held at full occupancy in the final cycles. Na14 has very small and K8 very large thermal parameters but their occupancies did not deviate from unity by more than 2σ when varied. The largest residual peaks in the final difference Fourier map were 1.9 e/Å^3, 1.96 Å from In20, and -1.73 e/Å^3. The final refined composition of the compound is $K_{15}Na_8In_{39}$.

Physical properties

Electric resistivity and magnetic susceptibility data were obtained for nearly single phase samples of the rhombohedral $A_{22}In_{39}$ from reaction loaded as $K_2Na_5In_{12}$ (K : Na : In = 6.5 : 16.25 : 39), and of the orthorhombic $A_{23}In_{39}$ from a reaction loaded as $K_5Na_2In_{12}$ (K : Na : In = 16.25 : 6.5 : 39). The electrodeless "Q" method[12] was again used for the resistivity measurements, and data were taken at 170 and 295K. The magnetizations of 25 mg samples were measured at a field of 3 Tesla over 6–295K on a Quantum Design MPMS SQUID magnetometer. The techniques for the measurements and the sample holder are described elsewhere.[3]

RESULTS AND DISCUSSION

Structure description

$K_{8.2}Na_{13.8}In_{39}$. The final positional and thermal parameters and the important distances are listed in Tables II and III, respectively.

This phase is isostructural with the rhombohedral $Na_{21}Ga_{39}$[8] if one more cation is added in the latter. It contains two types of icosahedra (Figure 1) and a 15-atom "spacer" of interconnected indium atoms (Figure 2b). The first type icosahedron (In1, 2, 6, 7, Figure 1a) has C_{2h} symmetry and is 12-bonded to 4 icosahedra of the same type (In1 to In1), 2 icosahedra of the second type (In6 to In10), and 6 spacers (In2 to In3 and In7 to In8). The second type icosahedron (In9, 10, Figure 1b) has D_{3d} symmetry and is 6-bonded to 6 icosahedra of the first type (In10 to In6). The 15-atom spacer (In3, 4, 5, 8, Figure 2b) is 15-bonded to 6 icosahedra of the first type (In3 to In2 and In8 to In7) and 9 other spacers (In4 to In5). The indium network can be viewed as rhombohedrally distorted MgCu2- type Laves phase where the Cu sites are occupied by the icosahedra and the Mg sites by the 15-atom spacers. All alkali-metal atoms except K1 are positioned in the voids between the building blocks of indium. K1 occupies the centers of the 15 atom spacers. This position is the one left empty in $Na_{21}Ga_{39}$.[8] On the other hand, the Na2 position which is between 6 icosahedra and 2 spacers was refined with mixed K and In occupancy in $K_{22.33}In_{39.67}$.[10]

$K_{15}Na_8In_{39}$. The final positional and isotropic displacement parameters are listed in Table IV, the anisotropic displacement parameters for the indium atoms in Table V, and the important distances in Table VI. A general view of the unit cell in Figure 3 outlines all In–In distances less than 4.0 Å.

The structure is very similar to that of $Na_{22}Ga_{39}$[7] and the orthorhombic $Na_{21}Ga_{39}$.[9] (The latter would be isostructural with $Na_{22}Ga_{39}$ when one empty position is occupied by a

sodium atom.) All these structures have one and the same space group (*Pnma*) and similar lattice parameter ratios. Also, they are very similar with the above rhombohedral $A_{22}In_{39}$ in the types of the building blocks and the connectivity between them.

The indium network in $K_{15}Na_8In_{39}$ is again built of two types icosahedra (Figure 4) and a 15 atom "spacer" (Figure 2c). The first type icosahedron (In1, 6, 7, 10, 12, 16, Figure 4a) is centered the *4a* (0,0,0; 0,1/2,0; 1/2,0,1/2; 1/2,1/2,1/2; Figure 3) type positions and has C_i symmetry. It is 12-bonded to 2 icosahedra of the same type (In16 to In16), 4 icosahedra of the second type (In10 to In8 and In7 to In2), and 6 spacers (In1 to In9, In6 to In15, and In12 to In11). This icosahedron corresponds to the first type of icosahedron in $A_{22}In_{39}$ (Figure 1a) as well as in $Na_{22}Ga_{39}$.[7]

The second type icosahedron (In2, 3, 5, 8, 17, 18, 19, 20, Figure 4b) is centered at *4c* (x,1/4,z; $x \approx 1/4$, $z \approx 1/4$; Figure 3) type positions and has C_s symmetry. It is 7-bonded to 4 icosahedra of the first type (In2 to In7 and In10 to In8), 2 icosahedra of the same type (In17 to In20), and 1 spacer (In18 to In21). This icosahedron corresponds to the second type of icosahedron in $A_{22}In_{39}$ (Figure 1b) in which it is six- instead of seven-bonded with the bond to the spacer missing. It also corresponds to a 9-bonded icosahedron in $Na_{22}Ga_{39}$ which has two additional bonds to two more 15-atom spacers.

The 15-atom spacer (In4, 9, 11, 13, 14A, 14B, 15, 22, 23, Figure 2c) is centered at *4c* (x,1/4,z; $x \approx 1/2$, $z \approx 7/8$; Figure 3) type positions and has C_s symmetry. It is 15-bonded to 6 icosahedra of the first type (In9 to In1, In11 to In12, and In15 to In6), 1 icosahedron of the second type (In21 to In18), and 4 other spacers (In4 to In 13, In14A to In22, and In14B to In23).

The two types icosahedra are positioned in the same manner as in the rhombohedral $A_{22}In_{39}$ and in $Na_{22}Ga_{39}$, that is, they occupy the Cu positions in a $MgCu_2$-type Laves phase.

Furthermore, in this respect all of the above structures are related to the structures of $Na_7In_{11.8}$,[3] $Na_{15}In_{27.4}$,[5] and phases found in ternary Na–In–Zn, Na–In–Au, Na–In–Cd, and Na–In–Sn systems.[13] All these contain icosahedra connected to each other in a similar network, and the major differences come from the type and the bonding of the "spacer" that occupies the Mg sites in $MgCu_2$. In $Na_7In_{11.8}$ we find an 8-bonded *closo*-In_{16} as a spacer, in $Na_{15}In_{27.4}$ the same spacer is 12-bonded, and in a Zn substituted compound we find again the same spacer but this time 16-bonded. Another, Au-substituted structure has a 15-bonded *closo*-In_{15} cluster for a spacer, in a Cd-substituted structure it is a 12-bonded *arachno*-In_{18}, and in a Sn-substituted compound we find 9-bonded *closo*-In_{18}. In $Na_{22}Ga_{39}$, the 15-atom spacer is 13-bonded (Figure 2a), in $A_{22}In_{39}$ the same spacer is 15-bonded (Figure 2b), and finally in $A_{23}In_{39}$, the spacer has a different shape although it has again 15 atoms and is 15-bonded (Figure 2c).

All three spacers shown on Figure 2 have at least one mirror plane which is approximately perpendicular to the view direction. It can be seen that the only difference between the spacers on Figures 2a and 2b is that the first one has two exo bonds fewer than the second one, and therefore two three bonded atoms. On the other hand, the spacer on Figure 1c has a different geometry. A pair of atoms marked as 14 on Figure 2a and as 3 on Figure 2b are in general type positions with respect to the mirror plane in these two spacers. The same pair of atoms becomes two atoms on two special positions on the mirror plane in the third spacer (marked as 14A and 14B on Figure 2c). (In order to keep the numbering of the atoms as in the reported $Na_{22}In_{39}$, we used letters in addition to the number for atoms 14A and 14B.) The rest of the spacer remains the same, and the number of In atoms also does not change since one 8-fold position becomes two 4-fold positions. This switch of the direction of the pair of atoms leaves two 3-bonded indium atoms (marked as 13 in Figure 2c). Also, the pair of atoms 14A and 14B, instead of being exo bonded to icosahedra as in $Na_{22}Ga_{39}$, are exo bonded to another

spacer. This is the reason why we find 9-bonded icosahedron and 13-bonded spacer in $Na_{22}Ga_{39}$, and 7-bonded icosahedron and 15-bonded spacer in $A_{23}In_{39}$.

The alkali metal cations are positioned in between the building blocks of the indium network in a similar way as in $Na_{22}Ga_{39}$ and $A_{22}In_{39}$. The only major difference in $A_{23}In_{39}$ is the position of Na11. This cation caps the hexagonal ring of the spacers from the outside in $Na_{22}Ga_{39}$ and $A_{22}In_{39}$ (Figure 2a and 2b) and lies on a special position on the mirror plane through the spacers. In A_{23}In39 there is no hexagon in the spacer, and the cation becomes on a general position above and below the mirror plane (Figure 2c). This leads to 23 instead of 22 cations per 39 indium atoms in the formula. We should point out here that this position is occupied preferentialy by the smaller cation sodium.

Electronic structure and electron count

It has been shown by R. B. King[14] and confirmed by Burdett and Canadell[15] that there is a double Ga=Ga bond between the two three bonded atoms in the 15-atom spacer in $Na_{22}Ga_{39}$ (atoms 22 and 23 on Figure 2a). Also, calculations show that there is a 3-center 2-electron bonding within the triangles that share all edges in the spacers of the three structures (atoms 11, 11, 21 in Figure 2c, as an example). With this and the Wade's rules in mind, we can calculate the numbers of electrons needed for bonding in $Na_{22}Ga_{39}$, $A_{22}In_{39}$ and $A_{23}In_{39}$ in the following way:

a) $Na_{22}Ga_{39}$ - Each formula unit has one 12-bonded icosahedron which requires 26 (skeletal) + 12 (exo bonds) = 38 electrons, one 9-bonded icosahedron which requires 26 (skeletal) + 9 (exo bonds) + 3 × 2 (lone pairs) = 41 electrons, and one 13-bonded 15-atom spacer which requires 20 × 2 (2-center, 2-electron bonds) + 1 × 4 (double bond) + 1 × 2 (3-center, 2-electron bond) + 13 (exo bonds) = 59 electrons. The total is **138** electrons.

b) $A_{22}In_{39}$ - Each formula unit has one and a half 12-bonded icosahedron which requires 1.5 × [26 (skeletal) + 12 (exo bonds)] = 1.5 × 38 = 57 electrons, one half of a 6-bonded icosahedron which requires 0.5 × [26 (skeletal) + 6 (exo bonds) + 6 × 2 (lone pairs)] = 0.5 × 44 = 22 electrons, and one 15-bonded 15 atom spacer which requires 21 × 2 (2-center-2-electron bonds) + 1 × 2 (3-center-2-electron bond) + 15 (exo bonds) = 59 electrons. The total is **138** electrons.

Both structures have also one and the same stoichiometry and, therefore, the same number of electrons available, which is 22 + 39 × 3 = 139. This means that the two structures have one extra electron per formula (assuming full occupancy of all sites).

c) $A_{23}In_{39}$ - In a similar way one can count the number of electrons needed for bonding in the orthorhombic $A_{23}In_{39}$. For the 12- and 7-bonded icosahedra we get 26 (skeletal) + 12 (exo bonds) = 38 and 26 (skeletal) + 7 (exo bonds) + 5 × 2 (lone pairs) = 43 electrons, respectively. A problem arises with counting the electrons needed for bonding within the 15-atom spacer, and particularly with In13 which is 3-bonded. If one were to assign an additional lone pair of electrons to each In13, the number of electrons becomes 20 × 2 (2-center, 2-electron bonds) + 1 × 2 (3-center, 2-electron bond) + 2 × 2 (lone pairs on In13) + 15 (exo bonds) = 61. In this case the total number of electrons needed per formula unit will be 38 + 43 + 61 = 142. On the other hand, if the lone pairs on In3 are left off, the total becomes 138. The number of electrons available is 23 + 39 × 3 = 140. This means that the number of needed electrons cannot possibly exceed this number, and the case in which the lone pairs on all In13 are filled automatically becomes impossible.

In order to determine correctly the number of electrons needed for bonding in $A_{23}In_{39}$, we performed extended-Hückel MO calculations on the 6-bonded square In4, 13, 4, 13 which connects two spacers (Figures 2 and 5). The result showed that the two lone pairs on In13 are

predominantly p_z orbitals and are involved in π-bonding interactions with the p_z orbitals on the In4 atoms. Before going further on discussing the consequences of this, we should explain how the p_z orbitals on In4 become available for the π-bonding.

More detailed study of the bonding at In4 shows that, although four bonded, its coordination deviates very much from tetrahedral. Since In11 and In21 (Figures 2 and 5) are not only bonded to In4 but also to each other (3.15 (1) Å), they form triangle together with In4. This leads to a very small angle at In4, 63.3 (3)°. The angles In11–In4–In13 and In21–In4–In13, on the other hand, become very close to 120° (129.7(3)°, 122.3(3)°, 128.5(3)°, and 123.9(3)°). This means that the hybridization on In4 is much closer to sp^2 than to sp^3. The small angle In11–In4–In21 will cause smaller participation of the In4 p_z orbitals in the In4–In11 and In4–In21 exo bonding, and therefore free up these orbitals to some extend for π-bonding within the square. The latter (Figure 5) is perfectly flat (with an inversion center), and although not perfect square, it is very close to a rectangle. Its edges are 2.83(1) and 3.04(1) Å, and the angles on In4 and In13 are 92.3(3)° and 87.7(3)°, respectively.

The availability of π-type p_z orbitals on In4 and In13 and the planar and nearly square arrangement resembles to great extend a molecule of cyclobutadiene. The facts that In4 is 4-bonded, and 3-bondd In13 is not planar makes this formation also similar to cyclobutane. The results from the extended-Hückel MO calculations show four π-type molecular orbitals as in cyclobutadiene. The lowest one energetically (a_{2u} in ideal D_{4h}) is π-bonding within the square and σ-bonding to the exo atoms. The next two orbitals correspond to the e_g type orbitals in idealized cyclobutadiene. These are nonbonding within the square (2 nodes) but bonding to the exo atoms. In our case, as in cyclobutadiene, this doubly degenerate orbital experience an Jahn-Teller distortion and becomes two nondegenerate orbitals. This, of course, leads to distortion of the ideal square to a rectangle-like shape with two short and two long edges. Again, as in

cyclobutadiene, the orbital that is bonding along the shorter edge and antibonding along the longer edge becomes with lower energy (not shown) than the one opposite to this. The latter is left empty in cyclobutadiene, but in our case it is stabilized to some extent by σ-bonding to the exo atoms and becomes the HOMO (Figure 5a). Finally, the fourth and highest orbital in energy (b_{1u} in ideal D_{4h}) is π-antibonding (4 nodes) within the square and σ-bonding to the exo atoms (Figure 5b). The antibonding interactions are quite strong and overcome the bonding ones, and this orbital becomes the LUMO *ca.* 1.0 eV higher in energy than the HOMO. This orbital would have been stabilized further and eventually filled had the In13 atoms had two instead of one exo neighbors.

Such a case where all four atoms of a square are 4-bonded is presented by another formation in the very same structure. The atoms In14A, 14B, 22, 23 form such a square (Figure 2c) in which each atom is bonded in a similar manner to In4 to 2 exo atoms together with which it forms a nearly equilateral triangle (ΔIn15–In14A–In15, ΔIn9–In14B–In9, ΔIn15–In22–In15 and ΔIn11–In23–In11). The angle formed with the two exo atoms is close to 60° for all of the atoms in the square meaning that their p_z orbitals are freed up for π-type interactions. The square is again perfectly flat (all atoms are in a mirror plane). The extended-Hückel calculations showed the same set of four π-type molecular orbitals. This time, because of additional stabilization through σ-bonding to 8 rather than 6 exo atoms, even the highest in energy, π-antibonding orbital has a lower energy and is filled. The square also experiences Jahn-Teller distortion and becomes again more rectangle-like with edges of 2.83(1), 2.87(2), 2.97(1) and 3.01(1) Å and angles of 92.0(4)°, 88.8(4)°, 90.5(4)° and 88.7(4)°. The π-interactions of the p_z orbitals are also responsible for the quite shorter In–In distances of around the squares, 2.83 to 2.87 Å compared to the usual 2.95 Å and above.

We saw earlier that the molecular orbital in the square In4, 13, 4, 13 that involves the lone pairs on In13 is left empty. This means that, formally, only one out of every two In13 atoms will have a filled lone pair of electrons, the lone pair on the other one will remain empty. Now we can determine correctly the number of electrons needed for bonding in the 15-bonded 15-atom spacer in $A_{23}In_{39}$. They become 20×2 (2-center-2-electron bonds) + 1×2 (3-center-2-electron bond) + 1×2 (filled lone pair on one In13) + 15 (exo bonds) = 59 electrons. Surprisingly, this is the same number as for the spacers in $Na_{22}Ga_{39}$ and $A_{22}In_{39}$. This number combined with the numbers of electrons needed for bonding in the two types icosahedra (38 and 43, above) totals 140 electrons. The same, $23 + 39 \times 3 = 140$, is the number of electrons available, as we saw before, and this means that the structure should be electronically balanced, a Zintl phase.

Properties

The resistivities of $A_{22}In_{39}$ (loaded composition $K_2Na_5In_{12}$) and of $A_{23}In_{39}$ (loaded composition $K_5Na_2In_{12}$) at 295 K are about 280 and 360 μΩ-cm. Another measurement on the same samples at 170 K showed smaller resistivities of about 200 and 230 μΩ-cm for $A_{22}In_{39}$ and $A_{23}In_{39}$. This is indicative of metallic type conductivity and, assuming a linear ρ *vs.* T relation, we can calculate approximate temperature coefficients of +0.24 and +0.28% K^{-1}, respectively, for the two phases. The room temperature values are comparable to those of the metallic $Na_7In_{11.8}$ and $Na_{15}In_{27.4}$, 540 and 290 μΩ-cm, respectively, and also to that of the electronically balanced Na_2In, 270 μΩ-cm.

Magnetic measurements gave temperature independent susceptibilities for the two phases, -1.65×10^{-3} and -1.73×10^{-3} emu mol^{-1} for $A_{22}In_{39}$ and $A_{23}In_{39}$, respectively, over 30–295 K. Two types of diamagnetic corrections are appropriate. Those for K^+, Na^+ and In^{3+} ion cores[16] total -9.17×10^{-4} emu mol^{-1} for $A_{22}In_{39}$ and -9.76×10^{-4} emu mol^{-1} for $A_{23}In_{39}$. As before,[3]

correction for the Larmor precession of the electron pairs in cluster orbitals is appropriate. For r_{ave}, we used 2.4 Å calculated for an icosahedron in $Na_7In_{11.8}$. This gives -4.2×10^{-4} emu mol^{-1} per cluster additional diamagnetic correction for each of the two icosahedra per formula unit. The corrected susceptibilities become $\chi_M = +1.1 \times 10^{-4}$ and $+0.9 \times 10^{-4}$ emu mol^{-1} for $A_{22}In_{39}$ and $A_{23}In_{39}$, respectively. These values are consistent with small Pauli paramagnetic terms, as also observed for $Na_7In_{11.8}$ and Na_2In.

The electric resistivity and the magnetic susceptibility measured for $A_{22}In_{39}$ are consistent with the electronic expectations for this structure (above). The $A_{23}In_{39}$ structure, on the other hand, is expected to be semiconducting from straightforward electron counting (above), but the weak metallic conductivity and the small positive magnetic susceptibility measured contradict the expectations. Such mismatch between expected and measured properties has already been observed for a few other compounds. Na_2In,[5] Rb_2In_3[4] and $K_8In_{10}Zn$[6] are diamagnetic but metallic, although all are expected to be electronically balanced, Zintl phases. Also, calculations based on an augmented spherical wave method involving both Na and Sn states show that β-NaSn should be a semiconductor.[17] Conducitvity measurements show a contrary metallic property. In our case there are two major sources of possible errors in the measurements. One comes from the quite approximate numbers used for diamagnetic ion core corrections.[16] This combined with the small magnetic susceptibilities measured for these compounds will lead to large uncertainty in the corrected values. The second source of error comes from measuring the electrical conductivity by a very approximate technique, the "Q" method, which is accurate by a factor of three. Semiconductors with small gaps could give magnetic susceptibility and electrical conductivity results that would place them in a category with the metals. Also, mixing of alkali-metal states in and broadening of the conduction and valence bands may lead to some small but nonzero density of states at the Fermi level.

Ranges of existence of $A_{22}In_{39}$ and $A_{23}In_{39}$

All loaded compositions and the lattice parameters of the major product in each are listed in Table VII. Also added there is the result from treating reaction 16 under similar conditions which we reported before.[3] The reactions are listed in order of decreasing K to In atomic ratio.

The rhombohedral $A_{22}In_{39}$ forms at the binary K–In end, as expected, but also at the potassium-poor side of the ternary system. The orthorhombic $A_{23}In_{39}$ does not form without Na, but only a small amount (reaction 2, K : Na = 7 : 1) is sufficient. The two phases have quite wide ranges of stability in terms of the K to Na ratio. O–$A_{23}In_{39}$ exists at least from K : Na = 6 : 1 to 2.5 : 1, and R–$A_{22}In_{39}$ has minimum ranges of K : Na = 1.33 : 1 to 0.40 : 1. It is clear from the Table that the alkali metal to indium ratio is not the controlling factor for the phases' existences since all reactions were loaded with similar A : In proportions. It appears that the principal factor responsible for which structure forms is the K : Na atomic ratio. The $A_{22}In_{39}$ structure forms at the binary K–In end, but in the presence of Na it forms again only when the K to Na ratio falls below 1.33 : 1. (In reactions 5 and 8 the ratio K : Na is 1:1 but the product is the orthorhombic instead of the rhombohedral structure. Since these reactions are alkali metal-rich and give alkali metal as a side product, the real ratio K : Na in the major product is not clear.) Above this ratio, the orthorhombic structure is more stable. This means that the availability of a certain number of the large potassium cations is crucial for the stability of the orthorhombic $A_{23}In_{39}$ phase. Also, since the alternative rhombohedral structure can form with large cations in the K–In binary, the size of the cations should not be a reason for its nonexistence at the potassium-rich side. The conclusion is that there must be other reasons for the preferred formation of the orthorhombic structure at this side on the ternary system. One such reason could be that $A_{23}In_{39}$ is electronically balanced while $A_{22}In_{39}$ has an extra electron

per formula. It is plausible, therefore, to prefer the phase with lower absolute electronic energy over another otherwise possible phase but with higher energy.

The next question to be answered is what causes the disappearance of $A_{23}In_{39}$ at lower K to Na atomic ratios. As discussed above, the two structures are very similar. The major difference between them is that in $A_{23}In_{39}$ we find two indium atoms on different positions from $A_{22}In_{39}$. The changes lead to more space and two cavities large enough to accommodate two of the smaller sodium cations instead of one large potassium cation. Apparently, this is possible only in the presence of enough of the large cations of potassium to prop the structure open. When the number of potassium "pillars" exchanged by sodium atoms exceeds a critical number, the space needed to fit the extra sodium cation disappears, the two indium atoms change positions, and the structure switches to $A_{22}In_{39}$. When no sodium is present, although the structure is "open" by the potassium cations, it exists only as $A_{22}In_{39}$ since there are no small cations to fill an eventual small size cavity.

Decreasing the K to Na ratio even further leads next to formation of the line phase $K_3Na_{26}In_{39}$ in which three sites larger than the rest are occupied by potassium cations only.

The volume per atom of In (Table VII) is calculated by dividing the unit cell volume by the number of indium atoms in it. Within the range of existence of each of the two structures, the volume decreases with decreasing the K : Na ratio. When plotted versus the sodium atomic fraction, the volumes per atom indium fall on two straight lines, one for the orthorhombic (0.5 $Å^3$ maximum deviation) and one for the rhombohedral (0.25 $Å^3$ maximum deviation) structures. The second one, if projected, includes the binary $K_{22}In_{39}$ and passes near by $K_3Na_{26}In_{48}$ and $Na_7In_{11.8}$. The lattice parameters also follow this pattern. Some of them have quite large standard deviations because of broad lines in the observed powder pattern and also, sometimes, because of very closely positioned lines from a second phase.

The switch from $A_{22}In_{39}$ to $A_{23}In_{39}$, reactions 8 and 9, is accompanied by quite large decline of the volume per In atom, 47.90(2) to 46.009(1) $Å^3$, although the K to Na ratio in reaction 9 (1.33 : 1) is larger than that in reaction 8 (1 : 1). This proves once more that $A_{22}In_{39}$ indeed has fewer cations than $A_{23}In_{39}$. The same effect can be seen in comparing reactions 1 and 2 although it is less pronounced.

The formula of $K_3Na_{26}In_{48}$ can be rewritten as $A_{23.56}In_{39}$. It is richer in alkali metal even than $A_{23}In_{39}$, but the volume per In atom decreases further because it has smaller K to Na ratio. In $Na_7In_{11.8}$, which can be rewritten as $Na_{22.75}In_{39}$, this volume reaches a minimum because of the presence of sodium cations only.

More on the relations to $MgCu_2$

We have already discussed the similarities between $A_{22}In_{39}$, $A_{23}In_{39}$ and $MgCu_2$. Here, we will present more quantitative relationships between these structures. The rhombohedral cell of $A_{22}In_{39}$ can be converted to rhombohedrally-distorted face-centered cubic cell. As an example, the lattice parameters of the unit cell from reaction 9 can be rewritten as a = b = c = 24.31 Å and $\alpha = \beta = \gamma = 87.98°$. This would be a face-centered cubic cell that is stretched only a little bit along one of its body diagonals. The orthorhombic cell of $A_{23}In_{39}$ can be converted to monoclinically distorted face centered cubic cell. As an example, the lattice parameters of the unit cell from reaction 4 can be rewritten as a = b = 24.71, c = 25.01 Å, and $\alpha = \beta = 90°$, $\gamma = 87.81°$. This would be a face-centered cubic cell that is stretched a little along one of its face diagonals with also a slight compression along the edge perpendicular to the distorted face. The space groups $R\bar{3}m$ of $A_{22}In_{39}$ and *Pnma* of $A_{23}In_{39}$ are subgroups of $Fd\bar{3}m$ which is the space group for $MgCu_2$. This means that the two structures can be converted to each other by going through the cubic cell and without major structural rearrangements. It is not surprising then, that a binary potassium phase (around K : In = 1 : 1) with a space group $Fd\bar{3}m$ and lattice parameter

a ≈ 24.63 Å exists.[13] The compound has not been structurally characterized completely, but from the partial solution, it is clear that there are icosahedra positioned at the Cu sites in $MgCu_2$ and interconnected very similarly as in $A_{22}In_{39}$ and $A_{23}In_{39}$. Also, a cubic phase $Na_9In_{16.74(6)}Zn_{2.29}$ with space group $Fd\bar{3}m$ and lattice parameter a = 22.715(7) Å was found in the ternary Na–In–Zn system.[13] Again, it has icosahedra at the Cu sites in $MgCu_2$ structure, but also it has 16-bonded *closo*-In_{16} icosioctahedron at the Mg sites.

REFERENCES

1. Belin, C.; Charbonnel, M. T. *Prog. Sol. St. Chem.* **1993**, *22*, 59.
2. Sevov, S. C.; Corbett, J. D. *Inorg. Chem.* **1991**, *30*, 4875.
3. Sevov, S. C.; Corbett, J. D. *Inorg. Chem.* **1992**, *31*, 1895.
4. Sevov, S. C.; Corbett, J. D. *Z. Anorg. Allg. Chem.* **1993**, *619*, 128.
5. Sevov, S. C.; Corbett, J. D. *J. Sol. St. Chem.* **1993**, in press.
6. Sevov, S. C.; Corbett, J. D. *Inorg. Chem.* **1993**, *32*, in press.
7. Ling, R. G.; Belin, C. *Acta Cryst.* **1982**, *B38*, 1101.
8. Cordier, U. F.; Cordier, G.; Schäfae, H. *Z. Naturforsch.* **1982**, *37b*, 119.
9. Cordier, U. F.; Cordier, G.; Schäfer, H. *Z. Naturforsch.* **1982**, *37b*, 127.
10. Cordier, G.; Müller, V. *Z. Krist.* **1992**, *198*, 302.
11. *"Binary Alloy Phase Diagrams"* 2nd ed., American Society for Metals, Metals Park, Ohio 440073, vol. 3, pp. 2261, 2250, respectively.
12. Shinar, J.; Dehner, B.; Beaudry, B. J.; Peterson, D. T. *Phys. Rev.* **1988**, *37B*, 2066.
13. Sevov, S. C.; Corbett, J. D., unpublished research.
14. King, R. B. *Inorg. Chem.* **1989**, *28*, 2796.
15. Burdett, J. K.; Canadell, E. *J. Am. Chem. Soc.* **1990**, *112*, 7207.
16. Selwood, P. W. *Magnetochemistry*, Interscience Publishers: New York, 2nd ed., **1956**, p. 70.
17. Springelkamp, F.; De Groot, R. A.; Geertsma, W.; Van der Lugt, W; Mueller, F. M. *Phys. Rev.* **1985**, *32B*, 2319.

Table I. Data collection and refinement parameters for $K_{8.2(2)}Na_{13.8}In_{39}$ and $K_{15}Na_8In_{39}$.

Formula	$K_{8.2(2)}Na_{13.8}In_{39}$	$K_{15}Na_8In_{39}$
Formula weight	5115.8	5248.4
Crystal size, mm	0.3×0.2×0.05	0.15×0.2×0.08
Lattice parameters:[a]		
a, Å	16.620 (3)	17.69 (1)
b, Å		17.028 (5)
c, Å	42.904 (8)	24.82 (1)
V, Å^3	10263 (5)	7476 (9)
Space group, Z	$R\bar{3}m$, 6	*Pnma*, 4
d(calc.), g cm^{-3}	4.97	4.66
μ(Mo–Kα), cm^{-1}	132.56	124.79
Transmission range	0.8723–1.0962	0.6695–1.0575
Diffractometer	CAD4	Rigaku AFC6R
Radiation	Mo–Kα (λ = 0.71069 Å)	graphite-monochromated
Temperature, °C	23	23
Octants measured	±*h*, *k*, *l*	*h*, *k*, ±*l*
Scan method	ω–θ	ω–2θ
$2\theta_{max}$	50°	50°
Number of reflections:		
measured	6350	14419
observed ($I \geq 3\sigma_I$)	4686	2320
unique	1674	1150
Number of variables	117	244
R; R_w,[b] %	3.8; 5.3	4.8; 4.9
R_{ave}, %	5.4[c]	4.1
Goodness of fit indicator	1.97	1.08
Maximum shift/σ in final cycle	0.00	0.00
Largest peaks in final ΔF map	+2.86 e/Å^3 (1.48 Å from In10)	+1.91 e/Å^3 (1.96 Å from In20)
	-3.43 e/Å^3	-1.73 e/Å^3
Secondary ext. coeff.	1.4(5) × 10^{-9}	4(1) × 10^{-9}

[a] Room temperature Guinier data with Si as an internal standard (λ = 1.540562 Å).

[b] $R = \Sigma||F_o| - |F_c||/\Sigma|F_o|$; $R_w = [\Sigma w(|F_o| - |F_c|)^2/\Sigma w(F_o)^2]^{1/2}$; $w = \sigma_F^{-2}$.

[c] All data

Table II. Positional and thermal parameters for $K_{8.2(2)}Na_{13.8}In_{39}$.

Atom	N	x	y	z	B_{eq}	Occupancy
IN1	36i	0.15976(6)	0.49187(7)	0.00020(2)	2.50(3)	
IN2	36i	-0.00006(6)	0.34433(6)	0.03596(2)	1.95(3)	
IN3	36i	0.00205(6)	0.18754(6)	0.06971(2)	1.65(3)	
IN4	18h	0.12984(4)	0.2597	0.87641(3)	1.865(2)	
IN5	18h	0.22829(4)	0.4566	0.85361(3)	1.870(2)	
IN6	18h	0.55111(4)	1.1022	0.94196(3)	1.754(4)	
IN7	18h	0.44799(5)	0.8960	0.94200(3)	1.740(5)	
IN8	18h	0.39665(4)	0.7933	0.88347(3)	1.465(7)	
IN9	18h	0.22851(4)	0.4570	0.15387(3)	1.344(5)	
IN10	18h	0.39395(4)	0.7879	0.11607(2)	1.181(5)	
K1	6c	0	0	0.8703(2)	3.0(2)	
K2	36i	0.6230(2)	0.6239(2)	0.12206(7)	2.7(1)	
K3	18h	0.2055(4)	0.4110	0.0742(1)	2.70(8)	40(3)%
NA1	18h	0.2055	0.4110	0.0742	2.70	60%
NA2	6c	0	0	0.0391(3)	2.1(3)	
NA3	6c	0	0	0.2860(3)	2.7(3)	
NA4	6c	0	0	0.3789(3)	2.4(3)	
NA5	18h	0.1271(3)	0.2543	0.9992(2)	2.99(6)	
NA6	18h	0.4491(3)	0.8982	0.8104(2)	2.78(4)	
NA7	18h	0.2103(3)	0.4205	0.9295(2)	2.59(6)	

Atom	U_{11}	U_{22}	U_{33}	U_{12}	U_{13}	U_{23}
IN1	0.0280(4)	0.0425(5)	0.0287(4)	0.0208(3)	-0.0008(4)	-0.0006(4)
IN2	0.0362(4)	0.0222(4)	0.0202(4)	0.0180(3)	-0.0000(3)	0.0020(3)
IN3	0.0177(4)	0.0198(4)	0.0267(4)	0.0105(3)	0.0033(3)	0.0052(3)
IN4	0.0170(4)	0.0170	0.0180(5)	-0.0057(7)	0.0009(5)	-0.0009
IN5	0.0168(4)	0.0168	0.0181(5)	-0.0062(8)	0.0020(5)	-0.0020
IN6	0.0230(4)	0.0230	0.0172(5)	0.0089(6)	-0.0048(5)	0.0048
IN7	0.0216(4)	0.0216	0.0187(5)	0.0076(7)	0.0030(5)	-0.0030
IN8	0.0185(4)	0.0185	0.0207(5)	0.0108(6)	0.0012(5)	-0.0012
IN9	0.0124(3)	0.0124	0.0203(5)	0.0018(6)	0.0003(5)	-0.0003
IN10	0.0131(3)	0.0131	0.0166(5)	0.0049(5)	-0.0006(5)	0.0006
K1	0.026(2)	0.026	0.059(5)	0.013	0	0
K2	0.032(1)	0.032(1)	0.043(1)	0.019(1)	0.007(1)	0.003(1)
K3	0.042(2)	0.042	0.039(3)	0.037(3)	0.002(4)	-0.002
NA1	0.042	0.042	0.039	0.037	0.002	-0.002
NA2	0.014(4)	0.014	0.054(8)	0.007	0	0
NA3	0.033(4)	0.033	0.035(7)	0.017	0	0
NA4	0.029(3)	0.029	0.033(6)	0.017	0	0
NA5	0.047(3)	0.047	0.032(4)	0.033(4)	0.000(3)	-0.000
NA6	0.028(2)	0.028	0.041(4)	0.007(4)	0.004(4)	-0.004
NA7	0.042(2)	0.042	0.030(4)	0.033(3)	0.004(3)	-0.004

Table III. Distances to nearest neighbors about each atom in $K_{8.2}Na_{13.8}In_{39}$ ($d_{In-In} \leq 4.0$ Å, $d_{In-Na,K} \leq 4.5$ Å, $d_{K,Na-K,Na} \leq 4.5$ Å).

	In1			**In5**			**In10**			**Na3**	
	In1	2.864(2)		In4	2.998(2)		In6	2.950(2)	6	In1	3.542(7)
	In1	2.926(2)		In4	2.811(2)	2	In9	3.085(1)	3	In7	3.332(2)
	In2	2.985(1)	2	In8	2.932(1)		In9	3.003(2)	3	In8	3.48(1)
	In2	2.992(1)				2	In10	3.022(2)			
	In6	2.997(1)		K1	3.897(6)					Na4	3.99(2)
	In7	3.003(1)	2	K2	3.507(3)	2	K2	3.676(3)	3	Na7	3.680(9)
			2	Na6	3.689(6)	2	K3	3.66(1)			
	K3	3.673(6)		Na7	3.298(7)		Na4	3.49(1)			**Na4**
	Na3	3.542(7)									
	Na4	3.490(7)			**In6**			**K1**	6	In1	3.490(7)
	Na5	3.708(8)							3	In6	3.369(2)
	Na7	3.508(6)	2	In1	2.997(1)	6	In3	4.028(5)	3	In10	3.49(1)
			2	In2	3.124(1)	3	In4	3.747(2)			
		In2		In7	2.969(2)	3	In5	3.897(6)	3	K3	3.88(1)
				In10	2.950(2)	3	In8	4.159(8)		Na3	3.99(2)
	In1	2.864(2)									
	In1	2.926(2)	2	K2	3.725(3)		Na2	3.89(2)			**Na5**
	In2	3.085(2)	2	K3	3.584(7)	3	Na6	3.387(8)			
	In3	2.997(1)		Na4	3.369(2)				2	In1	3.708(8)
	In6	3.124(1)						**K2**	2	In2	3.516(5)
	In7	3.134(1)			**In7**				2	In2	3.484(5)
							In2	3.733(3)	2	In3	3.523(7)
	K2	3.733(3)	2	In1	3.003(1)		In3	3.875(3)	2	In3	3.492(7)
	K3	3.437(4)	2	In2	3.134(1)		In4	3.561(3)			
	Na5	3.516(5)		In6	2.969(2)		In5	3.507(3)		K3	3.93(1)
	Na5	3.484(5)		In8	2.914(2)		In6	3.725(3)	2	Na2	4.04(1)
	Na7	3.403(4)					In7	3.748(3)	2	Na5	3.661(9)
			2	K2	3.748(3)		In8	3.633(3)		Na7	3.83(1)
		In3		Na3	3.332(2)		In9	3.660(3)			
			2	Na7	3.470(5)		In9	3.592(3)			**Na6**
	In2	2.997(1)					In10	3.676(3)			
	In3	3.151(2)			**In8**				2	In3	3.579(7)
	In3	3.049(2)					K2	4.021(6)	2	In4	3.656(4)
	In4	2.994(1)	2	In5	2.932(1)		K2	4.104(6)	2	In5	3.689(6)
				In7	2.914(2)		K3	3.764(5)		In8	3.480(8)
	K1	4.028(5)	2	In8	3.157(2)		Na6	3.847(7)		In9	3.275(8)
	K2	3.875(3)					Na6	3.869(6)			
	K3	3.56(1)		K1	4.159(8)		Na7	3.895(5)		K1	3.387(8)
	Na2	3.367(5)	2	K2	3.633(3)				2	K2	3.847(7)
	Na5	3.523(7)		Na3	3.48(1)				2	K2	3.869(6)
	Na5	3.492(7)		Na6	3.480(8)			**K3**		K3	3.95(1)
	Na6	3.579(7)	2	Na7	3.650(7)						
	Na7	3.732(7)				2	In1	3.673(6)			**Na7**
					In9	2	In2	3.437(4)			
		In4				2	In3	3.56(1)	2	In1	3.508(6)
			2	In9	3.211(1)	2	In6	3.584(7)	2	In2	3.403(4)
2	In3	3.049(2)	2	In10	3.085(1)		In9	3.481(6)	2	In3	3.732(7)
	In5	2.998(2)		In10	3.003(2)	2	In10	3.66(1)		In5	3.298(7)
	In5	2.811(2)							2	In7	3.470(5)
			2	K2	3.660(3)	2	K2	3.764(5)	2	In8	3.650(7)
	K1	3.747(2)	2	K2	3.592(3)		Na4	3.88(1)			
2	K2	3.561(3)		K3	3.481(6)		Na5	3.93(1)	2	K2	3.895(5)
2	Na6	3.656(4)		Na6	3.275(8)		Na6	3.95(1)		Na3	3.680(9)
	Na7	3.248(8)								Na5	3.83(1)
								Na2			
						6	In3	3.367(5)			
							K1	3.89(2)			
							Na2	3.36(3)			
						6	Na5	4.04(1)			

Table IV. Positional and isotropic equivalent displacement parameters for $K_{15}Na_8In_{39}$.

Atom	N	x	y	z	B_{eq}
In(1)	8d	0.8552(4)	0.5767(5)	0.9626(3)	1.9(4)
In(2)	8d	1.1862(4)	0.3372(5)	0.8312(3)	1.6(3)
In(3)	8d	1.1866(4)	0.0959(6)	0.7160(3)	1.4(3)
In(4)	8d	1.4296(4)	0.5934(5)	0.9906(3)	2.6(4)
In(5)	8d	0.8356(4)	0.0965(6)	0.7086(3)	1.7(4)
In(6)	8d	1.0044(5)	0.5784(3)	0.8925(2)	1.8(2)
In(7)	8d	1.0945(4)	0.4255(5)	0.9173(3)	1.8(4)
In(8)	8d	0.8367(4)	0.3406(5)	0.8260(3)	1.2(3)
In(9)	8d	0.7075(4)	0.6581(5)	0.9272(3)	1.8(3)
In(10)	8d	0.9191(4)	0.4272(5)	0.9140(3)	1.4(4)
In(11)	8d	1.2888(4)	0.6575(5)	0.9408(3)	1.8(4)
In(12)	8d	1.1435(4)	0.5781(6)	0.9705(3)	1.9(4)
In(13)	8d	0.5701(4)	0.5561(4)	0.9426(3)	2.8(4)
In(14A)	4c	0.6469(5)	3/4	0.7318(4)	1.8(5)
In(14B)	4c	0.7363(6)	3/4	0.8263(4)	1.8(5)
In(15)	8d	1.0097(4)	0.6527(4)	0.7808(2)	1.8(3)
In(16)	8d	0.9970(5)	0.6629(3)	0.9989(2)	2.1(3)
In(17)	4c	0.9232(6)	1/4	0.7391(4)	1.7(5)
In(18)	4c	1.1930(6)	1/4	0.6431(4)	1.2(5)
In(19)	4c	0.8347(6)	1/4	0.6353(5)	1.7(5)
In(20)	4c	1.0975(6)	1/4	0.7438(4)	1.3(5)
In(21)	4c	1.1248(6)	1/4	0.5318(4)	2.2(5)
In(22)	4c	0.8752(6)	3/4	0.7564(4)	1.8(5)
In(23)	4c	0.7829(6)	3/4	0.6614(4)	2.1(5)
K(1)	8d	0.828(1)	0.558(1)	0.8137(8)	1.9(4)
Na(2)	8d	0.906(2)	-0.080(2)	0.664(1)	1.6(6)
K(3)	8d	1.282(1)	0.560(2)	1.0780(9)	3.9(6)
K(4)	8d	0.809(1)	0.063(1)	0.5634(8)	2.1(4)
K(5)	8d	0.513(2)	0.373(1)	0.8703(7)	3.4(5)
K(6)	8d	1.011(1)	0.442(1)	0.7801(6)	1.7(3)
K(7)	8d	1.195(1)	0.940(1)	0.8232(8)	1.9(4)
K(8)	4c	0.991(3)	1/4	0.377(1)	5.2(8)
K(9)	4c	1.014(2)	1/4	0.871(1)	2.4(6)
Na(10)	4c	-0.177(3)	1/4	-0.046(2)	1.9(9)
Na(11)	8d	1.121(2)	-0.084(2)	0.684(1)	1.3(6)
K(12)	4c	1.192(2)	1/4	0.967(1)	2.5(7)
Na(13)	4c	-0.114(3)	1/4	-0.894(2)	1.6(9)
Na(14)	4c	-0.899(2)	1/4	-0.892(2)	0.5(8)
Na(15)	4c	0.914(3)	1/4	0.511(2)	1.9(9)

Table V. Anisotropic displacement parameters for $K_{15}Na_8In_{39}$.

Atom	U_{11}	U_{22}	U_{33}	U_{12}	U_{13}	U_{23}
In(1)	0.026(5)	0.022(7)	0.022(4)	0.002(4)	0.000(4)	-0.000(5)
In(2)	0.021(4)	0.018(5)	0.022(4)	0.004(4)	-0.003(4)	-0.001(4)
In(3)	0.021(4)	0.016(5)	0.018(4)	-0.003(4)	0.006(3)	-0.006(4)
In(4)	0.027(4)	0.030(5)	0.043(4)	0.005(4)	-0.002(4)	0.005(4)
In(5)	0.021(4)	0.030(6)	0.016(3)	0.005(4)	0.002(3)	0.003(4)
In(6)	0.024(4)	0.021(3)	0.024(2)	0.004(4)	-0.002(4)	0.002(3)
In(7)	0.017(4)	0.033(7)	0.018(4)	0.004(4)	0.006(3)	0.000(4)
In(8)	0.019(4)	0.012(5)	0.013(4)	0.002(3)	-0.003(3)	0.006(4)
In(9)	0.024(4)	0.026(5)	0.018(3)	-0.005(4)	-0.004(3)	0.004(4)
In(10)	0.015(4)	0.016(6)	0.022(4)	-0.005(3)	0.002(3)	-0.003(4)
In(11)	0.020(4)	0.025(5)	0.024(4)	0.004(4)	-0.001(3)	0.002(4)
In(12)	0.027(5)	0.029(7)	0.016(4)	-0.010(4)	-0.006(3)	-0.005(4)
In(13)	0.036(5)	0.031(5)	0.038(4)	-0.003(4)	0.008(4)	0.001(4)
In(14A)	0.015(6)	0.027(8)	0.027(6)	0	-0.007(5)	0
In(14B)	0.019(6)	0.025(8)	0.026(6)	0	-0.007(5)	0
In(15)	0.022(4)	0.021(3)	0.026(3)	-0.005(4)	0.004(4)	-0.001(3)
In(16)	0.033(4)	0.018(3)	0.027(3)	-0.001(5)	0.007(4)	0.004(2)
In(17)	0.019(6)	0.027(9)	0.018(6)	0	-0.002(5)	0
In(18)	0.023(6)	0.004(6)	0.017(5)	0	-0.010(5)	0
In(19)	0.010(6)	0.027(8)	0.029(6)	0	0.009(5)	0
In(20)	0.024(6)	0.012(7)	0.014(5)	0	0.002(5)	0
In(21)	0.045(8)	0.015(6)	0.022(5)	0	-0.001(6)	0
In(22)	0.024(6)	0.022(8)	0.023(6)	0	-0.002(5)	0
In(23)	0.033(7)	0.022(7)	0.023(6)	0	0.009(5)	0

Table VI. Distances to nearest neighbors about each atom in $K_{15}Na_8In_{39}$ ($d_{In\text{-}In} \leq 4.0$ Å, $d_{In\text{-}Na,K} \leq 4.5$ Å, $d_{K,Na\text{-}K,Na} \leq 4.5$ Å).

	In1		**In5**		**In9**		**In13**			**In16**
In6	3.16(1)	In2	3.04(1)	In1	3.09(1)	In4	2.83(1)		In1	3.04(1)
In7	3.11(1)	In3	3.23(1)	In9	3.13(2)	In4	3.04(1)		In6	3.01(1)
In9	3.09(1)	In8	3.10(1)	In13	3.01(1)	In9	3.01(1)		In7	3.04(1)
In10	3.04(1)	In17	3.13(1)	In14B	3.00(1)				In10	3.04(1)
In12	3.12(1)	In19	3.18(1)			Na2	3.96(3)		In12	3.05(1)
In16	3.04(1)			K1	3.91(2)	K3	3.32(3)		In16	2.97(1)
		K1	3.71(2)	K3	3.72(3)	K4	3.69(2)			
K1	3.74(2)	Na2	3.44(3)	K4	3.76(2)	K5	3.74(2)		K9	3.56(2)
K3	3.50(3)	K4	3.68(2)	K8	4.03(5)	K8	3.84(2)		Na10	3.71(5)
K4	3.84(2)	K5	3.73(3)	Na11	3.40(3)	Na11	3.30(3)		K12	3.76(3)
K12	3.54(2)	K6	3.63(2)	K12	3.54(3)	Na15	3.73(2)		Na13	3.64(5)
Na14	3.52(3)	K7	3.74(2)	Na14	3.83(4)				Na14	3.50(4)
				Na15	3.38(4)		**In14A**			
	In2		**In6**							**In17**
					In10		In14B	2.83(1)		
In2	2.97(2)	In1	3.1691)			2	In15	2.95(1)	2	In5	3.13(1)
In3	3.08(1)	In10	3.03(1)	In1	3.04(1)		In23	2.97(1)	2	In8	3.09(2)
In5	3.04(1)	In12	3.13(1)	In6	3.03(1)					In19	3.01(1)
In7	3.07(1)	In15	3.05(1)	In7	3.10(1)	2	K7	3.60(2)		In20	3.08(1)
In19	3.13(1)	In16	3.01(1)	In8	3.01(1)		K8	4.34(4)			
In20	3.06(1)			In12	3.08(1)	2	Na11	3.55(3)	2	K5	3.78(2)
		K1	3.71(2)	In16	3.04(1)		Na13	3.18(5)	2	K6	3.76(2)
K4	3.79(2)	K6	3.64(2)							K9	3.64(3)
K6	3.79(2)	K7	3.79(2)	K1	3.72(2)		**In14B**				
K7	3.81(2)	Na13	3.51(3)	K3	3.56(3)					**In18**	
K9	3.53(3)	Na14	3.47(2)	K6	3.71(2)	2	In9	3.00(1)			
K12	3.67(3)			K9	3.61(2)		In14A	2.83(1)	2	In3	3.19(1)
			In7	Na10	3.60(3)		In22	3.01(1)	2	In8	3.07(1)
	In3									In20	3.02(2)
		In1	3.11(1)		**In11**	2	K1	3.65(2)		In21	3.01(1)
In2	3.08(1)	In2	3.07(1)				K8	4.20(5)			
In5	3.23(1)	In6	3.11(1)	In4	2.99(1)	2	Na11	3.50(3)	2	K3	3.65(3)
In8	3.05(1)	In10	3.10(1)	In11	3.15(2)		Na14	3.31(5)	2	K5	3.83(3)
In18	3.19(1)	In12	3.04(1)	In12	3.00(1)					Na10	3.32(5)
In20	3.14(1)	In16	3.04(1)	In21	3.15(1)		**In15**				
				In23	2.99(1)					**In19**	
K1	3.70(2)	K4	3.82(2)				In6	3.05(1)			
K3	3.53(2)	K6	3.72(2)	Na2	3.57(3)		In14A	2.95(1)	2	In2	3.13(1)
K5	3.78(3)	K7	3.73(2)	K3	3.79(2)		In15	3.31(1)	2	In5	3.18(1)
K6	3.55(2)	K9	3.51(2)	K4	3.78(2)		In22	2.96(1)		In17	3.01(1)
K7	3.77(2)	K12	3.66(2)	K7	3.74(2)						
Na11	3.37(3)			Na10	3.64(4)				2	K4	3.67(2)
			In8	Na13	3.65(5)		K1	3.69(2)	2	K5	3.79(3)
	In4						Na2	3.64(3)		K12	3.57(3)
		In3	3.05(1)		**In12**		K6	3.59(2)		Na15	3.38(5)
In11	2.99(1)	In5	3.10(1)				K7	3.78(2)			
In13	2.83(1)	In8	3.09(2)	In1	3.12(1)		K8	4.25(3)		**In20**	
In13	3.04(1)	In10	3.01(1)	In6	3.13(1)		Na11	3.32(3)			
In21	3.01(1)	In17	3.06(1)	In7	3.04(1)		Na13	3.76(5)	2	In2	3.06(1)
		In18	3.07(1)	In10	3.08(1)		Na14	3.77(4)	2	In3	3.14(1)
Na2	3.87(3)			In11	3.00(1)					In17	3.08(1)
K3	3.45(2)	K1	3.73(3)	In16	3.05(1)					In18	3.02(2)
K4	3.67(2)	K3	3.60(3)								
K5	3.64(2)	K6	3.71(2)	K3	3.63(3)				2	K5	3.83(2)
K8	4.13(3)	K9	3.66(3)	K4	3.88(2)				2	K6	3.71(2)
Na15	3.88(4)	Na10	3.53(4)	K7	3.78(2)					K9	3.48(3)
				Na10	3.53(3)						
				Na13	3.52(3)						

Table VI. (continued)

		In21			**Na2**			**K5**			**K8**			**K12**	
2	In4	3.01(1)		In4	3.87(3)		In3	3.78(3)	2	In4	4.13(3)	2	In1	3.54(2)
2	In11	3.15(1)		In5	3.44(3)		In4	3.64(2)	2	In9	4.03(5)	2	In2	3.67(3)
	In18	3.01(1)		In11	3.57(3)		In5	3.73(3)	2	In13	3.84(2)	2	In7	3.66(2)
				In13	3.96(3)		In13	3.74(2)		In14A	4.34(4)	2	In9	3.54(3)
2	K3	3.81(3)		In15	3.64(3)		In17	3.78(2)		In14B	4.20(5)	2	In16	3.76(3)
2	K5	3.77(2)		In22	3.72(3)		In18	3.83(3)	2	In15	4.25(3)		In19	3.57(3)
	Na10	3.52(5)		In23	3.61(3)		In19	3.79(3)		In22	4.07(4)			
	Na15	3.76(5)					In20	3.83(2)		In23	4.12(5)	2	K4	3.86(3)
				K1	3.98(3)		In21	3.77(2)					K9	3.96(4)
				K4	3.90(4)				2	Na2	3.57(4)		Na14	3.86(5)
		In22		K5	4.10(4)		Na2	4.10(4)	2	Na11	3.77(4)		Na15	3.96(6)
				K6	4.16(3)		K4	4.11(3)		Na15	3.60(6)			
	In14B	3.01(1)		K7	3.76(4)		K5	4.19(4)						**Na13**
2	In15	2.96(1)		K8	3.57(4)		K6	3.91(2)			**K9**			
	In23	2.87(2)		Na11	3.84(4)		Na11	4.29(4)				2	In6	3.51(3)
							Na15	4.01(4)	2	In2	3.53(3)	2	In11	3.65(5)
2	K1	3.66(3)			**K3**				2	In7	3.51(2)	2	In12	3.52(3)
2	Na2	3.72(3)						**K6**	2	In8	3.66(3)		In14A	3.18(5)
	K8	4.07(4)		In1	3.50(3)				2	In10	3.61(2)	2	In15	3.76(5)
	Na14	3.39(5)		In3	3.53(2)		In2	3.79(2)	2	In16	3.56(2)	2	In16	3.64(5)
				In4	3.45(2)		In3	3.55(2)		In17	3.64(3)		In23	3.29(5)
		In23		In8	3.60(3)		In5	3.63(2)		In20	3.48(3)			
				In9	3.72(3)		In6	3.64(2)				2	K7	3.95(4)
2	In11	2.99(1)		In10	3.56(3)		In7	3.72(2)	2	K6	3.96(2)		Na10	3.93(7)
	In14A	2.97(1)		In11	3.79(2)		In8	3.71(2)		Na10	3.95(6)		Na14	3.81(5)
	In22	2.87(2)		In12	3.63(3)		In10	3.71(2)		K12	2.96(4)			
				In13	3.32(3)		In15	3.59(2)						**Na14**
2	Na2	3.61(3)		In18	3.65(3)		In17	3.76(2)			**Na10**			
2	K7	3.61(2)		In21	3.81(3)		In20	3.71(2)				2	In1	3.52(3)
	K8	4.12(5)							2	In8	3.53(4)	2	In6	3.47(2)
	Na13	3.29(5)		K1	3.87(3)		K1	3.90(3)	2	In10	3.60(3)	2	In9	3.83(4)
				K4	4.12(3)		Na2	4.16(3)	2	In11	3.64(4)		In14B	3.31(5)
		K1		K5	4.02(4)		K5	3.91(2)	2	In12	3.53(3)	2	In15	3.77(4)
				Na10	3.81(4)		K7	3.97(3)	2	In16	3.71(5)	2	In16	3.50(4)
	In1	3.74(2)		Na11	3.99(4)		K9	3.96(2)		In18	3.32(5)		In22	3.39(5)
	In3	3.70(2)					Na11	3.91(4)		In21	3.52(5)			
	In5	3.71(2)			**K4**							2	K1	4.00(3)
	In6	3.71(2)						**K7**	2	K3	3.81(4)		K12	3.86(5)
	In8	3.73(3)		In1	3.84(2)					K9	3.95(6)		Na13	3.81(5)
	In9	3.91(2)		In2	3.79(2)		In2	3.81(2)		Na13	3.93(7)			
	In10	3.72(2)		In4	3.67(2)		In3	3.77(2)						**Na15**
	In14B	3.65(2)		In5	3.68(2)		In5	3.74(2)			**Na11**			
	In15	3.69(2)		In7	3.82(2)		In6	3.79(2)				2	In4	3.88(4)
	In22	3.66(3)		In9	3.76(2)		In7	3.73(2)		In3	3.37(3)	2	In9	3.38(4)
				In11	3.78(2)		In11	3.74(2)		In9	3.40(3)	2	In13	3.73(2)
	Na2	3.98(3)		In12	3.88(2)		In12	3.78(2)		In13	3.30(3)		In19	3.38(5)
	K3	3.87(3)		In13	3.69(2)		In14A	3.60(2)		In14A	3.55(3)		In21	3.76(5)
	K6	3.90(3)		In19	3.67(2)		In15	3.78(2)		In14B	3.50(3)			
	K7	4.13(2)					In23	3.61(2)		In15	3.32(3)	2	K4	3.90(4)
	Na11	3.68(4)		Na2	3.90(4)							2	K5	4.01(4)
	Na14	4.00(3)		K3	4.12(3)		K1	4.13(2)		K1	3.68(4)		K8	3.60(6)
				K5	4.11(3)		Na2	3.76(4)		K3	3.99(4)		K12	3.96(6)
				K7	4.05(3)		K4	4.05(3)		K5	4.29(4)			
				K12	3.86(3)		K6	3.97(3)		K6	3.91(4)			
				Na15	3.90(4)		Na11	3.71(3)		K7	3.71(3)			
							Na13	3.95(4)		K8	3.77(4)			

Table VII. Results from reactions in the ternary K–Na–In system

rxn	Loaded composition	Atomic ratios K : Na : In	K : Na	Major phase	Lattice parameters of the major phase, Å a	b	c	Volume per one In, Å^3	Minor phase
1	K_7In_{11}	24.8: 0.0: 39	7.00:0	R	17.242(4)		44.72(2)	49.203(3)	K_8In_{11}
2	K_7NaIn_{11}	24.8: 3.5: 39	7.00:1	O	17.221(4)	17.875(8)	25.17(1)	49.666(2)	A
3	$K_6Na_2In_{11}$	21.3: 7.1: 39	3.00:1	O	17.134(5)	17.800(5)	25.01(2)	48.895(3)	A
4	K_6NaIn_{12}	19.5: 3.3: 39	6.00:1	O	17.206(3)	17.878(3)	25.154(3)	49.600(1)	-
5	$KNaIn_2$	19.5:19.5: 39	1.00:1	O	17.028(5)	17.69(1)	24.82(1)	47.926(3)	A
6	$K_5Na_3In_{11}$	17.7:10.6: 39	1.67:1	O	16.964(5)	17.677(6)	24.798(6)	47.668(1)	A
7	$K_5Na_2In_{12}$	16.3: 6.5: 39	2.50:1	O	17.24(1)	17.73(1)	26.07(1)	49.122(6)	-
8	$K_4Na_4In_{11}$	14.2:14.2: 39	1.00:1	O	16.95(2)	17.59(4)	25.06(4)	47.90(2)	A
9	$K_4Na_3In_{12}$	13.0: 9.8: 39	1.33:1	R	16.8906(2)		43.575(1)	46.009(1)	-
10	$K_3Na_5In_{11}$	10.6:17.7: 39	0.60:1	R	16.721(5)		43.23(3)	44.733(3)	O
11	$K_3Na_4In_{12}$	9.8:13.0: 39	0.75:1	R	16.717(5)		43.20(3)	44.680(3)	O
12	$K_2Na_6In_{11}$	7.1:21.3: 39	0.33:1	R	16.58(1)		43.10(1)	43.850(4)	C
13	$K_2Na_5In_{12}$	6.5:16.3: 39	0.40:1	R	16.620(3)		42.904(8)	43.861(1)	-
14	KNa_7In_{11}	3.5:24.8: 39	0.14:1	C	16.0640(4)			43.181(1)	-
15	KNa_6In_{12}	3.3:19.5: 39	0.17:1	C	16.047(2)			43.044(5)	R
16	Na_7In_{12}	0.0:22.8: 39	0.00:1	T	16.093(4)		23.384(8)	42.055(3)	-

R - rhombohedral $A_{22}In_{39}$, O - orthorhombic $A_{23}In_{39}$ C - cubic $K_3Na_{26}In_{48}$ A - alkali metal T - $Na_7In_{11.8}$

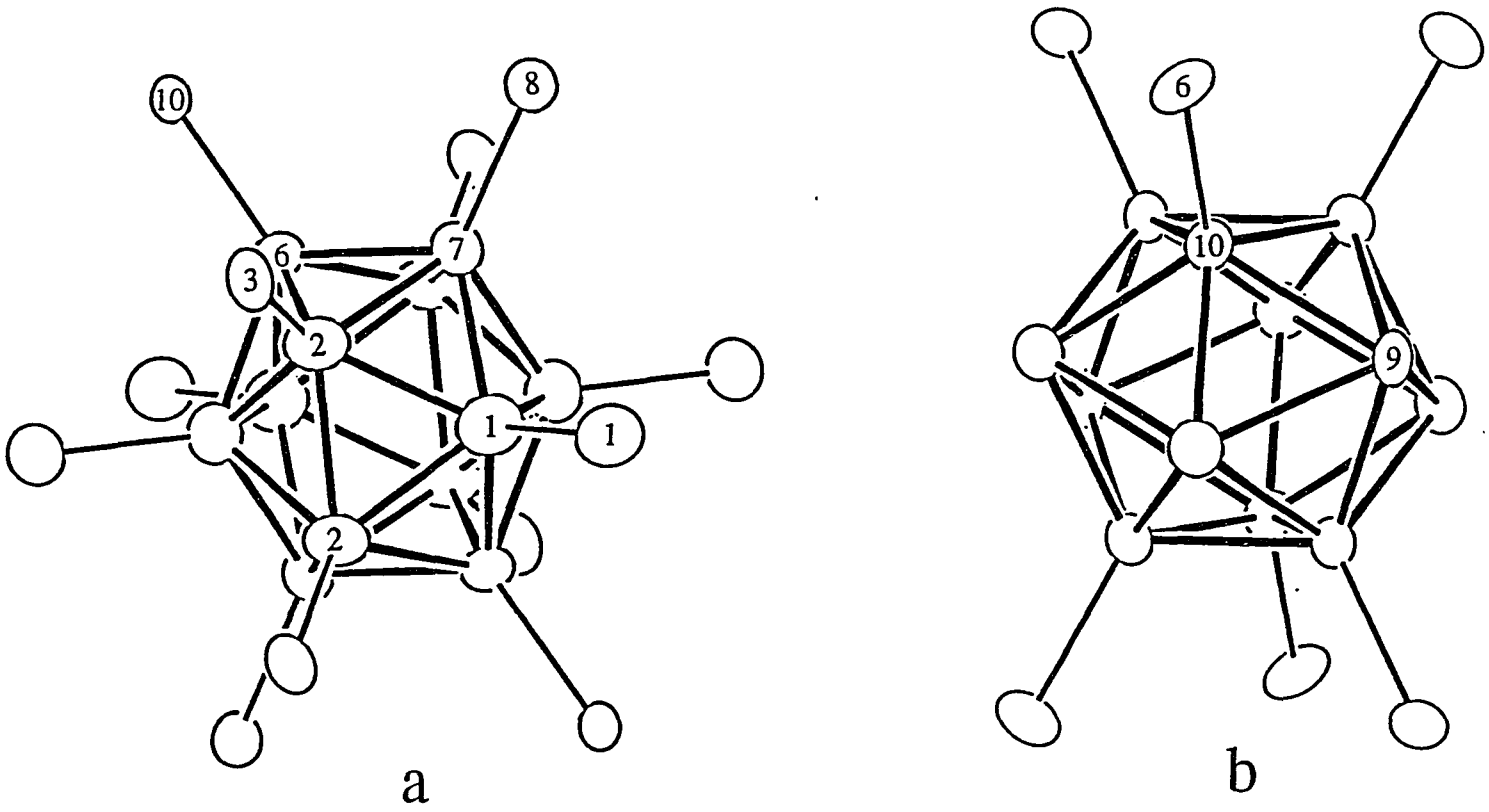

Figure 1. The two types of icosahedra in the rhombohedral $A_{22}In_{39}$: a) 12-bonded In_{12} (C_{2h}, the two-fold axis bisects the pair of In2 atoms) and b) 6-bonded In_{12} (D_{3d}, the three-fold axis is vertical). The thermal ellipsoids are drawn at 94% probability level.

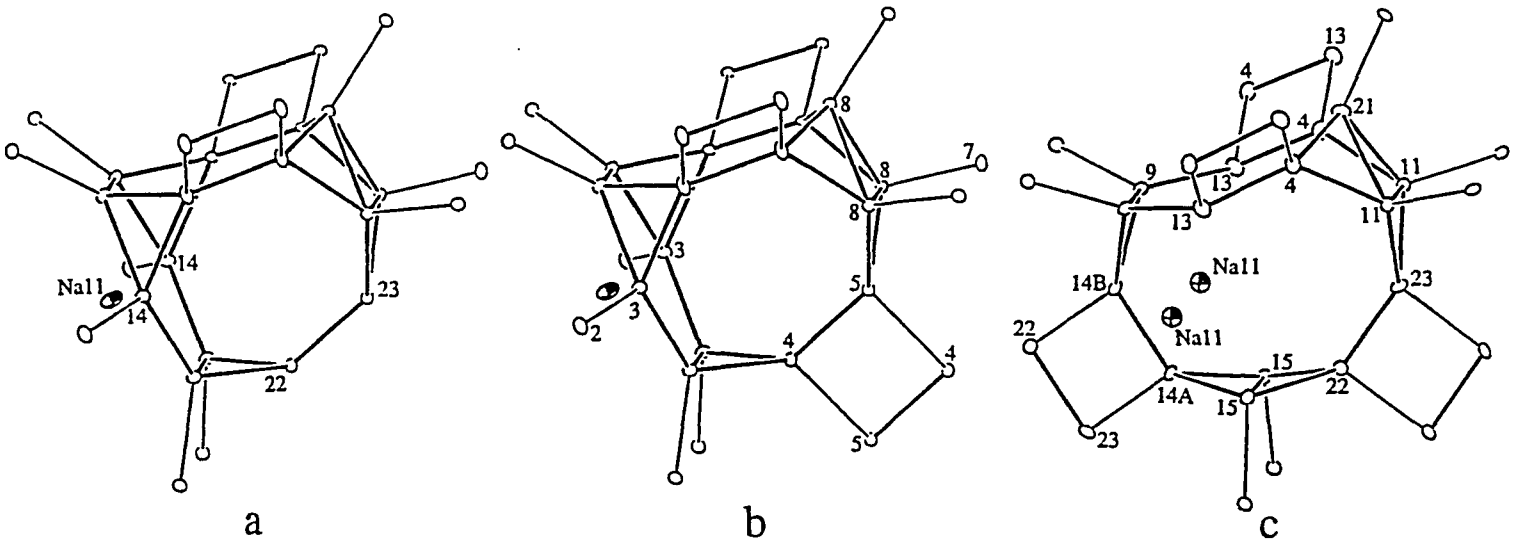

Figure 2. The individual "spacers" in a) $Na_{22}Ga_{39}$, b) the rhombohedral $A_{22}In_{39}$, and c) the orthorhombic $A_{23}In_{39}$. The two three and four squares that can be seen in a), b) and c), respectively, are formed from parallel exo bonds to other spacers. (50% thermal ellipsoids)

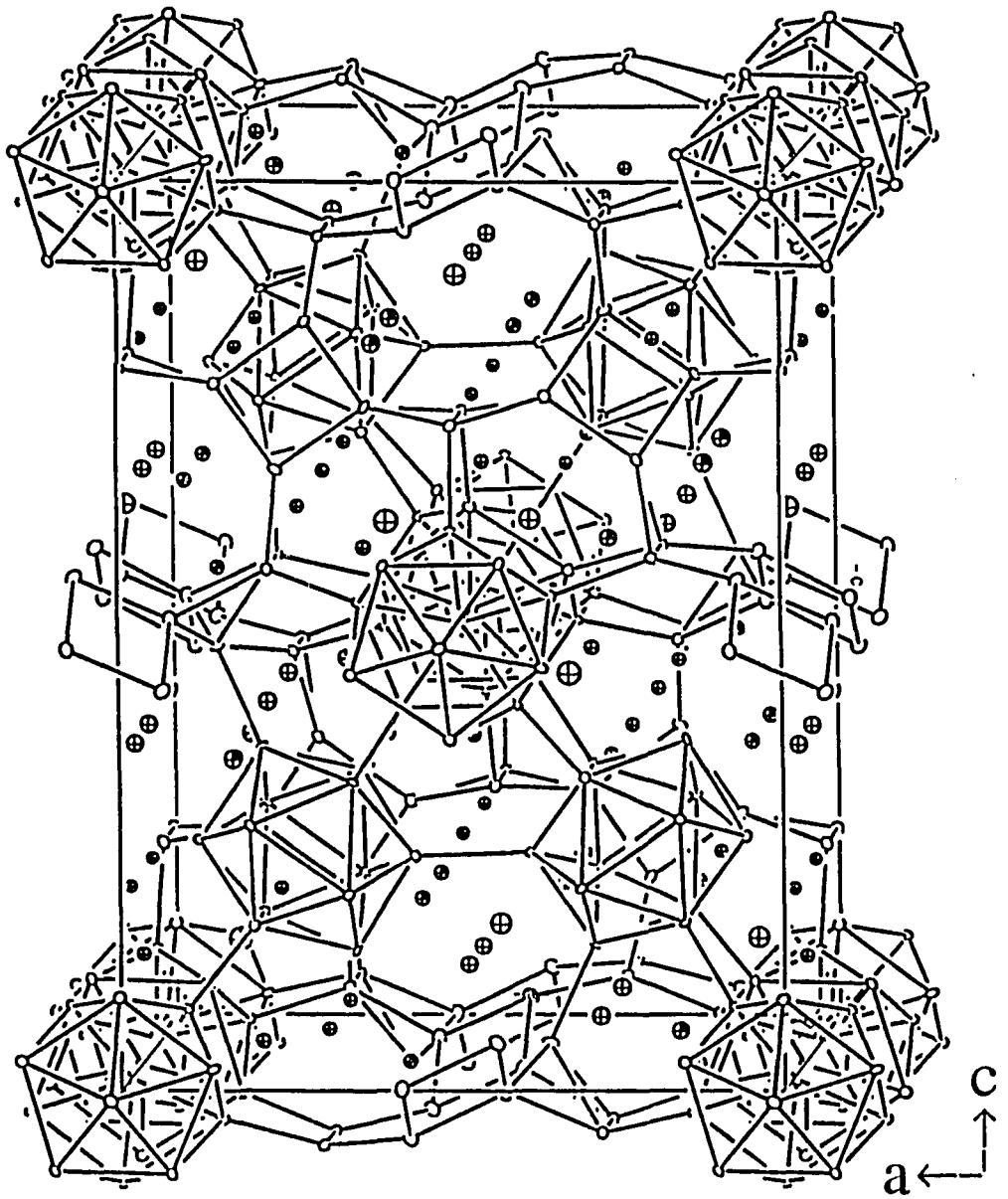

Figure 3. A view of the unit cell of the orthorhombic $K_{15}Na_8In_{39}$. Lines connect all indium atoms less than 4.0 Å apart, while the alkali metal atoms are shown as crossed ellipsoids. (30% probabilty for the thermal ellipsoids)

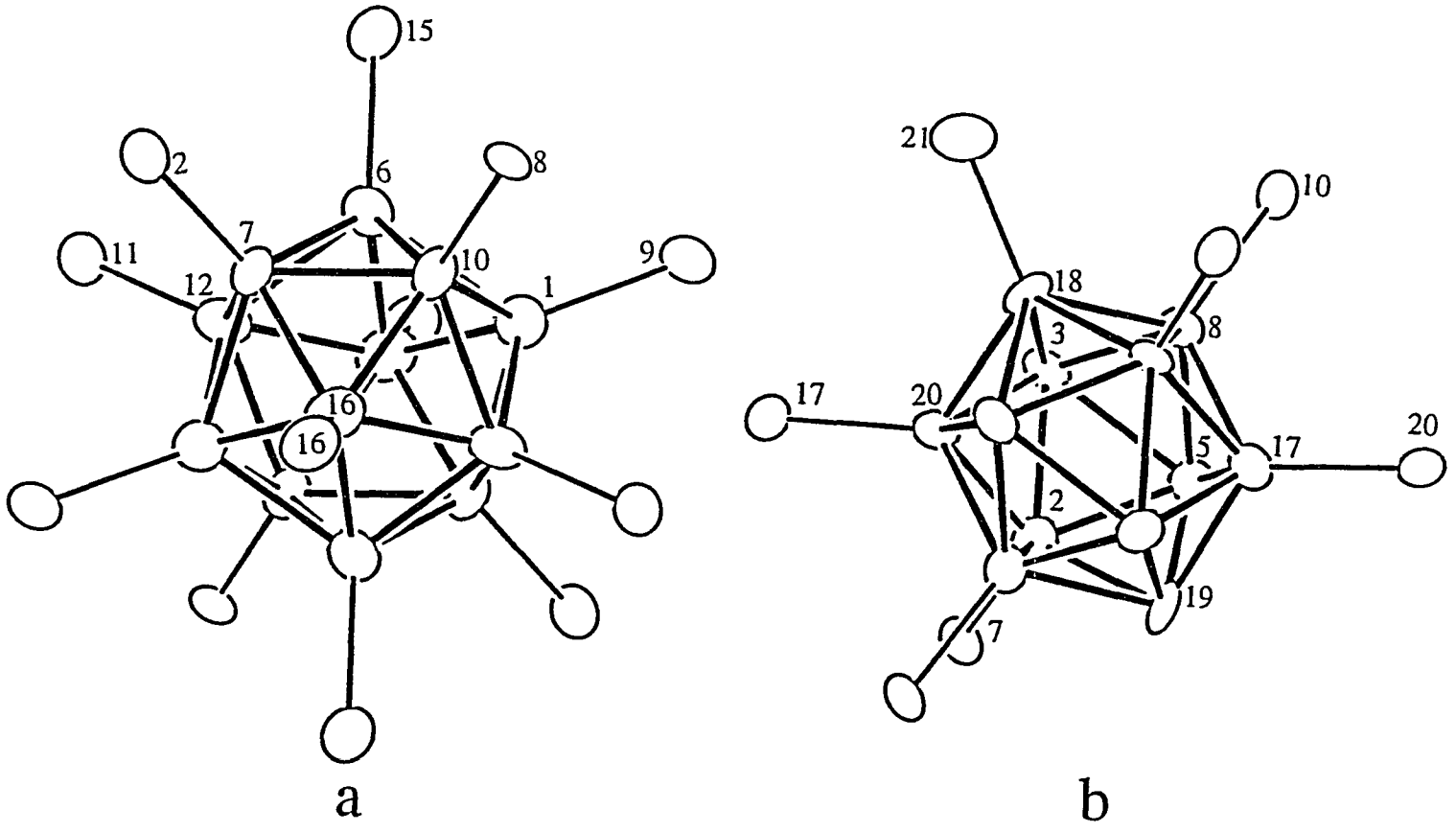

Figure 4. The two types of icosahedra in the orthorhombic $A_{23}In_{39}$: a) 12-bonded In_{12} (C_i) and b) 7-bonded In_{12} (C_s, In17 to 20 are on the mirror plane). The thermal ellipsoids are drawn at 94% probability level.

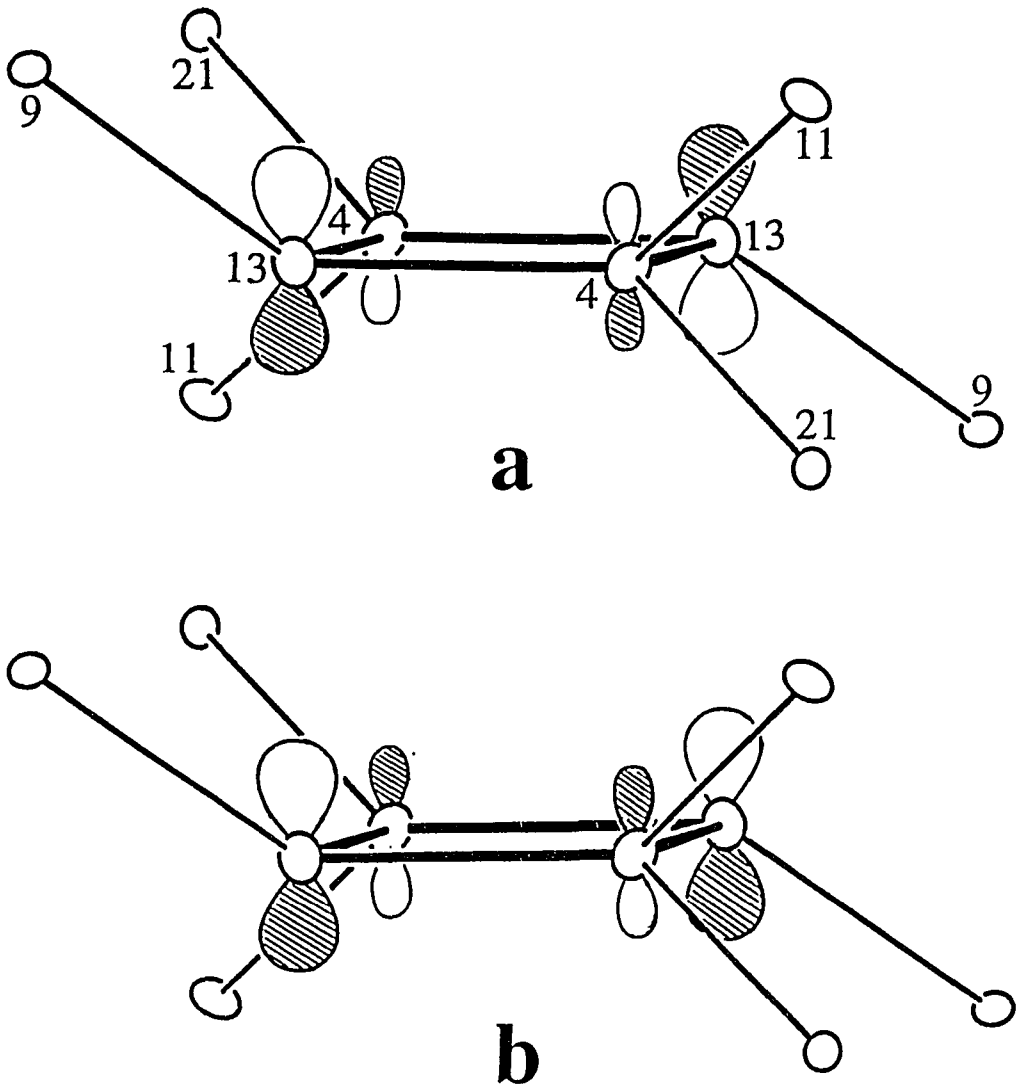

Figure 5. The HOMO (a) and LUMO (b) molecular orbitals in the square In4, 13, 4, 13. Notice the π-antibonding character of the latter and also the larger contribution of the lone pairs on In13.

PAPER 8. SYNTHESIS, CHARACTERIZATION AND BONDING OF INDIUM CLUSTERS: $A_3NA_{26}IN_{48}$ (A = K, RB, CS) WITH A NOVEL CUBIC NETWORK OF *ARACHNO-* AND *CLOSO*-IN_{12} CLUSTERS

Slavi C. Sevov and John D. Corbett*

ABSTRACT

The title compounds are obtained in high yield by slow cooling of the appropriate fused mixture of elements in welded Ta. They occur in the cubic space group $Pm\bar{3}n$, $Z = 2$, with a = 16.0640 (4), 16.101 (1), 16.130 (1) Å for A = K, Rb, Cs, respectively. The structure was refined by single crystal means for A = K, Rb to R,R_w = 2.5, 3.3 and 2.0, 2.5%. The structure contains *closo*-In_{12} icosahedra (T_h symmetry) plus *arachno*-In_{12} (D_{2d}) as approximate (D_{6d}) hexagonal antiprisms (drums) with 12 exo In–In bonds about each cluster. Nonintersecting chains of "drums" lie in the faces of the cubic cell and parallel to the cell edges. Adjacent arachno clusters are interconnected only indirectly at chain crossings via the closo polyhedra that define a body-centered cube. The structure is A15 (Cr_3Si)-like with *arachno*- and *closo*-In_{12} clusters, respectively, replacing the metal and nonmetal atoms of the parent. The larger A cations order in, and appear required for, the larger cavities lying between drums in each chain. The compounds are electron-rich by 5.5% according to theory, and the potassium example is metallic (ρ_{295} ~ 23 μohm-cm) and Pauli paramagnetic (2.2×10^{-3} emu mol^{-1}) by measurement.

INTRODUCTION

Even the binary compounds in the alkali metal–gallium[1-3] and –indium[4-9] systems are remarkable in their structural novelty and complexity. The most striking lesson to be gained from these is the very considerable driving force shown by these post-transition "metallic" elements in negative oxidation states to localize electrons in covalent bonds and the fascinating variety of ways this can be accomplished. The generic shortage of electrons with these elements means that either large negative charges or delocalized bonding (or both) will pertain. Characteristically, the delocalized versions feature either familiar or new varieties of naked clusters. A few isolated and hypoelectronic clusters are found for indium,[4,6] while the alternative linkage of clusters into networks via simple exo bonds is frequently observed for both elements. The networks may be remarkably complex and diverse in response to an evident parallel tendency to achieve bonding situations that are close to valence (Zintl) phases. For example, we have earlier completed a study of the entire Na–In system and find that it contains four phases: $Na_{15}In_{27.4}$ with interconnected *closo*-In_{16}, *nido*-In_{11}, *arachno*-In_{10}, and four-bonded In units;[6] $Na_7In_{11.8}$ with somewhat related cluster units in a different network;[5] the traditional Zintl phase NaIn with a diamond-like anionic array,[10] and Na_2In with isolated tetrahedra.[6] The second phase is especially noteworthy in that it comes within 0.6% of being electron-precise. It is also noteworthy that the K–In system contains four completely different phases.[4,9]

The subtle but important effects of cation size and number suggest that mixed cations may produce yet other arrangements. Such have already been observed for gallium,[11] but it also seems likely that the differences between gallium and indium structures in this sort of chemistry may be greater than their similarities. Three phases are found in the K_8In_{11}–$Na_7In_{11.8}$ pseudobinary system, and this article reports on the most distinctive of these, the cubic $K_3Na_{26}In_{48}$ and its analogues with other cations in place of rubidium.

EXPERIMENTAL SECTION

Synthesis

All materials were handled in a N_2-filled glovebox that had a typical H_2O level of < 0.1 ppm vol. The surfaces of the indium (Cerac, 99.999%), sodium (Alpha, 99.9+%, sealed under Ar) and potassium (J. T. Baker, lump under oil, purified 98+%) were cut clean with a scalpel before use. The potassium lump was washed with hexane and dried under vacuum before introduction into the glovebox. Rubidium (Alpha, 99.9%, sealed under Ar) and cesium (Alpha, 99.98%, sealed under Ar) were used as received, the amounts loaded being weighed by difference. (Loss of alkali metal on transfer is the most probable error.) All reactions were carried in welded tantalum tubes jacketed in sealed SiO_2 containers. The techniques are described elsewhere.[5,6]

Samples with atomic ratios of K:Na:In = 1:7:11, Rb:Na:In = 2:6:11 and Cs:Na:In 3:26:48 were prepared, and the mixtures were melted at 550 °C for 10 hours. (The highest melting points in the Na–In, K–In and Rb–In systems are about 441, 478 and 522 °C, respectively.[12]) The samples were then slowly cooled to room temperature at 3° per hour. The products had gray metallic appearances and were very brittle.

Powder patterns were obtained from ground samples that were mounted between pieces of cellophane tape. An Enraf-Nonius Guinier Camera, Cu Kα radiation (λ = 1.540562 Å), and NBS (NIST) silicon as internal standard were employed for this purpose. X-ray powder patterns calculated on the basis of the refined positional parameters for A = K (below) matched the respective ones measured for the Rb-Na-In and Cs-Na-In products very well, leading to the conclusion that the same structure pertained to all three. (That for Rb showed ~15–20% of Rb_2In_3[7] as a second phase.) A least-squares refinement of the measured 2θ values together with those of the standard Si lines resulted in a = 16.0640 (4) Å for $K_3Na_{26}In_{48}$, a = 16.101 (1) Å for

$Rb_3Na_{26}In_{48}$ and a = 16.130 (1) Å for $Cs_3Na_{26}In_{48}$. All the patterns also contained weak lines for indium metal, probably from adventitious oxidation or hydrolysis of the very sensitive samples during the X-ray exposure.

Structure determination

Diffraction data for $K_3Na_{26}In_{48}$ and $Rb_3Na_{26}In_{48}$ were collected on a CAD4 single crystal diffractometer at 21° C with monochromated Mo Kα radiation up to $2\theta = 50°$. The structures were refined with the aid of the TEXSAN package. Some details of the data collection and refinement for the two structures are listed in Table I. Unique aspects of the crystallography follow:

$K_3Na_{26}In_{48}$. A few small pieces of the crushed sample were picked, sealed in thin-walled glass capillaries, and checked for singularity by means of oscillation photographs. A plate-like example, 0.1 × 0.2 × 0.2 mm, was studied by Weissenberg photography, which showed that the cell was primitive cubic with a systematic absence condition hhℓ: $\ell = 2n$ consistent with two possible space groups, $P4\bar{3}n$ and $Pm\bar{3}n$. The same crystal was mounted on the diffractometer, and reflections from a random search were indexed with a cubic cell of the expected dimension. Data from one octant of reciprocal space confirmed the two possible space groups after correction for Lorentz and polarization effects and for absorption with the aid of the average of four ψ-scans at different angles. The Wilson plot indicated a centrosymmetric distribution, and therefore $Pm\bar{3}n$ was chosen for the first trial.

Direct methods provided seven peaks, but only the first three had distances to each other appropriate for indium atoms, and they were so assigned. A few cycles of least-squares refinement and a difference Fourier synthesis revealed the last four plus one more that had A–In distances in the range seen before for A = K or Na. One had relatively higher weight and was assigned to K, the rest to sodium. Refinement, finally with anisotropic thermal parameters and a

secondary extinction correction, converged at R = 2.5%. The largest residual peaks in the final difference Fourier map were 1.8 e/Å^2, 1.25 Å from In1, and −1.2 e/Å^2. The occupancies of the atoms did not deviate from unity by more than 2% (2σ) for In when the cations were held constant, and by more than 4% (2σ) for K and Na with In fixed, so all were held at full occupancy.

$Rb_3Na_{26}In_{48}$. The fact that the lattice parameters determined from powder data varied so slightly in the three compounds, ~0.066 Å over the range, produced some concern about whether the compounds were really ternary. In order to rule out any possibility that they might be only binary, data were also collected on a larger single crystal of the Rb product. The structure was refined to final residuals R = 2.0, R_w = 2.5% with the Rb atoms occupying the K position in $K_3Na_{26}In_{48}$ (Table I). All sites were fully occupied to within 1.5 σ. Later, some crystallites of the K and Rb compounds were checked by SEM/EDS and the compositions confirmed.

Physical properties

Electric resistivity and magnetic susceptibility data were obtained for a single phase sample of $K_3Na_{26}In_{48}$. The electrodeless "Q" method[13] was again used for the resistivity measurements on a powdered and sized sample mixed with chromatographic Al_2O_3. Data were taken every 10 degrees over the 160–295 K range. The magnetization of a 25 mg sample was measured at a field of 3T over 6–295 K on a Quantum Design MPMS SQUID magnetometer. The techniques for the measurements and the sample holder are described elsewhere.[5]

RESULTS AND DISCUSSION

Structure description

The final positional and isotropic-equivalent displacement parameters for the isostructural $K_3Na_{26}In_{48}$, and $Rb_3Na_{26}In_{48}$ are reported in Table II, and important distances are listed in Table III. A partial view of the unit cell is shown in Figure 1 with only In–In distances less than 3.5 Å drawn. The seemingly complex structure is in fact a three-dimensional network built of only two different In_{12} building blocks: arachno-12-vertex polyhedra ("drums") and closo-icosahedra, each of which are shown isolated in Figure 2. Every vertex is bonded to another cluster via an exo In–In intercluster bond, this being, as usual, somewhat shorter than In–In distances within the clusters where delocalized bonding is operative.

The cluster arrangement shown in Fig. 1 is in fact simple and well-known. Each icosahedron is, naturally, icosahedrally bonded to 12 separate *arachno*-In_{12} (Fig. 2). Each of the latter "drums" is surrounded by and bonded to four closo and eight arachno clusters to form a larger hexagonal antiprism. Two additional arachno units formally cap this antiprism to generate the chains, but these are not directly bonded to the central one. The structure is seen to consist of three nonintersecting chains of *arachno*-clusters that lie in the middle of all faces of the cube and parallel to the different cell edges. These are interconnected to each other where they overlap (but do not intersect), e.g., around 1, ½, ¾ in Figure 1. (Note that the horizontal chain lying in the front face of the cube has been omitted.) All six chains that are so placed in the unit cell are also bonded to the closo icosahedra that lie at the body center and at the corners of the cell. The structure is isotypic with the A15 (Cr_3Si or W_3O) type structure[14] *if* we equate metal atoms with the arachno groups and the nonmetals with closo-icosahedra.

The *arachno*-In_{12} (In1, 3) has D_{2d} ($\bar{4}$m2) point group symmetry but is close to D_{6d} symmetry (Fig. 2, top). This polyhedron appears to be the first example of an *arachno*

derivative of a 14-vertex closo-species that would result from capping the two hexagonal faces of the observed cluster. The unknown *closo*-In_{14} has 24 triangular faces and could be called an icositetrahedron (twenty-four-hedron). The hexagons that make up the *arachno* unit are not exactly planar, the In1 atoms in each being 0.056 (3) Å (K) or 0.044 (2) Å (Rb) outside of the plane defined by the four In3 atoms. The distances around the hexagons also differ slightly, 3.048 (1) (In3–In3) vs 3.063 (1) Å (In1–In3) for K and 3.0398 (7) vs 3.0751 (4) Å for Rb derivatives. This combined with the out-of-plane displacement leads to ~126° angles at In1 and ~125° at In3. The distances between members of adjoining hexagons in a single drum are longer than those within them by 0.06 to 0.1 Å. This difference is probably caused by the lack of capping atoms on the rings, similar shortening of distances in open faces having been observed in other *nido*- and *arachno*-clusters.[5,6,9] Each of the In1 atoms lies trans to one another in the hexagons and is exo-bonded to an icosahedron, while each In3 atom is bonded to another *arachno*-In_{12} polyhedron in a separate, perpendicular chain. The arachno clusters are centered by the Na2 ions.

The closo-icosahedra have the rare T_h point group symmetry and are built of In2 atoms only. There are two different bond distances: the six edges parallel to the unit cell axes (Fig. 2 bottom) are shorter than the remaining fourteen: 2.948 (2) vs 3.019 (1) Å (K) and 2.981 vs 3.0480 (6) Å (Rb). The vertices in each icosahedron are bonded to 12 different *arachno*-In_{12} polyhedra and thus also serve to interlink the chains. The distance differences within the *closo*-In_{12} clusters with K vs Rb are greater than elsewhere even though these cations are not nearest neighbors to this unit, doubtlessly reflecting packing requirements of the networks. Other examples of the T_h symmetry for twelve-atom polyhedra are $(Al,Zn)_{12}$ units in $Mg_{11}Zn_{11}Al_6$,[15] zinc-centered Zn_{12} in Mg_2Zn_{11}[16] and $NaZn_{13}$,[17] centered $Al_{12}W$ in WAl_{12},[18] and Ga_{12} in $Li_{13}Cu_6Ga_{21}$.[19]

The cations are not shown in the figure, and generalities are sufficient to analyze these. All sodium atoms except Na2 cap triangular faces of the polyhedra. The Na2 and K (Rb) cations alternate along the cylindrical chains of arachno-clusters, with Na2 lying within these and K (Rb,Cs) between them and centered on the cell faces (1, ½, ½, etc). These A ions also alternate with Na1 ions at 1, ¼, ¾, etc. in cation chains that run in a perpendicular direction. The size of cavity about Na2 within the drum is not particularly distinctive relative to those containing the other types of sodium whereas the A site between them is 0.60 Å larger. These features are doubtlessly what limit this structure to the $Na_{26}A_3$ proportion with A = K, Rb or Cs. Continued substitution of potassium for sodium does not fill the next larger site (Na3, 0.17 Å larger) but rather produces a series of three closely related structures.[9] The first is rhombohedral $K_xNa_{22-x}Ga_{39}$ ($\sim 7 < x < \sim 14$) (analogous to Na_7Ga_{13}[20]) with 2 of the 9 cation sites mixed, the second is a partially ordered orthorhombic $K_xNa_{22-x}Ga_{39}$ ($\sim 14 < x < \sim 19$) structured like $Na_{22}Ga_{39}$[21] and, finally, the rhombohedral $K_{22}In_{39}$ reappears with a single type of cation.

Properties

The resistivity of $K_3Na_{26}In_{48}$ is linear with temperature over 160 – 295 K with a coefficient of +0.13% per degree and ρ_{295}~23 μohm-cm. Such a resistivity is characteristic of a typical metal (21 μohm-cm for lead, for example[22]).

The magnetic susceptibilities of $K_3Na_{26}In_{48}$ over the 6–295 K range were temperature-independent and, after holder corrections, fell in the ranges of $-(13.40 \text{ to } 14.42) \times 10^{-4}$ emu/mol. As before,[4,5] two types of diamagnetic corrections may be applied to these numbers. The first one, for the ion cores of the constituent elements, totals -10.81×10^{-4} emu/mol. The second correction is for the Larmor precession of the electron pairs in the cluster orbitals. We estimate 2.14 Å for the average orbital radius in *closo*-In_{12} and 2.96 Å for *arachno*-In_{12}, which give -3.36 and -7.42×10^{-4} emu/mol-cluster, respectively. According to the proportion of

each cluster per formula unit, the total correction becomes $\chi_L = [1(3.36) + 3(7.42)] \times 10^{-4} = -25.62 \times 10^{-4}$ emu/mol. Combination of these and the measured susceptibilities provides $\chi_M = + (2.2 - 2.3) \times 10^{-3}$ emu/mol for $K_3Na_{26}In_{48}$. This result is typical for a moderate Pauli-type paramagnetism and is consistent with both the measured metal-like conductivity and the electron count based on theory (below).

Electronic structure and electron count

Extended-Hückel calculations were performed on the separate 12-bonded *closo*-In_{12} and *arachno*-In_{12}. The procedure is described elsewhere.[5,23] These confirmed the expected (Wade's rule) n+1 and n+3 skeletal bonding orbitals in the respective closo- and arachno-species. Combination of these with the number of two-electron exo-bonds for each cluster leads to local charge of −2 for the *closo*-In_{12}, and −6 for the *arachno*-In_{12}. Rough HOMO–LUMO gaps in each cluster are 3.7 and 1.9 eV, respectively. A band calculation for the anion network was not pursued.

The electron count for $K_3Na_{26}In_{48}$ can be done in the following way. Each unit cell contains two 12-bonded *closo*-In_{12}, which require 26 skeletal and 12 exo-bond electrons each, and six 12-bonded *arachno*-In_{12}, which need 30 skeletal and 12 exo-bond electrons each. The total number of valence electrons becomes 2(26 + 12) + 6(30 + 12) = 328. Since each In atom provides three and each alkali metal atom one valence electron, the number of available electrons is 2(3 + 26 + 48·3) = 346. This means that the compound is electron-rich with 18 (5.5%) extra electrons per unit cell. These are presumably delocalized in a conduction band, consistent with the observed metallic properties (above).

This novel structure once again illustrates the driving force for covalent bonding that is present in the anionic compounds of indium, both when delocalized in cluster units and in what can be described as simple two-center bonds between these. Many cluster types appear possible

in these network structures beyond *closo*-In_{12}, *nido*-In_{11}, *arachno*-In_{10}, including octahedra, *closo*-In_{16} units and the present *arachno*-In_{12}. Even more examples can be captured when heteroatoms are used to alter the electronic requirements.[4,8,9] The structural variety and complexity of these solids arise from the problems of fitting clusters and spacers into ordered, space-filling, three-dimensional arrays with sufficient room for cations, while at the same time responding to an evidently strong electronic tendency to approach (or achieve) closed-shell, semiconducting configurations.

Acknowledgement. We are indebted to J. Shinar for the use of the "Q" resistivity apparatus and J. E. Ostenson for the measurement of the magnetic data.

Supplemental Material Available. Tables of data collection and refinement details and of anisotropic displacement parameters for $A_3Na_{26}In_{48}$, A = K, Rb (2 pages). Ordering information is given on any current masthead page.

REFERENCES

(1) Belin, C.; Ling, R. G. *J. Solid State Chem.* **1983**, *48*, 40.

(2) Schäfer, H. *J. Solid State Chem.* **1985**, *57*, 97.

(3) Burdett, J. K.; Canadell, E. *J. Am. Chem. Soc.* **1990**, *112*, 7207.

(4) Sevov, S. C.; Corbett, J. D. *Inorg. Chem.* **1991**, *30*, 4875.

(5) Sevov, S. C.; Corbett, J. D. *Inorg. Chem.* **1992**, *31*, 1895.

(6) Sevov, S. C.; Corbett, J. D. J. Solid State Chem. **1993**, *103*, in press.

(7) Sevov, S. C.; Corbett, J. D. *Z. Anorg. Allg. Chem.* **1993**, in press.

(8) Sevov, S. C.; Corbett, J. D. *Inorg. Chem.* **1993**, *32*, accepted.

(9) Sevov, S. C.; Corbett, J. D., unpublished research.

(10) Zintl, E.; Neumayr, S. *Z. Phys. Chem.* **1933**, *B20*, 270.

(11) Belin, C.; Charbonnel, M. *J. Solid State Chem.* **1986**, *64*, 57.

(12) "Binary Alloy Phse Diagrams" 2nd ed., American Society for Metals, Metals Park, Ohio 44073, vol. 3, pp. 2261, 2250, 2280, respectively.

(13) Shinar, J.; Dehner, B.; Beaudry, B. J.; Peterson, D. T. *Phys. Rev.* **1988**, *37B*, 2066.

(14) Hyde, B. G.; Andersson, S. *Inorganic Crystal Structures*: John Wiley and Sons, New York, New York, **1989**, p. 330.

(15) Bergman, C.; Waugh, J. L. T.; Pauling, L. *Acta Crystallogr.* **1957**, *10*, 254.

(16) Samson, S. *Acta Chem. Scand.* **1949**, *3*, 835.

(17) Shoemaker, D. P.; Marsh, R. E.; Ewing, F. J.; Pauling, L. *Acta Crystallogr.* **1952**, *5*, 637.

(18) Adam, J.; Rich, J. B. *Acta Crystallogr.* **1954**, *7*, 813.

(19) Tillard-Charbonnel, M.; Belin, C. *J. Solid State Chem.* **1991**, *90*, 270.

(20) Frank-Cordier, U.; Cordier, G.; Schäfer, H. *Z. Naturforsch*, **1982**, *37B*, 119.

(21) Ling, R. G.; Belin, C. *Acta Crystallogr.* **1982**, *B38*, 1101.

(22) Handbook of Chemistry and Physics, CRC Press, Boca Raton, Florida, 65th ed. **1985**, p. F-120.

(23) Hoffmann, R. *J. Chem. Phys.* **1963**, *39*, 1397.

Table I. Selected Data Collection and Refinement Parameters for $K_3Na_{26}In_{48}$ and $Rb_3Na_{26}In_{48}$

Formula	$K_3Na_{26}In_{48}$	$Rb_3Na_{26}In_{48}$
space group, Z	$Pm\bar{3}n$ (no. 223), 2	$Pm\bar{3}n$ (no. 223), 2
a,[a] Å	16.0640 (4)	16.101 (1)
V, Å^3	4145.3 (1)	4174.1 (3)
d(calc), g. cm^{-3}	4.99	5.06
absorp coeff, (Mo Kα) cm^{-1}	131.5	146.0
trans coeff range	0.429 – 1.000	0.405 – 1.000
no indep obs refl, variables	479, 39	578, 39
R, R_w[b] %	2.5, 3.3	2.0, 2.5

[a] Room temperature Guinier data with Si as an internal standard (λ = 1.540562 Å).

[b] $R = \Sigma||F_o| - |F_c||/\Sigma|F_o|$; $R_w = [\Sigma w(|F_o| - |F_c|)^2 / \Sigma w(F_o)^2]^{1/2}$; $w = \sigma_F^{-2}$.

Table II. Positional and Isotropic Equivalent Displacement Parameters for $A_3Na_{26}In_{48}$

atom	position	*x*	*y*	*z*	B_{eq},[a] Å^2
$K_3Na_{26}In_{48}$					
In1	24 k	0	0.16357 (7)	0.31861 (7)	2.01 (5)
In2	24 k	0	0.09176 (7)	0.15237 (7)	2.26 (5)
In3	48 l	0.33289 (5)	0.33010 (5)	0.09488 (4)	1.81 (4)
K	6 b	0	½	½	2.5 (3)
Na1	6 c	¼	0	½	1.5 (3)
Na2	6 d	¼	½	0	2.8 (4)
Na3	16 i	0.1892 (3)	x	x	2.27 (4)
Na4	24 k	0	0.2958 (4)	0.1356 (4)	2.6 (3)
$Rb_3Na_{26}In_{48}$					
In1	24 k	0	0.16415 (3)	0.31863 (3)	1.76 (2)
In2	24 k	0	0.09257 (3)	0.15348 (3)	1.67 (2)
In3	48 l	0.33314 (2)	0.32961 (2)	0.09512 (2)	1.69 (2)
Rb	6 b	0	½	½	1.89 (5)
Na1	6 c	¼	0	½	1.9 (1)
Na2	6 d	¼	½	0	2.1 (1)
Na3	16 i	0.1898 (1)	x	x	2.43 (5)
Na4	24 k	0	0.2961 (2)	0.1349 (2)	2.4 (1)

[a] $B_{eq} = (8\pi^2/3)\Sigma_i\Sigma_j U_{ij} a_i^* a_j^* \vec{a}_i \vec{a}_j$.

Table III. Distances of nearest neighbors about each atom in $A_3Na_{26}In_{48}$, A = K, Rb

atom1	atom2	$K_3Na_{26}In_{48}$	$Rb_3Na_{26}In_{48}$	atom1	atom2	$K_3Na_{26}In_{48}$	$Rb_3Na_{26}In_{48}$
In1 -	In2	2.909(2)	2.8981(7)	**A** -	4 In1	3.924(1)	3.9386(5)
	2 In3	3.0633(9)	3.0751(4)		8 In3	4.1205(8)	4.1340(4)
	2 In3	3.123(1)	3.1274(6)		2 Na1	4.0160(1)	4.0252(3)
	A	3.924(1)	3.9386(5)		2 Na2	4.0160(1)	4.0252(3)
	Na2	3.228(1)	3.2308(5)		4 Na4	3.938(6)	3.936(3)
	2 Na3	3.706(2)	3.7163(8)				
	2 Na4	3.433(4)	3.440(2)	**Na1** -	8 In3	3.3443(7)	3.3476(4)
	Na4	3.627(7)	3.643(3)		2 A	4.0160(1)	4.0252(3)
					4 Na4	3.760(6)	3.770(3)
In2 -	In1	2.909(2)	2.8981(7)				
	In2	2.948(2)	2.981(1)	**Na2** -	4 In1	3.228(1)	3.2308(5)
	4 In2	3.019(1)	3.0480(6)		8 In3	3.3978(7)	3.4153(4)
	2 Na3	3.471(6)	3.482(3)		2 A	4.0160(1)	4.0252(3)
	Na4	3.289(6)	3.291(3)				
	2 Na4	3.497(6)	3.495(3)	**Na3** -	3 In1	3.706(2)	3.7163(8)
					3 In2	3.471(6)	3.482(3)
In3 -	In1	3.0633(9)	3.0751(4)		3 In3	3.500(3)	3.497(2)
	In1	3.123(1)	3.1274(6)		3 In3	3.570(4)	3.567(2)
	In3	3.048(1)	3.0398(7)		Na1	3.38(1)	3.360(7)
	In3	3.052(2)	3.0632(7)		3 Na4	3.594(4)	3.613(2)
	In3	3.162(2)	3.1788(7)				
	A	4.1205(8)	4.1340(4)	**Na4** -	2 In1	3.433(4)	3.440(2)
	Na1	3.3443(7)	3.3476(4)		In1	3.627(7)	3.643(3)
	Na2	3.3978(7)	3.4153(4)		In2	3.289(6)	3.291(3)
	Na3	3.500(3)	3.497(2)		2 In2	3.497(6)	3.495(3)
	Na3	3.570(4)	3.567(2)		2 In3	3.255(4)	3.257(2)
	Na4	3.255(4)	3.257(2)		2 In3	3.527(6)	3.540(3)
	Na4	3.527(6)	3.540(3)		A	3.938(6)	3.936(3)
					Na1	3.760(6)	3.770(3)
					2 Na3	3.594(4)	3.613(2)

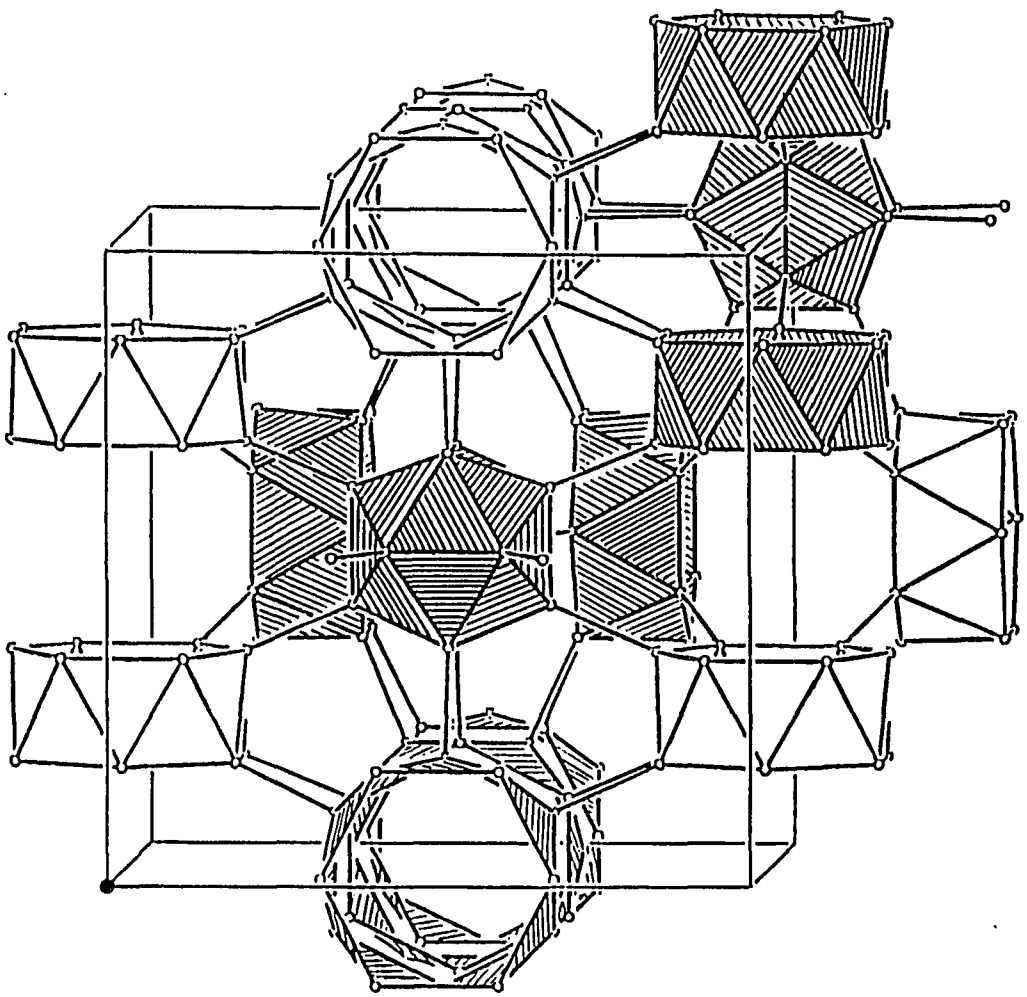

Figure 1. A portion of the indium network in the structure of $A_3Na_{26}In_{48}$. Some of the polyhedra are shaded to emphasize the building blocks: *closo*-In_{12} icosahedra and *arachno*-In_{12} hexagonal antisprisms (drums). Arachno clusters are connected via other clusters into chains lying in all faces of the cube, but the chain across the front face is not shown. The A atoms are centered in the larger cavity at 1, ½, ½ between arachno clusters in the same chain.

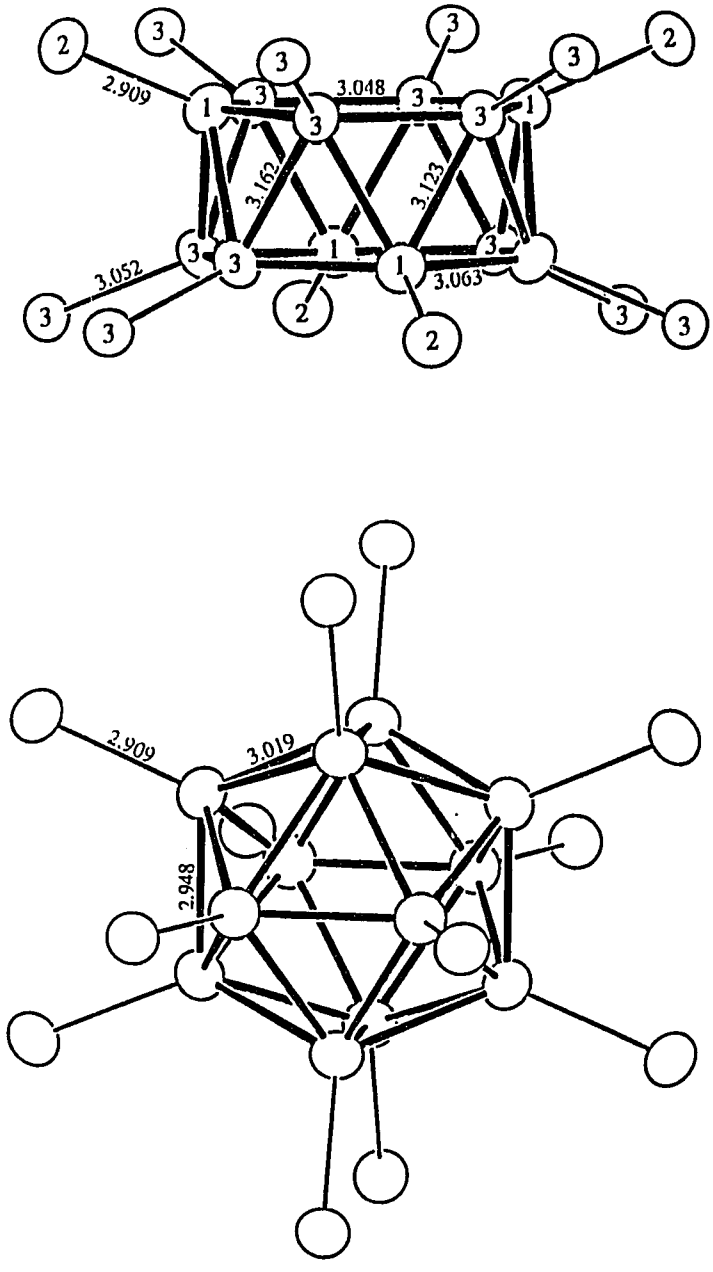

Figure 2. The separate *arachno*-In_{12} (top) and *closo*-In_{12} (bottom) cluster units with independent distances and the numbering system. All cluster atoms in the latter are In2. (94% probability thermal ellipsoids.)

SUPPLEMENTARY MATERIAL

Empirical formula	$K_3Na_{26}In_{48}$	$Rb_3Na_{26}In_{48}$
Formula weight	6226.4	6365.5
Crystal size	0.1 x 0.2 x 0.2 mm	0.07 x 0.15 x 0.22 mm
Lattice parameters: a, Å V, Å^3	16.0640 (4) 4145.3 (1)	16.101 (1) 4174.1 (3)
Space group, Z	$Pm\bar{3}n$ (#223), 2	$Pm\bar{3}n$ (#223), 2
D(calc), g/cm^3	4.99	5.06
Diffractometer	CAD4	CAD4
Radiation	Mo Kα, Graphite-monochr.	Mo Kα Graphite-monochr.
Temperature, °C	21	21
Octants measured	h, k, ℓ	h, k, ℓ
Scan method	Ω–θ	Ω–θ
2θ (max), deg.	50	50
No. reflections measured	4062	4077
Obs. (I>3.00 σ_I)	2293	3003
Indep. obs.	479	578
abs. coeff. (Mo Kα) cm^{-1}	131.54	146.05
Transm. factor range	0.429 – 1.000	0.405 –1.000
No. variables	39	39
Residuals: R, R_w,[a] %	2.5; 3.3	2.0; 2.5
R(ave.),[b] %	5.7	3.3
Goodness of fit indicator	1.498	1.136
Max. shift in final cycle	0.00	0.00
Largest peaks in final ΔF, e/Å^3	+1.8 (1.25 Å from In1), –1.2	+1.5 (center of c-In_{12}), –1.2
Sec. Ext. Coeff. (10^{-9})	7(3)	18 (3)

a $R = \Sigma||F_o| - |F_c||/ \Sigma|F_o|$; $R_w = [\Sigma w(|F_o| - |F_c|)^2 / \Sigma w(F_o)^2]^{1/2}$; $w = \sigma_F^{-2}$.

b All data.

Anisotropic displacement parameters

atom	U_{11}[a]	U_{22}	U_{33}	U_{12}	U_{13}	U_{23}
$K_3Na_{26}In_{48}$						
In1	0.0269(7)	0.0251(7)	0.0243(7)	0	0	–0.0052(5)
In2	0.0339(7)	0.0291(7)	0.0228(7)	0	0	–0.0051(5)
In3	0.0244(5)	0.0226(5)	0.0217(4)	0.0047(3)	–0.0017(3)	–0.0006(3)
K	0.030(4)	0.030(5)	0.033(5)	0	0	0
Na1	0.023(7)	0.017(4)	U_{22}	0	0	0
Na2	0.05(1)	0.027(5)	U_{22}	0	0	0
Na3	0.0288(2)	U_{11}	U_{11}	–0.000(2)	U_{12}	U_{12}
Na4	0.027(4)	0.030(4)	0.041(4)	0	0	–0.005(3)
$Rb_3Na_{26}In_{48}$						
In1	0.0227(3)	0.0231(3)	0.0209(3)	0	0	–0.0043(2)
In2	0.0232(3)	0.0214(3)	0.0189(3)	0	0	–0.0020(2)
In3	0.0229(2)	0.0206(2)	0.0205(2)	0.0037(1)	–0.0027(1)	–0.0002(1)
Rb	0.0239(7)	0.0230(7)	0.0251(7)	0	0	0
Na1	0.028(3)	0.021(2)	U_{22}	0	0	0
Na2	0.042(3)	0.020(2)	U_{22}	0	0	0
Na3	0.0308(1)	U_{11}	U_{11}	–0.0018(9)	U_{12}	U_{12}
Na4	0.027(1)	0.026(1)	0.037(2)	0	0	–0.003(1)

a $T = \exp[-2\pi^2(U_{11}h^2a^{*2} + U_{22}k^2b^{*2} + U_{33}\ell^2c^{*2} + 2U_{12}hka^*b^* + 2U_{13}h\ell a^*c^* + 2U_{23}k\ell b^*c^*)]$.

PAPER 9. SYNTHESIS, CHARACTERIZATION AND BONDING OF INDIUM CLUSTERS: RB_2IN_3, A ZINTL PHASE WITH LAYERS OF CLOSO-INDIUM OCTAHEDRA

Slavi C. Sevov and John D. Corbett*

ABSTRACT

The Rb–In system contains only $RbIn_4$ ($BaAl_4$ type) and Rb_2In_3 in the 0–80 at.% In region. The structure of Rb_2In_3 consists of rubidium ions between layers of *closo*-In_6 clusters joined into sheets through exo bonds at four coplanar vertices (I4/mmm, a = 6.8735 (4) Å, c = 15.899 (1) Å, $R(F)/R_w$ = 3.2/3.5 %). The phase is isostructural with Cs_2In_3 when a probable error in the earlier space group assignment is corrected. Rb_2In_3 is a poor conductor ($\rho > 10^3$ μohm·cm) with a temperature-independent magnetic susceptibility of $(0\pm4) \times 10^{-6}$ 10 emu/mol after core and orbital corrections. The corresponding Zintl phase (closed shell configuration) predicted on the basis of conventional electron counting for the cluster network is supported by extended-Hückel MO calculations. The structures of Rb_4In_6 and In_4Rb show a close, inverse relationship in the same space group.

INTRODUCTION

Elements in the boron family exhibit some remarkable structural and bonding properties via homoatomic cluster units, results deriving principally from the presence of fewer valence electrons than good bonding orbitals. Borane analogues in which clusters of Al, Ga, etc. have exo bonds to H, R, etc. are evidently not stable, which means that any classical "naked" clusters obeying Wade's rules will require unusually high charges, viz., *closo*-M_n^{-n-2}. Of course distortions may lead to unusual hypoelectronic alternatives like In_{11}^{7-} [1], but a much more common result is the formation of networks of clusters via normal intercluster bonds. Each such bond reduces the local cluster charge by one, effectively through oxidation of the otherwise "inert s-pair " at that vertex. Many examples have been discovered for gallium and the bonding accounted for fairly well by classical cluster bonding treatments [2–4] (and references therein). Indium and thallium systems are less well known, but several new alkali-metal–indium phases with network structures involving *nido*-In_{11}, *arachno*- and *closo*-In_{12} and *closo*-In_{16} clusters have recently been described that exhibit very nearly closed-shell bonding [5–7].

The Rb–In system has not received much synthetic and structural attention. The phases Rb_4In_5 [8], Rb_5In_8, and $RbIn_4$ [9] have been reported on the basis of thermal analysis and X-ray powder diffraction, but only the last has a known structure type, $BaAl_4$ [10]. A recent phase diagram summary [11] left the first composition uncertain, and replaced the estimated Rb_5In_8 with Rb_2In_3 on the basis that a compound with the corresponding composition and a unique structure had been defined for Cs_2In_3 by Yatsenko, et al. [12].

The present article reports our results for the Rb–In system.

EXPERIMENTAL SECTION

Syntheses

All materials were handled in a N_2-filled glovebox that had typical moisture levels of <0.1 ppm vol. The surface of the indium (Cerac, 99.999%) was cleaned with a scalpel before use, while the rubidium (Alpha, 99.9%, sealed under Ar) was used as received. The weight of Rb loaded from the ampule was determined by difference. All reactions were carried out in welded tantalum tubing as described elsewhere [5].

A reaction designed to produce Rb_2In_3 was loaded (60 at.% In), and the contents held at 530°C for 5 hours. (The highest melting point in the Rb–In system is about 522°C [11].) The sample was successively annealed at 400, 300 and 250°C for 2.5, 2 and 2 days, respectively, and then was slowly cooled (10°/hour) to room temperature. Other samples containing 56, 58 and 75 at.% In were treated similarly.

Powder patterns were obtained after grinding the samples and mounting the powder between pieces of cellophane tape. An Enraf-Nonius Guinier camera, Cu Kα radiation (λ = 1.540562 Å), and NBS (NIST) silicon as an internal standard were employed for this purpose. The pattern for the Rb_2In_3 composition matched that calculated for Cs_2In_3 very well although the lines were naturally shifted to higher 2Θ angles because of the smaller lattice parameters. The yield of the dark gray and very brittle phase appeared quantitative, and a least-squares refinement of the positions of the indexed lines and those of the standard silicon afforded the lattice constants listed in Table 1. Patterns of the other samples synthesized contained only Rb, this phase and/or $RbIn_4$. Thus, a phase near Rb_4In_5 (55.6 at.% In) [8] does not exist, in agreement with the conclusions of Thümmel and Klemm [9]

Structure determination

An additional refinement of the structure type seemed necessary judging from the relatively poor refinement of Cs_2In_3 [12] (R = 9.9%, with some extreme thermal ellipsoids) and a clear suggestion of a centrosymmetric tetragonal space group rather than the assigned $I\bar{4}m2$. The reported coordinates of the two Cs atoms, 0, ½, ¼ and 0, ½, ¾, can be related by an inversion center, and such a center is also allowed for the In atom refined at 0.295 (1), 0, −0.0059 (6) if $z = 0$.

Single bar-like crystals were picked from the crushed reaction product and sealed in thin-walled glass capillaries. One was selected after checking for singularity by means of oscillation photographs. Diffraction data were collected for two octants on a Rigaku AFC6R single crystal diffractometer at room temperature with the aid of monochromated Mo Kα radiation and with the absence condition for body-centering imposed. The Wilson plot statistics after correction for Lorentz and polarization effects and for absorption with the aid of one Ψ-scan indicated a centrosymmetric space group, and therefore I4/mmm was chosen. The structure was refined with the aid of the TEXAN package [13]. Some details regarding the cell, the data collection, and refinement are listed in Table I. Unique aspects of the crystallography follow.

The corresponding atomic coordinates from Cs_2In_3 were used as a starting model, and refinement with isotropic thermal parameters proceeded smoothly, converging at R = 10.2%. The final residuals listed in Table 1 were obtained after a better empirical absorption correction (DIFABS) [14] and the anisotropic refinement of all atoms. Structure factor data are available from J.D.C. The next step was to refine the structure in the $I\bar{4}m2$ space group originally assigned to Cs_2In_3. However, this led to neither lower residuals nor more accurate parameters. The deviation from $z = 0$ with one In atom on the x, 0, z type position was less than 0.5 σ. All the results support the correctness of the centrosymmetric space group I4/mmm.

Property measurements

The resistivity of Rb_2In_3 was examined, as before, by the electrodeless "Q" method [15] for 330 mg. of a 300–380 μm diameter powder mixed with Al_2O_3. Measurements were made at 35 MH_z and at 160 and 295 K. The magnetization of a 25 mg. sample was measured at 3T over the range 6–295 K on a Quantum Design MPMS SQUID magnetometer. Additional measurements were made at 100 Oe and 2–10 K to check for superconductivity, which was not found.

RESULTS AND DISCUSSION

Structure description

The final positional and anisotropic displacement parameters for Rb_2In_3 are reported in Table 2 and important distances are listed in Table 3. A general view of the structure is shown in Fig. 1, where the solid lines represent bonding interactions between the indium atoms (open ellipsoids) while rubidium atoms (crossed ellipsoids) are shown isolated.

The anion structure is composed of *closo*-In_6 octahedra that are each exo-bonded to four others about their waists to form quasi-infinite planar sheets. These layers are nested by the I-centering and are well separated by rubidium, the two types of cations falling in the valleys within each layer. The In_6 octahedra are centered at 4/mmm type positions and thus have D_{4h} point symmetry. The In1 atoms occupy the apical positions and do not have exo-bonds but are four-bonded to In2 atoms within each cluster. The In2 atoms in the waist of the octahedra are each exo-bonded to an In2 atom in an adjoining octahedron as well as to two In1 and two In2 atoms. The intercluster distances (2.808 (2) Å) are shorter than the intracluster separations (2.875 (2) to 3.094 (2) Å), a behavior that has been observed in many other condensed cluster compounds of the gallium family elements [2,3,5–7]. The octahedra are elongated toward the four-bonded In1 apices, the distances around the waist being 0.219 (3) Å less. The shortest interlayer In–In distance is 5.86 Å between In1 apices in adjacent layers. The indium thermal ellipsoids (Table 2) are consistent with some torsional or wave motion within the layers as the apex In1 appears larger normal to $\vec{c}$ while In2 is larger along $\vec{c}$. The values for Rb1 also correlate with such a motion of the closer In1.

The compound is evidently isostructural with Cs_2In_3 [12] presuming the minor change in space group is correct there as well. We also confirm by powder pattern data the $BaAl_4$-type

structure of $RbIn_4$ (a = 4.9092 (5), c = 12.640 (3) Å, *I4/mmm*)), but with a somewhat smaller c dimension than reported before (12.82 Å) [10].

Properties

The resistivity of Rb_2In_3 could only be estimated as larger than 1000 μohm-cm. The reason for this ambiguity is that the sample did not produce any deflections of the "Q"-meter. We should point out here that measurements made on the meter are proportional to the conductivity of the sample, and the smallest measurable signal corresponds to a resistivity of at least 1000 μohm·cm. Such a value certainly suggests that Rb_2In_3 is a semiconductor, consistent with bonding expectations (below). Of course, the temperature coefficient of the resistivity for Rb_2In_3 is unknown. In passing, we note that the magnitude of this resistivity is also quite consistent with 450–900 μohm-cm maxima near 1:1 compositions measured for liquid Cs and K systems with Ga, In and Tℓ [16,17]. The liquids apparently always give lower ρ values and are presumably simpler than the neighboring solids, while the ρ values appear to depend only on the alkali metal [18]. We have previously found ρ values of 270 to 600 μohm·cm and metal-like dependencies for several phases with indium network structures where bonding calculations and electron counting indicate very small fractions of excess electrons. The latter data also correlate well with small net Pauli-like paramagnetic remnants [1,5,6].

The magnetic susceptibilities of Rb_2In_3 over 12–295 K were temperature independent, amounting to $-1.42\ (4) \times 10^{-4}$ emu/mol after holder corrections. As before, two types of diamagnetic corrections can be applied to this number. The first one, for the cores of the constituent cations [19], totals -0.97×10^{-4} emu/mol for Rb_2In_3. A second correction for the Larmor precession of the electron pairs in the cluster orbitals is estimated from $\chi_L = -0.79 \times 10^{-6}\ Z_i\ (r_{ave}/a_0)^2$ emu/mol-cluster, where Z_i is the number of skeletal electrons in the cluster, r_{ave} is the average radius of their molecular orbitals, and a_0 = 0.529 Å [20]. We assume this applies

only to the octahedra, and r_{ave} = 1.51 Å gives -0.90×10^{-4} emu/mol-cluster. The combination of these results in $(0 \pm 4) \times 10^{-6}$ emu/mol for Rb_2In_3, that is, effectively zero. This is very consistent with the minimal resistivity and the predicted closed-shell electronic structure (below), but of course the magnetic susceptibility result does not necessarily guarantee a semiconducting property. A similar result for Na_2In with isolated closed-shell indium tetrahedra is coupled with ρ_{295} ~ 270 μohm-cm and a metal-like temperature coefficient [6]. Other magnetic contributions or the absence of a gap between expected filled valence and empty conduction bands can be sources of contradiction.

Electronic structure

Isolated octahedral In_6 units would require 2n+2 = 14 skeletal bonding electrons according to Wade's rules [21]. This applies to valence p electrons, with an inert s pair or an exo bond to hydrogen etc. at each vertex (e.g., In_6^{8-}, $B_6H_6^{2-}$). Formation of exo homoatomic bonds serve to expand the valence states at each such vertex to include s, to oxidize the cluster, and to reduce the charge for the naked cluster by one for each exo bond [2,4,5]. (The mixing of s with p also produces shorter bonds at such atoms.) Thus the observed $^2_\infty[In_6^{4-}]$ sheets in Rb_4In_6 are completely consistent with this expectation, a closed valence shell, and the measured properties. Extended-Hückel calculations were performed as before [1,5,6] on isolated 4-bonded *closo*-In_6 units with the observed dimensions, and these confirmed the expectations for skeletal bonding and a –4 charge per octahedron. The presence of low-lying, localized and mainly 5s pairs on the octahedral apices (In1) was clear in the results. The calculated HOMO-LUMO gap was 2.2 eV.

In contrast, Yatsenko et al. [12] predicted four excess electrons per octahedron in Cs_4In_6 and thence a metallic behavior or Cs–Cs binding. Their error was the omission of the inert s pairs at the two In1 vertices in each octahedron.

Both theory and experiment indicate that Rb_2In_3 and probably Cs_2In_3 as well are likely Zintl (valence) compounds. They are evidently the only examples of this novel, extended structure. The absence of K_2In_3 [7] can presumably be attributed to the inadequate interlayer separation provided by the smaller cation, but whether there are thallium analogues remains to be seen. Finally, we observe an interesting interrelationship exists between this and the $BaAl_4$ structure type [22], that is, between what are evidently the only rubidium–indium phases, Rb_4In_6 and $RbIn_4$. These two structures occur in the same space group (I4/mmm), and the first can be converted to the second by replacement of (a) the cation positions in Rb_4In_6 by indium and (b) the In_6 clusters in the former by Rb atoms at their centers (0,0,0), i.e., $Rb_4In_6 \rightarrow In_4Rb$. Figure 2 emphasizes this with open interconnections between the rubidium atoms in Rb_2In_3. (The horizontal lines defining the square net are distinctly longer ($a/\sqrt{2}$) and could be omitted.) Judging from recent band calculations [23], $RbIn_4$ with separate layers should have an incomplete valence band and be metallic whereas $BaIn_4$ [10] should be a Zintl (valence) compound or close to it.

Acknowledgements: We thank J. E. Ostenson for the magnetic susceptibility data. This research was supported by the U.S. Department of Energy, Office of Basic Energy Sciences, Materials Sciences Division. The Ames Laboratory is operated for the Department of Energy by Iowa State University under contract No. W-7405-Eng-82.

REFERENCES

[1] *S. C. Sevov, J. C. Corbett:* Inorg. Chem. **30**, (1991) 4875.

[2] *C. Belin, R. G. Ling:* J. Solid State Chem. **48**, (1983) 40.

[3] *H. Schäfer:* J. Solid State Chem. **57** (1987) 210.

[4] *J. K. Burdett, E. Canadell:* J. Am. Chem. Soc. **112** (1990) 7207.

[5] *S. C. Sevov, J. D. Corbett:* Inorg. Chem. **31** (1992) 1895.

[6] *S. C. Sevov, J. D. Corbett:* J. Solid State Chem. (1992) submitted.

[7] *S. C. Sevov, J. D. Corbett:* to be submitted for publication.

[8] *S. P. Yatsenko, K. A. Chuntonov, V. D. Bushmanov, V. N. Dieva:* Struktura Faz. Fazovye Prevrascheniya i Diagramma Sostoyaniya Metallicheskikh Sistem, Nauka, Moscow (1974) **198.**

[9] *R. Thümmel, W. Klemm:* Z. Anorg. Allg. Chem. **376** (1970) 44.

[10] *G. Bruzzone:* Acta Crystallogr. **B25** (1969) 1206.

[11] Binary Alloy Phase Diagrams, *Massalski, T. B.*, ed., 2nd edition, Amer. Soc. Metals: Metals Park, Ohio (1991) vol. 3, p. 2280.

[12] *S. P. Yatsenko, K. A. Tschuntonow, A. N. Orlow, Ya. P. Yarmolyuk, Yu. N. Hryn:* J. Less-Common Met. **108** (1985) 343.

[13] TEXAN, Version 6.0 package; Molecular Structure Corp., The Woodlands, Texas (1990).

[14] *N. Walker, D. Stuart:* Acta Crystallogr. **A39** (1983) 158.

[15] *J. Shinar, B. Dehner, B. J. Beaudry, D. T. Peterson:* Phys. Rev. **B37** (1988) 2066.

[16] *M. Kitajima, M. Shimji:* Inst. Phys. Conf. Ser. **30** (1977) 226.

[17] *J. A. Meijer, W. Geertsma, W. van der Lugt:* J. Phys. F: Met. Phys. **15** (1985) 899.

[18] *J. A. Meijer*: Doctoral Thesis, University of Groningen, The Netherlands (1988).

[19] *P. W. Selwood:* Magnetochemistry, 2nd ed.; Interscience Publishers: New York (1956) p. 70.

[20] *N. W. Ashcroft, D. N. Mermin:* Solid State Physics; Holt, Rinehart and Winston: Philadephia (1976), p. 649.

[21] *K. Wade:* Adv. Inorg. Chem. Radiochem. **18** (1976) 1.

[22] *R. M. Andress, E. Albertini:* Z. Metallk. **27** (1935) 126.

[23] *C. Zheng, R. Hoffmann:* Z. Naturforsch. **41b** (1986) 292.

Table 1. Selected data collection, reduction and refinement parameters for Rb_2In_3

space group, Z	I4/mmm (no. 139), 4
cell parameters (Guinier)	
a	6.8735 (4) Å
c	15.899 (1) Å
V	751.15 (9) $Å^3$
d(calc)	4.56 g/cm^3
crystal dimens	0.1 × 0.1 × 0.3 mm
octants measured	± h, k, ℓ
2θ(max)	50°
reflections	
measured	731
observed ($I/\sigma(I) > 3.0$)	555
indep	176
R_{ave} (all data)	9.0%
abs. coeff. (Mo Kα)	214.2 cm^{-1}
transm. coeff. range	0.622 – 1.28
no. variables	14
sec. extinct. coeff.	$9(6)\cdot10^{-8}$
R[a]	3.2%
R_w[b]	3.5%
largest ΔF peaks	1.9 e/$Å^3$, 1.7 Å from Rb1; −1.1 e/$Å^3$

[a] $R = \Sigma||F_o| - |F_c||/ \Sigma|F_o|$.

[b] $R_w = [\Sigma w(|F_o| - |F_c|)^2 / \Sigma w(F_o)^2]^{1/2}$; $w = [\sigma(F)]^{-2}$.

Table 2. Positional and Thermal Parameters for Rb_2In_3[a]

Atom	Posn.	*x*	*y*	*z*	B_{eq} (Å^2)	U_{11}	U_{22}	U_{33}
In1	4 (e)	0	0	0.1467(1)	2.28(5)	37.3(8)	U_{11}	12(1)
In2	8 (i)	0.2957(2)	0	0	2.14(6)	16.4(8)	27.3(8)	37.7(9)
Rb1	4 (e)	0	0	0.3907(2)	3.61(8)	59(1)	U_{11}	19(2)
Rb2	4 (d)	0	½	¼	3.21(8)	38(1)	U_{11}	45(2)

[a] Space group *I*4/*mmm*.

[b] $U_{ii} \times 10^3$; $U_{12} = U_{13} = U_{23} = 0$; $T = \exp[(2\pi^2(U_{11}h^2a^{*2} + U_{22}k^2b^{*2} + U_{33}\ell^2c^{*2})$.

Table 3. Nearest Neighbor Distances About Each Atom in Rb_2In_3 (Å)[a]

In1	In2	Rb1	Rb2
4 In2 3.094(2)	2 In1 3.094(2)	In1 3.879(3)	4 In1 3.8090(9)
Rb1 3.879(3)	In2 2.808(2)	8 In2 4.099(1)	4 In2 4.2155(4)
4 Rb2 3.8090(8)	2 In2 2.875(2)	Rb1 3.477(6)	4 Rb1 4.100 (2)
	4 Rb1 4.099(1)	4 Rb2 4.100(2)	4 Rb2 4.8603(3)
	2 Rb2 4.2155(4)		

[a] < 4.06 Å for In–In.

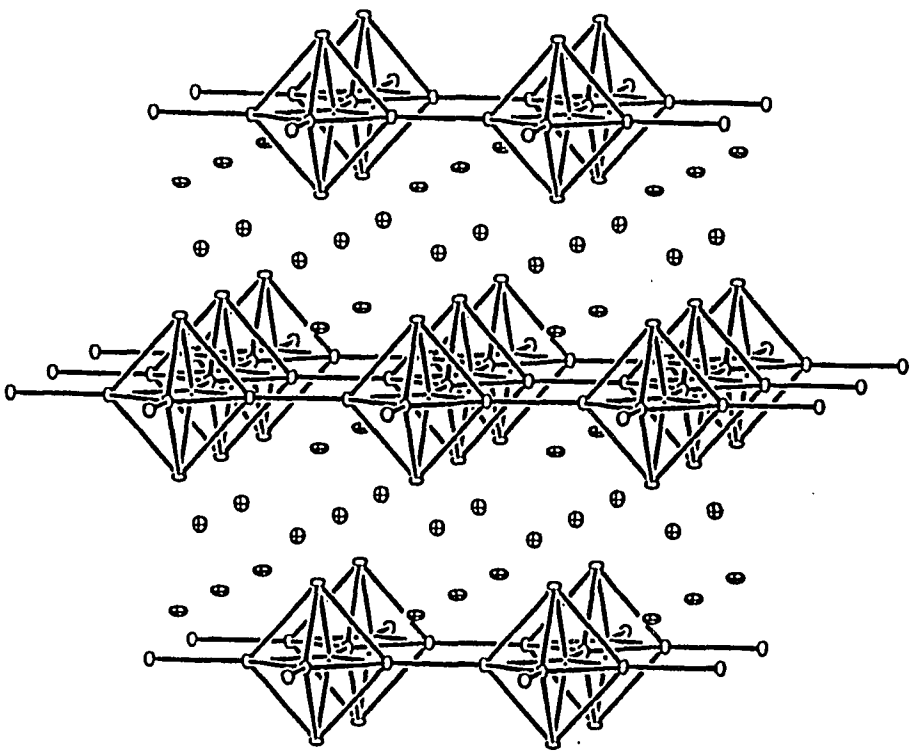

Figure 1. A section of the structure of Rb_2In_3 (*I4/nmm*) with indium as open and rubidium as crossed ellipsoids and the *c* axis vertical. The indium octahedra are joined with normal two-center exo bonds to form quasi-infinite square nets.

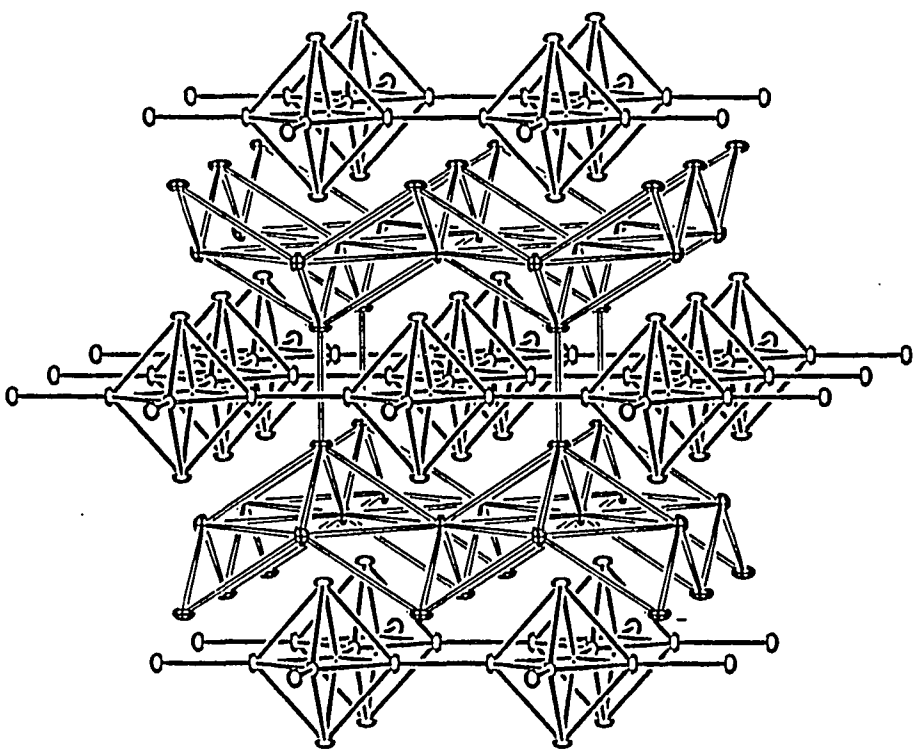

Figure 2. The Rb_2In_3 structure with neighboring rubidium atoms joined by open lines to emphasize the close relationship to the aluminum network in the $BaAl_4$ type structure of $RbIn_4$.

PAPER 10. SYNTHESIS, CHARACTERIZATION AND BONDING OF INDIUM CLUSTERS: FIVE NEW NETWORK STRUCTURES IN TERNARY ALKALI-METAL–INDIUM–THIRD ELEMENT SYSTEMS

ABSTRACT

Five new structures with complex networks of interconnected clusters were found in the systems (Na or K)–In–(Si, Ge, Sn, Pb, Zn, Cd, Hg, Cu, Ag or Au) where the third element substitutes for In. The structures have been refined by single crystal means: (I) $Na_{23}In_{38.4}Zn_{4.6}$ and $Na_{23}In_{39.8}Au_{3.4}$ – *P6/mmm*, Z = 2, a = 16.183 (2), 16.236 (1) Å and c = 15.723 (4), 15.733 (4) Å , R/R_w = 2.8/3.2 and 2.7/3.1% for the Zn and Au compound, respectively; (II) $Na_9In_{16.8}Zn_{2.3}$ – $Fd\bar{3}m$, Z = 16, a = 22.715 (7) Å, R/R_w = 2.6/3.0%; (III) $KIn_{2-x}Cd_x$ – *P6/mmm*, Z = 30, a = 17.4851 (8) and c = 10.4461 (7) Å, R/R_w = 3.5/5.8%; (IV) $K_{37}In_{69-x}Cd_x$ – $R\bar{3}m$, Z = 6, a = 17.301 (3) and c = 76.18 (3) Å, R/R_w = 3.1/4.5%; (V) $Na_{49}In_{80.9}Sn_{9.1}$ – $R\bar{3}m$, Z = 3, a = 16.209 (5) and c = 51.70 (3) Å, R/R_w = 4.5/5.1%. Structures I and III can be related to the structure of the σ-phase $CaCu_5$ and structures II and V, to the structure of the Laves phase $MgCu_2$ by substitution of indium clusters with different sizes for the Ca, Cu and Mg atoms. Structure IV is an intergrowth structure of III and $K_{22}In_{39}$ (related similarly to $MgCu_2$-type structure) and can be related in the same way to the structure of $NbBe_3$ which, in turn, is an intergrowth structure of the $CaCu_5$- and $MgCu_2$-type structures. A novel deltahedron of 18 indium atoms, a *closo*-In_{18}, is present in V. Apparently, a major factor ruling the stability of the different phases is the number of available electrons as modified by the amount and the kind of a neighboring element. The compounds with refined formulae, I, II and V, are Zintl phases according to the electron count while compounds III and IV could be such if their compositions are $KIn_{1.733}Cd_{0.267}$ and $K_{37}In_{64}Cd_5$, respectively.

INTRODUCTION

The chemistry of indium with negative oxidation states has shown to be remarkably diverse even in the binary alkali-metal–indium systems. It spans from a simple (noncluster) network of 8-bonded indium atoms in KIn_4[1] (oxidation state of -0.25 for In) through complicated structures of networks of clusters with 7-, 6- and 5-bonded indium atoms ($Na_7In_{11.4}$ as an example,[2] oxidation state of -0.65 for In) and isolated clusters of 5- and 4-bonded indium atoms in K_8In_{11}[3] (oxidation state of -0.72 for In), to the extreme case of isolated clusters of 3-bonded indium atoms in Na_2In[4] (oxidation state of -2 for In). Such fertile soil in the binary systems provokes an obvious next step of exploring ternary systems. Two paths have been undertaken, one in which cations are mixed and another, where indium atom is substituted or indium cluster is centered by a third element. Both have provided yet more new and structurally novel compounds. A few examples are the mixed cation compound $K_3Na_{26}In_{48}$ with *closo*- and *arachno*-In_{12},[5] the isolated $In_{10}Hg$ cluster in $K_8In_{10}Hg$ with one indium atom substituted by mercury,[6] and the Zn- and Ni-centered isolated clusters $In_{10}Zn$ and $In_{10}Ni$ in $K_8In_{10}Zn$[7] and $K_{10}In_{10}Ni$[8], respectively.

This article presents five more structure types found for ternary alkali-metal–indium–third element compounds. All five are networks of clusters where some of the indium sites are substituted by the third element.

EXPERIMENTAL SECTION

Synthesis

All materials were handled in a N_2-filled glovebox. The surfaces of Na (Alpha, 99.9+%, sealed under Ar), K (J.T.Baker, lump under oil, 98+%) and In (Cerac, granules, 99.999%) were cleaned with scalpel before use. Si (Johnson Matthey, rod, 99.9999%), Ge (Johnson Matthey, broken ingot, 99.9999%), Sn (Baker's Analyzed, drops, 99.999%), Pb (Johnson Matthey, electrolytic bar, 99.999%), Zn (Fisher, granules, 99.99%), Cd (Comico Products, strips, 99.999%), Hg (Fisher, instrument grade), Cu (J.T.Baker, turnings, 99.99%), Ag (G. Frederic Smith, granules, reagent) and Au (government issue, reagent) were used as received. Listed in Table I are the compositions of the mixtures of alkali-metal–indium–third element and the products obtained. Each mixture was loaded in a container of Ta-tubing that was welded at both ends under He at negative pressure. The containers, jacketed in evacuated and sealed fused-silica tubes, were then heated at different temperatures. Reactions 4, 7 and 20 (Table I) were heated at 700°C for two days and then cooled to room temperature at a rate of 5° per hour. The rest of the reactions were heated at 600°C for two days and then cooled to room temperature at a rate of 3° per hour. All products were gray, brittle and with a metallic lustre.

Characterization

A powder pattern from each product was obtained from a small portion of a powdered sample mounted between pieces of cellophane tape. An Enraf-Nonius Guinier camera, Cu $K\alpha_1$ radiation (λ = 1.540562 Å) and NBS (NIST) silicon as an internal standard were employed for this purpose. Five new structure types and, sometimes, known binary compounds were present in the products. The new structures were refined for at least one compound (below), and powder patterns were calculated based on the refined parameters. The rest of the products were identified by matching the observed powder pattern with a calculated one, and the results are

presented in Table I. The lattice parameters for each phase were determined by a least square refinement of the measured 2θ values indexed on the basis of the corresponding calculated pattern.

Structure refinement

All structures were refined with the aid of the TEXSAN package.[9]

$Na_{23}In_{38.4}Zn_{4.6}$ and $Na_{23}In_{39.8}Au_{3.4}$ (**I**). The two compounds are isostructural. Data collection and refinement parameters for the two are listed in Table II. Following is a more detailed description of the determination of the structure.

The product of reaction 12 (loaded as $Na_8In_{10}Zn$) was crushed and a few small pieces were sealed in glass capillaries. These were checked for singularity by oscillation film techniques and some were aligned. A Weissenberg photograph of the zero layer of one of them (0.1 × 0.1 × 0.2 mm) revealed a hexagonal cell with a mirror plane perpendicular to *c* (the crystal happened to be aligned along the *a* axis). An oscillation photograph from another crystal showed layer spacings inconsistent with the hexagonal cell determined from the first crystal. Later, the symmetry of the second crystal was determined to be cubic, and the structure was refined (structure **II**, below). The crystal with the hexagonal cell was mounted on a CAD4 single crystal diffractometer and 25 reflections from a random search were indexed with a hexagonal cell with cell dimensions close to the ones estimated from the film methods. Data from two small octants of reciprocal space were collected at 23°C with monochromated Mo Kα radiation up to 2θ = 50°. Corrections were applied for Lorentz and polarization effects and for absorption with the aid of the average of three ψ-scans at different θ angles. No systematic extinction condition was observed and the Wilson plot statistics suggested a centrosymmetric space group. Thus *6/mmm* was chosen for the first trials and later showed to be the correct space group.

Direct methods provided seven peaks with distances appropriate for indium atoms, one (In7, below) with distances of ~1.77 Å to two of its symmetry related positions but with distances to the rest of the atoms appropriate for indium, and one (In1, below) with distances shorter by ~0.2 Å from the distances around the first seven peaks. The peak heights of the last two plus two of the first seven positions (In8, 9, below) were about half of the peak heights of the remaining five. Nevertheless, all were assigned as indium atoms for the first few least-square cycles. A difference Fourier map revealed all eight sodium atoms. The subsequent refinement with the sodium atoms included led to about twice as large thermal parameters for In7–9 and about 1.3 times larger thermal parameter for In1 than the remaining indium atoms. In2 and 3 had relatively large thermal parameters as well. Next, the occupancies of all indium atoms were freed to vary while the sodium occupancies were held fixed. The occupancies of In1, 7, 8 and 9 dropped down to 50–60% and those of In2 and 3 to 80-90%. In4–6 deviated only by ~2% (0.5σ) from full occupancy. It was clear that In7 is statistically half occupied in order to avoid the short distance of 1.77 Å to symmetry related positions. It was not clear, though, which of the remaining partially occupied positions had some zinc mixed with the indium. The fact that such compound does not exist in the binary Na–In system indicates that the structure is truly ternary but how much zinc is involved and where it is positioned was not clear at this point. Fortunately, a crystal from an isostructural Na–In–Au compound was found and was studied by single crystal means.

A few small pieces from the crushed product of reaction 17 (loaded as $Na_9In_{10}Au$) were sealed in glass capillaries and checked for singularity by oscillation film technique. One of them (0.15 × 0.2 × 0.2 mm) was aligned along the *a* axis, and Weissenberg photographs of the zero and the first layers proved the correctness of the chosen Laue class *6/mmm*. Data were collected on CAD4 single crystal diffractometer from one big octant of reciprocal space up to $2\theta = 50°$

with monochromated Mo Kα at 23°C. Corrections were applied for Lorentz and polarization effects and for absorption with the aid of the average of two ψ-scans at different θ angles. The positional parameters from the partially refined Na–In–Zn structure were used for the first few least-squares cycles. All indium atoms were initially kept at full occupancy. This time, the thermal parameters of In1–3 became smaller than those of In4–6 while the ones for In7–8 remained about twice the latter. When the occupancies of the indium atoms were freed to vary In1–3 showed occupancies larger than full and In7–9 showed occupancies of 50–60%. This is a very strong indication that the In1–3 sites have some of the third element Zn or Au mixed in while the In7–9 sites are truly partially occupied by indium only. Therefore, In and Au were refined in the In1–3 sites by keeping the occupancies at full. In the final least-squares cycles, the data were additionally corrected for absorption by DIFABS empirical absorption correction, and all atoms were refined with anisotropic displacement parameters. The refinement converged at R, R_w = 2.7, 3.1% with a refined formula $Na_{23}In_{39.8(1)}Au_{3.40(7)}$. The largest residual peaks in the final difference Fourier map were 2.01 e/Å^3 (0.8 Å from In8) and -1.73 e/Å^3.

After Zn was mixed in the In1–3 positions of the first structure and DIFABS empirical absorption correction applied to the data all atoms were refined with anisotropical displacement parameters. The final refinement converged at R, R_w = 2.8, 3.2% and gave a refined formula $Na_{23}In_{38.4(2)}Zn_{4.6(1)}$. The largest residual peaks in the final difference Fourier map were 1.76 e/Å^3 (0.9 Å from In8) and -1.94 e/Å^3.

The largest degree of mixing of Zn or Au with In occurs at the In1 site in both structures, 53(1)% Zn and 27.6(6)% Au. This site is a part of an icosahedron (below) and has a very short exo bond (2.662(4) Å in the Zn and 2.761(2) Å in the Au derivatives) to its symmetry related position, thus interconnecting the icosahedra into a network. It is important to note here

that similar sites occur in the other four structures, and usually they are the ones occupied by the third element.

$Na_9In_{16.8}Zn_{2.3}$ (II). It was mentioned above that a single crystal with cubic symmetry was found in the crushed product of reaction 12 (loaded as $Na_8In_{10}Zn$). The crystal (0.15 × 0.15 × 0.20 mm) was mounted on a CAD4 single crystal diffractometer and 25 reflections found from random search were indexed with a face-centered cubic cell. Data from one octant of reciprocal space were collected at 23°C up to $2\theta = 50°$ with monochromated Mo Kα radiation. The data were corrected for Lorentz and polarization effects and for absorption with the aid of the average of three ψ-scans at different θ angles. An additional systematic extinction condition *hk0*: $h + k \neq 4n$ was observed. The Wilson plot statistics showed presence of a center of symmetry and, therefore, $Fd\bar{3}m$ was chosen for the structure solution. Listed in Table III are some data collection and structure refinement parameters.

Direct methods provided four peaks with distances appropriate for indium, but two of them, In2 and 4 (below), were with lower heights, approximately 2/3 and 1/2, respectively, of the heights of the other two. Also, the distance between two symmetry related In2 sites was shorter by ~0.2 Å than the rest of the distances. All four peaks were assigned as indium and a few least-square cycles and a difference Fourier map revealed four sodium positions. The thermal parameters for In2 and 4 became much larger than those of the other two indium atoms. Next, the occupancies of all indium atoms were varied while those of the sodium atoms were kept fixed. The occupancies of In1 and 3 did not deviate by more than 4% (1σ) from 100%, but In2 and In4 became 75% (8σ from full occupancy) and 52% (40σ from full occupancy), respectively. It was not clear, as in the refinement of the previous Zn-containing structure (above), which of the two positions contained zinc. A closer look at the bonding of In2 and 4 revealed that the first one corresponds to the In1 site from the previous structure (the site with

the biggest Zn mixing), that is, a part of an icosahedron that is exo bonded via a very short bond of 2.652(3) Å to an equivalent symmetry-related atom. In4, on the other hand, is a part of an icosioctahedron (In_{16}) and is six-bonded within the cluster. Moreover, if fully occupied this atom would be exo bonded (a seventh bond) to a symmetry equivalent atom. From previous experience, such a situation is very unlikely. From the two factors above it was quite clear that the In2 site has some Zn mixed in while the In4 site is partially occupied. The final refinement with Zn added to give a full occupancy of the In2 site, varied occupancy of the In4 site, anisotropic displacement parameters for all atoms and refined secondary extinction coefficient converged at R, R_w = 2.6, 3.0%. The largest residual peaks in the final difference Fourier map were 1.01 e/Å^3 (0.76 Å from In3) and -1.34 e/Å^3. The refined formula is $Na_9In_{16.8(3)}Zn_{2.3(3)}$.

$KIn_{2-x}Cd_x$ **(III).** A few small pieces from the crushed product of reaction 18 (loaded as K_2In_2Cd) were sealed in glass capillaries and checked for singularity by oscillation film technique. One of them (0.1 × 0.1 × 0.2 mm) was chosen, aligned and a Weissenberg photograph of the zero layer taken. This combined with a lattice parameter determined from the oscillation photograph defined a hexagonal unit cell and a *6/mmm* Laue class (the crystal happened to be aligned along the *a* axis). The same crystal was mounted on the CAD4 single crystal diffractometer, and 25 reflections found during a random search were indexed with the expected hexagonal cell. Data were collected from one large octant at 23°C up to 2θ = 50° with monochromated Mo Kα radiation. These were corrected for Lorentz and polarization effects and for absorption with the aid of the average of four ψ-scans at different θ angles. The Wilson plot statistics suggested a centrosymmetric space group, and since no systematic extinction condition was observed *P6/mmm* was chosen for the structure solution. The data collection and the structure refinement parameters are listed in Table IV.

Direct methods provided six peaks with distances appropriate for indium and they were so assigned. A few least-square cycles and a difference Fourier map revealed five positions with distances appropriate for potassium. One of them, K5 (below), was relatively smaller than the rest. They were assigned as potassium atoms and a few least-square cycles led to thermal parameter for K5 about six times larger than the rest. The thermal parameters of In5 and 6 were also larger than those of the rest of the indium atoms, three and two times, respectively. Next, anisotropic displacement parameters were refined for all atoms. This showed that K5 tends to be elongated along the *c* axis. This atom is positioned at the center of a hexagonal prism of In5 face-centered by In6 (below). The hexagonal ends of the prism are quite large openings normal to the *c* axis. The prisms are stacked on top of each other and form a cylindrical channel along which the potassium atoms are apparently free to "travel". In order to examine the environment around K5 more closely, a Fourier map was calculated based on F_{obs} with phases from the model. A section of it, passing through K5 and In5, is shown in Figure 1 (*c* vertical). The four black spots are the positions of In5 and at the center is the K5 position. It can be seen that there are two quite elongated satellites above and below K5, approximately 2.5 Å from it. A closer look reveals that the satellites are near the planes of the ends of the hexagonal prism and have two maxima with heights of approximately 16 and 13 e/Å^3. Initially, two potassium atoms were placed at the maxima but the subsequent refinement showed very strong coupling between their thermal parameters, one becoming very large and the other negative. Next, one potassium atom, K6, was refined somewhere between the two maxima. This time coupling occurred with the thermal parameter of the central potassium atom. The problem was approached by constraining each of the anisotropic displacement parameters of K6 to be equal to the corresponding one of K5 and, also, the sum of the occupancies of the two sites to be equal to one potassium atom per hexagonal prism. This led to a non-positive definite thermal parameter for the two potassium

atoms. This result and the fact that two potassium atoms were refined in a similar hexacapped hexagonal prism found in $K_{36}In_{69-x}Cd_x$ led to the conclusion that the total electron density inside the indium formation should be approximated with two rather than one potassium atoms. Subsequently, the sum of the occupancies of K5 and 6 was constrained to 2 atoms per indium cluster and the refinement converged at R, R_w = 3.5, 5.8%. This gives an approximate formula $KIn_{2-x}Cd_x$ for the compound. The largest residual peaks in the final difference Fourier map are 6.2 e/Å^3 (at K5, which could not be approximated better) and -3.56 e/Å^3. The K5 position refined with 80(4)% occupancy and this means that there is one potassium atom in 80% of the indium hexagonal prisms. This, of course, is inconsistent with the assumption that there are two potassium atoms in each prism but it is not possible to refine the sum of the occupancies of K5 and 6 since they have to be constrained to a fixed number. Therefore, the total content of potassium in the compound might be slightly less than estimated.

The thermal parameters of In5 and 6 are larger than those of the rest of the indium atoms. In order to check whether these two atoms might be partially occupied, the occupancies of all indium atoms were freed to vary while those of the potassium atoms were kept fixed. This resulted in a maximum deviation of 2% (1σ) from full occupancy and therefore all indium atoms were refined as fully occupied. The same procedure performed on the occupancies of K1–4 showed a maximum deviation of 8% (4σ), and therefore these atoms were also kept with full occupancies in the final refinement.

A second data set was collected from the same crystal at a temperature of -60°C. The idea was that if K5 and 6 move more or less freely along the channel of stacked hexacapped hexagonal prisms, their movement might be reduced at the lower temperature. Unfortunately, no significant improvement was achieved for the thermal parameters of these two atoms in the

refined structure. As expected, all atoms had smaller thermal motions but K5 and 6 retained their elongated thermal ellipsoids and a split type position for K6.

Since In and Cd differ only by one electron, it was not possible to determine how much and where the cadmium atoms are positioned. It was clear, though, that the phase is ternary since the binary K–In system has been studied quite extensively and no similar compound has been found. As can be seen from Table I, a compound with the same structure forms in the K–In–Hg system. Diffraction data set was collected from a single crystal of this compound (reaction 22, loaded as K_7In_9Hg), but it could not be refined to a satisfactory result. Nevertheless, even when partially refined to R = ~7%, the structure of the compound suggested quite clearly that Hg is mixed in the In2, 3 and 4 sites. These atoms form icosahedra (below) interconnected in a similar manner as the ones in the hexagonal **I** and cubic **II** structures (above). Similarly, all icosahedral sites in the former and one such site in the latter were refined with third-element content (above). It is logical, therefore, to have the same type sites with mixed In and Cd in the present compound, although how much of each element is present is impossible to determine. The result from the partial refinement of the corresponding Hg-substituted compound suggests an approximate formula $KIn_{1.64(3)}Hg_{0.36}(3)$ (~K_3In_5Hg).

$K_{36}In_{69-x}Cd_x$ (**IV**). A few pieces from the crushed product of reaction 20 (loaded as $K_8In_9Cd_2$) were sealed in glass capillaries and checked by oscillation film technique for singularity. Two of them were aligned, and Weissenberg photographs were taken from the corresponding zero layers. These combined with the layer spacing determined from the oscillation photographs revealed an R-centered hexagonal cell (the two crystals happened to be aligned along the *a* axis) with a very long *c* axis of approximately 76 Å. One of these crystals (0.2 × 0.15 × 0.1 mm) was mounted on a CAD4 single crystal diffractometer and 25 reflections found during random search were indexed with a rhombohedral cell with the expected

dimensions. Data from one big octant of reciprocal space were collected with ω-scans at 23°C up to $2\theta = 50°$ with monochromated Mo Kα radiation. Although the *c* axis is very long, because of the rhombohedral systematic extinction, no overlap of reflections was observed. The data were corrected for Lorentz and polarization effects and for absorption with the aid of the average of four ψ-scans at different θ angles. No additional systematic extinction condition was observed, and since the Wilson plot statistics suggested a centrosymmetric space group $R\bar{3}m$ was chosen. The data collection and structure refinement parameters are listed in Table V.

Direct methods provided 17 positions with distances appropriate for indium, and they were assigned as such. A few least-square cycles followed by a difference Fourier map revealed sixteen positions with environments and heights appropriate for potassium atoms, and they were so assigned. The refinement with isotropic thermal parameters proceeded smoothly to $R \approx 9\%$ but K16 and, to some extent, K14 and 15 had thermal parameters somewhat larger than the rest. Next, all atoms were refined with anisotropic displacement parameters. This led to very large ratios of $U_{33} : U_{11} = 3$, 4.5 and 12 for K14, 15 and 16, respectively. A more detailed study of the environment and the electron density around these positions was performed. The three atoms are surrounded by a cylinder of indium atoms, a hexacapped hexagonal prism, and they have each other for neighbors along the axis of the cylinder, the *c* axis. K14 and 15 are above and below and K16 is inside the hexacapped hexagonal prism. A Fourier map calculated from F_{obs} with phases defined by the refined structure revealed that K14 and 15 are truly single atoms elongated along *c* but that the third one, K16, has two maxima very close to each other. A section of the Fourier map passing through K16 and two of the capping atoms In15 of the hexagonal prism is shown in Figure 2 (*c* horizontal). The number of electrons in the elongated formation inside the prism was determined by integrating the electron density over the surface of the different isoelectronic contours. The resulting number of 36(1) electrons indicated that there

were two potassium atoms disordered inside the hexagonal prism. The fact that the latter has a mirror plane perpendicular to *c* through the capping In15 atoms means that one potassium atom is in one-half of the prism and the second, generated by the mirror, is in the other half. The approximation of the unique potassium atom was done by refining two atoms with partial occupancies at the two maxima of the electron density, K16 at the higher and K17 at the lower maximum. The sum of the two occupancies was constrained to two potassium atoms per hexagonal prism. In contrast to the refinement of the previous structure **III**, which has the same hexacapped hexagonal prisms, the two partially occupied potassium positions inside the prisms, K16 and 17, were successfully refined with independent thermal parameters. The final R and R_w became 3.1 and 4.5%, respectively, after the data were corrected for absorption by a DIFABS empirical absorption correction and all atoms refined with anisotropic displacement parameters. The largest residual peaks in the final difference Fourier map were 3.7 e/Å^3 (0.8 Å from K17) and -1.8 e/Å^3. The positions and the number of cadmium atoms could not be determined because of the negligible difference in the scattering power compared to that of indium and, therefore, the formula of the compound can be written only approximately as $K_{37}In_{69-x}Cd_x$. When varied, the occupancies for the indium positions did not deviate by more than 4% (1σ) when the occupancies of the potassium positions were held fixed, and by more than 8% (5σ) for the potassium positions (except K16 and 17) when the occupancies of the indium positions were held fixed.

$Na_{49}In_{80.9}Sn_{9.1}$ (V). A few crystals from the crushed product of reaction 7 (loaded as $Na_{21}In_{32}Sn_4$) were sealed in glass capillaries and checked for singularity by oscillation film technique. Some of them turned out to be of the $KIn_{2-x}Cd_x$-type structure according to lattice parameters determined from the oscillation photographs, but some showed layer spacings inconsistent with that structure. One of the latter (0.3 × 0.1 × 0.08 mm) was chosen, mounted

on a Rigaku AFC6R rotating anode single crystal diffractometer, and the 25 reflections found during a random search were indexed with a rhombohedral cell with a quite long *c* axis of ~52 Å. Data from one big octant of reciprocal space were collected at 23°C up to $2\theta = 50°$ with monochromated Mo Kα radiation. These were corrected for Lorentz and polarization effects and for absorption with the aid of the average of three ψ-scans at different θ angles. The Wilson plot suggested a centrosymmetric space group and therefore $R\bar{3}m$ was chosen. Data collection and refinement parameters are listed in Table VI.

Direct methods provided fourteen positions with distances appropriate for indium but four of them with somewhat smaller heights than the rest. All were assigned as indium and after a few least-square cycles and a difference Fourier map, ten positions appropriate for sodium were found and assigned as such. The subsequent refinement led to quite large thermal parameters for four indium positions, In6 and In12–14. The occupancies of these were freed to vary and showed values substantially lower than 100%. Next, the data were corrected for absorption by a DIFABS empirical absorption correction, and all atoms were refined with anisotropic displacement parameters. The final residuals and the largest peaks in the final difference Fourier map were R, R_w = 4.5, 5.1% and +2.11 e/Å^3 (1.4 Å from In14) and -2.53 e/Å^3, respectively. The approximate formula at this stage was $Na_{49}In_{90}$. It was clear, though, that some Sn is mixed in some of the In sites since no such structure occurs in the binary Na–In system. Again, the small difference of one electron between In and Sn made the questions of amount and locations of the tin atoms unanswerable.

The structure contains icosahedra connected to each other in a very similar manner to all four of the structure described above. The position of In14 is the one via which these clusters are bonded and this type of position contains a third element mixed in for structures **I** and **II**. Moreover, the distance from In14 to its symmetry related position in another icosahedron,

2.806(7) Å, is shorter than the "normal" range of In–In distances of 2.85 to 3.1 Å. Also, the distance from this position to its symmetry related position in the same icosahedron, 2.853(7) Å, is unusually short for an intracluster In–In distance. These observations suggest that the six-bonded In14 may be a tin position and, therefore, a tin atom was refined there. The occupancy, 76(1)%, remained below full and gave final formula $Na_{49}In_{80.9(1)}Sn_{9.1(1)}$.

RESULTS AND DISCUSSION

Structure description

$Na_{23}In_{38.4}Zn_{4.6}$ and $Na_{23}In_{39.8}Au_{3.4}$ (I). The final positional and thermal parameters for each of the two compounds and the important distances are listed in Tables VII, VIII and IX, respectively. A general view of the anionic network of the structure is shown in Figure 3 where all distances less than 3.5 Å are drawn and the building blocks are shaded.

It can be seen from Figure 3 that the structure is built of two types of clusters, In_{12} and In_{15}, and a quite open formation of 21 atoms, a "spacer", all interconnected via exo bonds. The first type of clusters, a 12-bonded icosahedron with D_{2h} symmetry (Figure 4a) is centered on the *3g* (*mmm*) position. It is built of In1, 2 and 3, the sites with some mixing from the third element Zn or Au. The cluster is bonded to four clusters of the same type through In1–In1 bonds, to four In_{15} clusters through In3–In4 bonds, and to four spacers through In2–In5 bonds. Many of the intra- and inter-cluster distance are very short for In–In, the shortest of them associated with the site with the largest amount of third element mixed in, In1. One intra- and one inter-cluster distances from this site to two symmetry equivalent positions are only 2.662(4) Å for the Zn-substituted compound and 2.761(2) Å for the Au-substituted one. The latter is apparently larger because of the larger Au atom and also because Au substitutes 27.6(6)% for the indium in this position while Zn does 53(1)%. The other four intracluster distances from In1 are also short, 2.923(2)–2.939(1) and 2.9275(8)–2.948(1) Å for the Zn and Au derivatives, respectively. In2 and 3 have smaller amounts of Zn (6(1) and 18(1)%, respectively) or Au (13.4(6) and 15.6(6)%, respectively), and therefore the contraction of the distances to these positions is not as pronounced. The intracluster bonds around In2 are in the ranges 2.939(1)–3.011(1) and 2.9275(8)–3.071(2) Å and the exo bonds are 2.937(2) and 2.913(1) Å for the Zn and the Au derivatives, respectively. In3, which has more of the third element mixed

in than In2, has even shorter intracluster, 2.923(2)–3.011(1) Å for the Zn compound and 2.9265(2)–3.0403(9) Å for the Au compound, and intercluster distances, 2.878(2) and 2.866(1) Å for the Zn and Au derivatives, respectively.

The next building block, a 15-bonded *closo*-In_{15} cluster centered on the *2c* ($\bar{6}m2$) position, has D_{3h} symmetry (Figure 4b). It is built of In4, 6 and 9 and its geometry can be viewed as tricapped truncated trigonal prism. It has 26 hexagonal faces and can be called icosihexahedron. The atoms of the truncated prism (In4, 6) are 5-bonded within the cluster and the ones capping the hexagonal faces (In9) are 6-bonded. The distances from the 6-bonded In9 atom, 3.265(1) and 3.263(1) Å to In4 and 3.440(2) and 3.445(1) to In6 in the Zn and Au compounds, respectively, are quite longer than those from the 5-bonded atoms. Such differences have been seen for 6-bonded atoms in other clusters and this is normal since more but longer bonds can equate to fewer but short ones. All of the atoms are also exo bonded, In4 to In3 from six icosahedra, In6 to In8 from three 21-atom spacers (2 bonds to each spacer) and In9 to In9 from three other In_{15} clusters. The In9 site refines as 63.1(4) and 64.4(4)% In in the Zn and Au compounds, respectively. The two numbers are equal within 3σ, a good indication that no Zn or Au are mixed with indium in this site. The fact that it is partially occupied is not surprising since similar 7-bonded (6 intra- and 1 inter-cluster bonds), partially occupied indium positions are common features in other large clusters. Examples are found in 8-bonded *closo*-In_{16}, 12-bonded *closo*-In_{18} and 16-bonded *closo*-In_{16}. Since the exo bond is In9–In9, half occupancy of this site would mean that when one site is occupied, the other is left empty so that no exo bond is present and, therefore, the atom at the filled position has a lone pair pointing at the empty position. A 63–64% occupancy means that some 26–28% of the In9–In9 pairs will have both sites filled and therefore an exo bond will exist.

The 21-atom "spacer" is shown in Figure 4c. It is centered on the position *1a* (*6/mmm* type) with a 6-fold axis and six mirror planes containing that axis. Figure 4c shows only one of the two possible orientations for the spacer while Figure 5 shows how the formation required by the symmetry of the *6/mmm* position is generated by overlapping two equivalent spacers rotated 60° from each other. The In5 position is common to both orientations and has full occupancy in both Zn and Au compounds. One-half of the In7 and In8 positions belong to one orientation and the other half, to the second. Moreover, an occupied In7 position in one orientation excludes the possibility of having the same position occupied in the other orientation because this would lead to impossibly short In–In separations of 1.775 Å. In a very good agreement with this is the fact that this position refines with half occupancy for both Zn and Au compounds, 49.8(6) and 50.3(5)%, respectively. The In8 position does not necessarily have to be with half occupancy since it can be occupied in both orientations at the same time. The distance from In8 from one orientation to In8 from the other orientation is 3.471(2) Å for the Zn compound and 3.485(2) Å for the Au compound. These are quite long In–In distances and are comparable to the distances between similar but fully occupied positions forming the two ends of a hexacapped hexagonal prisms present in **III**, d(In–In) = 3.624(2) Å, and in **IV**, d(In–In) = 3.567(3) Å. In8 refined with equal within 2σ occupancies for the Zn and the Au compounds, 60.8(6) and 62.1(6)%, respectively. Again, this proves that no third element mixes with indium at this position. The fact that In8 is about 11–12% more than half occupied means that when three In7 and six In8 atoms are with one orientation, additional In8 atoms from the other orientation may be present as well. These extra atoms will have different bonding than the other six In8 atoms since no bond can be formed to In7.

The geometry of the 21-atom spacer can be viewed as two truncated tetrahedra fused through one triangular face. Some of the hexagonal faces near the waist may be capped by In8.

It is 18-bonded to 12 icosahedra (In5–In2) and 3 In_{15} clusters (two In8–In6 to each In_{15}). The two orientations are equivalent and equivalently bonded and, therefore, the energy difference between them will be zero. This probably is the reason why preferred orientation and subsequently a formation of a superstructure do not occur. Attempts to refine the structure in lower symmetry space groups did not produce a new result.

Finally, the structure can be viewed as somewhat related to a very common structure among the intermetallic compounds, that of $CaCu_5$. The latter is called a σ-phase and is very closely related to the Laves phase $MgCu_2$. The structure is composed of a network of tetrahedra of Cu atoms fused through one face and through all four vertices and "interstitial"-like Ca atoms in the big voids of the network. The relation of the structure of **I** to that of $CaCu_5$ is such that the centers of the In_{12} and In_{15} clusters in the former are at the positions of the Cu atoms in the latter, and the centers of the 21-atom spacers in the former are at the positions of the Ca atoms in the latter. A condensed view of the structure presented in Figure 6 clearly shows this relation. Crossed circles represent the 21-atom spacers (Ca in $CaCu_5$), octant-shaded circles are used for the In_{15} clusters (2-fold Cu position in $CaCu_5$) and open circles are used for the icosahedra (3-fold Cu position in $CaCu_5$). The icosaehdra form Kagomé nets and these are joined via bonding to the icosihexahedra.

All sodium cations except Na1 and 2 are in the voids between the building blocks and cap their faces. Na1 centers the In_{15} cluster and Na2, the two fused truncated tetrahedra of the 21-atom spacer.

As can be seen in Table I, this structure occurs not only when the third element is electron-poorer, e.g. Cu, Ag, Au, Zn, Hg, but also when it is electron-richer than indium, e.g. Si, Ge, Sn. It is not clear why and how this happens and also why the same structure does not exist in the corresponding binary alkali-metal–indium systems.

$Na_9In_{16.8}Zn_{2.3}$ (**II**). The final positional and thermal parameters and important distances are listed in Tables X and XI, respectively. A general view of the anionic network of the structure is shown in Figure 7 where all distances less than 4.0 Å are drawn and the building blocks are shaded.

The anionic structure is a network of two kinds of building blocks: a 12-bonded icosahedron, In_{12}, and a 16-bonded icosioctahedron, In_{16}. The icosahedron (Figure 8a) is centered on the *16c* ($\bar{3}m$) position and has D_{3d} symmetry. It is built of In1 and 2 and is 12-bonded to 6 icosahedra (In2–In2) and 6 icosioctahedra (In1–In3). The icosahedra form Kagomé nets. In2, the site via which the icosahedra are interconnected, corresponds to the In1 site in structure **I**. Not surprisingly then, like In1 in **I**, In2 in this structure is the site which has some Zn mixed in, 38(5)%. Also, like In1 in **I**, the distances from In2 to the surrounding atoms are shorter than the other In–In distances. These include two intracluster In2–In2 distances of 2.881(3) Å, two intracluster In2–In1 distances of 2.955(2) Å, one intracluster In2–In1 distance of 2.889(2) Å and one very short intercluster In2–In2 distance of 2.652(3) Å.

The icosioctahedron In_{16} (Figure 8b) is centered on the *8b* ($\bar{4}3m$) position and has T_d symmetry. It is built of In3 and 4 and is 16-bonded to 12 icosahedra (In3–In1) and 4 icosioctahedra (In4–In4). Its geometry is a truncated tetrahedron of In3 tetracapped by In4. The same cluster but 8- and 12-bonded has been found in $Na_7In_{11.7}$ and $Na_{15}In_{27.5}$, respectively. Again, the intracluster distances from the 6-bonded In4, 3.399(5) Å, are longer than those between the 5-bonded In3 atoms, 3.013(3) and 3.062(2) Å. In4 refines with occupancy of 52(1)%, one-half within 2σ. If fully occupied it would be exo bonded (a seventh bond) to In4 from another icosioctahedron and, as discussed above, this is apparently an unfavorable situation. Instead, when the In4 site in one icosioctahedron is filled, the neighboring equivalent site in the

adjacent icosioctahedron is presubably empty and no exo bond is formed. A lone pair on the filled site would be pointing towards the empty one.

The structure can be viewed as related to the well known Laves phase $MgCu_2$ which is built of Cu tetrahedra sharing all corners with each other and "interstitial"-like Mg atoms in the voids of the Cu network. The relation with **II** is such that the icosahedra are centered on the Cu positions and the icosioctahedra are centered on the Mg positions. A condensed view of the structure shown in Figure 9 illustrates this. All sodium cations except Na4 are in the voids between the clusters and cap their faces. Na4 centers the icosioctahedron.

The same structure type has been reported by Charbonnel and Belin for the compound $Na_{8.75(3)}Ga_{14.06(5)}Cd_{5.94}$.[10] There are two differences in their refinement compared with that presented here. Firstly, the third element Cd was refined mixed with Ga in all of the icosioctahedral sites, 70.7(7) and 85(1)% Cd in the corresponding In3 and In4 sites, respectively. No partially occupied sites on the icosahedra were observed. Secondly, the Na1 site which is located in the tetrahedral void between four icosahedra was refined with 49(5)% occupancy. From our experience, a partially occupied alkali-metal site is a very unlikely situation. (No such site has been encountered by us in any of the alkali-metal–indium–(third element) structures.) The composition of the compound provides 1.25 electrons fewer than the needed 64, and this has been explained by "hypoelectronic interpolyhedral bonding", a phrase invented especially for this compound since no other compound in the Ga or In systems has such bonding. The refined formula for $Na_9In_{16.8}Zn_{2.3}$ provides $9 + 16.8 \times 3 + 2.3 \times 2 = 64$ electrons (below) and is more likely to be the right composition.

$KIn_{2-x}Cd_x$ (**III**). The final positional and thermal parameters and the important distances are listed in Tables XII and XIII, respectively. A general view of the anionic network of the

structure is shown in Figure 10 where the building blocks are shaded and all distances below 4.0 Å are drawn.

The network of this structure is assembled of three building blocks: a 12-bonded icosahedron, a 6-bonded triangle and a 12-bonded 18-atom "spacer" with a shape of a hexacapped hexagonal prism (a "Big Mac"). The icosahedra (Figure 11a) are centered on the *3g* (*mmm*) positions and have D_{2h} symmetry. They are built of In2, 3 and 4 and are bonded to 4 icosahedra (In2–In2), 4 triangles (In4–In1) and 4 spacers (In3–In5). Interconnected via In2, the icosahedra form the same Kagomé nets as found in **I** and **II**. The In2 site corresponds to In1 and In2 in **I** and **II**, respectively. The distances around this position in the latter two structures are too short for In–In distances and a third element Zn or Au was found mixed with In in the site. In contrast, the distances around In2 in this structure, 2.995(2)–3.123(1) Å, are in the "normal" In–In range. Similar to **I**, **II** and the partially refined Hg derivative, it is thought that Cd substitutes for In in some of the icosahedral sites.

The second building block, a 6-bonded triangle (Figure 11b), is centered on the *2d* ($\bar{6}m2$) position and has D_{3h} symmetry. Each In1 atom of the triangle is 4-bonded, two bonds in the triangle and two exo bonds to two icosahedra (In1–In4).

The 18-atom spacer (Figure 11c) is centered on the *1b* (*6/mmm*) position and has D_{6h} symmetry. It can be considered as a hexagonal prism formed of In5 that is face-centered (rectangular faces) or hexacapped by In6. It is 12-bonded to 12 icosahedra (In5–In3). The distances between In5 and In6, 2.920(1) Å, are in the "normal" In–In range, but the distances within the hexagonal rings of In5 and In6 are quite longer, 3.624(2) and 3.267(2) Å, respectively. The shorter bonds within the middle hexagon of In5 compared with those within the end hexagons of In6 make it somewhat squeezed at the waist. The distance between the In5 atoms is practically out of the bonding range, and therefore these atoms are only three-bonded.

Bonds between these atoms are shown in Figure 11c only to clarify the shape of the formation. The length of the exo bond at In5, 3.001(2) Å, is typical for In–In. It looks like the surrounding icosahedra pull the In5 atoms outward and they, in turn, pull the In6 atoms outward. The impact of this is more strongly pronounced on the hexagons of In5 than on the hexagons of In6. Indeed, what we find is a prism more expanded at the ends than at the waist. All of this suggests that the shape and the distances of this so-called spacer are determined to a great extent by external and not so much by internal factors. This conclusion is also supported by the fact that the same formation but with somewhat shorter In5–In5 and In6–In6 distances, 3.567(3) and 3.191(2) Å, respectively, exists in $K_{37}In_{69-x}Cd_x$ (**IV**) where the decrease is apparently a result of a more densely packed Kagomé net of icosahedra.

Like **I**, this structure can also be viewed as related to the σ-phase $CaCu_5$. A condensed view of the structure is shown in Figure 12. Again, icosahedra are centered on the 3-fold Cu positions, but this time triangles instead of In_{15} clusters are centered on the 2-fold Cu positions. The Ca position is the center of the 18-atom spacer. As Ca in $CaCu_5$, the spacers in this structure form chains along the *c* axis. The hexagonal prisms are stacked on top of each other and form a cylindrical channel (Figure 10).

All potassium atoms except K5 and 6 are in the voids between the building blocks and cap their triangular faces. K5 and 6 are inside the 18-atom spacer and are disordered along the axis of the cylindrical channel.

As in structure **I**, this structure also exists with elements electron-poorer or electron-richer than indium (Table I). The partially refined structure of $KIn_{1.64(3)}Hg_{0.36}$ provides the 202 (within 3σ) electrons needed for bonding (below) and, therefore, the compounds with Si, Ge, Sn or Pb would have some antibonding states filled. On the other hand, although listed under this structure type in Table I, the electron richer compounds may have some slight modifications of

the structure that are undetectable by powder diffraction. Moreover, a partial structure refinement of the Ge analogue has shown that although the bulk part of the structure is the same as $KIn_{2-x}Cd_x$, the two ends of the hexacapped hexagonal prism may be capped by Ge atoms. Also, the prism is expanded rather than squeezed at the waist. These differences may lead to different electronic requirements, but practically the same powder pattern. Again, it is not clear why the structure does not form in the binary alkali-metal–indium systems.

$K_{37}In_{69-x}Cd_x$ (**IV**). The final positional and equivalent isotropic thermal parameters, the anisotropic displacement parameters and the important distances are listed in Tables XIV, XV and XVI, respectively. A general view of the anionic network of the structure is shown in Figure 13 where the building blocks are shaded, and all distances less than 4.0 Å are drawn.

The structure is composed of five different building blocks: 12-bonded icosahedra, 6-bonded icosahedra, 6-bonded triangles, 15-bonded 15-atom spacers and 12-bonded 18-atom spacers. The 12-bonded icosahedra (Figure 14a) are centered on *18h* (*m*: ~1/6, 2x, 0.1) positions and have C_s symmetry. They are built of In2, 3, 5, 6, 7, 8, 9 and 10, and are bonded to four icosahedra of the same type (In3–In3 and In7–In7), one 6-bonded icosahedron (In9–In4), two triangles (In2–In1 and In5–In1), three 15-atom spacers (In10–In11 and In8–In12) and to two 18-atom spacers (In6–In17). These clusters form Kagomé nets like the 12-bonded icosahedra in structures **I–III**. Atoms In3 and 7 provide the intralayer bonding between the clusters and therefore correspond to the In1 position in **I** and the In2 position in **II**, the sites with mixed In and Zn or Au occupancies. In contrast with **I** and **II**, though, the distances from In3 and In7 to their equivalent positions, 2.982(2) and 3.007(2) Å for the intercluster In3–In3 and In7–In7, respectively, and 3.002(2) and 3.017(2) Å for the intracluster In3–In3 and In7–In7, respectively, are "normal" for In–In. The In3–In3 distances are slightly shorter than the corresponding inter- and intra-cluster distances in **III**, 2.995(2) and 3.015(2), respectively, and this leads to slightly

shorter distances within the hexagons of the 18-atom spacer (below). Similarly to **I–III** the sites of In3 and 7 are thought to have some Cd mixed in.

The 6-bonded icosahedron (Figure 14b) is centered on the *3a* ($\bar{3}m$) position and has D_{3d} symmetry. It is built of In4 and 13 and is bonded to six 12-bonded icosahedra (In4–In9). The In13 atoms do not have exo bonds. The clusters provide some of the bonding between every other pair of Kagomé nets and correspond to the In_{15} clusters in **I** and to the triangles in **III**.

The 6-bonded triangle (Figure 14c) is centered on a *6c* (*3m*: 0, 0, 0.83345) position and has C_{3v} symmetry. It is composed of three In1 atoms, each of which is four bonded, 2 bonds within the triangle and 2 exo bonds to two 12-bonded icosahedra (In1–In2 and In1–In5). The triangles provide some of the bonding between the Kagomé nets but only between the ones that are not already joined via a 6-bonded icosahedron. In other words, triangles and 6-bonded icosahedra alternate between the Kagomé nets. The same kind of 6-bonded triangles is present in structure **III**.

The 15-bonded 15-atom spacer (Figure 15a) is centered on a *6c* (*3m*; 0, 0, 0.6403) position and has C_{3v} symmetry. It is built of In11, 12, 14, 16 and is bonded to nine 12-bonded icosahedra (In11–In10 and In12–In8) and three spacers of the same type (two bonds In14–In16 to each). The spacer is positioned between every other pair of Kagomé nets, the same pairs between which the 6-bonded icosahedra are positioned. The same type spacer has been found in $K_{22}In_{39}$.[11]

The 12-bonded 18-atom spacer (Figure 15b) is centered on the *3b* ($\bar{3}m$) position and has D_{3d} symmetry, but it is very close to D_{6h}. The same type spacer was found in **III** (above). The distances within the hexagons of this hexacapped hexagonal prism, 3.191(2) Å for In15–In15 and 3.567(3) Å for In17–In17, are longer than the usually seen range of In–In distances while the distances between the hexagons, 2.992(2) and 2.994(2), and the exo distances, 3.014(2) Å,

are within that range. Again, it looks like the In17 atoms are pulled radially outward by In6 from the surrounding icosahedra and they, in turn, pull out the atoms in the waist hexagon, In15.

All potassium cations except K14–17 occupy the voids between the building blocks and cap their triangular faces. K14 centers the 15-atom spacer, K16 and 17 are disordered inside the 18-atom spacer, and K15 lies between the two types of spacers and caps a hexagonal face of each.

Finally, the structure can be viewed as related to another σ-phase, $NbBe_3$. The latter is actually an intergrowth structure of the σ-phase $CaCu_5$ and the Laves phase $MgCu_2$. Stacking alternating layers of the two on each other gives the $NbBe_3$ structure. Structure **IV** is built in a similar manner. We have already shown that structures **II** and **III** can be related to $MgCu_2$ and $CaCu_5$, respectively. A layer of **III** provides one of the two kinds of building layers of **IV**. The second type of layer could not be a layer of **II** since the latter contains 16-atom clusters. On the other hand, the structure of $K_{22}In_{39}$[11] is also related to $MgCu_2$ and at the same time has the same 15-atom spacer as the one found in **IV**. A condensed view of **IV** together with a condensed view of $K_{22}In_{39}$ are shown in Figure 16. Stacking alternating layers of $K_{22}In_{39}$ (Figure 16b) and of **III** (Figure 12) on each other gives structure **IV**.

$Na_{49}In_{80.9}Sn_{9.1}$ (**V**). The final positional and isotropic thermal parameters, the anisotropic displacement parameters and the important distances are shown in Tables XVII, XVIII and XIX, respectively. A general view of the anionic network of the structure is shown in Figure 17 where the building blocks are striped and all distances less than 4.0 Å are drawn.

The structure is composed of four interconnected building blocks: two types of 12-bonded icosahedra, 12-bonded *closo*-In_{18} deltahedra and 24-bonded 20-atom spacers. The first type of icosahedron, A-type (Figure 18a), is centered on the *9d* (*2/m*) position and has C_{2h} symmetry. It is built of the atoms In8, 9, 11 and Sn and is bonded to four A-type and two B-

type icosahedra (Sn–Sn and In8–In1, respectively), two 20-atoms spacers (two In9–In7 bonds to each), and two In_{18} clusters (In11–In4). Again, these icosahedra interconnected to each other via Sn–Sn bonds form Kagomé nets. Although Sn and In are undistinguishable by X-ray diffraction, Sn was refined at this particular site because the corresponding site in **I** and **II** has shown a third element mixed in. Also, the inter- and intra-cluster Sn–Sn distances, 2.806(7) and 2.853(7) Å, respectively, are less than the rest of the distances in the structure.

The 12-bonded *closo*-In_{18} cluster (Figure 18b) is centered on the *3a* ($\bar{3}m$) position and has D_{3d} symmetry. It is built of In4, 10 and 13 and is bonded to 6 A-type and 6 B-type icosahedra (In4–In11 and In13–In3, respectively). Its geometry could be considered as that of a hexacapped (In13) truncated trigonal antiprism (In4 and 10). Since it has 32 faces it can be named icosidodecahedron. This is the largest deltahedron found and is the first example of this size. The capping atom In13 is 6-bonded within the cluster and has an exo bond. As in many other clusters with similar 7-bonded atoms, In13 refines partially occupied, 45(1)%. The cluster has the same function as the *closo*-In_{15} in **I**, the triangles in **III**, and the 6-bonded icosahedra in **IV**: it joins the Kagomé nets of 12-bonded icosahedra.

The second type icosahedron, B-type (Figure 19a), is centered on a *6c* (*3m*: 0, 0, ~0.3) position and has C_{3v} symmetry. It is built of In1, 2, 3 and 6 and is bonded to three A-type icosahedra (In1–In8), four 20-atom spacers (three In2–In5 bonds to one and three In6–In5 bonds to three others) and three In_{18} clusters (In3–In13). In6, which is exo bonded to In5 from a 20-atom spacer, was refined with 80(1)% occupancy meaning that In5 (Figure 19b) is only 3-bonded 20% of the time. This will not change the electronic requirements for this particular bonding (below) since a 2-electron bond In5–In6 is replaced by a 2-electron lone pair on In5 when the In6 site is empty.

The 24-bonded 20-atom spacer (Figure 19b) is centered on the *3b* ($\bar{3}m$) positions. It is composed of In5, 7, 9 and 12 and is bonded to six A-type icosahedra (two bonds In7–In9 to each) and eight B-type icosahedra (two icosahedra with three bonds In5–In2 to each and six icosahedra with one bond In5–In6 to each). The spacer can be viewed as built of two parts of monocapped truncated tetrahedron. One of the triangles of what would be a complete truncated tetrahedron, the triangle of In2 atoms, is actually a triangular face of the B-type icosahedron. The In12 atom caps the face of six In7 atoms making it 6-bonded within the truncated tetrahedron. If fully occupied it would have a seventh bond to another In12 from the other half of the spacer. As seen many times, such atoms tend to be partially occupied and In12 is not an exception. It refines with 70(2)% occupancy which means that in some of the spacers the exo bond In12–In12 exists and in some it is replaced by a lone pair on one of the In12 atoms.

A condensed view of the structure with the building blocks represented as spheres with different sizes is shown in Figure 20a. The network of Kagomé nets of In12 (A-type) connected via In_{18} can be seen. The B-type icosahedra and the 20-atom spacer are filling voids in this network.

Another, perhaps better, way to look at the structure is to consider the B-type icosahedron and monocapped truncated tetrahedron (half of the 20-atom spacer) fused via triangle as one building block of 22 atoms (In1, 2, 3, 5, 6, 7, 12). It is 19-bonded to 9 A-type icosahedra (In1–In8 and In7–In9), 3 In_{15} clusters (In3–In13) and 7 spacers of the same sort (In5–In6 and In12–In12). Figure 20b shows another condensed view of the structure where the centers of this 22-atom formation are represented as spheres. It can be seen that the structure can be considered as again related to the Laves phase $MgCu_2$. The network of Cu atoms in the latter is replaced by network of A-type icosahedra and *closo*-In_{18} clusters while the 22-atom

spacers are centered on the Mg sites. Since In_{18} via which the Kagomé nets are joined is quite large and elongated the spacers that occupy the Mg site have to be large and long.

All sodium cations except Na2 and 9 are positioned between the building blocks and cap their faces. Na2 centers the monocapped truncated tetrahedra of the spacers and Na9 centers the *closo*-In_{18}.

Electronic structure and electron count

Structure I. Extended-Hückel MO calculations were performed on the *closo*-In_{15} cluster (Figure 4b) and the resulting diagram is shown in Figure 21. It can be seen that there is one nonbonding orbital which could be filled or empty. When empty the cluster has $2n + 2$ skeletal electrons below a gap of ~1 eV and obeys the Wade's rule. When the orbital is filled the cluster has $2n + 4$ skeletal electrons and a gap of ~2 eV. The HOMO is tangential with only p_x and p_y orbitals on In4 and 6 involved in the interactions. It is antibonding within the triangles of In4 but is σ-bonding between In4 and In6 and is also π-antibonding along the In6–In6 bonds. The atoms at the waist have zero coefficients since the orbital has a node there. If the cluster is considered as built of two equivalent parts above and below the waist, this orbital then is bonding within each part but antibonding between them. The same type of orbital for the smaller tricapped trigonal prism, In_9, is well into the antibonding region because it is antibonding within and between the two ends of the prism (the capping atoms do not contribute). When the cluster gets larger and more elongated the two parts get further apart, more bonding interactions are available and the antibonding ones are not so pronounced. The orbital is nonbonding for In_{15} and already bonding for the larger In_{18} (Figure 21).

The In_{15} cluster is always at least 6-bonded (In4–In3, Figure 4b). Six additional exo bonds In6–In8 are formed every time the 21-atom spacer is in a proper orientation (above). The 2 electrons needed for such bond will be replaced by 2 electrons needed for a lone pair on In6

when the exo bonds are not available and therefore the number of needed electrons would not change. In9 may or may not be exo bonded to another In9. Again, a pair of electrons is needed in both cases, either for a bond or a lone pair. It is very unlikely that two In9 atoms from two neighboring clusters will be missing at the same time so that there will be no need for this pair of electrons. This means that the number of exo electrons will be independent of the exo bonding of the cluster, and so we can consider it always as 15-bonded for simplicity. The number of electrons required for skeletal bonding within the cluster will be the same whatever the occupancy of the In9 site may be.

All atoms of the 21-atom spacer are 4-bonded and therefore require 4 electrons each. We can count the number of needed electrons for each building block in the following way. Each of the three 12-bonded icosahedra requires 26 (skeletal) + 12 (exo bonds) = 38 electrons. Each of the two 15-bonded In_{15} clusters requires 32 or 34 (skeletal) + 15 (exo bonds) = 47 or 49 electrons depending upon whether the nonbonding orbital is filled or not. Each spacer has 21 4-bonded atoms and therefore requires $21 \times 4 = 84$ electrons. The sum per unit cell becomes $3 \times 38 + 2 \times 47$ (or 49) + 84 = 292 or 296 needed electrons.

The numbers of available electrons from the two refined formulae $Na_{23}In_{38.4(2)}Zn_{4.6}$ and $Na_{23}In_{39.8(1)}Au_{3.4}$ are $2 \times (23 + 38.4 \times 3 + 4.6 \times 2) = 294.8(1.2)$ and $2 \times (23 + 39.8 \times 3 + 3.4) = 291.6(1.2)$, respectively. These numbers suggest that the Au compound could be balanced electronically while the Zn derivative has some extra electrons, presumably on the nonbonding levels of the In_{15} cluster. The number of available electrons in a hypothetical binary Na–In compound with the same structure would have been around 304 which means that 8 electrons would be in antibonding levels. On the other hand, the structure exists with the electron richer Si, Ge and Sn according to their powder patterns. One possible explanation for this is that the occupancies of some sites may be even lower so that the formula would provide fewer electrons.

Another possibility is that the main framework of the structure is the same, so that the powder pattern looks similar, but the spacer may be different.

Structure II. We have done EHMO calculation on an icosioctahedron before and have found that because of the T_d symmetry it intrinsically requires $2n + 4 = 36$ rather than the usual $2n + 2$ electrons.[2] The In4 atom, 6-bonded within the cluster and exo bonded to the same atom from the next icosioctahedron, refines with half occupancy. This means that either a 2-electron exo bond or a lone pair is associated with this atom and, therefore, the occupancy does not affect the electron count. We can think of the cluster as 16-bonded for simplicity.

Since each 12-bonded icosahedron requires 26 (skeletal) + 12 (exo bonds) = 38 and each 16-bonded icosioctahedron, 36 (skeletal) + 16 (exo bonds) = 52 electrons, and there are one icosahedron and a half icosioctahedron per formula, the number of needed electrons is 38 + 52/2 = 64 per formula. The refined formula $Na_9In_{16.8(3)}Zn_{2.3}$ provides $9 + 16.8 \times 3 + 2.3 \times 2 =$ 64(1) electrons and therefore the compound should be a Zintl phase.

Structure III. Extended-Hückel Mo calculations performed on the 12-bonded 18-atom spacer showed that it has 20 bonding skeletal orbitals below a gap of 0.8 eV. This leads to a requirement of $40 = 2n + 4$ skeletal electrons. If we assume that the spacer is the *arachno* derivative of a *closo*-In_{20} then the latter should have $2n$ electrons. This comparison is probably inappropriate since the spacer has quite long distances In5–In5 and In6–In6 and thus deviates too much from the geometry expected for species derived from a deltahedron.

The numbers of electrons needed for each of the building blocks are as follows: 26 (skeletal) + 12 (exo bonds) = 38 for each of the three icosahedra, $3 \times 4 = 12$ for each of the triangles (all are 4-bonded atoms) and 40 (skeletal) + 12 (exo bonds) + 2×6 (lone pairs) = 64 for the 18-atom spacer. The total per unit cell becomes $3 \times 38 + 2 \times 12 + 64 = 202$ electrons needed for bonding. The electronically balanced compound would have the formula

$KIn_{1.733}Cd_{0.267}$. We should point out now that the formula of the partially refined Hg compound is $KIn_{1.64(3)}Hg_{0.36}(3)$ and provides 199(3) electrons which is equal within 1σ to the number of needed electrons.

Structure IV. The 12-bonded 18-atom spacers are the same as in structure **III** and therefore require 40 (skeletal) + 12 (exo bonds) + 2 × 6 (lone pairs) = 64 electrons each. We have done EHMO calculations on a 15-bonded 15-atom spacer before and have found that it requires 44 (skeletal) + 15 (exo bonds) = 59 electrons.[11] For the 12- and 6-bonded icosahedra the numbers are 26 (skeletal) + 12 (exo bonds) = 38 and 26 (skeletal) + 6 (exo bonds) + 2 × 6 (lone pairs) = 44, respectively. Since there are 18 12-bonded and 6 6-bonded icosahedra, 3 18-atom spacers, 6 15-atom spacers and 18 isolated 4-bonded indium atoms, the total number of needed electrons becomes 18 × 38 + 3 × 44 + 3 × 64 + 6 × 59 + 18 × 4 = 1434 per unit cell. This means that the formula of the compound should be $K_{37}In_{64}Cd_5$ in order to provide that number of electrons.

Structure V. Extended-Hückel MO calculations performed on the *closo*-In18 cluster (Figure 18b) showed that it requires $2n + 4 = 40$ electrons to fill the bonding orbitals below a gap of 2 eV, and together with In_{15} and In_{16} it is in the class of hyperelectronic clusters (Figure 21). The extra orbital (seventh below the HOMO) is of the same type as the nonbonding orbital in In_{15} but this time it is quite strongly bonding and is almost 1 eV below the HOMO. The cluster can be viewed as built of two equivalent parts above and below a plane trough the center of the cluster and perpendicular to the 3-fold axis. The orbital in question is antibonding within the triangles of In4 but σ-bonding between In4 and In10 and between In10 and In13 of the same half. It is π-antibonding between In10 from one half and In13 from the other or, in other words, the orbital is bonding within each half but antibonding between them. Since the cluster is quite elongated, the antibonding interaction will be quite weak compared to the bonding ones. The

partial occupancy of the In13 site will not affect the number of needed skeletal electrons. It also will not affect the number of exo electrons needed since when an In13 atom is missing and the In13–In3 bond not present the corresponding 2 electrons will be needed for a lone pair on the In3 atom. For purpose of simplicity we can think of the cluster as 12-bonded and therefore needs 40 (skeletal) + 12 (exo bonds) + 2 × 6 (lone pairs) = 64 electrons.

The same line of consideration leads to the conclusion that the partial occupancies of the Sn, In6 and In12 sites will not affect the total electron count.

Extended-Hückel calculations were performed on the 24-bonded 20-atom spacer (Figure 19b). It was found that each triangle In7–In7–In12 that has all of its edges shared with other triangles contains a 3-center-2-electron bond. The rest of the bonds within the spacer are 2-center-2-electron bonds. This gives 6 × 2 (3-center-2-electron bonds) + 19 × 2 (2-center-2-electron bonds) + 24 (exo bonds) = 74 electrons required for the intra- and inter-spacer bonding.

There are 9 A-type and 6 B-type 12-bonded icosahedra, 3 In_{18} clusters and 3 20-atom spacers per unit cell and therefore the total number of bonding electrons is (9 + 6) × 38 + 3 × 64 + 3 × 74 = 984. The refined formula $Na_{49}In_{80.9(1)}Sn_{9.1(1)}$ provides 3 × (49 + 80.9 × 3 + 9.1 × 4) = 984.3(1.5) electrons and the structure is electronically balanced.

REFERENCES

1. Bruzzone, G. *Acta Cryst.* **1969**, *25B*, 1206.
2. Sevov, S. C.; Corbett, J. D. *Inorg. Chem.* **1992**, *31*, 1895.
3. Sevov, S. C.; Corbett, J. D. *Inorg. Chem.* **1991**, *30*, 4875.
4. Sevov, S. C.; Corbett, J. D. *J. Sol. St. Chem.* **1993**, *103*, 114.
5. Sevov, S. C.; Corbett, J. D. *Inorg. Chem.* **1993**, *32*, in press.
6. Sevov, S. C.; Ostenson, J. E.; Corbett, J. D. *J Alloys Comp.* **1993**, submitted.
7. Sevov, S. C.; Corbett, J. D. *Inorg. Chem.* **1993**, *32*, 1059.
8. Sevov, S. C.; Corbett, J. D. *J. Am. Chem. Soc.* **1993**, submitted.
9. TEXSAN, version 6.0 package, Molecular Structure Corp., The woodlands: Texas (1990).
10. Charbonnel, M. T.; Belin, C. *Mat. Res. Bull.* **1992**, *27*, 1277.
11. Sevov, S. C.; Corbett, J. D., unpublished research.

Table I. Results from reactions in the ternary systems alkali-metal–indium–main-group element

Loaded compositions	Structure types and lattice parameters, Å (Guinier)					Side product
	$Na_{23}In_{38.4}Zn_{4.6}$	$KIn_{2-x}Cd_x$	$Na_9In_{16.8}Zn_{2.3}$	$K_{36}In_{69-x}Cd_x$	$Na_{49}In_{80.9}Sn_{9.1}$	
1. $Na_{16}In_{20}Si$	a = 16.217(6) c = 15.71(1)					NaIn
2. $Na_6In_{10}Ge$		a = 16.586(3) c = 9.867(4)				NaGe
3. $Na_{9.3}In_{20}Ge$		a = 16.618(2) c = 9.932(1)				
4. $Na_{21}In_{32}Ge_4$		a = 16.584(5) c = 9.914(5)				NaGe
5. $Na_{16}In_{16}Ge$	a = 16.230(2) c = 15.770(5)					NaIn
6. $Na_{16}In_{20}Ge$	a = 16.236(3) c = 15.774(7)					
7. $Na_{21}In_{32}Sn_4$		a = 16.588(5) c = 9.835(6)			a = 16.209(5) c = 51.70(3)	
8. $Na_7In_{12}Sn_2$		a = 16.641(5) c = 9.888(5)				
9. Na_9In_9Sn	a = 16.247(5) c = 15.793(9)					NaIn
10. Na_3InPb		a = 16.61(1) c = 9.92(1)				unknown

Table I. (continued)

11. $Na_9In_{17}Zn_3$			a = 22.735(4)			
12. $Na_8In_{10}Zn$	a = 16.183(2) c = 15.723(4)		a = 22.715(7)			
13. $Na_{18}In_{16}Zn$	a = 16.192(2) c = 15.691(7)		a = 22.727(5)			
14. $Na_8In_{10}Hg$	a = 16.221(3) c = 15.756(3)					
15. $Na_9In_{10}Cu$	a = 16.220(3) c = 15.74(1)					NaIn
16. $Na_9In_{10}Ag$	a = 16.258(3) c = 15.759(7)					NaIn
17. $Na_9In_{10}Au$	a = 16.236(1) c = 15.733(4)		a = 22.576(7)			
18. K_2In_2Cd		a = 17.4851(8) c = 10.4461(7)				KCd_{13}
19. K_4In_4Cd		a = 17.419(6) c = 10.57(1)				
20. $K_8In_9Cd_2$		a = 17.419(1) c = 10.537(1)		a = 17.301(3) c = 76.18(3)		
21. K_4In_6Cd				a = 17.308(2) c = 76.03(1)		
22. K_7In_9Hg		a = 17.394(1) c = 10.508(1)				

Table II. Data collection and refinement parameters for $Na_{23}In_{38.4(2)}Zn_{4.6(1)}$ and $Na_{23}In_{39.8(1)}Au_{3.40(7)}$

Formula	$Na_{23}In_{38.4(2)}Zn_{4.6(1)}$	$Na_{23}In_{39.8(1)}Au_{3.40(7)}$
Formula weight	5241.2	5762.5
Crystal size, mm	0.1 × 0.1 × 0.2	0.15 × 0.2 × 0.2
Lattice parameters:[a]		
a, Å	16.183 (2)	16.236 (1)
c, Å	15.723 (4)	15.733 (4)
V, Å^3	3566 (1)	3592 (1)
Space group, Z	*P6/mmm*, 2	*P6/mmm*, 2
d(calc.), g cm^{-3}	4.88	5.33
μ(Mo–Kα), cm^{-1}	136.72	193.27
Transmission range	0.8037–1.1036	0.8968–1.0678
Diffractometer	CAD4	CAD4
Radiation	Mo–Kα (λ = 0.71069 Å) graphite-monochromated	
Temperature, °C	23	23
Octants measured	*h, k, ±l*	*±h, k, l*
Scan method	ω-θ	ω-θ
$2\theta_{max}$	50°	50°
Number of reflections:		
measured	4644	6767
observed ($I \geq 3\sigma_I$)	2409	4075
unique	722	1160
Number of variables	88	88
R; R_w,[b] %	2.8; 3.2	2.7; 3.1
R_{ave},[c] %	10.1	7.1
Goodness of fit indicator	1.11	1.14
Maximum shift/σ in final cycle	0.00	0.00
Largest peaks in final ΔF map	+1.76 e/Å^3 (0.9 Å from In8)	+2.01 e/Å^3 (0.8 Å from In8)
	-1.94 e/Å^3	-1.73 e/Å^3

[a] Room temperature Guinier data with Si as an internal standard (λ = 1.540562 Å).

[b] $R = \Sigma||F_o| - |F_c||/\Sigma|F_o|$; $R_w = [\Sigma w(|F_o| - |F_c|)^2/\Sigma w(F_o)^2]^{1/2}$; $w = \sigma_F^{-2}$.

[c] All data

Table III. Data collection and refinement parameters for $Na_9In_{16.8(3)}Zn_{2.3(3)}$

Formula weight	2278.7
Crystal size, mm	0.15 × 0.15 × 0.2
Lattice parameters:[a]	
a, Å	22.715 (7)
V, Å^3	11720 (4)
Space group, Z	$Fd\bar{3}m$ (#227, origin at $\bar{3}m$), 16
d(calc.), g cm^{-3}	5.17
μ(Mo–Kα), cm^{-1}	147.11
Transmission range	0.5577–1.0000
Diffractometer	CAD4
Radiation	Mo–Kα (λ = 0.71069 Å) graphite-monochromated
Temperature, °C	23
Octants measured	*h, k, l*
Scan method	ω–2θ
$2\theta_{max}$	50°
Number of reflections:	
measured	2765
observed ($I \geq 3\sigma_I$)	1348
unique observed ($I \geq 3\sigma_I$)	319
Number of variables	36
R_{ave} (all data), %	10.6
R; R_w,[b] %	2.6; 3.0
Goodness of fit indicator	1.12
Maximum shift/σ in final cycle	0.00
Largest peaks in final ΔF map	+1.01 e/Å^3 (0.76 Å from In3) -1.34 e/Å^3
Secondary extinction cofficient	1.5(4) × 10^{-9}

[a] Room temperature Guinier data with Si as an internal standard (λ = 1.540562 Å).

[b] $R = \Sigma||F_o| - |F_c||/\Sigma|F_o|$; $R_w = [\Sigma w(|F_o| - |F_c|)^2/\Sigma w(F_o)^2]^{1/2}$; $w = \sigma_F^{-2}$.

Table IV. Data collection and refinement parameters for $KIn_{2-x}Cd_x$

Formula weight	268.74
Crystal size, mm	0.1 × 0.1 × 0.2
Lattice parameters:[a]	
a, Å	17.4851 (8)
c, Å	10.4461 (7)
V, Å^3	2765.8(3)
Space group, Z	*P6/mmm* (#191), 30
d(calc.), g cm^{-3}	4.84
μ(Mo–Kα), cm^{-1}	131.88
Transmission range	0.4639–1.0000
Diffractometer	CAD4
Radiation	Mo–Kα (λ = 0.71069 Å) graphite-monochromated
Temperature, °C	23
Octants measured	±*h*, *k*, *l*
Scan method	ω–2θ
$2\theta_{max}$	50°
Number of reflections:	
measured	5326
observed ($I \geq 3\sigma_I$)	4246
unique observed ($I \geq 3\sigma_I$)	858
Number of variables	55
R_{ave} (all data), %	4.4
R; R_w,[b] %	3.5; 5.8
Goodness of fit indicator	2.8
Maximum shift/σ in final cycle	0.00
Largest peaks in final ΔF map	+6.2 e/Å^3 (at K5)
	-3.56 e/Å^3

[a] Room temperature Guinier data with Si as an internal standard (λ = 1.540562 Å).

[b] $R = \Sigma||F_o| - |F_c||/\Sigma|F_o|$; $R_w = [\Sigma w(|F_o| - |F_c|)^2/\Sigma w(F_o)^2]^{1/2}$; $w = \sigma_F^{-2}$.

Table V. Data collection and refinement parameters for $K_{37}In_{69-x}Cd_x$

Formula weight	9369.2
Crystal size, mm	0.2 × 0.15 × 0.1
Lattice parameters:[a]	
a, Å	17.301 (3)
c, Å	76.18 (3)
V, Å^3	19747(11)
Space group, Z	$R\bar{3}m$ (#166), 6
d(calc.), g cm^{-3}	4.72
μ(Mo–Kα), cm^{-1}	128.25
Transmission range	0.9236–1.0316
Diffractometer	CAD4
Radiation	Mo–Kα (λ = 0.71069 Å) graphite-monochromated
Temperature, °C	23
Octants measured	±*h*, *k*, *l*
Scan method	ω
$2\theta_{max}$	50°
Number of reflections:	
measured	12075
observed ($I \geq 3\sigma_I$)	7723
unique observed ($I \geq 3\sigma_I$)	2793
Number of variables	202
R_{ave} (all data), %	5.1
R; R_w,[b] %	3.1; 4.5
Goodness of fit indicator	1.68
Maximum shift/σ in final cycle	0.00
Largest peaks in final ΔF map	+3.7 e/Å^3 (0.8 Å from K17) -1.8 e/Å^3

a Room temperature Guinier data with Si as an internal standard (λ = 1.540562 Å).

b $R = \Sigma||F_o| - |F_c||/\Sigma|F_o|$; $R_w = [\Sigma w(|F_o| - |F_c|)^2/\Sigma w(F_o)^2]^{1/2}$; $w = \sigma_F^{-2}$.

Table VI. Data collection and refinement parameters for $Na_{49}In_{80.9(1)}Sn_{9.1(1)}$

Formula weight	11496
Crystal size, mm	0.30 × 0.10 × 0.08 (wedge-like)
Lattice parameters:[a]	
a, Å	16.209 (5)
c, Å	51.70 (3)
V, Å^3	11763(10)
Space group, Z	$R\bar{3}m$ (#166), 3
d(calc.), g cm^{-3}	4.87
μ(Mo–Kα), cm^{-1}	130.24
Transmission range	0.8123–1.2191
Diffractometer	Rigaku AFC6R/RA
Radiation	Mo–Kα (λ = 0.71069 Å) graphite-monochromated
Temperature, °C	23
Octants measured	±*h*, *k*, *l*
Scan method	ω
$2\theta_{max}$	50°
Number of reflections:	
measured	7249
observed ($I \geq 3\sigma_I$)	2628
unique observed ($I \geq 3\sigma_I$)	1003
Number of variables	143
R_{ave} (all data), %	15
R; R_w,[b] %	4.5; 5.1
Goodness of fit indicator	1.40
Maximum shift/σ in final cycle	0.00
Largest peaks in final ΔF map	+2.11 e/Å^3 (1.4 Å from Sn) -2.53 e/Å^3

[a] Room temperature Guinier data with Si as an internal standard (λ = 1.540562 Å).

[b] $R = \Sigma||F_o| - |F_c||/\Sigma|F_o|$; $R_w = [\Sigma w(|F_o| - |F_c|)^2/\Sigma w(F_o)^2]^{1/2}$; $w = \sigma_F^{-2}$.

Table VII. Positional and thermal parameters for $Na_{23}In_{38.4(2)}Zn_{4.6(1)}$

atom	N	x	y	z	B_{eq}	Occupancy
In1	12q	0.1645(1)	0.4936(1)	1/2	1.76(6)	47(1)% In + 53(1)% Zn
In2	12n	0.34724(7)	0	0.40462(8)	1.67(7)	94(1)% In + 6(1)% Zn
In3	12o	0.55217(5)	2x	0.65276(8)	1.71(7)	82(1)% In + 18(1)% Zn
In4	12o	0.60329(5)	2x	0.8115(1)	1.85(6)	
In5	12n	0.18842(8)	0	0.31419(9)	1.74(6)	
In6	12o	0.22424(5)	2x	0.90564(8)	2.09(7)	
In7	6l	0.0630(1)	2x	0	1.6(2)	49.8(6)% In
In8	12o	0.12383(9)	2x	0.1514(1)	2.5(1)	60.8(6)% In
In9	6l	0.5544(1)	2x	0	3.2(2)	63.1(4)% In
Na1	2c	1/3	2/3	0	1.7(4)	
Na2	2e	0	0	0.191(1)	2.9(6)	
Na3	12o	0.2084(3)	2x	0.6929(5)	2.5(4)	
Na4	4h	1/3	2/3	0.6228(8)	2.3(3)	
Na5	2e	0	0	0.401(1)	2.2(5)	
Na6	12n	0.3814(5)	0	0.1911(5)	2.9(4)	
Na7	6m	0.1321(4)	2x	1/2	3.0(6)	
Na8	6j	0.2976(7)	0	0	3.3(6)	

atom	U_{11}	U_{22}	U_{33}	U_{12}	U_{13}	U_{23}
In1	0.022(1)	0.0217(9)	0.022(1)	0.0106(7)	0.0	0.0
In2	0.0190(7)	0.0237(8)	0.0224(7)	$U_{22}/2$	-0.0019(5)	0.0
In3	0.0217(6)	0.0211(8)	0.0219(8)	$U_{22}/2$	-0.0015(3)	$2U_{13}$
In4	0.0203(5)	0.0227(7)	0.0283(7)	$U_{22}/2$	-0.0012(3)	$2U_{13}$
In5	0.0203(5)	0.0174(7)	0.0274(7)	$U_{22}/2$	-0.0039(5)	0.0
In6	0.0324(6)	0.0217(8)	0.0215(7)	$U_{22}/2$	0.0001(3)	$2U_{13}$
In7	0.025(2)	0.016(2)	0.016(2)	$U_{22}/2$	0.0	0.0
In8	0.030(1)	0.031(1)	0.036(2)	$U_{22}/2$	0.006(1)	$2U_{13}$
In9	0.053(2)	0.020(2)	0.036(2)	$U_{22}/2$	0.0	0.0
Na1	0.030(6)	U_{11}	0.005(8)	$U_{11}/2$	0.0	0.0
Na2	0.027(7)	U_{11}	0.06(1)	$U_{11}/2$	0.0	0.0
Na3	0.035(3)	0.035(5)	0.026(4)	$U_{22}/2$	0.001(1)	$2U_{13}$
Na4	0.032(5)	U_{11}	0.023(7)	$U_{11}/2$	0.0	0.0
Na5	0.029(7)	U_{11}	0.03(1)	$U_{11}/2$	0.0	0.0
Na6	0.035(3)	0.033(5)	0.040(5)	$U_{22}/2$	-0.004(4)	0.0
Na7	0.032(4)	0.047(8)	0.041(7)	$U_{22}/2$	0.0	0.0
Na8	0.039(5)	0.060(9)	0.034(6)	$U_{22}/2$	0.0	0.0

Table VIII. Positional and thermal parameters for $Na_{23}In_{39.8(1)}Au_{3.40(7)}$

atom	N	x	y	z	B_{eq}	Occupancy
In1	12q	0.16051(5)	0.49105(6)	1/2	1.45(3)	72.4(6)%In + 27.6(6)%Au
In2	12n	0.34564(5)	0	0.40241(5)	1.45(5)	86.6(6)%In + 13.4(6)%Au
In3	12o	0.55203(3)	2x	0.65519(5)	1.47(5)	84.4(6)%In + 15.6(6)%Au
In4	12o	0.60378(3)	2x	0.81214(6)	1.62(4)	
In5	12n	0.18761(6)	0	0.31477(6)	1.61(4)	
In6	12o	0.22425(3)	2x	0.90595(6)	1.91(5)	
In7	6l	0.0631(1)	2x	0	1.7(1)	50.3(5)% In
In8	12o	0.12393(7)	2x	0.1511(1)	2.4(1)	62.1(6)% In
In9	6l	0.55458(9)	2x	0	3.2(1)	64.4(4)% In
Na1	2c	1/3	2/3	0	1.4(3)	
Na2	2e	0	0	0.190(1)	2.9(4)	
Na3	12o	0.2096(2)	2x	0.6908(4)	2.3(3)	
Na4	4h	1/3	2/3	0.6177(6)	2.1(3)	
Na5	2e	0	0	0.4001(8)	1.8(4)	
Na6	12n	0.3825(4)	0	0.1929(4)	2.5(3)	
Na7	6m	0.1337(3)	2x	1/2	2.0(4)	
Na8	6j	0.2985(6)	0	0	3.1(5)	

atom	U_{11}	U_{22}	U_{33}	U_{12}	U_{13}	U_{23}
In1	0.0180(4)	0.0183(4)	0.0193(5)	0.0093(3)	0.0	0.0
In2	0.0173(4)	0.0173(5)	0.0204(5)	$U_{22}/2$	-0.0019(3)	0.0
In3	0.0202(4)	0.0176(5)	0.0170(5)	$U_{22}/2$	-0.0004(2)	$2U_{13}$
In4	0.0204(4)	0.0203(5)	0.0209(5)	$U_{22}/2$	-0.0023(2)	$2U_{13}$
In5	0.0201(4)	0.0174(5)	0.0228(5)	$U_{22}/2$	-0.0048(3)	0.0
In6	0.0318(5)	0.0197(5)	0.0170(5)	$U_{22}/2$	-0.0001(2)	$2U_{13}$
In7	0.030(1)	0.020(2)	0.011(2)	$U_{22}/2$	0.0	0.0
In8	0.0292(8)	0.030(1)	0.032(1)	$U_{22}/2$	0.006(4)	$2U_{13}$
In9	0.053(2)	0.022(1)	0.036(2)	$U_{22}/2$	0.0	0.0
Na1	0.024(4)	U_{11}	0.006(6)	$U_{11}/2$	0.0	0.0
Na2	0.039(5)	U_{11}	0.033(9)	$U_{11}/2$	0.0	0.0
Na3	0.027(2)	0.041(4)	0.023(3)	$U_{22}/2$	0.001(1)	$2U_{13}$
Na4	0.026(3)	U_{11}	0.027(5)	$U_{11}/2$	0.0	0.0
Na5	0.021(4)	U_{11}	0.029(8)	$U_{11}/2$	0.0	0.0
Na6	0.035(3)	0.028(3)	0.030(3)	$U_{22}/2$	-0.003(2)	0.0
Na7	0.028(3)	0.026(4)	0.020(4)	$U_{22}/2$	0.0	0.0
Na8	0.046(4)	0.052(6)	0.021(4)	$U_{22}/2$	0.0	0.0

Table IX. Distances to nearest neighbors about each atom in $Na_{23}In_{38.4}Zn_{4.6}$ and $Na_{23}In_{39.8}Au_{3.4}$ ($d_{In\text{-}In} \leq 3.50$, $d_{In,Na\text{-}Na} \leq 4.00$ Å)

	Na–In–Zn	Na–In–Au		Na–In–Zn	Na–In–Au		Na–In–Zn	Na–In–Au
	In1			**In4**			**In7**	
2	In1 2.662(4)	2.761(2)		In3 2.878(2)	2.866(1)2	2	In7 3.0584(4)	3.0747(2)
2	In2 2.939(1)	2.9275(8)	2	In4 3.0767(4)	3.0629(2)	2	In7 1.766(3)	1.775(3)
2	In3 2.923(2)	2.948(1)	2	In6 3.043(1)	3.0481(9)	2	In8 2.929(2)	2.928(1)
				In9 3.265(1)	3.263(1)			
2	Na3 3.482(7)	3.454(5)				2	Na2 3.49(2)	3.47(1)
2	Na4 3.375(7)	3.381(5)		Na1 3.455(1)	3.444(1)	2	Na8 3.40(1)	3.426(9)
	Na7 3.479(3)	3.434(2)	2	Na3 3.561(4)	3.567(3)			
				Na4 3.46(1)	3.534(8)		**In8**	
	In2		2	Na6 3.474(4)	3.488(3)			
						2	In5 3.092(2)	3.110(2)
2	In1 2.939(1)	2.9275(8)		**In5**			In6 2.9541(9)	2.9603(6)
	In2 2.999(3)	3.071(2)					In7 2.929(2)	2.928(1)
2	In3 3.011(1)	3.0403(9)		In2 2.937(2)	2.913(1)	2	In8 3.471(2)	3.485(2)
	In5 2.937(2)	2.913(1)	2	In5 3.049(1)	3.0460(9)			
			2	In8 3.092(2)	3.110(2)		Na2 3.528(4)	3.538(3)
2	Na3 3.346(5)	3.331(4)					Na3 3.407(6)	3.465(4)
	Na6 3.402(8)	3.350(6)		Na2 3.61(1)	3.626(8)	2	Na6 3.664(7)	3.695(5)
2	Na7 3.391(6)	3.382(4)	2	Na3 3.547(1)	3.597(1)	2	Na8 3.458(6)	3.468(5)
				Na5 3.342(7)	3.328(5)			
	In3			Na6 3.674(8)	3.700(6)		**In9**	
			2	Na7 3.462(3)	3.474(2)			
2	In1 2.923(2)	2.948(1)				2	In4 3.265(1)	3.263(1)
2	In2 3.011(1)	3.0403(9)		**In6**		4	In6 3.440(2)	3.445(1)
	In3 2.9247(4)	2.9265(2)					In9 3.0489(4)	3.0696(2)
	In4 2.878(2)	2.866(1)	2	In4 3.043(1)	3.0481(9)			
				In6 2.967(3)	2.959(2)		Na1 3.1472(4)	3.1521(2)
2	Na3 3.424(4)	3.405(3)		In8 2.9541(9)	2.9603(6)	4	Na6 3.877(7)	3.900(5)
	Na4 3.244(2)	3.277(2)	2	In9 3.440(2)	3.445(1)	2	Na8 3.61(1)	3.614(8)
2	Na6 3.442(7)	3.390(5)						
				Na1 3.3987(7)	3.4058(5)		**Na1**	
				Na3 3.374(7)	3.410(6)			
			2	Na6 3.567(3)	3.595(3)	6	In4 3.455(1)	3.444(1)
			2	Na8 3.532(2)	3.537(2)	6	In6 3.3987(7)	3.4058(5)
						3	In9 3.1472(4)	3.1521(2)

Table IX. (continued)

	Na–In–Zn	Na–In–Au		Na–In–Zn	Na–In–Au
	Na2			**Na6**	
6	In5 3.61(1)	3.626(8)		In2 3.402(8)	3.350(6)
6	In7 3.49(2)	3.47(1)	2	In3 3.442(7)	3.390(5)
6	In8 3.528(4)	3.538(3)	2	In4 3.474(4)	3.488(3)
				In5 3.674(8)	3.700(6)
	Na5 3.30(3)	3.31(2)	2	In6 3.567(4)	3.595(3)
			2	In8 3.664(7)	3.695(5)
	Na3		2	In9 3.877(7)	3.900(5)
2	In1 3.482(7)	3.454(5)	2	Na3 3.619(7)	3.641(5)
2	In2 3.346(5)	3.331(4)		Na6 3.84(1)	3.82(1)
2	In3 3.424(4)	3.405(3)		Na8 3.297(9)	3.327(7)
2	In4 3.561(4)	3.567(3)			
2	In5 3.547(2)	3.597(1)		**Na7**	
	In6 3.374(7)	3.410(6)			
	In8 3.407(6)	3.465(4)	2	In1 3.479(3)	3.434(2)
			4	In2 3.391(6)	3.382(4)
	Na4 3.671(4)	3.663(3)	4	In5 3.462(3)	3.474(2)
2	Na6 3.619(7)	3.641(5)			
	Na7 3.711(6)	3.683(5)	2	Na3 3.711(6)	3.683(5)
			2	Na7 3.70(1)	3.760(8)
	Na4				
				Na8	
6	In1 3.375(7)	3.381(5)			
3	In3 3.244(2)	3.277(2)	4	In6 3.532(2)	3.537(2)
3	In4 3.46(1)	3.534(8)	2	In7 3.40(1)	3.426(9)
			4	In8 3.458(6)	3.468(5)
3	Na3 3.671(4)	3.663(3)	2	In9 3.61(1)	3.614(8)
	Na4 3.86(2)	3.70(2)			
			2	Na6 3.29&(9)	3.327(7)
	Na5				
6	In5 3.342(7)	3.328(5)			
	Na2 3.30(3)	3.31(2)			
	Na5 3.11(3)	3.14(3)			

Table X. Positional and thermal parameters for $Na_9In_{16.8(3)}Zn_{2.3(3)}$

atom	N	x	y	z	B_{eq}	Occupancy
In1	96g	0.03819(4)	x	0.88438(5)	1.58(3)	
In2	96g	0.33373(4)	x	0.00596(6)	1.57(4)	62(5)% In + 38(5)% Zn
In3	96g	0.07810(4)	x	0.76723(5)	1.65(3)	
In4	32e	0.4611(1)	x	x	2.846(2)	52(1)% In
Na1	8a	1/8	x	x	1.429(5)	
Na2	32e	0.2182(3)	x	x	1.922(3)	
Na3	96g	0.0651(2)	x	0.3708(3)	2.43(2)	
Na4	8b	3/8	x	x	3.186(7)	

atom	U_{11}	U_{22}	U_{33}	U_{12}	U_{13}	U_{23}
In1	0.0211(5)	U_{11}	0.0178(7)	-0.0013(5)	0.0002(4)	U_{13}
In2	0.0205(6)	U_{11}	0.0187(9)	0.0005(7)	0.0013(4)	U_{13}
In3	0.0226(5)	U_{11}	0.0177(7)	-0.0059(6)	-0.0013(4)	U_{13}
In4	0.03605(2)	U_{11}	U_{11}	-0.006(1)	U_{12}	U_{12}
Na1	0.01810(7)	U_{11}	U_{11}	0.0	0.0	0.0
Na2	0.02434(4)	U_{11}	U_{11}	0.001(3)	U_{12}	U_{12}
Na3	0.025(2)	U_{11}	0.043(5)	0.004(3)	-0.001(3)	U_{13}
Na4	0.0403(1)	U_{11}	U_{11}	0.0	0.0	0.0

Table XI. Distances to nearest neighbors about each atom in $Na_9In_{16.8(3)}Zn_{2.3}$ ($d \leq 4.00$ Å)

In1	**In3**	**Na1**	**Na3**
2 In1 3.033(2)	In1 2.954(2)	12 In2 3.257(2)	2 In1 3.390(4)
2 In2 2.955(2)	2 In3 3.062(2)		2 In1 3.392(5)
In2 2.889(2)	In3 3.013(3)	4 Na2 3.67(1)	2 In2 3.502(7)
In3 2.854(2)	2 In4 3.399(5)		2 In3 3.526(7)
		Na2	2 In3 3.566(6)
Na2 3.238(2)	Na2 3.547(2)		In4 3.921(7)
2 Na3 3.392(5)	2 Na3 3.526(7)	6 In1 3.238(2)	In4 3.909(8)
2 Na3 3.390(4)	2 Na3 3.566(6)	3 In2 3.384(7)	
	Na4 3.565(2)	3 In3 3.547(2)	Na2 3.629(8)
In2/Zn			2 Na3 3.604(8)
	In4	Na1 3.67(1)	Na3 3.85(1)
2 In1 2.955(2)		3 Na3 3.629(8)	
In1 2.889(2)	6 In3 3.399(5)		**Na4**
2 In2 2.881(3)	In4 3.06(1)		
In2 2.652(3)			12 In3 3.565(2)
	3 Na3 3.921(7)		4 In4 3.390(5)
Na1 3.257(2)	3 Na3 3.909(8)		
2 Na2 3.384(7)	Na4 3.390(5)		
2 Na3 3.502(7)			

Table XII. Positional and thermal parameters for $KIn_{2-x}Cd_x$

atom	N	x	y	z	B_{eq}	Occup.
In1	6m	0.60686(6)	1.2137	1/2	1.4(1)	
In2	12p	0.66628(7)	0.16127(7)	0	1.21(4)	
In3	12n	0.35895(7)	0	0.1467(1)	1.38(6)	
In4	12o	0.55054(4)	1.1011	0.2474(1)	1.33(6)	
In5	12n	0.2072(1)	0	0.2812(2)	4.1(1)	
In6	6m	0.89212(7)	1.7842	1/2	2.6(1)	
K1	4h	1/3	2/3	0.1975(7)	1.4(2)	
K2	12o	0.2114(1)	0.4228	0.6955(4)	1.8(2)	
K3	6l	0.8637(2)	1.7275	0	2.3(4)	
K4	6k	0.3796(4)	0	1/2	2.4(3)	
K5	1b	0	0	1/2	8(1)	80(4)%
K6	2e	0	0	0.264(4)	8	60(2)%

atom	U_{11}	U_{22}	U_{33}	U_{12}	U_{13}	U_{23}
In1	0.027(2)	0.0168(8)	0.0136(9)	$U_{11}/2$	0.0	0.0
In2	0.0158(6)	0.0146(6)	0.0149(7)	0.0071(5)	0.0	0.0
In3	0.0202(5)	0.0166(6)	0.0145(7)	$U_{22}/2$	0.0017(4)	0.0
In4	0.0199(5)	0.0152(6)	0.0140(7)	$U_{22}/2$	-0.0002	$2U_{13}$
In5	0.0612(9)	0.062(1)	0.033(1)	$U_{22}/2$	0.0186(7)	0.0
In6	0.015(2)	0.041(1)	0.033(1)	$U_{11}/2$	0.0	0.0
K1	0.017(2)	U_{11}	0.020(3)	$U_{11}/2$	0.0	0.0
K2	0.021(1)	0.027(2)	0.023(2)	$U_{22}/2$	-0.001	$2U_{13}$
K3	0.022(5)	0.028(3)	0.037(4)	$U_{11}/2$	0.0	0.0
K4	0.039(3)	0.031(3)	0.017(3)	$U_{22}/2$	0.0	0.0
K5	0.014(3)	U_{11}	0.27(3)	$U_{11}/2$	0.0	0.0
K6	0.014	U_{11}	0.27	$U_{11}/2$	0.0	0.0

Table XIII. Distances to nearest neighbors about each atom in $KIn_{2-x}Cd_x$ ($d \leq 4.20$ Å)

In1		In4		K1		K4	
2	In1 3.137(3)		In1 3.142(1)	3	In1 3.642(6)	2	In1 3.861(4)
2	In4 3.142(1)	2	In2 3.123(1)	6	In2 3.645(4)	2	In3 3.708(1)
		2	In3 3.087(1)	3	In4 3.555(1)	4	In4 3.706(4)
2	K1 3.642(6)		In4 3.061(2)			2	In5 3.783(5)
4	K2 3.794(4)				K1 4.12(1)		
2	K4 3.861(4)		K1 3.555(1)	3	K2 3.858(4)	4	K2 3.951(3)
		2	K2 3.657(2)				K4 4.21(1)
In2		2	K4 3.706(4)	**K2**			
						K5	
	In2 2.995(2)	**In5**		2	In1 3.794(4)		
	In2 3.015(2)			2	In2 3.686(4)	6	In5 4.285(2)
2	In3 3.041(1)		In3 3.001(2)	2	In3 3.674(2)	6	In6 3.267(2)
2	In4 3.123(1)	2	In5 3.624(2)	2	In4 3.657(2)		
		2	In6 2.920(1)	2	In5 3.741(3)	2	K6 2.47(4)
2	K1 3.645(4)				In6 3.741(4)		
2	K2 3.686(4)	2	K2 3.741(3)				
	K3 3.690(5)	2	K3 3.590(2)		K1 3.858(4)	**K6**	
In3			K4 3.783(5)		K2 4.084(8)		
			K6 3.628(3)		K3 3.911(5)	6	In5 3.628(3)
2	In2 3.041(1)			2	K4 3.951(3)	6	In6 4.09(3)
	In3 3.065(2)	**In6**		**K3**			
2	In4 3.087(1)					**K5**	2.47(4)
	In5 3.001(2)	4	In5 2.920(1)	2	In2 3.690(5)		
		2	In6 3.267(2)	4	In3 3.729(2)		
2	K2 3.674(2)			4	In5 3.590(2)		
2	K3 3.729(2)	2	K2 3.741(4)				
	K4 3.708(1)		K5 3.267(2)	2	K2 3.911(5)		
				2	K3 4.127(6)		

Table XIV. Positional and equivalent displacement parameters for $K_{37}In_{69-x}Cd_x$

atom	N	x	y	z	B_{eq}	Occup.
In1	18h	0.06027(5)	2x	0.83345(2)	1.43(6)	
In2	18h	0.11625(5)	2x	0.86824(2)	1.38(5)	
In3	36i	0.17275(7)	0.99962(7)	0.09728(1)	1.21(4)	
In4	18h	0.05920(5)	2x	0.97039(2)	1.33(5)	
In5	18h	0.11677(5)	2x	0.79882(2)	1.34(5)	
In6	36i	0.33186(7)	0.02212(7)	0.11768(1)	1.39(4)	
In7	36i	0.17419(7)	0.17400(7)	0.23519(1)	1.14(4)	
In8	36i	0.33244(7)	0.01986(7)	0.07643(1)	1.33(4)	
In9	18h	0.11617(5)	2x	0.93655(2)	1.33(6)	
In10	18h	0.11664(5)	2x	0.73104(2)	1.21(5)	
In11	18h	0.06085(5)	2x	0.69738(2)	1.40(4)	
In12	36i	0.33559(8)	0.85729(8)	0.05565(1)	1.92(4)	
In13	18h	0.09968(6)	2x	0.00719(2)	1.56(5)	
In14	18h	0.10314(6)	2x	0.32132(2)	1.60(8)	
In15	18h	0.10643(6)	2x	0.49939(2)	2.03(7)	
In16	18h	0.46518(6)	2x	0.02393(2)	1.78(6)	
In17	36i	0.0049(1)	0.2013(1)	0.53202(2)	3.34(6)	
K1	6c	0	0	0.9290(1)	1.3(2)	
K2	6c	0	0	0.7922(1)	1.5(2)	
K3	6c	0	0	0.8751(1)	1.4(2)	
K4	6c	0	0	0.7392(1)	1.3(2)	
K5	18h	0.1259(2)	2x	0.05383(6)	1.8(3)	
K6	18g	0.3754(3)	0	1/2	2.2(3)	
K7	18h	0.4677(2)	2x	0.09680(6)	2.0(3)	
K8	18h	0.1226(2)	2x	0.27619(6)	1.5(3)	
K9	18h	0.1989(2)	2x	0.09545(6)	1.9(2)	
K10	18h	0.1229(2)	2x	0.13941(6)	1.7(1)	
K11	18h	0.1139(2)	2x	0.65385(6)	2.2(3)	
K12	36i	0.2841(3)	0.3310(2)	0.97307(4)	2.2(2)	
K13	18h	0.1241(2)	2x	0.19390(6)	1.9(2)	
K14	6c	0	0	0.6403(2)	5.7(5)	
K15	6c	0	0	0.5856(2)	5.2(5)	
K16	6c	0	0	0.5288(2)	2.7(4)	66(5)%
K17	6c	0	0	0.5108(2)	0.3(5)	34(5)%

Table XV. Anisotropic displacement parameters for $K_{37}In_{69-x}Cd_x$

atom	U_{11}	U_{22}	U_{33}	U_{12}	U_{13}	U_{23}
In1	0.0158(8)	0.0158	0.0167(7)	0.003(1)	-0.0000(6)	0.0000
In2	0.0152(8)	0.0152	0.0190(7)	0.005(1)	0.0004(6)	-0.0004
In3	0.0133(6)	0.0145(6)	0.0177(5)	0.0065(5)	0.0001(4)	0.0002(4)
In4	0.0164(8)	0.0164	0.0179(7)	0.008(1)	0.0016(6)	-0.0016
In5	0.0144(8)	0.0144	0.0173(7)	0.004(1)	-0.0010(6)	0.0010
In6	0.0152(6)	0.0184(6)	0.0173(5)	0.0070(5)	0.0004(4)	0.0012(4)
In7	0.0136(6)	0.0150(6)	0.0147(5)	0.0070(5)	0.0001(4)	0.0000(4)
In8	0.0147(6)	0.0167(6)	0.0186(5)	0.0074(5)	0.0001(4)	-0.0004(4)
In9	0.0141(8)	0.0141	0.0187(8)	0.004(1)	-0.0001(6)	0.0001
In10	0.0151(8)	0.0151	0.0158(7)	0.007(1)	0.0013(6)	-0.0013
In11	0.0187(9)	0.0187	0.0186(7)	0.011(1)	0.0002(6)	-0.0002
In12	0.0221(6)	0.0261(7)	0.0248(6)	0.0121(6)	0.0005(5)	-0.0032(5)
In13	0.020(1)	0.020	0.0181(7)	0.010(1)	-0.0003(6)	0.0003
In14	0.022(1)	0.022	0.0157(7)	0.010(1)	0.0020(6)	-0.0020
In15	0.032(1)	0.032	0.0250(9)	0.024(2)	-0.0007(7)	0.0007
In16	0.0211(9)	0.0211	0.0189(8)	0.005(1)	0.0039(7)	-0.0039
In17	0.0358(8)	0.054(1)	0.0371(7)	0.0223(8)	-0.0025(6)	-0.0210(7)
K1	0.020(3)	0.020	0.010(4)	0.010	0.0	0.0
K2	0.019(3)	0.019	0.018(4)	0.009	0.0	0.0
K3	0.015(3)	0.015	0.023(4)	0.008	0.0	0.0
K4	0.018(3)	0.018	0.015(4)	0.009	0.0	0.0
K5	0.022(3)	0.022	0.031(3)	0.014(5)	0.002(2)	-0.002
K6	0.032(2)	0.025(3)	0.025(3)	0.013	-0.001(1)	-0.002
K7	0.027(3)	0.027	0.026(3)	0.014(5)	0.007(2)	-0.007
K8	0.023(3)	0.023	0.018(2)	0.014(4)	-0.001(2)	0.001
K9	0.030(3)	0.030	0.025(3)	0.023(5)	-0.001(2)	0.001
K10	0.026(3)	0.026	0.021(2)	0.018(5)	0.002(2)	-0.002
K11	0.031(3)	0.031	0.027(3)	0.018(5)	0.003(2)	-0.003
K12	0.027(2)	0.023(2)	0.028(2)	0.009(2)	0.001(1)	0.001(2)
K13	0.022(3)	0.022	0.033(3)	0.015(5)	-0.000(2)	0.000
K14	0.040(5)	0.040	0.14(1)	0.02	0.0	0.0
K15	0.029(4)	0.029	0.14(1)	0.01	0.0	0.0
K16	0.016(5)	0.016	0.07(1)	0.01	0.0	0.0
K17	0.001(7)	0.001	0.01(1)	0.00	0.0	0.0

Table XVI. Distances to nearest neighbors about each atom in $K_{37}In_{69-x}Cd_x$ ($d \leq 4.50$ Å)

In1

2	In1	3.128(3)
	In2	3.137(2)
	In5	3.135(2)
	K2	3.626(7)
	K3	3.651(7)
2	K6	3.849(3)
2	K10	3.802(5)
2	K13	3.837(5)

In2

	In1	3.137(2)
2	In3	3.155(2)
	In5	3.006(2)
2	In6	3.092(1)
	K3	3.522(2)
2	K6	3.742(3)
2	K10	3.635(3)

In3

	In2	3.155(2)
	In3	2.982(2)
	In3	3.002(2)
	In6	3.012(2)
	In8	3.051(1)
	In9	3.113(2)
	K1	3.598(4)
	K3	3.658(5)
	K5	3.817(5)
	K9	3.684(5)
	K10	3.703(4)

In4

2	In4	3.072(3)
	In9	3.092(2)
	In13	3.055(2)
2	In13	3.113(2)
	K1	3.620(6)
2	K5	3.754(5)
2	K12	3.795(4)

In5

	In1	3.135(2)
	In2	3.006(2)
2	In6	3.116(1)
2	In7	3.125(2)
	K2	3.536(2)
2	K6	3.714(4)
2	K13	3.657(3)

In6

	In2	3.092(1)
	In3	3.012(2)
	In5	3.116(2)
	In7	2.996(1)
	In8	3.143(2)
	In17	3.014(2)
	K6	3.747(2)
	K7	3.719(3)
	K9	3.740(3)
	K10	3.610(3)
	K13	3.640(3)

In7

	In5	3.125(2)
	In6	2.996(1)
	In7	3.007(2)
	In7	3.017(2)
	In8	3.089(2)
	In10	3.108(2)
	K2	3.663(4)
	K4	3.589(4)
	K7	3.682(5)
	K8	3.628(4)
	K13	3.662(5)

In8

	In3	3.051(1)
	In6	3.143(2)
	In7	3.089(2)
	In9	3.105(1)
	In10	3.089(1)
	In12	3.251(2)
	K5	3.617(3)
	K7	3.666(3)
	K8	3.555(3)
	K9	3.608(3)
	K12	3.802(4)

In9

2	In3	3.113(2)
	In4	3.092(2)
2	In8	3.105(1)
	In10	3.013(2)
	K1	3.529(2)
2	K5	3.709(3)
2	K12	3.760(4)

In10

2	In7	3.108(2)
2	In8	3.089(1)
	In9	3.013(2)
	In11	3.061(2)
	K4	3.550(2)
2	K8	3.629(3)
	K12	3.834(4)

In11

	In10	3.061(2)
2	In11	3.158(3)
2	In14	3.045(2)
	K4	3.669(7)
2	K8	3.764(4)
	K11	3.678(5)
2	K12	3.817(4)

In12

	In8	3.251(2)
	In12	3.337(2)
	In12	3.220(2)
	In16	3.103(2)
	K5	3.784(5)
	K7	3.713(4)
	K8	3.818(5)
	K9	3.665(4)
	K11	3.712(5)
	K12	3.977(4)
	K14	3.964(9)
	K15	3.809(8)

In13

	In4	3.055(2)
2	In4	3.113(2)
2	In13	3.182(2)
	K5	3.639(5)
	K11	3.613(6)
2	K12	3.854(4)
2	K12	3.816(4)

In14

2	In11	3.045(2)
	In14	4.224(5)
	In16	2.870(2)
	In16	3.084(2)
	K8	3.487(5)
2	K11	3.773(4)
2	K12	3.717(4)
	K14	4.2565

In15

2	In15	3.191(2)
2	In17	2.992(2)
2	In17	2.994(2)
2	K6	4.0595
	K10	3.770(5)
	K13	3.687(5)
	K16	3.896(9)
	K16	3.843(9)
	K17	3.306(5)
	K17	3.283(5)

Table XVI. (continued)

In16

2	In12	3.103(2)
	In14	2.870(2)
	In14	3.084(2)
	K8	3.464(5)
2	K11	3.807(3)
2	K12	3.767(4)
	K14	3.955(2)

In17

	In6	3.014(2)
2	In15	2.992(2)
2	In17	3.567(3)
	K6	3.910(5)
	K7	3.559(4)
	K9	3.562(4)
	K10	3.701(5)
	K13	3.791(5)
	K16	3.450(2)
	K17	3.801(8)

K1

6	In3	3.598(4)
3	In4	3.620(6)
3	In9	3.529(2)
	K3	4.10(1)
3	K5	3.994(6)

K2

3	In1	3.626(6)
3	In5	3.536(2)
6	In7	3.663(4)
	K4	4.04(1)
3	K13	3.868(5)

K3

3	In1	3.651(7)
3	In2	3.522(2)
6	In3	3.658(5)
	K1	4.10(1)
3	K10	3.846(5)

K4

6	In7	3.589(4)
3	In10	3.550(2)
3	In11	3.669(7)
	K2	4.04(1)3
3	K8	3.854(5)

K5

2	In3	3.817(5)
2	In4	3.754(5)
2	In8	3.617(3)
2	In9	3.709(3)
2	In12	3.784(5)
	In13	3.639(5)
	K1	3.994(6)
	K9	3.852(7)
	K11	4.196(7)
2	K12	3.889(4)

K6

2	In1	3.849(3)
2	In2	3.742(3)
2	In5	3.714(4)
2	In6	3.747(2)
2	In15	4.059(5)
2	In17	3.910(5)
	K6	4.31(1)
2	K10	3.914(3)
2	K13	3.907(3)

K7

2	In6	3.719(3)
2	In7	3.682(5)
2	In8	3.666(3)
2	In12	3.713(4)
2	In17	3.559(4)
	K8	3.791(7)
2	K9	4.028(4)
	K13	3.948(7)
	K15	4.199(7)

K8

2	In7	3.628(4)
2	In8	3.555(3)
2	In10	3.629(3)
2	In11	3.764(4)
2	In12	3.818(5)
	In14	3.487(5)
	In16	3.464(5)
	K4	3.854(5)
	K7	3.791(7)
2	K12	4.095(4)

K9

2	In3	3.684(5)
2	In6	3.740(3)
2	In8	3.608(3)
2	In12	3.665(4)
2	In17	3.562(4)
	K5	3.852(7)
2	K7	4.028(4)
	K10	4.049(7)
	K15	4.174(7)

K10

2	In1	3.802(5)
2	In2	3.635(3)
2	In3	3.703(4)
2	In6	3.610(3)
	In15	3.770(5)
2	In17	3.701(5)
	K3	3.846(5)
2	K6	3.914(3)
	K9	4.049(7)
	K13	4.151(7)

K11

	In11	3.678(5)
2	In12	3.712(5)
	In13	3.613(6)
2	In14	3.773(4)
2	In16	3.807(3)
	K5	4.196(7)
2	K12	4.149(6)
2	K12	3.998(6)
	K14	3.568(7)

K12

	In4	3.795(4)
	In8	3.802(4)
	In9	3.760(4)
	In10	3.834(4)
	In11	3.817(4)
	In12	3.977(4)
	In13	3.854(4)
	In13	3.816(4)
	In14	3.717(4)
	In16	3.767(4)
	K5	3.889(4)
	K8	4.095(4)
	K11	4.150(5)
	K11	3.998(6)
	K12	4.103(8)
	K12	4.337(7)

K13

2	In1	3.837(5)
2	In5	3.657(3)
2	In6	3.640(3)
2	In7	3.662(5)
	In15	3.687(5)
2	In17	3.791(5)
	K2	3.868(5)
2	K6	3.907(3)
	K7	3.948(7)
	K10	4.151(7)

K14

6	In12	3.964(9)
3	In14	4.26(1)
3	In16	3.955(2)
3	K11	3.568(7)
	K15	4.16(2)

K15

6	In12	3.809(8)
3	K7	4.199(7)
3	K9	4.174(7)
	K14	4.16(2)
	K16	4.33(2)

K16

3	In15	3.896(9)
3	In15	3.843(9)
6	In17	3.450(2)
	K15	4.33(2)
	K16	4.38(3)
	K17	1.36(2)
	K17	3.02(2)

K17

3	In15	3.306(5)
3	In15	3.283(5)
6	In17	3.801(8)
	K16	1.36(2)
	K16	3.02(2)
	K17	1.65(4)

Table XVII. Positional and isotropic equivalent displacement parameters for $Na_{49}In_{80.9(1)}Sn_{9.1(1)}$

atom	N	x	y	z	B_{eq}	Occup.	No.at./formula
In1	18h	0.2710(1)	-x	0.92860(7)	2.1(2)		
In2	18h	0.6030(1)	-x	0.98805(7)	2.3(2)		
In3	18h	0.2250(1)	-x	0.98019(7)	2.2(2)		
In4	18h	0.2704(1)	-x	0.73798(7)	2.1(2)		
In5	18h	0.5415(1)	-x	0.94200(8)	2.4(2)		
In6	18h	0.5616(2)	-x	0.04185(9)	2.1(3)	80(1)%	4.80(7)
In7	36i	0.6678(2)	0.1477(2)	0.89359(5)	2.3(1)		
In8	18h	0.2182(1)	-x	0.88075(7)	2.6(2)		
In9	36i	0.6669(2)	0.9913(2)	0.86320(5)	3.0(1)		
In10	18h	0.5623(1)	-x	0.29080(7)	2.4(2)		
In11	18h	0.2191(1)	-x	0.78617(8)	2.9(2)		
In12	6c	0	0	0.4691(3)	5.3(5)	70(2)%	1.40(3)
In13	18h	0.1137(4)	-x	0.9837(2)	4.0(7)	45(1)%	2.70(7)
Sn	36i	0.4926(3)	0.3343(2)	0.16662(6)	2.6(1)	76(1)%	9.1(1)
Na1	6c	0	0	0.4041(7)	2(1)		
Na2	18h	0.5389(7)	-x	0.1057(4)	3(1)		
Na3	18h	0.1282(8)	-x	0.1037(5)	4(1)		
Na4	18h	0.2139(6)	-x	0.0468(4)	3(1)		
Na5	18h	0.5427(8)	-x	0.8343(4)	3(1)		
Na6	36i	0.290(1)	0.331(1)	0.9318(3)	3.2(6)		
Na7	6c	0	0	0.2046(7)	3(1)		
Na8	6c	0	0	0.1280(7)	3(1)		
Na9	3a	0	0	0	4(2)		
Na10	18f	0.372(2)	0	0	7(2)		

Table XVIII. Anisotropic displacement parameters for $Na_{49}In_{80.9(1)}Sn_{9.1(1)}$

atom	U_{11}	U_{22}	U_{33}	U_{12}	U_{13}	U_{23}
In1	0.030(2)	U_{11}	0.029(2)	0.021(2)	-0.0005(8)	$-U_{13}$
In2	0.030(2)	U_{11}	0.027(2)	0.015(2)	-0.002(1)	$-U_{13}$
In3	0.028(2)	U_{11}	0.027(2)	0.013(2)	0.002(1)	$-U_{13}$
In4	0.023(1)	U_{11}	0.035(2)	0.013(2)	0.000(1)	$-U_{13}$
In5	0.029(2)	U11	0.032(2)	0.015(2)	-0.003(1)	$-U_{13}$
In6	0.022(2)	U11	0.034(3)	0.011(2)	0.004(1)	$-U_{13}$
In7	0.023(1)	0.027(1)	0.035(1)	0.012(1)	0.001(1)	-0.009(1)
In8	0.036(2)	U11	0.025(2)	0.017(2)	-0.005(1)	$-U_{13}$
In9	0.064(2)	0.031(2)	0.027(1)	0.031(2)	-0.000(2)	-0.005(1)
In10	0.037(2)	U11	0.025(2)	0.025(2)	-0.0014(9)	$-U_{13}$
In11	0.043(2)	U11	0.030(2)	0.024(2)	0.004(1)	$-U_{13}$
In12	0.081(8)	U11	0.040(8)	$U_{11}/2$	0.0	0.0
In13	0.063(6)	U11	0.039(6)	0.040(7)	-0.001(3)	$-U_{13}$
Sn	0.030(2)	0.027(2)	0.027(2)	0.004(2)	0.001(2)	-0.000(2)
Na1	0.03(1)	U11	0.02(2)	$U_{11}/2$	0.0	0.0
Na2	0.03(1)	U_{11}	0.06(2)	0.02(1)	-0.003(5)	$-U_{13}$
Na3	0.04(1)	U_{11}	0.06(2)	0.02(1)	0.000(6)	$-U_{13}$
Na4	0.023(8)	U_{11}	0.06(1)	0.02(1)	0.008(5)	$-U_{13}$
Na5	0.032(9)	U_{11}	0.03(1)	0.00(1)	0.004(6)	$-U_{13}$
Na6	0.04(1)	0.032(8)	0.05(1)	0.018(8)	0.016(8)	0.016(8)
Na7	0.04(1)	U_{11}	0.03(2)	$U_{11}/2$	0.0	0.0
Na8	0.05(1)	U_{11}	0.03(2)	$U_{11}/2$	0.0	0.0
Na9	0.07(3)	U_{11}	0.02(3)	$U_{11}/2$	0.0	0.0
Na10	0.09(2)	0.04(2)	0.11(3)	$U_{22}/2$	-0.02(2)	$2U_{13}$

Table XIX. Distances to nearest neighbors about each atom in $Na_{49}In_{80.9}Sn_{9.1}$ (d ≤ 4.20 Å)

	In1			In5			In9			In13			Na3			Na6	
2	In1	3.033(7)		In2	2.940(5)		In7	2.977(4)		In3	3.13(1)	2	In4	3.54(2)		In1	3.59(1)
	In3	2.963(5)		In6	3.013(6)		In8	3.078(3)		In4	3.18(1)	2	In7	3.48(2)		In3	3.63(1)
2	In6	2.989(5)	2	In7	3.067(4)		In9	3.088(6)	2	In10	3.355(7)	2	In9	3.39(1)		In4	3.52(1)
	In8	2.882(5)					In11	3.083(4)		In10	3.05(1)		In10	3.23(2)		In5	3.56(1)
				Na1	3.575(7)		Sn	2.941(5)	2	In13	3.61(1)	2	In11	3.51(1)		In6	3.55(1)
2	Na2	3.57(2)		Na2	3.34(2)		Sn	2.945(5)				2	Sn	3.72(2)		In7	3.64(1)
2	Na6	3.59(1)	2	Na4	3.48(1)				2	Na6	3.66(2)					In8	3.64(1)
	Na7	3.44(3)	2	Na6	3.56(1)		Na2	3.35(1)		Na9	3.30(1)		Na4	3.80(3)		In9	3.59(1)
			2	Na10	3.83(2)		Na3	3.39(1)	2	Na10	3.73(3)	2	Na6	3.55(2)		In10	3.48(1)
	In2						Na5	3.42(1)					Na8	3.81(3)		In11	3.63(1)
				In6			Na5	3.46(1)		Sn						In13	3.66(2)
2	In2	3.097(7)					Na6	3.59(1)					Na4				
2	In3	3.115(4)	2	In1	2.989(5)					In8	2.942(5)					Na2	3.67(2)
	In5	2.940(5)		In2	3.014(6)		In10			In9	2.941(5)	2	In2	3.42(2)		Na3	3.55(2)
	In6	3.014(6)	2	In3	3.206(3)					In9	2.945(5)		In3	3.45(2)		Na4	3.74(2)
				In5	3.013(6)	2	In4	2.956(4)		In11	2.928(5)	2	In5	3.48(1)		Na10	3.71(2)
	Na1	3.53(3)				2	In13	3.355(7)		Sn	2.853(7)	2	In7	3.50(2)			
2	Na4	3.42(2)		Na2	3.36(2)		In13	3.05(1)		Sn	2.806(7)		In10	3.08(2)		Na7	
2	Na10	3.61(2)	2	Na6	3.55(1)												
			2	Na10	3.46(2)		Na3	3.23(2)		Na2	3.63(2)		Na1	3.57(2)	3	In1	3.44(3)
	In3						Na4	3.08(2)		Na3	3.72(2)		Na3	3.80(3)	3	In8	3.268(7)
				In7		2	Na6	3.48(1)		Na5	3.70(2)	2	Na6	3.74(2)	6	Sn	3.44(2)
	In1	2.963(5)					Na9	3.662(4)		Na7	3.44(2)	2	Na10	3.94(1)			
2	In2	3.115(4)		In5	3.067(4)					Na8	3.47(2)				3	Na2	3.78(2)
2	In6	3.206(3)		In7	3.045(5)		In11						Na5			Na8	3.96(5)
	In13	3.13(1)		In7	2.991(5)					Na1							
				In9	2.977(4)		In4	2.876(5)				2	In7	3.60(2)		Na8	
	Na4	3.45(2)		In12	3.379(6)		In8	2.921(6)	3	In2	3.53(3)	2	In7	3.53(2)			
2	Na6	3.63(1)				2	In9	3.083(4)	3	In5	3.575(7)	2	In9	3.42(1)	3	In4	3.42(3)
2	Na10	3.367(5)		Na1	3.53(2)	2	Sn	2.928(5)	6	In7	3.53(2)	2	In9	3.46(1)	3	In11	3.236(7)
				Na2	3.51(2)					In12	3.36(4)		In12	3.85(2)	6	Sn	3.47(2)
	In4			Na3	3.48(2)	2	Na3	3.51(1)					In12	3.81(2)			
				Na4	3.50(2)	2	Na6	3.63(1)	3	Na4	3.57(2)	2	Sn	3.70(2)	3	Na3	3.81(3)
2	In4	3.063(6)		Na5	3.53(2)		Na8	3.236(7)								Na7	3.96(5)
2	In10	2.956(4)		Na5	3.60(2)					Na2			Na2	3.86(3)			
	In11	2.876(5)		Na6	3.64(1)		In12					2	Na5	3.48(2)		Na9	
	In13	3.18(1)							2	In1	3.57(2)						
				In8		6	In7	3.379(6)		In5	3.34(2)				6	In4	4.089(4)
2	Na3	3.54(2)					In12	3.19(3)		In6	3.36(2)				6	In10	3.662(4)
2	Na6	3.52(1)		In1	2.882(5)				2	In7	3.51(2)				6	In13	3.30(1)
	Na8	3.42(3)	2	In9	3.078(3)		Na1	3.36(3)	2	In8	3.49(1)						
				In11	2.921(6)	3	Na5	3.81(2)	2	In9	3.35(1)					Na10	
			2	Sn	2.942(5)	3	Na5	3.85(2)	2	Sn	3.63(2)						
															2	In2	3.61(2)
			2	Na2	3.49(1)					Na5	3.86(3)				2	In3	3.367(5)
			2	Na6	3.64(1)				2	Na6	3.67(2)				2	In5	3.83(2)
				Na7	3.268(7)					Na7	3.78(2)				2	In6	3.46(2)
															2	In13	3.73(3)
															2	Na4	3.94(1)
															2	Na6	3.71(2)

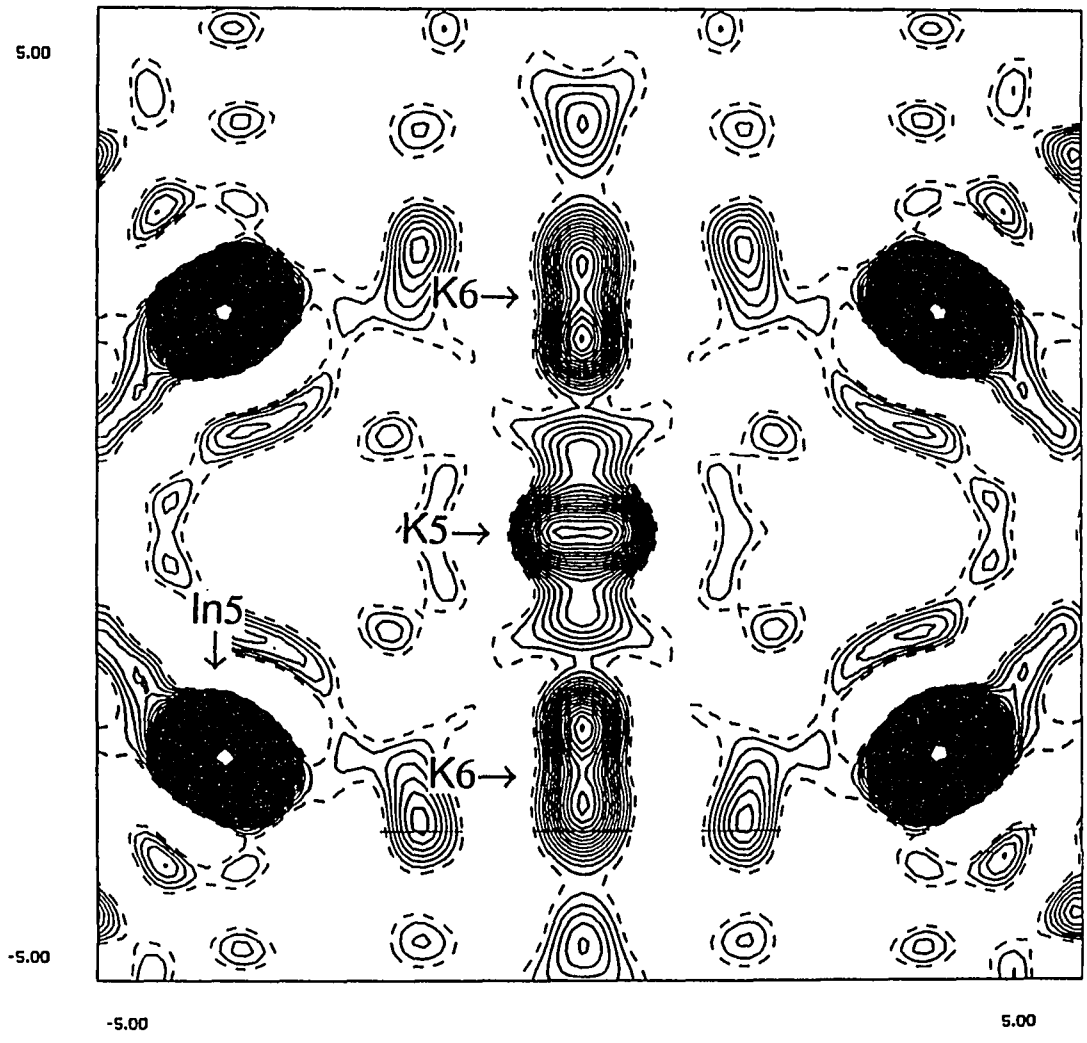

Figure 1. A section of a Fourier map calculated from F_{obs} with phases from the refined structure **III**. The plane contains four In5 atoms, part of a hexagonal prism (black spots), and K5 and K6 which are disordered along the *c* axis (vertical). The contour interval is 1 e/Å^3.

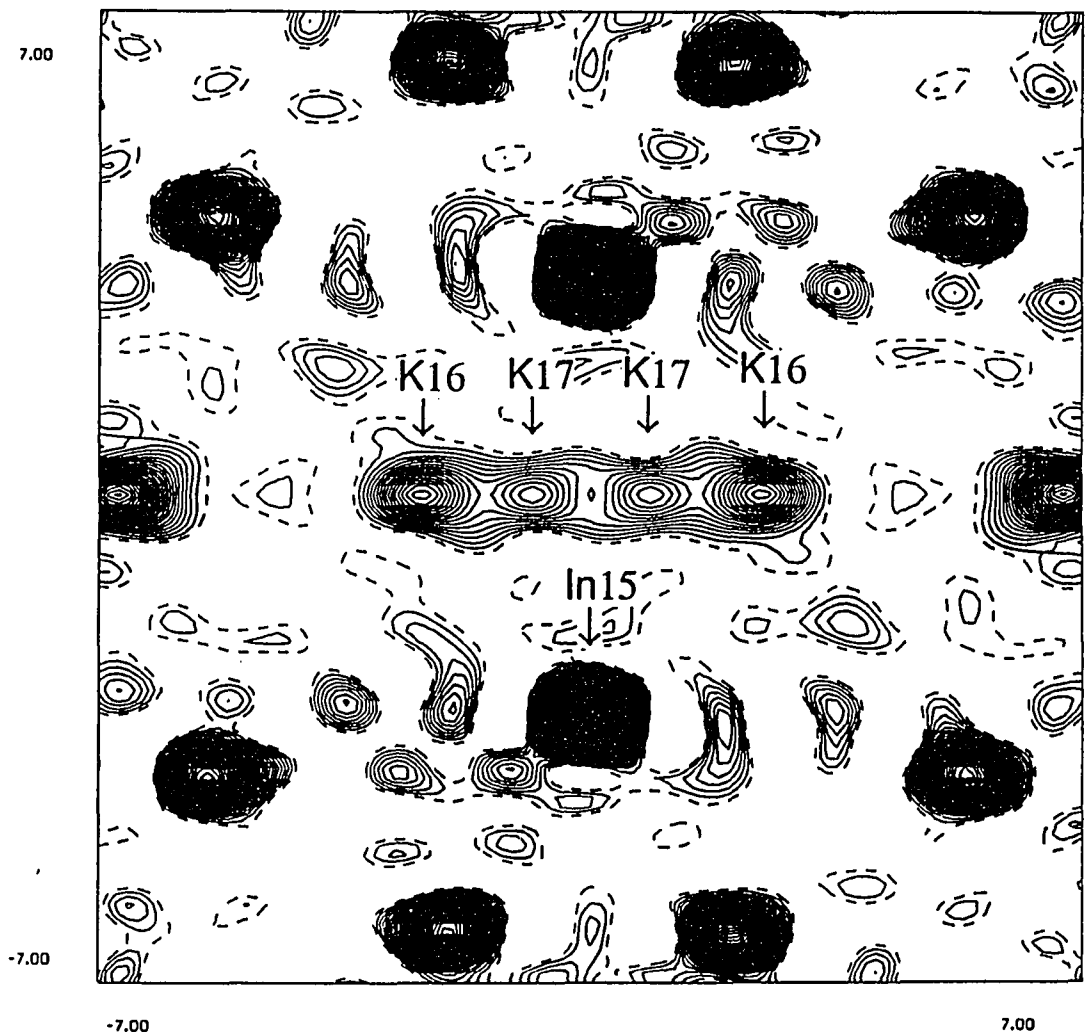

Figure 2. A section of a Fourier map calculated from F_{obs} with phases from the refined structure **IV**. The plane contains two of the capping atoms, In15, of a hexacapped hexagonal prism and K16 and K17 which are disordered along the *c* axis (horizontal). The contour interval is 1 e/Å^3.

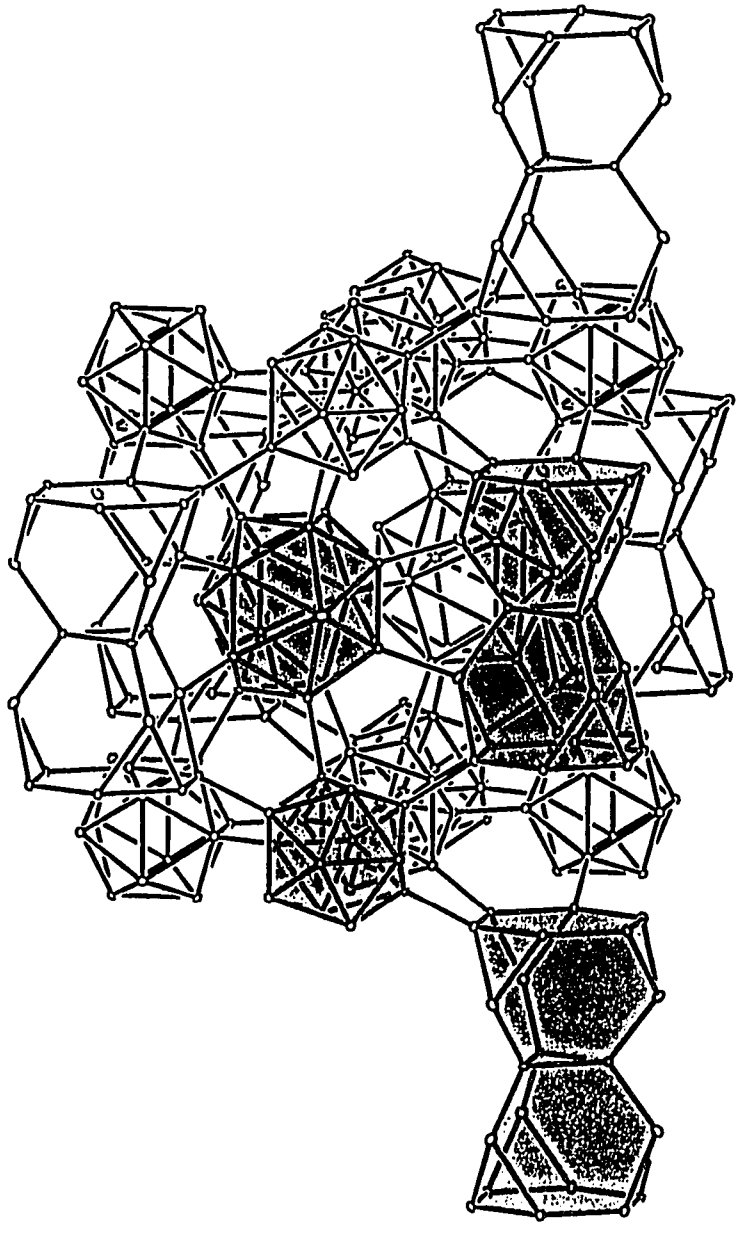

Figure 3. The anionic network of structure I (*c* vertical). All distances less than 3.5 Å are drawn and the building blocks of In_{12}, In_{15} and 21-atom spacer are shaded. (20% ellipsoid probability)

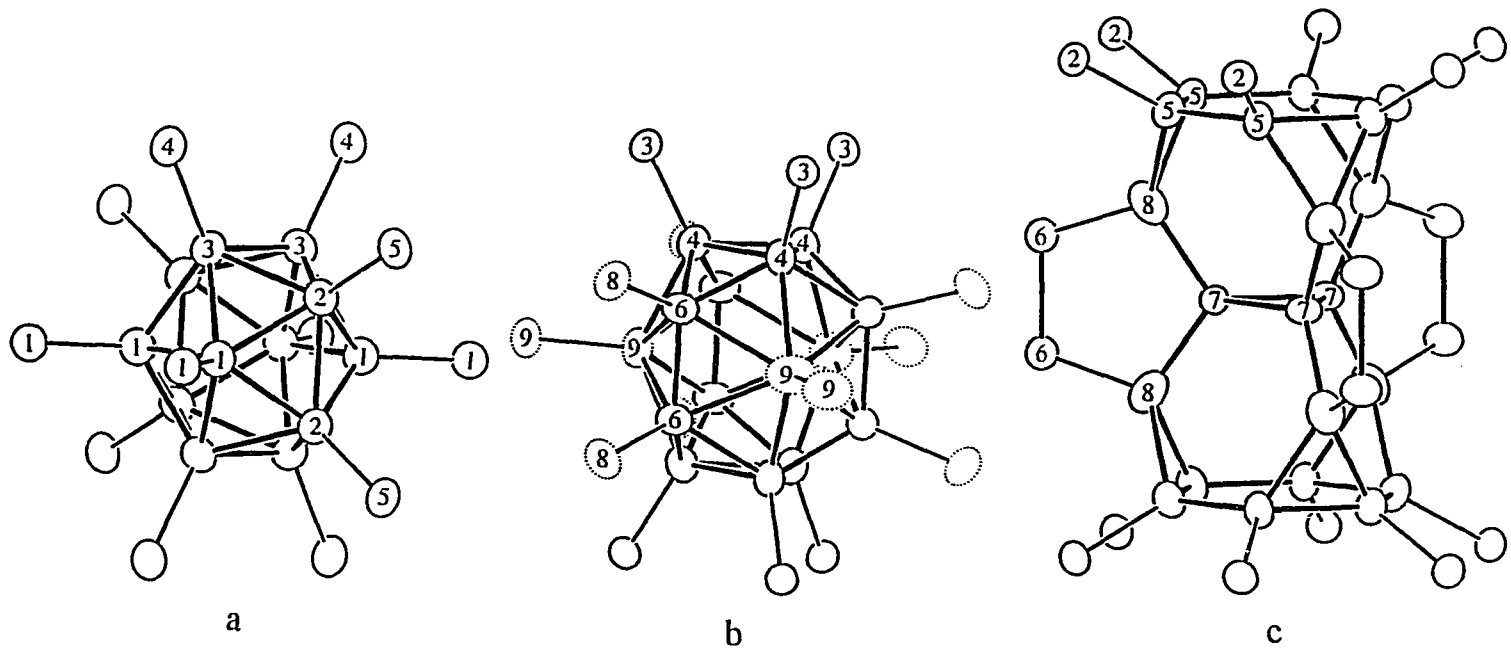

Figure 4. The three building blocks of structure I: a) 12-bonded icosahedron; b) 15-bonded *closo*-In_{15}; c) 18-bonded 21-atom spacer in one of two possible orientations. In1, 2, 3 have mixed In and Zn or Au occupancy. The partially occupied sites are shown as dotted ellipsoids. (94% probability thermal ellipsoids)

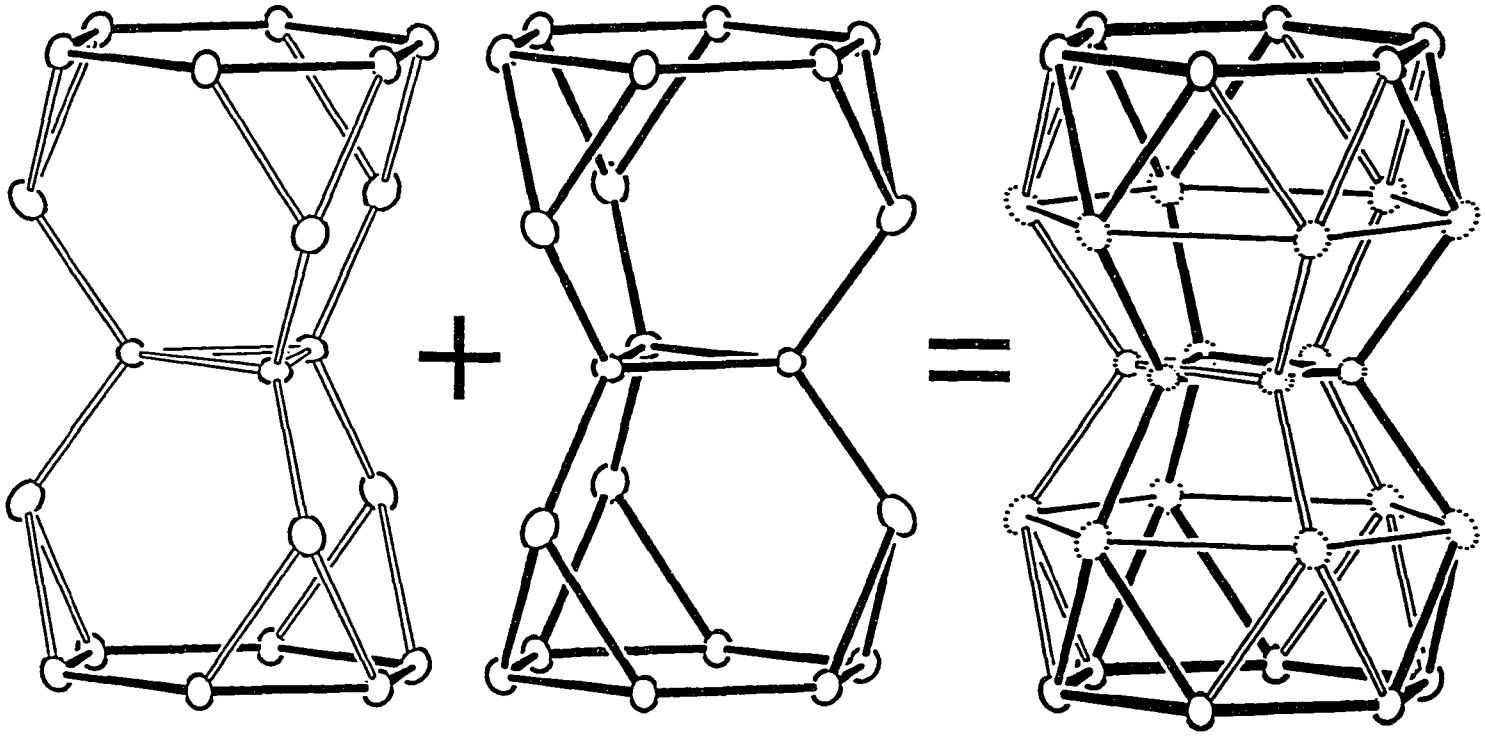

Figure 5. Shown is how the refined formation (right) with D_{6h} symmetry is generated by superimposing two 21-atom spacers with two orientations. The atoms of the two end hexagons are common for both orientations (solid ellipsoids) while the rest belong to one orientation only (dotted ellipsoids).

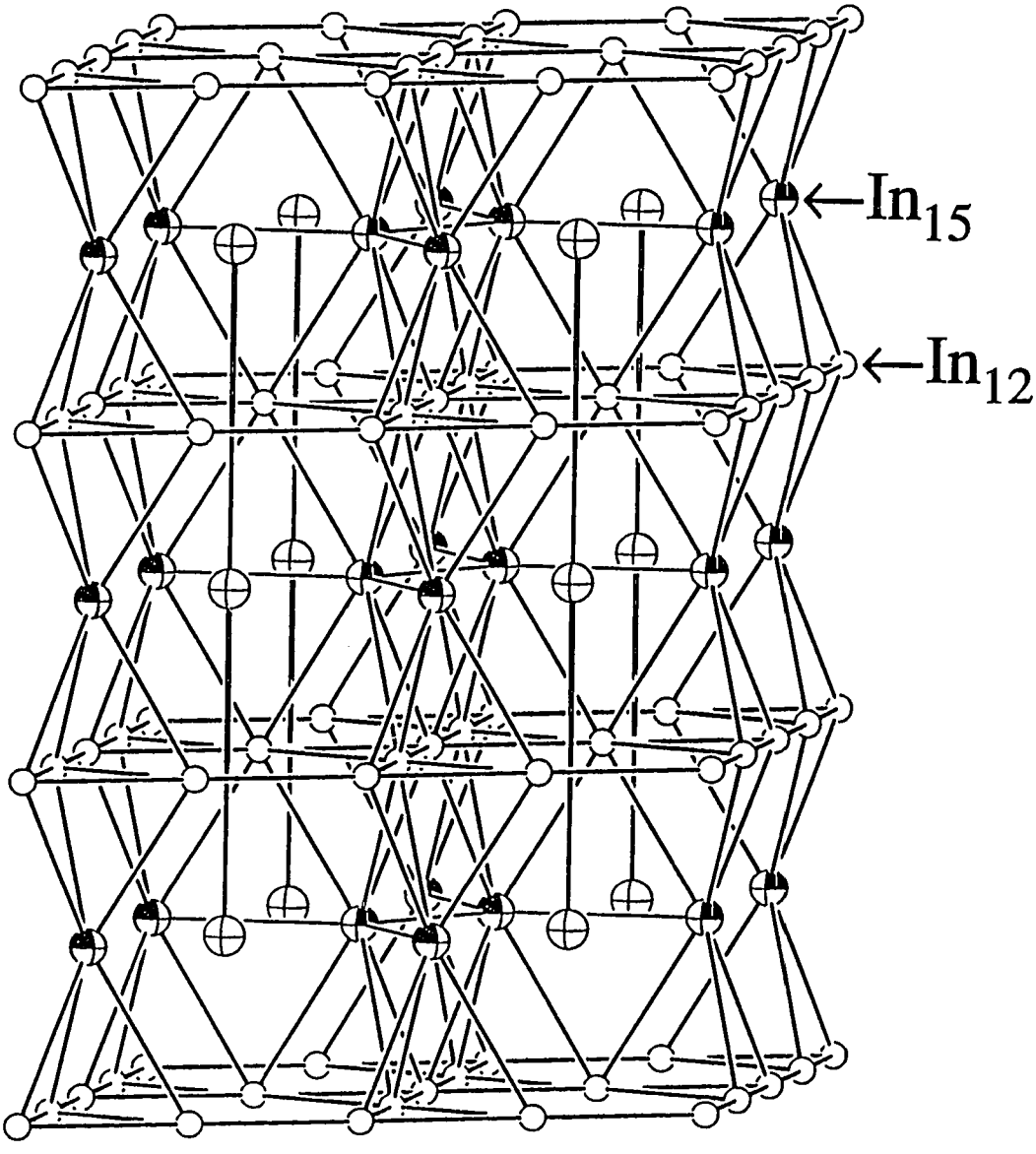

Figure 6. A condensed view of structure I (*c* vertical). The Kagomé nets of In_{12} (open circles) are joined via In_{15} (octant-shaded circles) and the voids are filled with the 21-atom spacers (crossed circles). The structure can be related to $CaCu_5$ by replacing In_{12} and In_{15} with Cu and the 21-atom spacer, with Ca atoms.

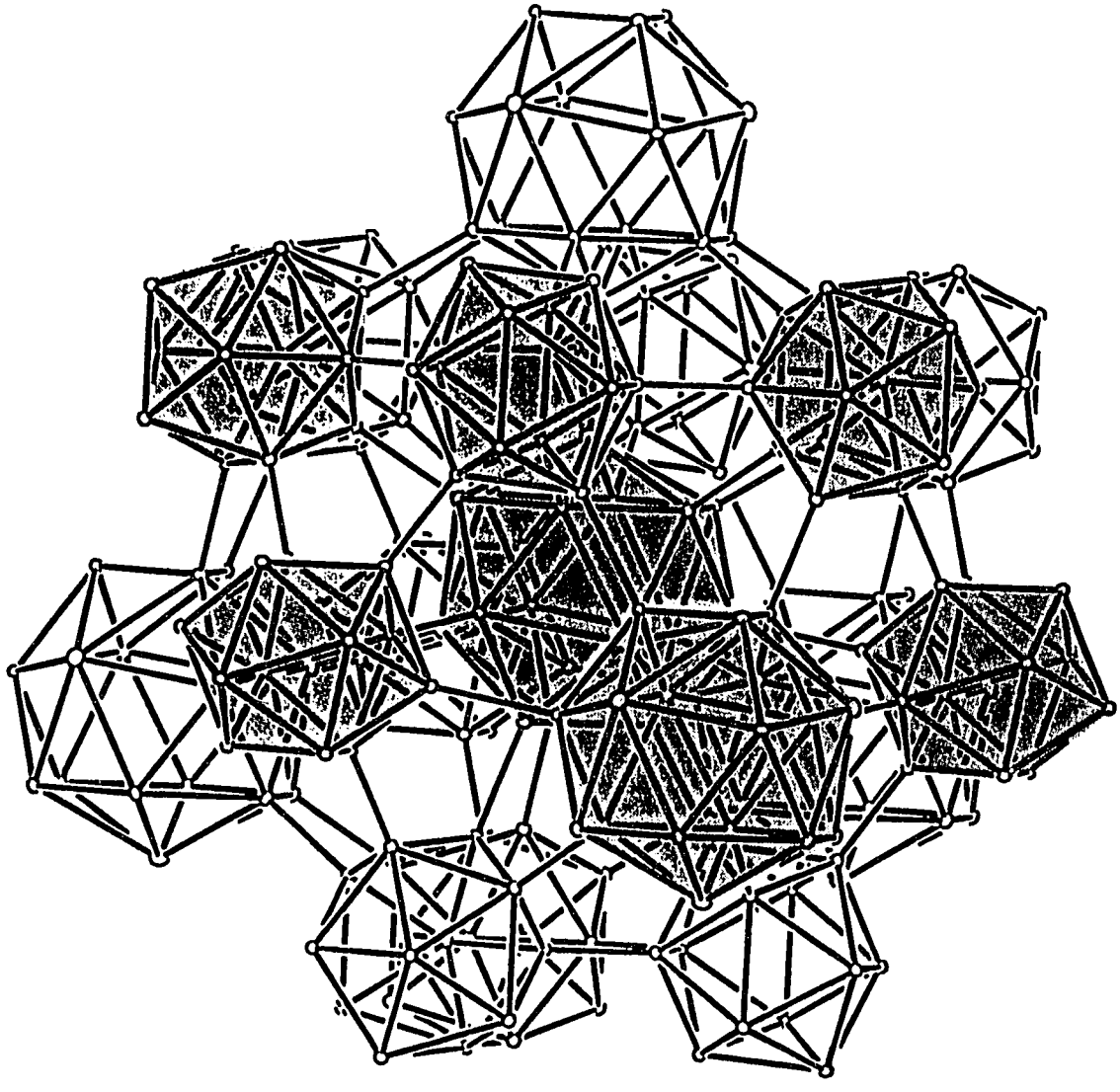

Figure 7. A view of the anionic network of structure II ([111] vertical). All distances less than 4.0 Å are drawn and the building blocks of $In_{12}$and In_{16} are shaded. (20% probability thermal ellipsoids)

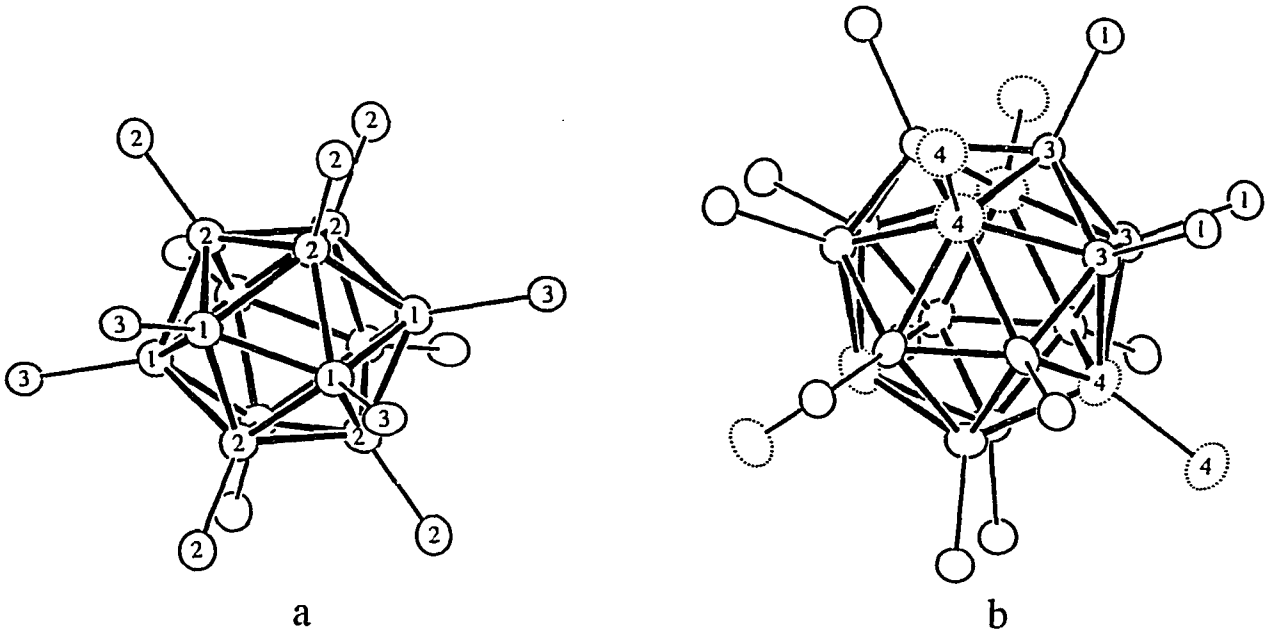

Figure 8. The two building blocks of structure **II**: a) 12-bonded In_{12}; b) 16-bonded In_{16}. In1 has mixed In and Zn occupancy. The partially occupied positions are shown with dotted ellipsoids. (94% probability thermal ellipsoids)

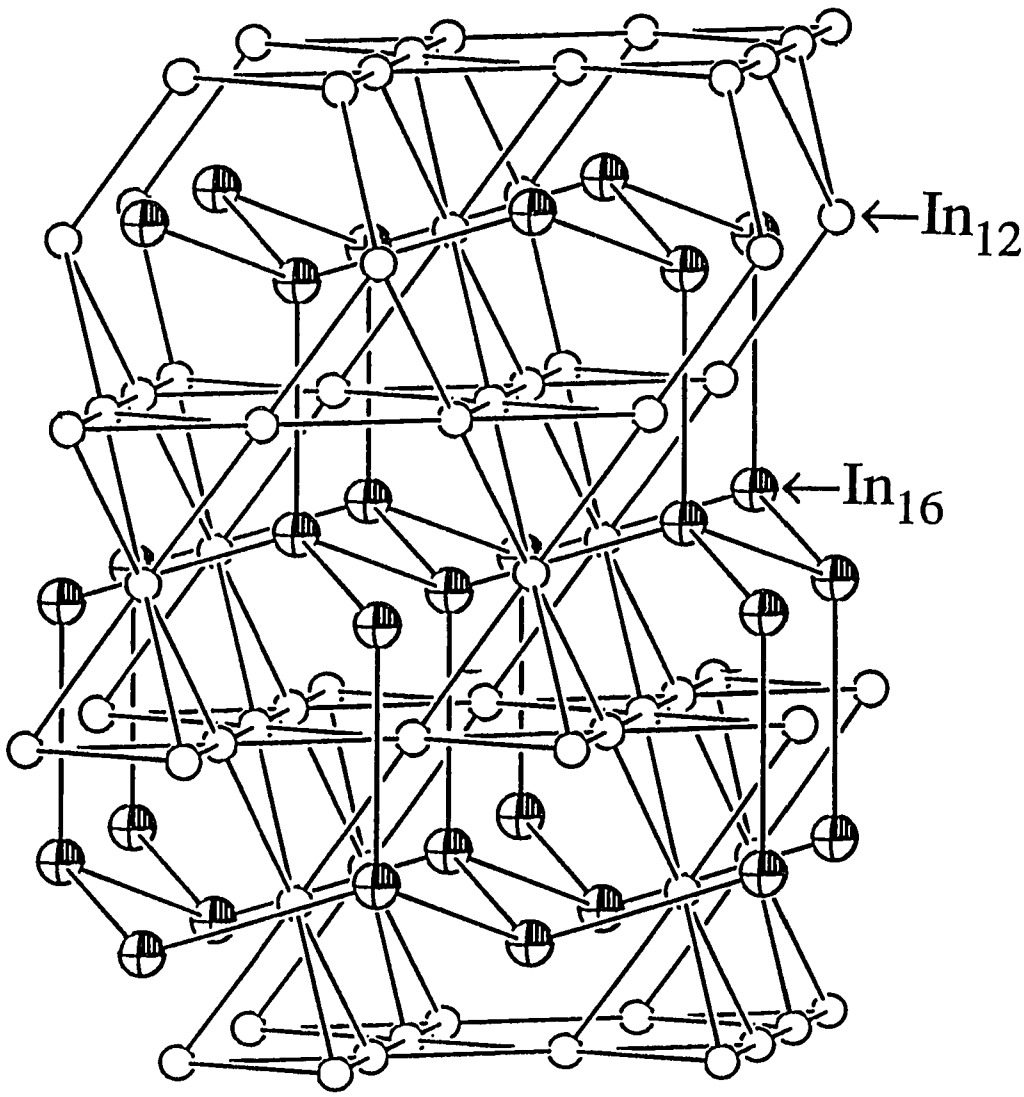

Figure 9. A condensed view of structure II ([111] vertical). The voids between the Kagomé nets of In_{12} (open circles) are filled by In_{16} (octant-shaded circles). The structure can be related to the Laves phase $MgCu_2$ by replacing In_{12} and In_{16} with Cu and Mg atoms, respectively.

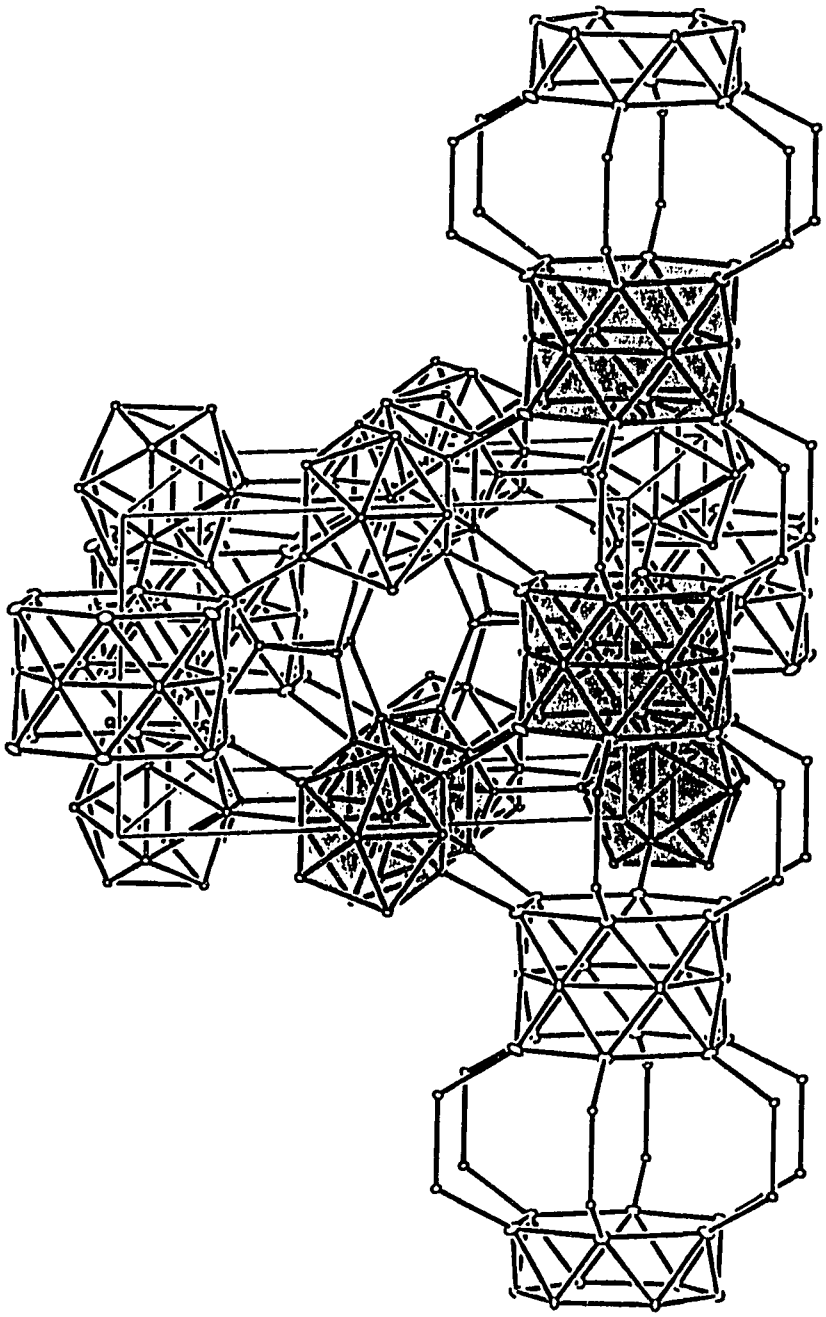

Figure 10. The anionic network of structure **III** (*c* vertical). All distances less than 4.0 Å are drawn, and the building blocks of In_{12}, In_3 and 18-atom spacer are shaded. The latter form chains along the *c* axis. (20% probability thermal ellipsoids)

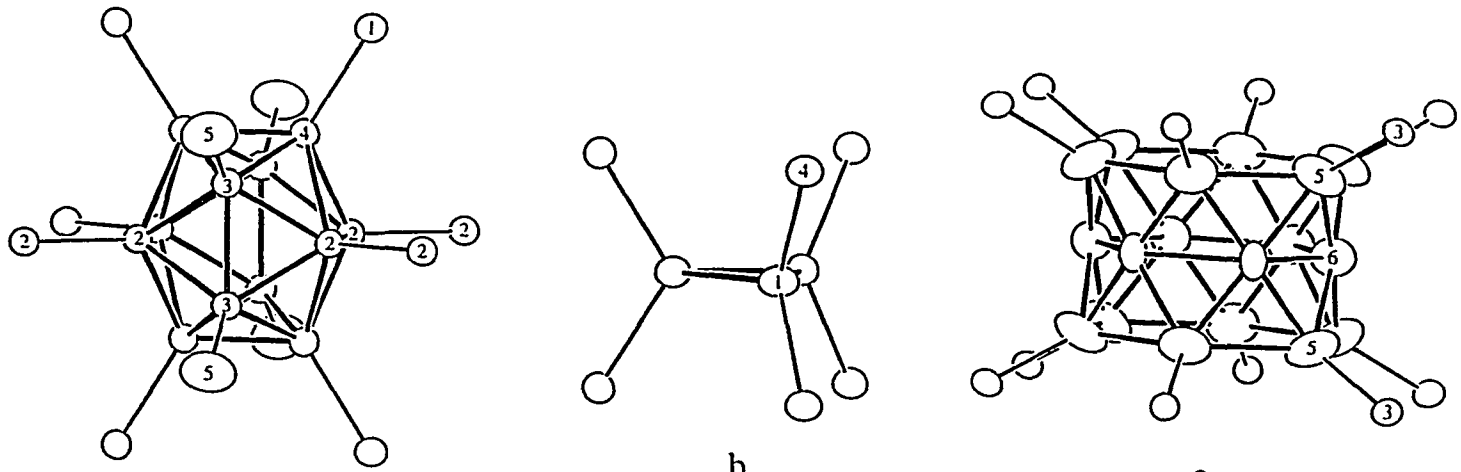

Figure 11. The three building blocks of structure **III**: a) 12-bonded icosahedron; b) 6-bonded triangle; c) 12-bonded 18-atom spacer (a "Big Mac") with a geometry of a hexacapped (In6) hexagonal prism (In5). (94% probability thermal ellipsoids)

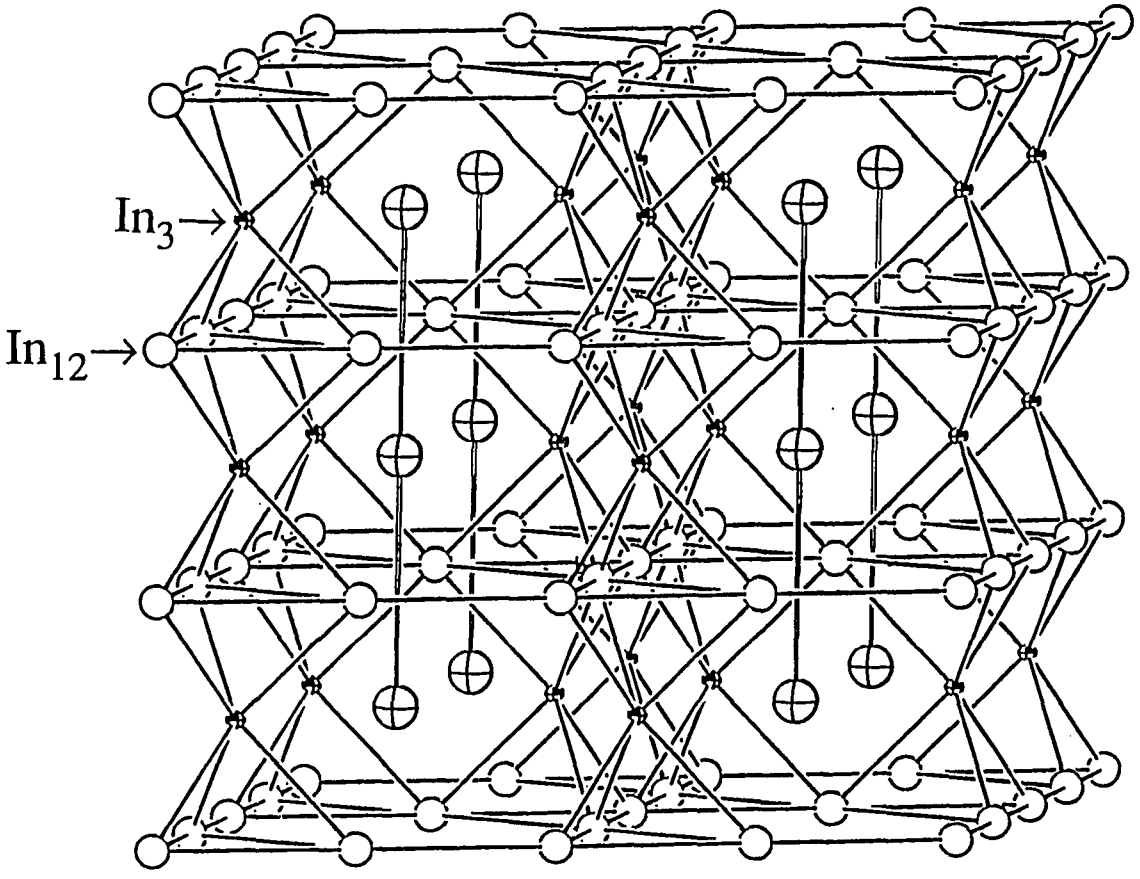

Figure 12. A condensed view of structure **III** (*c* vertical). The Kagomé nets of In_{12} (open circles) are joined via indium triangles (small shaded circles). The voids are occupied by the 18-atom spacers (crossed circles) which form chains along *c*.

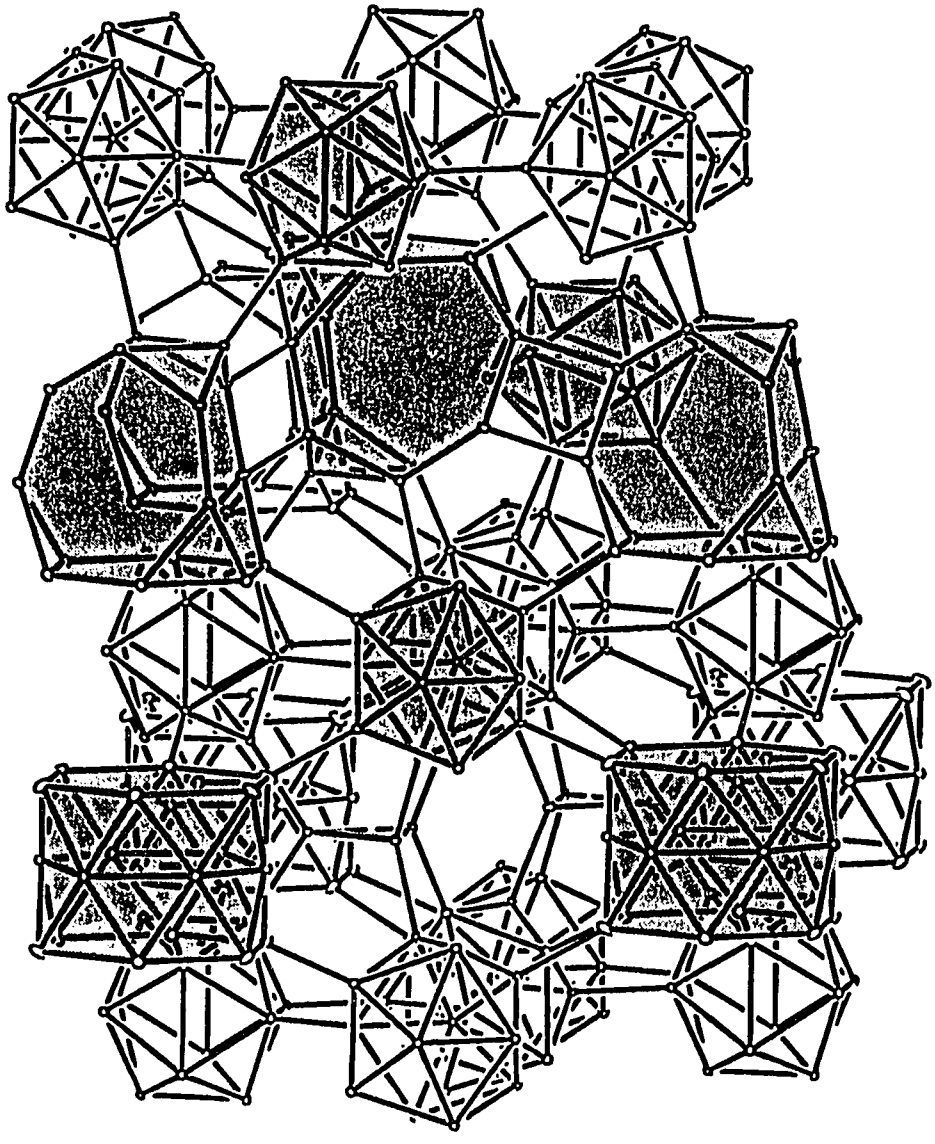

Figure 13. The anionic network of structure IV (*c* vertical). All distances less than 4.0 Å are drawn, and the building blocks of 12- and 6-bonded In_{12}, In_3 and 15- and 18-atom spacers are shaded. (20% probability thermal ellipsoids)

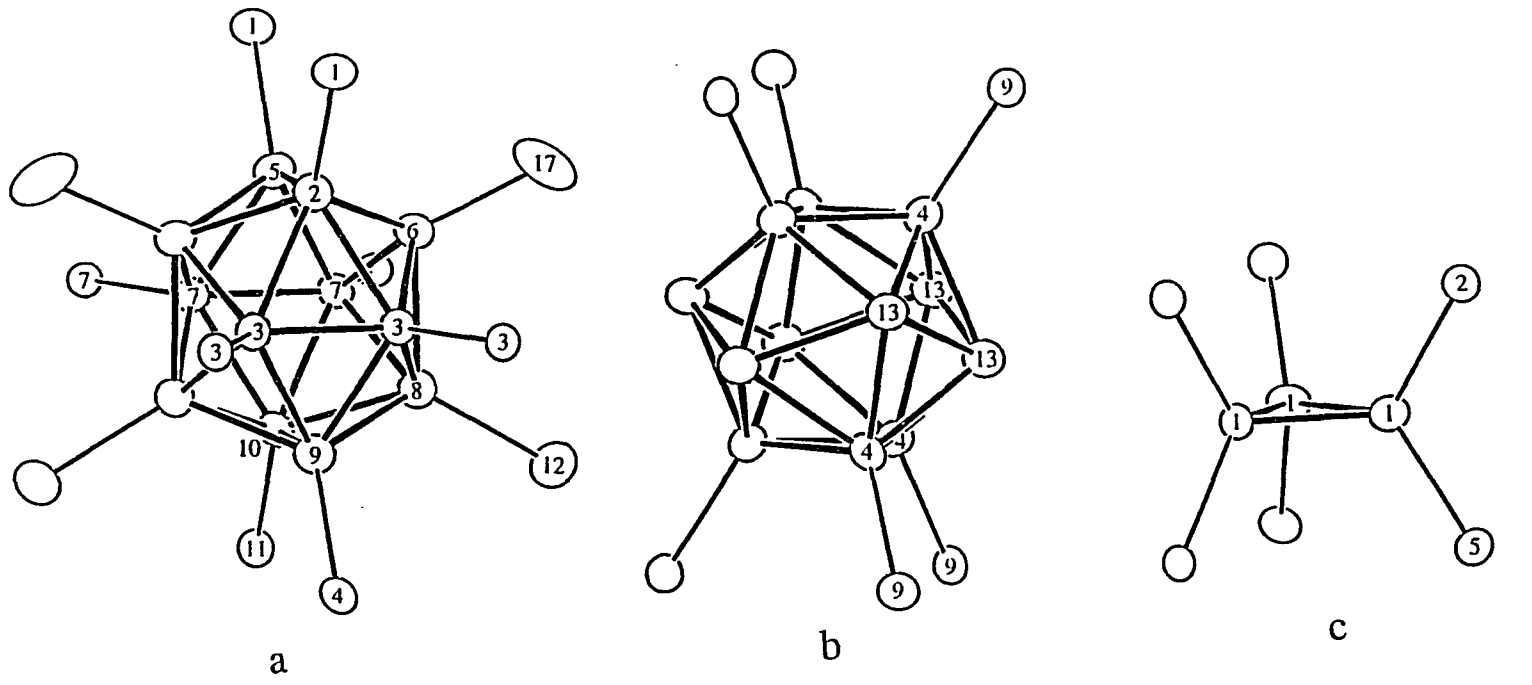

Figure 14. Three of the five building blocks of structure **IV** are shown: a) 12-bonded In_{12}; b) 6-bonded In_{12}; c) 6-bonded triangle. (94% probability thermal ellipsoids)

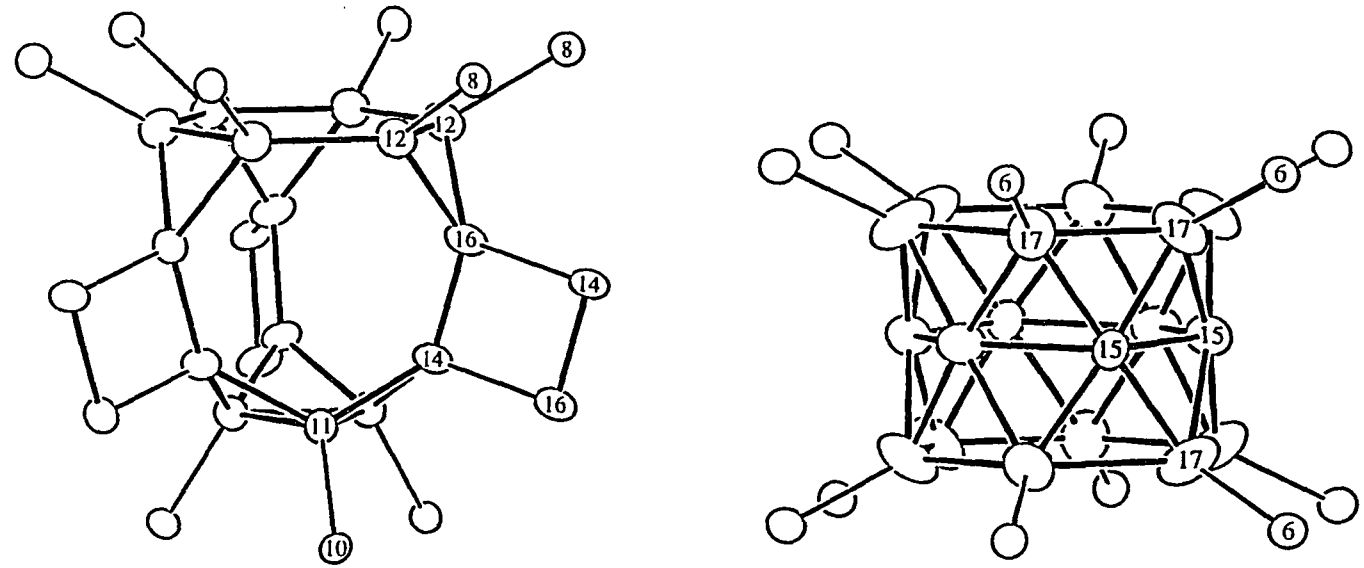

Figure 15. The two spacers in structure IV: a) 15-bonded 15-atom spacer with C_{3v} symmetry; b) 12-bonded 18-atom spacer with D_{3d} symmetry. (94% probability thermal ellipsoids)

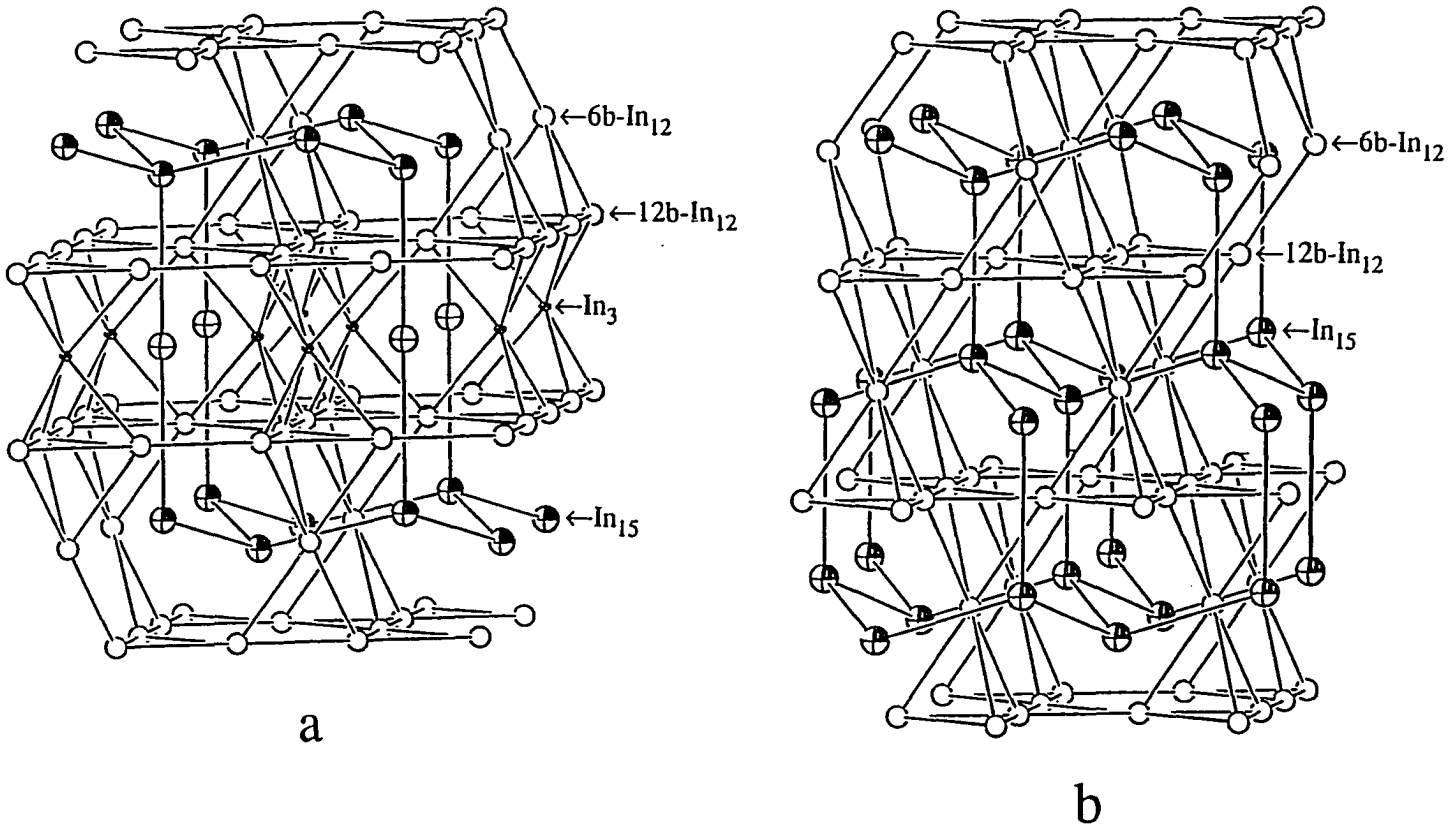

Figure 16. Condensed views of structure **IV** (a) and $K_{22}In_{39}$ (b). The Kagomé nets of 12-bonded In_{12} (open circles) are joined by 6-bonded In_{12} (open circles) in $K_{22}In_{39}$ and by alternating 6-bonded In_{12} and In_3 (small shaded circles) in **IV**. The voids are filled by 15-atom spacers (octant shaded circles) in $K_{22}In_{39}$ and by alternating 15- and 18-atom (crossed circles) spacers in **IV**. Structure **IV** is an intergrowth structure of layers of $K_{22}In_{39}$ (top and bottom layers) and of structure **III** (middle layer). It can be related to the structure of $NbBe_3$ by replacing In_{12} and In_3 with Be and the spacers, with Nb atoms.

296

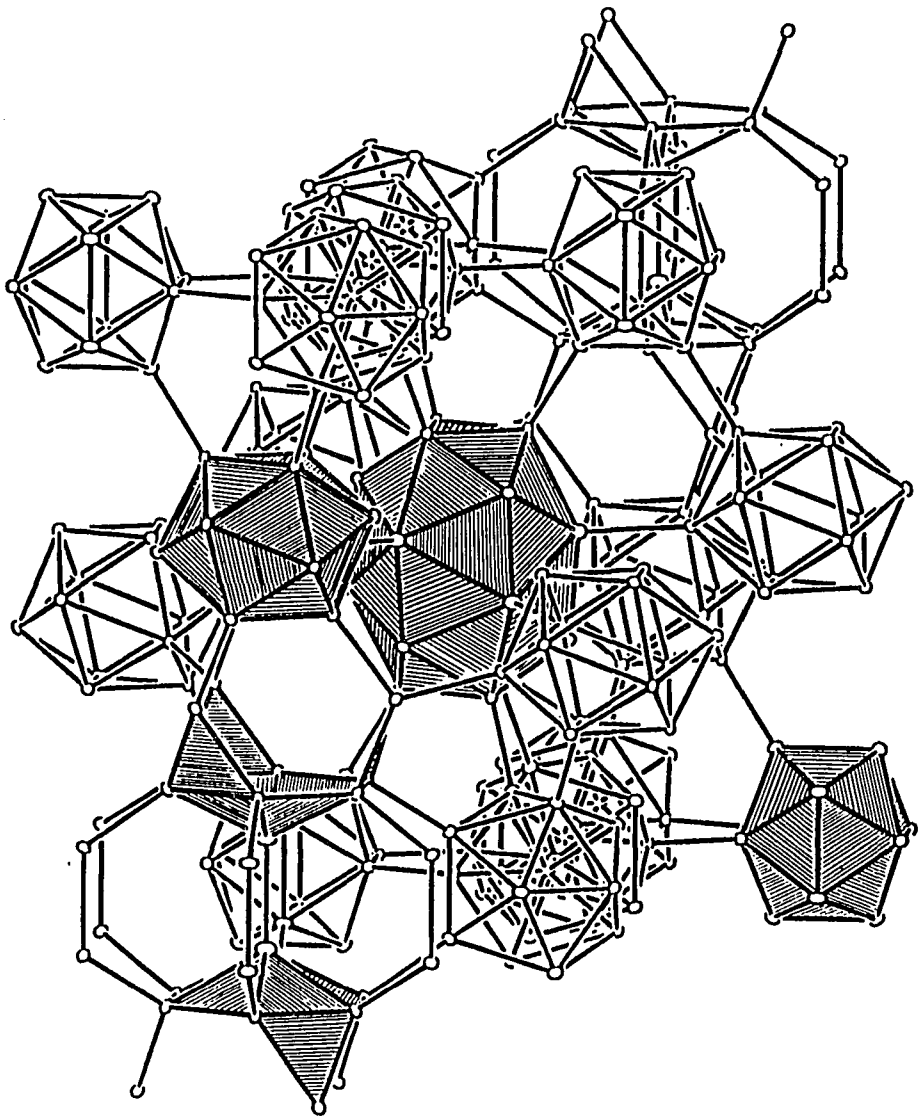

Figure 17. The anionic network of structure V (*c* vertical). All distances less than 4.0 Å are drawn and the building blocks of 12-bonded icosahedra (A- and B-type), *closo*-In_{18} (center) and 20-atom spacer (down left) are striped. (20% probability thermal ellipsoids)

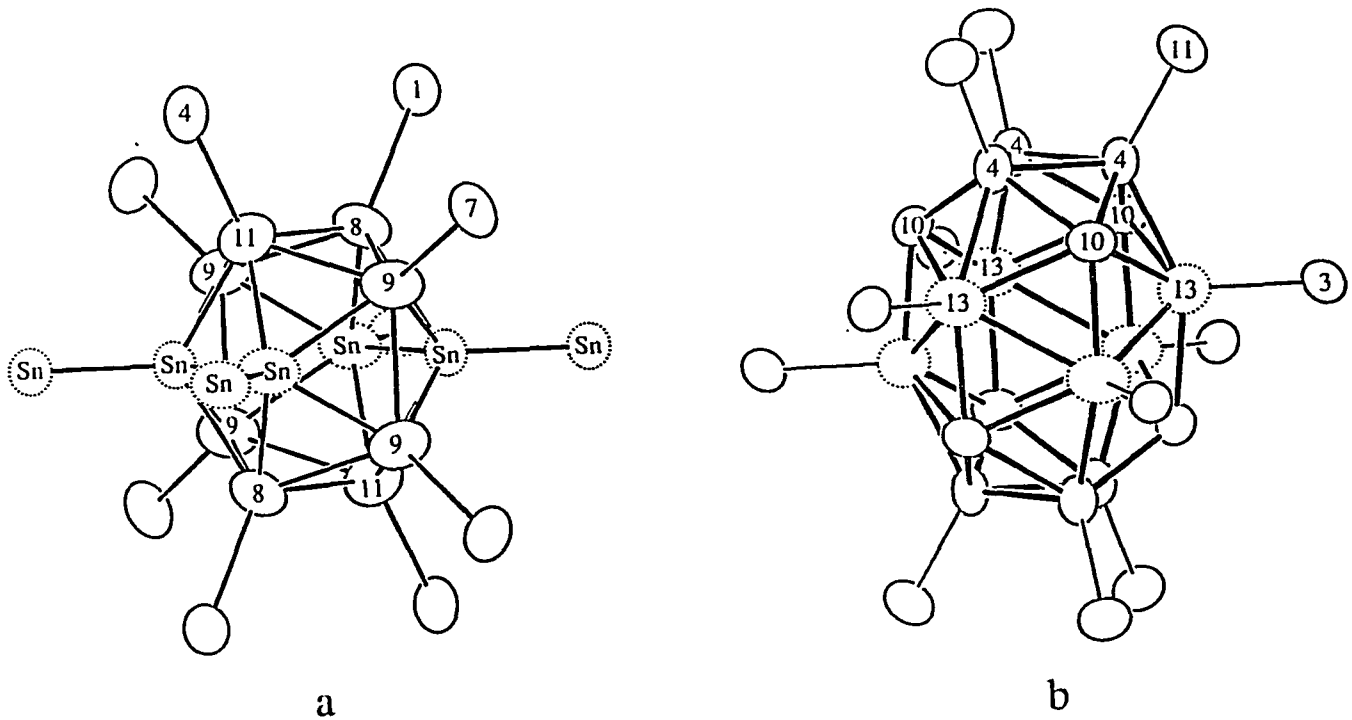

Figure 18. Two of the four building blocks of structure **V**: a) 12-bonded In_{12} (A-type); b) 12-bonded *closo*-In_{18} with D_{3d} symmetry. The partially occupied sites are shown with dotted ellipsoids. (94% probability thermal ellipsoids)

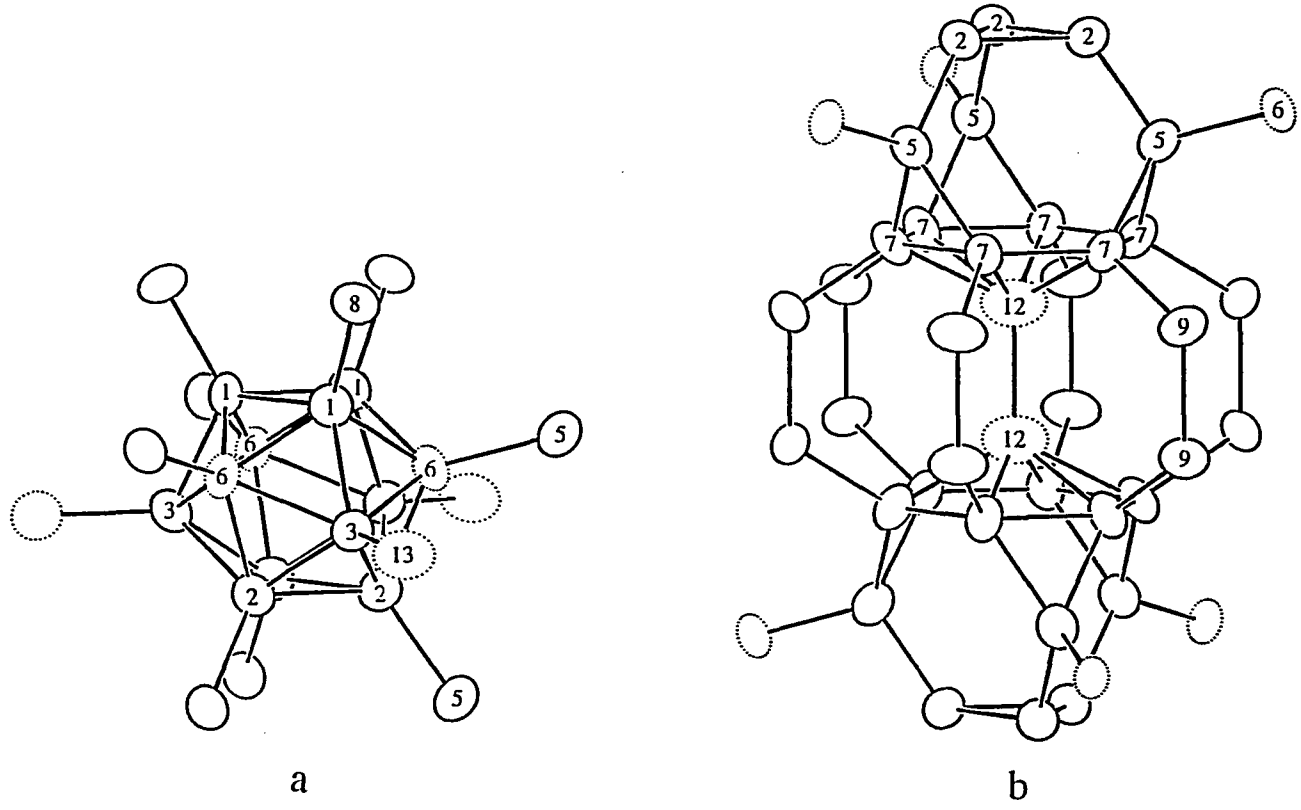

Figure 19. Two of the four building blocks of structure V: a) 12-bonded In_{12} (B-type); b) 24-bonded 20-atom spacer. The partially occupied sites are shown with dotted ellipsoids. (94% probability thermal ellipsoids)

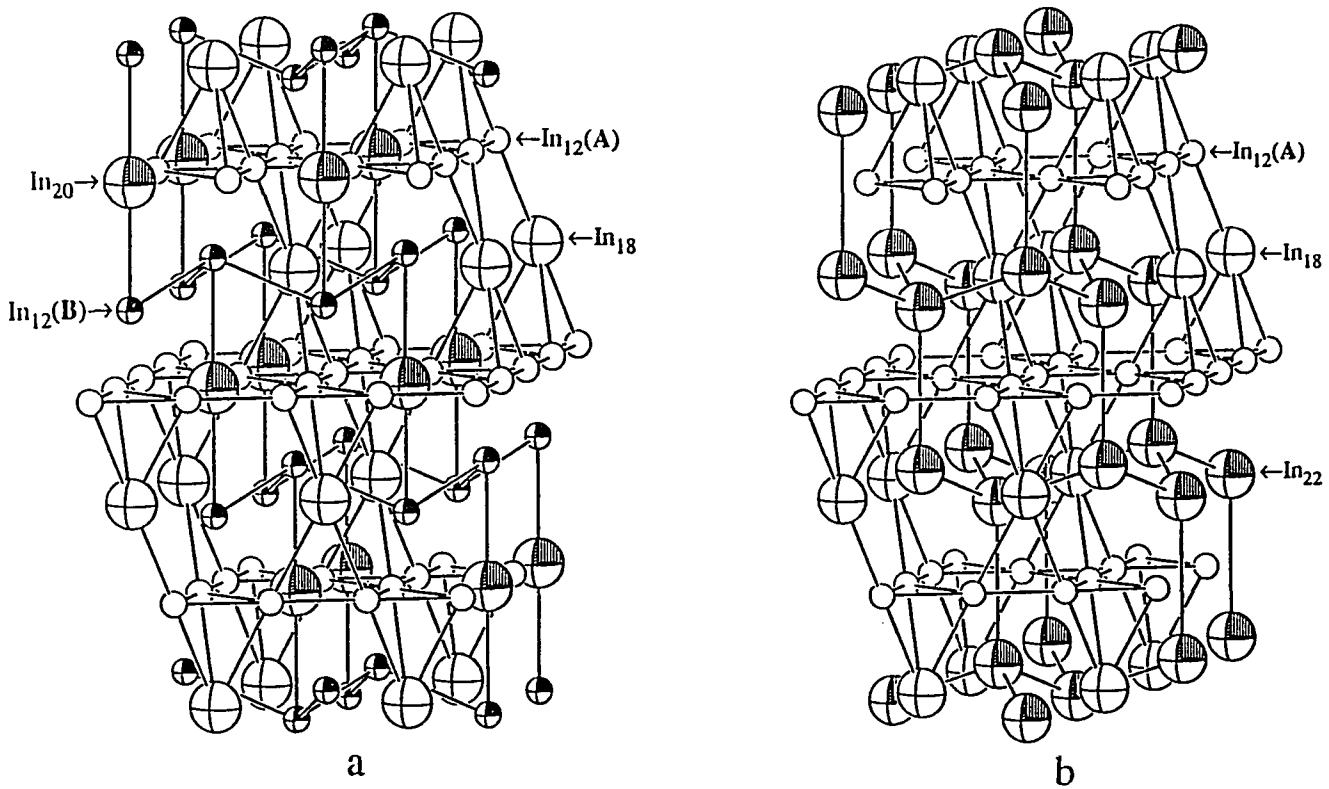

Figure 20. Two condensed interpretattions of structure V. The Kagomé nets of A-type In_{12} are joined via In_{18} and the voids are filled by: a) the B-type In_{12} and the 20-atom spacers; b) 22-atom spacers made of one B-type In_{12} and a half of the 20-atom spacer (Figure 19b). The second version can be considered as related to the structure of the Laves phase $MgCu_2$ by replacing In_{12} and In_{18} with Cu and the 22-atom spacers, with Mg atoms.

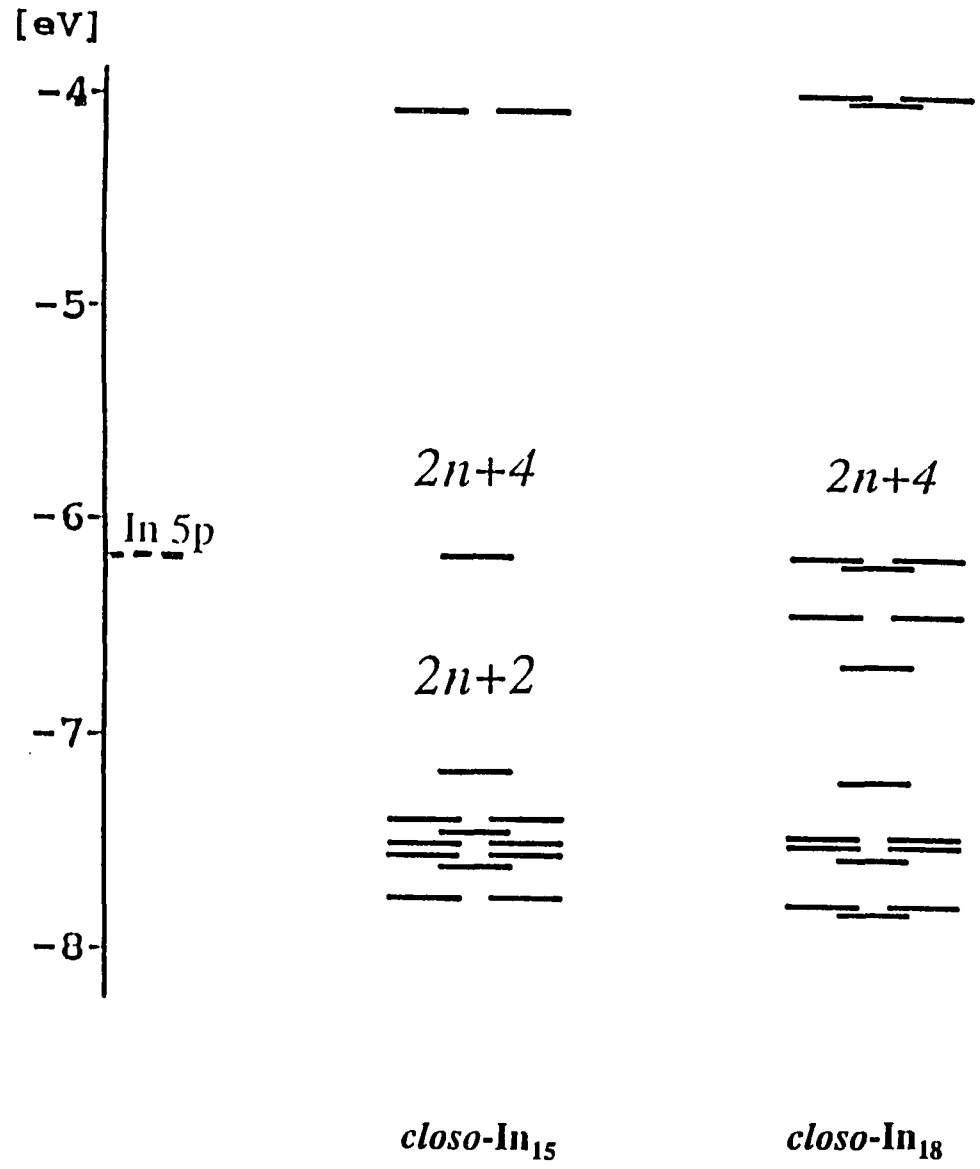

Figure 21. Molecular orbital diagrams for *closo*-In_{15} (left) and *closo*-In_{18} (right) obtained from extended-Hückel calculations.

PART III. COMBINATIONS OF ISOLATED AND INTERCONNECTED INDIUM CLUSTERS – FULLERENES OF INDIUM

PAPER 11. SYNTHESIS, CHARACTERIZATION AND BONDING OF INDIUM FULLERENES: LAYERS OF FUSED In_{74} WITH ENCAPSULATED CLUSTERS

ABSTRACT

Ternary compounds $Na_{96}In_{\sim 97}Z_2$ where Z=Ni, Pd or Pt are obtained in high yield by slow cooling of the appropriate fused mixtures of the elements in welded Ta. They occur in the hexagonal space group $P6_3/mmc$, Z = 2 with a = 15.969 (9), 15.963 (2), 15.950 (2) Å and c = 47.39 (8), 47.57 (1), 47.45 (1) Å for Z = Ni, Pd, Pt respectively. The structure was refined for the Ni and Pd derivatives to R, R_w = 4.5, 5.2% and 3.2, 3.1% respectively. It contains layers of fullerene-type spheres of 74 indium atoms, In_{74}. Each sphere (D_{3h}) shares the equatorial six of its twelve pentagonal faces with six other spheres of the same type. The layers are separated by sodium cations and naked Z-centered $In_{\sim 10}$ clusters in octahedral type voids. The indium spheres are centered by isolated Z-centered $In_{\sim 10}$ clusters as well as sphere of sodium cations between the surface of the indium sphere and the central cluster. Each indium atom of the network is bonded to a fourth indium, which, for those in the equatorial belt of the spheres, is accomplished through bonding between two spheres. The atoms near the poles of the spheres gain a fourth or more bonds through bonding to a triangle of indium atoms added above each pole or to hexagons of indium atoms placed above and below every other point of the layer where three spheres meet. Extended-Hückel band calculations on a single layer and the refined composition indicate that the most likely place of the Fermi level is between slightly bonding and slightly antibonding combinations of mainly lone pairs of electrons on the added triangles and hexagons of indium atoms. This would require a total of -23 charge distributed between the two types of isolated Z-centered indium clusters. The latter have nearly spherical geometry with nearly continuous distribution of the electron density on the surface. The refinement with partially occupied indium positions of the cluster showed a total of approximately 10 indium atoms per cluster. The compounds are diamagnetic (-2.6, -2.0, -1.2 × 10^{-3} emu mol^{-1} for Z = Ni, Pd, Pt respectively).

INTRODUCTION

A considerable amount of work has been done on studying different sizes of carbon fullerenes and their derivatives obtained by substitution, addition, intercalation and insertion.[1] There have been reports on mass-spectrometric detection of boron substituted fullerenes B_nC_{60-n} ($n \leq 6$) as well as on failed attempts to prepare cages of noncarbon atoms only, B-N as an example.[2] Another part of the research has been directed toward synthesis of fullerenes with encapsulated metal atoms, and recently the metallofullerenes $M@C_{82}$ (M = La, Y, Sc) and $Sc_3@C_{82}$ have been identified by mass spectrometry and electron paramagnetic resonance.[3-8] The scandium atoms in the latter are thought to form a triangular cluster inside the 82-atom cage. Alkali metal intercalated fullerenes of C_{60} and C_{70} have shown superconductivity.[1] In these compounds, the carbon cages carry negative charges of up to -6 or in other words, there are 6 more electrons on the cluster orbitals than the needed for skeletal bonding within the cages.

This article reports on compounds containing Buckminster Fuller type cages of indium atoms only. Moreover, these 74 atom cages have an isolated Ni, Pd or Pt-centered clusters of *ca.* 10 indium atoms encapsulated at the center as well as 39 sodium atoms placed between the surface of the sphere and the isolated central cluster which are capping from inside the 12 pentagonal and 27 hexagonal faces of the cage. Following the nomenclature proposed by Smalley *et al*,[2] the formula of one cage should be written as $Z@In_{10}@Na_{39}@In_{74}$ where Z = Ni, Pd or Pt. Although these cages are not isolated but rather fused with each other via six of the pentagonal faces and lack the characteristic for the C_{60} delocalized π-bonding system, we still can call them fullerenes since they resemble the structures proposed by the late Fuller.

We have already studied the binary alkali metal–indium systems and discovered novel compounds containing isolated clusters (In_{11}^{7-}, In_4^{8-})[9, 10] or networks of clusters (8-bonded-In_{16}^{12-}, 4-bonded-In_6^{4-} etc.)[11, 12] of indium. Later we worked on ternary systems and found that

some elements like Zn, Ni, Pd, Pt center isolated clusters of 10 indium atoms such as $In_{10}Zn^{8-}$ in $K_8In_{10}Zn$ or $In_{10}Z^{10-}$ in $K_{10}In_{10}Z$ where Z = Ni, Pd, Pt.[13, 14] The next step was to try to make similar ternary phases using Na instead of K. This led to the compounds presented here which are in fact a combination of a network of indium atoms and isolated and centered indium clusters.

EXPERIMENTAL SECTION

Synthesis.

All materials were handled in a N_2-filled glovebox with a typical H_2O level of less than 0.1 ppm vol. The surface of the indium (Cerac, 99.999%) and sodium (Alpha, 99.9+%, sealed under Ar) were cut clean with a scalpel before use. Nickel sheet (Matheson Coleman & Bell, reagent), palladium wire (Johnson Matthey, 99.995%) and platinum sheet (Government issue, reagent) were used as received. All reactions were carried out in welded tantalum tubes jacketed in sealed silica containers. The techniques are described elsewhere.[11]

Initially the phases $Na_{96}In_{\sim 97}Z_2$ were identified in the products from reactions loaded with compositions $Na_{10}In_{10}Z$ and heated at 600°C. After the structure of the Ni derivative was partially refined and approximate composition determined, samples with atomic ratio of Na : In : Ni, Pd or Pt = 96 : 98 : 2 were prepared. The mixtures were melted at 700°C for one day (the highest melting point in the Na–In system is about 440°C) and then slowly cooled to room temperature at 5° per hour. The compounds form bar- and gem-like crystals with dark gray color but metallic luster.

Powder patterns were obtained from ground samples that were mounted between pieces of cellophane tape. An Enraf-Nonius Guinier camera, Cu $K\alpha_1$ radiation (λ = 1.540562 Å), and NBS (NIST) silicon as internal standard were employed for this purpose. X-ray powder patterns calculated on the basis of the refined positional parameters for $Na_{96}In_{\sim 97}Ni_2$ matched the respective ones measured for the Pd and Pt products very well, leading to the conclusion that the same structure pertained to all three. A least-square refinement of the measured 2θ values together with those of the standard Si lines resulted in a = 15.969 (9), c = 47.39 (8) Å for $Na_{96}In_{\sim 97}Ni_2$, a = 15.963 (2), c = 47.57 (1) Å for $Na_{96}In_{\sim 97}Pd_2$ and a = 15.950 (2), c = 47.45 (1) Å for $Na_{96}In_{\sim 97}Pt_2$. The quite large standard deviations of the lattice parameters of the Ni

derivative resulted from very diffuse lines on the experimental powder pattern. All the patterns contained also weak lines for minor phases of NaIn, $Na_{10}In_{10}Z$ and In metal (total mass fraction of less than *ca.*10%) probably formed from eventual incongruent formation of the major compound upon the slow cooling.

Structure Determination.

Diffraction data for $Na_{96}In_{\sim 97}Ni_2$ and $Na_{96}In_{\sim 97}Pd_2$ were collected on CAD4 and SIEMENS/RA single crystal diffractometers, respectively, at 21°C with monochromated Mo Kα radiation up to $2\theta = 50°$. The structures were refined with the aid of the TEXSAN software package. Some details of the data collection and refinement for the two compounds are listed in Table I. Unique aspects of the crystallography follow:

$Na_{96}In_{\sim 97}Ni_2$. A few bar-like crystals of the first sample (Na : In : Ni = 10 : 10 : 1) were sealed in thin-walled capillaries and checked for singularity by means of oscillation photographs. One of them, 0.1 × 0.1 × 0.2 mm, was chosen, mounted on CAD4 single crystal diffractometer, and 25 reflections found from random search were indexed with a hexagonal unit cell. Data collected from one small octant of reciprocal space were corrected for Lorentz and polarization effects and for absorption with the aid of the average of four ψ-scans at different 2θ angles. The observed extinction condition, *hhl*: $l \neq 2n$ suggested three possible space groups — $P6_3mc$, $P62c$ and $P6_3/mmc$. The Wilson plot corresponded to a centrosymmetric distribution and therefore $P6_3/mmc$ was chosen. The reflections were very sharp (*ca.* 0.4° along ω) and although the *c* axis is quite long no overlap of reflections was observed (collection was done with 0.5° width ω-scans).

Direct methods (SHELXS-86) provided eleven peaks that had distances to each other appropriate for indium atoms, and they were so assigned. A few cycles of least-squares refinement and a difference Fourier synthesis revealed two atoms at special positions with many

peaks surrounding them at distances appropriate for Ni–In distances and also fourteen other positions with distances appropriate for sodium. After assigning the first two positions to Ni atoms and the latter fourteen to Na atoms, the subsequent refinement and difference Fourier map revealed four more Na atoms, and the electron density around the Ni atoms remained. These remaining peaks were of relatively low height, and some of them were too close to each other although all of them were at appropriate distances to the central Ni atoms. A few of them were assigned as indium, and the following least-square refinement led to unusually high thermal parameters for them. At this point the well behaved indium atoms and all 18 sodium atoms were refined with anisotropic thermal parameters which resulted R of 9.5%. Next, all remaining peaks around the Ni atoms were input as In atoms and their anisotropic thermal parameters as well as their multiplicities were refined. The R and R_w factors dropped to 4.5 and 5.2% respectively after refining a secondary extinction coefficient as well. The largest residual peaks in the final difference Fourier map were 2.56 e/Å^3, 1.2 Å from Na1, and -3.23 e/Å^3. The total numbers of In atoms around Ni(A) and Ni(B) are 9.86 (9) and 10.19 (9) respectively. This leads to a final refined composition of $Na_{96}In_{96.9(1)}Ni_2$.

$Na_{96}In_{\sim 97}Pd_2$. The fact that the data from the Ni-containing compound were refined with few partially occupied indium atoms with quite anisotropic and large thermal parameters produced some concern about whether the space group chosen was correct. In order to check for a possible lower symmetry space group a single crystal (gem-like, 0.15 × 0.15 × 0.15 mm) of the Pd compound was studied by oscillation and Weissenberg photography with Cu Kα radiation. The crystal was aligned along the *a* axis of the hexagonal setting and Weissenberg pictures of the *0kl* and *1kl* layers were taken. Three mirror planes perpendicular to *a*, to *b* and to *c* and an extinction condition *00l*: $l \neq 2n$ were revealed. Later the same crystal was mounted on SIEMENS/RA single crystal diffractometer, and this time a larger data set of a quarter of a

sphere of reciprocal space was collected. After corrections for Lorentz and polarization effects and for absorption with the aid of a θ-dependent curve derived from six ψ-scans, the data confirmed the extinction condition for *P6$_3$/mmc* and averaged very well in the corresponding Laue class (4.6% on all data with I > 0). The atomic positions for the well behaved In atoms and those for the Ni and Na atoms in $Na_{96}In_{\sim 97}Ni_2$ were used to refine the structure. A difference Fourier map revealed again many low height (*ca.* 20 to 25 e/Å^3) peaks around the Pd atoms, but some of them were too close to each other. After assigning all of them as In atoms and refining their multiplicities and anisotropic thermal parameters for all atoms, the final residues became R, R_w = 3.2, 3.1% respectively. The largest peaks in the final difference Fourier map were 1.57 e/Å^3, 1.3 Å from InA3, and -1.24 e/Å^3. The total numbers of the In atoms around Pd(A) and Pd(B), 9.45 (6) and 10.07 (7) respectively, are very close (within 4σ) to those around Ni(A) and Ni(B) in the Ni derivative. At this point, it was thought that maybe some of the symmetry elements implied by *P6$_3$/mmc* were artificial for the problematic indium atoms, although they may be real for the remaining atoms (only ~17% of the scattering is due to the indium atoms around the palladium positions). Consequently, a much lower symmetry space group *P2$_1$/m* was assigned, and atomic positions were calculated from the well refined atoms in *P6$_3$/mmc*. The difference Fourier map based on this model revealed the same problem around the palladium atoms. There were again peaks with low height, some very close to each other. The same result was obtained using the acentric *P2$_1$* and this led to the conclusion that these problematic atoms experience real disorder throughout the crystal.

Physical Properties.

About 25 mg of nearly single phase $Na_{96}In_{\sim 97}$(Ni, Pd or Pt)$_2$ were prepared by selectively collecting relatively large crystals of the corresponding compound from each product. These were ground, loaded in special holders and sealed under He atmosphere. The

magnetization was measured at a field of 3 T over 6–295 K and of 100 Oe over 1.4–6 K on a Quantum Design MRMS SQUID magnetometer.

RESULTS AND DISCUSSION

Structure Description.

The final positional and isotropic-equivalent displacement parameters as well as the occupancy of the partially occupied sites are reported in Tables II and III for $Na_{96}In_{\sim 97}Ni_2$ and $Na_{96}In_{\sim 97}Pd_2$, respectively. The anisotropic displacement parameters for the two compounds are listed in Tables IV and V, respectively. The important distances around the In, Ni and Pd atoms are reported in Table VI and those around the Na atoms, in Table VII. A general view of the unit cell is shown in Figure 1 with all In–In distances less than 4.0 Å drawn, for clarity, only one cluster between the layers and the contents of one cage are shown.

The structure is built of layers perpendicular to the *c* axis with two layers per unit cell. Each layer is a close packed arrangement of equivalent and nearly spherical cages and is perfectly flat. The cages (Fig. 2) are 74-atom indium fullerenes built of 12 pentagonal (as in all sizes of carbon fullerenes) and 27 hexagonal faces, and have D_{3h} point group symmetry. Each atom of the cage has three bonds on its surface. Each of the six equatorial (the equatorial plane of the ball is perpendicular to the *c* axis and the corresponding poles are pointing along *c*) pentagons of a cage is shared with a neighboring cage so that the atoms of these pentagons (In2, 4, 7, Figure 2) belong to two cages and are four-bonded. The two atoms of each of the three equatorial hexagons that do not belong to a pentagon (In5) form two additional bonds to the same type atoms from two neighboring spheres and become five-bonded (Figure 3). At higher latitude, In6 atoms have one additional bond each to In6 atoms in another sphere and are four-bonded (Figure 3). The atoms near and at the poles (In1, 3, 8, 9) do not have close neighbors from surrounding spheres in order to form more than three bonds. In contrast to the carbon atoms in the carbon fullerenes which have only three σ bonds, the indium atoms appear to require four or more bonds. In order to satisfy this requirement, triangles of In11 are added

above each pole, and hexagons of In10 are inserted above and below every other point of the layer where three spheres meet (Figures 1 and 3). This leads to formation of three additional bonds for the polar (In9) atoms and one more bond from their nearest neighbors (In8) to the triangles (Figure 3). The atoms forming the triangles become also four-bonded. In1 and 3 from the spheres form two and one additional bonds to each hexagon and become five- and four-bonded, respectively. The atoms from the hexagons are four-bonded.

The layers of the fullerenes are stacked in a hexagonal (ABA...) fashion along the *c* axis at z = 1/4 and 3/4. Since the hexagons of In10 (above) are inserted only in B positions in A-type layers and in A positions in B-type layers, those In11 triangles added above each pole of the spheres are right above or below these hexagons (Fig. 1, near 1/3, 2/3, 1/2 and Fig. 3). The shortest distance between two layers occurs between In10 and In11 and is 5.434 (9) Å for the Ni derivative and 5.458 (2) Å for the Pd one.

The layers are separated by sodium cations and also by isolated Z-centered indium clusters nested at the octahedral sites that are the C positions for both layers (Fig. 1, at 0, 0, 1/2). From Figure 1 can be seen that these octahedral sites are surrounded by indium hexagons and pentagons from above and below which remind one to some extend of a broken sphere. If we zoom in on this place, we find that there is one sodium atom, Na7, which, if connected to its nearest indium neighbors, completes the sphere to a M_{60}-type fullerene (Figure 4) built of 48 indium (In3, 6, 8, 10, 11) and 12 sodium atoms. This fullerene has the geometry of the known C_{60} molecule although with somewhat reduced point group symmetry of D_{3d}. Notice on Figure 4 that the sodium atoms are positioned quite a bit above the surface of the sphere defined by the indium atoms, and the reason for this is the longer Na–In bonds (*ca.* 3.4 Å) compared with the In–In bonds (*ca.* 3.0 Å). All six Na7–Na7 edges are shared with other M_{60} cages in the *a,b* plane, and thus another type of close-packed layer (at z = 0 and 1/2) emerges. The M_{60} shares

six of its pentagons (In3, 6, 8) with In_{74}, and the two cages contain the two types of isolated Z-centered indium clusters at their centers.

The above considerations suggest a different representation of the whole structure. It now can be viewed as built of alternating close packed layers of In_{74} and M_{60} ($In_{48}Na_{12}$) fullerenes stacked along the *c* axis which follow a double hexagonal CACB... sequence with M_{60} always at the C level (Figure 5a). The number of the M_{60} cages equals the number of the In_{74} cages, and if we imagine that each M_{60} is a Ni atom and each In_{74} is an As atom, then the compound is isotypic with the very well known NiAs type structure.

The positioning of the sodium atoms throughout this structure is novel, that is, all the sodiums except Na7 (above) cap all of the hexagonal and pentagonal faces of the two cages from both sides (Figures 6 and 7). Following is a list of the capping sodium atoms and the faces they cap:

a) in In_{74}

- Na13	inside and	Na2	outside cap the	hexagon In1, 3, 3, 8, 8, 9;
- Na18	inside and	Na17	outside cap the	pentagon In3, 3, 6, 6, 8;
- Na4	inside and	Na8	outside cap the	hexagon In1, 3, 4, 5, 6, 7;
- Na12	inside and	Na1	outside cap the	hexagon In2, 2, 4, 4, 6, 6;
- Na9	inside and	Na14	outside cap the	hexagon In5, 5, 7, 7, 7, 7;
- Na16	inside and	Na16	outside cap the	pentagon In2, 4, 4, 7, 7;

b) in M_{60}

- Na6	inside and	Na1	outside cap the	hexagon In6, 6, 6, 6, 6, 6;
- Na17	inside and	Na18	outside cap the	pentagon In3, 3, 6, 6, 8;
- Na10	inside and	Na8	outside cap the	hexagon In3, 3, 6, 6, 10, 10;
- Na15	inside and	Na2	outside cap the	hexagon In3, 8, 10, 11, Na7, 7;
- Na11	inside and	Na5	outside cap the	pentagon In10, 10, 11, Na7, 7.

There are 39 sodium atoms (12 × Na4 + 3 × Na9 + 6 × Na12 + 6 × Na13 + 6 × Na16 + 6 × Na18) inside the 39 faces of In_{74} and 32 sodium atoms (2 × In6 + 6 × In10 + 6 × Na11 + 12 × In15 + 6 × In17) inside the 32 faces of M_{60}. The sodium atoms that are outside both cages are Na1, 2, 3, 5, 8, 14.

If lines are drawn between the inside sodium atoms (endo-Na) of the two spheres as it is done with open bonds in Figures 6 and 7, additional nearly spherical formations inside the fullerenes are revealed. These are correspondingly 39 and 32 atom regular deltahedra (triangular faces only) of five and six "bonded" sodium atoms (within the deltahedron). Figure 5b shows part of the cell with only the sodium atoms (except Na7). The atoms of the indium fullerenes can now be viewed as capping all faces of each inside deltahedron. Since each "six-bonded" sodium atom has six adjacent triangles and each "five-bonded" sodium atom has five, they cap respectively a hexagon and a pentagon from the fullerene.

One very important consideration for the further discussion is that the "six-bonded" endo-Na atoms need to be closer to the surface of the fullerene, or in other words further from its center than the "five-bonded" endo-Na atoms, in order to keep reasonable and more or less equal Na–In distances. This also leads to shorter exo-endo Na-Na distances for the hexagon capping atoms than for the pentagon capping ones. (As an example, 4.34 (1) Å for Na17–Na18 *vs.* 3.48 (1) Å for Na13–Na2). All of this means in effect that all of the sodium positions in the structure are fixed (determined) by the positions of the atoms building the fullerenes, and this has a dramatic effect on the isolated indium clusters at the center of the cages.

There are two different isolated and Z-centered clusters in the structure. The central atoms (Ni or Pd) have two crystallographically different positions with very high symmetry, $\bar{6}m2$ (D_{3h} point group) and $\bar{3}mm$ (D_{3d} point group). The first one is at the center of the In_{74} fullerene (NiA and PdA) and the second one is at the center of M_{60} cage (NiB and PdB).

During the refinement of the structures (above), it was found that each of these positions is surrounded by a shell of electron density with no well defined maxima (Figure 8). These shells are quite spherical and with average radii (2.78 and 2.66 Å around NiA and B, respectively, and 2.80 and 2.70 Å around PdA and B, respectively) appropriate for Ni–In and Pd–In.distances (2.77 Å is the average for Ni–In in $In_{10}Ni^{10-}$ and 2.81 Å is the Pd–In distance in PdIn with CsCl type structure[14, 16]). The electron density of these shells was approximated by placing indium atoms at all maxima and refining them anizotropically and with partial occupancies. Figure 9 shows the clusters with the ellipsoids of the indium atoms drawn at the 94% probability level. It can be seen that all the ellipsoids are quite two dimensional disks and also that all of them are tangential to a sphere around the center of the cluster. The same clusters are shown with 50% probability thermal ellipsoids on Figure 10 where one can see more clearly the supposed positions of the indium atoms.

The electron density around NiA (within In_{74}) was refined with five independent indium positions, InA1, A11, A2, A3, A31, while only four positions , InA1, A11, A2, A3, were enough (the criterium was achieving comparable positive and negative peaks in the difference Fourier map) around PdA. Nevertheless, the totals of the indium atoms (the partial occupancies are accounted for) in the two clusters are equal within 4σ, 9.86 (9) and 9.45 (6) around NiA and PdA, respectively. For both clusters, InA3 (Figure 11) can be considered as a split atom around a position that defines a trigonal prism. InA2 is split around a position that caps the rectangular faces of that prism. InA1 caps the corresponding triangular ends. In addition to these, InA11 and InA31 are satellites of InA1 and InA3, respectively. From Table VI can be seen that many of the positions are very close to each other but also that there are many separations appropriate to be In–In distances. The shortest distances from these clusters to the In_{74} fullerene are 5.00 (2) and 4.988 (7) Å for the Ni and Pd compounds, respectively, and occur between InA1 and In9.

Indium atoms in three different positions (InB1, B11, B2) around NiB and four different positions (InB1, B11, B2, B3) around PdB in the M_{60}-type cages were refined. The two clusters refined to the same numbers of indium atoms within 1σ, 10.19 (9) and 10.07 (7) around NiB and PdB, respectively. The InB1 and B3 positions in the palladium cluster form an icosahedron-like deltahedron. InB2 can be considered as a split atom around each InB3 position. InB11 is like a satellite to InB1. Again, many of the distances on the surface of the cluster are reasonable for In–In distances. The shortest distance from the cluster to the indium atoms of the M_{60} cage is 5.137 (6) Å (InB2 to In11) for the Ni compound and 4.867 (8) Å (InB3 to In11) for the Pd compound. All our attempts to model 10-atom A or B type clusters with fully occupied positions and "normal" In–In distances, disordered or not, failed.

A closer look at the electron density distribution on the surface of the clusters (see Figures 8 and 9) reveals that there are only a few islands which have near zero electron density. Most of the surface is otherwise covered by the thermal ellipsoids of the atoms. Another interesting observation is that these islands of zero electron density are always located below a "five-bonded" sodium atom from the outer deltahedron (Figures 12 and 13). We already discussed the fact that the "five-bonded" sodium atoms are closer to the center of the deltahedron than the six "bonded" ones (above). (One can see on Figure 12 that the "five-bonded" sodium atoms are much closer to the plane of the pentagons they are bonded to than the "six-boned" atoms to the corresponding hexagons). As a result of this, it is evidently impossible to locate an indium atom anywhere in the nearest vicinity between the central atom and a "five-bonded" sodium atom because it would be to close to one of them. On the other hand, the "six-bonded" sodium atoms could have indium atoms underneath at although very short but still possible distances. The observed distances of 3.06(1), 3.18(2) and 2.906(8) Å within the pairs of atoms InA11–Na13, InB11–Na6 and InB1–Na10, respectively, in $Na_{96}In_{\sim 97}Pd_2$ as an example, are

comparable with the shortest Na–In distances in Na_7In_{12}, 3.06 and 3.12 Å.[11] The distance between InB2 and Na15 in both compounds, 2.80(1) and 2.759(7) Å for the Ni and Pd derivatives,respectively, is on the other hand extremely short but evidently possible in this quite compressed from outside formation. The rest of the surface of the cluster is allowed in terms of distances considerations. The final result of all of this is that the inner indium atoms are pinned radially by the Z atoms from inside and by the sodium atoms from outside, and at the same time are not restricted at particular positions on the surface of the cluster and can "float". This gives the observed disk-like thermal ellipsoids which cover most of the surface of the cluster.

The discussed above situation also reminds one very much the so called incommensurate structures. In the latter, a mismatch between two layers or two rows of atoms with different periodicities occurs, and this causes similar problems when refining the structure as commensurate. In our case the mismatch is between the atoms of two spheres one of which has fixed position (the sodium) and the other one is free to take different orientations in respect to the first one. The incommensurability could be visualized as two infinite incommensurate rows of atoms wrapped an infinite number of times around a sphere and can be called circular or angular incommensurability.

Properties

Since the compounds are very air sensitive it is very difficult to measure their resistivities by the conventional four probe method. They also could not be measured by "Q" measurements technique used by us before because that requires quite large size particles in large quantities and such were not formed for these products.

The magnetic susceptibilities of the three $Na_{96}In_{\sim 97}Z_2$ compounds over the range 6–295 K were temperature independent. As before, after corrections for the holder two types of diamagnetic corrections were applied. The first one, for the ion cores of the constituent

elements, totals -2.39, -2.41 and -2.44 × 10^{-3} emu mol^{-1} for the Ni, Pd and Pt derivatives, respectively. The second correction is for the Larmor precession of the electron pairs in the orbitals of the isolated clusters. This was calculated by using an estimated average orbital radius of 2.4 Å for all isolated clusters and assuming a charge of -10 (20 skeletal electrons) on each of them. This gave an additional correction of -0.32 × 10^{-3} emu mol^{-1} per cluster. The corrected values for χ_M are plotted on Figure 14 and are *ca.* -2.6, -2.0 and -1.2 × 10^{-3} emu mol^{-1} for the Ni, Pd and Pt derivatives, respectively. These are quite large negative (diamagnetic) susceptibilities but one should keep in mind that large diamagnetic contributions from bonding electron pairs in the condensed indium cages have not been accounted for. If applied they would lift the numbers of χ_M closer to zero and may even make them positive (eventually Pauli paramagnetism). No superconductivity was detected at field 100 Oe down to 1.4K in any of the three compounds.

Electronic Structure

Extended–Hückel band calculations were performed on a single layer of the structure with only the indium atoms included.[17] The resulting distributions of the density of states (DOS) and the total crystal orbital overlap population (COOP) curve are plotted on Figure 15. A strongly bonding band of predominantly In p character is located between -10.2 and -6.3 eV while the s levels form an wider band between -17.6 and -10.2 eV. It is clear from the COOP curve that the levels between -6.3 and -4.0 eV are nonbonding or slightly antibonding. Since the Z-centered isolated indium clusters could not be modeled with a particular rigid geometry a precise electron count for the compound can not be done and therefore the position of the Fermi level can not be determined unambiguously. Its position in Figure 15 (broken line) has been chosen because of some indirect considerations presented below.

Figure 16 shows on the left a magnified section of DOS near the Fermi level and on the right the corresponding bands plotted throughout the Brillouin zone (Γ is at 0, 0, K is at 0.5, 0.0, and M is at 0.5, 0.5). One can see that the bands closest to the Fermi level are very flat and this suggests very weak and also localized interactions associated with them. The bands further above and below are more and more dispersed which is the effect of stronger bonding or antibonding interactions. Another observation is that the valence and conduction bands as assigned by us form peaks that are very similar in shape and height in the density of states plot. This similarity hinted that we should check more carefully the types of the corresponding orbitals. A further magnified picture of this part of the diagram is shown on Figure 17. It can be seen that the conduction band consists of two doubly degenerate orbitals at Γ point that are very close in energy. The lower one is e′ type and the upper one is e″ type in the D_{3h} point group symmetry which the layer possesses. Moving away from the Γ point the degeneracy is removed and two orbitals, one of each pair, go through a minimum at the K point. Now turning our attention to the valence band, we find the same, a pair of doubly degenerate e′ (upper) and e″ (lower) orbitals (see insert). Through the Brillouin zone these look very much like a mirror image of the pair of orbitals forming the conduction band but are less dispersed. The gap between the two bands is *ca.* 0.5 eV.

Further exploration of the orbital vectors and the atoms associated with the valence and conduction band orbitals revealed that mainly only four types of atoms, In3, 8, 10 and 11, participate in them. The rest of the atoms have very small weight in these orbitals. In10 and 11 are the atoms that build the hexagons and the triangles outside the In_{74} fullerenes and are bonded to them, the former to In1 and 3 and the latter to In8 and In9 (Figures 2, 3 and 4). These two atoms have bonds in only relatively small sectors of the space around them (see Figure 3) and this is a good indication that they have lone pairs of electrons pointing more or less away from

the bonds' main direction. Indeed, the conduction and valence band orbitals are combinations of such lone pairs. The ones in the valence band are slightly more bonding combinations. Also, the p_z orbitals of the In8 atoms of the fullerene are in phase with the lone pairs on In11. The conduction band orbitals are more antibonding in character within the triangles and the hexagons, and the p_z orbitals on In3 and 8 are also somewhat out of phase with the lone pairs on In10 and 11. This situation, in which one and the same atomic orbitals form bonding and antibonding orbitals, usually means that the most likely place for the Fermi level is between the two combinations. We should mention here that the next two bands above the conduction band around -4.5 eV are also combinations of lone pairs but almost purely on In10 and with an out-of-phase contribution from In3. The bands below -6.0 and above -4.0 Ev are all skeletal electrons.

Assuming that the position for the Fermi level of the indium layer is correct, the number of electrons needed to fill the bands for the layer to this level becomes 304. Since each repeating unit of the layer has 77 indium atom, the number of electrons provided is $77 \times 3 = 231$, or $304 - 231 = 73$ short from the required. These 73 electrons will come from the same number of sodium atoms. Since each formula unit has 96 sodium atoms, the remaining 23 will evidently supply electrons to the two isolated indium clusters per formula unit. This in turn means that the sum of the charges on the two clusters must be -23. Also, according to the magnetic susceptibility results, neither cluster nor the network has unpaired and localized electrons. The charge may seem too high, but we have already seen a charge of -10 on Ni-, Pd- or Pt-centered *closo*-$In_{10}Z$ clusters in $K_{10}In_{10}Z$ which require 20 skeletal electrons for bonding.[14] The isolated clusters in the fullerenes are refined to consist of approximately 10 indium atoms each and are centered by the same elements but their configurations are not clear. In case one (or both) of them is *nido* or even *arachno* derivative of 11 or 12 atom *closo* clusters,

respectively, the charge will need to be even larger than -10 and a sum of the two of -23 is plausible.

Since the position of the Fermi level is only estimated, we should explore the situations if it might be lower or higher. Lowering it will lead to fewer needed electrons for the bonding within the indium layers and accordingly fewer electrons from sodium atoms to balance the deficit. This in turn will lead to more remaining sodium atoms to donate electrons to the isolated clusters, meaning that the latter should have even higher charges, which is very unlikely. Moving the Fermi level upward will lead to the opposite result, which is lower charges on the isolated clusters or, in other words, fewer electrons available for In–In skeletal bonding within them. One problem with this situation is that the atoms of the fullerenes will have to carry quite high charges (may have to exceed -2 charge on some atoms). Another problem is that isolated clusters presumably require particular minimum numbers of bonding electrons according to the Wade-like rules for borane type deltahedra, although we have found hypoelectronic clusters, as an example In_{11}^{7-}, which deviate from these principles.[9] Furthermore, the clusters in the fullerenes are *encapsulated* within them and could be considered as forced by the outside environment of sodium deltahedron and indium fullerene to have the particular sizes and quasi-commensurate shapes. If this is the case, there may be no need of electrons for the indium bonding, although the In–In distances are well within the bonding ranges of distances found in other indium clusters. This would be a case in which the positions of the indium atoms of the clusters are solely determined by the mentioned above external factors and not in any degree by the atoms of the clusters themselves. If this is so, lower charges are quite possible and subsequently a higher energy Fermi level is conceivable.

At this point we should recall that only the indium atoms were included in the extended–Hückel band calculations since alkali metal atoms can not be handled reliably by this

method. Also we should note that a sodium atom (Na7) is involved in completing the M_{60} fullerene (see Figure 4). It is "bonded" to In10 and In11 from the side where the lone pairs (above) on these atoms point. If one would turn on the Na–In interactions, the most affected bands would be the assumed valence and conduction bands as well as the one right above the conduction band (around -4.5 eV) since they are combinations of mainly the lone pairs, as mentioned. This most likely will lower their energies through mixing with the sodium atomic orbitals and they may very well become all filled. This would open quite large gap below *ca.* -3.3 eV. The effect of this for the electron counting will be exactly equivalent to raising the Fermi level and will lead to high charges on the indium atoms of the layer and low charges on the encapsulated clusters.

REFERENCES

1. *Fullerenes: Synthesis, Properties, and Chemistry of Large Carbon Clusters*, American Chemical Society series, vol. 481, Washington, DC **1992.**

2. Guo, T.; Jin, Ch.; Smalley, R. E. *J. Phys. Chem.* **1991**, *95*, 4948.

3. Chai, Y.; Guo, T.; Jin, Ch.; Haufler, R. E.; Chibante, L. P. F.; Fure, J.; Wang, L.; Alford, J. M.; Smalley, R. E. *J. Phys. Chem.* **1991**, *95*, 7564.

4. Johnson, R. D.; de Vries, M. S.; Salem, J.; Bethune, D. S.; Yannony, C. S. *Nature* **1992**, *355*, 239.

5. Weaver, J. H.; Chai, Y.; Kroll, G. H.; Jin, C.; Ohno, T. R.; Haufler, R. E.; Guo, T.; Alford, J. M.; Conceicao, J.; Chibante, L. P. F.; Jain, A.; Palmer, G.; Smalley, R. E. *Chem. Phys. Letters* **1990**, *190*, 460.

6. Shinohara, H.; Sato, H.; Saito, Y.; Ohkohchi, M.; Ando, Y. *J. Phys. Chem.* **1992**, *96*, 3571.

7. Yannoni, C. S.; Hoinkis, M.; de Vries, M. S.; Bethune, D. S.; Salem, J. R.; Crowder, M. S.; Johnson, R. D. *Science* **1992**, *256*, 1191.

8. Shinohara, H.; Sato, H.; Saito, Y.; Ohkohchi, M.; Ando, Y.; Kato, T.; Kodama, T.; Shida, T. *Nature* **1992**, *357*, 52.

9. Sevov, S. C.; Corbett, J. D. *Inorg. Chem.* **1991**, *30*, 4875.

10. Sevov, S. C.; Corbett, J. D. *J. Sol. St. Chem.* **1993**, in press.

11. Sevov, S. C.; Corbett, J. D. *Inorg. Chem.* **1992**, *31*, 1895.

12. Sevov, S. C.; Corbett, J. D. *Z. Anorg. Allg. Chem.* **1993**, *619*, 128.

13. Sevov, S. C.; Corbett, J. D. *Inorg. Chem.* **1993**, *32*, in press.

14. Sevov, S. C.; Corbett, J. D. unpublished research.

15. There were lines on the powder patterns that matched some calculated for $K_{10}In_{10}Z$.[14]

16. Harris, I. R.; Norman, M.; Bryant, A. W. *J. Less-Common Met.* **1968**, *16*, 427.

17. Orbital parameters and energies from Janiak, C.; Hoffman, R. *J. Am. Chem. Soc.* **1990**, *112*, 5924.

Table I. Data collection and refinement parameters for $Na_{96}In_{96.9(1)}Ni_2$ and $Na_{96}In_{96.5(1)}Pd_2$

Formula	$Na_{96}In_{96.9(1)}Ni_2$	$Na_{96}In_{96.5(1)}Pd_2$
Formula weight	13462	13502
Crystal size, mm	0.1 × 0.1 × 0.3	0.1 × 0.1 × 0.2
Lattice parameters:[a]		
a, Å	15.969 (9)	15.963 (2)
c, Å	47.39 (8)	47.57 (1)
V, Å^3	10465 (23)	10497 (3)
Space group, Z	*P6$_3$/mmc*, 2	*P63/mmc*, 2
d(calc.), g cm^{-3}	4.27	4.27
μ(Mo–Kα), cm^{-1}	106.76	105.82
Transmission range	0.771–1.000	0.706–0.782
Diffractometer	CAD4	SIEMENS/RA
Radiation	Mo–Kα (λ = 0.71069 Å) graphite-monochromated	
Temperature, °C	23	23
Octants measured	*h, k, l*	±*h, k, l*
Scan method	ω	ω
$2\theta_{max}$	50°	50°
Number of reflections:		
measured	6291	19727
observed ($I \geq 3\sigma_I$)	3225	7616
unique	1737	1896
Number of variables	229	231
R; R_w,[b] %	4.5; 5.2	3.2; 3.1
R_{ave}, %	4.0[c]	4.6
Goodness of fit indicator	1.50	1.10
Maximum shift/σ in final cycle	0.05	0.04
Largest peaks in final ΔF map	+2.46 e/Å^3 (1.2 Å from Na1)	+1.57 e/Å^3 (1.3 Å from InA3)
	-3.23 e/Å^3	-1.24 e/Å^3
Secondary ext. coeff.	6(1) × 10^{-9}	11(1) × 10^{-9}

[a] Room temperature Guinier data with Si as an internal standard (λ = 1.540562 Å).

[b] $R = \Sigma||F_o| - |F_c||/\Sigma|F_o|$; $R_w = [\Sigma w(|F_o| - |F_c|)^2/\Sigma w(F_o)^2]^{1/2}$; $w = \sigma_F^{-2}$.

[c] All data

Table II. Positional and isotropic equivalent displacement parameters for $Na_{96}In_{\sim 97}Ni_2$.

Atom	x	y	z	B_{eq}	N	Occup.	#at./clust
In(1)	0.54067(8)	1.0813	-0.13170(4)	1.4(1)	12k		
In(2)	0.0637(1)	0.1275	1/4	1.6(2)	6h		
In(3)	0.6445(1)	0.9756(1)	-0.11507(3)	1.52(5)	24l		
In(4)	0.12711(8)	0.2542	0.20015(4)	1.5(1)	12k		
In(5)	0.60180(8)	1.2036	-0.18408(4)	1.5(1)	12k		
In(6)	0.8084(1)	0.9987(1)	-0.14958(3)	1.56(4)	24l		
In(7)	0.22792(8)	0.4558	0.21841(4)	1.5(1)	12k		
In(8)	0.77297(8)	1.5459	0.09284(4)	1.5(1)	12k		
In(9)	1/3	2/3	-0.08673(7)	1.4(1)	4f		
In(10)	0.4765(1)	1.1424(1)	-0.07721(3)	1.56(5)	24l		
In(11)	0.73155(8)	1.4631	0.03139(4)	1.8(1)	12k		
Ni(A)	1/3	2/3	3/4	1.6(2)	2d		
In(A1)	1/3	2/3	-0.1923(3)	7.8(5)	4f	43(1)%	0.86(2)
In(A11)	0.3881(8)	0.7761	-0.2036(3)	11(1)	12k	27.8(8)%	1.67(5)
In(A2)	0.2318(3)	0.4636	-0.2394(3)	9.9(9)	12k	45.5(6)%	2.73(4)
In(A3)	0.442(1)	0.8354(6)	-0.2198(2)	12.7(5)	24l	36.3(5)%	4.36(6)
In(A31)	0.438(2)	0.8763	-1/4	4(3)	6h	8(1)%	0.24(3)
Ni(B)	0	0	0	0.8(2)	2a		
In(B1)	0.0634(3)	0.1268	0.0438(1)	7.1(4)	12k	54.6(8)%	3.28(5)
In(B11)	0.966(1)	1.9324	0.0511(4)	16(3)	12k	19.5(8)%	1.17(5)
In(B2)	1.0331(6)	1.1750(4)	-0.0151(2)	14.4(5)	24l	47.8(5)%	5.74(6)
Na(1)	0	0	0.1870(5)	3.2(6)	4e		
Na(2)	0.5426(4)	1.0852	0.0708(2)	2.6(6)	12k		
Na(3)	1/3	2/3	0.1183(5)	2.9(7)	4f		
Na(4)	0.6200(6)	1.0080(6)	-0.1859(2)	3.0(3)	24l		
Na(5)	1/3	2/3	0.0437(5)	2.4(6)	4f		
Na(6)	0	0	-0.1156(4)	2.0(5)	4e		
Na(7)	0.5582(4)	1.1163	-0.0131(2)	2.3(6)	12k		
Na(8)	0.2104(4)	0.4208	0.1441(2)	2.0(6)	12k		
Na(9)	0.5459(7)	1.0918	3/4	3(1)	6h		
Na(10)	0.1330(5)	0.2661	-0.5888(3)	3.1(7)	12k		
Na(11)	0.1902(5)	0.3804	-0.5214(2)	3.0(7)	12k		
Na(12)	0.1156(5)	0.2311	-0.2107(2)	2.7(7)	12k		
Na(13)	0.5855(4)	1.1710	0.1403(3)	2.5(6)	12k		
Na(14)	1/3	2/3	1/4	1.6(7)	2c		
Na(15)	0.3383(7)	0.0485(7)	0.0418(2)	4.1(4)	24l		
Na(16)	0.309(1)	0.015(1)	3/4	3.5(5)	12j		
Na(17)	0.1108(5)	0.2215	-0.0897(3)	3.4(7)	12k		
Na(18)	0.2033(5)	0.4066	-0.1625(3)	3.8(8)	12k		

Table III. Positional and isotropic equivalent displacement parameters for $Na_{96}In_{\sim 97}Pd_2$.

Atom	x	y	z	B_{eq}	N	Occup.	#at./clust
In(1)	0.54054(4)	1.0811	-0.13175(2)	1.68(6)	12k		
In(2)	0.06338(6)	0.1268	1/4	1.6(1)	6h		
In(3)	0.64433(5)	0.97550(5)	-0.11497(2)	1.64(3)	24l		
In(4)	0.12700(4)	0.2540	0.20003(2)	1.62(5)	12k		
In(5)	0.60195(4)	1.2039	-0.18394(3)	1.77(6)	12k		
In(6)	0.80855(5)	0.99875(5)	-0.14938(2)	1.62(2)	24l		
In(7)	0.22787(4)	0.4557	0.21847(2)	1.69(5)	12k		
In(8)	0.77303(4)	1.5461	0.09273(2)	1.65(5)	12k		
In(9)	1/3	2/3	-0.08668(4)	1.44(5)	4f		
In(10)	0.47669(6)	1.14256(6)	-0.07734(2)	1.78(3)	24l		
In(11)	0.73140(4)	1.4628	0.03139(3)	1.95(6)	12k		
Pd(A)	1/3	2/3	3/4	2.17(9)	2d		
In(A1)	1/3	2/3	-0.1915(1)	6.1(2)	4f	45.3(8)%	0.91(2)
In(A11)	0.3799(6)	0.7597	-0.2007(2)	19(1)	12k	24.7(5)%	1.48(3)
In(A2)	0.2312(2)	0.4623	-0.2357(1)	9.8(4)	12k	42.3(4)%	2.54(2)
In(A3)	0.4504(5)	0.8402(3)	-0.2205(1)	13.6(3)	24l	37.7(3)%	4.52(4)
Pd(B)	0	0	0	0.90(7)	2a		
In(B1)	0.0649(1)	0.1298	0.04384(8)	7.2(2)	12k	55.2(5)%	3.31(3)
In(B11)	0.9674(7)	1.9348	0.0519(2)	19(2)	12k	19.6(5)%	1.18(3)
In(B2)	1.0219(4)	1.1719(3)	-0.0171(1)	10.5(3)	24l	32.7(3)%	3.92(4)
In(B3)	0.0964(3)	0.1928	-0.0101(3)	15(1)	12k	27.6(6)%	1.66(4)
Na(1)	0	0	0.1862(3)	2.7(3)	4e		
Na(2)	0.5419(2)	1.0837	0.0710(2)	2.9(4)	12k		
Na(3)	1/3	2/3	0.1185(2)	2.1(3)	4f		
Na(4)	0.6231(3)	1.0093(3)	-0.1850(1)	3.3(2)	12k		
Na(5)	1/3	2/3	0.0438(3)	4.2(5)	4f		
Na(6)	0	0	-0.1160(3)	2.5(3)	4e		
Na(7)	0.5588(3)	1.1176	-0.0132(2)	3.1(4)	12k		
Na(8)	0.2109(2)	0.4218	0.1443(1)	2.6(4)	12k		
Na(9)	0.5463(4)	1.0927	3/4	2.8(6)	6h		
Na(10)	0.1346(3)	0.2692	-0.5896(2)	3.1(4)	12k		
Na(11)	0.1903(3)	0.3806	-0.5217(1)	3.3(4)	12k		
Na(12)	0.1161(3)	0.2321	-0.2105(1)	3.0(4)	12k		
Na(13)	0.5848(3)	1.1696	0.1398(2)	3.0(4)	12k		
Na(14)	1/3	2/3	1/4	3.4(5)	2c		
Na(15)	0.3397(4)	0.0491(3)	0.0420(1)	4.2(2)	24l		
Na(16)	0.3096(5)	0.0148(5)	3/4	3.5(3)	12j		
Na(17)	0.1110(3)	0.2220	-0.0893(1)	2.9(4)	12k		
Na(18)	0.2039(3)	0.4077	-0.1630(2)	4.1(4)	12k		

Table IV. Anisotropic displacement parameters for $Na_{96}In_{\sim 97}Ni_2$.

Atom	U_{11}	U_{22}	U_{33}	U_{12}	U_{13}	U_{23}
In(1)	0.0180(8)	0.022(1)	0.016(1)	0.011	0.001	0.002(1)
In(2)	0.030(3)	0.019(1)	0.016(1)	0.015	0	0
In(3)	0.0178(7)	0.0165(7)	0.0249(7)	0.0096(5)	0.0026(6)	0.0029(6)
In(4)	0.0235(9)	0.016(1)	0.016(1)	0.008	0.000	0.000(1)
In(5)	0.0179(8)	0.020(1)	0.019(1)	0.010	0.003	0.006(1)
In(6)	0.0200(6)	0.0186(6)	0.0218(7)	0.0105(5)	0.0045(7)	0.0021(7)
In(7)	0.0230(9)	0.017(1)	0.017(1)	0.008	-0.000	-0.001(1)
In(8)	0.0150(8)	0.019(1)	0.024(1)	0.009	-0.001	-0.001(1)
In(9)	0.017(1)	0.017	0.020(2)	0.008	0	0
In(10)	0.0175(7)	0.0195(7)	0.0240(6)	0.0105(5)	-0.0014(7)	-0.0042(7)
In(11)	0.025(1)	0.016(1)	0.023(1)	0.008	0.002	0.005(1)
Ni(A)	0.028(4)	0.028	0.005(4)	0.014	0	0
In(A1)	0.14(1)	0.14	0.022(7)	0.069	0	0
In(A11)	0.119(9)	0.23(2)	0.10(1)	0.12	-0.071(5)	-0.141
In(A2)	0.109(6)	0.030(4)	0.21(2)	0.02	0.012(3)	0.023
In(A3)	0.14(1)	0.106(6)	0.144(7)	-0.007(8)	-0.015(8)	-0.089(5)
In(A31)	0.01(2)	0.03(3)	0.13(6)	0.02	0	0
Ni(B)	0.010(3)	0.010	0.012(4)	0.005	0	0
In(B1)	0.117(5)	0.076(5)	0.061(4)	0.038	-0.025(2)	-0.051
In(B11)	0.29(4)	0.23(4)	0.06(1)	0.12	0.038(8)	0.076
In(B2)	0.244(7)	0.069(3)	0.26(1)	0.096(3)	0.065(6)	0.087(4)
Na(1)	0.05(1)	0.05	0.02(1)	0.03	0	0
Na(2)	0.036(6)	0.029(8)	0.031(7)	0.015	0.004	0.009(6)
Na(3)	0.026(8)	0.026	0.06(2)	0.01	0	0
Na(4)	0.048(5)	0.040(4)	0.034(4)	0.029(4)	0.020(4)	0.013(4)
Na(5)	0.022(7)	0.022	0.04(1)	0.01	0	0
Na(6)	0.023(7)	0.023	0.03(1)	0.01	0	0
Na(7)	0.037(5)	0.024(7)	0.022(6)	0.012	0.003	0.006(6)
Na(8)	0.023(5)	0.020(7)	0.033(6)	0.010	-0.009	-0.017(5)
Na(9)	0.07(2)	0.03(1)	0.03(1)	0.04	0	0
Na(10)	0.037(6)	0.030(8)	0.048(8)	0.015	-0.006	-0.012(7)
Na(11)	0.039(6)	0.06(1)	0.024(6)	0.029	0.005(3)	0.011
Na(12)	0.031(5)	0.05(1)	0.028(6)	0.026	-0.001	-0.002(6)
Na(13)	0.028(5)	0.031(8)	0.037(7)	0.016	0.005	0.011(6)
Na(14)	0.03(1)	0.03	0.01(1)	0.01	0	0
Na(15)	0.077(7)	0.043(5)	0.035(5)	0.030(5)	0.016(5)	0.010(4)
Na(16)	0.035(7)	0.054(8)	0.032(6)	0.013(6)	0	0
Na(17)	0.038(6)	0.045(9)	0.048(7)	0.022	-0.016	-0.032(7)
Na(18)	0.037(6)	0.05(1)	0.064(9)	0.023	-0.004	-0.008(8)

Table V. Anisotropic displacement parameters for $Na_{96}In_{\sim 97}Pd_2$.

Atom	U_{11}	U_{22}	U_{33}	U_{12}	U_{13}	U_{23}
In(1)	0.0203(4)	0.0260(7)	0.0194(6)	0.0130	0.0016	0.0031(6)
In(2)	0.028(1)	0.0190(8)	0.0146(8)	0.0142	0	0
In(3)	0.0201(3)	0.0189(3)	0.0250(4)	0.0109(2)	0.0035(4)	0.0030(4)
In(4)	0.0259(5)	0.0188(6)	0.0145(6)	0.0094	-0.0008	-0.0015(5)
In(5)	0.0212(4)	0.0229(7)	0.0238(6)	0.0115	0.0021	0.0042(6)
In(6)	0.0217(3)	0.0188(3)	0.0216(4)	0.0107(3)	0.0046(4)	0.0020(4)
In(7)	0.0277(5)	0.0170(6)	0.0160(6)	0.0085	-0.0000	-0.0001(6)
In(8)	0.0186(4)	0.0194(6)	0.0247(6)	0.0097	-0.0016	-0.0032(6)
In(9)	0.0177(6)	0.0177	0.019(1)	0.009	0	0
In(10)	0.0207(4)	0.0220(4)	0.0258(4)	0.0113(3)	-0.0017(4)	-0.0041(4)
In(11)	0.0273(5)	0.0225(7)	0.0226(6)	0.0112	0.0010	0.0019(6)
Pd(A)	0.034(1)	0.034	0.014(2)	0.017	0	0
In(A1)	0.107(4)	0.107	0.017(3)	0.054	0	0
In(A11)	0.189(6)	0.48(2)	0.160(7)	0.241	-0.132(4)	-0.264
In(A2)	0.113(4)	0.036(3)	0.196(8)	0.018	0.015(2)	0.030
In(A3)	0.166(8)	0.097(3)	0.140(4)	-0.019(4)	-0.011(4)	-0.075(3)
Pd(B)	0.0137(9)	0.0137	0.007(1)	0.007	0	0
In(B1)	0.117(3)	0.078(3)	0.066(2)	0.039	-0.029(1)	-0.058
In(B11)	0.36(2)	0.28(2)	0.041(6)	0.139	0.049(4)	0.097
In(B2)	0.123(3)	0.058(2)	0.237(7)	0.059(2)	0.018(4)	0.075(3)
In(B3)	0.27(2)	0.014(4)	0.21(1)	0.01	0.008(3)	0.016
Na(1)	0.031(4)	0.031	0.039(7)	0.016	0	0
Na(2)	0.036(3)	0.021(4)	0.048(5)	0.011	-0.001	-0.002(4)
Na(3)	0.034(4)	0.034	0.013(6)	0.017	0	0
Na(4)	0.058(3)	0.050(2)	0.033(3)	0.039(2)	0.009(3)	0.005(2)
Na(5)	0.038(5)	0.038	0.08(1)	0.02	0	0
Na(6)	0.024(4)	0.024	0.046(8)	0.012	0	0
Na(7)	0.042(3)	0.041(5)	0.036(4)	0.020	0.001	0.003(4)
Na(8)	0.030(3)	0.028(4)	0.042(4)	0.014	0.001	0.002(3)
Na(9)	0.013(7)	0.050(7)	0.031(6)	0.006	0	0
Na(10)	0.036(3)	0.032(4)	0.049(5)	0.016	-0.011	-0.022(4)
Na(11)	0.044(3)	0.050(5)	0.035(4)	0.025	-0.004(2)	-0.008
Na(12)	0.041(3)	0.050(5)	0.025(4)	0.025	0.001	0.001(4)
Na(13)	0.030(3)	0.038(4)	0.050(5)	0.019	0.001	0.002(4)
Na(14)	0.049(7)	0.049	0.03(1)	0.02	0	0
Na(15)	0.071(4)	0.035(3)	0.041(3)	0.019(2)	0.010(3)	0.002(3)
Na(16)	0.029(3)	0.059(5)	0.034(4)	0.014(3)	0	0
Na(17)	0.033(3)	0.040(4)	0.040(4)	0.020	-0.005	-0.010(4)
Na(18)	0.042(3)	0.054(5)	0.061(5)	0.027	-0.012	-0.024(4)

Table VI. Distances to nearest neighbors ($d_{In-In} \leq 4.0$ Å, $d_{In-Na} \leq 4.5$ Å) about each In, Ni and Pd atoms in $Na_{96}In_{\sim 97}Z_2$, Z = Ni, Pd.

	$Na_{96}In_{97}Pd_2$	$Na_{96}In_{97}Ni_2$		$Na_{96}In_{97}Pd_2$	$Na_{96}In_{97}Ni_2$		$Na_{96}In_{97}Pd_2$	$Na_{96}In_{97}Ni_2$
	In1			**In5**			**In9**	
2	In3 3.003(1)	3.003(3)		In1 3.007(2)	3.004(5)	3	In8 2.955(1)	2.955(3)
	In5 3.007(2)	3.004(5)	2	In5 3.099(2)	3.108(4)	3	In11 3.181(2)	3.178(5)
2	In10 3.115(1)	3.109(4)	2	In7 3.031(1)	3.023(3)			
						3	Na2 3.530(7)	3.51(1)
	Na2 3.679(7)	3.69(1)		Na3 3.592(9)	3.60(2)	3	Na13 3.391(8)	3.39(1)
	Na3 3.544(2)	3.543(5)	2	Na4 3.289(5)	3.280(9)			
2	Na4 3.313(5)	3.326(9)	2	Na8 3.487(6)	3.50(1)		**In10**	
2	Na8 3.489(3)	3.493(6)		Na9 3.499(5)	3.49(1)			
	Na13 3.486(7)	3.51(1)		Na14 3.616(1)	3.603(5)		In1 3.115(1)	3.109(4)
							In3 3.085(1)	3.085(3)
	In2			**In6**			In10 3.020(2)	3.023(4)
							In10 3.058(2)	3.063(4)
2	In2 3.035(3)	3.054(6)		In3 2.952(1)	2.949(3)			
2	In4 2.957(2)	2.942(4)		In4 2.991(1)	2.983(4)		Na2 3.487(6)	3.50(1)
				In6 3.016(2)	3.018(3)		Na3 3.615(6)	3.61(1)
2	Na1 3.50(1)	3.47(2)		In6 3.076(2)	3.082(3)		Na5 3.433(8)	3.43(1)
4	Na12 3.359(6)	3.34(1)					Na7 3.424(7)	3.41(1)
2	Na16 3.373(8)	3.37(1)		Na1 3.515(7)	3.53(1)		Na8 3.615(7)	3.60(1)
				Na4 3.488(5)	3.533(9)		Na10 3.302(6)	3.33(1)
	In3			Na6 3.435(6)	3.45(1)		Na11 3.334(7)	3.3391)
				Na8 3.560(6)	3.55(1)		Na15 3.453(6)	3.45(1)
	In1 3.003(1)	3.003(3)		Na10 3.414(6)	3.43(1)			
	In6 2.952(1)	2.949(3)		Na12 3.321(6)	3.31(1)		**In11**	
	In8 2.993(1)	2.995(2)		Na17 3.258(6)	3.24(1)			
	In10 3.085(1)	3.085(3)		Na18 3.411(7)	3.39(1)		In8 3.137(2)	3.129(5)
							In9 3.181(2)	3.178(5)
	Na2 3.360(5)	3.371(8)		**In7**		2	In11 3.100(2)	3.109(4)
	Na4 3.419(5)	3.45(1)						
	Na8 3.567(4)	3.554(6)		In4 2.924(2)	2.920(3)	2	Na2 3.534(6)	3.51(1)
	Na10 3.377(3)	3.400(6)	2	In5 3.031(1)	3.023(3)		Na5 4.00(1)	3.98(2)
	Na13 3.415(5)	3.435(9)		In7 3.000(2)	2.994(6)	2	Na7 3.354(7)	3.36(1)
	Na15 3.516(6)	3.52(1)					Na11 3.325(7)	3.31(1)
	Na17 3.300(5)	3.30(1)	2	Na4 3.474(5)	3.474(8)	2	Na15 3.380(5)	3.39(1)
	Na18 3.424(6)	3.40(1)		Na8 3.559(7)	3.55(1)			
			2	Na9 3.481(6)	3.49(1)		Pd(A)	Ni(A)
	In4			Na14 3.279(1)	3.278(3)			
			2	Na16 3.365(6)	3.37(1)	2	InA1 2.781(7)	2.73(1)
	In2 2.957(2)	2.942(4)				6	InA11 2.673(9)	2.67(1)
2	In6 2.991(1)	2.983(4)		**In8**		6	InA2 2.905(4)	2.853(7)
	In7 2.924(2)	2.920(3)				12	InA3 2.822(4)	2.766(7)
			2	In3 2.993(1)	2.995(2)	3	InA31	2.90(5)
	Na1 3.572(3)	3.570(5)		In9 2.955(1)	2.955(3)			
2	Na4 3.530(5)	3.563(8)		In11 3.137(2)	3.129(5)		Pd(B)	Ni(B)
	Na8 3.522(7)	3.52(1)						
2	Na12 3.407(3)	3.404(6)	2	Na2 3.387(5)	3.379(8)	6	InB1 2.751(3)	2.716(6)
2	Na16 3.352(6)	3.34(1)	2	Na13 3.482(5)	3.484(9)	6	InB11 2.63(1)	2.59(2)
			2	Na15 3.468(5)	3.48(1)	12	InB2 2.711(4)	2.669(6)
				Na17 3.210(7)	3.22(1)	6	InB3 2.708(8)	.....
				Na18 3.402(8)	3.36(2)			

Table VI. (continued)

	$Na_{96}In_{97}Pd_2$	$Na_{96}In_{97}Ni_2$
	InA1	
3	InA11 1.36(2)	1.61(2)
6	InA3 2.808(6)	2.70(1)
	Z(A) 2.781(7)	2.73(1)
3	Na13 3.345(9)	3.33(2)
3	Na18 3.829(9)	3.86(2)
	InA11	
	InA1 1.36(2)	1.61(2)
2	InA11 2.23(3)	2.62(4)
2	InA2 2.961(8)	2.97(1)
2	InA3 1.53(2)	1.19(2)
2	InA3 3.25(1)	3.32(2)
	Z(A) 2.673(9)	2.67(1)
2	Na4 4.00(1)	3.80(2)
	Na13 3.06(1)	3.09(2)
2	Na13 4.26(2)	4.44(2)
2	Na18 3.618(9)	3.69(2)
	InA2	
2	InA11 2.961(8)	2.97(1)
	InA2 1.36(1)	1.00(2)
2	InA3 2.314(8)	2.44(2)
2	InA3 3.028(8)	2.97(2)
2	InA3 3.175(8)	3.11(2)
2	InA31 -------	2.90(3)
	Z(A) 2.905(4)	2.853(7)
2	Na4 4.145(6)	4.21(1)
	Na12 3.402(8)	3.49(1)
	Na12 4.085(9)	3.99(2)
2	Na16 3.540(8)	3.52(1)
	Na18 3.54(1)	3.73(2)
	InA3	
	InA1 2.808(6)	2.70(1)
	InA11 1.53(2)	1.19(2)
	InA11 3.25(1)	3.32(2)
	InA2 2.314(8)	2.44(2)
	InA2 3.028(8)	2.97(2)
	InA2 3.175(8)	3.11(2)
	InA3 0.97(2)	0.77(3)
	InA3 2.81(1)	2.87(2)
	InA3 2.97(1)	2.97(2)
	InA31 -------	1.59(2)
	Z(A) 2.822(4)	2.766(7)
	Na4 3.208(7)	3.23(1)
	Na4 3.734(8)	3.64(2)
	Na9 3.79(1)	3.84(2)
	Na13 3.872(9)	3.79(2)
	Na16 3.87(1)	3.99(2)
	Na18 3.83(1)	3.89(2)
	InA31	
2	InA11 -------	2.60(3)
4	InA2 -------	2.90(3)
4	InA3 -------	1.59(2)
	Z(A) -------	2.90(5)
4	Na4 -------	4.00(3)
	Na9 -------	2.98(6)
2	Na16 -------	3.69(3)
	InB1	
2	InB1 3.108(7)	3.04(1)
	InB11 2.72(2)	2.71(3)
2	InB11 1.601(4)	1.559(8)
2	InB2 2.022(6)	2.157(9)
2	InB2 3.128(7)	3.00(1)
2	InB2 3.231(6)	3.151(9)
	InB3 2.71(1)	--------
2	InB3 2.85(1)	--------
	Z(B) 2.751(3)	2.716(6)
	Na6 3.87(1)	3.83(2)
	Na10 2.906(8)	2.87(1)
	Na11 3.624(9)	3.66(2)
2	Na15 3.818(6)	3.82(1)
2	Na17 3.437(7)	3.44(1)
	InB11	
	InB1 2.72(2)	2.71(3)
2	InB1 1.601(4)	1.559(8)
2	InB11 1.56(3)	1.62(5)
2	InB2 2.44(2)	2.42(3)
2	InB2 3.285(9)	3.35(2)
	InB3 2.66(2)	
	Z(B) 2.63(1)	2.59(2)
	Na6 3.18(2)	3.20(3)
2	Na10 3.811(9)	3.76(2)
2	Na15 4.28(2)	4.23(3)
	Na17 2.81(2)	2.81(3)
2	Na17 4.02(1)	4.06(3)
	InB2	
	InB1 2.022(6)	2.157(9)
	InB1 3.128(7)	3.00(1)
	InB1 3.231(6)	3.151(9)
	InB11 2.44(2)	2.42(3)
	InB11 3.285(9)	3.35(2)
	InB2 1.73(1)	1.70(2)
	InB2 2.04(1)	1.74(2)
2	InB2 3.055(7)	2.943(9)
	InB2 3.094(9)	3.32(1)
	InB3 1.112(7)	-------
	InB3 2.102(9)	-------
	Z(B) 2.711(4)	2.669(6)
	Na10 4.12(1)	4.23(2)
	Na11 3.551(9)	3.44(1)
	Na11 3.573(9)	3.71(2)
	Na15 2.759(7)	2.80(1)
	Na15 3.864(9)	3.81(1)
	Na15 3.935(8)	3.84(1)
	Na17 3.65(1)	3.70(2)
	InB3	
	InB1 2.71(1)	-------
2	InB1 2.85(1)	-------
	InB11 2.66(2)	-------
2	InB2 1.112(7)	-------
2	InB2 2.102(9)	-------
2	InB3 2.83(1)	-------
	Z(B) 2.708(8)	-------
	Na11 3.00(1)	-------
2	Na15 3.18(1)	-------
2	Na15 4.20(1)	-------
	Na17 3.79(2)	-------

Table VII. Distances to nearest neighbors ($d_{In-In} \leq 4.0$ Å, $d_{In-Na} \leq 4.5$ Å) about each sodium atom in $Na_{96}In_{\sim 97}Z_2$, Z = Ni, Pd.

		$Na_{96}In_{97}Pd_2$	$Na_{96}In_{97}Ni_2$			$Na_{96}In_{97}Pd_2$	$Na_{96}In_{97}Ni_2$			$Na_{96}In_{97}Pd_2$	$Na_{96}In_{97}Ni_2$
	Na1				Na4				Na7		
3	In2	3.50(1)	3.47(2)		In1	3.313(5)	3.326(9)	2	In10	3.424(7)	3.41(1)
3	In4	3.572(3)	3.570(5)		In3	3.419(5)	3.45(1)	2	In11	3.354(7)	3.36(1)
6	In6	3.515(7)	3.53(1)		In4	3.530(5)	3.563(8)				
					In5	3.289(5)	3.280(9)		Na2	3.92(1)	3.91(2)
	Na6	3.34(2)	3.39(3)		In6	3.488(5)	3.533(9)		Na2	4.03(1)	4.00(2)
3	Na12	3.409(9)	3.39(1)		In7	3.474(5)	3.474(8)		Na5	3.32(1)	3.33(2)
									Na7	3.48(1)	3.45(2)
	Na2				InA11	4.00(1)	3.80(2)	2	Na11	3.592(6)	3.60(1)
					InA2	4.145(6)	4.21(1)	2	Na15	3.988(8)	3.98(1)
	In1	3.679(7)	3.69(1)		InA3	3.208(7)	3.23(1)	2	Na15	4.061(8)	4.06(1)
2	In3	3.360(5)	3.371(8)		InA3	3.734(8)	3.64(2)				
2	In8	3.387(5)	3.379(8)		InA31	-------	4.00(3)		Na8		
	In9	3.530(7)	3.51(1)								
2	In10	3.487(6)	3.50(1)		Na4	3.78(1)	3.71(2)	2	In1	3.489(3)	3.493(6)
2	In11	3.534(6)	3.51(1)		Na8	3.550(6)	3.60(1)	2	In3	3.567(4)	3.554(6)
					Na9	3.803(6)	3.74(1)		In4	3.522(7)	3.52(1)
	Na7	3.92(1)	3.91(2)		Na12	3.929(7)	3.95(1)	2	In5	3.487(6)	3.50(1)
	Na7	4.03(1)	4.00(2)		Na13	3.784(8)	3.77(1)	2	In6	3.560(6)	3.55(1)
	Na13	3.48(1)	3.50(2)		Na16	3.342(6)	3.31(1)		In7	3.559(7)	3.55(1)
2	Na15	3.293(7)	3.31(1)		Na18	3.353(6)	3.37(1)	2	In10	3.615(7)	3.60(1)
	Na3				Na5				Na3	3.601(7)	3.61(1)
								2	Na4	3.550(6)	3.60(1)
3	In1	3.544(2)	3.543(5)	6	In10	3.433(8)	3.43(1)		Na10	3.35(1)	3.38(2)
3	In5	3.592(9)	3.60(2)	3	In11	4.00(1)	3.98(2)				
6	In10	3.615(6)	3.61(1)						Na9		
					Na3	3.55(2)	3.54(3)				
	Na5	3.55(2)	3.54(3)	3	Na7	3.32(1)	3.33(2)	2	In5	3.499(5)	3.49(1)
3	Na8	3.601(7)	3.71(2)	3	Na11	4.092(9)	4.10(2)	4	In7	3.481(6)	3.49(1)
					Na6			4	InA3	3.79(1)	3.84(2)
									InA31	-------	2.98(6)
				6	In6	3.435(6)	3.45(1)				
								4	Na4	3.803(6)	3.74(1)
				3	InI11	3.87(1)	3.83(2)		Na14	3.339(1)	3.34(2)
				3	InI111	3.18(2)	3.20(3)	2	Na16	3.337(8)	3.34(1)
					Na1	3.34(2)	3.39(3)				
				3	Na10	3.929(8)	3.89(1)				
				3	Na17	3.322(9)	3.30(1)				

Table VII. (continued)

	$Na_{96}In_{97}Pd_2$	$Na_{96}In_{97}Ni_2$		$Na_{96}In_{97}Pd_2$	$Na_{96}In_{97}Ni_2$		$Na_{96}In_{97}Pd_2$	$Na_{96}In_{97}Ni_2$
	Na10			**Na13**			**Na16**	
2	In3 3.377(3)	3.400(6)		In1 3.486(7)	3.51(1)		In2 3.373(8)	3.37(1)
2	In6 3.414(6)	3.43(1)	2	In3 3.415(5)	3.435(9)	2	In4 3.352(6)	3.34(1)
2	In10 3.302(6)	3.33(1)	2	In8 3.482(5)	3.484(9)	2	In7 3.365(6)	3.37(1)
				In9 3.391(8)	3.39(1)			
	InB1 2.906(8)	2.87(1)				2	InA2 3.540(8)	3.52(1)
2	InB11 3.811(9)	3.76(2)		InA1 3.345(9)	3.33(2)	2	InA3 3.87(1)	3.99(2)
2	InB2 4.12(1)	4.23(2)		InA11 3.06(1)	3.09(2)		InA31 -------	3.69(3)
			2	InA11 4.26(2)	4.44(2)			
	Na6 3.929(8)	3.89(1)	2	InA3 3.872(9)	3.79(2)	2	Na4 3.342(6)	3.31(1)
	Na8 3.35(1)	3.38(2)					Na9 3.337(8)	3.34(1)
	Na11 3.58(1)	3.56(2)		Na2 3.48(1)	3.50(2)	2	Na12 3.316(7)	3.31(1)
2	Na15 3.852(7)	3.82(1)	2	Na4 3.784(8)	3.77(1)		Na16 4.47(2)	4.48(3)
2	Na17 3.442(5)	3.41(1)	2	Na13 3.92(1)	3.89(2)			
			2	Na18 3.325(7)	3.32(1)		**Na17**	
	Na11							
				Na14		2	In3 3.300(5)	3.30(1)
2	In10 3.334(7)	3.33(1)				2	In6 3.258(6)	3.24(1)
	In11 3.325(7)	3.31(1)	6	In5 3.616(1)	3.603(5)		In8 3.210(7)	3.22(1)
			6	In7 3.279(1)	3.278(3)			
	InB1 3.624(9)	3.66(2)				2	InB1 3.437(7)	3.44(1)
2	InB2 3.551(9)	3.44(1)	3	Na9 3.33(1)	3.34(2)		InB11 2.81(2)	2.81(3)
2	InB2 3.573(9)	3.71(2)				2	InB11 4.02(1)	4.06(3)
	InB3 3.00(1)	-------		**Na15**		2	InB2 3.65(1)	3.70(2)
							InB3 3.79(2)	-------
	Na5 4.092(9)	4.10(2)		In3 3.516(6)	3.52(1)			
2	Na7 3.592(6)	3.60(1)		In8 3.468(5)	3.48(1)	2	Na10 3.442(5)	3.41(1)
2	Na15 3.481(6)	3.47(1)		In10 3.453(6)	3.45(1)	2	Na15 3.380(8)	3.39(1)
2	Na15 3.634(8)	3.61(1)		In11 3.380(5)	3.39(1)		Na18 4.34(1)	4.29(2)
	Na12			InB1 3.818(6)	3.82(1)		**Na18**	
				InB11 4.28(2)	4.23(3)			
2	In2 3.359(6)	3.34(1)		InB2 2.759(7)	2.80(1)	2	In3 3.424(6)	3.40(1)
2	In4 3.407(3)	3.404(6)		InB2 3.864(9)	3.81(1)	2	In6 3.411(7)	3.39(1)
2	In6 3.321(6)	3.31(1)		InB2 3.935(8)	3.84(1)		In8 3.402(8)	3.36(2)
				InB3 3.18(1)	-------			
	InA2 3.402(8)	3.49(1)		InB3 4.20(1)	-------		InA1 3.829(9)	3.86(2)
	InA2 4.085(9)	3.99(2)				2	InA11 3.618(9)	3.69(2)
				Na2 3.293(7)	3.31(1)		InA2 3.54(1)	3.73(2)
	Na1 3.409(9)	3.39(1)		Na7 3.988(8)	3.98(1)	2	InA3 3.83(1)	3.89(2)
2	Na4 3.929(7)	3.95(1)		Na7 4.061(8)	4.06(1)			
	Na12 3.76(1)	3.73(2)		Na10 3.852(7)	3.82(1)	2	Na4 3.353(6)	3.37(1)
2	Na16 3.316(7)	3.31(1)		Na11 3.481(6)	3.47(1)		Na12 3.32(1)	3.33(2)
	Na18 3.32(1)	3.33(2)		Na11 3.634(8)	3.61(1)	2	Na13 3.325(7)	3.32(1)
				Na15 3.85(1)	3.85(2)		Na17 4.34(1)	4.29(2)
				Na15 4.22(1)	4.18(2)			
				Na17 3.380(8)	3.39(1)			

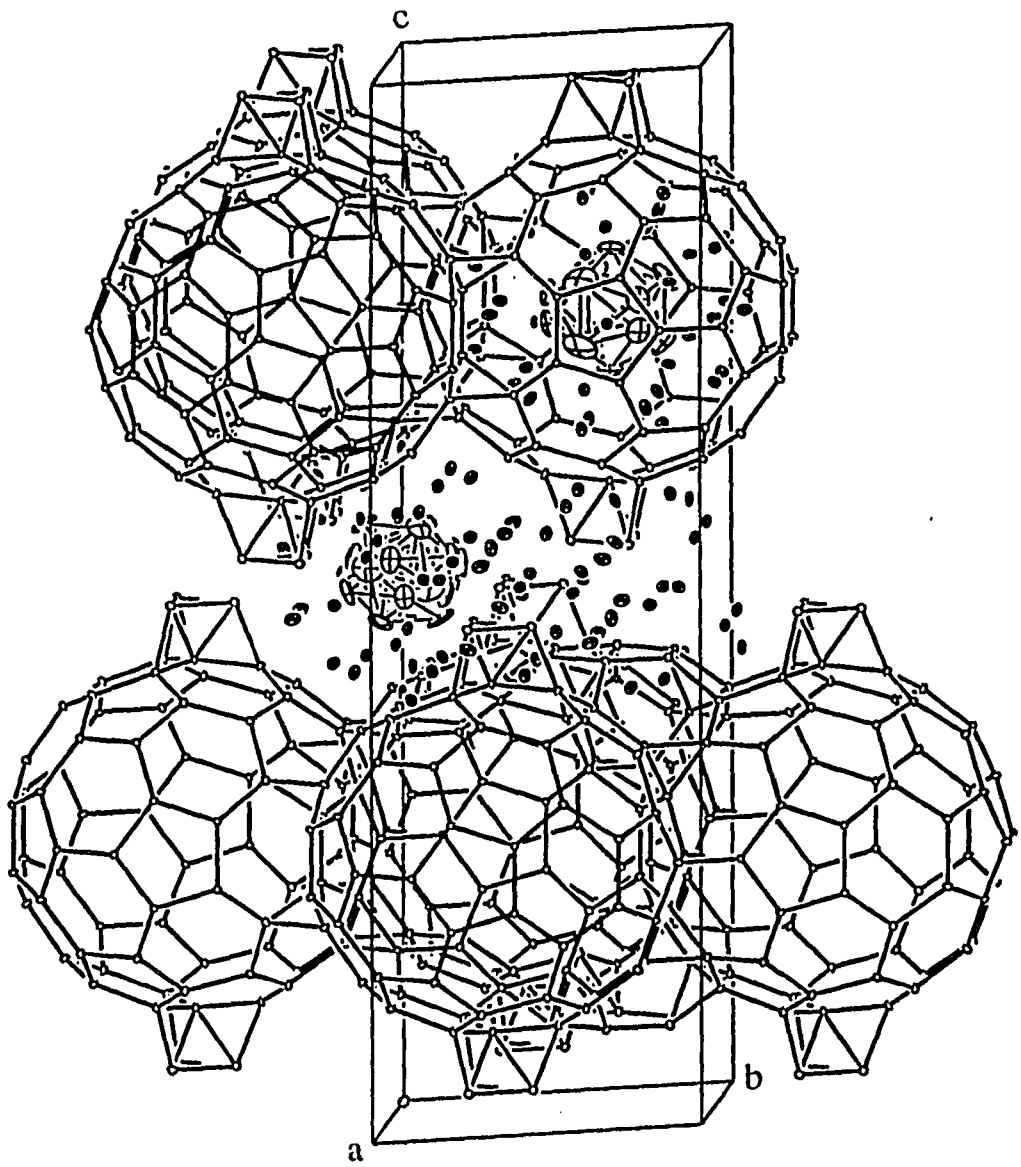

Figure 1. A general view of the unit cell of $Na_{96}In_{\sim 97}Z_2$, Z = Ni, Pd, Pt with all In–In bonds less than 4.00 Å drawn. The contents of only one sphere and only one cluster between the layers are shown. The indium atoms from the network are shown as open circles, the ones from the isolated interstitial clusters as crossed circles, and the sodium atoms as shaded ellipsoids. The Z atoms are at the centers of the isolated clusters. All atoms are drawn with real thermal ellipsoids at 20% probability level.

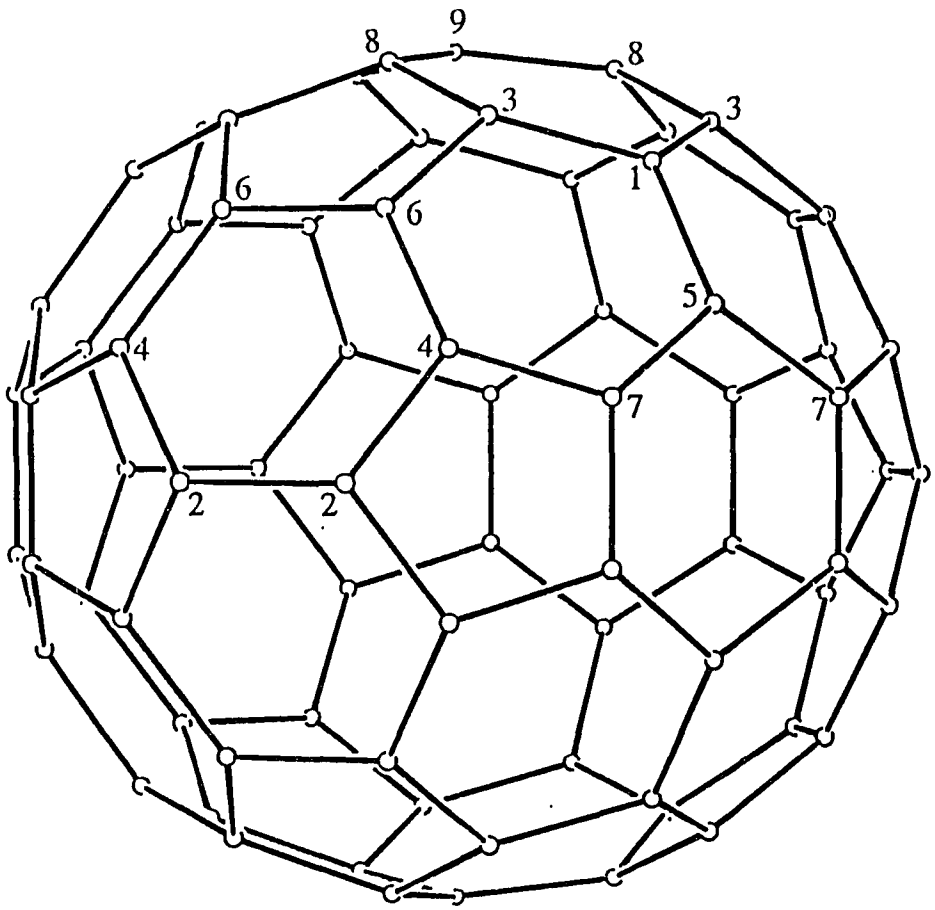

Figure 2. A view of the In_{74} fullerene (D_{3h}). The equatorial plane (at the waist) contains six pentagons (In2, 4, 7) shared with six other In_{74} fullerenes, and three hexagons. The three-fold axis (*c* axis) is vertical and goes through the poles which are In9.

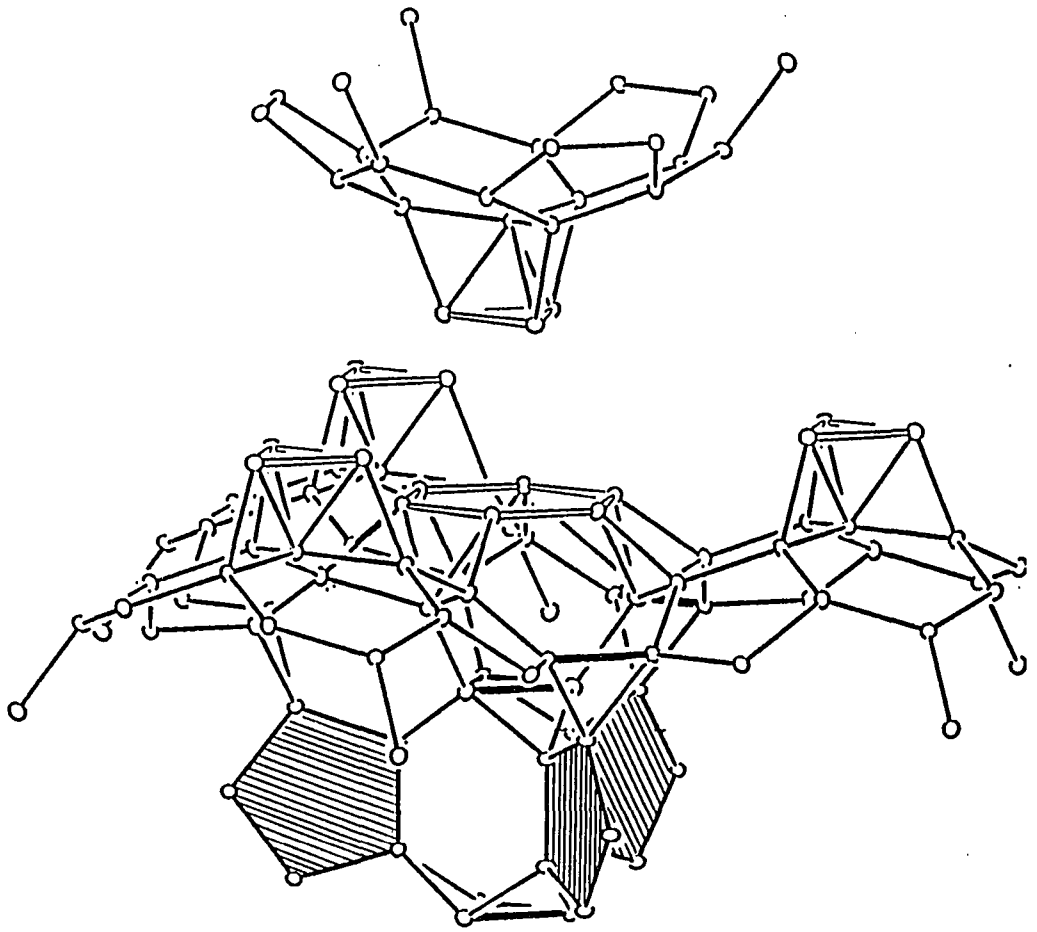

Figure 3. An enlarged section of the unit cell of $Na_{96}In_{\sim 97}Z_2$ (near 1/3, 2/3, 1/2) where three spheres from one layer are in contact (along the striped pentagons of In2, 4, 7, Fig. 2) and a part of a sphere from the layer above. The intersphere bonds (In5-In5 and In6-In6, Fig. 2) are drawn as thicker lines, and the inserted hexagons of In10 and the added triangles of In11 (see text) are shown with open lines.

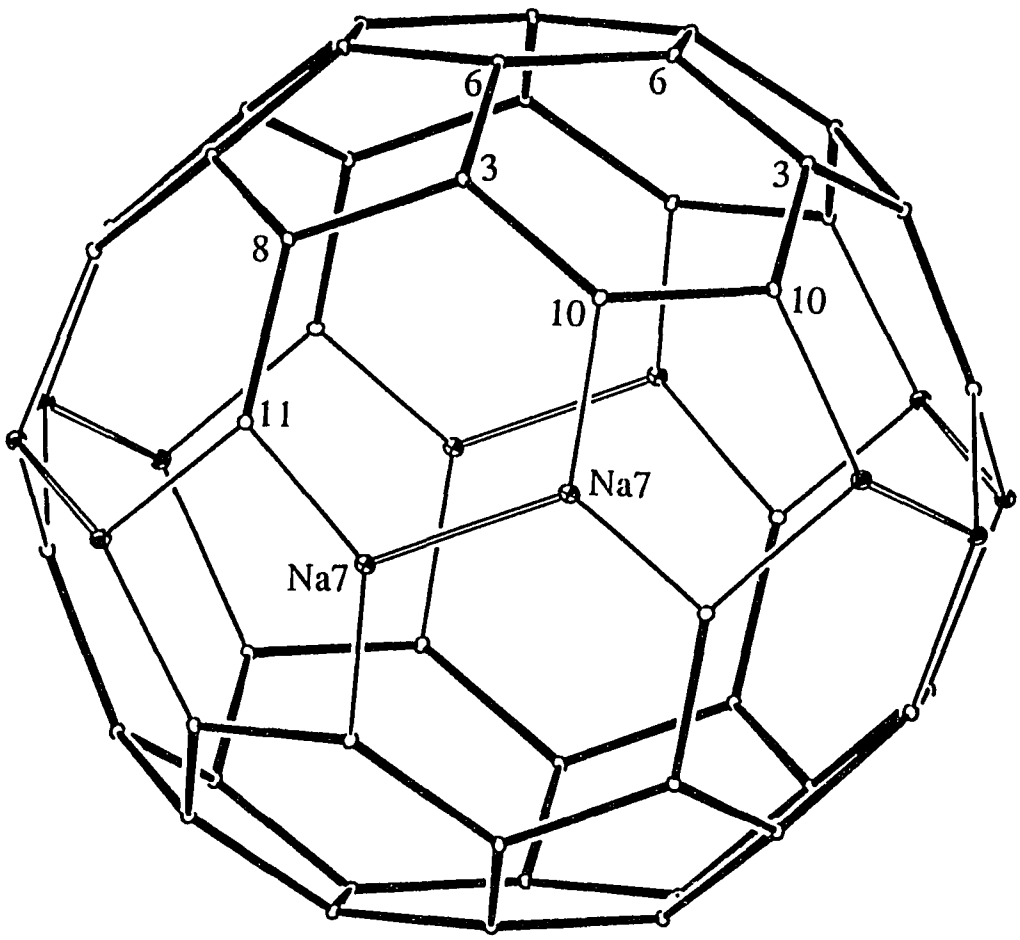

Figure 4. A view of the M_{60} (D_{3d}) fullerene of 48 indium and 12 sodium atoms. The six edges at the waist (open bonds) are shared with six other M_{60} cages. The six pentagons near the top and the bottom are shared with six In_{74} fullerenes. The three-fold axis (*c* axis) goes through the top and bottom hexagons.

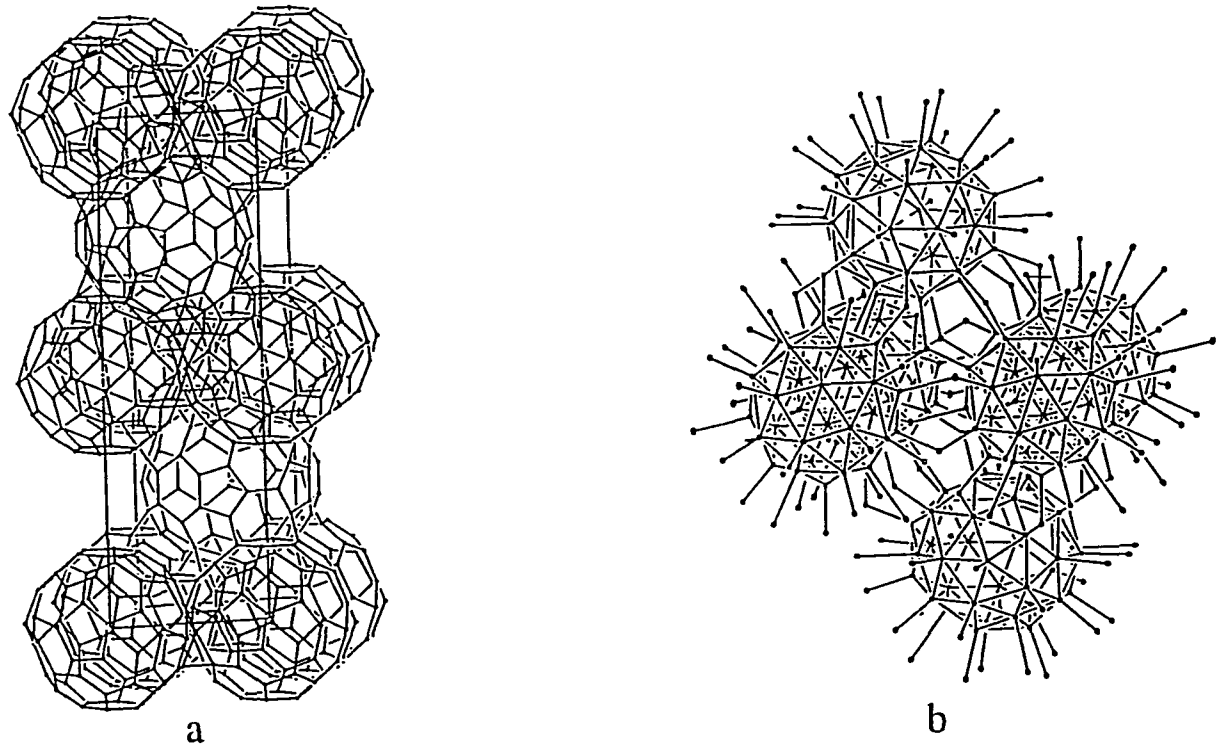

Figure 5. a) A view of the unit cell with all indium atoms and Na7 shown. The close packed layers of M_{60} (C level) are at z = 0, 1/2, 1 and those of In_{74} (A and B levels) are at z = 1/4, 3/4. b) Only the sodium atoms (except Na7) are shown. The sodium deltahedra inside M_{60} and In_{74} are connected to each other through the fullerenes' faces (the exo bonds around each deltahedron).

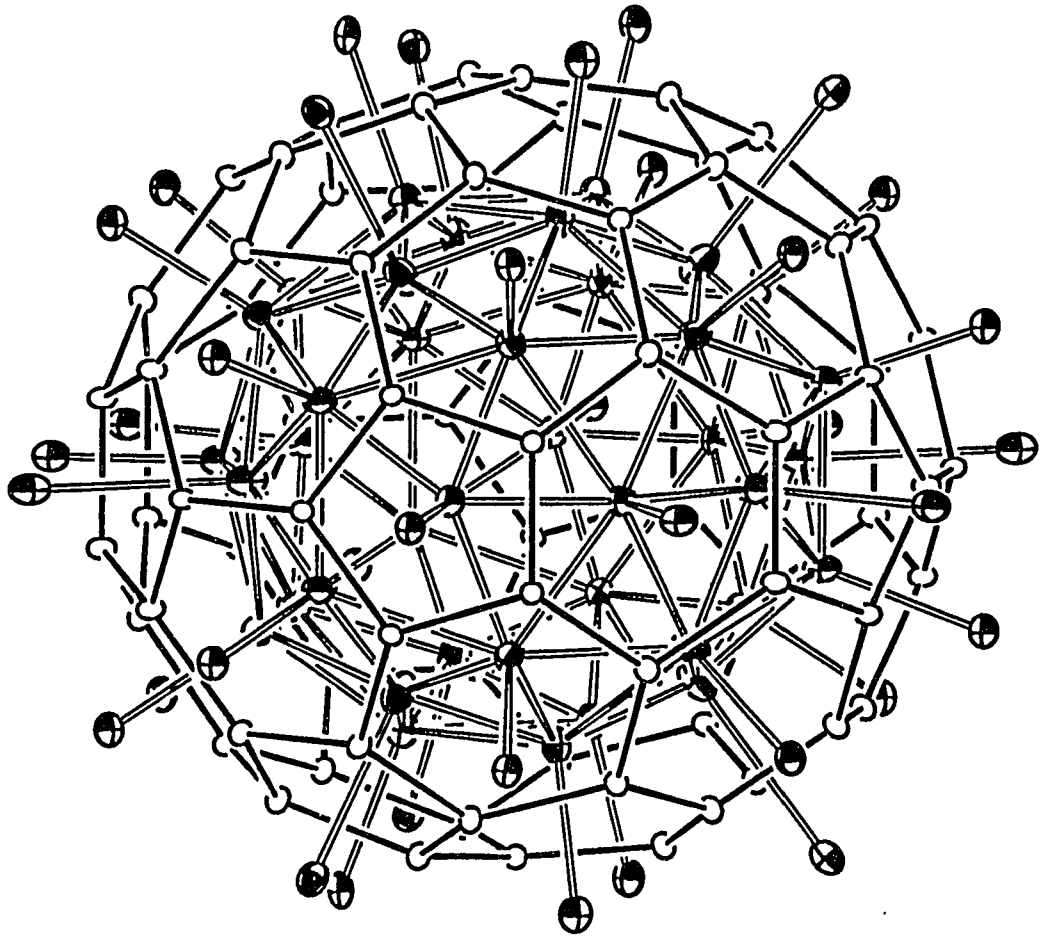

Figure 6. A view of the In_{74} fullerene (open circles) together with all nearest sodium atoms interconnected (shaded circles). All pentagonal and hexagonal faces of the fullerene are capped from in and outside by sodium atoms. The sodium atoms inside form a 39 atom deltahedron (open lines).

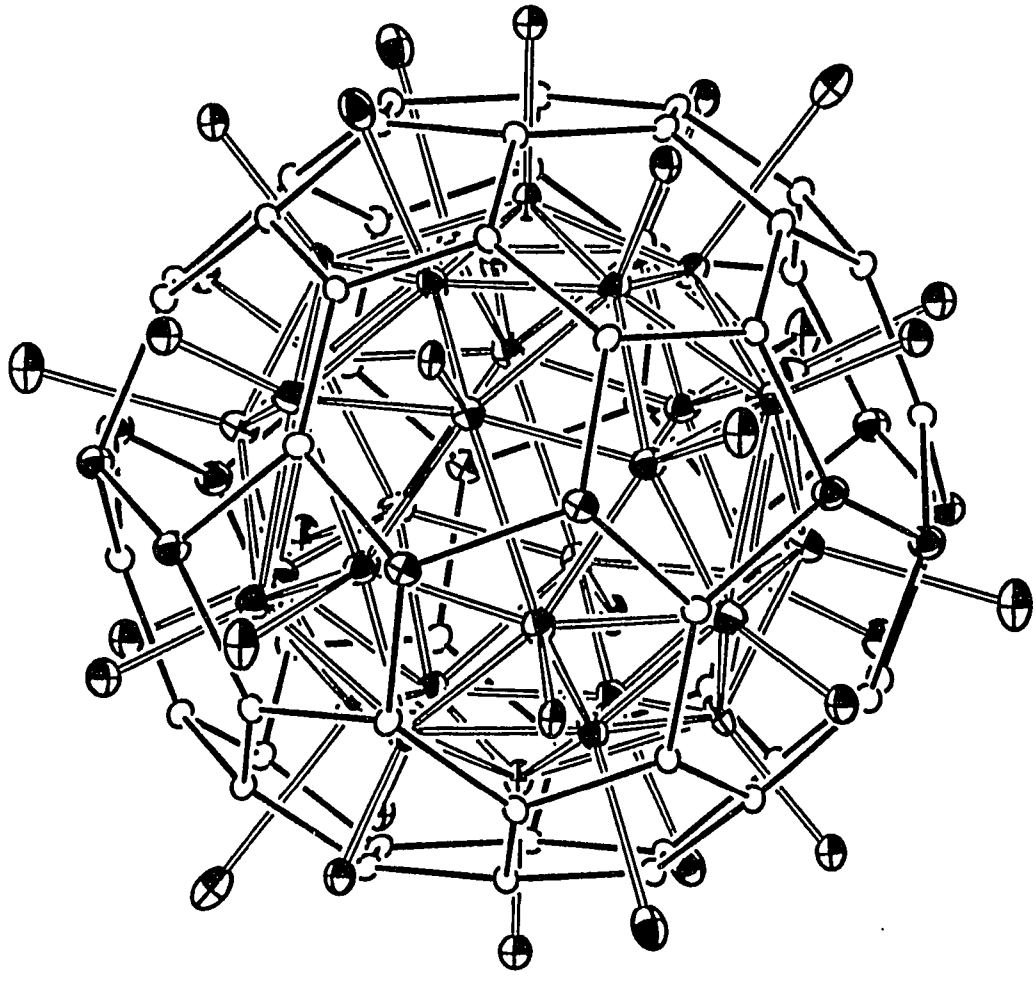

Figure 7. A view of the M_{60} ($In_{48}Na_{12}$) fullerene together with all nearest sodium atoms interconnected (shaded circles). All pentagonal and hexagonal faces of the fullerene are capped from in and outside by sodium atoms. The sodium atoms inside form a 32 atom deltahedron (open lines).

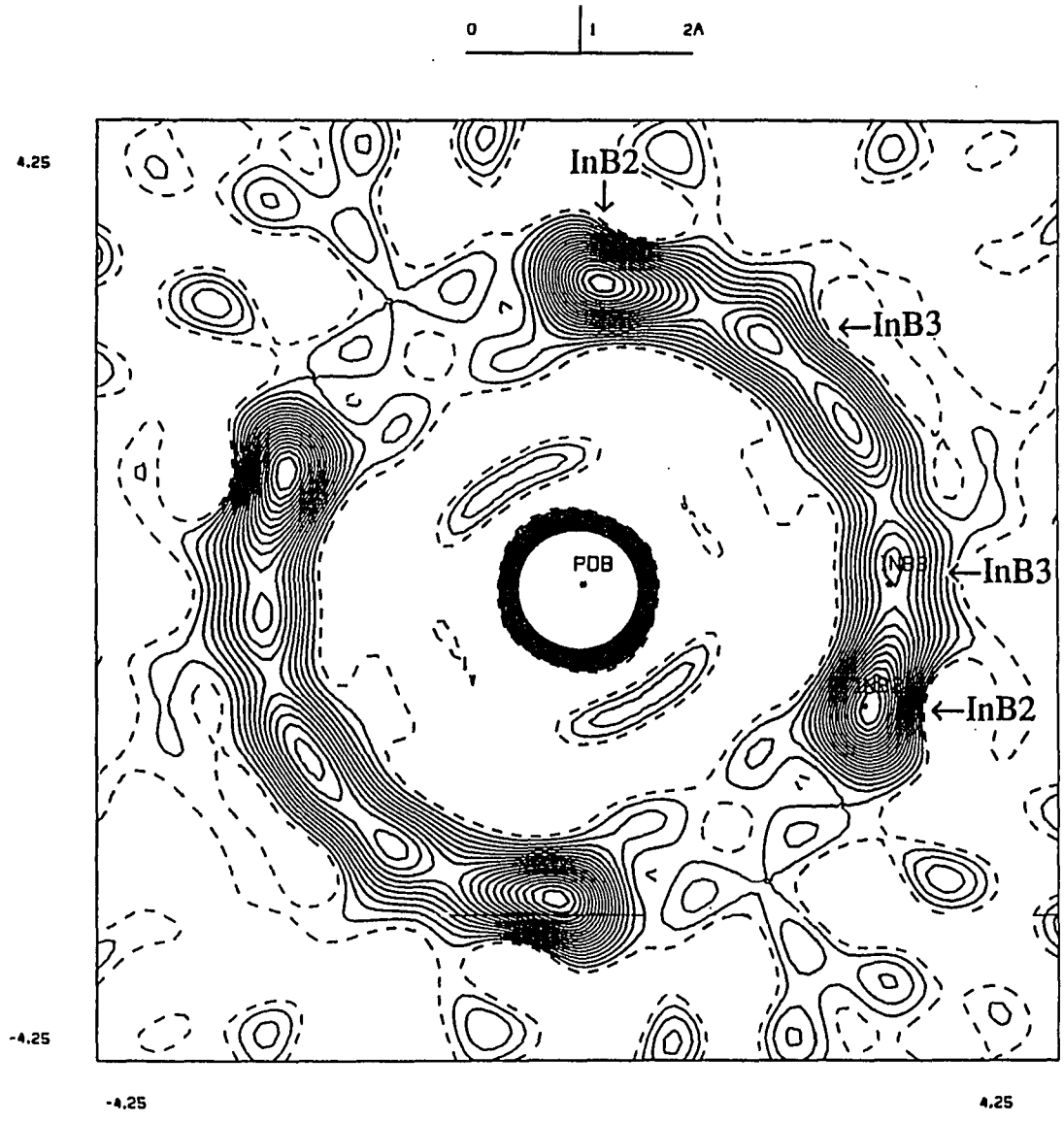

Figure 8. A plot (8.5 × 8.5 Å) of the electron density around PdB (D_{3d} symmetry position) calculated from F_{obs}. The plane is defined by InB2, InB3 and PdB (Fig. 10). The refined atoms at the electron density maxima are shown. The maximum between the two InB3 atoms is the remaining electron density from two other InB2 atoms above and below the plane. The "gaps" in the circle are directly under a "five-bonded" sodium atoms positioned outside the cluster (see text).

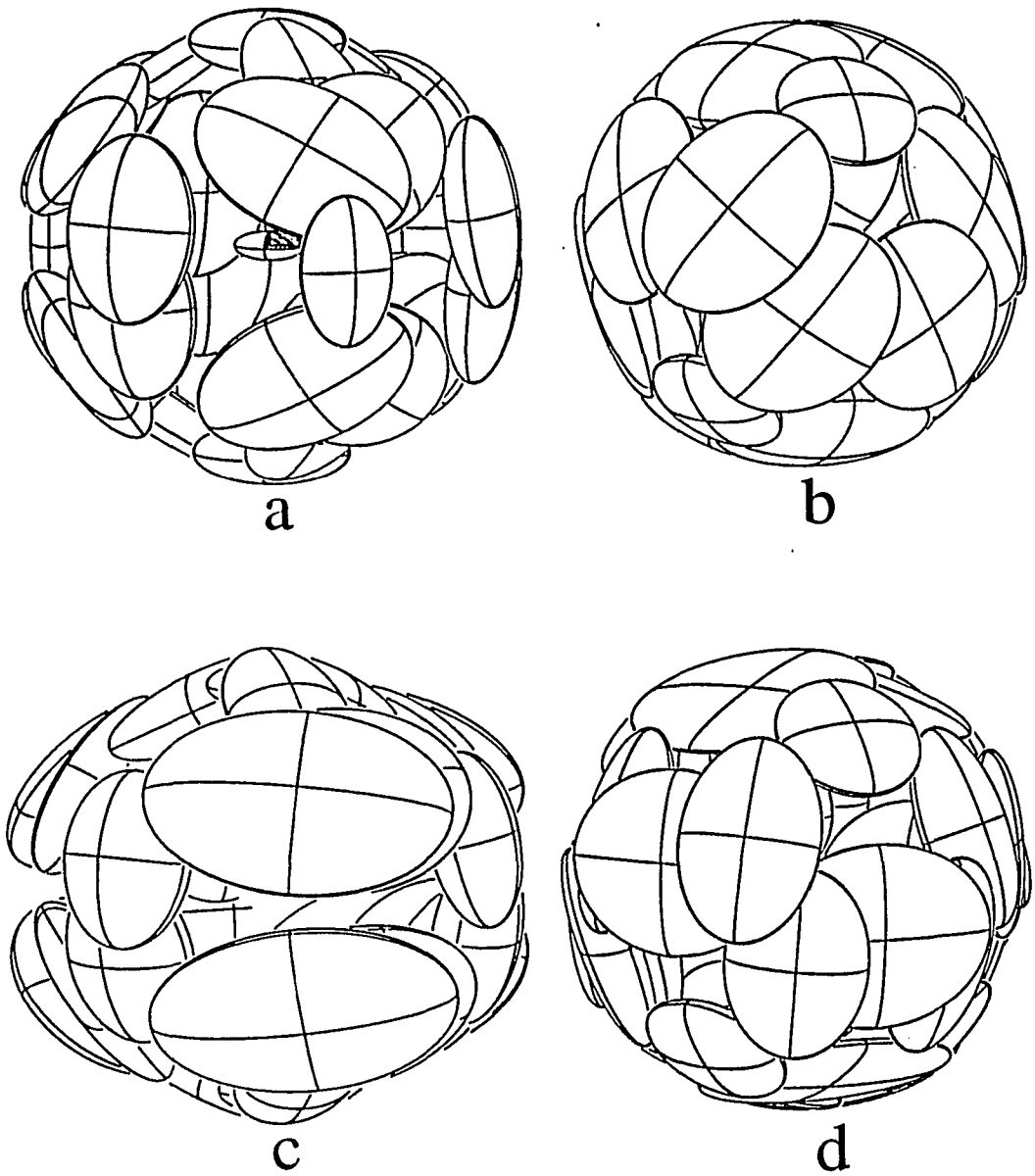

Figure 9. A 94% probability thermal ellipsoids drawing of the isolated clusters (the 3-fold axis vertical) centered by a) NiA, b) NiB, c) PdA, and d) PdB inside the fullerenes. Only a few islands on the surface of the spheres have nearly zero electron density.

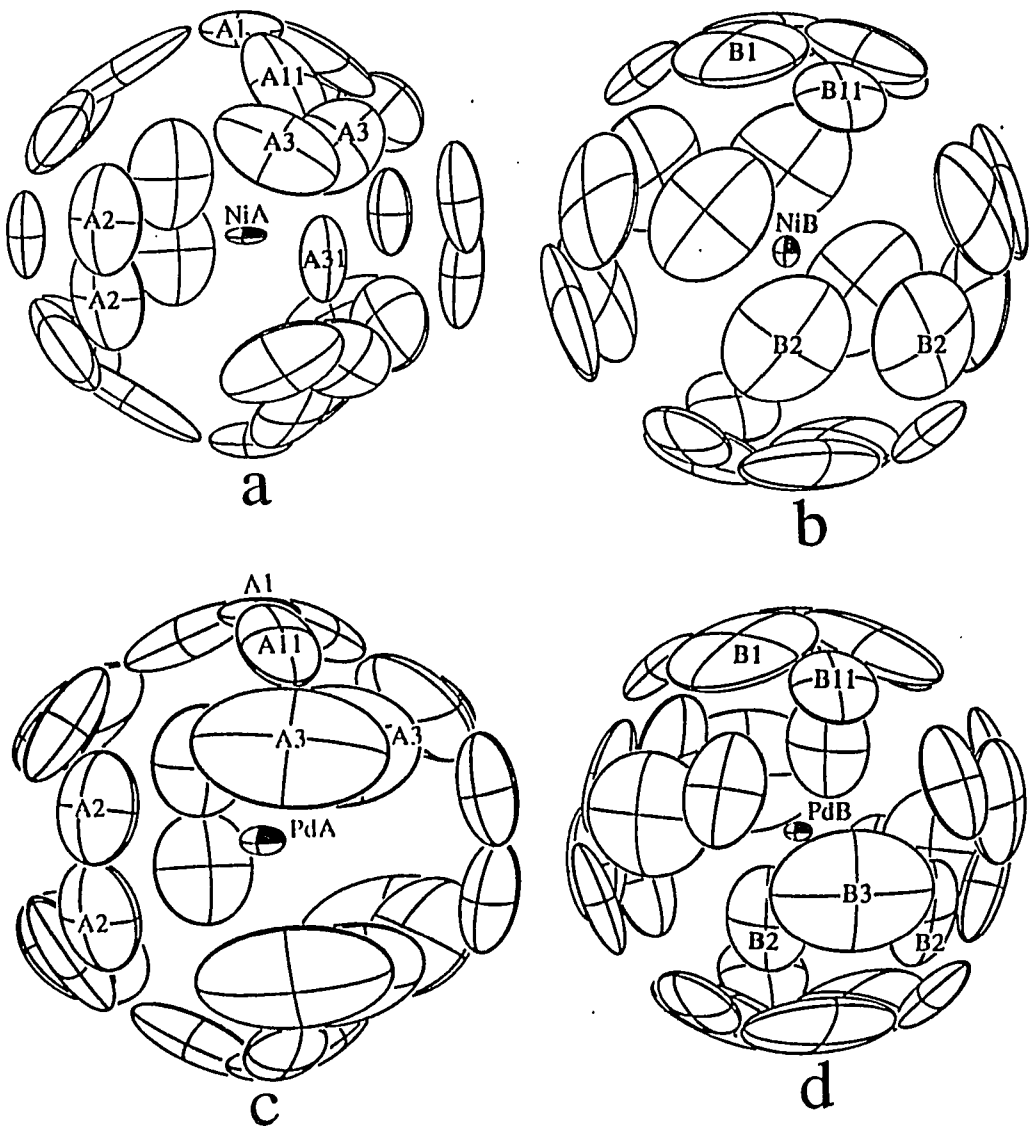

Figure 10. A 50% probability thermal ellipsoids drawing of the isolated clusters centered by a) NiA, b) NiB, c) PdA, and d) PdB inside the fullerenes. The positioning of the indium atoms around the central atoms can be seen.

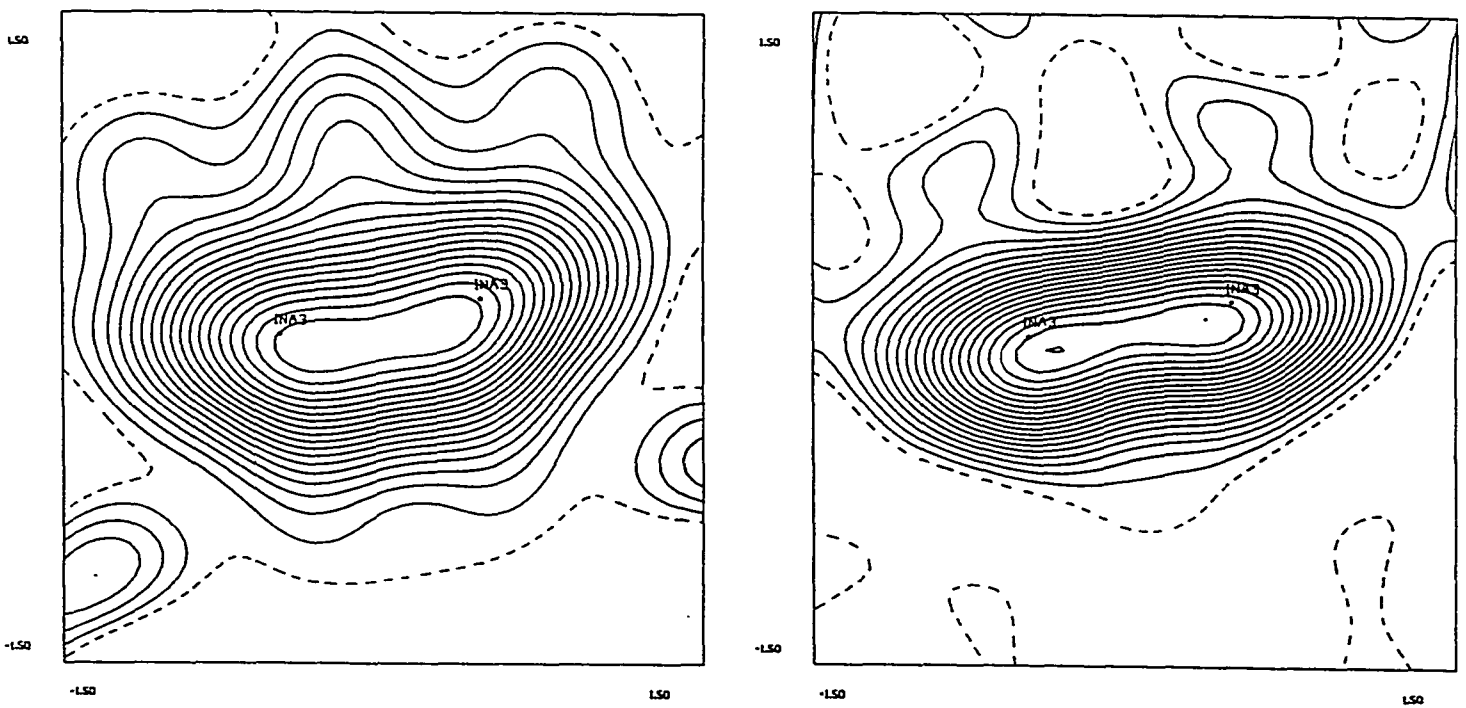

Figure 11. Nearly tangential (left) and radial (right) two dimensional plots of the electron density distribution (calculated from F_{obs}) around the InA3 positions of the cluster around PdA. The two quite broad maxima can be seen.

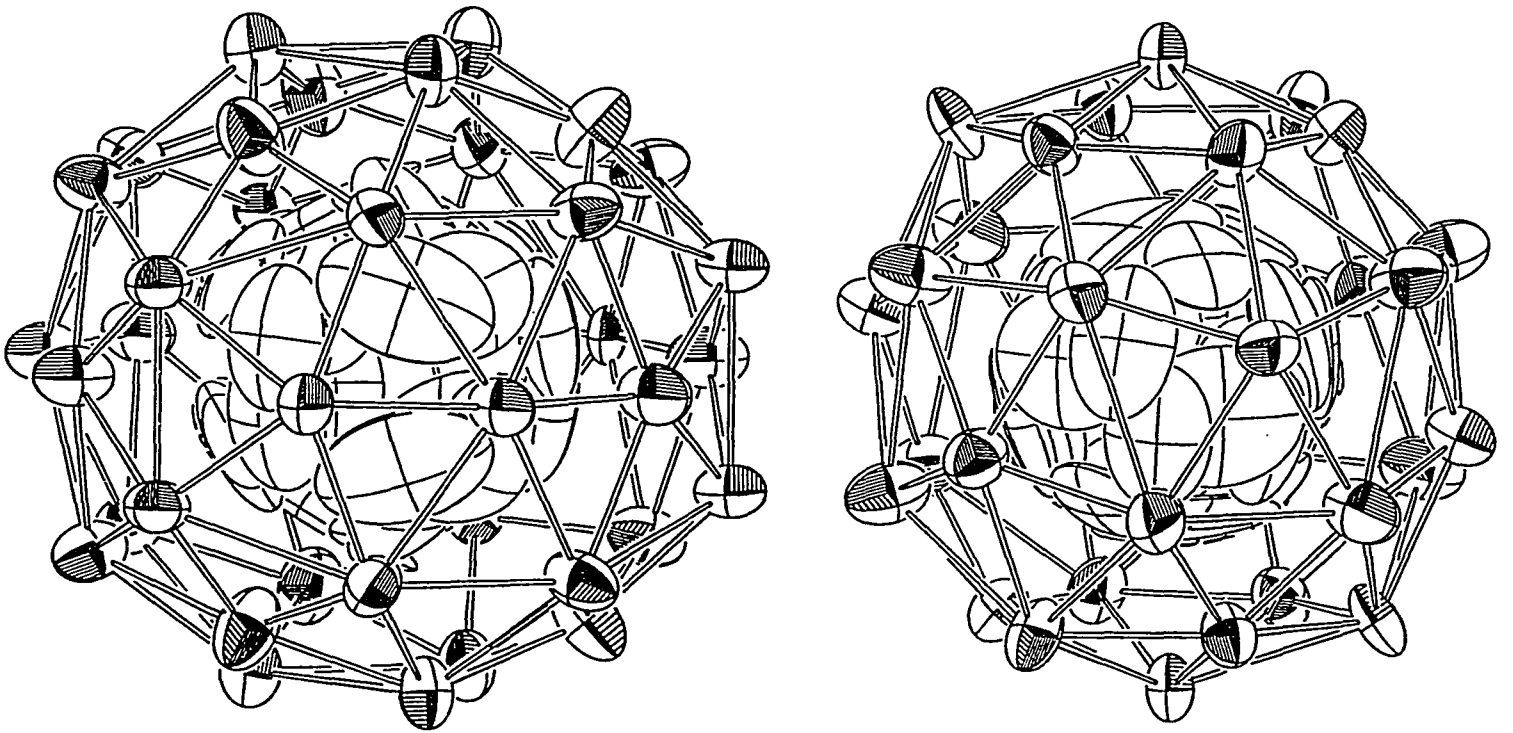

Figure 12. The positioning of the sodium atoms (shaded ellipsoids) around the isolated clusters (crossed ellipsoids) inside In_{74} (left) and M_{60} (right) in $Na_{96}In_{\sim 97}Pd_2$. All "five-bonded" (open bonds) sodium atoms are right above "openings" in the electron density on the surface of the clusters. (94% thermal ellipsoids)

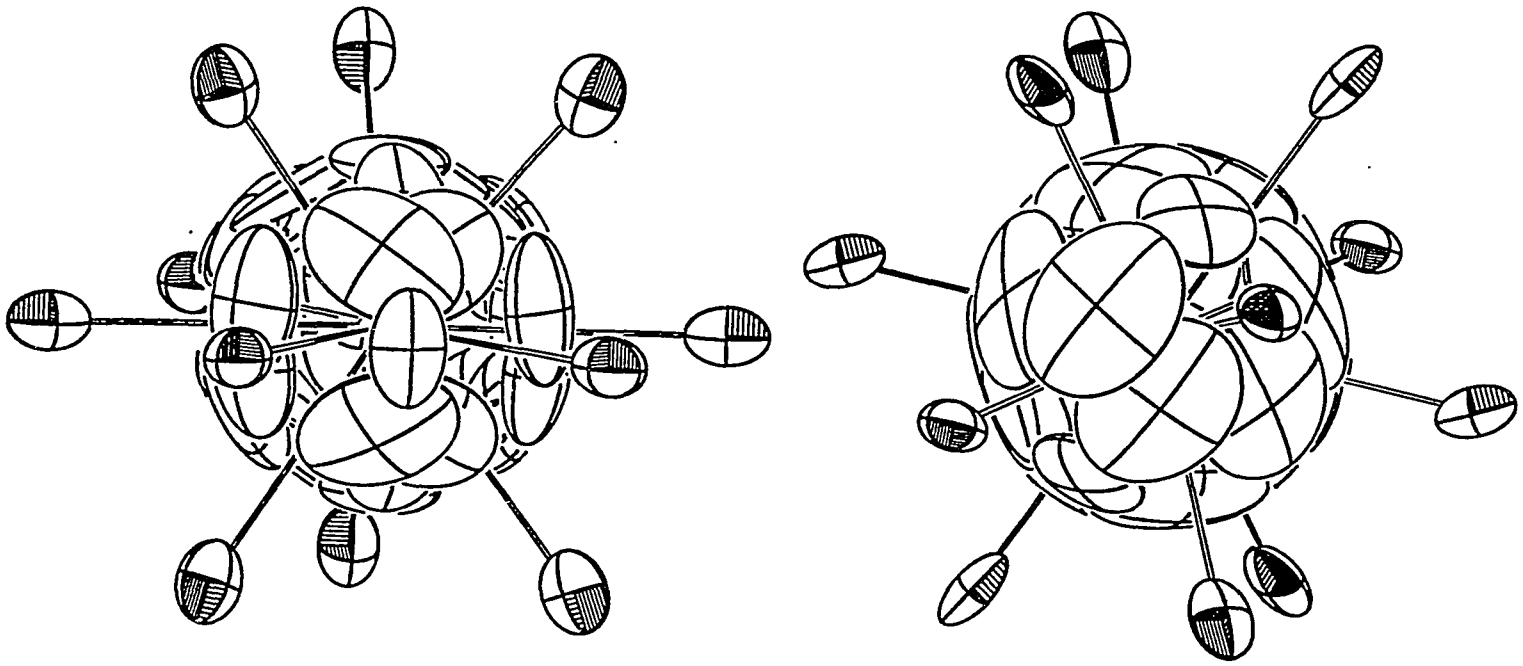

Figure 13. All of the "five-bonded" sodium atoms (shaded ellipsoids) around the NiA (left) and NiB (right) centered clusters are radially above islands of nearly zero electron density on the indium cluster (crossed ellipsoids). Open lines drawn between the central atoms and the sodium atoms intersect those islands.

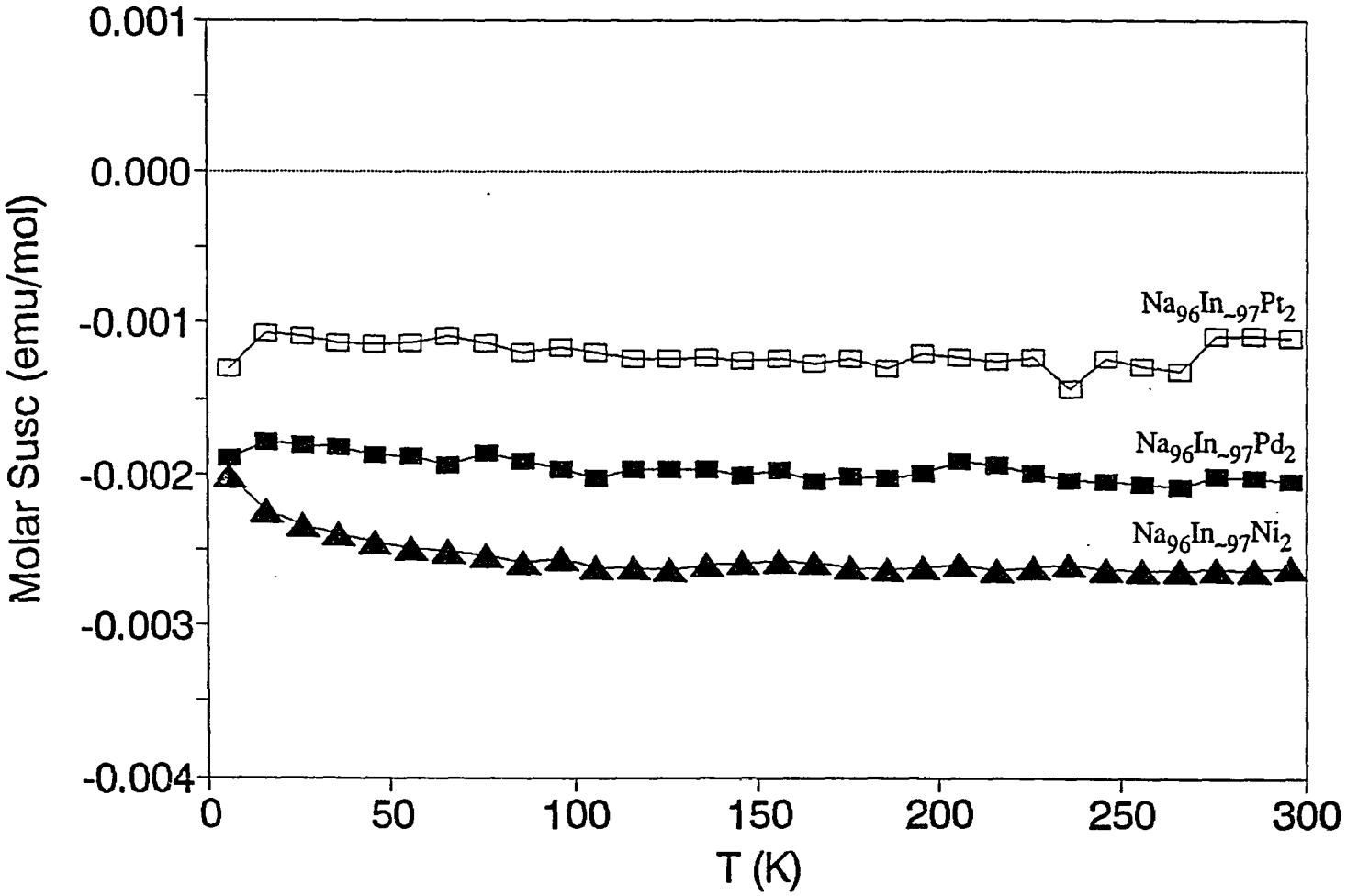

Figure 14. Plots of the molar magnetic susceptibilities of $Na_{96}In_{\sim 97}Z_2$, Z = Ni, Pd, Pt, corrected for ion core and Larmor precession on cluster orbitals diamagnetism (see text). All compounds show quite strong diamagnetism.

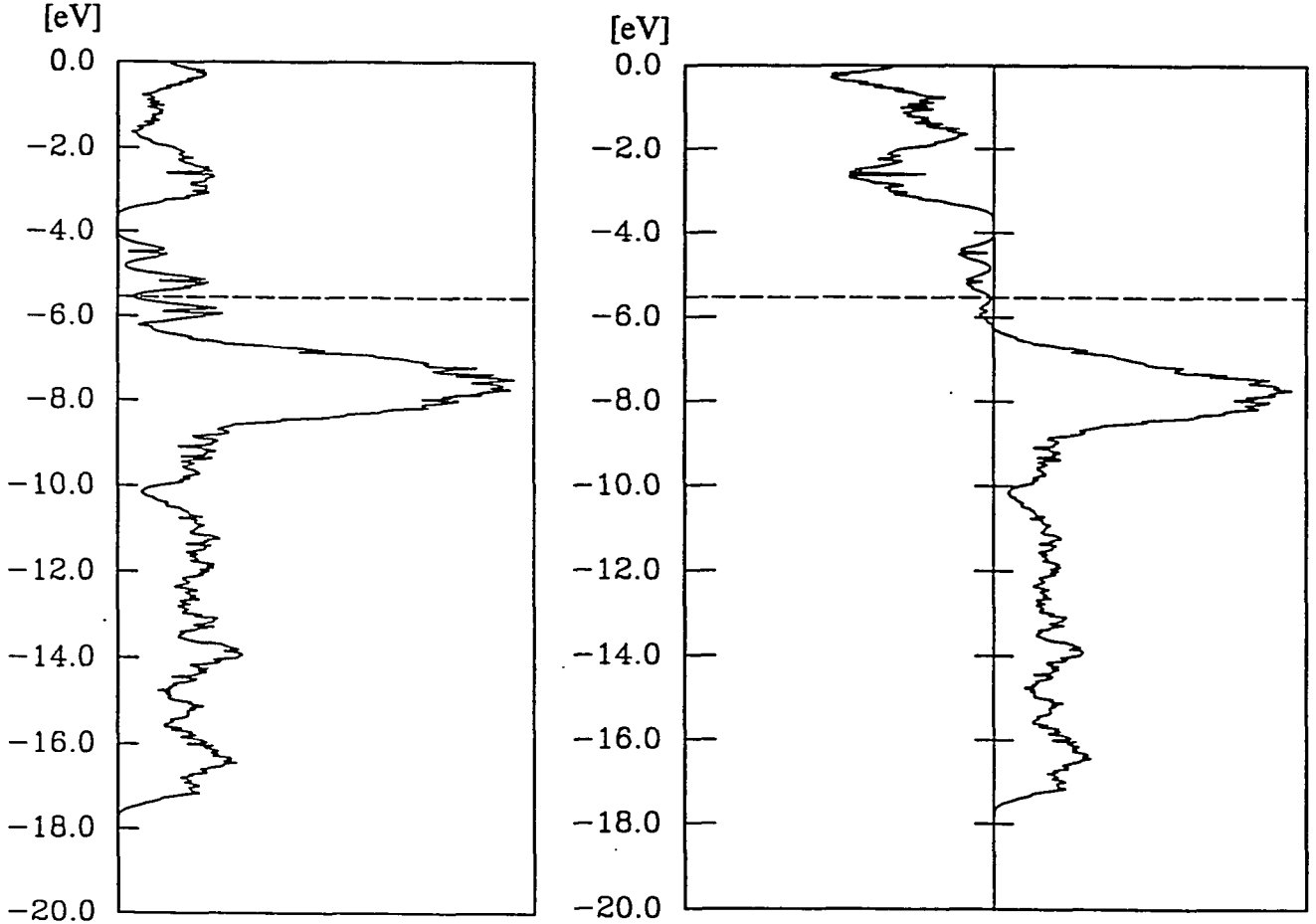

Figure 15. Plots of the DOS (left) and the total COOP curve (right) distributions for an indium layer of the structure of $Na_{96}In_{\sim 97}Ni_2$ (0.2 eV was used for Gaussian smoothing). Only the indium atoms were included in the extended-Hückel band calculations. The Fermi level is shown as broken line.

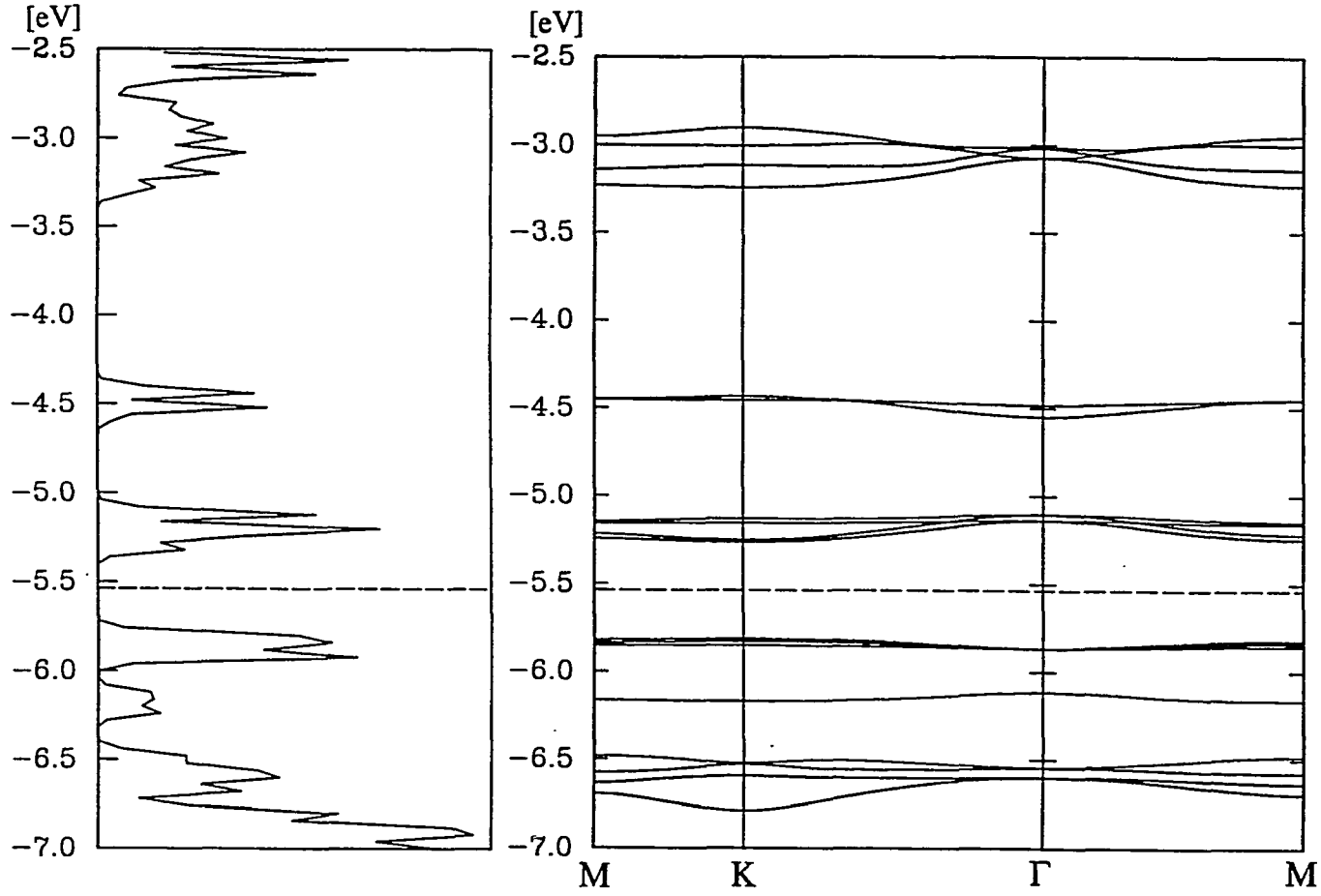

Figure 16. Portions of the density of states (left) near Fermi level (broken line) and the energy band diagram (right). A factor of 0.05 eV was used for Gaussian smoothing.

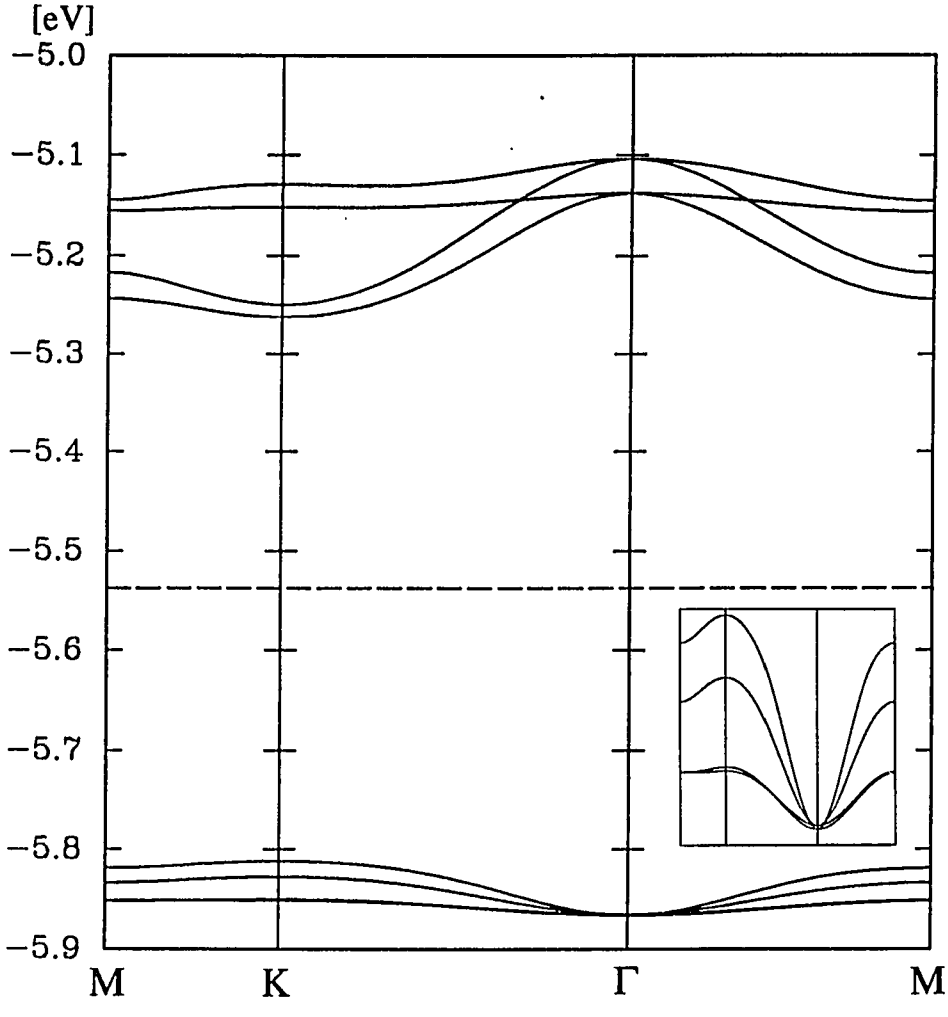

Figure 17. A magnified portion of the energy band diagram near Fermi level (broken line) with the valence band magnified even further in the insert. Notice in the insert that the valence band is a pair of doubly degenerate orbitals at Γ.

PAPER 12. SYNTHESIS, CHARACTERIZATION AND BONDING OF INDIUM FULLERENES: LAYERS OF FUSED In_{70} ANDd In_{78} CAGES WITH ENCAPSULATED INDIUM CLUSTERS

ABSTRACT

Ternary compounds $Na_{\sim 172}In_{\sim 197}Z_2$ with Z=Ni, Pd or Pt are obtained by slow cooling of the appropriate fused mixtures of the elements in welded Ta. They occur in the orthorhombic space group *Pmmn*, Z = 2 with a = 15.988 (5), b = 26.102 (7), and c = 47.59 (6) Å and R, R_w = 6.0, 6.7% for Z = Ni. The structure contains puckered double layers built of fullerene-type spheres of 70 and 78 indium atoms. Each of the spheres shares six of the twelve pentagonal faces with six other spheres, two of the same type and four of the other type. The layers are separated by sodium cations and naked Z-centered $In_{\sim 10}$ clusters (Z = Ni, Pd, Pt). The latter are nested in M_{60} spheres built of 48 indium and 12 sodium atoms that have the geometry of the C_{60} fullerene (C_{2v} symmetry, reduced from the ideal I_h). The M_{60} cages share six of their pentagonal faces with two In_{70} cages (C_{2v} symmetry, reduced from the ideal D_{5h}) and four In_{78} cages (C_{2v} symmetry, reduced from the ideal D_{3h}). The spheres of In_{70} are centered by another type of isolated Z-centered $In_{\sim 10}$ clusters, and the spheres of In_{78} are centered by ca. 14-atom indium clusters that are 2-bonded to the surface of the spheres and contain central Na atom. All three spheres, In_{70}, In_{78} and M_{60}, have deltahedra of sodium cations on the inside surfaces that screen the encapsulated clusters from the spheres. Two of the pentagonal faces in In_{78} are parts of icosahedra such that two indium atoms (through which the encapsulated cluster is connected to the surface) cap those faces from inside, while the rest of each icosahedron is outside the cage. Except those two faces, all faces in all three spheres are capped by sodium atoms from inside and outside.

The encapsulated clusters have nearly spherical geometry with nearly continuous distribution of the electron density on the surface partially restricted by interior for the fullerenes sodium atoms. This distribution was approximated by refining many partially occupied and closely positioned indium atoms on their surfaces.

No properties have been measured since the compounds have not been synthesized in 100% yield. Also, the electronic structure of the compounds has not been studied since the number of atoms in the unit cell exceeds the maximum that the available programs for calculations could handle.

INTRODUCTION

Since the breakthrough in the synthesis of large quantities of carbon fullerenes[1] a myriad of scientists have focused their efforts on experimental and theoretical studies on them. A considerable amount of work has been done on different sizes of molecules of this new form of carbon and their derivatives obtained by substitution, addition, intercalation and insertion.[2] The structural characterization of the fullerenes has been quite difficult owing to the rotation of the molecules even in solid state, and so far this has relied mainly on NMR results. Only products from addition reactions where a large organic moiety is attached to the fullerene cage and stops the spinning have been fully characterized structurally on atomic level by X-ray diffraction.[3,4] The relatively smaller fullerenes up to 76 atoms have only one isomer according to the isolated-pentagon rule (each pentagon is surrounded only by hexagons) and their geometries have been very easy to predict.[5-9] Unlike them, the larger fullerenes have many possible isomers, and their theoretical prediction and experimental confirmation are still an open challenge.

Another part of the research has been directed toward synthesis of fullerenes with encapsulated metal atoms, and recently the metallofullerenes $M@C_{82}$ (M = La, Y, Sc) and $Sc_3@C_{82}$ have been identified by mass spectrometry and electron paramagnetic resonance.[10-15] The scandium atoms in the latter are thought to form a triangular cluster inside the 82-atom cage. Fullerenes of C_{60} and C_{70} intercalated by alkali metal have shown superconductivity.[16] In these compounds, the carbon cages carry negative charges of up to -6, or in other words, 6 more electrons in cluster orbitals than needed for skeletal bonding within the cages.

This article reports on compounds containing Buckminster Fuller-type cages of indium atoms only. Moreover, the cages contain smaller sodium cages which, in turn, contain indium clusters.

EXPERIMENTAL SECTION

Synthesis.

All materials were handled in a N_2-filled glovebox with a typical H_2O level of less than 0.1 ppm vol. The surfaces of the indium (Cerac, 99.999%) and sodium (Alpha, 99.9+%, sealed under Ar) were cut clean with a scalpel before use. Nickel sheet (Matheson Coleman & Bell, reagent), palladium wire (Johnson Matthey, 99.995%) and platinum sheet (Government issue, reagent) were used as received. All reactions were carried out in welded tantalum tubes jacketed in sealed silica containers. The techniques are described elsewhere.[17]

Initially phase **II**, $Na_{\sim 172}In_{\sim 197}Z_2$, was identified by the specific bar-like shape of the crystals in the product from a reaction loaded with compositions $Na_{10}In_{10}Ni$ and heated at 600°C. After its structure was partially refined and the approximate composition determined, samples with atomic ratio of Na : In : Ni, Pd or Pt = 174 : 194 : 2 were prepared. The mixtures were melted at 700°C for one day (the highest melting point in the Na–In system is about 440°C) and then slowly cooled to room temperature at 5° per hour. Compound **II** forms bar-like crystals with Z = Ni and needle-like crystals with Z = Pd or Pt. The crystals are with dark gray color but metallic luster. The crystals of the Ni derivative of **II** can be distinguished easily from the bar-like crystals of **I**, $Na_{96}In_{\sim 97}Z_2$, by the direction of the striations that can be seen on the faces of the crystals with a conventional optical microscope. In the latter, these run perpendicular to the bar direction (the *c* axis of the hexagonal unit cell a = 15.969 (9), c = 47.39 (8) Å), normal to the layers of fused In_{74}, while in **II** the striations are parallel to the bar length, which lies along the shortest axis, and are perhaps normal to the longest axis (*c*) and parallel to the layers of In_{70} and In_{78}. The needle-like crystals of the Pd and Pt derivatives of **II** are also very easily distinguishable from the bar-like crystals of **I**. Unfortunately, the reactions loaded close to the stoichiometry of **II** did not provide high yield of the phase. Probably the

compounds are incongruently melting and slow cooling leads to formation of other phases as well. Quenching and subsequent annealing at proper temperature could provide better yields. Another difficulty encountered with the characterization of **II** was that their lines on the X-ray powder patterns could not be identified in the presence of **I** since two of the lattice parameters of the two phases are very close to each other and many of the diffraction lines overlap. Moreover, phase **II** has its strongest line at an extremely low 2θ angle which is buried in the high film background in this region. The rest of the lines are so weak (the next strongest one is about 15 on a 0–100 scale) and so close to each other that they can be hardly identified in the presence of other phases and that is why the phase identification was done by visual inspection of the morphology of the samples.

Powder patterns were obtained from ground samples that were mounted between pieces of cellophane tape. An Enraf-Nonius Guinier camera, Cu $K\alpha_1$ radiation (λ = 1.540562 Å), and NBS (NIST) silicon as internal standard were employed for this purpose. All powder patterns of **II** contained lines from **I**, NaIn and In and, in addition, samples loaded as $Na_{10}In_{10}Z$ (Z = Ni, Pd, Pt) contained also lines from the isolated cluster-type phase $Na_{10}In_{10}Z$.[18] Since the lines could not be distinguished as discussed above, the lattice parameters were not determined from these powder patterns and also the yield could not be estimated from them. The yield by eye inspection was assessed to be around 60 to 70% in the samples loaded at approximately the right composition. In order to determine the lattice parameters, crystals of the Ni derivative of **II** were selectively collected and ground. The measured X-ray powder pattern displayed sections with nearly continuous intensity and these on the calculated powder pattern appeared as groups of many lines with nearly equal 2θ angles and intensities. Assigning correct Miller indices for most of them was practically impossible. Indices for only 21 lines could be assigned with relatively greater certainty. A least-square refinement of the measured 2θ values of these lines

together with those of the standard Si lines resulted in a = 15.988 (5), b = 26.102 (7) and c = 47.59 (6) Å.

Structure determination.

Diffraction data for $Na_{\sim 172}In_{\sim 197}Ni_2$ were collected on CAD4 single crystal diffractometer at 23°C with monochromated Mo Kα radiation up to 2θ = 50°. The structure was refined with the aid of the TEXSAN software package. Some details of the data collection and refinement are listed in Table I.

A few bar-like crystals from the sample loaded as $Na_{10}In_{10}Ni$ were sealed in thin-walled capillaries and checked for singularity by means of oscillation photographs. One of them, 0.15 × 0.2 × 0.3 mm, was chosen, mounted on CAD4 single crystal diffractometer, and 25 reflections found from random search were indexed with a primitive orthorhombic unit cell. Data collected from one octant of reciprocal space were corrected for Lorentz and polarization effects and for absorption with the aid of the average of five ψ-scans at different 2θ angles. The observed extinction condition, *hk0*: $h + k \neq 2n$ suggested three possible space groups – $Pm2_1n$, $P2_1mn$ and *Pmmn*. The Wilson plot corresponded to a centrosymmetric distribution and therefore *Pmmn* was chosen. The reflections were very sharp (*ca.* 0.4° ω width) and although the *c* axis is quite long no overlap of reflections was observed (collection was done with 0.4° wide ω-scans).

Direct methods (SHELEX-86) provided 57 peaks that had distances to each other appropriate for indium atoms, and they were so assigned. A few cycles of least-squares refinement and a difference Fourier synthesis revealed two atoms at special positions with many peaks surrounding them at distances appropriate for Ni–In distances and also many other positions with distances appropriate for sodium. After assigning the first two positions to Ni atoms and the latter to Na atoms, the subsequent refinement and difference Fourier map revealed

a few more Na atoms, and the electron density shell around the Ni atoms remained. These peaks were of relatively low height, and some of them were too close to each other although all of them were at distances appropriate for In–Ni. By repeating the sequence of least-squares refinement, difference Fourier synthesis and addition of new atoms, all 68 sodium atoms were located. At this point almost all indium atoms from the fused fullerenes (In1 to In52, except In53) and some of the cluster within In_{78} (InC1 to InC5) had been located and refined. In52, InC3 to InC5 and Na37 had abnormally large thermal parameters, Na1 had negative thermal parameter, and an electron density of relatively low height (*ca.* 20 to 30 e/Å^3) remained around the two nickel positions as well as near InC3, C4 and C5. A few of these maxima were assigned as indium, and a subsequent least-squares refinement led to unusually high thermal parameters for them. At this point the well behaved indium atoms were refined with anisotropic thermal parameters and In52 and InC3, C4, C5 were refined with partial occupancies. This gave an R of around 15%. Next, all remaining peaks around the Ni atoms and those near InC3, C4 and C5 were input as In atoms and their anisotropic thermal parameters as well as their multiplicities were refined. All sodium atoms were refined anisotropically as well. This led to non-positive-definite parameters for Na1, 3, 30, 37 and 51, and so they were converted back to isotropic. The R and R_w factors at this point dropped to 6.3 and 7.0%, respectively, but there was a large positive peak of about 10 e/Å in the difference Fourier map. This peak was located about 1.4 Å from Na37 (the one with relatively large thermal parameter) and about 2.8 Å from In19, 40, 43 and was paired with its symmetry equivalent position generated by a mirror plane. A map calculated from F_{obs} clearly showed two nearly spherical "islands" of electron density at the two symmetry-related positions around Na37. More careful study of their environment revealed that they are parts of two otherwise *arachno* indium icosahedra (see Structure Description). The two positions, if filled, connect what become two *nido* icosahedra and are also

a part of an In_{78} fullerene-type cage and make it *closo*-type. Na37 is on the mirror plane generating the two positions. Since the distances to the surrounding indium atoms suggested that the two positions are more appropriate for indium atoms, In53 was refined there with partial occupancy and also the multiplicity of Na37 was freed. This resulted in a 85(5)% occupied Na37 site and a 30(2)% occupied In53 site. The sum of the two occupancies, 115(5)%, is within 3σ of 100%. This suggests that when Na37 is not present the two nearby sites of In53 are occupied.

Na1 remained with a negative thermal parameter but within 1σ of zero in the final refinement. It centers a *ca.* 14-atom indium deltahedron built of InC1–C7 with distances to these atoms ranging from 3.23 to 3.52 Å. Such large distances dismiss the possibility of having In or Ni as central atom but are reasonable for Na–In. Moreover, sodium atoms with relatively small thermal parameters have always been found at the center of relatively large clusters like 15-bonded *closo*-In_{15} in a Na-In-Au compound,[19] 8- and 12-bonded *closo*-In_{16} in $Na_7In_{11.8}$ and $Na_{15}In_{27.4}$,[17,20] respectively, and 12-bonded *closo*-In_{18} in a Na-In-Sn compound.[19] The reasons why the sodium atom refines with negative thermal parameter in this case may come from the fact that the surrounding InC3–C7 atoms are refined with partial occupancies and InC6 and C7 have extremely anisotropic thermal parameters.

The occupancy of In52 is 59(1)% in the final refinement. This site is 6-bonded within a *nido*-In_{14} cluster (see Structure Description) and, if fully occupied, it would have an additional exo bond to its symmetry-related counterpart. This seems to be unfavorable according to our experiences with other systems with similarly positioned atoms. Usually, such positions are with close to a half occupancy, as in this case, so that when one position is occupied its symmetry-related counterpart is empty, and formation of the corresponding exo bond between the two atoms is avoided.

The final residuals are R, R_w = 6.0, 6.7%, respectively, and the largest residual peaks in the final difference Fourier map are 5.3 e/Å^3, 0.45 Å from Na30, and -4.1 e/Å^3. The total numbers of In atoms around NiA, NiB and Na1 are 10.0 (2), 10.08 (7) and 14.4 (1), respectively, if, of course, it is assumed that the single anisotropic description of each site gives a good representation of the total present. This leads to a final refined composition of $Na_{171.85(5)}In_{197.1(2)}Ni_2$ in the independent unit.

Since the electron density distributions around NiA, NiB and partially around Na1 were approximated by many closely positioned, partially occupied and quite anisotropic indium atoms, a reasonable question arises about the correctness of the chosen space group. Clearly, many of the atoms around NiA and to some extend around NiB and Na1 are too close to each other because of mirror planes passing through the central atoms. Although these may be artificial for the clusters, the mirror planes are definitely there for the rest of the atoms which account for about 88% of the scattering power (130 atoms out of the total of 141). From our experiences with isolated clusters with similar behaviors in $Na_{96}In_{\sim 97}Ni_2$, we concluded that a larger set of data and subsequent refinement in a lower symmetry space group does not solve the problem. (Reduction of the symmetry from $P6_3/mmc$ all the way to $P2_1$ did not lead to better results for $Na_{96}In_{\sim 97}(Ni \text{ or } Pd)_2$.) The large number of atoms that *have* the symmetry elements of the chosen space group will generate structure factors that are practically the same in any subgroup. The contribution from atoms that may not have some of the symmetry elements is so small that, although the real space group may be of lower symmetry, refinement in it is practically impossible.

Later, data were collected on a second crystal (0.1 × 0.2 × 0.2 mm) of this compound. It diffracted more weakly than the first crystal (6951 observed reflections), which caused about 50% larger standard deviations in the final refined parameters. The structure refined to R/R_w =

6.4, 7.2% (GOF = 1.68, 960 variables, largest peaks in ΔF = +5.1 and -3.8, absorption range 0.598–1.000) and the resulted composition was $Na_{171.8(1)}In_{197.5(3)}Ni_2$. All atoms except Na3, 5, 8, 17, 19, 21, 23, 37, 39, 45, 51, 52, 60, 62, 63 and In53 were refined with anisotropic thermal parameters. These were refined as isotropic since these parameters became nonpositive-definite when converted to anisotropic. The final thermal parameter for Na1 was slightly negative (-0.2 (4)), as in the first crystal. The indium atoms forming the isolated clusters around the nickel atoms and some of those around Na1 had very anisotropic, two-dimensional thermal ellipsoids as before. The occupancies of all of the sites of the encapsulated indium clusters were within 3σ of those refined for the first crystal. Also, In52 refined with 54(1)%, In53 with 17(1)% and Na37 with 84(7)% occupancies.

RESULTS AND DISCUSSION

Structure description.

The final positional and isotropic-equivalent displacement parameters as well as data on the partially occupied sites are reported in Table II. The anisotropic displacement parameters and the important distances are listed in Tables III and IV, respectively. A general view of the unit cell is shown in Figure 1 where the In_{70} and In_{78} cages are represented as spheres, and lines for separations less than 4.0 Å for the indium atoms between the spheres are drawn.

The structure can be viewed in two ways. In the first, only bonding between the indium atoms is considered and in the second some sodium atoms are added to the "bonding" scheme. Starting from the first, the structure is viewed as built of puckered double layers perpendicular to the *c* axis with one such per unit cell and with gaps between the layers at z = 0 and 1 (Figure 1). There is no In–In bonding between the double layers. Each layer is a close packed arrangement of face-sharing In_{70} and In_{78} cages. The sequence of these cages is such that rows of each type along the *a* axis (nearly the view direction in Figure 1) alternate along the *b* axis (horizontal in Figure 1) and are puckered to form waves along the latter. Two layers are bonded together to form a double-layer formation through quite complicated In–In bonding (near z = 1/2). Some of the atoms in the cages (near z = 0 and 1) also have exo bonds pointing approximately outward from the double layers to other indium atoms that do not belong to a cage and do not interconnect cages.

Figure 2 shows the cage **A** built of 70 indium atoms with the unique atoms labeled. It has C_{2v} point group symmetry (the 2-fold axis is vertical in Figure 2) but is very close to D_{5h} (the pseudo 5-fold axis is nearly along the view direction in Figure 2), the symmetry of the C_{70} fullerene. All atoms exhibit small, well behaved ellipsoids. The two pentagons generated by In1, 34, 50 plus a mirror plane (Figure 2) are shared with two other In_{70} cages along the *a* axis.

The four pentagons near the waist composed of In9, 27, 36, 44, 47 are shared with four In_{78} cages. The two hexagons near the top, In16, 29, 31, 45, are parts of *nido* 14-atom clusters (not shown) which will be discussed later.

An In_{78} cage (cage **C**) is shown in Figure 3 with all unique atoms labeled. It also has C_{2v} point group symmetry (the 2-fold axis is vertical) but very close to D_{3h} (the pseudo 3-fold axis is nearly along the view direction). We can compare its geometry with that predicted for some isomers of C_{78}. The latter has five allowed isomers according to the isolated-pentagon rule (each pentagon is surrounded only by hexagons), C_{2v}-**I**, C_{2v}-**II**, D_3, D_{3h}-**I** and D_{3h}-**II**,[21] with close energies, and different authors have predicted different orders of stability based on different calculational methods. Fowler et al.[21] predicted D_{3h}-**II** to be the most stable isomer based on the largest HOMO–LUMO gap. The same approach but combined with the π-resonance energy of the systems gives D_{3h}-**II** and C_{2v}-**II** as the most stable isomers.[22] Tight-binding molecular dynamics used by Ho et al.[23] predicted the order of stability as C_{2v}-**I** > D_{3h}-**I** > C_{2v}-**H** > D_3 > D_{3h}-**II**, and finally, both Diederich et al.[24] from force field calculations and Colt and Scuseria[25] from an *ab initio* study, gave the order of stability as C_{2v}-**I** > C_{2v}-**II** > D_3 > D_{3h}-**I** > D_{3h}-**II**. Experimental NMR studies on C_{78} fullerenes isolated by chromatography have also produced different results. Diederich et al.[24] found C_{2v}-**II** and D_3 in ratio 5 : 1, while Kikuchi et al.[26] obtained C_{2v}-**I**, C_{2v}-**II** and D_3 in a ratio 5 : 2 : 2. In our case, In_{78} has the geometry of the D_{3h}-**I** isomer with the symmetry slightly reduced to C_{2v}. (The C_{2v} symmetry here is coincidental with the symmetry of the first two isomers of C_{78}. It results from a removal of the 3-fold axis in the *isomer* D_{3h}-**I** without any atomic rearrangements.) We should point out that the D_{3h}-**I** is the only nearly spherical isomer, the rest are quite oblong-like.

The two pentagons at the waist of In_{78} are generated by In5, 17, 46 and a mirror plane, and are shared with two other In_{78} cages along the *a* axis, as before. The four pentagons of In9,

27, 36, 44, 47, two in front and two in back, are shared with four In_{70} cages. As can be seen from Figure 3, the two pentagons of In13, 40 and 53 are parts of two *nido*-icosahedra. In19 caps each pentagon from inside the cage and is bonded to InCl which is part of an encapsulated cluster at the center of the cage (the rest of the cluster is not shown). The remaining atoms of the icosahedra are outside the cage and all are exo bonded. In53 is the atom that refined to 30(2)% occupancy (17(1)% for the second crystal) and is 1.4 Å from Na37, which refined with 85(5)% occupancy (84(7) for the second crystal). The fact that the In53 and Na37 sites are so close means that when one is occupied, the other is empty. This combined with the fact that the sum of the occupancies of the two positions, 115(5)% (101(7)% for the second crystal), is within 3σ of 100% suggests that only *arachno*-In_{76} and *closo*-In_{78} exist throughout the structure. Presence of *nido*-In_{77} would lead to lower occupancy of the In53 site. For purpose of clarity the cage will be referred to as In_{78} in the text. The distance between the two In53 atoms (2.72(4) Å) and between each In53 and the nearest atoms of the icosahedron (2.75(2) Å to In19, 2.82(2) Å to In43, 2.83(1) Å to In40) are shorter compared to the usual 2.85 Å and above. A similar situation with a row of very close *arachno*-icosahedra was encountered in $Na_{15}In_{27.4}$.[20] In that case, a pair of indium atoms, that each refined with 54.1(9)% occupancy cap a pair of *arachno*-polyhedra. These are also very close to the polyhedral atoms (2.788(6), 2.889(3), 2.841(5) Å) and to each other (2.76(1) Å). It was not clear though in that structure whether some of the icosahedra are bonded via such atoms or simply alternating *closo* and *arachno* species are present. A comparison between the distances distributions in In_{78} and in the D_{3h}-I isomer of C_{78} results in a surprising similarity. Colt and Scuseria[25] calculated by an *ab initio* method the distances between all carbon atoms of the five possible isomers for C_{78}. They found that the corresponding to In53–In53 distance in the D_{3h}-I isomer is shorter than the rest of the distances, 1.338 vs. 1.381–1.493 Å.

A magnified section of the unit cell near z = 1/2 in Figure 4 shows the connectivity between the two layers that generate the double layers of fused fullerenes. Figure 5 shows the two cages with the atoms forming the "attachments" labeled. Figure 5a is practically the same as Figure 3 but the cage is represented as a sphere and the view is rotated about 90° around the vertical *c* axis from Figure 3. As mentioned above, the hexagons of In16, 29, 31, 45 in In_{70} (Figures 2 and 5b) are also parts of *nido*-In_{14}. The corresponding *closo*-deltahedron is a tricapped truncated trigonal prism. The two triangular faces formed by truncation are ΔIn45, 38, 38 on one side and ΔIn16, 39, 39 on the other side (Figure 5b). The triangles formed from the truncated corners are ΔIn33, 38, 38, 2ΔIn31, 45, 38, Δ26, 39, 39 and 2ΔIn16, 29, 39 (Figure 5b). The *nido* derivative in our case has one capping atom missing, the atom that would cap the hexagonal face In16, 29, 31, 45 from inside the fullerene. Instead, a sodium atom is positioned there. The other 6-bonded capping atoms are two In52 (Figure 5b). This deltahedron is 12-bonded, six from In16, 29, 31, 45 to other atoms of the fullerene. The two In39 atoms connect the In_{70} fullerene to two In_{78} fullerenes in the same layer through exo bonds to In20 of the attached *nido*-icosahedra (Figures 4, 5a and b). The two In38 atoms connect the In_{70} fullerene to two In_{78} fullerenes but in the next layer via In43 in the *nido*-icosahedra.

The capping atoms In52 are exo bonded to the same type of atoms in clusters attached to In_{70} in the next layer. These atoms refine with nearly half occupancy (59(1)%) which suggests that probably when one position is occupied, the symmetry related one in the neighboring cluster is empty so that no In52–In52 bonds exist in the structure. A similar outcome has been observed in other compounds – nearly half occupied positions with 6 nominal bonds within the cluster and also an exo "bond" to its symmetry equivalent atom in another cluster. Such examples are the six-bonded atoms in a 15-bonded *closo*-In_{15} cluster found in a ternary Na–In–Au compound, those in a 12-bonded *closo*-In_{18} cluster found in a ternary Na–In–Sn

compound and the six-bonded atoms in a 16-bonded *closo*-In_{16} found in a ternary Na–In–Zn compound.[19] On the other hand, such in a 12-bonded *closo*-In_{16} cluster found in $Na_{15}In_{27.4}$ were refined with full occupancy, although they are exo bonded to their equivalents from the next cluster.[20] Nevertheless, it seems that 7-bonded state for the indium atoms is quite unfavorable. Two atoms, In26, 33, of the *nido*-In_{14} on the In_{70} fullerene are without exo bonds, and presumably lone pairs of electrons are associated with them.

One more connection between the two layers within a double layer is achieved through an exo bond from In14 of the *nido*-icosahedra to In4 atom. The latter is also bonded to two In42 atoms from the In_{70} cage and another In4 which, in turn, is bonded to the next In_{70} cage.

In summary, the bonding pattern **inside** the double layer (Figure 4) discussed above is as follows: a) each In_{70} is connected to two other In_{70} cages within one layer by sharing two pentagonal faces and also through the In4–In4 pair of exo atoms; b) the same cage is connected to four In_{78} cages within one layer by sharing four pentagonal faces and also through the In39–In20 pair of exo atoms; c) the same cage is connected to one In_{78} cage from the next layer of a bilayer through the two In38–In43 and In4–In14 pairs of exo atoms; d) the same cage would had been connected to four other In_{70} cages from the next layer had In52 (59(1)% occupancy) been fully occupied; e) each In_{78} cage is connected to two other In_{78} cages within the same layer via two shared pentagonal faces, but no additional bonding through exo atoms occurs; f) the same cage is connected to one In_{70} from the next layer through six pairs of exo atoms, 2 × In14–In4 and 4 × In43–In38.

Next, we turn our attention to the bonding pattern **outside** the double layers. Figure 6 shows a magnified section of the unit cell near z = 0 where parts of two neighboring bilayers can be seen. The space between them is filled with sodium cations and also the NiB-centered isolated clusters of *ca.* 10 indium atoms. If no exo indium atoms had been present at this side

of the In_{70} and In_{78} cages, many atoms on their surfaces would have been only 3-bonded. (As a matter of fact, the exo atoms between the two layers forming the bilayers play the same role for the atoms on the inward-facing surface of the cages.) Unlike carbon in the carbon fullerenes where each atom has 3 σ-bonds but is also π-bonded, the indium atoms require at least four σ-bonds. A 3-bonded state is very unlikely for indium, although a precedent was found in the structure of $K_{15}Na_8In_{39}$ where two 3-bonded indium atoms form a rectangle by alternating with two 4-bonded ones.[19] This is the only case, so far, where formally sp^2 hybridized indium atoms are involved in relatively well pronounced π-bonding.

Hexagons and triangles of exo atoms (open bonds) can be seen in Figure 6. Each triangle (In48, 51) is bonded to one In_{78} cage (In49, 22, 23), while each hexagon (In8, 18, 35) is bonded to two In_{78} cages (In3, 12, 28) and one In_{70} cage (In21, 32). Notice that each triangle has an opposed hexagon from the next layer such that the planes of the two are nearly parallel. The closest approach of the two layers occurs between the atoms of these triangles and hexagons with distances of 5.412 (7) Å for In35–In48, 5.455 (6) Å for In8–In48 and 5.462 (6) for In18–In51. The same formations of hexagons and triangles with similar arrangement are found on the surface of and between the In_{74} cages in $Na_{96}In_{97}Z_2$. It can be seen in Figure 6 that four In_{78} and two In_{70} cages, four hexagons, and four triangles surround a cavity with nearly spherical coordination. At its center we find the isolated NiB-centered indium cluster.

At this point, the second way of describing the structure is needed in order to ease its further comprehension. It was mentioned above that sodium cations fill the space between the bilayers. Two among them, Na12 and 48, have special positioning, such that if connected to the nearest indium atoms, another type of a fullerene cage is revealed, Figure 7 with the unique atoms labeled. This cage (M_{60}) is built of 60 atoms (48 indium and 12 sodium atoms) and is isotypic with the C_{60} fullerene. Its symmetry is C_{2v} reduced from the ideal I_h. It is centered by

the NiB-centered indium cluster and fills the cavity discussed in the previous paragraph (Figure 6). Each cage is connected to six other M_{60} cages by sharing the Na12–Na12 and Na48–Na48 edges. It is fused to two In_{78} fullerenes from one layer (the upper layer in Figure 6) by sharing the pentagons In6, 22, 28, and to two In_{78} fullerenes from the next layer (the lower layer in Figure 6) by sharing the pentagons In2, 3, 23. It is also fused to two In_{70} fullerenes from one layer (the upper layer in Figure 6) by sharing the pentagons In10, 21, 30. Notice in Figure 7 that the sodium atoms are a bit above the surface of the sphere defined by the indium atoms and the pentagons In18, 51, Na48 as an example, are puckered outward. This is caused by the longer Na–Na and Na–In distances compared with the In–In distances.

Since the bonding between the two layers of a double layer of In_{70} and In_{78} fullerenes has already been discussed in detail, we will omit the corresponding, interconnecting exo atoms in the further discussion as well as in the following figures. Condensed views of the structure along or nearly along the axes *a*, *b* and *c* are shown in Figures 8, 9 and 10, respectively, with the different sized fullerenes labeled and the unit cell outlined. (The empty space around z = 1/2 is where the omitted indium exo atoms first discussed as well as some sodium atoms are positioned.) In order to show the positioning of the different cages rather than the way they are fused with each other, the sizes of the spheres that represent them have been chosen slightly smaller than they are supposed to be. Also we should remember that each type cage is fused along *a* (Figure 9) with two members through pentagons for In_{78} and In_{70} and through pairs of sodium atoms for M_{60}. Also fused through pentagons are four M_{60} and four In_{70} cages to each In_{78} cage, two M_{60} and four In_{78} to each In_{70}, and four more M_{60}, two In_{70} and four In_{78} to each M_{60}. From Figure 10 one can see that the individual layers of In_{70} and In_{78} (normal to *c*) are of a close-packed type, that is, there are six spheres around each sphere, two of the same and four of the other type. The spheres of each type form straight rows along the *a* axis (Figure 9)

and these alternate and pucker along the *b* axis forming a wave-like surface (Figure 8). However, the neighboring layers of the same type along *c* are positioned exactly on the top of each other (Figures 8 and 9). Close-packed layers of M_{60} are placed between every other pair of layers and take the wave-like shape defined by the latter. Within the M_{60} layer, each cage of M_{60} is fused with six other M_{60} cages.

We should point out here that In_{70} and, alike, C_{70} with their D_{5h} (or pseudo D_{5h}) symmetry have oblong-like rather than spherical shape. The long axis of the ellipsoid of In_{70} is along the *a* axis of the unit cell and happens to be equal to the diameter of the nearly spherical In_{78} of pseudo D_{3h} symmetry (both are equal to the *a* axis of the unit cell, 15.988 (5) Å). This, and the fact that both cages have two diametrically opposed equatorial (in the *a*, *b* plane) pentagons (along *a*) that can be shared with other cages of the same type, are the grounds for forming commensurate rows of In_{70} and In_{78} along the *a* axis. The reason why the rows are ordered in a wave-like rather that planar fashion along the *b* direction is probably the absence of four more equatorial pentagons on these cages. Unlike In_{74} (D_{3h}) found in $Na_{96}In_{\sim 97}Ni_2$ which has six pentagons in an equatorial plane and forms perfectly flat layers by sharing them with other In_{74} cages, these two cages have four additional pentagons outside the waist. The layer formed by sharing them with other cages will become puckered, automatically.

Let us imagine that the layers of In_{78} and In_{70} were flat. Since they stack exactly on top of each other in pairs, as mentioned above (Figures 8–10), there will be trigonal prismatic sites between them as sites for M_{60}. The puckering of the layers is such that one vertical edge of each trigonal prism is shifted up or down along the *c* axis. A logical result is that the centering units are pushed toward the opposed rectangular face of the trigonal prism, and in the extreme case these species will center that face. The latter is the positioning of the M_{60} cages at the center of the rectangular faces formed between two vertical edges In_{78}–In_{70} in a pseudo trigonal

prism. The third (displaced) vertical edge is another pair of In_{70} and In_{78}. The packing scheme of the layers along the *c* axis is ABA␣ABA␣... where A is a In_{70}, In_{78} layer, B is a M_{60} layer and ␣ designates the position of the interconnecting indium atoms (Figure 1, 4, 5 and left empty in Figures 8 and 9).

The positioning of the sodium atoms throughout the structure is similar to that in $Na_{96}In_{\sim 97}Z_2$. Most of them are used to cap all of the hexagonal and pentagonal faces of the cages from both sides (Figures 11 to 13). Following is a list of the capping atoms and the faces they cap:

a) in In_{70} (Figure 11)

- Na5	inside and	Na6	outside cap the	hexagon	In21, 21, 21 , 21, 32, 32;
- Na20	inside and	Na42	outside cap the	hexagon	In21, 10, 32, 11, 44, 47;
- Na29	inside and	Na53	outside cap the	pentagon	In21, 21, 10, 10, 30;
- Na14	inside and	Na59	outside cap the	hexagon	In1, 30, 10, 47, 9, 34;
- Na45	inside and	Na45	outside cap the	pentagon	In1, 34, 34, 50, 50;
- Na62	inside and	Na3	outside cap the	hexagon	In9, 34, 50, 25, 24, 27;
- Na54	inside and	Na41	outside cap the	pentagon	In9, 47, 44, 36, 27;
- Na31	inside and	Na34	outside cap the	hexagon	In7, 11, 36, 36, 44, 44;
- Na33	inside and	Na52	outside cap the	hexagon	In7, 36, 27, 24, 29, 16;
- Na50	inside and	Na8	outside cap the	hexagon	In50, 50, 25, 25, 42, 42;
- Na40	inside and	Na7	outside cap the	pentagon	In25, 42, 31, 29, 24;
- Na36	inside and	Na2	outside cap the	hexagon	In16, 45, 29, 29, 31, 31;
- Na13	inside and	Na4	outside cap the	hexagon	In45, 45, 31, 31, 42, 42;

b) in In_{78} (Figure 3)

- In19	inside		caps the	pentagon	In13, 13, 40, 40, 53;

- Na15 inside and Na30 outside cap the hexagon In13, 13, 15, 15, 46, 46;
- Na38 inside and Na38 outside cap the pentagon In46, 46, 5, 5, 17;
- Na60 inside and Na25 outside cap the hexagon In53, 53, 40, 40, 41, 41;
- Na16 inside and Na3 outside cap the hexagon In41, 41, 27, 27, 9, 9;
- Na65 inside and Na52 outside cap the hexagon In40, 41, 27, 36, 15, 13;
- Na41 inside and Na54 outside cap the pentagon In9, 27, 36, 44, 47;
- Na19 inside and Na59 outside cap the hexagon In9, 9, 47, 47, 6, 6;
- Na63 inside and Na42 outside cap the hexagon In44, 47, 6, 28, 12, 37;
- Na44 inside and Na34 outside cap the hexagon In15, 36, 44, 37, 5, 46;
- Na17 inside and Na28 outside cap the pentagon In6, 6, 28, 28, 22;
- Na68 inside and Na9 outside cap the hexagon In2, 3, 12, 37, 5, 17;
- Na56 inside and Na24 outside cap the hexagon In22, 49, 23, 3, 12, 28;
- Na26 inside and Na35 outside cap the pentagon In2, 3, 3, 23, 23;
- Na51 inside and Na61 outside cap the hexagon In23, 23, 49, 49, 23, 23;

c) in M_{60} (Figure 7)

- Na35 inside and Na26 outside cap the pentagon In2, 3, 3, 23, 23;
- Na66 inside and Na61 outside cap the hexagon In48, 48, 23,23,Na12, 12;
- Na27 inside and Na9 outside cap the hexagon In2, 2, 3, 3, 18, 18;
- Na64 inside and Na24 outside cap the hexagon In3, 23, 48, 18,Na48, 48;
- Na46 inside and Na55 outside cap the pentagon In48, 8, 35, Na12, 48;
- Na67 inside and Na55 outside cap the pentagon In18, 18, 51, Na48, 48;
- Na58 inside and Na24 outside cap the hexagon In8, 28, 22, 51,Na48, 48;
- Na43 inside and Na6 outside cap the hexagon In35, 35, 21,21,Na12, 12;
- Na22 inside and Na42 outside cap the hexagon In21, 35, 8, 28, 6, 10;

- Na28	inside and	Na17	outside cap the	pentagon	In6, 6, 28, 28, 22;
- Na21	inside and	Na59	outside cap the	hexagon	In6, 6, 10, 10, 30, 30;
- Na53	inside and	Na29	outside cap the	pentagon	In21, 21, 10, 10, 30.

There are 37 sodium atoms (1 × Na5 + 2 × Na13 + 4 × Na14 + 4 × Na20 + 2 × Na29 + 2 × Na31 + 4 × Na33 + 2 × Na36 + 4 × Na40 + 2 × Na45 + 2 × Na50 + 4 × Na54 + 4 × 62) inside the 37 faces of In_{70}, 39 sodium atoms (2 × In15 + 2 × In16 + 2 × Na17 + 2 × In19 + 2 × In26 + 2 × Na38 + 4 × Na41 + 4 × Na44 + 1 × Na51 + 4 × Na56 + 2 × Na60 + 4 × Na63 + 4 × Na65 + 4 × Na68) and 2 indium atoms (2 × In19) inside the 41 faces of In_{78}, and 32 sodium atoms (2 × Na21 + 4 × Na22 + 2 × Na27 + 2 × Na28 + 2 × Na35 + 2 × Na43 + 4 × Na46 + 2 × Na53 + 4 × Na58 + 4 × Na64 + 2 × Na66 + 2 × Na67) inside the 32 faces of M_{60}.

The remaining few sodium atoms that do not cap faces of fullerenes (Na10, 11, 23, 32, 37, 39, 47, 49, 57) are located near Z = 1/2. They cap the faces of the deltahedra positioned there. One more sodium atom, Na18, caps the exo hexagon In8, 8, 18, 18, 35, 35 (Figure 6), that connects two In_{70} and one In_{78} cages.

If lines are drawn between the sodium atoms (endo-Na) inside the three spheres, as it is done with open bonds in Figures 11, 12 and 13, additional nearly spherical formations inside the fullerenes are revealed. These are correspondingly 37-, 39- and 32-atom regular deltahedra (triangular faces only) constructed of five and six "bonded" sodium atoms. The deltahedron in Figure 12 (inside the In_{78} cage) is *arachno*-type if only the sodium atoms are considered, but it becomes *closo*-type when the two In19 atoms inside the In_{78} cage (labeled in Figure 3) are included. The atoms in the fullerenes can now be viewed as capping all triangles of each inner deltahedron from the outside. Since each "six-bonded" sodium atom has six adjacent triangles and each "five-bonded" sodium atom has five, they cap, respectively, hexagons and a pentagons in the fullerene.

One very important consideration for later discussion is that the "six-bonded" endo-Na atoms need to be closer to the surface of the fullerene, or in other words further from its center, than the "five-bonded" endo-Na atoms in order to keep reasonable and more or less equal Na–In distances. This also leads to shorter exo-endo Na-Na distances across the hexagons than across the pentagons. This, in turn, means that the positions of all of the inner sodium atoms in the fullerenes are fixed (determined) by the positions of the atoms building the fullerenes, and this has a dramatic effect on the isolated indium clusters at the center of the cages.

There are two different isolated and Ni-centered clusters and one Na-centered (Na1) cluster in the structure. NiA, NiB and Na1 are at the centers of the In_{70}, M_{60} and In_{78} fullerenes, respectively. During the refinement of the structures (above), it was found that these core positions are surrounded by shells of electron density with no well-defined maxima. These shells are quite spherical and with average radii of 2.73 (3), 2.86 (3) and 3.38 (5) Å around NiA, NiB and Na1, respectively. The first two lengths are quite appropriate for Ni–In distances (2.77 Å is the average for Ni–In in $In_{10}Ni^{10-}$)[19] and the third is common for Na–In (see Table IV). The electron density within these shells was approximated by placing indium atoms at all maxima and refining them anisotropically and with partial occupancies. Figure 14 shows the clusters with the ellipsoids of the indium atoms drawn at the 94% probability level. It can be seen that all the ellipsoids around NiA and NiB and some around Na1 appear as two dimensional disks that are tangential to a sphere around the cluster center. The same clusters are shown with 50% probability thermal ellipsoids on Figure 15 where one can see more clearly the positions of the indium atoms.

NiA-centered cluster. The electron density around NiA (within In_{70}) was refined with six independent indium positions, A1 to A6 (Figure 15a). All these atoms refined with 50% occupancy (within 1σ) and gave total of 10.0 (2) indium atoms per cluster (see Table II). Some

of the distances between them are quite small but some are reasonable for In–In distances. All of them are at proper distances from the central atom, NiA (2.68 (1) to 2.801 (8) Å). The fact that each of the atoms of the cluster refined with half occupancy suggested to us that a good model might be a cluster of 10 indium atoms that exists disordered throughout the structure. The best model that we could find, Figure 16a, is achieved by removing the two vertical mirror planes through the center of the cluster that are required by the space group . The view in Figure 16a is slightly off from the one in Figure 15a, but still one can see that this 10-atom cluster has half of each type of refined atoms. All In–In distances (from 2.95 (1) to 3.35(1) Å), except one, are within the normal range. The only one exception is the distance InA2–InA3 which is 2.30 (1) Å, impossibly short distance for two indium atoms. Nevertheless, since all of the atoms of the cluster refine with such extreme thermal motions, it is possible that in each In_{10} cluster the atoms InA2 and A3 are not actually at the centers of the refined thermal ellipsoids. Each of these two atoms would need to move away only about 0.3 Å in order to establish a reasonable bond length. Notice that the radii of the disks approximating the distribution of InA2 and A3 are ~0.7 Å even when drawn at only 50% probability. Since the positions of all InA1 to A6 atoms have been refined as the average positions of a cluster disordered throughout the structure, it is possible to artificially refine sometimes an atom centered between two maxima in the electron density that are very close (~0.3 Å) to each other.

Assuming that the model we proposed is correct, we can discuss the geometry of this cluster. Shown in Figure 16b is a Ni-centered isolated $In_{10}Ni^{10-}$ cluster found in $K_{10}In_{10}Ni$.[19] Its geometry is very close to the modeled cluster in Figure 16a, and both can be considered as tetracapped trigonal prisms (vertical in the Figures). The trigonal prism in Figure 16a is constructed of atoms A4, A6, A6 (lower triangle) and A1, A2, A3 (upper large triangle). A5 caps the upper triangular face (A5 is bonded to A1, A2, A3), and another three atoms, A1, A3,

A4, cap all trapezoidal (formerly rectangular) faces of the trigonal prism. Since all atoms should be nearly equidistant from the central nickel atom, the capping atom A5 becomes very close to the upper triangle and causes expansion of the latter. Extended-Hückel MO calculations performed on the cluster of Figure 16b have shown that clusters with this geometry require $2n$ = 20 electrons (n is the number of indium atoms) for skeletal bonding. This will result in a charge of -10 associated with the clusters encapsulated in In_{70}.

NiB-centered cluster. The electron density around NiB (within M_{60}) was refined with five independent indium positions, B1 to B5 (Figure 15b). B1 and B2 refined with 100% occupancy (within 1σ), and B3, B4 and B5 refined with 57(1), 35(1) and 70(1)% occupancies, respectively (see Table II). This gave a total of 10.08(7) indium atoms per cluster. Again, some of the distances between the atoms of the cluster are quite short but some are reasonable for In–In distances, and also, all of the indium atoms are at proper distances from the central NiB atom (from 2.64 (1) to 2.699 (8) Å). As for the NiA-centered cluster, this cluster also can be modeled as a 10-atom indium cluster disordered throughout the structure. The model in a different orientation from Figure 15b is shown in Figure 17. It is achieved by using all of the B1 and B2 atoms (100% occupancy) and one half each of the B3, B4 and B5 atoms. It can be seen that this cluster resembles the NiA-centered cluster (Figure 16a) and also the $In_{10}Ni^{10-}$ cluster found in $K_{10}In_{10}Ni$.[19] Except a few short distances, the In–In range is 2.94 (1) to 3.37 (1) Å. There are six relatively short distances, two of 2.68 (1) Å between InB1 and B3, two of 2.76 (1) Å between InB2 and B4, and two of 2.78 (2) Å between InB3 and B4. Again, as in the NiA-centered cluster, since all of the atoms of the cluster refine with very large tangential disks, it is possible that in each cluster the atoms B1, B2, B3 and B4 are slightly off the centers of the refined positions. Displacements of only ~0.1 Å for each of these atoms would make the distances "normal".

The geometry of the cluster (Figure 17) is again a tetracapped trigonal prism (vertical) similar to that for the NiA-centered cluster. The trigonal prism is built of B3, B2, B5 (lower triangle) and B1, B1, B4 (upper large triangle). The capping atoms are B1 which caps the upper triangular face and InB1, B3, B4 which cap all quasi-rectangular faces of the trigonal prism. The upper triangle has opened so that the capping atom InB1 can approach the central Ni atom. Since both clusters are isotypic with $In_{10}Ni^{10-}$, each should require 20 electrons for skeletal bonding and therefore would have a charge of -10.

This model for the NiB-centered cluster implies that InB1 and B2 are 100% occupied, as they are, and InB3, B4 and B5 are 50% occupied. The latter three were refined with 57 (1), 35 (1) and 70 (1)% occupancies,respectively, which are, correspondingly, 7σ, 15σ and 20σ deviations from the required value. The last two numbers are quite large but, again, we should keep in mind that all so-called atoms of the refined cluster are very much imperfect and they , of course, will affect the refined parameters of each other.

Na1-centered cluster. This cluster (Figure 15c) is nested at the center of the In_{78} fullerene, but it is unusual since it "hangs" on two adjacent indium atoms. Some of the maxima in the electron density distribution around the central Na1 atom were quite well defined and with reasonable heights for In atoms. On the other hand, some sections of the electron density had no clear maxima and almost continuous (plato-like) distribution with relatively low but not negligible heights. Atoms C1 to C3 refined with relatively "normal" thermal parameters and with nearly full occupancies, 100 (1)%, 100 (1)% and 88 (1)%, respectively. The two C1 atoms have exo bonds to two In19 atoms through which the cluster communicates with the "outside world". The latter are the indium atoms that cap two pentagonal faces of the In_{78} fullerene from the inside (see Figure 3). C4 and C5 refined with smaller occupancies, 86 (2) and 78 (2)%, respectively, (within 7σ and 11σ of full occupancy). Their thermal parameters are quite

large but not extreme. Finally, C6 and C7 gave very large and considerably elongated thermal ellipsoids with refined occupancies of 80 (1) and 50 (1)%, respectively. Two different cross-sections of the electron density distribution near InC6 and C7 are shown by Figures 18 and 19, both from Fourier syntheses based on F_{obs} and the assigned phases. The plane of the plot in Figure 18 is defined by the atoms InC4, C6, and C7, and the one in Figure 19, by InC4, C5 and C7 (see also Figure 15c). It is clear that there are no well defined maxima in the electron density near the positions refined for InC6 and C7. There is a continuum of electron density in the shape of an arc which extends from InC4 through InC7, C6, C7 to another InC4. This causes great problems when one tries to approximate it with a few discrete positions. The result is large anisotropic thermal ellipsoids and large ambiguity in the correct positions of the atoms. Also, an artificial symmetry element (or elements) that passes through the center of the cluster will generate further problems when refining these atoms since the refined positions will be average and not necessarily correct.

We tried to model this cluster in a similar way to the other two discussed above. A model that is relatively reasonable is shown in Figure 20a. In it, all atoms C1 to C6 are assumed fully occupied and C7 is half occupied. The result is 2-bonded *closo*-In_{16} which has one of the two mirror planes through the center missing. Of course, lower occupancies of C1 to C6 may lead to different *nido*, *arachno*, *hypho* etc. species. Shown in Figure 20b, for comparison, is a 12-bonded *closo*-In_{16} found in $Na_{15}In_{27.4}$.[20] It can be seen that the geometries of the two are very similar.

Most of the distances in the modeled cluster as well as the two exo bonds are within the range of "normal" In–In distances and span from 2.80 (2) to 3.320 (9) Å. The two distances from InC6 to In4 (in front in Figure 20a) are very long, 4.49 Å, but are marked in the figure. There are only six relatively short distances in the whole formation. These are two distances of

2.36 (2) Å between InC6 and C7, two of 2.47 (2) Å between InC5 and C7, and two of 2.58 (2) Å between InC4 and C7. Notice that all of them include InC7, the atom with half occupancy and most anisotropic thermal ellipsoid. The arguments that we used to rationalize short distances associated with atoms with large thermal ellipsoids in the other two clusters are valid here as well.

A closer look at the electron density distributions on the entire surface of the Ni-centered clusters and the "upper" part of the surface of the Na1-centered cluster (see Figure 14) reveals that there are only a few islands that have near-zero electron density. Most of the surface is otherwise covered by the thermal ellipsoids of the atoms, especially at 94%. Another interesting observation is that these islands of zero electron density are always located directly below a "five-bonded" sodium atom from the outer deltahedron (Figures 21 to 23). Exactly the same positioning of "five-bonded" sodium atoms was also observed around isolated Z-centered indium clusters in $Na_{96}In_{\sim 97}Z_2$ (Z = Ni, Pd or Pt). We already discussed the fact that such sodium atoms are closer to the center of the deltahedra than the six "bonded" ones (above). (One can see in Figures 21 to 23 that the "five-bonded" sodium atoms are much closer to the plane of the pentagons to which they are bonded than the "six-bonded" atoms to the corresponding hexagons.) As a result of this, it is evidently impossible to locate an indium atom anywhere near both the central atom and a "five-bonded" sodium atom. On the other hand, the "six-bonded" sodium atoms can have indium atoms underneath although sometimes with very short but apparently possible distances. Such short distances are the following: 3.05 (1) Å for InA1–Na33, 2.92 (2) Å for InA5–Na13, 3.08 (1) Å for InA6–Na20, 3.04 (1) Å for InB1–Na22, 3.03 (2) Å for InB3–Na58, 2.86 (2) Å for InB4–Na64, 2.89 (2) Å for InB5–Na66, 3.12 (2) Å for InC2–Na16, 3.01 (1) Å for InC3–Na44, and 3.11 (2) Å for InC7–Na63. All are comparable with the shortest Na–In distances in $Na_7In_{11.8}$, 3.06 and 3.12 Å.[17] Even shorter distances of

about 2.8 Å were observed in $Na_{96}In_{\sim 97}Ni_2$. Such distances should not be surprising since the encapsulated indium clusters in sodium deltahedra are apparently compressed considerably by the outer fullerenes.

Since all isolated clusters found so far in the different sized fullerenes appear to contain 10 indium atoms, we can comprehend the different degree of compression they experience by comparing their average Ni–In distances. The ranges of Ni–In distances in M_{60} found in $Na_{96}In_{\sim 97}Ni_2$ and in $Na_{\sim 172}In_{\sim 197}Ni_2$ are 2.59(2)–2.716(6) (2.66(3) Å average) and 2.64(1)–2.699(8) Å (2.67(3) Å average), respectively. Although the clusters there have different geometries, the distances are practically identical and suggest that are defined to some extend by surrounding sodium atoms which, in turn, are fixed by the atoms of the fullerenes. Furthermore, we find longer Ni–In distances in larger sized fullerenes, 2.68(1)–2.801(8) Å (2.73(3) Å average) in In_{70} and 2.67(1)–2.90(5) Å (2.78(3) Å average) in In_{74}. This means that the In_{10} clusters may be quite flexible in terms of Ni–In distances. Smaller fullerenes apply higher degree of compression on the encapsulated sodium deltahedra. The sodium atoms in these deltahedra get, accordingly, close to the indium atoms in the encapsulated clusters and effectively compress them. This results in disk-like thermal ellipsoids for the indium atoms, shorter Ni–In contacts and also smaller In–In distances on the surface of the clusters.

The final result of all of the above considerations is that the inner indium atoms appear excluded from some regions but can be anywhere else on the surface of the cluster or, in other words, they "float". The only restricted places are the "islands" radially below "five-bonded" sodium atoms (Figure 24). This explains the observed disk-like thermal ellipsoids which cover most of the surface of the clusters. In summary, the positions of the pentagonal faces of the fullerene determine the positions of the "five-bonded" sodium atoms and they, in turn, define the positions of the "islands" of zero electron density on the surface of the cluster. That is why the

clusters inside the different fullerenes have seemingly different geometries although all appear to be of 10 indium atoms. Also, although each fullerene has 12 pentagonal faces, they have different location in the different sized fullerenes.

The situation discussed above also reminds one very much the so called incommensurate structures. In the latter, a mismatch between two layers or two rows of atoms with different periodicities occurs, and this causes similar problems when refining the structure as commensurate. In our case, the mismatch is between the atoms of two spheres, one of which has fixed position (the sodium) and the other one is free to take different, but not all orientations in respect to the first one. The incommensurability could be visualized as two infinite incommensurate rows of atoms wrapped an infinite number of times around a sphere and could be called circular or angular incommensurability.

Following the nomenclature proposed by Smalley et al,[27] the formula of one In_{70} cage, as an example, could be written as $Z@In_{10}@Na_{37}@In_{70}$ where Z = Ni, Pd or Pt. Although these cages are not isolated but rather fused with each other and lack the characteristic delocalized π-bonding system of C_{60} etc., we still can call them fullerenes because they resemble the structures proposed by the late Fuller.

Besides $Na_{96}In_{\sim 97}Z_2$ and $Na_{\sim 172}In_{\sim 197}Z_2$, there is another precedent of a cage-built structure. Nesper in his *Habilitationsschrift* describes very briefly an unpublished structure containing fused Al_{76} cages.[28] The compound has an approximate composition $LiMgAl_2$ and although the structure has been refined down to R/R_w = 6.6/5.6%, there are many uncertainties remaining. It is built of Al_{76} cages fused through all twelve pentagonal faces to other cages of the same type. Each cage has C_{3v} symmetry (no center of symmetry). Six of the pentagonal faces are in the equatorial plane of the cage and are nearly equidistant from each other. The remaining six pentagons are near the poles, three in each hemisphere. They define two triangles

that are staggered to each other and parallel to the equatorial plane with the other six pentagons. If the cage is sliced through the three planes (the equatorial plus the two triangles of pentagons) the positions of the pentagons in these planes form close-packed layers stacked in a cubic ABC-type order. Since each pentagon is shared with another Al_{76} cage, the cages also form close-packed layers stacked in a cubic order. Unfortunately, only the Al sites building the cages and a few Li and Mg sites have been unambiguously identified. Most of the cationic sites have been refined with mixed Li and Mg contents, some partially occupied. Also, the aluminum cages apparently contain some kind of isolated aluminum cluster at the center. The refinement of the latter experienced similar problems to those in our refinement of the central clusters in the indium cages. In the case of the Al_{76} cages, though, it was not clear what kind of atoms were building the central cluster. These have been refined with 6 Al atoms in a trigonal prism centered by partially occupied Mg site. The rectangular faces and the triangular ends of the prism are capped and bridged, respectively, by partially occupied Mg sites. Like those building the clusters inside the indium cages, the atoms in the encapsulated clusters inside the aluminum cages refine with large highly anisotropic thermal ellipsoids and also with partial occupancies. The clusters are thought to be disordered throughout the structure, and a model for a cluster with reasonable atomic distances was not found. Furthermore, it seems that two spherical shells of cations between the central cluster and the aluminum cage are proposed, and from our experience with the indium cages this seems to be very unlikely. Usually, alternating cationic and anionic shells are observed. The number of cations in the inner shell is only estimated by refining many sites close to each other with partial magnesium occupancies. The shell closer to the cage was refined with 40 atomic positions, many of them of mixed Li and Mg content, that cap from within all 40 faces of the aluminum cage. Other sites, partially occupied by Mg cap the faces of the cage from the outside. This is remarkably similar to the positioning of the

sodium cations inside and outside the indium cages. The uncertainties in the contents of many of the cationic sites as well as the central cluster hindered the determination of the real formula of Nesper's compound. Nevertheless, his structure is another example of the diversity in the chemistry of the elements of the boron family. By adding Al_{76}, the list of different size cages that are known becomes impressive: M_{60} ($In_{48}Na_{12}$), In_{70}, In_{74}, Al_{76} and In_{78}. We can say "so long" to the uniqueness of the carbon fullerenes.

The chemistry of indium with negative oxidation states has shown remarkable diversity. It spans from truly intermetallic compounds, such as KIn_4 and $RbIn_4$[29] ($BaAl_4$-type structures), with metallic and more or less nondirectional type bonding of 8-coordinate indium atoms to indeed molecular ions in Na_2In where covalent (directional) type bonding of 3-bonded In atoms forming In_4^{8-} "molecules" takes place.[20] Moreover, this range of oxidation states is covered quite densely by a large number of compounds with different structures and similar stoichiometries. The ability of indium to exist as three-, four-, five-, six- and even seven-bonded in one and the same compound has produced an amazing structural variety. Simply by increasing or decreasing the ratio of less-bonded to more-bonded atoms, the compounds can in parallel accommodate more or fewer electrons. This, in other words, means that if space is available for any particular number of cations, an almost continuous range of compounds would be possible between the structures of KIn_4 and Na_2In. A very good example is the existence of the compounds $K_{22}In_{39}$ and $K_{15}Na_8In_{39}$ where one additional electron in the second causes two 4-bonded indium atoms to become 3-bonded and two 6-bonded indium atoms to become 5-bonded while the rest of the structure remains the same.[19] Notice that the difference in the stoichiometries of the two compounds is only one cation per total of 61 atoms.

Another structural benefit for indium (but not only for indium) is the ability to mimic some of the structural specificities of the elements of main group four (tetralides, Tt). As an

example, In^{1-} (electronically equivalent to Tt) forms a diamond-type network in NaIn[30] (NaTl-type) and In^{2-} (electronically equivalent to Tt^{1-}) forms tetrahedra like Sn^{1-} in NaSn.[31] It is not so surprising then that indium with an oxidation state approximately -1 can form fullerene-type structures related to those that carbon forms. Different sizes fullerene-type cages of indium can form around isolated central clusters in the presence of elements (Ni, Pd, Pt) known to have a tendency for cluster centering and enough alkali-metal atoms to provide a nearly -1 formal charge on the indium atoms (mostly 4-bonded). The sizes of these cages and the connectivity between them will probably depend upon many factors one of which will be the formal oxidation state of indium, that is the atomic ratio Na : In. The formal oxidation state on the indium atoms in $Na_{96}In_{\sim 97}Ni_2$ is practically -1 (Na : In ≈ 1 : 1), and therefore mainly 4-bonded indium atoms are expected throughout the structure. Indeed, only 14 of the 77 (18%) indium atoms in the fused 74-atom fullerene network have more than four bonds (12 are 5- and 2 are 6-bonded). In $Na_{\sim 172}In_{\sim 197}Z_2$ the ratio Na : In is less, 0.9 : 1.0, and therefore more indium atoms with more bonds are found. Out of the 174 (41%) building the fused 70- and 78-atom fullerenes, 46 are 5- and 26 are 6-bonded.

REFERENCES

1. Krätschmer, W.; Lamb, L. D.; Fostiropoulos, K.; Huffman, D. R. *Nature* **1990**, *347*, 354.

2. *Fullerenes: Synthesis, Properties, and Chemistry of Large Carbon Clusters*, American Chemical Society Symposium Series, vol. 481, Washington, DC **1992**.

3. Hawkins, J. M.; Meyer, A.; Lewis, T. A.; Loren, S. in *Fullerenes: Synthesis, Properties, and Chemistry of Large Carbon Clusters*, American Chemical Society Symposium Series, vol. 481, Washington, DC **1992**, p. 91.

4. Balch, A. L.; Catalano, V. J.; Lee, J. W.; Olmstead, M. M.; Parkin, S. R. *J. Am. Chem. Soc.* **1991**, *113*, 3704.

5. Schmalz, T. G.; Seitz, W. A.; Klein, D. J.; Hite, G. E. *J. Am. Chem. Soc.* **1988**, *110*, 1113.

6. Fowler, P. W.; Cremona, J. E.; Steer, J. I. *Theor. Chim. Acta* **1988**, *73*, 1.

7. Kroto, H. W., Heath, J. R.; O'Brien, S. C.; Curl, R. F.; Smalley, R. E. *Nature* **1985**, *318*, 162.

8. Kroto, H. W. *Nature*, **1987**, *329*, 529.

9. Manolopoulos, D. E. *J. Chem. Soc. Faraday Trans.* **1991**, *87*, 2861.

10. Chai, Y.; Guo, T.; Jin, C.; Haufler, R. E.; Chibante, L. P. F.; Fure, J.; Wang, L.; Alford, J. M.; Smalley, R. E. *J. Phys. Chem.* **1991**, *95*, 7564.

11. Johnson, R. D.; de Vries, M. S.; Salem, J.; Bethune, D. S.; Yannony, C. S. *Nature* **1992**, *355*, 239.

12. Weaver, J. H.; Chai, Y.; Kroll, G. H.; Jin, C.; Ohno, T. R.; Haufler, R. E.; Guo, T.; Alford, J. M.; Conceicao, J.; Chibante, L. P. F.; Jain, A.; Palmer, G.; Smalley, R. E. *Chem. Phys. Letters* **1990**, *190*, 460.

13. Shinohara, H.; Sato, H.; Saito, Y.; Ohkohchi, M.; Ando, Y. *J. Phys. Chem.* **1992**, *96*, 3571.

14. Yannoni, C. S.; Hoinkis, M.; de Vries, M. S.; Bethune, D. S.; Salem, J. R.; Crowder, M. S.; Johnson, R. D. *Science* **1992**, *256*, 1191.

15. Shinohara, H.; Sato, H.; Saito, Y.; Ohkohchi, M.; Ando, Y.; Kato, T.; Kodama, T.; Shida, T. *Nature* **1992**, *357*, 52.

16. Haddon, R. C.; Hebard, A. F.; Rosseinsky, M. J.; Murphy, D. W.; Glarum, S. H.; Palstra, T. T. M.; Ramirez, A. P.; Duclos, S. J.; Fleming, R. M.; Siegrist, T, Tycko, R. in *Fullerenes: Synthesis, Properties, and Chemistry of Large Carbon Clusters*, American Chemical Society Symposium Series, vol. 481, Washington, DC **1992**, p. 71.

17. Sevov, S. C.; Corbett, J. D. *Inorg. Chem.* **1992**, *31*, 1895.

18. Some of the lines on the powder patterns matched some calculated for $K_{10}In_{10}Z$.[19]

19. Sevov, S. C.; Corbett, J. D. unpublished research.

20. Sevov, S. C.; Corbett, J. D. *J. Sol. State Chem.* **1993**, *103*, in press.

21. Fowler, P. W.; Batten, R. C.; Manolopoulos, D. E. *J. Chem. Soc. Faraday Trans.* **1991**, *87*, 3103.

22. Liu, X.; Schmalz, T. G.; Klein, D. J. *Chem. Phys. Lett.* **1992**, *188*, 550.

23. Zhang, B. L.; Wang, C. Z.; Ho, K. M. *Chem. Phys. Lett.* **1992**, *193*, 225.

24. Diederich, F.; Whetten, R. L.; Thilgen, C.; Ettl, R.; Chao, I.; Alvarez, M. M. *Science* **1991**, *254*, 1768.

25. Colt, J. R.; Scuseria, G. E. *Chem. Phys. Lett.* **1992**, *199*, 505.

26. Kikuchi, K.; Nakahara, N.; Wakabayashi, T.; Suzuki, S.; Shiromaru, H.; Miyake, Y.; Saito, K., Ikemoto, I.; Kainosho, M.; Achiba, Y. *Nature*, **1992**, *357*, 142.

27. Guo, T.; Jin, C.; Smalley, R. E. *J. Phys. Chem.* **1991**, *95*, 4948.

28. Nesper, R. *Habilitationsschrift* **1988**, Universität Stuttgart.

29. Thümmel, R.; Klemm, W. *Z. Anorg. All. Chem.* **1970**, *376*, 44.

30. Zintl, E.; Neumayr, S. *Z. Phys. Chem.* **1933**, *20B*, 272.

31. Müller, W.; Volk, K. *Z. Naturforsch.* **1977**, *32B*, 709.

Table I. Data collection and refinement parameters for $Na_{171.85(5)}In_{197.1(2)}Ni_2$

Formula weight	26705
Crystal size, mm	0.15 × 0.20 × 0.30
Lattice parameters:[a]	
a, Å	15.988(5)
b, Å	26.102(7)
c, Å	47.59(6)
V, Å^3	19860(36)
Space group, Z	*Pmmn* (#59), 2
d(calc.), g cm^{-3}	4.46
μ(Mo–Kα), cm^{-1}	113.12
Transmission range	0.6742–1.0000
Diffractometer	CAD4
Radiation	Mo–Kα (λ = 0.71069 Å) graphite-monochromated
Temperature, °C	23
Octants measured	*h, k, l*
Scan method	ω
$2\theta_{max}$	50°
Number of reflections:	
measured	18823
indep. observed ($I \geq 3\sigma_I$)	8120
Number of variables	1000
R; R_w,[b] %	6.0; 6.7
Goodness of fit indicator	1.62
Maximum shift/σ in final cycle	0.03
Largest peaks in final ΔF map	+5.3 e/Å^3 (0.45 Å from Na30) -4.1 e/Å^3
Secondary ext. coeff.	1.2(2) × 10^{-9}

[a] Room temperature Guinier data with Si as an internal standard (λ = 1.540562 Å).

[b] $R = \Sigma||F_o| - |F_c||/\Sigma|F_o|$; $R_w = [\Sigma w(|F_o| - |F_c|)^2/\Sigma w(F_o)^2]^{1/2}$; $w = \sigma_F^{-2}$.

Table II. Positional and isotropic equivalent displacement parameters for $Na_{171.85(5)}In_{197.1(2)}Ni_2$

atom	N	x	y	z	B_{eq}	occup.	No. at./clust.
In1	2b	3/4	1/4	0.26040(9)	1.4(2)		
In2	4f	0.3443(2)	3/4	0.11108(6)	1.6(1)		
In3	8g	0.4369(1)	0.65645(9)	0.09142(4)	1.4(1)		
In4	4f	0.3448(2)	3/4	0.51146(6)	1.3(1)		
In5	4e	1/4	0.6581(1)	0.20301(6)	1.5(1)		
In6	8g	0.6548(1)	0.4373(1)	0.17040(4)	1.34(9)		
In7	4e	1/4	0.5385(1)	0.32785(6)	1.5(1)		
In8	8g	0.4400(1)	0.4654(1)	0.08901(4)	1.5(1)		
In9	8g	0.6556(1)	0.4379(1)	0.27854(4)	1.36(9)		
In10	8g	0.5576(1)	0.34286(9)	0.18883(4)	1.4(1)		
In11	4e	1/4	0.4663(1)	0.20202(7)	1.5(1)		
In12	8g	0.4397(1)	0.5623(1)	0.12826(4)	1.47(9)		
In13	8g	0.4148(1)	0.6944(1)	0.35840(4)	1.5(1)		
In14	4f	0.4141(2)	3/4	0.45390(6)	1.4(1)		
In15	8g	0.3466(1)	0.63719(9)	0.30998(4)	1.4(1)		
In16	4e	1/4	0.5025(1)	0.38973(6)	1.4(1)		
In17	2b	1/4	3/4	0.1666(1)	1.7(2)		
In18	8g	0.3453(1)	0.5599(1)	0.07085(4)	1.6(1)		
In19	4f	0.5847(2)	3/4	0.34852(7)	1.9(1)		
In20	8g	0.4133(1)	0.65989(9)	0.41703(4)	1.4(1)		
In21	8g	0.4044(1)	0.30830(9)	0.15867(4)	1.3(1)		
In22	4e	3/4	0.5325(1)	0.09087(6)	1.5(1)		
In23	8g	0.5888(1)	0.69289(9)	0.06053(4)	1.5(1)		
In24	8g	0.5627(1)	0.46102(9)	0.38271(4)	1.31(9)		
In25	8g	0.6553(1)	0.36602(9)	0.39894(4)	1.34(9)		
In26	4e	1/4	0.5598(1)	0.49237(6)	1.9(1)		
In27	8g	0.5624(1)	0.4979(1)	0.32145(4)	1.4(1)		
In28	8g	0.5957(1)	0.4984(1)	0.12171(4)	1.5(1)		
In29	8g	0.4106(1)	0.4610(1)	0.41652(4)	1.5(1)		
In30	4f	0.6543(2)	1/4	0.20652(6)	1.3(1)		
In31	8g	0.4105(1)	0.36757(9)	0.45389(4)	1.5(1)		
In32	4e	1/4	0.3728(1)	0.16407(6)	1.4(1)		
In33	4e	1/4	0.4673(1)	0.52916(6)	2.0(2)		
In34	4e	3/4	0.3418(1)	0.29589(6)	1.5(1)		
In35	8g	0.3445(1)	0.3684(1)	0.10680(4)	1.6(1)		
In36	8g	0.4094(1)	0.5342(1)	0.29340(4)	1.5(1)		
In37	8g	0.3463(1)	0.5636(1)	0.18350(4)	1.6(1)		
In38	8g	0.3450(1)	0.36979(9)	0.51270(4)	1.5(1)		
In39	8g	0.3449(1)	0.5621(1)	0.43639(4)	1.6(1)		
In40	8g	0.5844(1)	0.65772(9)	0.38386(4)	1.6(1)		
In41	8g	0.6546(1)	0.5580(1)	0.36605(4)	1.5(1)		
In42	8g	0.4367(1)	0.69103(9)	0.55649(4)	1.4(1)		
In43	8g	0.5843(1)	0.69348(9)	0.44227(4)	1.5(1)		
In44	8g	0.4088(1)	0.4987(1)	0.23248(4)	1.5(1)		
In45	4e	1/4	0.3084(1)	0.46672(6)	1.5(1)		
In46	4e	1/4	0.6936(1)	0.26430(7)	1.7(1)		
In47	8g	0.5612(1)	0.4389(1)	0.22441(4)	1.35(9)		

Table II. (continued)

atom	N	x	y	z	B_{eq}	occup.	No. at./clust.
In48	8g	0.6522(2)	0.6340(1)	0.00691(4)	1.8(1)		
In49	4e	3/4	0.6361(1)	0.06511(6)	1.3(1)		
In50	4e	3/4	0.3065(1)	0.35420(6)	1.3(1)		
In51	4e	3/4	0.5380(1)	0.02541(7)	1.7(1)		
In52	8g	0.4155(3)	0.4825(2)	0.48714(9)	2.7(2)	59(1)%	
In53	4f	0.665(1)	3/4	0.3997(4)	2.0(10)	30(2)%	
NiA	2a	1/4	1/4	0.3114(1)	0.8(3)		
InA1	8g	0.2198(5)	0.1530(2)	0.3290(1)	6.5(5)	50(1)%	2.00(4)
InA2	4f	0.3759(8)	1/4	0.3505(3)	10.2(9)	50(4)%	1.00(8)
InA3	8g	0.1075(6)	0.1883(4)	0.3165(3)	11.5(7)	50(2)%	2.00(8)
InA4	8g	0.1083(5)	0.2084(4)	0.2879(2)	8.5(5)	50(2)%	2.00(8)
InA5	4f	0.196(1)	1/4	0.3647(2)	8.8(7)	50(4)%	1.00(8)
InA6	8g	0.2224(6)	0.1924(3)	0.2652(1)	7.6(5)	50(1)%	2.00(4)
							10.0(2)
NiB	2b	3/4	1/4	0.0492(1)	1.0(3)		
InB1	8g	0.6576(3)	0.1936(2)	0.0847(1)	10.7(3)	100(1)%	4.00(4)
InB2	2b	3/4	1/4	0.9937(1)	13.2(8)	100(1)%	1.00(1)
InB3	8g	0.7062(8)	0.1558(3)	0.0349(3)	19.0(10)	57(1)%	2.28(4)
InB4	8g	0.634(1)	0.1932(7)	0.0235(3)	14.0(10)	35(1)%	1.40(4)
InB5	4f	0.5901(5)	1/4	0.0310(2)	8.8(6)	70(1)%	1.4(2)
							10.08(7)
InC1	4f	0.6559(3)	3/4	0.29277(8)	3.4(2)	100(1)%	2.00(2)
InC2	4e	3/4	0.6497(2)	0.2738(1)	4.0(2)	100(1)%	2.00(2)
InC3	8g	0.0826(2)	0.1864(2)	0.75463(9)	7.5(2)	88(1)%	3.52(4)
InC4	4e	1/4	0.1210(3)	0.7853(1)	15.0(7)	86(2)%	1.72(4)
InC5	4e	1/4	0.1963(4)	0.8364(1)	18.0(8)	78(2)%	1.56(4)
InC6	4f	0.0801(5)	1/4	0.8109(1)	23.0(10)	80(1)%	1.60(2)
InC7	8g	0.1263(9)	0.1640(8)	0.8109(3)	27.0(10)	50(1)%	2.00(4)
							14.4(1)
Na1	2a	1/4	1/4	0.7740(4)	-0.2(3)		
Na2	4e	1/4	0.4452(7)	0.4579(3)	2.0(8)		
Na3	4e	3/4	0.4408(7)	0.3453(3)	2.0(3)		
Na4	4f	0.563(1)	3/4	0.5073(3)	3.0(10)		
Na5	2a	1/4	1/4	0.1969(5)	2.0(10)		
Na6	2a	1/4	1/4	0.1226(5)	3.0(10)		
Na7	8g	0.5946(8)	0.0615(5)	0.4533(3)	2.6(6)		
Na8	2b	3/4	1/4	0.4195(5)	2.0(10)		
Na9	4e	3/4	0.1307(9)	0.8712(4)	3.0(10)		
Na10	4e	3/4	0.0186(7)	0.4119(3)	2.1(8)		
Na11	8g	0.0574(8)	0.0611(5)	0.5673(2)	2.2(5)		
Na12	4e	1/4	0.1848(7)	0.0504(4)	2.5(9)		
Na13	4f	0.126(1)	1/4	0.4215(4)	3.0(10)		
Na14	8g	0.5757(8)	0.1761(5)	0.2560(2)	2.5(6)		
Na15	4f	0.560(1)	1/4	0.7081(4)	4.0(10)		
Na16	4e	1/4	0.0448(6)	0.6945(3)	1.7(8)		
Na17	4e	1/4	0.0497(8)	0.8394(4)	3.0(10)		
Na18	4e	1/4	0.0093(8)	0.1272(4)	2.3(9)		

Table II. (continued)

atom	N	x	y	z	B_{eq}	occup.	No. at./clust.
Na19	4e	3/4	0.0036(8)	0.2238(4)	3.0(10)		
Na20	8g	0.1294(8)	0.1291(5)	0.2203(2)	2.7(6)		
Na21	4e	3/4	0.1775(7)	0.1572(4)	1.7(8)		
Na22	8g	0.5442(8)	0.1277(6)	0.1210(2)	2.7(6)		
Na23	4e	3/4	0.1275(7)	0.6213(3)	1.6(3)		
Na24	8g	0.0619(8)	0.0653(6)	0.9381(3)	3.2(7)		
Na25	4e	1/4	0.1187(7)	0.5785(4)	3.0(10)		
Na26	4f	0.052(1)	1/4	0.8767(3)	3.0(10)		
Na27	4e	3/4	0.1735(7)	0.9395(4)	2.2(8)		
Na28	4e	3/4	0.0877(7)	0.1099(3)	2.0(8)		
Na29	4f	0.054(1)	1/4	0.2211(4)	2.1(8)		
Na30	2b	3/4	1/4	0.6666	5.0(8)		
Na31	4e	1/4	0.057(1)	0.2770(4)	4.0(10)		
Na32	2a	1/4	1/4	0.5282(5)	2.0(10)		
Na33	8g	0.1265(7)	0.0553(6)	0.3451(2)	2.6(6)		
Na34	4e	3/4	0.0664(8)	0.7464(3)	2.3(9)		
Na35	4f	0.588(1)	1/4	0.9549(4)	3.0(10)		
Na36	4e	1/4	0.1311(8)	0.4009(4)	3.0(10)		
Na37	2a	3/4	3/4	0.3994(6)	1.8(7)	85(5)%	
Na38	4f	0.605(1)	1/4	0.7787(3)	3.0(10)		
Na39	2b	3/4	1/4	0.5967(6)	4.0(20)		
Na40	8g	0.0461(8)	0.1496(5)	0.3868(3)	2.7(6)		
Na41	8g	0.0882(9)	0.0551(6)	0.7429(3)	3.5(7)		
Na42	8g	0.0665(9)	0.0535(6)	0.1636(2)	3.3(7)		
Na43	4f	0.051(1)	1/4	0.0924(4)	3.0(10)		
Na44	8g	0.5785(8)	0.1268(5)	0.7579(3)	3.0(7)		
Na45	4f	0.605(1)	1/4	0.3131(4)	3.0(10)		
Na46	8g	0.0353(8)	0.1415(5)	0.0504(3)	3.0(6)		
Na47	4e	3/4	0.1476(7)	0.4630(4)	2.1(8)		
Na48	8g	0.088(1)	0.0211(5)	0.0192(2)	3.1(7)		
Na49	8g	0.5559(8)	0.1348(5)	0.5102(2)	2.4(6)		
Na50	4f	0.577(1)	1/4	0.3815(3)	1.8(8)		
Na51	2a	1/4	1/4	0.8997(6)	2.9(6)		
Na52	8g	0.5594(8)	0.0634(6)	0.6327(2)	2.5(6)		
Na53	4f	0.581(1)	1/4	0.1435(4)	3.0(10)		
Na54	8g	0.0490(9)	0.0855(5)	0.2824(2)	2.8(6)		
Na55	4e	1/4	0.055(1)	0.0585(4)	5.0(10)		
Na56	8g	0.1258(9)	0.1286(5)	0.8778(3)	3.0(7)		
Na57	4e	3/4	0.1721(7)	0.5380(4)	2.5(9)		
Na58	8g	0.6315(8)	0.0555(6)	0.0551(2)	3.4(7)		
Na59	4e	3/4	0.1336(9)	0.2236(4)	3.0(10)		
Na60	4e	1/4	0.1707(9)	0.6574(3)	3.0(10)		
Na61	2a	1/4	1/4	0.9718(6)	3.0(10)		
Na62	8g	0.5766(8)	0.1296(6)	0.3323(2)	2.8(6)		
Na63	8g	0.0514(9)	0.0540(7)	0.8132(2)	4.2(7)		
Na64	8g	0.557(1)	0.1327(6)	0.9806(2)	3.9(7)		
Na65	8g	0.0569(9)	0.1321(5)	0.6868(2)	3.0(6)		
Na66	4f	0.073(1)	1/4	0.0050(4)	4.0(10)		
Na67	4e	3/4	0.0693(9)	0.9903(4)	3.0(10)		
Na68	8g	0.571(1)	0.1736(6)	0.8361(3)	3.7(8)		

Table III. Anisotropic displacement parameters for $Na_{\sim 172}In_{\sim 197}Ni_2$

atom	U_{11}	U_{22}	U_{33}	U_{12}	U_{13}	U_{23}
In1	0.019(2)	0.014(3)	0.019(2)	0.0	0.0	0.0
In2	0.019(2)	0.015(2)	0.026(2)	0.0	0.006(2)	0.0
In3	0.018(1)	0.014(1)	0.021(1)	0.001(1)	0.003(1)	0.004(1)
In4	0.016(2)	0.020(2)	0.012(1)	0.0	0.000(1)	0.0
In5	0.025(2)	0.017(2)	0.016(2)	0.0	0.0	0.002(2)
In6	0.018(1)	0.018(1)	0.015(1)	0.001(1)	0.002(1)	0.005(1)
In7	0.017(2)	0.020(2)	0.019(2)	0.0	0.0	0.003(2)
In8	0.017(1)	0.017(1)	0.024(1)	0.003(1)	-0.004(1)	0.002(1)
In9	0.018(1)	0.019(1)	0.014(1)	0.001(1)	-0.000(1)	-0.003(1)
In10	0.022(1)	0.015(1)	0.017(1)	0.000(1)	-0.003(1)	0.000(1)
In11	0.018(2)	0.014(2)	0.024(2)	0.0	0.0	-0.005(2)
In12	0.020(1)	0.018(1)	0.017(1)	0.003(1)	0.002(1)	0.001(1)
In13	0.023(1)	0.018(1)	0.015(1)	-0.005(1)	-0.002(1)	0.000(1)
In14	0.024(2)	0.012(2)	0.018(2)	0.0	0.002(2)	0.0
In15	0.020(1)	0.014(1)	0.020(1)	-0.000(1)	-0.002(1)	-0.002(1)
In16	0.020(2)	0.020(2)	0.014(1)	0.0	0.0	0.002(2)
In17	0.025(3)	0.017(3)	0.022(2)	0.0	0.0	0.0
In18	0.019(1)	0.017(1)	0.026(1)	-0.002(1)	-0.003(1)	0.000(1)
In19	0.021(2)	0.018(2)	0.034(2)	0.0	0.005(2)	0.0
In20	0.024(1)	0.015(1)	0.014(1)	-0.002(1)	-0.001(1)	-0.000(1)
In21	0.015(1)	0.014(1)	0.021(1)	0.000(1)	-0.003(1)	-0.001(1)
In22	0.018(2)	0.017(2)	0.022(2)	0.0	0.0	0.004(2)
In23	0.018(1)	0.015(1)	0.025(1)	0.003(1)	0.002(1)	-0.001(1)
In24	0.016(1)	0.014(1)	0.019(1)	0.002(1)	0.003(1)	0.003(1)
In25	0.017(1)	0.016(1)	0.017(1)	0.002(1)	0.003(1)	0.004(1)
In26	0.037(2)	0.018(2)	0.016(2)	0.0	0.0	-0.002(2)
In27	0.019(1)	0.019(1)	0.014(1)	0.003(1)	-0.002(1)	-0.005(1)
In28	0.017(1)	0.019(1)	0.018(1)	0.001(1)	-0.000(1)	0.003(1)
In29	0.019(1)	0.017(1)	0.021(1)	0.003(1)	0.004(1)	0.001(1)
In30	0.019(2)	0.015(2)	0.014(1)	0.0	-0.003(1)	0.0
In31	0.019(1)	0.016(1)	0.022(1)	0.005(1)	0.004(1)	0.001(1)
In32	0.017(2)	0.019(2)	0.017(2)	0.0	0.0	-0.005(1)
In33	0.045(2)	0.015(2)	0.015(2)	0.0	0.0	0.000(1)
In34	0.026(2)	0.013(2)	0.017(2)	0.0	0.0	-0.003(1)
In35	0.018(1)	0.021(1)	0.020(1)	-0.001(1)	0.001(1)	0.003(1)
In36	0.018(1)	0.022(1)	0.018(1)	0.007(1)	-0.002(1)	-0.002(1)
In37	0.021(1)	0.020(1)	0.019(1)	0.003(1)	0.003(1)	0.002(1)
In38	0.018(1)	0.021(1)	0.016(1)	0.002(1)	-0.000(1)	0.000(1)
In39	0.021(1)	0.014(1)	0.026(1)	-0.003(1)	0.005(1)	-0.001(1)
In40	0.026(1)	0.016(1)	0.017(1)	0.005(1)	0.001(1)	-0.001(1)
In41	0.021(1)	0.014(1)	0.022(1)	0.000(1)	-0.000(1)	-0.003(1)
In42	0.018(1)	0.014(1)	0.020(1)	0.002(1)	0.003(1)	0.004(1)
In43	0.025(1)	0.016(1)	0.018(1)	0.003(1)	-0.003(1)	-0.001(1)
In44	0.020(1)	0.020(1)	0.016(1)	0.003(1)	-0.001(1)	-0.002(1)
In45	0.019(2)	0.014(2)	0.023(2)	0.0	0.0	-0.001(2)
In46	0.029(2)	0.013(2)	0.022(2)	0.0	0.0	-0.000(2)
In47	0.020(1)	0.019(1)	0.012(1)	0.005(1)	-0.001(1)	-0.001(1)
In48	0.023(1)	0.023(1)	0.021(1)	0.000(1)	-0.003(1)	0.000(1)
In49	0.017(2)	0.015(2)	0.017(2)	0.0	0.0	0.003(1)
In50	0.025(2)	0.014(2)	0.012(2)	0.0	0.0	0.000(1)

Table III. (continued)

atom	U_{11}	U_{22}	U_{33}	U_{12}	U_{13}	U_{23}
In51	0.031(2)	0.012(2)	0.023(2)	0.0	0.0	-0.001(2)
In52	0.025(2)	0.040(3)	0.038(2)	-0.001(2)	-0.007(2)	-0.011(2)
In53	0.02(1)	0.02(1)	0.02(1)	0.0	0.00(1)	0.0
NiA	0.012(4)	0.010(4)	0.009(4)	0.0	0.0	0.0
InA1	0.13(1)	0.025(3)	0.096(5)	-0.019(4)	0.020(4)	0.030(3)
InA2	0.12(1)	0.19(2)	0.086(8)	0.000	-0.081(7)	0.0
InA3	0.077(6)	0.114(8)	0.25(1)	-0.066(6)	0.013(8)	0.036(8)
InA4	0.054(5)	0.132(8)	0.136(7)	-0.034(5)	-0.041(5)	-0.048(6)
InA5	0.23(2)	0.054(7)	0.048(5)	0.0	0.075(7)	0.0
InA6	0.18(1)	0.060(4)	0.047(3)	0.025(6)	-0.044(5)	-0.036(3)
NiB	0.020(4)	0.016(4)	0.001(3)	0.0	0.0	0.0
InB1	0.124(3)	0.102(3)	0.183(4)	0.032(3)	0.111(3)	0.090(3)
InB2	0.15(1)	0.33(2)	0.015(4)	0.0	0.0	0.0
InB3	0.29(2)	0.046(5)	0.37(1)	-0.048(7)	-0.10(1)	-0.083(7)
InB4	0.17(1)	0.18(1)	0.19(1)	-0.15(1)	-0.132(9)	0.08(1)
InB5	0.031(4)	0.18(1)	0.129(7)	0.0	-0.022(5)	0.0
InC1	0.035(2)	0.048(3)	0.048(2)	0.0	0.008(2)	0.0
InC2	0.062(3)	0.034(3)	0.057(3)	0.0	0.0	0.008(2)
InC3	0.055(2)	0.099(3)	0.133(3)	-0.034(2)	0.021(2)	-0.035(3)
InC4	0.44(2)	0.048(4)	0.089(5)	0.0	0.0	0.018(4)
InC5	0.47(2)	0.153(8)	0.065(4)	0.0	0.0	0.041(5)
InC6	0.068(6)	0.76(4)	0.037(4)	0.0	0.037(4)	0.0
InC7	0.13(1)	0.60(2)	0.29(1)	-0.07(1)	-0.01(1)	0.35(1)
Na1	-0.003(4)					
Na2	0.03(1)	0.02(1)	0.02(1)	0.0	0.0	-0.007(9)
Na3	0.025(4)					
Na4	0.03(1)	0.06(1)	0.02(1)	0.0	0.007(9)	0.0
Na5	0.02(1)	0.02(2)	0.02(1)	0.0	0.0	0.0
Na6	0.04(2)	0.06(2)	0.01(1)	0.0	0.0	0.0
Na7	0.028(7)	0.024(7)	0.047(7)	-0.021(7)	-0.015(7)	0.011(7)
Na8	0.04(2)	0.03(2)	0.02(1)	0.0	0.00	0.0
Na9	0.02(1)	0.06(2)	0.04(1)	0.0	0.00	0.00(1)
Na10	0.03(1)	0.03(1)	0.017(9)	0.0	0.0	-0.006(9)
Na11	0.030(7)	0.034(8)	0.017(6)	-0.000(8)	-0.004(6)	0.013(6)
Na12	0.04(1)	0.01(1)	0.05(1)	0.0	0.00	0.00(1)
Na13	0.06(1)	0.03(1)	0.03(1)	0.0	-0.02(1)	0.0
Na14	0.031(8)	0.042(9)	0.022(6)	-0.011(7)	-0.019(6)	-0.001(6)
Na15	0.03(1)	0.06(2)	0.05(1)	0.0	-0.00(1)	0.0
Na16	0.04(1)	0.01(1)	0.017(9)	0.0	0.0	-0.006(7)
Na17	0.03(1)	0.04(1)	0.04(1)	0.0	0.00	0.01(1)
Na18	0.02(1)	0.03(1)	0.03(1)	0.0	0.0	0.01(1)
Na19	0.02(1)	0.06(1)	0.03(1)	0.0	0.00	0.00(1)
Na20	0.043(9)	0.036(9)	0.023(7)	0.005(8)	0.009(6)	0.003(7)
Na21	0.004(8)	0.02(1)	0.04(1)	0.0	0.0	-0.006(9)
Na22	0.036(8)	0.06(1)	0.007(6)	-0.001(8)	-0.007(6)	-0.005(6)
Na23	0.020(4)					

Table III. (continued)

atom	U_{11}	U_{22}	U_{33}	U_{12}	U_{13}	U_{23}
Na24	0.027(7)	0.037(9)	0.056(8)	-0.010(8)	-0.014(7)	0.000(8)
Na25	0.03(1)	0.02(1)	0.06(1)	0.0	0.00	-0.01(1)
Na26	0.07(1)	0.03(1)	0.008(8)	0.0	0.00(1)	0.0
Na27	0.05(1)	0.01(1)	0.03(1)	0.0	0.00	0.011(8)
Na28	0.03(1)	0.02(1)	0.03(1)	0.0	0.0	-0.001(9)
Na29	0.02(1)	0.02(1)	0.04(1)	0.0	-0.016(9)	0.0
Na30	0.06(1)					
Na31	0.05(1)	0.07(2)	0.04(1)	0.0	0.00	-0.03(1)
Na32	0.01(1)	0.04(2)	0.03(1)	0.0	0.0	0.0
Na33	0.020(7)	0.06(1)	0.019(6)	0.013(8)	0.003(5)	-0.008(7)
Na34	0.03(1)	0.04(1)	0.03(1)	0.0	0.0	-0.00(1)
Na35	0.02(1)	0.02(1)	0.08(1)	0.0	-0.01(1)	0.0
Na36	0.04(1)	0.03(1)	0.05(1)	0.0	0.0	-0.00(1)
Na37	0.023(8)					
Na38	0.06(1)	0.04(1)	0.02(1)	0.0	0.01(1)	0.0
Na39	0.07(2)	0.01(2)	0.05(2)	0.0	0.0	0.0
Na40	0.039(8)	0.015(7)	0.048(8)	-0.007(7)	-0.011(7)	-0.005(7)
Na41	0.041(9)	0.05(1)	0.039(8)	0.010(9)	-0.001(7)	0.010(7)
Na42	0.04(1)	0.05(1)	0.029(7)	-0.014(8)	0.010(7)	-0.014(7)
Na43	0.07(1)	0.01(1)	0.03(1)	0.0	0.00(1)	0.0
Na44	0.029(8)	0.027(8)	0.057(9)	-0.002(7)	-0.009(7)	0.004(7)
Na45	0.05(1)	0.05(1)	0.02(1)	0.0	0.02(1)	0.0
Na46	0.034(8)	0.04(1)	0.038(8)	-0.001(8)	0.000(7)	0.003(7)
Na47	0.008(9)	0.04(1)	0.04(1)	0.0	0.00	-0.00(1)
Na48	0.06(1)	0.04(1)	0.016(6)	-0.007(9)	-0.003(7)	-0.001(6)
Na49	0.035(8)	0.033(8)	0.025(7)	-0.004(8)	0.000(6)	0.003(6)
Na50	0.03(1)	0.002(9)	0.04(1)	0.0	0.014(9)	0.0
Na51	0.037(7)					
Na52	0.021(7)	0.046(9)	0.029(7)	-0.005(8)	-0.003(6)	0.015(7)
Na53	0.05(1)	0.02(1)	0.03(1)	0.0	-0.00(1)	0.0
Na54	0.042(8)	0.039(9)	0.027(7)	0.007(8)	0.001(7)	-0.002(7)
Na55	0.07(2)	0.07(2)	0.04(1)	0.00	0.00	-0.01(1)
Na56	0.05(1)	0.029(8)	0.040(8)	0.006(8)	0.001(7)	-0.013(7)
Na57	0.03(1)	0.02(1)	0.04(1)	0.0	0.00	0.01(1)
Na58	0.043(9)	0.06(1)	0.025(7)	0.019(9)	0.014(6)	-0.003(7)
Na59	0.03(1)	0.06(2)	0.02(1)	0.0	0.00	0.02(1)
Na60	0.05(1)	0.06(2)	0.005(8)	0.0	0.0	-0.00(1)
Na61	0.01(1)	0.04(2)	0.05(2)	0.0	0.00	0.0
Na62	0.034(8)	0.04(1)	0.029(7)	0.006(8)	0.002(6)	-0.008(7)
Na63	0.045(9)	0.10(1)	0.012(6)	0.03(1)	-0.006(6)	-0.007(8)
Na64	0.06(1)	0.07(1)	0.019(7)	0.03(1)	0.017(7)	0.011(7)
Na65	0.050(9)	0.04(1)	0.025(7)	0.015(8)	0.012(7)	0.006(7)
Na66	0.08(2)	0.02(1)	0.04(1)	0.0	-0.03(1)	0.0
Na67	0.03(1)	0.06(2)	0.03(1)	0.0	0.00	0.01(1)
Na68	0.04(1)	0.024(8)	0.07(1)	0.001(8)	0.011(8)	-0.005(8)

Table IV. Distances to nearest neighbors about each atom in $Na_{\sim 172}In_{\sim 197}Ni_2$ ($d \leq 4.00$ Å)

In1

2	In30	2.986(6)
2	In34	2.932(4)
4	Na14	3.40(1)
2	Na45	3.42(2)
2	Na59	3.51(2)

In2

	In2	3.016(7)
2	In3	3.005(3)
	In17	3.041(6)
2	Na9	3.56(2)
	Na26	3.37(2)
2	Na27	3.47(2)
	Na35	3.32(2)
2	Na68	3.49(2)

In3

	In2	3.005(3)
	In12	3.019(3)
	In18	3.074(3)
	In23	2.994(3)
	Na9	3.54(1)
	Na24	3.41(1)
	Na26	3.41(1)
	Na27	3.36(8)
	Na35	3.31(1)
	Na56	3.43(1)
	Na64	3.49(1)
	Na68	3.48(1)

In4

	In4	3.030(7
	In14	2.955(5)
2	In42	3.020(4)
	Na4	3.50(2)
	Na8	3.62(2)
2	Na47	3.30(2)
2	Na49	3.55(1)
2	Na57	3.46(2)

In5

	In17	2.961(4)
2	In37	3.052(4)
	In46	3.061(6)
	Na9	3.60(2)
	Na34	3.40(2)
2	Na38	3.44(2)
2	Na44	3.41(1)
2	Na68	3.44(1)

In6

	In6	3.043(4)
	In10	3.044(3)
	In28	2.967(4)
	In47	2.975(4)
	Na17	3.34(2)
	Na19	3.34(2)
	Na21	3.42(2)
	Na22	3.39(1)
	Na28	3.32(2)
	Na42	3.56(1)
	Na59	3.49(2)
	Na63	3.55(2)

In7

2	In15	3.121(4)
	In16	3.092(5)
2	In36	3.033(3)
	Na23	3.35(2)
	Na31	3.47(2)
2	Na33	3.25(1)
	Na34	3.61(2)
2	Na52	3.64(1)

In8

	In12	3.143(4)
	In18	3.020(3)
	In28	3.059(3)
	In35	3.077(3)
	Na18	3.60(1)
	Na22	3.32(1)
	Na24	3.50(1)
	Na42	3.58(1)
	Na46	3.37(1)
	Na48	3.37(1)
	Na55	3.41(1)
	Na58	3.50(1)

In9

	In9	3.018(4)
	In27	2.974(3)
	In34	3.041(4)
	In47	2.986(4)
	Na3	3.52(1)
	Na14	3.41(1)
	Na16	3.42(1)
	Na19	3.37(2)
	Na41	3.40(1)
	Na54	3.33(1)
	Na59	3.55(2)
	Na62	3.35(1)

In10

	In6	3.044(3)
	In21	2.979(3)
	In30	3.000(3)
	In47	3.025(3)
	Na14	3.25(1)
	Na20	3.42(1)
	Na21	3.466(8)
	Na22	3.32(1)
	Na29	3.38(1)
	Na42	3.56(1)
	Na53	3.27(1)
	Na59	3.548(9)

In11

	In32	3.036(5)
2	In37	3.097(4)
2	In44	3.044(3)
	Na18	3.62(2)
2	Na20	3.26(1)
	Na31	3.62(2)
	Na34	3.59(2)
2	Na42	3.50(1)

In12

	In3	3.019(3)
	In8	3.143(4)
	In18	3.122(4)
	In28	3.017(3)
	In37	3.024(4)
	Na9	3.52(1)
	Na18	3.56(1)
	Na24	3.71(1)
	Na42	3.46(1)
	Na56	3.45(1)
	Na63	3.32(1)
	Na68	3.37(1)

In13

	In13	2.903(4)
	In15	2.954(4)
	In19	3.116(4)
	In20	2.932(4)
	In40	3.121(3)
	Na15	3.50(2)
	Na23	3.30(1)
	Na30	3.235(2)
	Na39	3.69(2)
	Na52	3.47(1)
	Na65	3.52(1)

In14

	In4	2.955(5)
2	In20	2.935(3)
2	In43	3.144(4)
	Na4	3.49(2)
	Na39	3.56(2)
2	Na49	3.49(1)
2	Na57	3.34(1)

In15

	In7	3.121(4)
	In13	2.954(4)
	In15	3.089(5)
	In36	2.977(3)
	In46	3.046(4)
	Na15	3.41(1)
	Na23	3.62(1)
	Na30	3.507(2)
	Na34	3.60(2)
	Na44	3.46(1)
	Na52	3.66(1)
	Na65	3.37(1)

In16

	In7	3.091(5)
2	In29	3.064(3)
2	In39	3.107(4)
	Na2	3.57(2)
	Na23	3.30(2)
2	Na33	3.27(1)
	Na36	3.53(2)
2	Na52	3.60(1)

In17

2	In2	3.041(6)
2	In5	2.961(4)
2	Na9	3.59(2)
2	Na38	3.49(2)
4	Na68	3.49(1)

In18

	In3	3.074(3)
	In8	3.020(3)
	In12	3.122(4)
	In18	3.047(5)
	Na9	3.65(2)
	Na18	3.57(2)
	Na24	3.49(1)
	Na27	3.37(2)
	Na48	3.41(1)
	Na55	3.42(2)
	Na64	3.47(1)
	Na67	3.29(2)

Table IV. (continued)

In19

2 In13 3.116(4)
2 In40 2.938(3)
In53 2.75(2)
InCl 2.887(6)

Na15 3.55(2)
Na37 3.58(2)
2 Na60 3.37(1)
2 Na65 3.53(1)

In20

In13 2.932(4)
In14 2.935(3)
In39 2.925(3)
In40 3.159(3)
In43 3.112(3)

Na11 3.54(1)
Na23 3.29(1)
Na39 3.574(6)
Na49 3.56(1)
Na52 3.48(1)
Na57 3.39(1)

In21

In10 2.979(3)
In21 3.043(5)
In32 2.999(3)
In35 3.077(4)

Na5 3.42(1)
Na6 3.37(1)
Na20 3.40(1)
Na22 3.32(1)
Na29 3.40(1)
Na42 3.64(1)
Na43 3.57(2)
Na53 3.29(2)

In22

2 In28 3.006(3)
In49 2.971(5)
In51 3.119(6)

Na17 3.35(2)
2 Na24 3.42(1)
Na28 3.26(2)
2 Na56 3.53(1)
2 Na58 3.43(1)

In23

In3 2.994(3)
In23 2.981(5)
In48 3.146(4)
In49 2.980(3)

Na24 3.36(1)
Na26 3.39(1)
Na35 3.28(2)
Na51 3.53(1)
Na56 3.43(1)
Na61 3.35(1)
Na64 3.42(1)
Na66 3.46(2)

In24

In25 2.990(3)
In27 3.070(4)
In29 2.916(3)
In41 3.032(3)

Na3 3.523(9)
Na7 3.45(1)
Na10 3.344(8)
Na11 3.53(1)
Na33 3.54(1)
Na40 3.38(1)
Na52 3.39(1)
Na62 3.37(1)

In25

In24 2.990(3)
In25 3.028(5)
In42 2.980(4)
In50 3.040(4)

Na3 3.55(2)
Na7 3.35(1)
Na8 3.524(7)
Na10 3.43(2)
Na40 3.30(1)
Na47 3.42(1)
Na50 3.378(8)
Na62 3.41(1)

In26

In33 2.982(5)
2 In39 3.067(4)
2 In52 3.337(5)

Na2 3.41(2)
2 Na7 3.58(1)
Na47 3.12(2)
2 Na49 3.67(1)
Na57 3.27(2)

In27

In9 2.974(3)
In24 3.070(4)
In36 2.943(3)
In41 3.024(4)

Na3 3.53(1)
Na16 3.328(7)
Na33 3.51(1)
Na41 3.43(1)
Na52 3.39(1)
Na54 3.37(1)
Na62 3.37(1)
Na65 3.53(1)

In28

In6 2.967(4)
In8 3.059(3)
In12 3.017(3)
In22 3.006(3)

Na17 3.36(1)
Na22 3.39(1)
Na24 3.38(1)
Na28 3.38(1)
Na42 3.54(1)
Na56 3.43(1)
Na58 3.51(1)
Na63 3.49(1)

In29

In16 3.064(3)
In24 2.916(3)
In31 3.019(3)
In39 2.993(3)
In52 3.408(6)

Na2 3.26(1)
Na7 3.47(1)
Na11 3.59(1)
Na33 3.48(1)
Na36 3.59(1)
Na40 3.29(1)
Na52 3.58(1)

In30

In1 2.986(5)
2 In10 2.996(3)
In30 3.059(7)

2 Na14 3.29(1)
2 Na21 3.38(1)
Na29 3.41(2)
Na53 3.22(2)
2 Na59 3.50(2)

In31

In29 3.019(3)
In38 2.989(4)
In42 2.925(3)
In45 3.056(3)
In52 3.392(5)

Na2 3.27(1)
Na4 3.605(9)
Na7 3.48(1)
Na13 3.482(9)
Na36 3.60(1)
Na40 3.30(1)
Na49 3.55(1)

In32

In11 3.036(5)
2 In21 3.000(3)
2 In35 3.119(4)

Na5 3.56(1)
Na6 3.76(1)
Na18 3.54(2)
2 Na20 3.30(1)
2 Na42 3.51(1)

In33

In26 2.982(5)
2 In38 3.066(4)
2 In52 3.340(5)

Na2 3.44(2)
2 Na7 3.59(1)
Na10 3.11(2)
2 Na11 3.65(1)
Na25 3.25(2)

In34

In1 2.932(4)
2 In9 3.041(4)
In50 2.925(5)

Na3 3.49(2)
2 Na14 3.40(1)
2 Na45 3.43(1)
Na59 3.50(2)
2 Na62 3.35(1)

Table IV. (continued)

In35		In38		In41		In44		In47	
In8	3.077(3)	In31	2.989(4)	In24	3.032(3)	In11	3.044(3)	In6	2.975(4)
In21	3.077(4)	In33	3.066(4)	In27	3.024(4)	In36	3.043(4)	In9	2.986(4)
In32	3.119(4)	In38	3.037(5)	In40	2.959(3)	In37	3.049(4)	In10	3.025(3)
In35	3.022(5)	In43	2.933(4)	In41	3.049(5)	In47	2.919(3)	In44	2.919(3)
		In45	3.108(4)						
Na6	3.521(5)	In52	3.377(5)	Na3	3.56(2)	Na20	3.44(1)	Na14	3.36(1)
Na12	3.38(2)			Na10	3.33(1)	Na31	3.61(1)	Na19	3.37(1)
Na18	3.66(2)	Na2	3.60(1)	Na11	3.53(1)	Na34	3.25(1)	Na20	3.53(1)
Na22	3.26(1)	Na4	3.582(9)	Na16	3.28(1)	Na41	3.43(1)	Na41	3.44(1)
Na42	3.67(1)	Na11	3.53(1)	Na25	3.43(2)	Na42	3.57(1)	Na42	3.55(1)
Na43	3.58(1)	Na25	3.49(2)	Na52	3.42(1)	Na44	3.38(1)	Na54	3.33(1)
Na46	3.31(1)	Na32	3.553(6)	Na60	3.50(2)	Na54	3.30(1)	Na59	3.56(1)
Na55	3.40(2)	Na49	3.38(1)	Na65	3.54(1)	Na63	3.46(1)	Na63	3.50(2)
In36		**In39**		**In42**				**In48**	
						In45			
In7	3.033(3)	In16	3.107(4)	In4	3.020(4)			In23	3.146(4)
In15	2.977(3)	In20	2.925(3)	In25	2.980(4)	2	In31 3.056(3)	In48	3.126(5)
In27	2.943(3)	In26	3.067(4)	In31	2.925(3)	2	In38 3.108(4)	In49	3.181(4)
In44	3.043(4)	In29	2.993(3)	In42	3.079(5)		In45 3.050(7)	In51	3.083(4)
		In39	3.036(5)						
Na31	3.57(2)	In52	3.380(5)	Na4	3.46(1)		Na2 3.59(2)	Na12	3.41(2)
Na33	3.44(1)			Na7	3.45(1)	2	Na4 3.57(2)	Na24	3.49(1)
Na34	3.28(1)	Na2	3.56(2)	Na8	3.547(8)	2	Na13 3.30(2)	Na46	3.31(1)
Na41	3.38(1)	Na11	3.40(1)	Na13	3.55(2)		Na32 3.30(2)	Na48	3.36(1)
Na44	3.44(1)	Na23	3.57(1)	Na40	3.39(1)		Na36 3.51(2)	Na61	3.554(8)
Na52	3.63(1)	Na49	3.55(1)	Na47	3.325(9)			Na64	3.39(1)
Na54	3.23(1)	Na52	3.63(1)	Na49	3.50(1)		**In46**	Na66	3.33(1)
Na65	3.60(1)	Na57	3.47(2)	Na50	3.33(1)				
							In5 3.061(6)		
In37		**In40**		**In43**		2	In15 3.046(4)	**In49**	
							In46 2.943(7)		
In5	3.052(4)	In13	3.121(3)	In14	3.144(4)				In22 2.971(5)
In11	3.097(4)	In19	2.938(3)	In20	3.112(3)	2	Na15 3.62(2)	2	In23 2.980(3)
In12	3.024(4)	In20	3.159(3)	In38	2.933(4)		Na30 3.60(5)	2	In48 3.181(4)
In37	3.078(5)	In41	2.959(3)	In40	2.932(4)		Na34 3.36(2)		In51 3.184(5)
In44	3.049(4)	In43	2.932(4)	In43	2.950(5)	2	Na38 3.42(2)		
		In53	2.83(1)	In53	2.82(2)	2	Na44 3.42(1)	2	Na24 3.53(1)
Na9	3.49(2)								Na51 3.41(1)
Na18	3.63(2)	Na11	3.46(1)	Na4	3.45(1)			2	Na56 3.37(1)
Na34	3.68(1)	Na25	3.35(1)	Na11	3.51(1)				Na61 3.45(1)
Na42	3.49(1)	Na37	3.655(6)	Na25	3.44(1)				
Na44	3.46(1)	Na52	3.46(1)	Na32	3.34(1)				
Na63	3.29(1)	Na60	3.31(1)	Na37	3.65(1)				
Na68	3.30(1)	Na65	3.45(1)	Na49	3.53(1)				

Table IV. (continued)

In50

2	In25	3.040(4)
	In34	2.925(5)
	In50	2.948(7)
	Na3	3.53(2)
	Na8	3.44(2)
2	Na45	3.37(2)
2	Na50	3.39(1)
2	Na62	3.40(1)

In51

	In22	3.119(6)
2	In48	3.083(4)
	In49	3.184(5)
2	Na24	3.55(1)
2	Na48	3.38(1)
2	Na58	3.40(1)
	Na67	3.26(2)

In52

	In26	3.337(5)
	In29	3.408(6)
	In31	3.392(5)
	In33	3.340(5)
	In38	3.377(5)
	In39	3.380(5)
	In52	3.104(8)
	Na2	3.14(1)
	Na7	3.48(1)
	Na7	3.51(1)
	Na49	3.95(1)

In53

	In19	2.75(2)
2	In40	2.83(1)
2	In43	2.82(2)
	In53	2.72(4)
2	Na25	3.83(2)
	Na32	3.69(3)
	Na37	1.36(2)
2	Na60	3.68(2)

NiA

4	InA1	2.711(6)
2	InA2	2.74(1)
4	InA3	2.801(8)
4	InA4	2.750(7)
2	InA5	2.68(1)
4	InA6	2.700(8)

InA1

	NiA	2.711(6)
	InA1	0.97(1)
	InA2	3.70(1)
	InA2	3.13(1)
	InA3	2.10(1)
	InA3	2.97(1)
	InA4	3.02(1)
	InA4	3.67(1)
	InA5	3.074(8)
	InA5	3.334(9)
	InA6	3.208(9)
	InA6	3.338(9)
	Na31	3.56(2)
	Na33	3.05(1)
	Na33	3.62(1)
	Na36	3.50(2)
	Na40	3.91(1)
	Na54	3.93(1)

InA2

	NiA	2.74(1)
2	InA1	3.70(1)
2	InA1	3.13(1)
2	InA3	2.30(1)
2	InA4	3.18(1)
	InA5	2.95(2)
	InA5	1.33(2)
	Na13	3.38(2)
2	Na40	3.38(1)
	Na50	3.54(2)

InA3

	NiA	2.801(8)
	InA1	2.10(1)
	InA1	2.97(1)
	InA2	2.30(1)
	InA3	3.22(2)
	InA4	1.46(1)
	InA4	3.02(1)
	InA5	3.14(1)
	InA6	3.06(1)
	InA6	3.66(1)
	Na33	3.74(2)
	Na40	3.63(2)
	Na45	3.76(2)
	Na54	3.27(2)
	Na62	3.40(1)

InA4

	NiA	2.750(7)
	InA1	3.02(1)
	InA1	3.67(1)
	InA2	3.18(1)
	InA3	1.46(1)
	InA3	3.02(1)
	InA4	2.17(1)
	InA6	2.16(1)
	InA6	2.94(1)
	InA6	3.35(1)
	InA6	3.90(1)
	Na14	3.41(1)
	Na20	3.84(1)
	Na29	3.47(2)
	Na45	3.77(2)
	Na54	3.35(2)

InA5

	NiA	2.68(1)
2	InA1	3.074(8)
2	InA1	3.334(9)
	InA2	2.95(2)
	InA2	1.33(2)
2	InA3	3.14(1)
	InA5	1.73(3)
2	Na13	2.92(2)
2	Na36	3.65(2)
2	Na40	3.70(1)

InA6

	NiA	2.700(8)
	InA1	3.208(9)
	InA1	3.338(9)
	InA3	3.06(1)
	InA3	3.66(1)
	InA4	2.16(1)
	InA4	2.94(1)
	InA4	3.35(1)
	InA4	3.90(1)
	InA6	0.88(2)
	InA6	3.01(1)
	InA6	3.13(1)
	Na5	3.61(2)
	Na20	3.08(1)
	Na20	3.59(1)
	Na29	3.72(2)
	Na31	3.61(2)

NiB

4	InB1	2.685(5)
	InB2	2.64(1)
4	InB3	2.645(8)
4	InB4	2.67(1)
2	InB5	2.699(8)

InB1

	NiB	2.685(6)
	InB1	2.944(9)
	InB1	2.954(9)
	InB3	2.68(1)
	InB3	3.37(1)
	InB4	2.94(1)
	InB5	3.141(9)
	Na21	3.78(2)
	Na22	3.04(1)
	Na28	3.36(2)
	Na43	3.66(2)
	Na46	3.74(1)
	Na53	3.39(2)
	Na58	3.89(1)

InB2

	NiB	2.64(1)
4	InB3	3.22(1)
4	InB4	2.76(1)
2	InB5	3.11(1)
2	Na27	3.26(2)
2	Na35	3.18(2)

InB3

	NiB	2.645(8)
	InB1	2.68(1)
	InB1	3.37(1)
	InB2	3.22(1)
	InB3	1.40(3)
	InB4	1.60(2)
	InB4	2.78(2)
	InB5	3.09(1)
	Na46	3.95(2)
	Na58	3.03(2)
	Na58	3.81(2)
	Na64	3.57(2)
	Na67	3.18(2)

InB4

	NiB	2.67(1)
	InB1	2.94(1)
	InB2	2.76(1)
	InB3	1.60(2)
	InB3	2.78(2)
	InB4	2.96(3)
	InB4	3.70(3)
	InB5	1.68(2)
	Na35	3.66(2)
	Na46	3.29(2)
	Na58	3.90(2)
	Na64	2.86(2)
	Na66	3.74(3)

Table IV. (continued)

InB5

	NiB	2.699(8)
2	InB1	3.141(9)
	InB2	3.11(1)
2	InB3	3.09(1)
2	InB4	1.68(2)
	Na35	3.62(2)
	Na43	3.69(2)
2	Na46	3.59(1)
2	Na64	3.92(2)
	Na66	2.89(2)

InC1

	In19	2.887(6)
	InC1	3.009(8)
2	InC2	3.151(5)
2	InC3	3.036(6)
	Na1	3.52(2)
	Na15	3.45(2)
2	Na60	3.49(2)
2	Na65	3.59(1)

InC2

2	InC1	3.151(5)
2	InC3	3.149(5)
	InC4	2.911(8)
	Na1	3.47(1)
	Na16	3.12(2)
2	Na41	3.66(1)
	Na60	3.32(2)
2	Na65	3.64(1)

InC3

	InC1	3.036(6)
	InC2	3.150(5)
	InC3	3.320(9)
	InC4	3.493(6)
	InC6	3.150(8)
	InC7	2.83(1)
	Na1	3.282(6)
	Na15	3.59(2)
	Na38	3.61(2)
	Na41	3.47(2)
	Na44	3.01(1)
	Na65	3.55(1)

InC4

	InC2	2.911(8)
2	InC3	3.493(6)
	InC5	3.13(1)
2	InC7	2.58(2)
	Na1	3.409(7)
	Na17	3.18(2)
	Na19	3.28(2)
2	Na41	3.70(1)
2	Na63	3.86(2)

InC5

	InC4	3.13(1)
	InC5	2.80(2)
2	InC6	3.290(9)
2	InC7	2.47(2)
	Na1	3.28(2)
	Na17	3.83(2)
2	Na26	3.96(2)
	Na51	3.32(2)
2	Na56	3.31(1)

InC6

2	InC3	3.150(8)
2	InC5	3.290(9)
2	InC7	2.36(2)
	Na1	3.23(1)
	Na26	3.16(2)
	Na38	3.33(2)
2	Na68	3.35(1)

InC7

	InC3	2.83(1)
	InC4	2.58(2)
	InC5	2.47(2)
	InC6	2.36(2)
	InC7	3.95(3)
	Na1	3.47(1)
	Na17	3.83(2)
	Na56	3.32(2)
	Na63	3.11(2)
	Na68	3.38(2)

Na1

2	InC1	3.52(2)
2	InC2	3.47(1)
4	InC3	3.282(6)
2	InC4	3.409(7)
2	InC5	3.28(2)
2	InC6	3.23(1)
4	InC7	3.47(1)

Na2

	In16	3.57(2)
	In26	3.41(2)
2	In29	3.26(1)
2	In31	3.27(1)
	In33	3.44(2)
2	In38	3.60(1)
2	In39	3.56(2)
	In45	3.59(2)
2	In52	3.14(1)
	Na36	3.36(2)

Na3

2	In9	3.52(1)
2	In24	3.523(9)
2	In25	3.55(2)
2	In27	3.53(1)
	In34	3.49(2)
2	In41	3.56(2)
	In50	3.53(2)
	Na10	3.34(2)
	Na16	3.31(2)
2	Na62	3.38(2)

Na4

	In4	3.50(2)
	In14	3.49(2)
2	In31	3.605(9)
2	In38	3.582(9)
2	In42	3.46(1)
2	In43	3.45(1)
2	In45	3.57(2)
	Na13	3.53(2)
	Na32	3.43(2)
2	Na49	3.66(2)

Na5

4	In21	3.42(1)
2	In32	3.56(1)
4	InA6	3.61(2)
	Na6	3.53(3)
4	Na20	3.86(1)
2	Na29	3.33(2)

Na6

4	In21	3.37(1)
2	In32	3.76(1)
4	In35	3.521(5)
	Na5	3.53(3)
2	Na12	3.84(3)
2	Na43	3.49(2)

Na7

	In24	3.45(1)
	In25	3.35(1)
	In26	3.58(1)
	In29	3.47(1)
	In31	3.48(1)
	In33	3.59(1)
	In42	3.45(1)
	In52	3.48(1)
	In52	3.51(1)
	Na10	3.36(2)
	Na11	3.40(2)
	Na47	3.38(2)
	Na49	3.37(2)

Na8

2	In4	3.62(2)
4	In25	3.524(7)
4	In42	3.547(8)
2	In50	3.44(2)
2	Na47	3.38(2)
2	Na50	3.30(2)

Na9

2	In2	3.56(2)
2	In3	3.54(1)
	In5	3.60(2)
2	In12	3.52(1)
	In17	3.59(2)
2	In18	3.65(2)
2	In37	3.49(2)
	Na18	3.65(3)
	Na27	3.44(2)
2	Na68	3.50(2)

Na10

2	In24	3.344(8)
2	In25	3.43(2)
	In33	3.11(2)
2	In41	3.33(1)
	Na3	3.34(2)
2	Na7	3.36(2)
2	Na11	3.85(2)
	Na25	3.61(3)

Na11

	In20	3.54(1)
	In24	3.53(1)
	In29	3.59(1)
	In33	3.65(1)
	In38	3.53(1)
	In39	3.40(1)
	In40	3.46(1)
	In41	3.53(1)
	In43	3.51(1)
	Na7	3.40(2)
	Na10	3.85(2)
	Na25	3.47(1)
	Na49	3.79(2)
	Na52	3.63(2)

Table IV. (continued)

Na12

2	In35	3.38(2)
2	In48	3.41(2)
	Na6	3.84(3)
	Na12	3.40(3)
2	Na46	3.61(1)
	Na55	3.40(3)
2	Na66	3.94(2)

Na13

2	In31	3.482(9)
2	In42	3.55(2)
2	In45	3.30(2)
	InA2	3.38(2)
	InA5	2.92(2)
	InA5	3.93(2)
	Na4	3.53(2)
	Na13	3.98(4)
2	Na36	3.81(2)
2	Na40	3.35(2)
	Na50	3.76(2)

Na14

	In1	3.40(1)
	In9	3.41(1)
	In10	3.25(1)
	In30	3.29(1)
	In34	3.40(1)
	In47	3.36(1)
	InA4	3.41(1)
	Na14	3.86(3)
	Na20	3.89(2)
	Na29	3.29(2)
	Na45	3.36(2)
	Na54	3.34(2)
	Na59	3.37(2)
	Na62	3.83(2)

Na15

2	In13	3.50(2)
2	In15	3.41(1)
	In19	3.55(2)
2	In46	3.62(2)
	InC1	3.45(2)
2	InC3	3.59(2)
	Na30	3.62(2)
	Na38	3.44(3)
2	Na65	3.74(2)

Na16

2	In9	3.42(1)
2	In27	3.328(7)
2	In41	3.28(1)
	InC2	3.12(2)
	Na3	3.31(2)
2	Na41	3.47(2)
	Na60	3.73(3)
2	Na65	3.85(2)

Na17

2	In6	3.34(2)
	In22	3.35(2)
2	In28	3.36(1)
	InC4	3.18(2)
	InC5	3.83(2)
2	InC7	3.83(2)
	Na19	3.31(3)
2	Na56	3.39(2)
2	Na63	3.41(1)

Na18

2	In8	3.60(1)
	In11	3.62(2)
2	In12	3.56(1)
2	In18	3.57(2)
	In32	3.54(2)
2	In35	3.66(2)
2	In37	3.63(2)
	Na9	3.65(3)
2	Na42	3.60(2)
	Na55	3.48(3)

Na19

2	In6	3.34(2)
2	In9	3.37(2)
2	In47	3.37(1)
	InC4	3.28(2)
	Na17	3.31(3)
2	Na41	3.40(2)
	Na59	3.39(3)
2	Na63	3.93(2)

Na20

	In10	3.42(1)
	In11	3.26(1)
	In21	3.40(1)
	In32	3.30(1)
	In44	3.44(1)
	In47	3.53(1)
	InA4	3.84(1)
	InA6	3.08(1)
	InA6	3.59(1)
	Na5	3.86(2)
	Na14	3.89(2)
	Na20	3.85(3)
	Na29	3.38(1)
	Na31	3.82(2)
	Na42	3.49(2)
	Na54	3.42(2)

Na21

2	In6	3.42(2)
2	In10	3.466(8)
2	In30	3.38(1)
2	InB1	3.78(2)
	Na21	3.78(3)
2	Na22	3.93(1)
	Na28	3.25(2)
2	Na53	3.36(2)
	Na59	3.36(2)

Na22

	In6	3.39(1)
	In8	3.32(1)
	In10	3.32(1)
	In21	3.32(1)
	In28	3.39(1)
	In35	3.26(1)
	InB1	3.04(1)
	Na21	3.93(1)
	Na28	3.49(1)
	Na42	3.31(2)
	Na43	3.79(2)
	Na46	3.61(2)
	Na53	3.42(1)
	Na58	3.92(2)

Na23

	In7	3.35(2)
2	In13	3.30(1)
2	In15	3.62(1)
	In16	3.30(2)
2	In20	3.29(1)
2	In39	3.57(1)
	Na30	3.86(2)
	Na39	3.40(2)
2	Na52	3.52(1)

Na24

	In3	3.41(1)
	In8	3.50(1)
	In12	3.71(1)
	In18	3.49(1)
	In22	3.42(1)
	In23	3.36(1)
	In28	3.38(1)
	In48	3.49(1)
	In49	3.53(1)
	In51	3.55(1)
	Na48	3.86(2)
	Na56	3.46(2)
	Na58	3.36(2)
	Na64	3.28(2)

Na25

	In33	3.25(2)
2	In38	3.49(2)
2	In40	3.35(1)
2	In41	3.43(2)
2	In43	3.44(1)
2	In53	3.83(2)
	Na10	3.61(3)
2	Na11	3.47(1)
	Na37	3.58(2)
	Na60	3.99(2)

Na26

	In2	3.37(2)
2	In3	3.41(1)
2	In23	3.39(1)
2	InC5	3.96(2)
	InC6	3.16(2)
	Na51	3.35(2)
2	Na56	3.38(1)
2	Na68	3.40(2)

Na27

2	In2	3.47(1)
2	In3	3.362(8)
2	In18	3.37(2)
	InB2	3.26(2)
	Na9	3.44(2)
	Na27	3.99(3)
2	Na35	3.35(2)
2	Na64	3.81(2)
	Na67	3.64(3)

Na28

2	In6	3.32(1)
	In22	3.26(2)
2	In28	3.38(1)
2	InB1	3.36(2)
	Na21	3.25(2)
2	Na22	3.49(1)
2	Na58	3.33(2)

Table IV. (continued)

Na29		Na33		Na36		Na40		Na42	
2	In10 3.38(1)		In7 3.25(1)		In16 3.53(2)		In24 3.38(1)		In6 3.56(1)
2	In21 3.40(1)		In16 3.27(1)	2	In29 3.59(1)		In25 3.30(1)		In8 3.58(1)
	In30 3.41(2)		In24 3.54(1)	2	In31 3.60(1)		In29 3.29(1)		In10 3.56(1)
2	InA4 3.47(2)		In27 3.51(1)		In45 3.51(2)		In31 3.30(1)		In11 3.50(1)
2	InA6 3.72(2)		In29 3.48(1)	2	InA1 3.50(2)		In42 3.39(1)		In12 3.46(1)
			In36 3.44(1)	2	InA5 3.65(2)		InA1 3.91(1)		In21 3.64(1)
	Na5 3.33(2)		InA1 3.05(1)				InA2 3.38(1)		In28 3.54(1)
2	Na14 3.29(2)		InA1 3.62(1)		Na2 3.36(2)		InA3 3.63(2)		In32 3.51(1)
2	Na20 3.38(1)		InA3 3.74(2)	2	Na13 3.81(2)		InA5 3.70(1)		In35 3.67(1)
				2	Na33 3.86(2)				In37 3.49(1)
	Na30		Na31 3.79(2)	2	Na40 3.36(1)		Na13 3.35(2)		In44 3.57(1)
			Na33 3.95(2)				Na33 3.41(2)		In47 3.55(1)
4	In13 3.235(2)		Na36 3.86(2)		Na37		Na36 3.36(1)		
4	In15 3.507(2)		Na40 3.41(2)				Na50 3.29(2)		Na18 3.60(2)
2	In46 3.601(5)		Na52 3.44(2)	2	In19 3.58(2)		Na62 3.29(2)		Na20 3.49(2)
			Na54 3.32(2)	4	In40 3.655(6)				Na22 3.31(2)
2	Na15 3.62(2)		Na62 3.83(2)	4	In43 3.65(1)		Na41		Na63 3.56(2)
2	Na23 3.86(2)			2	In53 1.36(2)				
	Na39 3.33(3)		Na34				In9 3.40(1)		Na43
				2	Na25 3.58(2)		In27 3.43(1)		
	Na31		In5 3.39(2)		Na32 3.44(4)		In36 3.38(1)	2	In21 3.57(1)
			In7 3.61(2)	2	Na60 3.40(3)		In44 3.43(1)	2	In35 3.58(1)
	In7 3.47(2)		In11 3.59(2)				In47 3.44(1)	2	InB1 3.66(2)
	In11 3.62(2)	2	In15 3.60(2)		Na38		InC2 3.66(1)		InB5 3.69(2)
2	In36 3.57(2)	2	In36 3.28(1)				InC3 3.47(2)		
2	In44 3.61(1)	2	In37 3.68(1)	2	In5 3.45(1)		InC4 3.70(1)		Na6 3.49(2)
2	InA1 3.56(2)	2	In44 3.25(1)		In17 3.49(2)			2	Na22 3.79(2)
2	InA6 3.61(2)		In46 3.36(2)	2	In46 3.42(2)		Na16 3.47(2)	2	Na46 3.47(2)
				2	InC3 3.61(2)		Na19 3.40(2)		Na53 3.22(3)
2	Na20 3.82(2)		Na31 3.40(3)		InC6 3.33(2)		Na44 3.33(2)		
2	Na33 3.79(2)	2	Na44 3.21(2)				Na63 3.40(2)		Na44
	Na34 3.40(3)				Na15 3.44(3)		Na65 3.38(2)		
2	Na54 3.31(1)		Na35	2	Na44 3.39(1)				In5 3.41(1)
				2	Na68 3.43(2)				In15 3.46(1)
	Na32		In2 3.32(2)						In36 3.44(1)
		2	In3 3.31(1)		Na39				In37 3.46(1)
4	In38 3.553(6)	2	In23 3.28(2)						In44 3.38(1)
4	In43 3.34(1)		InB2 3.18(2)	4	In13 3.69(2)				In46 3.42(1)
2	In45 3.30(2)	2	InB4 3.66(2)	2	In14 3.56(2)				InC3 3.01(1)
2	In53 3.69(3)		InB5 3.62(2)	4	In20 3.574(6)				
									Na34 3.21(2)
2	Na4 3.43(2)	2	Na27 3.35(2)	2	Na23 3.40(2)				Na38 3.39(1)
	Na37 3.44(4)	2	Na64 3.34(2)		Na30 3.33(3)				Na41 3.33(2)
			Na66 3.52(3)	2	Na57 3.45(3)				Na63 3.85(2)
									Na68 3.91(2)

Table IV. (continued)

Na45

	In1	3.41(2)
2	In34	3.43(1)
2	In50	3.37(2)
2	InA3	3.76(2)
2	InA4	3.77(2)
2	Na14	3.36(2)
	Na50	3.28(2)
2	Na62	3.30(1)

Na46

	In8	3.37(1)
	In35	3.31(1)
	In48	3.31(1)
	InB1	3.74(1)
	InB3	3.95(2)
	InB4	3.29(2)
	InB5	3.59(1)
	Na12	3.61(1)
	Na22	3.61(2)
	Na43	3.47(2)
	Na48	3.57(2)
	Na58	3.49(2)
	Na64	3.64(2)
	Na66	3.61(2)

Na47

2	In4	3.30(2)
2	In25	3.42(1)
	In26	3.12(2)
2	In42	3.325(9)
2	Na7	3.38(2)
	Na8	3.38(2)
2	Na49	3.84(2)
	Na57	3.63(2)

Na48

	In8	3.37(1)
	In18	3.41(1)
	In48	3.36(1)
	In51	3.38(1)
	Na24	3.86(2)
	Na46	3.57(2)
	Na48	3.52(3)
	Na55	3.32(2)
	Na58	4.00(2)
	Na67	3.54(2)

Na49

	In4	3.55(1)
	In14	3.49(1)
	In20	3.56(1)
	In26	3.67(1)
	In31	3.55(1)
	In38	3.38(1)
	In39	3.55(1)
	In42	3.50(1)
	In43	3.53(1)
	In52	3.95(1)
	Na4	3.66(2)
	Na7	3.37(2)
	Na11	3.79(2)
	Na47	3.84(2)
	Na57	3.51(1)

Na50

2	In25	3.378(8)
2	In42	3.33(1)
2	In50	3.39(1)
	InA2	3.54(2)
	Na8	3.30(2)
	Na13	3.76(2)
2	Na40	3.29(2)
	Na45	3.28(2)
2	Na62	3.92(2)

Na51

4	In23	3.53(1)
2	In49	3.41(1)
2	InC5	3.32(2)
2	Na26	3.35(2)
4	Na56	3.88(1)
	Na61	3.43(4)

Na52

	In7	3.64(1)
	In13	3.47(1)
	In15	3.66(1)
	In16	3.60(1)
	In20	3.48(1)
	In24	3.39(1)
	In27	3.39(1)
	In29	3.59(1)
	In36	3.63(1)
	In39	3.63(1)
	In40	3.46(1)
	In41	3.42(1)
	Na11	3.63(2)
	Na23	3.52(1)
	Na33	3.44(2)
	Na65	3.64(2)

Na53

2	In10	3.27(1)
2	In21	3.29(2)
	In30	3.22(2)
2	InB1	3.39(2)
2	Na21	3.36(2)
2	Na22	3.42(1)
	Na43	3.22(3)

Na54

	In9	3.33(1)
	In27	3.37(1)
	In36	3.23(1)
	In44	3.30(1)
	In47	3.33(1)
	InA1	3.93(1)
	InA3	3.27(2)
	InA4	3.35(2)
	Na14	3.34(2)
	Na20	3.42(2)
	Na31	3.31(1)
	Na33	3.32(2)
	Na62	3.32(2)

Na55

2	In8	3.41(1)
2	In18	3.42(2)
2	In35	3.40(2)
	Na12	3.40(3)
	Na18	3.48(3)
2	Na48	3.32(2)
	Na67	4.00(3)

Na56

	In3	3.43(1)
	In12	3.45(1)
	In22	3.53(1)
	In23	3.43(1)
	In28	3.43(1)
	In49	3.37(1)
	InC5	3.31(1)
	InC7	3.32(2)
	Na17	3.39(2)
	Na24	3.46(2)
	Na26	3.38(1)
	Na51	3.88(1)
	Na56	3.97(3)
	Na63	3.83(2)
	Na68	3.90(2)

Na57

2	In4	3.46(2)
2	In14	3.34(1)
2	In20	3.39(1)
	In26	3.27(2)
2	In39	3.47(2)
	Na39	3.45(3)
	Na47	3.63(2)
2	Na49	3.51(1)

Na58

	In8	3.50(1)
	In22	3.43(1)
	In28	3.51(1)
	In51	3.40(1)
	InB1	3.89(1)
	InB3	3.03(2)
	InB3	3.81(2)
	InB4	3.90(2)
	Na22	3.92(2)
	Na24	3.36(2)
	Na28	3.33(2)
	Na46	3.49(2)
	Na48	4.00(2)
	Na58	3.79(3)
	Na67	3.64(2)

Na59

	In1	3.51(2)
2	In6	3.49(2)
2	In9	3.55(2)
2	In10	3.547(9)
2	In30	3.50(2)
	In34	3.50(2)
2	In47	3.56(1)
2	Na14	3.37(2)
	Na19	3.39(3)
	Na21	3.36(2)

Table IV. (continued)

Na60		Na63		Na65		Na68	
2	In19 3.37(1)	In6	3.55(2)	In13	3.52(1)	In2	3.48(1)
2	In40 3.31(1)	In12	3.32(1)	In15	3.37(1)	In3	3.48(1)
2	In41 3.50(2)	In28	3.49(1)	In19	3.53(1)	In5	3.44(1)
2	In53 3.68(2)	In37	3.29(1)	In27	3.53(1)	In12	3.37(1)
2	InC1 3.49(2)	In44	3.46(1)	In36	3.60(1)	In17	3.49(1)
	InC2 3.32(2)	In47	3.50(2)	In40	3.45(1)	In37	3.30(1)
		InC4	3.86(2)	In41	3.54(1)	InC6	3.35(1)
	Na16 3.73(3)	InC7	3.11(2)	InC1	3.59(1)	InC7	3.39(2)
	Na25 3.99(2)			InC2	3.64(1)		
	Na37 3.40(3)	Na17	3.41(1)	InC3	3.55(1)	Na9	3.50(2)
2	Na65 3.54(2)	Na19	3.93(2)			Na26	3.40(2)
		Na41	3.40(2)	NaI5	3.74(2)	Na38	3.43(2)
	Na61	Na42	3.56(2)	Na16	3.85(2)	Na44	3.91(2)
		Na44	3.85(2)	Na41	3.38(2)	Na56	3.90(2)
4	In23 3.35(1)	Na56	3.83(2)	Na52	3.64(2)	Na63	3.84(2)
4	In48 3.554(8)	Na68	3.84(2)	Na60	3.54(2)	Na68	3.99(3)
2	In49 3.45(1)						
		Na64		**Na66**			
	Na51 3.43(4)						
2	Na66 3.23(3)	In3	3.49(1)	2	In23 3.46(2)		
		In18	3.47(1)	2	In48 3.33(1)		
	Na62	In23	3.42(1)	2	InB4 3.74(3)		
		In48	3.39(1)		InB5 2.89(2)		
	In9 3.35(1)	InB3	3.57(2)				
	In24 3.37(1)	InB4	2.86(2)	2	Na12 3.94(2)		
	In25 3.41(1)	InB5	3.92(2)		Na35 3.52(3)		
	In27 3.37(1)			2	Na46 3.61(2)		
	In34 3.35(1)	Na24	3.28(2)		Na61 3.23(3)		
	In50 3.40(1)	Na27	3.81(2)	2	Na64 3.88(2)		
	InA3 3.40(1)	Na35	3.34(2)				
		Na46	3.64(2)		**Na67**		
	Na3 3.38(2)	Na66	3.88(2)				
	Na14 3.83(2)	Na67	3.53(2)	2	In18 3.29(2)		
	Na33 3.83(2)				In51 3.26(2)		
	Na40 3.29(2)			2	InB3 3.18(2)		
	Na45 3.30(1)						
	Na50 3.92(2)				Na27 3.64(3)		
	Na54 3.32(2)			2	Na48 3.54(2)		
					Na55 4.00(3)		
				2	Na58 3.64(2)		
				2	Na64 3.53(2)		

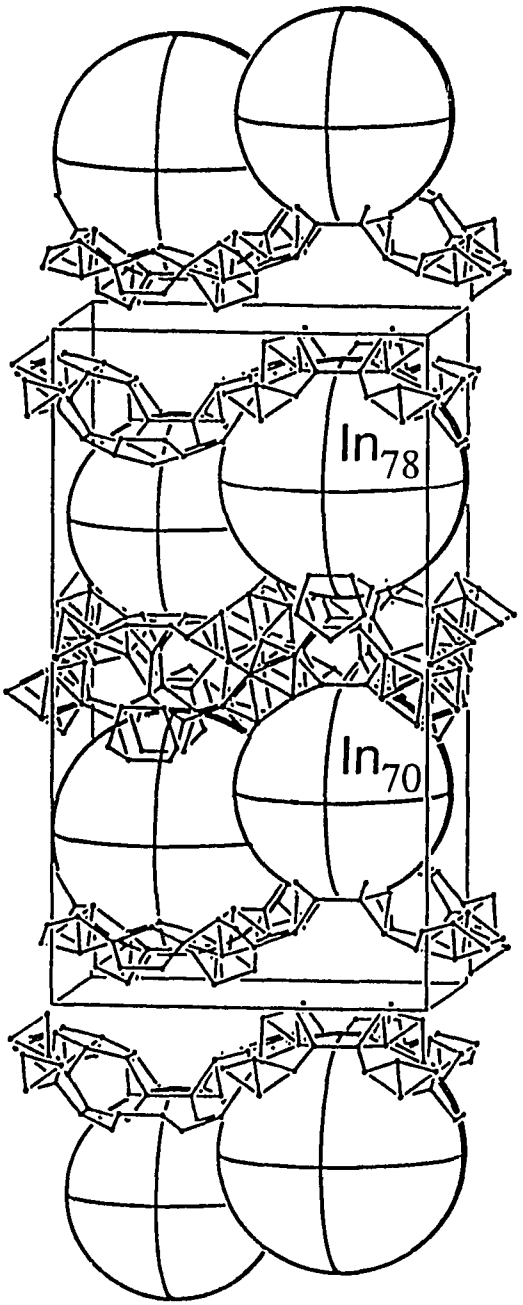

Figure 1. A general view of the unit cell of $Na_{\sim 172}In_{\sim 197}Ni2$ approximately along the *a* axis (*c* is vertical). The In_{70} and In_{78} fullerenes are shown as two large spheres. All In–In bonds less that 4.00 Å between the spheres are drawn.

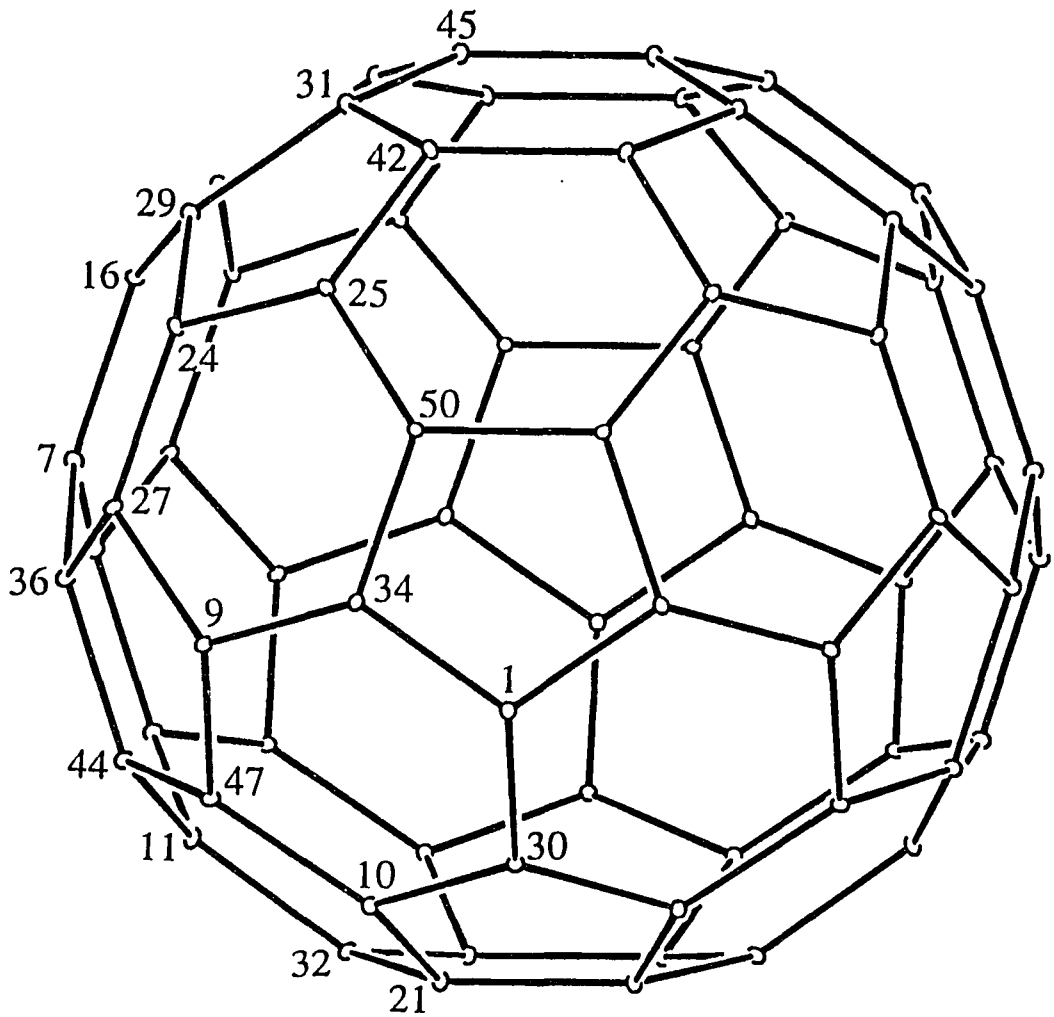

Figure 2. A nearly [100] view of the In_{70} fullerene with C_{2v} symmetry (the 2-fold axis is vertical). It has a pseudo D_{5h} symmetry (as C_{70}) with the pseudo 5-fold axis approximately along the view direction. (30% thermal ellipsoids)

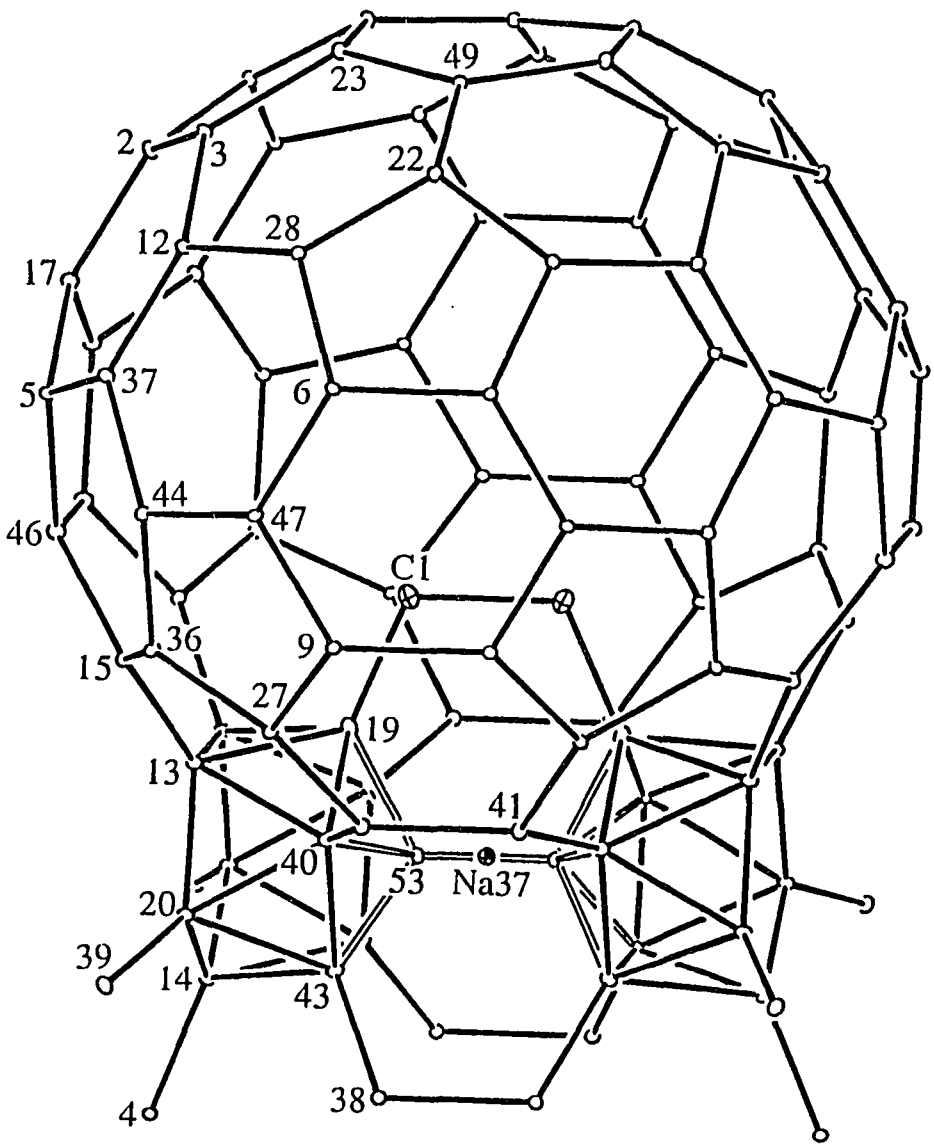

Figure 3. A nearly [010] view of the In_{78} fullerene with C_{2v} symmetry (the 2-fold axis is vertical). It has pseudo D_{3h} symmetry (as one of the C_{78} isomers, see text) with the pseudo 3-fold axis approximately along the view direction (through the hexagons made of In6, 9, 47 and a mirror plane). The two lower pentagons are parts of two *nido*-In_{11} (shown left and right). The exo bonds from the icosahedra provide connectivity to In_{70} fullerenes. In19 provides connection to InCl (labeled as Cl) which is part of encapsulated 2-bonded indium cluster (not shown). In53 and Na37 (open bonds) are refined with occupancies of 30(2) and 85(5)%, respectively. (30% thermal ellipsoids)

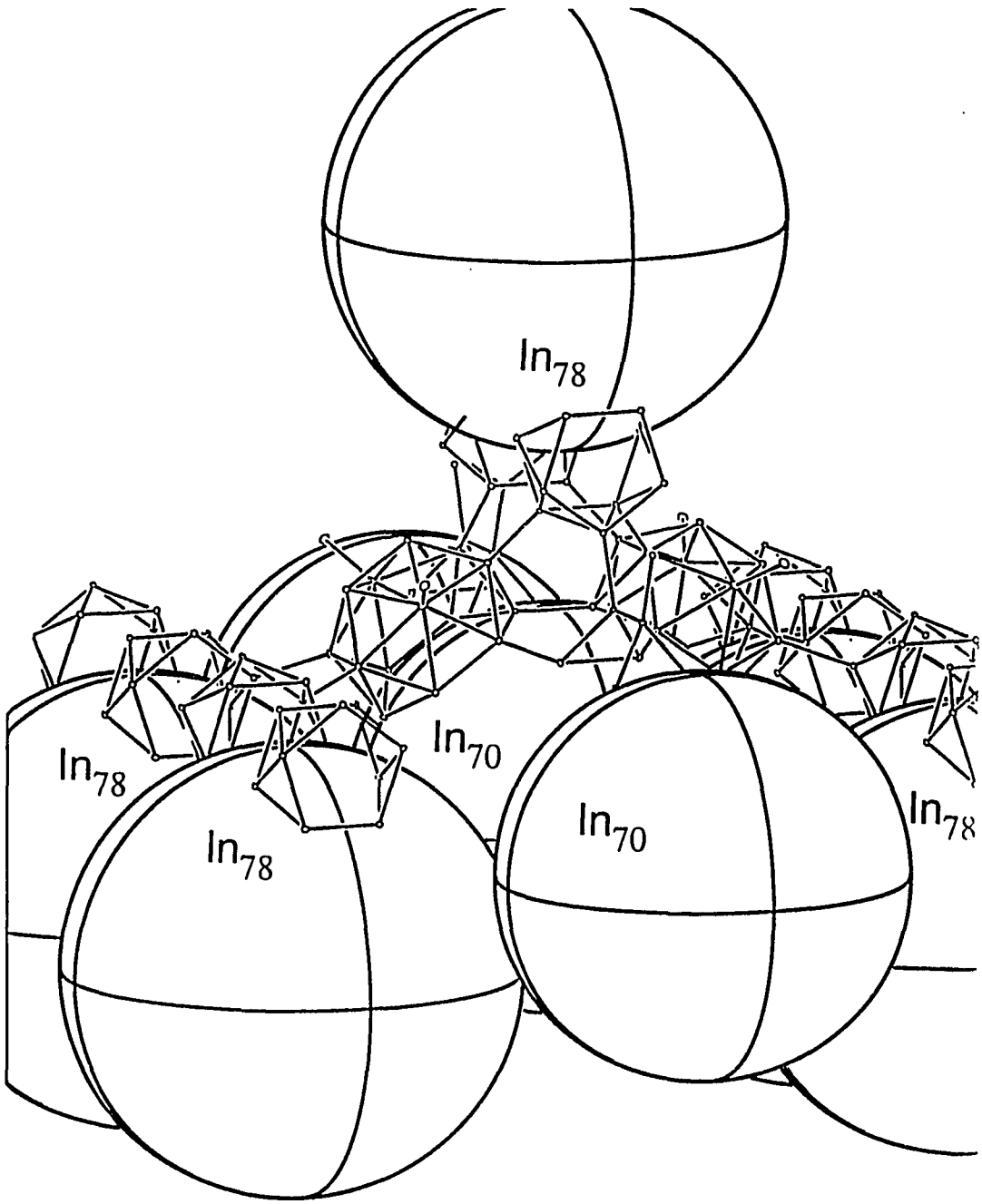

Figure 4. An enlarged section of the unit cell of $Na_{\sim 172}In_{\sim 197}Ni_2$ (near z = 1/2) where two layers of fullerenes are connected through exo indium atoms and form a double layer .

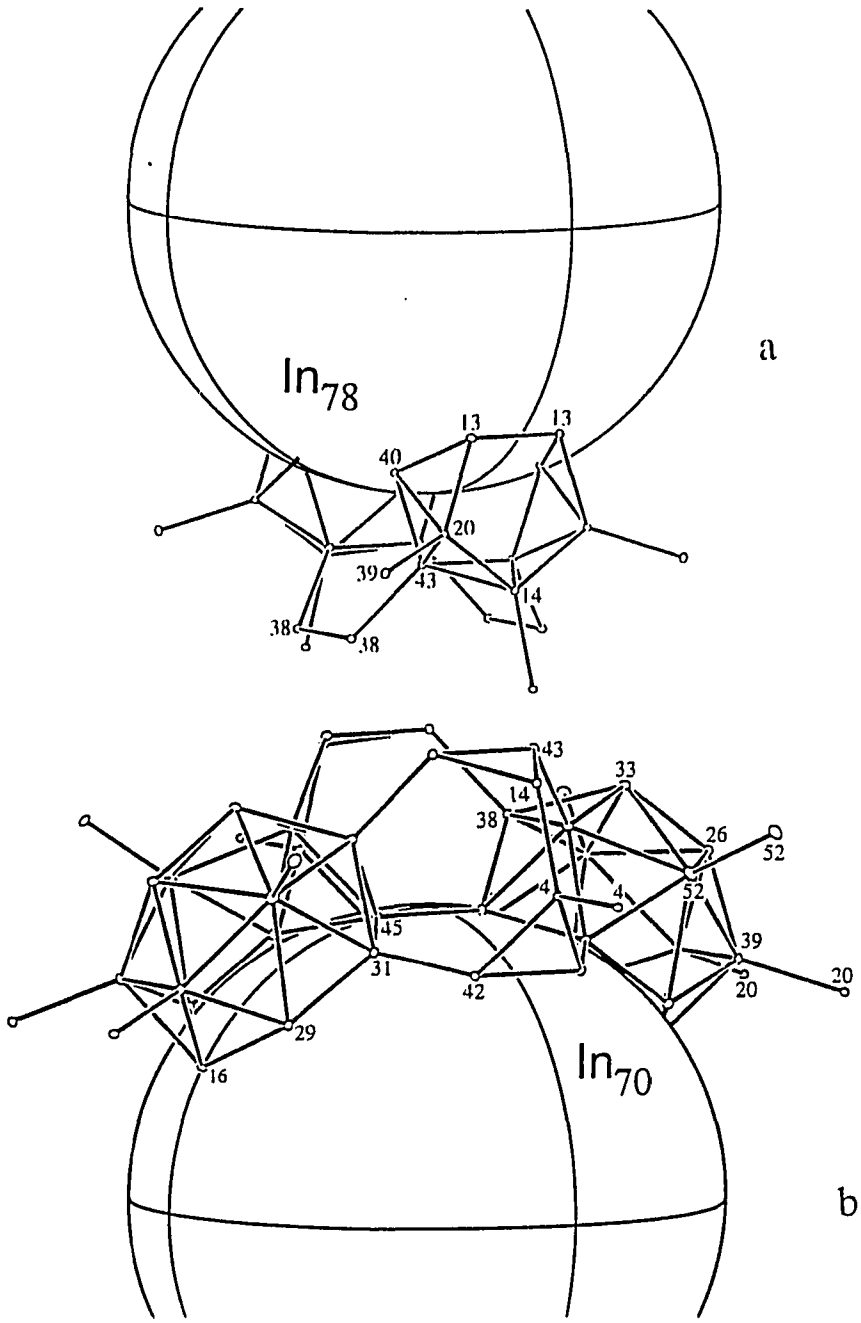

Figure 5. In_{78} (a) and In_{70} (b) shown separated with the *nido*-In_{11} and *nido*-In14, respectively, "attached" to them. The exo indium atoms (labeled) provide the connectivity between two layers of fullerenes. Two mirror planes through the centers of the spheres are defiend by In4, 14, and by In26, 33, respectively.

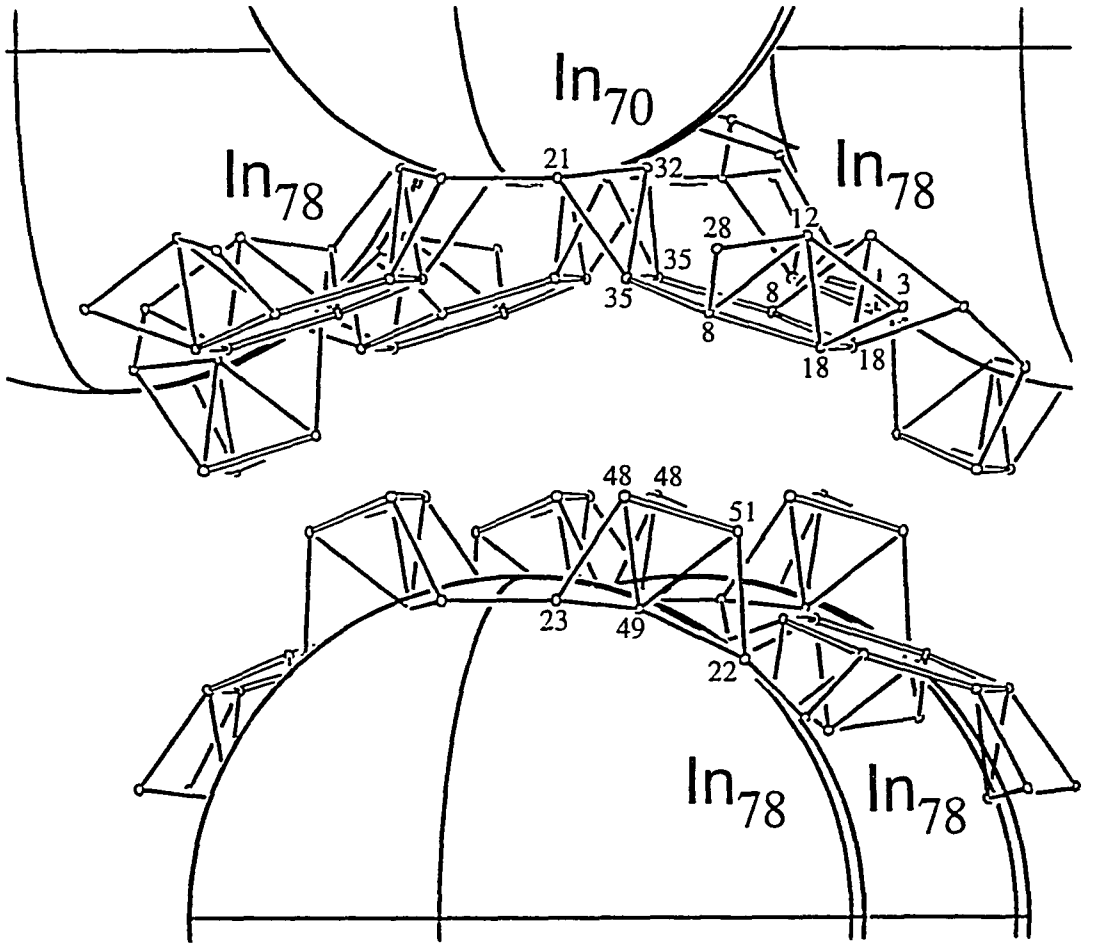

Figure 6. An enlarged section of the unit cell of $Na_{\sim 172}In_{\sim 197}Ni_2$ near z = 0 where four spheres from one layer (top, one In_{70} in the back can not be seen) approach two spheres from another layer (the bottom section). The bonds within the hexagonal and triangular formations of exo indium atoms are drawn as open lines.

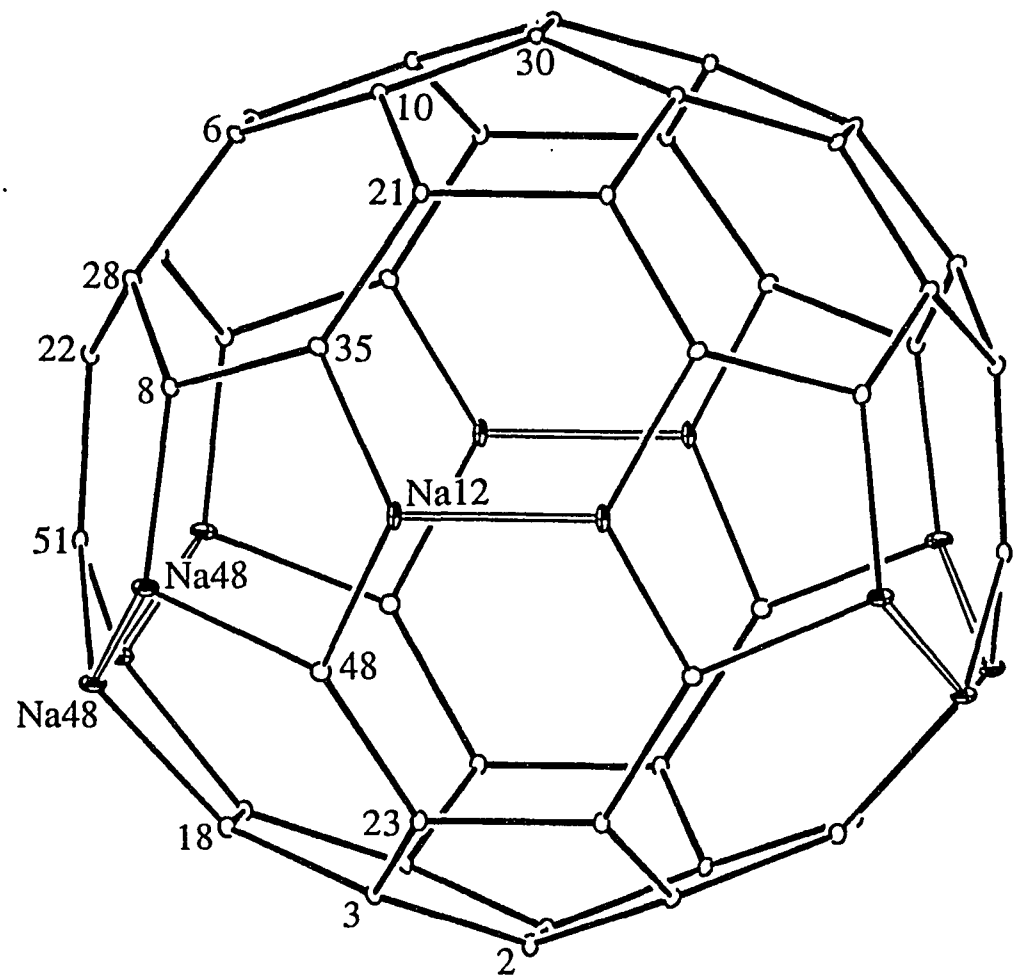

Figure 7. A nearly [100] view of the M_{60} fullerene (C_{2v} symmetry, reduced from the ideal I_h) of 48 indium and 12 sodium (crossed) atoms. The six edges of Na12 and Na48 near the waist (open bonds) are shared with six other M_{60} cages. All six pentagons that do not contain sodium atoms are shared with six fullerenes, four In_{78} and two In_{70}. The two-fold axis (*c* axis) is vertical. (30% thermal ellipsoids)

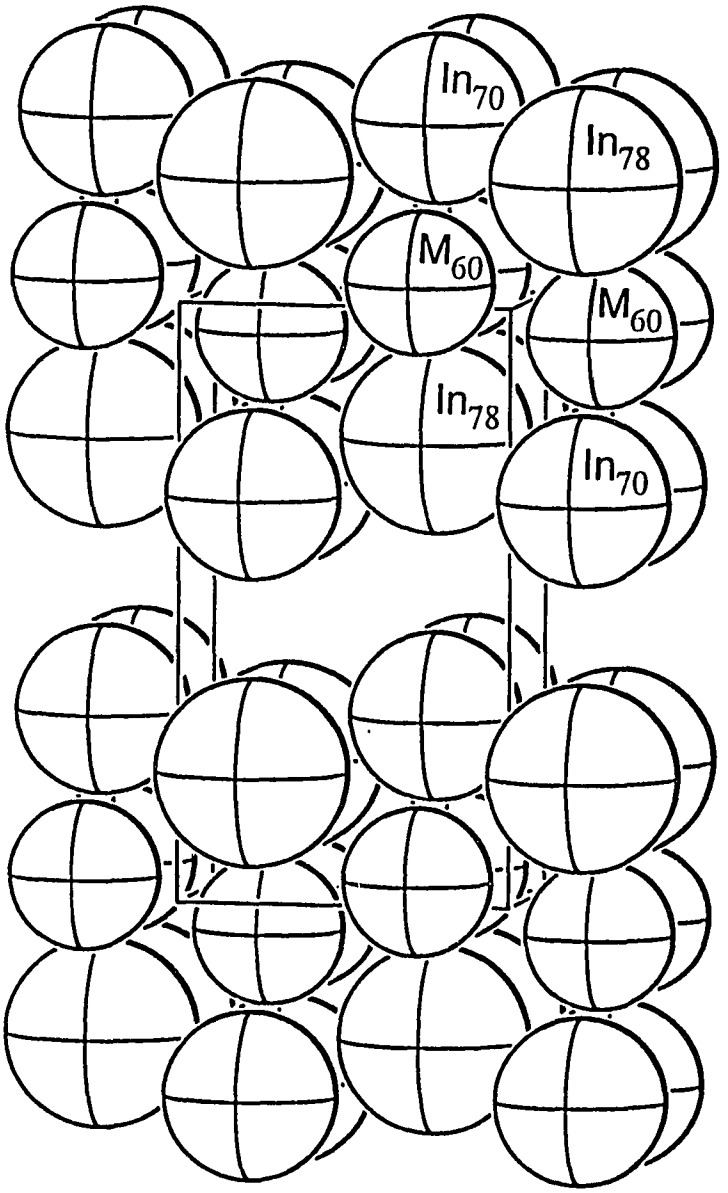

Figure 8. A condensed view of the unit cell along approximately [100] (the same as in Figure 1). Straight rows of fullerenes of each type run parallel to the *a* axis. The rows of In_{70} and In_{78} alternate along the *b* axis (horizontal) and form close-packed but puckered layers that stack on top of each other. Layers of M_{60} fill the space between every other pair of In_{70} and In_{78} layers, and assume the same wave-like pattern. The order of the stacking is ABA␣ where B is the M_{60} position and ␣ marks the omitted indium exo atoms (see text).

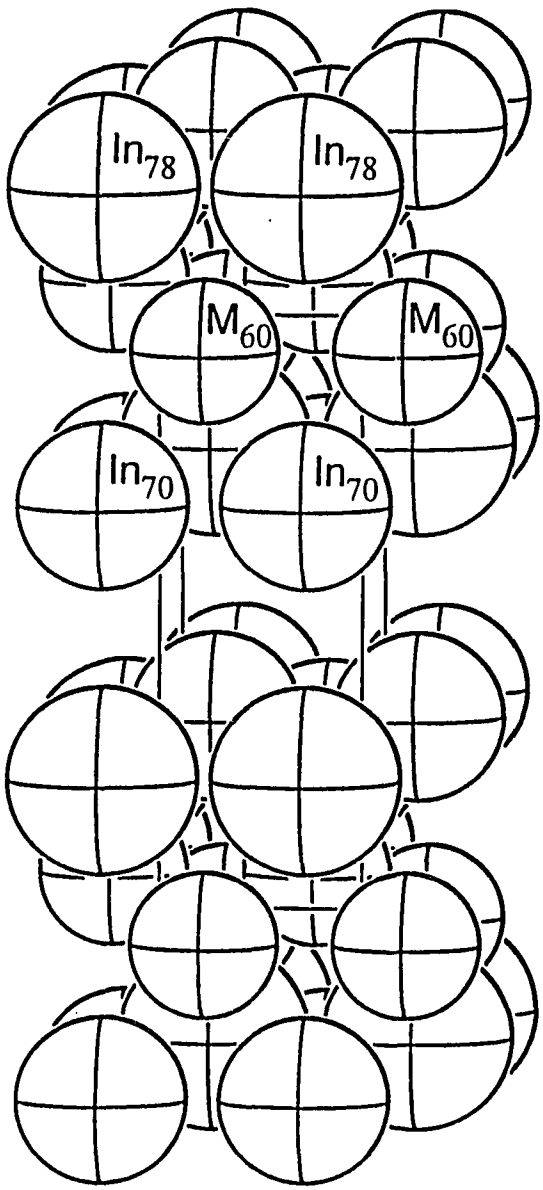

Figure 9. A condensed view of the unit cell along approximately [010]. The rows of equivalent-sized fullerenes parallel to the *a* axis (horizontal) can be seen. Also, the stacking of the layers of fused In_{70} and In_{78} on top of each other is clear.

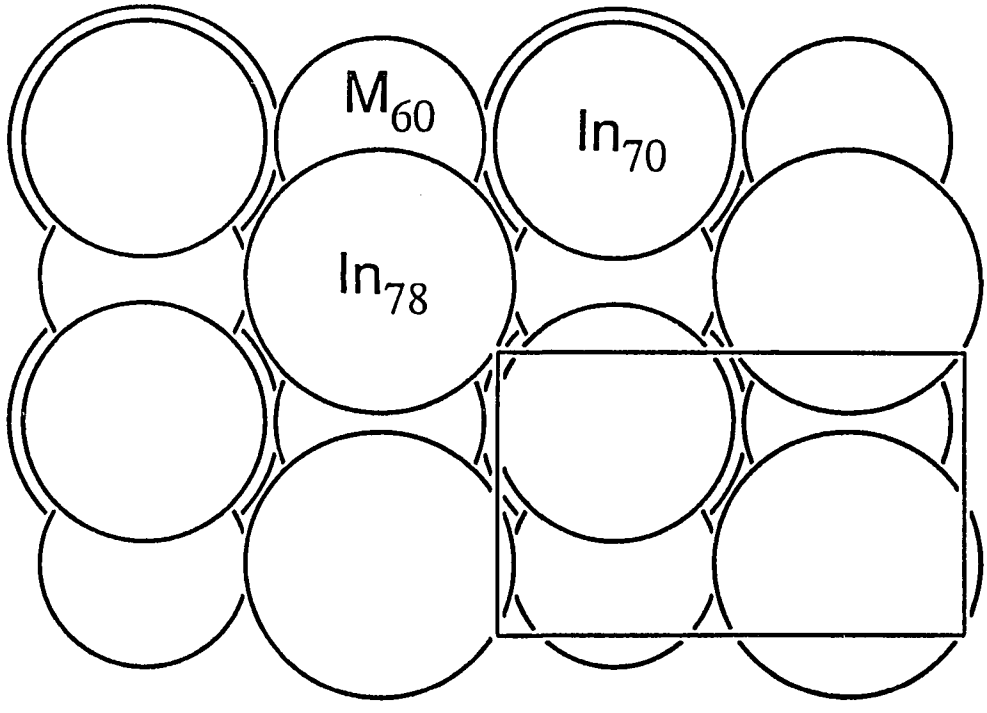

Figure 10. A condensed projection of the unit cell along the *c* axis. Notice that the layers of fused In_{70} and In_{78} as well as the ones of M_{60} between them are close-packed, although puckered.

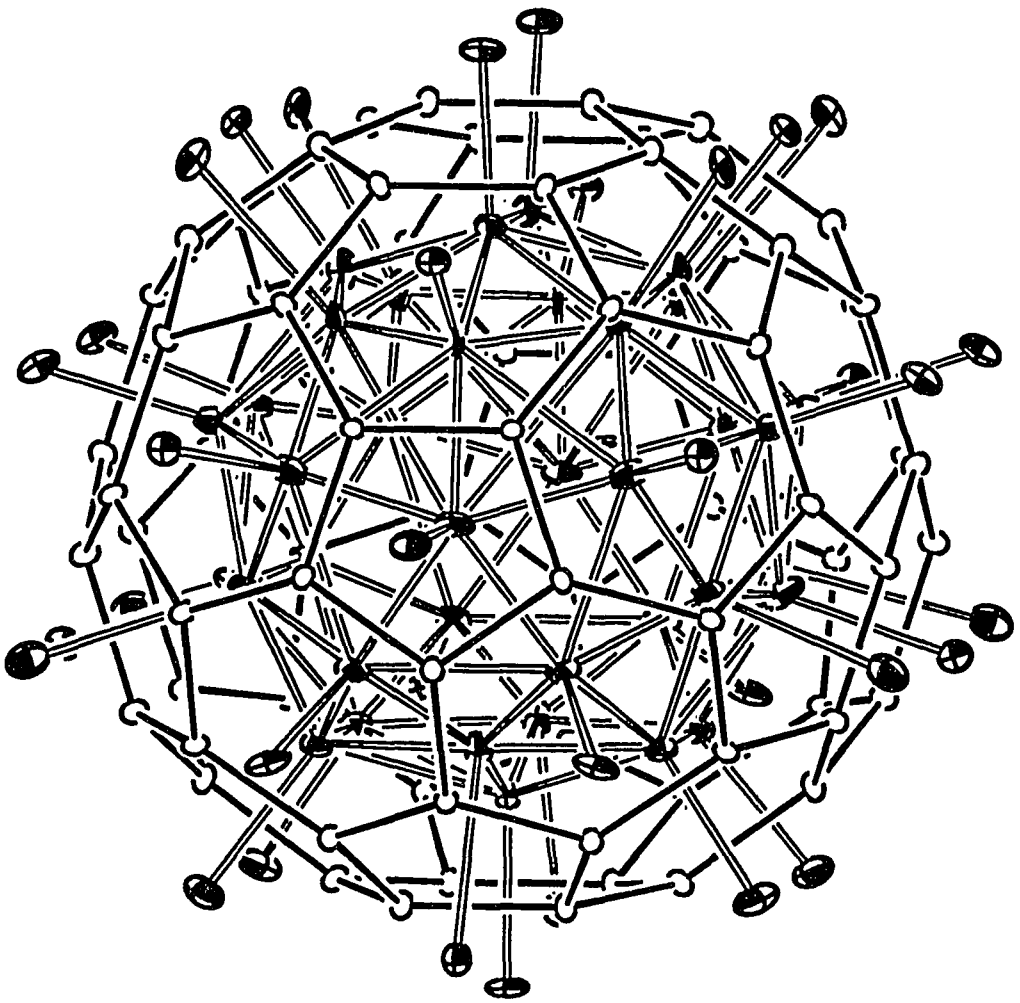

Figure 11. A view of the In_{70} fullerene (open circles, solid bonds) together with all nearest sodium atoms interconnected (shaded circles, open bonds). All 37 pentagonal and hexagonal faces of the fullerene are capped from inside and outside by sodium atoms. The sodium atoms inside form a 37-atom deltahedron (triangular faces only). Each of the 70 triangular faces of that deltahedron are capped by In.

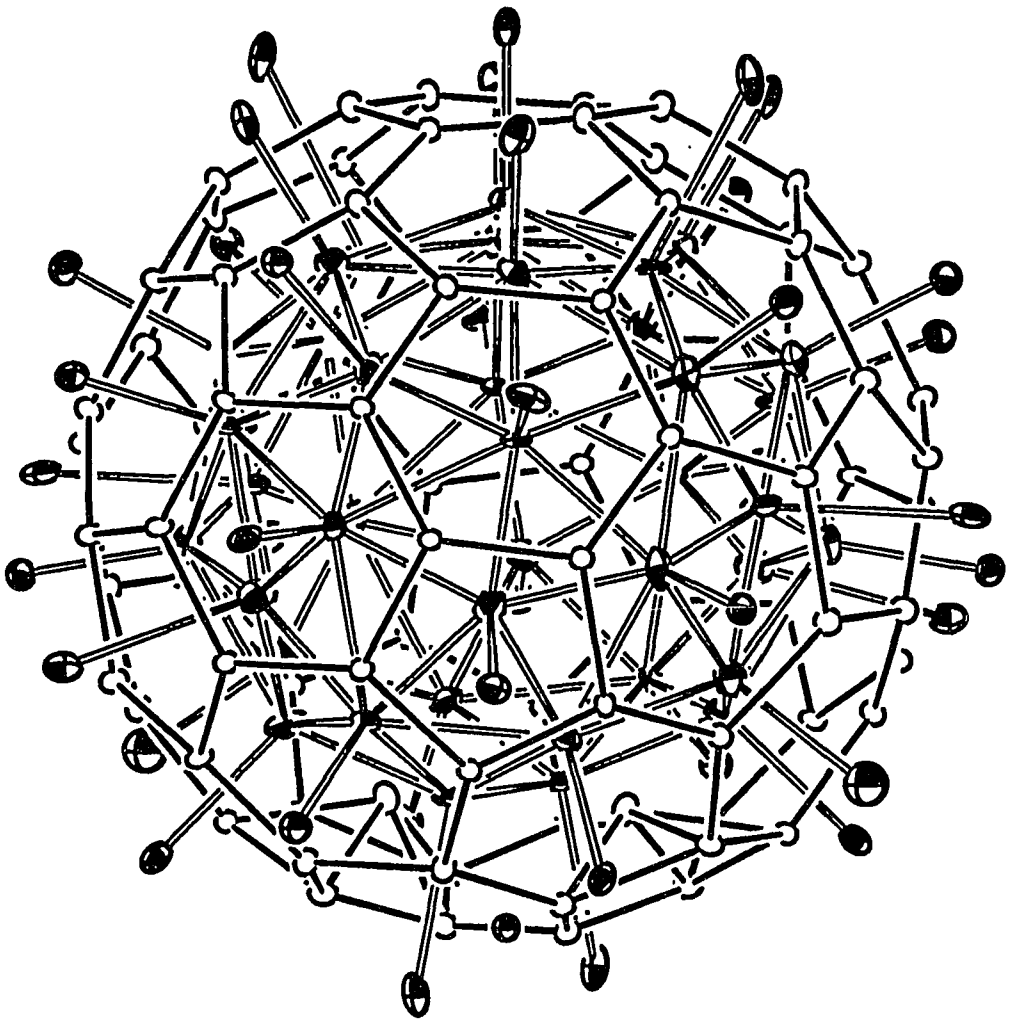

Figure 12. A view of the In_{78} fullerene (open circles, solid bonds) together with all nearest sodium atoms interconnected (shaded circles, open bonds). All 41 faces of the fullerene are capped from inside by 39 sodium and 2 indium (In19) atoms which form 41-atom *closo* deltahedron if the inside indiums are included, or a 39-atom *arachno* deltahedron if they are not. All In_{78} faces capped from inside are capped from the outside by sodium atoms as well. Each of the 78 triangular faces of the 41-atom *closo* deltahedron are capped by the atoms of the fullerene.

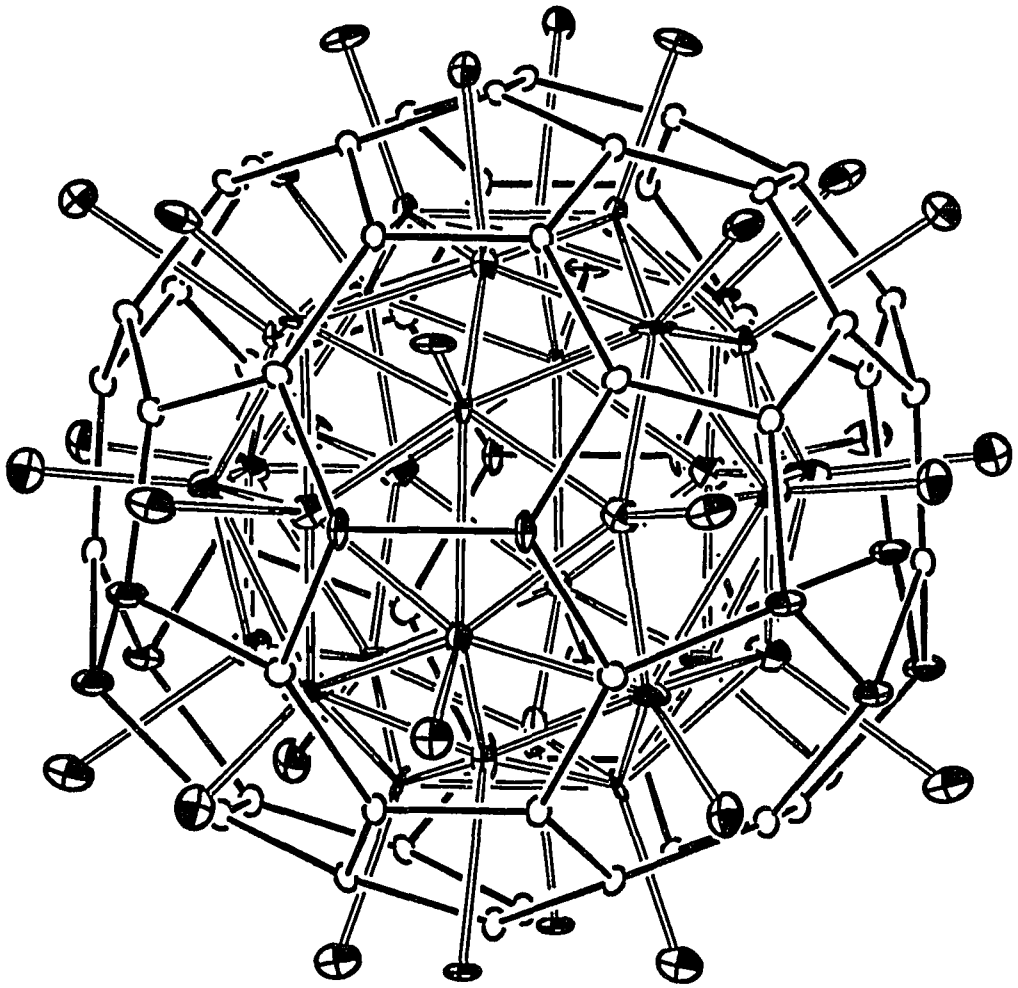

Figure 13. A view of the M_{60} ($In_{48}Na_{12}$) fullerene (In-open circles, Na-shaded circles) together with all nearest sodium atoms interconnected (shaded circles). All 32 pentagonal and hexagonal faces of the fullerene are endo- and exo-capped by sodium atoms. The sodium atoms inside form the 32 atom deltahedron marked with open lines. All 60 triangular faces of that deltahedron are capped by atoms of the fullerene from outside

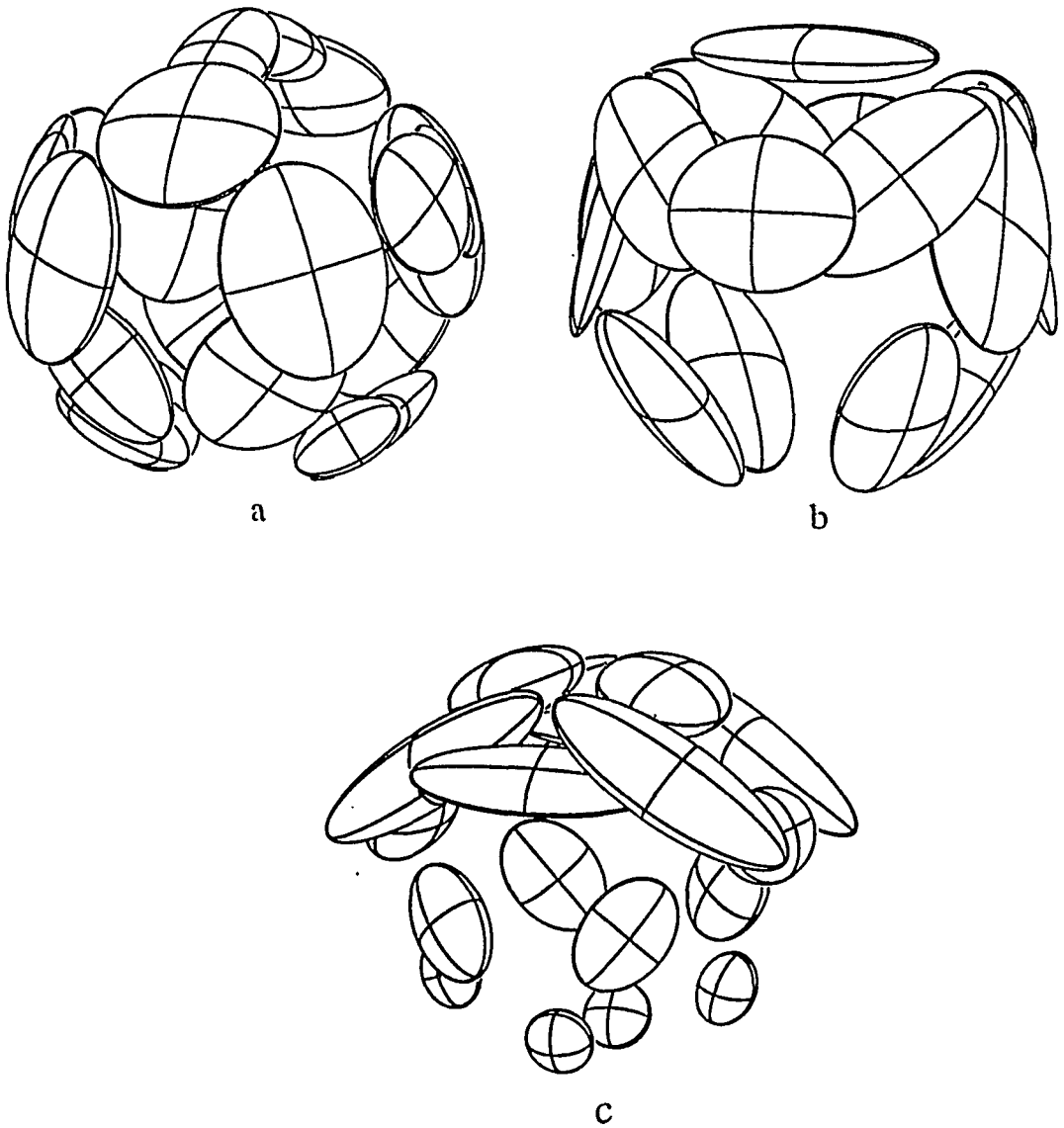

Figure 14. A drawing with 94% probability thermal ellipsoids of the indium clusters encapsulated in the fullerenes that are centered by a) NiA, b) NiB and c) Na1. Only a few islands on the surface of the first two and on the upper surface of the third one have nearly zero electron density.

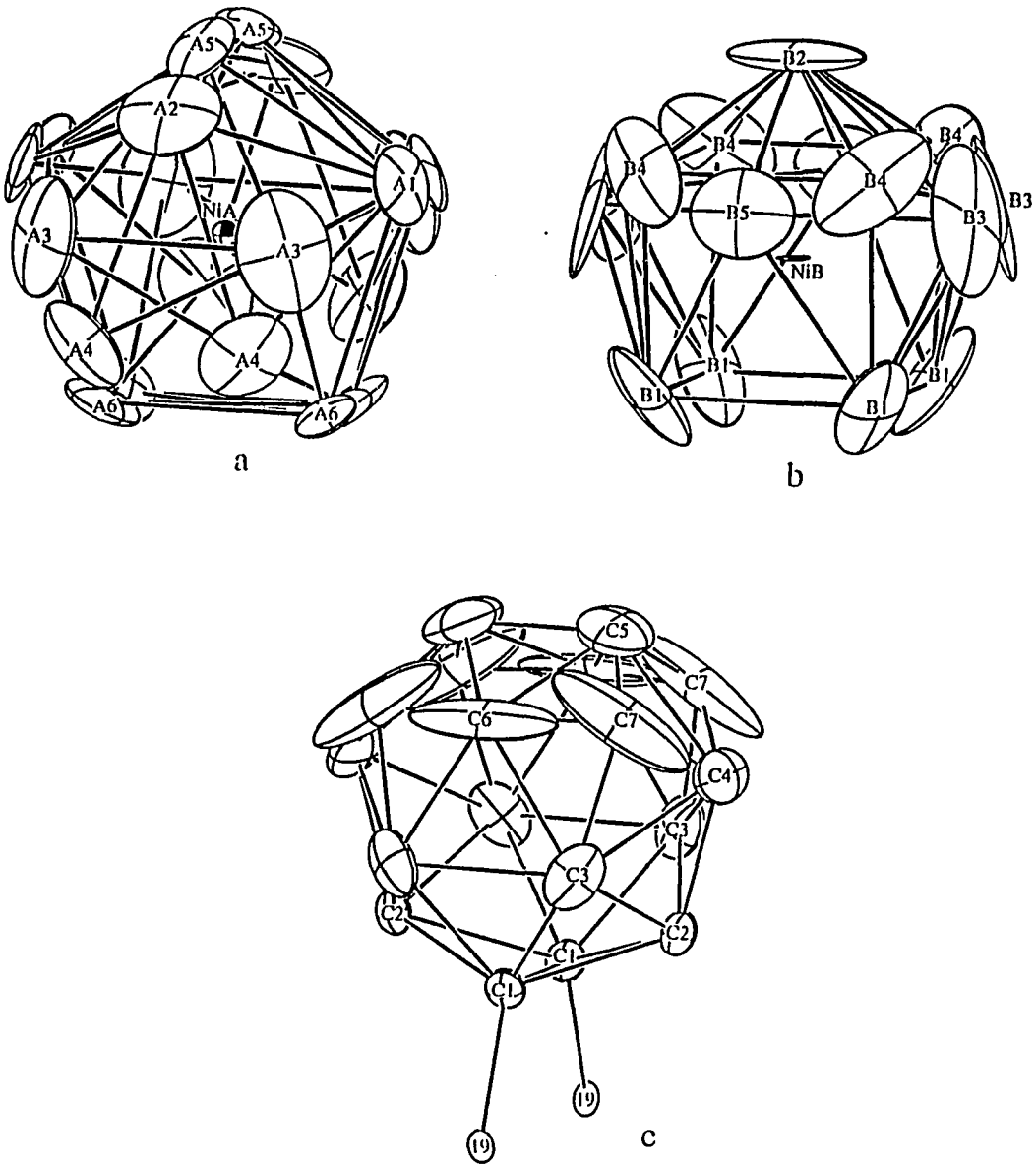

Figure 15. The 50% probability thermal ellipsoids for the encapsulated clusters centered by a) NiA, b) NiB and c) Na1 with neighbors interconnected. Notice that the Na1-centered cluster (c) is 2-bonded with exo bonds to In19 which, in turn, are bonded to the In_{78} fullerene. It is clear that many such "atoms" are too close to each other.

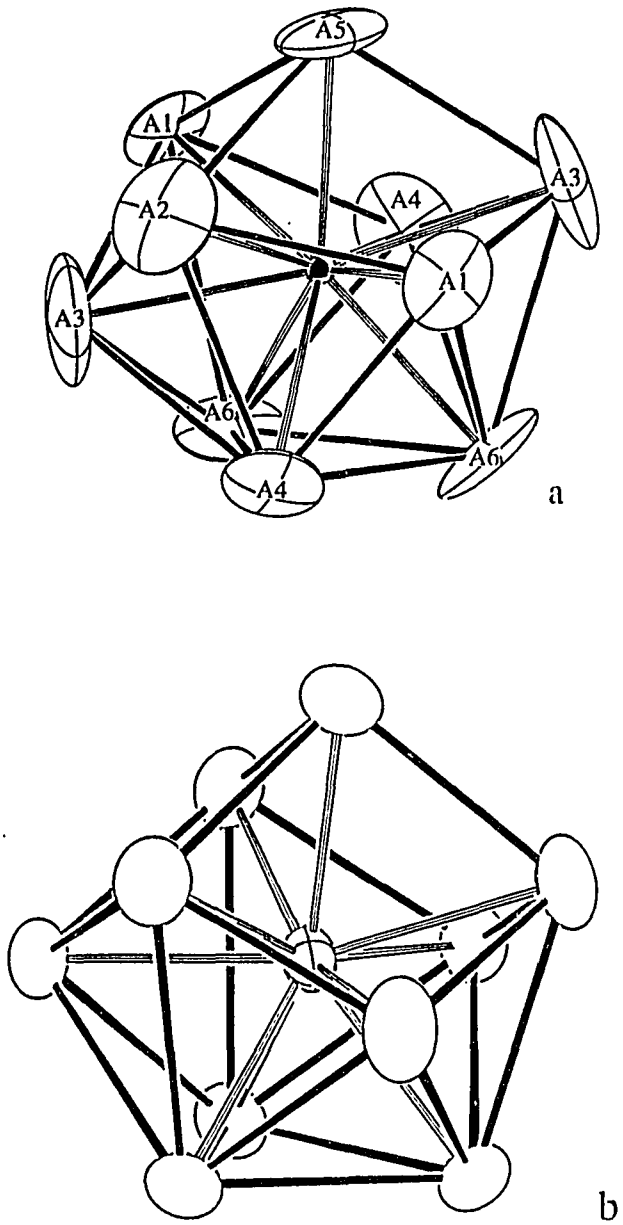

Figure 16. a) The geometry of a reasonable 10-atom model for the Ni(A)-centered cluster (50% thermal ellipsoids) compared with that of b) $In_{10}Ni^{10-}$ cluster (94% thermal ellipsoids) found in $K_{10}In_{10}Ni$.[26] Both are tetracapped trigonal prisms (vertical).

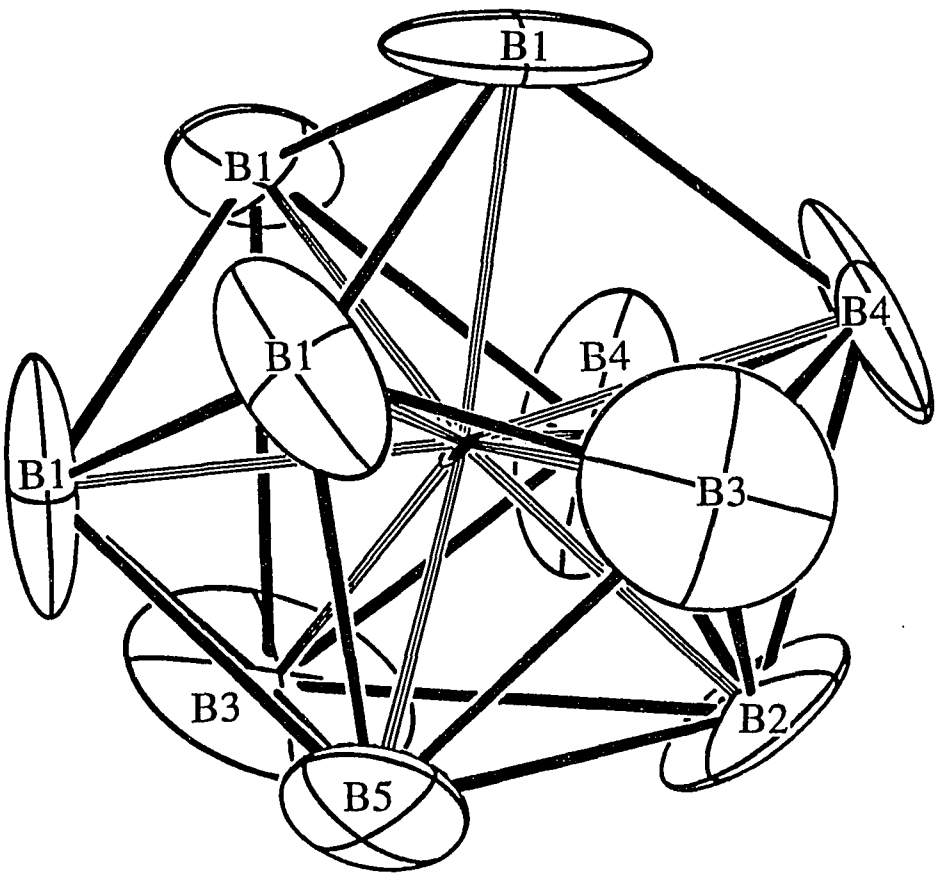

Figure 17. A 10-atom model for the NiB-centered cluster with reasonable In–In distances. Its geometry is similar to that of the model for the NiA-centered cluster (Figure 16a) as well as to the $In_{10}Ni^{10-}$ cluster in $K_{10}In_{10}Ni$ (Figure 16b). All are tetracapped trigonal prisms.

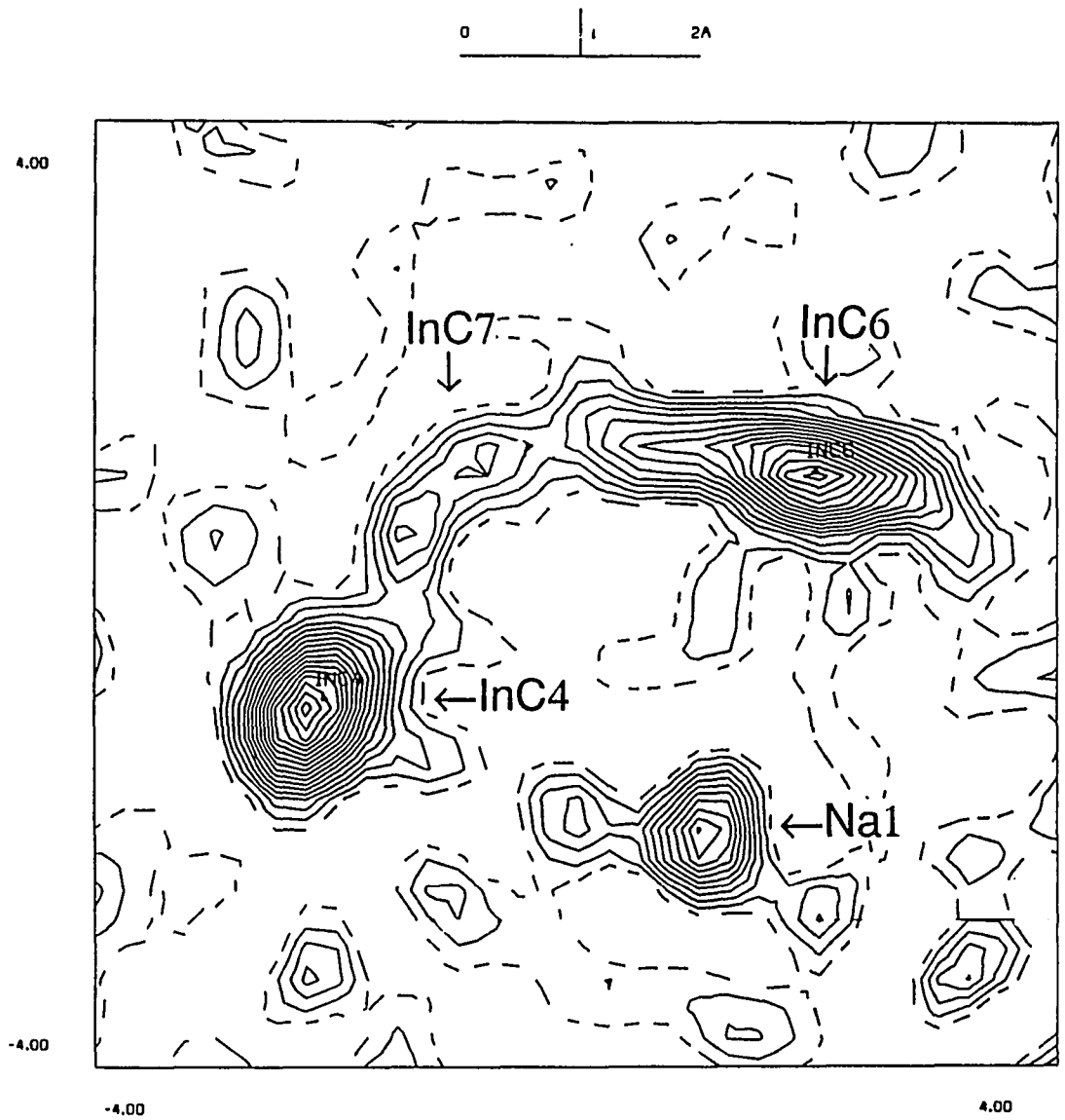

Figure 18. A plot (8 × 8 Å) of the electron density near Na1 calculated from F_{obs}. The plane is defined by InC4, InC6 and InC7 (Fig. 15c). The refined atoms at the electron density maxima are labeled. The contour interval is 2 e/Å^3.

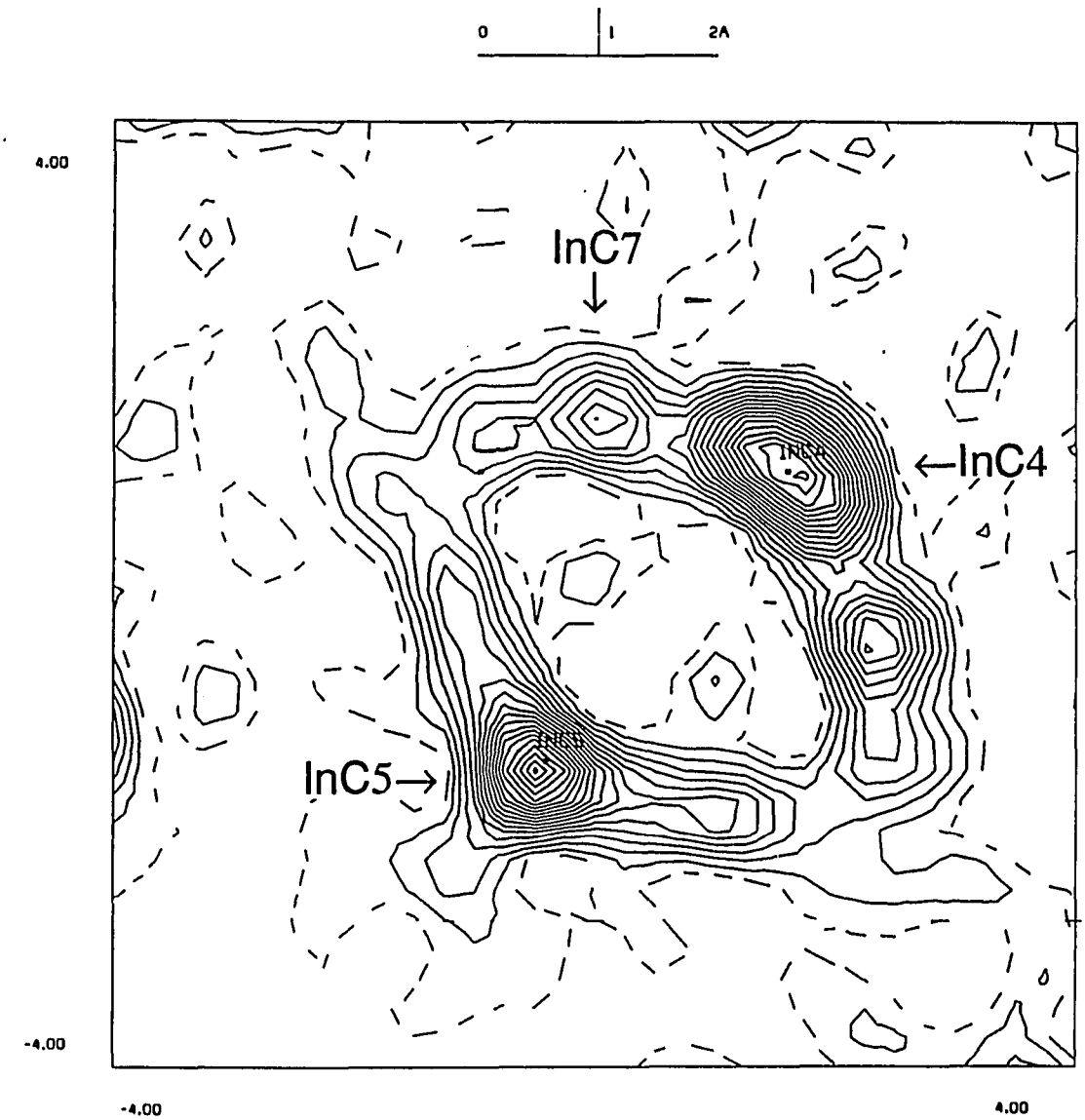

Figure 19. A plot (8 × 8 Å) of the electron density near Na1 calculated from F_{obs}. The plane is defined by InC4, InC5 and InC7 (Fig. 15c). The refined atoms at the electron density maxima are labeled. The contour interval is 2 e/Å^3.

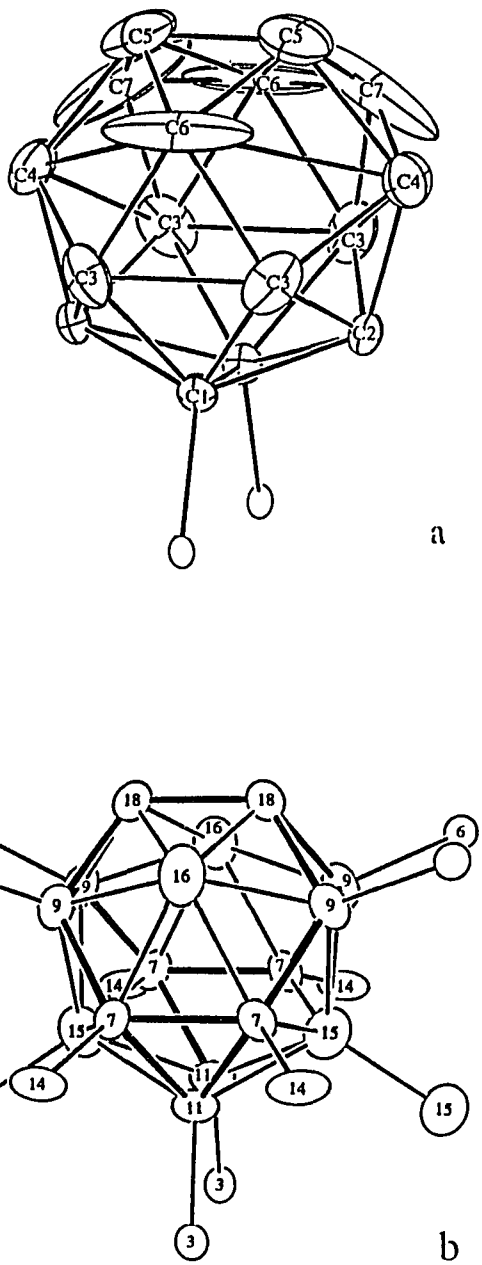

Figure 20. a) The geometry of a 16-atom model for the 2-bonded Na1-centered cluster with reasonable In–In distances, b) a similar 12-bonded *closo*-In_{16} found in $Na_{15}In_{27.4}$.[25]

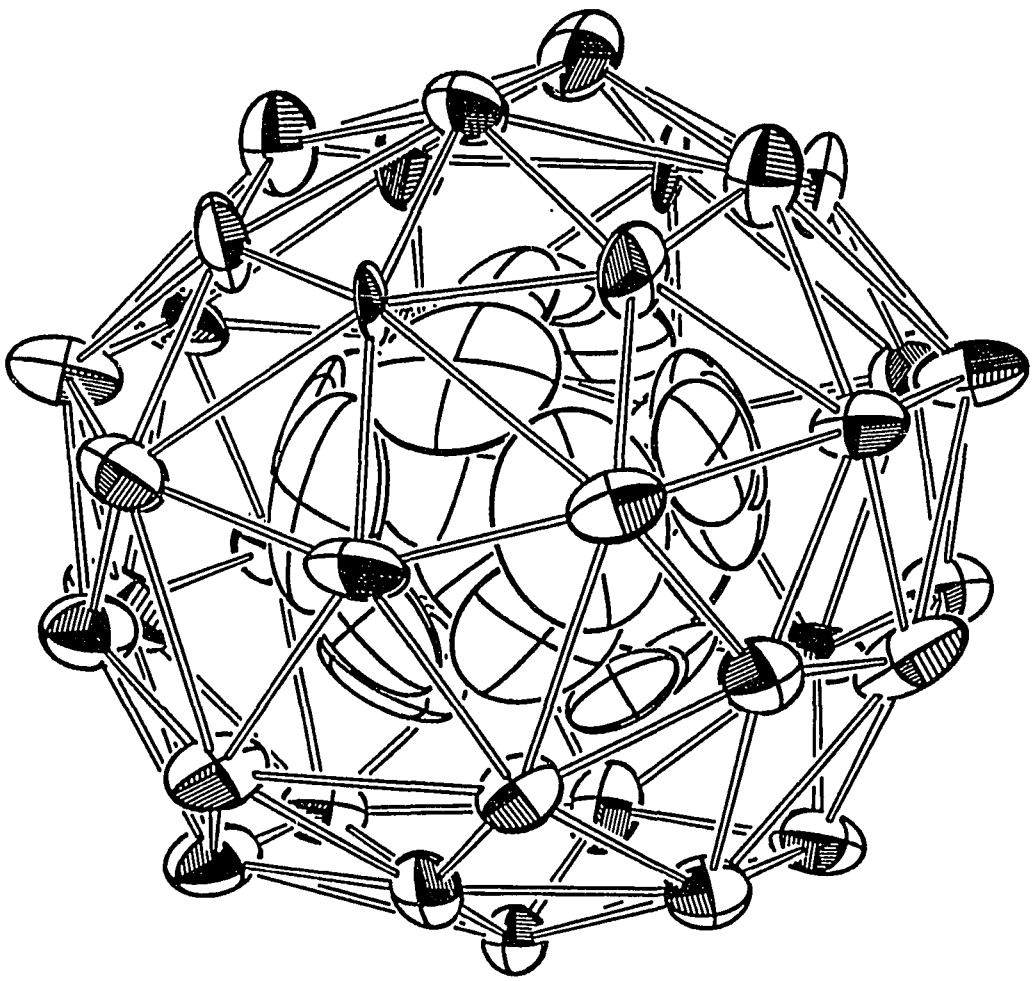

Figure 21. The positioning of the sodium atoms (shaded ellipsoids) around the isolated clusters (crossed ellipsoids) inside In_{70}. All "five-bonded" (open bonds) sodium atoms are right above "openings" in the electron density on the surface of the clusters. (94% thermal ellipsoids)

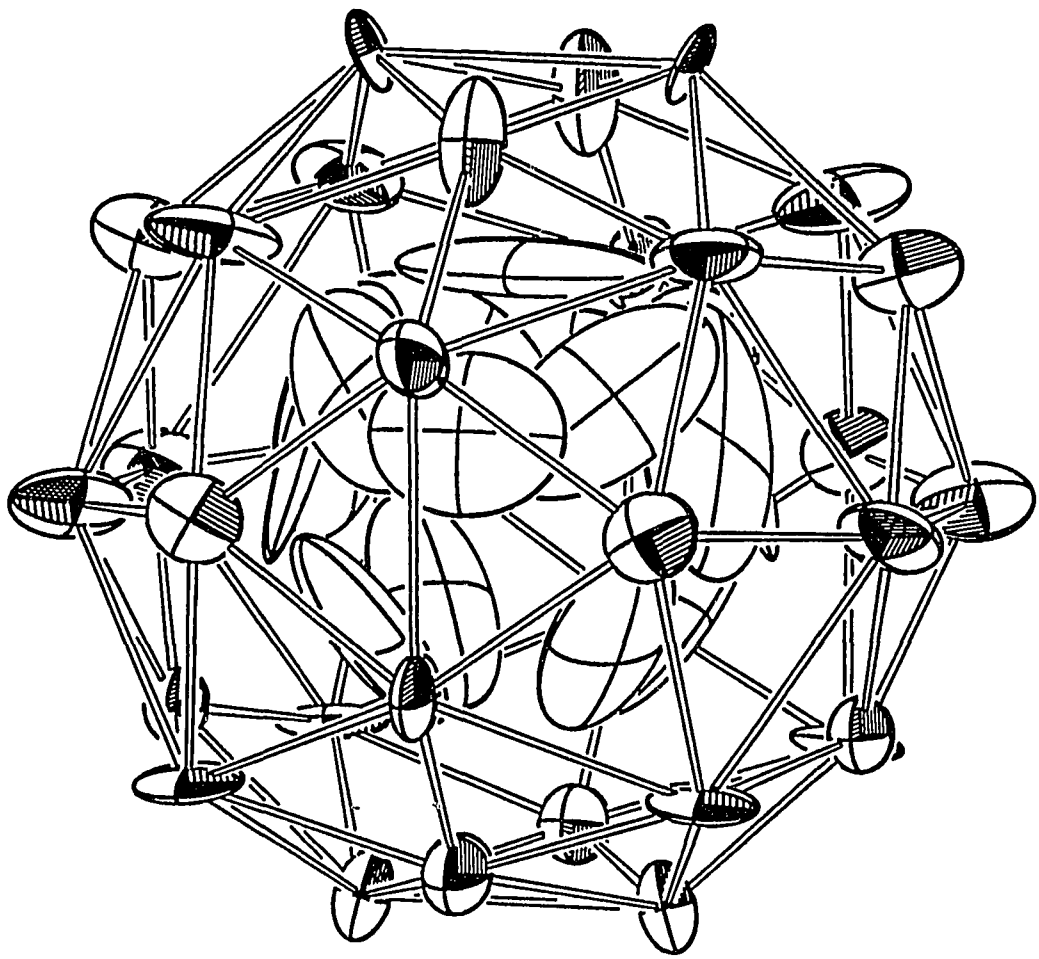

Figure 22. The positioning of the sodium atoms (shaded ellipsoids) around the isolated clusters (crossed ellipsoids) inside M_{60}. All "five-bonded" (open bonds) sodium atoms are right above "openings" in the electron density on the surface of the clusters. (94% thermal ellipsoids)

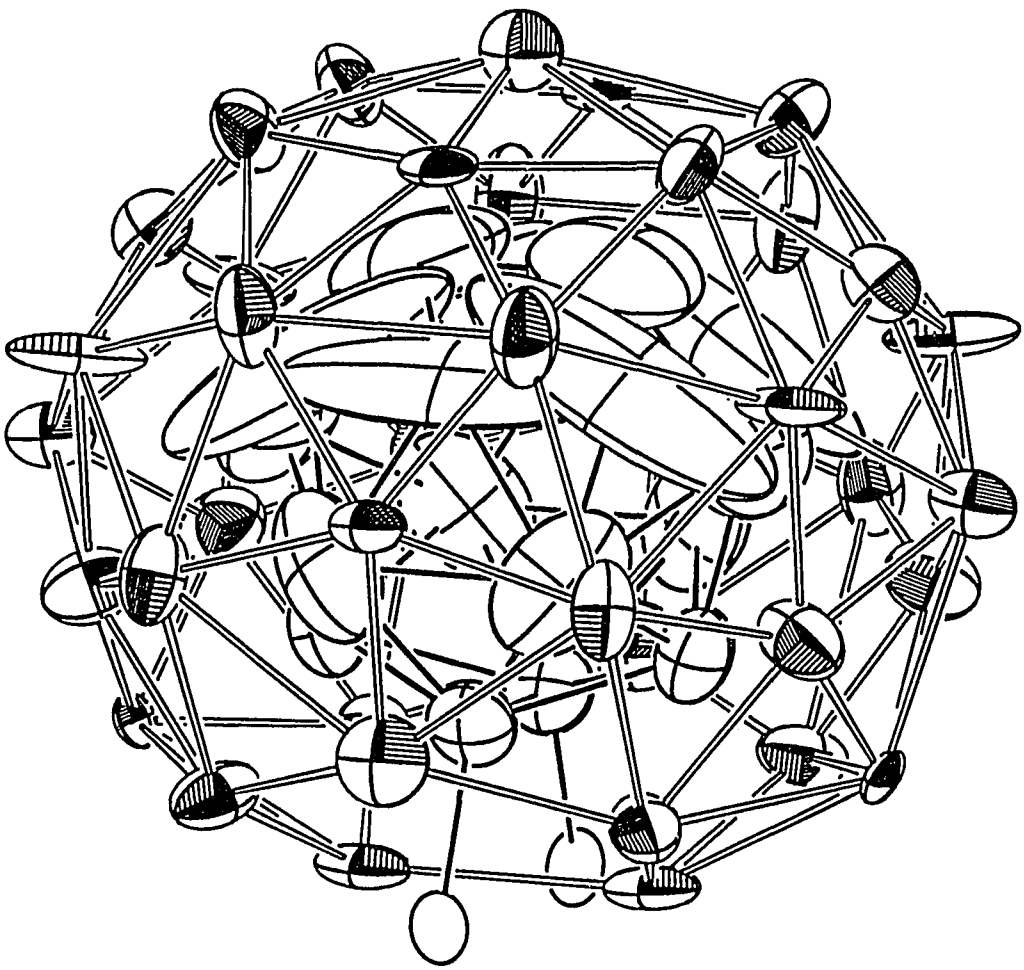

Figure 23. The positioning of the sodium atoms (shaded ellipsoids) around the isolated clusters (crossed ellipsoids) inside In_{78}. All "five-bonded" (open bonds) sodium atoms are right above "openings" in the electron density on the surface of the clusters. (94% thermal ellipsoids)

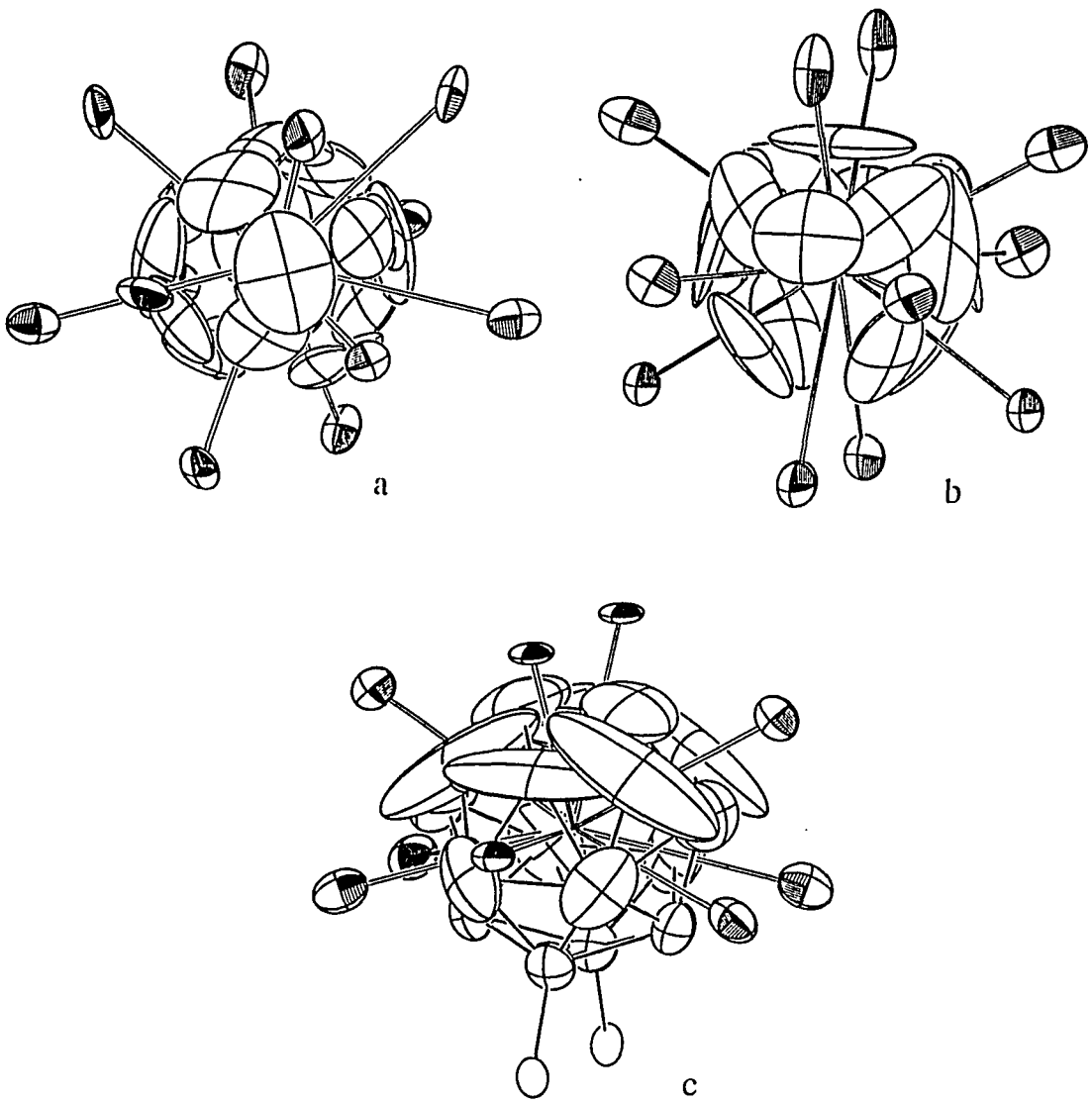

Figure 24. All of the "five-bonded" sodium atoms (shaded ellipsoids) around: a) the NiA-centered cluster, b) the NiB-centered cluster, c) the Na1-centered cluster. These lie radially above islands of nearly zero electron density on the indium cluster (crossed ellipsoids). Open lines drawn between the central atoms and the sodium atoms intersect those islands.

SUMMARY AND FUTURE WORK

General concepts

With the previous 12 papers on hand, we can deduce some general trends for the solid state chemistry of indium with negative oxidation states.

Firstly, we have to recognize the element's remarkable ability to form covalent homoatomic bonds. Moreover, this covers the range from 3-bonded all the way to 7-bonded atoms. This diversity of bonding states, of course, leads to a wide range of network structures. The proper energy separation of the s and p levels of indium is apparently responsible for the element's ability to form isolated clusters with stabilized lone pairs on the vertices and thence the applicability of Wade's (modified) rules. In addition, covalent bonding to third element makes possible the existence of centered clusters as well as substitution of indium atoms.

Secondly, we have to notice the quite contrasting structural behavior of indium compared to that of gallium. With one exception of a recently synthesized Ni-centered Ga_{10} cluster (not structurally characterized yet), no isolated clusters of the latter have been found. Although quite extensive, the networks of gallium contain only relatively small clusters that very often have partially occupied sites. Also, there is a tendency to form fused clusters, something very unusual for indium. (Only one compound, $Cs_6Na_{19}In_{59}$, has been found with two fused icosahedra.)

Thirdly, we should mention the ability of indium to imitate to some extend the structural chemistry of the tetralides when properly charged. The indium network in NaIn, as one example, is of a diamond type. Other examples are the indium tetrahedra found in Na_2In similar to the tin tetrahedra in NaSn. And a third example is the formation of fullerene-type cages of indium analogous to the well known carbon fullerenes.

Future work

As far as isolated clusters of indium are concerned, there are two structurally unfinished projects. The first one is a compound with approximate composition of "K_9In_{10}(Cu or Au)". The partial refinement of the structure shows that it contains Cu(Au)-centered clusters of In_{10} similar to the Ni-centered clusters. The problem is that a superstructure with quite large lattice parameters (in the order of 70 to 200 Å) is formed, and data collection and refinement would be nearly impossible with the available instrumentation. The second compound is with approximate formula "$Na_{10}In_{10}$(Ni, Pd or Pt) and from the partial refinement of the structure (either C-centered orthorombic or primitive monoclinic) looks like it contains Ni(Pd or Pt)-centered clusters of In_{10}. The problem is that all of the inspected crystals were twins or even maybe triplets. Perhaps different reaction conditions and subsequent inspection of large number of crystals would provide a single crystal.

Although theoretically it seems unfavorable, different approaches to form indium clusters centered by Co, Fe, Mn etc. should be undertaken. One such strategy would be to form a binary M_xIn_y intermetallic compound and use it as a precursor for the reaction with a proper alkali metal (the best bet would be potassium).

As far as new networks of clusters (some may be of novel sizes) are concerned, efforts should be concentrated on sodium and to some extend on potassium as countercations. Rubidium and cesium, in general, form a thermodynamically very stable compound A_2In_3, and the possibility of a ternary compound seems very slim. Nevertheless, in addition to $A_3Na_{26}In_{48}$, new compounds, one in the Cs–Na–In system ($Cs_6Na_{19}In_{59}$) and one in the Rb–In–Au systems, have been isolated. The structure of the first one has been solved fairly well (it contains fused icosahedra) while the second one (F-centered cubic) seems to have $MgCu_2$-type structure with icosahedra at the Cu positions and some kind of Au-centered clusters at the Mg positions.

Another phase with partially refined network-like structure, the only noncharacterized compound in the K–In system, has an approximate formula "KIn" (F-centered cubic). Again, it has $MgCu_2$-type structure with icosahedra at the Cu positions but problems at the Mg positions.

Two structure types in ternary compounds need some more work. One is a structure in the Na–In–(Ge, Sn or Pb) systems (primitive hexagonal). It has been refined partially for the Ge derivative and has been assigned as isostructural with a structure in the Na–In–Zn system, but it may not be exactly the same. The second one is in the K–In–(Sn or Pb) systems (primitive hexagonal). From a partial refinement it looks like a derivative of the structure of $K_{22}In_{39}$ but of a lower symmetry.

REFERENCES

1. Wade, K. Adv. Inorg. Chem. Radiochem. **1976**, 18, 1.
2. Schmettow, W.; von Schnering, H. G. *Angew. Chem.* **1977**, *89*, 895.
3. Hönle, W.; von Schnering, H. G. Z. *Kristallogr.* **1980**, *153*, 339.
4. Wichelhaus, W.; von Schnering, H. G. *Z. Naturwissen.* **1973**, *60*, 104.
5. Corbett, J. D. *Chem. Rev.* **1985**, *85*, 383.
6. Corbett, J. D. *Inorg. Chem.* **1968**, *7*, 198.
7. Corbett, J. D. *Prog. Inorg. Chem.* **1976**, *21*, 141.
8. Cisar, A.; Corbett, J. D. *Inorg. Chem.* **1977**, *16*, 2482.
9. Hershaft, A.; Corbett, J. D. *Inorg. Chem.* **1963**, *2*, 979.
10. Müller, W.; Volk, K. *Z. Naturforsch.* **1977**, *32b*, 709.
11. Edwards, P. A.; Corbett, J. D. *Inorg. Chem.* **1977**, *16*, 903.
12. Belin, C. H. E.; Corbett, J. D.; Cisar, A. *J. Am. Chem. Soc.* **1977**, *99*, 7163.
13. Corbett, J. D.; Edwards, P. A. *J. Am. Chem. Soc.* **1977**, *99*, 3313.
14. Belin, C.; Charbonnel, M. T. *Prog. Solid St. Chem.* **1993**, *22*, 59 and references therein.
15. Hansen, D. A.; Smith, J. F. *Acta. Cryst.* **1967**, *22*, 836.
16. Cordier, G.; Müller, V. *Z. Kristallogr.* **1992**, *198*, 281.
17. *Fullerenes: Synthesis, Properties, and Chemistry of Large Carbon Clusters*, American Chemical Society series, vol. 481, Washington, DC **1992**.